

Exploring mechanisms involved in the biosynthesis of cutaneous ceramides in health and disease

A thesis submitted to The University of Manchester for the degree of Doctor of Philosophy in the Faculty of Biology, Medicine and Health

2021

Norah N. Algazaq

School of Health Sciences

TABLE OF CONTENTS

LIST OF FIGURES	6
LIST OF TABLES	13
LIST OF ABBREVIATIONS	14
ABSTRACT	21
DECLARATION AND COPYRIGHT STATEMENT	23
ACKNOWLEDGMENTS	24
CHAPTER 1	25
1.1 SKIN STRUCTURE AND BIOLOGY	26
1.1.1 <i>Epidermal keratinocytes</i>	27
1.1.3 <i>Dermal fibroblasts</i>	29
1.2 CERAMIDES	30
1.2.1 <i>Ceramide structure and nomenclature</i>	31
1.2.2 <i>Ceramide metabolism</i>	34
1.2.2.1 Serine palmitoyltransferase	38
1.2.2.2 Ceramide synthase	38
1.2.2.3 Dihydroceramide delta 4-desaturase	40
1.2.2.4 <i>Sphingomyelin and glucosylceramide metabolising enzymes</i>	40
1.3 CUTANEOUS CERAMIDE BIOLOGY	41
1.3.1 <i>Cutaneous ceramides in diabetic dermopathies</i>	45
1.4 MEMBRANE LIPID BIOLOGY	46
1.4.2.1 Cholesterol, glycerolipids and glycerophospholipids	47
1.4.2.2 Endocannabinoids and their congeners	50
1.4.2.3 Fatty acids	53
1.5 OMEGA-3 AND OMEGA-6 PUFA IN SKIN HEALTH AND DISEASE	55
1.5.1 <i>PUFA and ceramide synthesis</i>	56
1.6 STUDY AIM AND OBJECTIVES	57
CHAPTER 2	60
2.1 CELL CULTURE	61
2.1.1 <i>Reagents and consumables</i>	61
2.1.1.1 Primary cells and cell lines	61
2.1.1.2 Reagents	62
2.1.1.3 Consumables and equipment	63
2.1.2 <i>Maintenance and subculture of cells</i>	63
2.1.2.1 Cryopreservation of cells	64
2.1.2.2 Cell count and seeding density determination	65
2.1.3 <i>Keratinocyte differentiation</i>	65
2.2 PUFA CELL TREATMENT AND TOXICITY ASSESSMENT	67
2.2.1 <i>Preparation of PUFA stock solutions</i>	67
2.2.1.1 Reagents and materials	67
2.2.1.2 PUFA stock solution preparation	67
2.2.2 <i>PUFA toxicity assessment</i>	68
2.2.2.1 Reagents and consumables	68
2.2.2.2 Preparation of PUFA doses for the MTT assay	69
2.2.2.3 MTT assay	69
2.2.3 <i>Treatment of cells with PUFAs</i>	70
2.3 REAL TIME QUANTITATIVE POLYMERASE-CHAIN REACTION (RT-QPCR) ANALYSIS	71
2.3.1 <i>Reagents and consumables</i>	71
2.3.2 <i>Method optimisation</i>	72
2.3.2.1 Housekeeping gene assessment	72
2.3.2.2 Primers target specificity validation	73
2.3.2.3 Determination of reaction volume and cDNA concentration	74
2.3.3 <i>Experimental protocol</i>	75

2.3.3.1 RNA extraction and quantification	75
RNA quantification	75
2.3.3.2 RNA conversion to cDNA	76
2.3.3.3 RT-qPCR analysis	76
2.3.4 <i>Gene expression quantification and analysis</i>	77
2.3.5 <i>Next-generation sequencing analysis</i>	78
2.4 LIPIDOMIC ANALYSIS USING UPLC/ESI-MS/MS	79
2.4.1 <i>Reagents and consumables</i>	81
2.4.1.1 Reagents.....	81
2.4.1.2 Consumables and equipment.....	82
2.4.2 <i>Preparation of internal standards and calibration samples</i>	82
2.4.2.1 Ceramide internal standards	82
2.4.2.2 Internal standards and quantitative calibration samples for endocannabinoids, N-acyl ethanolamines and monoacylglycerols.....	83
2.4.3 <i>Lipid extraction from skin and plasma samples</i>	84
2.4.4 <i>Targeted UPLC/ESI-MS/MS lipid analysis</i>	85
2.4.4.1 Analysis of skin and plasma ceramides.....	85
2.4.4.2 Analysis of skin and plasma endocannabinoids, N-acyl ethanolamines and monoacylglycerols.....	86
2.4.4.3 Protein content determination	87
2.4.5 <i>Data processing and quantitation</i>	89
2.4.5.1 Ceramide data processing and semi-quantitation.....	89
2.4.5.2 Endocannabinoids, N-acyl ethanolamines and monoacylglycerols data processing and quantitation	89
2.5 ANALYSIS OF MEMBRANE LIPIDS USING UHPSFC-MS ^E	90
2.5.1 <i>Reagents and consumables</i>	90
2.5.1.1 Reagents.....	90
2.5.1.2 Consumables and equipment.....	91
2.5.2 <i>Preparation of deuterated internal standards</i>	91
2.5.3 <i>Lipid extraction from skin cells</i>	91
2.5.4 <i>Untargeted membrane lipid analysis</i>	91
2.5.5 <i>Data processing and semi-quantitation</i>	92
2.6 STATISTICAL ANALYSIS	93
CHAPTER 3	95
3.1 INTRODUCTION	96
3.2 MATERIALS AND METHODS	98
3.2.1 <i>Analysis of keratinocyte ceramides using UPLC/ESI-MS/MS</i>	98
3.2.2 <i>Measurement of ceramide biosynthesis enzyme mRNA levels</i>	98
3.2.3 <i>Analysis of membrane lipids using UHPSFC-MS^E</i>	99
3.2.4 <i>Gene sequencing analysis</i>	99
3.3 RESULTS.....	100
3.3.1 <i>Effect of PUFA supplementation on ceramide levels</i>	100
3.3.1.1 Total ceramide levels were higher in differentiated NHEK.....	100
3.3.1.2 Ceramide levels in proliferating NHEK were significantly increased with DHA treatment	100
3.3.1.3 Treatment with DHA significantly enhanced the concentration of most ceramide classes in both cell types, whereas LA significantly increased CER[NDS] levels in differentiated NHEK.....	104
3.3.1.4 DHA significantly altered total carbon number in both cell types	121
3.3.1.5 DHA and LA significantly affected total sphingoid base-chain carbon number in proliferating NHEK.....	124
3.3.1.6 DHA and LA altered total fatty acyl-chain carbon number in proliferating NHEK.....	127
3.3.2 <i>n-3 PUFA significantly upregulated CERS3 and DES2 expression in proliferating NHEK</i>	130
3.3.2.1 DHA significantly upregulated CERS3 expression in proliferating NHEK at 48 hours post supplementation.....	130
3.3.2.2 n-3 PUFA significantly upregulated DES2 expression in proliferating NHEK.....	133
3.3.2.3 No change in CER biosynthesis enzyme gene expression was found in differentiated NHEK with PUFA	135

3.3.3 <i>n-3 PUFA significantly reduced membrane lipid levels in proliferating NHEK, whereas LA significantly increased lipid levels in differentiated NHEK</i>	138
3.3.3.1 EPA significantly reduced FFA 24:1 in proliferating NHEK, whereas LA significantly increased FFA 18:2 in differentiated NHEK.....	138
3.3.3.2 DHA significantly reduced SM levels in proliferating NHEK.....	146
3.3.3.3 DHA significantly reduced several TG species levels in proliferating NHEK.....	151
3.3.3.4 DHA reduced PC and LPC levels in proliferating NHEK, whereas LA significantly increased LPC 16:0 levels in differentiated NHEK.....	159
3.3.4 <i>Ceramide metabolism pathways were enriched in differentiated NHEK</i>	168
3.3.4.1 Ceramide metabolism pathways and differentiation-regulating genes were enriched in differentiated NHEK.....	168
3.3.5 <i>The expression of ceramide, membrane lipids and fatty acid metabolism genes was altered with differentiation</i>	172
3.3.5.1 Genes involved in S1P signalling, SPT activity and glucosylceramide metabolism were upregulated upon NHEK differentiation.....	172
3.3.5.2 DG and TG biosynthesis genes were highly expressed in differentiated NHEK whereas cholesterol degradation genes were downregulated.....	174
3.3.5.3 Fatty acid biosynthesis genes were upregulated upon NHEK differentiation.....	175
3.4 DISCUSSION.....	176
3.5 CONCLUSION.....	183
CHAPTER 4.....	185
4.1 INTRODUCTION.....	186
4.2 MATERIALS AND METHODS.....	187
4.2.1 <i>Analysis of fibroblast ceramides using UPLC/ESI-MS/MS</i>	187
4.2.2 <i>Measurement of ceramide biosynthesis enzyme mRNA levels</i>	188
4.2.3 <i>Analysis of complex membrane lipids using UHPSFC-MS^E</i>	188
4.3 RESULTS.....	189
4.3.1 <i>Supplementation with DHA and EPA for seven days significantly increased ceramide concentrations in primary HDF</i>	189
4.3.1.1 Total ceramide levels were increased in HDF cultured for seven days.....	189
4.3.1.2 Total CER[NS] levels were increased with DHA treatment for three days.....	189
4.3.1.3 Treatment with DHA or EPA for seven days significantly increased the concentration of several CER[NS], CER[NH] and CER[AH] species.....	193
4.3.1.4 DHA altered total carbon number of ceramides in HDF.....	201
4.3.1.5 DHA significantly affected total sphingoid base-chain carbon number at seven days post supplementation.....	204
4.3.1.6 DHA had a significant effect on total fatty acyl-chain carbon number.....	207
4.3.2 <i>n-3 PUFA downregulated CERS5 and CERS6 expression in HDF</i>	210
4.3.2.1 DHA and EPA significantly downregulated CERS5 and CERS6 expression at 24 and 48 hours post supplementation.....	210
4.3.2.2 No change was found in the expression of DES1 and DES2 expression in PUFA treated HDF.....	213
4.3.3 <i>n-3 and n-6 PUFA supplementation altered membrane lipid metabolism in HDF</i>	214
4.3.3.1 LA significantly reduced CE and TG levels, whereas DHA altered SM levels.....	214
4.3.3.2 DHA significantly reduced PE levels and increased PC levels, whereas LA significantly reduced PC and LPC levels in HDF.....	228
4.4 DISCUSSION.....	239
4.5 CONCLUSION.....	241
CHAPTER 5.....	242
5.1 INTRODUCTION.....	243
5.2 MATERIALS AND METHODS.....	246
5.2.1 <i>Animal model and tissue samples</i>	246
5.2.2 <i>Analysis of skin and plasma ceramides, endocannabinoids and their related mediators using UPLC/ESI-MS/MS</i>	247
5.3 RESULTS.....	247
5.3.1 <i>There was a significant decrease in CER[NH] levels in STZ-diabetic skin</i>	247
5.3.1.1 No differences were found in total ceramide levels between control and STZ-diabetic animals.....	248
5.3.1.2 Total CER[NH] levels were reduced with diabetes.....	249

5.3.1.3 Several CER[NH] species were decreased with diabetes.....	251
5.3.1.4 No difference in total carbon number was found.....	258
5.3.1.5 No difference in total sphingoid-base chains was observed.....	258
5.3.1.6 No difference in total fatty acyl-chain levels was observed.....	258
5.3.2 <i>There was a significant increase in CER[NDS] and CER[NS] levels in diabetic plasma compared with control</i>	262
5.3.2.1 No significant difference was found in total ceramide levels.....	262
5.3.2.2 There was a significant increase in total CER[NDS] with diabetes.....	263
5.3.2.3 Several CER[NDS] and CER[NS] species were elevated in diabetic plasma.....	265
5.3.2.4 Short chain ceramides were significantly increased in diabetic plasma.....	270
5.3.2.5 Total C24 sphingoid base-chain was increased in diabetic plasma.....	270
5.3.2.6 Total C16 fatty acyl-chains were elevated in diabetic plasma.....	270
5.3.3 <i>MAG and NAE species were reduced in diabetic skin</i>	274
5.3.4 <i>There was a significant decrease in NAE species in diabetic plasma</i>	277
5.4 DISCUSSION.....	280
5.5 CONCLUSION.....	286
CHAPTER 6	287
6.1 THESIS AIMS AND OBJECTIVES.....	288
6.2 EXPLORING THE PATHWAYS MEDIATING PUFA REGULATION OF CERAMIDE BIOSYNTHESIS IN PRIMARY HUMAN SKIN CELLS.....	289
6.2.1 <i>Proliferating NHEK</i>	290
6.2.2 <i>Differentiating NHEK</i>	291
6.2.3 <i>Primary HDF</i>	293
6.3 INVESTIGATING CHANGES IN CUTANEOUS CERAMIDE LEVELS IN AN STZ- DIABETIC RAT MODEL OF DPN.....	293
6.4 CONCLUSION AND FUTURE DIRECTIONS.....	295
REFERENCES	298
APPENDICES	318
APPENDIX 1.....	319
APPENDIX 2.....	319
APPENDIX 3.....	323
APPENDIX 4.....	342
APPENDIX 5.....	343
APPENDIX 6.....	354
APPENDIX 7.....	355
APPENDIX 8.....	357
APPENDIX 9.....	365
APPENDIX 10.....	377

Word count 74745

List of Figures

Figure 1.1 Skin structure.....	26
Figure 1.2 The layers of the epidermis.....	28
Figure 1.3 Sphingoid base structures.....	32
Figure 1.4 Ceramide biosynthesis pathways.....	36
Figure 1.5 Examples of two complex sphingolipids.....	37
Figure 1.6 The structure of cholesterol.....	47
Figure 1.7 The structure of glycerolipids.....	48
Figure 1.8 The structure of two abundant glycerophospholipids in skin.....	49
Figure 1.9 The structure of endocannabinoids.....	50
Figure 1.10 The synthesis of anandamide.....	51
Figure 1.11 The synthesis of 2-arachidonoylglycerol.....	52
Figure 1.12 The structure of <i>n</i> -3 and <i>n</i> -6 PUFAs.....	53
Figure 1.13 Enzymes regulating the biosynthesis of polyunsaturated fatty acids.....	55
Figure 2.1 Representative figures of primary NHEK and primary HDF.....	62
Figure 2.2 Representative figures of differentiated and proliferating NHEK.....	66
Figure 2.3 PUFA toxicity assessment for HDF treatment.....	70
Figure 2.4 Measurement of GAPDH and RPL27 in different cell types and conditions.....	73
Figure 2.5 Agarose gel electrophoresis for RT-qPCR primers.....	74
Figure 2.6 Schematic of the RT-qPCR steps.....	77
Figure 2.7 Schematic diagram of the UPLC-ESI-MS/MS principle.....	80
Figure 2.8 Representative UPLC/ESI-MS/MS chromatogram of ceramide internal standard and species.....	86
Figure 2.9 BSA standard calibration line.....	89
Figure 3.1 Total ceramide concentration in control proliferating and differentiated NHEK.....	101
Figure 3.2 The effect of PUFA supplementation on total ceramide levels per class in proliferating and differentiated NHEK.....	102
Figure 3.3 The effect of PUFA supplementation on CER[NS] species levels measured in proliferating NHEK.....	105
Figure 3.4 The effect of PUFA supplementation on CER[NS] species levels measured in differentiated NHEK.....	107
Figure 3.5 The effect of PUFA supplementation on CER[NDS] species levels measured in proliferating NHEK.....	109

Figure 3.6 The effect of PUFA supplementation on CER[NDS] species levels measured in differentiated NHEK.....	110
Figure 3.7 The effect of PUFA supplementation on CER[NH] species levels measured in proliferating NHEK.....	113
Figure 3.8 The effect of PUFA supplementation on CER[NH] species levels measured in differentiated NHEK.....	114
Figure 3.9 The effect of PUFA supplementation on CER[NP] species levels measured in proliferating NHEK.....	115
Figure 3.10 The effect of PUFA supplementation on CER[NP] species levels measured in differentiated NHEK.....	116
Figure 3.11 The effect of PUFA supplementation on CER[AH] species levels measured in proliferating NHEK.....	117
Figure 3.12 The effect of PUFA supplementation on CER[AH] species levels measured in differentiating NHEK.....	118
Figure 3.13 The effect of PUFA supplementation on CER[AS] species levels measured in proliferating NHEK.....	119
Figure 3.14 The effect of PUFA supplementation on CER[AS] species levels measured in differentiated NHEK.....	120
Figure 3.15 The effect of PUFA supplementation on CER[AP] species levels measured in differentiated NHEK.....	121
Figure 3.16 The effect of PUFA supplementation on CER total carbon chain number in proliferating and differentiated NHEK.....	122
Figure 3.17 The effect of PUFA supplementation on CER total spingoid base-chain length in proliferating and differentiated NHEK.....	125
Figure 3.18 The effect of PUFA supplementation on CER total fatty acyl-chain length in proliferating and differentiated NHEK.....	128
Figure 3.19 The effect of PUFA supplementation on CERS1-6 expression in proliferating NHEK.....	131
Figure 3.20 The effect of PUFA supplementation on DES1-2 expression in proliferating NHEK.....	134
Figure 3.21 The effect of PUFA supplementation on CERS1-4 expression in differentiated NHEK.....	136
Figure 3.22 The effect of PUFA supplementation on DES1-2 expression in differentiated NHEK.....	137
Figure 3.23 The effect of PUFA supplementation on total CE levels in proliferating and differentiated NHEK.....	139

Figure 3.24 The effect of PUFA supplementation on CE species levels measured in proliferating and differentiated NHEK.....	140
Figure 3.25 The effect of PUFA supplementation on total cholesterol levels in proliferating and differentiated NHEK.....	142
Figure 3.26 The effect of PUFA supplementation on total FFA levels in proliferating and differentiated NHEK.....	143
Figure 3.27 The effect of PUFA supplementation on FFA species levels measured in proliferating NHEK.....	144
Figure 3.28 The effect of PUFA supplementation on FFA species levels measured in differentiated NHEK.....	145
Figure 3.29 The effect of PUFA supplementation on total SM levels measured in proliferating and differentiated NHEK.....	146
Figure 3.30 The effect of PUFA supplementation on SM species levels measured in proliferating NHEK.....	147
Figure 3.31 The effect of PUFA supplementation on SM species levels measured in differentiated NHEK.....	149
Figure 3.32 The effect of PUFA supplementation on total DG levels measured in proliferating and differentiated NHEK.....	151
Figure 3.33 The effect of PUFA supplementation on DG species levels measured in proliferating and differentiated NHEK.....	153
Figure 3.34 The effect of PUFA supplementation on total TG levels measured in proliferating and differentiated NHEK.....	155
Figure 3.35 The effect of PUFA supplementation on TG species levels measured in proliferating NHEK.....	156
Figure 3.36 The effect of PUFA supplementation on TG species levels measured in differentiated NHEK.....	158
Figure 3.37 The effect of PUFA supplementation on total PC levels measured in proliferating and differentiated NHEK.....	160
Figure 3.38 The effect of PUFA supplementation on PC species levels measured in proliferating NHEK.....	161
Figure 3.39 The effect of PUFA supplementation on PC species levels measured in differentiated NHEK.....	163
Figure 3.40 The effect of PUFA supplementation on total LPC levels in proliferating and differentiated NHEK.....	165
Figure 3.41 The effect of PUFA supplementation on LPC species levels measured in proliferating and differentiated NHEK.....	166

Figure 3.42 Ceramide metabolism pathways regulating keratinocyte differentiation were enriched in differentiated NHEK.....	170
Figure 3.43 Ceramide metabolism gene expression in differentiated NHEK compared to proliferating NHEK.....	174
Figure 3.44 Sterol lipids, glycerolipid and glycerophospholipid metabolism gene expression in differentiated NHEK compared to proliferating NHEK.....	175
Figure 3.45 Fatty acid metabolism gene expression in differentiated NHEK compared to proliferating NHEK.....	176
Figure 3.46 Summary of the effects of PUFA treatment on lipid metabolism in NHEK.....	179
Figure 4.1 Total ceramide concentration in control HDF cultured for three and seven days.....	190
Figure 4.2 The effect of PUFA supplementation on total ceramide levels per class in HDF.....	191
Figure 4.3 The effect of PUFA supplementation on CER[NS] species levels measured in HDF.....	194
Figure 4.4 The effect of PUFA supplementation on CER[NDS] species levels measured in HDF.....	196
Figure 4.5 The effect of PUFA supplementation on CER[NH], CER[NP] and CER[AH] species measured in HDF.....	199
Figure 4.6 The effect of PUFA supplementation on CER total carbon chain number in HDF.....	202
Figure 4.7 The effect of PUFA supplementation on CER total spingoid base-chain length in HDF.....	205
Figure 4.8 The effect of PUFA supplementation on CER total fatty acyl-chain length in HDF.....	208
Figure 4.9 The effect of PUFA supplementation on CERS1-6 expression in HDF.....	211
Figure 4.10 The effect of PUFA supplementation on DES1-2 expression in HDF.....	213
Figure 4.11 The effect of PUFA supplementation on total CE levels in HDF.....	215
Figure 4.12 The effect of PUFA supplementation on CE species levels measured in HDF.....	216
Figure 4.13 The effect of PUFA supplementation on total cholesterol levels in HDF.....	218
Figure 4.14 The effect of PUFA supplementation on total FFA levels in HDF.....	218

Figure 4.15 The effect of PUFA supplementation on FFA species levels measured in HDF.....	220
Figure 4.16 The effect of PUFA supplementation on total SM levels measured in HDF.....	221
Figure 4.17 SM species levels measured in HDF after three days of PUFA supplementation.....	222
Figure 4.18 SM species levels measured in HDF after seven days of PUFA supplementation.....	223
Figure 4.19 The effect of PUFA supplementation on total DG levels measured in HDF.....	224
Figure 4.20 The effect of PUFA supplementation on DG species levels measured in HDF.....	225
Figure 4.21 The effect of PUFA supplementation on total TG levels measured in HDF.....	226
Figure 4.22 TG species levels measured in HDF after three days of PUFA supplementation.....	227
Figure 4.23 TG species levels measured in HDF after seven days of PUFA supplementation.....	228
Figure 4.24 The effect of PUFA supplementation on total PE levels measured in HDF.....	229
Figure 4.25 The effect of PUFA supplementation on PE species levels measured in HDF.....	230
Figure 4.26 The effect of PUFA supplementation on total PC levels measured in HDF.....	231
Figure 4.27 PC species levels measured in HDF after three days of PUFA supplementation.....	232
Figure 4.28 PC species levels measured in HDF after seven days of PUFA supplementation.....	234
Figure 4.29 The effect of PUFA supplementation on total LPC levels measured in HDF.....	236
Figure 4.30 The effect of PUFA supplementation on total LPC species levels measured in HDF.....	237
Figure 5.1 Total ceramide concentration in control and STZ- diabetic rat skin.....	248
Figure 5.2 Total CER classes measured in control and STZ-diabetic rat skin.....	250
Figure 5.3 CER[NDS] and CER[NS] species measured in control and STZ-diabetic rat skin.....	252

Figure 5.4 CER[NH] species measured in control and STZ-diabetic rat skin.....	254
Figure 5.5 CER[AS] and CER[AP] species measured in control and STZ-diabetic rat skin.....	255
Figure 5.6 CER[[EOH] measured in control and STZ-diabetic rat skin.....	256
Figure 5.7 Total carbon chain number in control and STZ-diabetic rat skin.....	259
Figure 5.8 Total sphingoid base-chain length in control and STZ-diabetic rat skin...	260
Figure 5.9 Total fatty acyl-chain length in control and STZ-diabetic rat skin.....	261
Figure 5.10 Total ceramide levels in control and STZ-diabetic rat plasma.....	262
Figure 5.11 Total CER per class measured in control and STZ-diabetic rat plasma...	264
Figure 5.12 CER[NDS] and CER[NS] species measured in control and STZ-diabetic rat plasma.....	266
Figure 5.13 CER[AS] and CER[AH] species measured in control and STZ-diabetic rat plasma.....	268
Figure 5.14 CER total carbon chains measured in control and STZ-diabetic rat plasma.....	271
Figure 5.15 Total CER sphingoid base-chains measured in control and STZ-diabetic rat plasma.....	272
Figure 5.16 Total CER fatty-acyl-chains measured in control and STZ-diabetic rat plasma.....	273
Figure 5.17 Endocannabinoid and NAE measured in control and STZ-diabetic rat skin.....	275
Figure 5.18 Endocannabinoids and N-acyl ethanolamines measured in control and STZ-diabetic rat plasma.....	278
Figure 6.1 Summary of the effects of PUFA treatment on lipid metabolism in NHEK and HDF.....	290
Figure 6.2 Summary lipid metabolism genes found altered in differentiating NHEK.....	292
Figure A 2.1 Experiment 1-a.....	320
Figure A 2.2 Experiment 1-b.....	321
Figure A 2.3 Experiment 1-c.....	321
Figure A 2.4 Experiment 2.....	322
Figure A 2.8 Experiment 3-a.....	322
Figure A 2.9 Experiment 3-b.....	323
Figure A 2.10 Experiment 3-c.....	323
Figure A 5.1,5.2 The individual Δ Ct values for CERS1-2 expression in proliferating NHEK.....	343

Figure A 5.3-5.4 The individual Δ Ct values for CERS3,4 expression in proliferating NHEK.....	344
Figure A 5.5 The individual Δ Ct values for CERS5 expression in proliferating NHEK.....	345
Figure A 5.6 The individual Δ Ct values for CERS6 expression in proliferating NHEK.....	345
Figure A 5.7 The individual Δ Ct values for DES1 expression in proliferating NHEK.....	346
Figure A 5.8 The individual Δ Ct values for DES2 expression in proliferating NHEK.....	346
Figure A 5.9 The individual Δ Ct values for CERS1 expression in differentiating NHEK.....	347
Figure A 5.10 The individual Δ Ct values for CERS2 expression in differentiating NHEK.....	347
Figure A 5.11 The individual Δ Ct values for CERS3 expression in differentiating NHEK.....	348
Figure A 5.12 The individual Δ Ct values for CERS4 expression in differentiating NHEK.....	348
Figure A 5.13 The individual Δ Ct values for DES1 expression in differentiating NHEK.....	349
Figure A 5.14 The individual Δ Ct values for DES2 expression in differentiating NHEK.....	349
Figure A 5.15 The individual Δ Ct values for CERS1 expression in HDF.....	350
Figure A 5.16 The individual Δ Ct values for CERS2 expression in HDF.....	350
Figure A 5.17 The individual Δ Ct values for CERS4 expression in HDF.....	351
Figure A 5.18 The individual Δ Ct values for CERS5 expression in HDF.....	351
Figure A 5.19 The individual Δ Ct values for CERS6 expression in HDF.....	352
Figure A 5.20 The individual Δ Ct values for DES1 expression in HDF.....	352
Figure A 5.21 The individual Δ Ct values for DES2 expression in HDF.....	353
Figure A 6.1 Growth curves.....	354
Figure A 7.1 Total CER measured in proliferating and differentiated NHEK, HDF, rat skin and plasma.....	355
Figure A 7.2 Total membrane lipids measured in proliferating NHEK, differentiated NHEK and HDF.....	356

List of tables

Table 1.1 Ceramide nomenclature.....	33
Table 1.2 CerS tissue distribution and acyl-chain length specificity.....	39
Table 1.3 Bioactive lipids and their derivatives.....	52
Table 2.1 The expression of differentiation and proliferation genes in differentiated NHEK.....	66
Table 2.2 Preparation of PUFA treatment stock solutions.....	68
Table 2.3 Details for the primers and probe mix used.....	72
Table 2.4 Δ Ct calculations for RT-qPCR data analysis.....	78
Table 2.5 BSA standard preparation.....	88
Table 2.6 The final concentration of standards in the ML IS- <i>d</i> cocktail.....	93
Table 3.1 Genes involved in CER signaling pathways controlling differentiation and apoptosis.....	171
Table A 1.1 Determination of cDNA concentration and reaction volume.....	319
Table A 3.1 MRM transitions and retention times used for the ceramide assay.....	324
Table A 4.1 MRM transitions and retention times used for the endocannabinoid assay.....	342
Table A 8.1 Ceramide species measured in proliferating NHEK (n= 3 individual donors).....	357
Table A 8.2 Ceramide species measured in differentiating NHEK (n= 3 individual donors).	358
Table A 8.3 Ceramide species measured in HDF (n= 3 individual donors).....	362
Table A 8.4 Ceramide species measured in rat skin (n=6 individual donors).....	363
Table A 8.5 Ceramides measured in rat plasma (n= 6 individual donors).....	365
Table A 9.1 Membrane lipids measured in proliferating NHEK (n= 3 individual donors).....	365
Table A 9.2 Membrane lipids measured in differentiating NHEK (n= 3 individual donors).....	369
Table A 9.3 Membrane lipids measured in HDF (n= 3 individual donors).....	373
Table A 10.1 Endocannabinoids and their congeners measured in rat skin (n= 6 individual donors).....	377
Table A 10.2 Endocannabinoids and their congeners measured in rat plasma (n= 6 individual donors).....	377

List of abbreviations

12-HEPE	12- Hydroxyeicosapentaenoic Acid
12-HETA	12- Hydroxyeicosatetraenoic Acid
18:1 DAG d5	Diacylglycerol Standard
2-AG	2-Arachidonoyl Glycerol
3-KDS	3-Ketodihydrosphingosine
46BR.1N	Immortalised Human Dermal Fibroblast Cell Line
A	Alpha-Hydroxy
AA	Arachidonic Acid
ACN	Acetone Nitrile
AD	Atopic Dermatitis
AE	Atopic Eczema
AEA	Arachidonoyl Ethanolamine
AGEs	Advanced Glycation End Products
AH	Alpha-Hydroxy 6-Hydroxysphingosine
AKT	Serine/Threonine Kinase 1, Protein Kinase B
ALA	Alpha-Linolenic Acid
ALEA	α -linolenoyl Ethanolamine
AP	Alpha-Hydroxy Phytoceramide
AP-1	Activator Protein-1 Transcription Factor
AS	Alpha-Hydroxy Ceramide
aSMase	Acidid Sphingomyelinase
BSA	Bovine Serum Albumin
C	Carbon Number
c-RAF	c-Rapidly Accelerated Fibrosarcoma
C1P	Ceramide-1-Phosphate
Ca ²⁺	Clacium
CaCl ₂	Calcium Chloride
CB1	Cannabinoid Receptor 1
CB2	Cannabinoid Receptor 2
cDNA	Complementary Deoxyribonucleic Acid
CDS1	Phosphatidate Cytidylyltransferase 1

CE	Cholesterol Ester
CER	Ceramide
CER 1 - 12	Ceramide 1 to 12
CER[ADS]	Alpha-Hydroxy Dihydroceramide
CER[AH]	Alpha-Hydroxy 6-Hydroxyceramide
CER[AP]	Alpha-Hydroxy Phytocermide
CER[AS]	Alpha-Hydroxy Ceramide
CER[DS]	Dihydroceramide
CER[EODS]	Ester-Linked Omega Hydroxy Dihydroceramide
CER[EOH]	Ester-Linked Omega-6-Hydroxysphingosine
CER[EOP]	Ester-Linked Omega-Hydroxy Phytoceramide
CER[EOS]	Ester-Linked Omega-Hydroxy Ceramide
CER[NDS]	Non-Hydroxy Dihydroceramide
CER[NH]	Non-Hydroxy 6-Hydroxyceramide
CER[NP]	Non-Hydroxy Phytoceramide
CER[NS]	Non-Hydroxyceramide
CerS	Ceramide Synthase
CerS1	Ceramide Synthase 1
CerS2	Ceramide Synthase 2
CerS3	Ceramide Synthase 3
CerS4	Ceramide Synthase 4
CerS5	Ceramide Synthase 5
CerS6	Ceramide Synthase 6
CETP	Cholesteryl Ester Transfer Protein
CH25H	Cholesterol 25-Hydroxylase
CHCl3	Chloroform
CIP	Ceramide 1 phosphate
CNS	Central Nervous System
CO2	Carbon Dioxide
Ct	Threshold Cycle
DAG	1,2-Diacylglycerol
DAGL	Diacylglycerol Lipase
DEA	Docosanoyl Ethanolamine

DEJ	Dermal-Epidermal Junction
DES1	Dihydroceramide-4 desaturase-1
DES2	Dihydroceramide-4 desaturase-2
DG	Diacylglycerol
DGKB	Diacylglycerol Kinase Beta
DGKG	Diacylglycerol Kinase Gamma
DGLEA	Dihomo- γ -Linolenoyl Ethanolamine
DHA	Docosahexaenoic Acid
DHCR24	24-Dehydrocholesterol Reductase
DHEA	Docosahexaenoyl Ethanolamine
DHEA	Docosahexaenoyl Ethanolamine
DM	Diabetes Mellitus
DMEM	Dulbecco's Modified Eagle's Medium
DMSO	Dimethyl Sulfoxide
DNA	Deoxyribonucleic Acid
DPEA	Docosapentaenoyl Ethanolamine
DPN	Diabetic Peripheral Neuropathy
DS	Dihydrophisphingosine
ECM	Extracellular Matrix
EDG	Endothelial Cell Differentiation Gene
EDGS	Epilife defined growth supplement
EDTA	Trypsin/Ethylenediaminetetraacetic Acid
ELOVL	Elongation of Very Long Chain Fatty Acids Protein
EOH	Ester-Linked Omega 6-Hydroxyceramide
EOS	Ester-Linked Omega-Hydroxy Sphingosine
EPA	Eicosapentaenoic Acid
EPEA	Endocannabinoid Cogeners Eicospentaenoyl Ethanolamine
EPEA	Eicosapentaenoyl Ethanolamine
ER	Endoplasmic Reticulum
ERK1	Extracellular Signal Regulated Kinase
FA	Fatty Acid
FA2H	Fatty Acid 2-Hydroxylase
FAAH	Fatty Acid Amide Hydrolase

FAN	Neutral Sphingomyelinase Activation Associated Factor
FBS	Foetal Bovine Serum
FFA	Free Fatty Acids
FPP	Farnesyl Pyrophosphate
GalCer	Galactosylceramide
GAPDH	Glyceraldehyde 3-Phosphate Dehydrogenase
GCase	Glycosidase
GlcCer	Glucosylceramide
GPAT2	Glycerol-3-phosphate acyltransferase 2
GPP	Geranyl Pyrophosphate
H	6-Hydroxysphingosine
HaCaT	Human Adult Low-Calcium High-Temperature Immortalised Keratinocytes
HDF	Human Dermal Fibroblasts
HEA	Heptadecanoyl Ethanolamine
HEPES	4-(2-Hydroxyethyl)-1-Piperazineethanesulfonic Acid
HMG-CoA	3-Hydroxy-3-Methylglutaryl CoA
HS	Hypertrophic Scar
ILoD	Instrumental Limit of Detection
ILoQ	Instrumental Limit of Quantification
IPA	Ingenuity Pathway Analysis
IPP	Isopentenyl Pyrophosphate
IRS-1	Insulin Receptor Substrate-1
IS-d9	Internal Standard Deuterated
JNK1	c-Jun N-Terminal Kinase 1
K1	Keratin 1
K10	Keratin 10
K14	Keratin 14
K5	Keratin 5
KDS	3-Ketodihydrospinosine
KSR	Kinase Suppressor of Ras
LA	Linoleic Acid
LC	Liquid Chromatography

LCAT	Lecithin-Cholesterol Acyltransferase
LEA	Lineoleoyl Ethanolamine
LGEA	Lignoceroyl Ethanolamine
LPA	Lysophosphatidic Acid
LPC	Lysophosphatidylcholine
LPCAT	Lysophosphatidylcholine Acyltransferase
LPCAT1	Lysophosphatidylcholine Acyltransferase 1
LPE	Lysophosphatidylethanolamine
LPS	Lipopolysaccharide Treatment
MAG	Monoacylglycerol
MAGL	Monoacylglycerol Lipase
MEA	Myristoyl Ethanolamide
MEK1	Mitogen-Activated Protein Kinase Kinase 1
MEKK1	Mitogen-Activated Protein Kinase Kinase Kinase 1
MEM	Minimum Essential Medium Eagle
MeOH	Methanol
MG	Monoacylglycerol
MKK4	Mitogen-Activated Protein Kinase Kinase 4
mRNA	Messenger Ribonucleic Acid
MTT	Tetrazolium Salt 3-(4, 5-dimethylthiazol-2-yl)-2,5-Diphenyltetrazolium Bromide
N	Non-Hydroxy
NAE	N-acyl Ethanolamine
NaOH	Sodium Hydroxide
NAPE	N-Acyl-Phosphatidylethanolamine
NAPE-PLD	NAPE-Specific Phospholipase D
NCEH1	Neutral Cholesterol Ester Hydrolase 1
NDS	Non-Hydroxy Dihydrosphingosine
NEA	Nervonoyl Ethanolamine
NFκB	Nuclear Factor Kappa B
NH	Non-Hydroxy 6-Hydroxysphingosine
NHEK	Primary Normal Human Epidermal Keratinocytes
NP	Non-Hydroxy Phytosphingosine

NS	Non-Hydroxy Sphingosine
nSMase	Neutral Sphingomyelinase
OA	Oleic Acid
OEA	Oleoylethanolamine
P	Phytoshingosine
PA	Phosphatidic Acid
PBS	Phosphate Buffered Saline
PC	Phosphatidylcholine
PDEA	Pentadecanoyl Ethanolamine
PE	Phosphatidylethanolamine
PE %	Process Efficiency
PEA	Palmitoyl Ethanolamine
PGE ₂	Prostaglandin E ₂
PGE ₃	Prostaglandin E ₃
pH	Potential of Hydrogen
PI	Phosphatidylinositol
PI3K	1-Phosphatidylinositol 3-Kinase
PIP ₂	Phosphatidylinositol (4,5)-Bisphosphate
PKC ζ	Protein Kinase C Zeta
PLC	Phospholipase C
PLP	Pyridoxal 5'-phosphate
POEA	Palmitoleoyl Ethanolamine
PP2A	Protein Phosphatase 2
PPAR- α	Peroxisome Proliferator-Activated Receptor-Alpha
PPAR- γ	Peroxisome Proliferator-Activated Receptor-Gamma
PUFA	Polyunsaturated Fatty Acid
RAS	Rat Sarcoma Gene Group
RFI	Relative Fold Increase
RNA	Ribonucleic Acid
RPL27	Ribosomal Protein L27
RT-qPCR	Real Time Quantitative Polymerase-Chain Reaction
S	Sphingosine
S1P	Sphingosine-1-Phosphate

SC	Stratum Corneum
SEA	Stearoyl Ethanolamine
SM	Sphingomyelin
SMase	Sphingomyelinase
SMPD	Sphingomyelin Cholinephosphohydrolase
SPHK	Sphingosine Kinase
SPT	Serine Palmitoyltransferase
SPTLC1	Serine Palmitoyltransferase Long Chain Base Subunit 1
SPTLC2	Serine Palmitoyltransferase Long Chain Base Subunit 2
SPTLC3	Serine Palmitoyltransferase Long Chain Base Subunit 3
sSMase	Secretory Sphingomyelinase
ssSPT	Small Subunit of Serine Palmitoyltransferase
STEA	Stearoyl Ethanolamine
STZ	Streptozotocin
TG	Triacylglycerol
TNF- α /	Tumor Necrosis Factor Alpha/Receptor 1
TNFR1	
TNS	Trypsin Neutralising Solution
UGCG	UDP-Glucose Ceramide Glucosyltransferase
UPLC/ESI- MS/MS	Electrospray Ionisation with Triple Quadrupole Tandem Mass Spectrometry
UVB	Ultraviolet B
UVR	Ultraviolet Radiation
VEA	Vaccenoyl Ethanolamine
Δ	Delta

The University of Manchester
Norah Algazaq
Doctor of Philosophy (PhD)

Exploring mechanisms involved in the biosynthesis of cutaneous ceramides in health and disease

Abstract

Ceramides are a dynamic group of bioactive lipids and major constituents of the epidermal permeability barrier. Alterations in their levels have been reported in skin conditions as well as in metabolic disorders with manifestations in the skin, such as diabetes. Polyunsaturated fatty acids (PUFAs) have been shown to affect ceramide concentration, the underlying mechanisms, however, require further investigation.

Aims: This project aims to explore mechanisms involved in the metabolism of cutaneous lipids in normal skin cells treated with PUFAs, and to examine differences in cutaneous and systemic bioactive lipid levels in a streptozotocin (STZ) -diabetic rat model of peripheral neuropathy when compared with control.

Methods: Proliferating and differentiating primary normal human epidermal keratinocytes (NHEK) and dermal fibroblasts (HDF) were treated with docosahexaenoic acid (DHA), eicosapentaenoic acid (EPA) and linoleic acid (LA) (10 μ M). Liquid chromatography coupled to mass spectrometry (UPLC-MS/MS) was used to measure ceramides (CERs), sterols, glycerolipids, free fatty acids (FFAs), glycerophospholipids, sphingomyelins (SM), endocannabinoids, N-acyl ethanolamines and monoacylglycerols. Gene expression of ceramide synthases 1-6 (*CERS1-6*) and dihydroceramide desaturases 1-2 (*DES1-2*), was achieved by RT-qPCR. Next generation sequencing was performed to determine the expression of lipid metabolism genes in differentiated and proliferating NHEK.

Results: Ceramide concentration was increased upon NHEK differentiation. CER signalling pathways and metabolism genes including serine palmitoyltransferase (SPT) and glucosylceramide, in addition to FFA and triacylglycerol (TG) metabolism genes were highly expressed in differentiated NHEK. Supplementation with DHA (10 μ M) increased ceramide CER[NS] concentration in proliferating and differentiated NHEK, and upregulated *CERS3* and *DES2* gene expression in proliferating NHEK. DHA reduced SM and TG levels, while EPA reduced FFA levels in proliferating NHEK at 72 hours post-supplementation. Neither *n-3* PUFA tested altered gene expression or membrane lipid levels in differentiated NHEK. LA increased some CERs, FFA and lysophosphatidylcholine (LPC) species in differentiated NHEK, but did not affect CER gene expression. Both EPA and DHA increased some CER species in HDF, and downregulated *CERS5* and *CERS6* mRNA expression. DHA also affected the levels of SM, phosphatidylethanolamine (PE) and phosphatidylcholine (PC) species. LA only had an effect on membrane lipids where it reduced cholesterol ester (CE), TG, PC and LPC levels in HDF. In the STZ-diabetic rat model, CER[NH] ceramides were significantly reduced in diabetic skin while short-chain ceramides were increased in plasma, 16 and 12

weeks post STZ, respectively. Significant decreases in palmitoleoyl ethanolamine (POEA) and vaccenoyl ethanolamine (VEA) levels in plasma, and pentadecanoyl ethanolamine (PDEA), oleoyl ethanolamine (OEA) and VEA in skin, were also observed.

Conclusion: This study demonstrates the differential effect of *n*-3 and *n*-6 PUFA supplementation on CER metabolism in human epidermal and dermal cells. This suggests that DHA may have a potential therapeutic benefit in the epidermis as it increased CER levels in cells representing the basal and granular layers, whereas LA may be essential for improving skin barrier function as it mainly enhanced CER concentration in differentiating cells. Based on these findings, future studies could focus on examining the effect of DHA and LA on the glucosylceramide recycling pathway in differentiated keratinocytes. In addition, investigating the effect of DHA on the SM degradation pathway in the dermis, could help to better understand the mechanisms by which DHA could alter dermal CER levels. The effect of LA on HDF lipids suggests that LA stimulates fibroblast growth, which is in agreement with previous reports on the role of *n*-6 PUFA in wound healing. Finally, the barrier critical CER[NH] ceramides were reduced in diabetic rat skin with disease progression; Future studies could investigate their potential role in diabetic dermopathies.

Declaration and copyright statement

I declare that no portion of the work referred to in the thesis has been submitted in support of an application for another degree or qualification of this or any other university or other institute of learning.

COPYRIGHT

i. The author of this thesis (including any appendices and/or schedules to this thesis) owns certain copyright or related rights in it (the “Copyright”) and s/he has given The University of Manchester certain rights to use such Copyright, including for administrative purposes.

ii. Copies of this thesis, either in full or in extracts and whether in hard or electronic copy, may be made only in accordance with the Copyright, Designs and Patents Act 1988 (as amended) and regulations issued under it or, where appropriate, in accordance with licensing agreements which the University has from time to time. This page must form part of any such copies made.

iii. The ownership of certain Copyright, patents, designs, trademarks and other intellectual property (the “Intellectual Property”) and any reproductions of copyright works in the thesis, for example graphs and tables (“Reproductions”), which may be described in this thesis, may not be owned by the author and may be owned by third parties. Such Intellectual Property and Reproductions cannot and must not be made available for use without the prior written permission of the owner(s) of the relevant Intellectual Property and/or Reproductions.

iv. Further information on the conditions under which disclosure, publication and commercialisation of this thesis, the Copyright and any Intellectual Property and/or Reproductions described in it may take place is available in the University IP Policy (see <http://documents.manchester.ac.uk/DocuInfo.aspx?DocID=24420>), in any relevant Thesis restriction declarations deposited in the University Library, The University Library’s regulations (see <http://www.library.manchester.ac.uk/about/regulations/>) and in The University’s policy on Presentation of Theses.

Acknowledgments

Firstly, I would like to thank my outstanding supervisory team, Prof Anna Nicolaou, Dr Alexandra Kendall and Dr Suzanne Pilkington. I am grateful for all your efforts and time and for your continuous support and guidance throughout my PhD project. I am lucky to have been part of such an amazing team and project.

I would also like to give special thanks to the brilliant past and present members of Prof Nicolaou's Lab. who have been a great source of encouragement and support; Dr Megan Uttley, Dr Kathryn McGurk, Dr Marta Koszyczarek, Dr Anggit L Sunarwidhi, Alya Başak, Grace Horne, Dr Loli Camacho-Muñoz, Dr Debbie Fisher, Mr Neil O'Hara, Dr Jonny Wray, Dr Adel Alghaith, Rayed Alqahtani, Dr Yousef Almoghrabi, Siriwat Sukphokkit and Yingxian Chen.

A huge thank you to Dr Leo Zeef, Dr Maya Haaker, Dr Natalie Gardiner and Dr Richard Unwin for their help in the gene sequencing and diabetic lipidomics studies.

To my dear friends Faye Aldehalan, Nada Al-Mohaisen, Hind Alrasheedi, Hanan Bukhari, Hajar Almoajel and Nora Aljindan; thank you for making this PhD journey enjoyable. I wish you all the best of luck with your studies and career.

I thank Imam Abdulrahman Bin Faisal University for funding my research. I would like to especially express my gratitude to the Division of Clinical Laboratory Sciences at IAU, and to Prof Layla Bashawri, Dr Faisal Al-Zahrani, Dr Afnan Alsultan and Dr Amani Owaidah for their continuous support and encouragement.

My heartfelt appreciation to my family. Thank you for your encouragement, prayers and endless support. Despite the miles between us, you gave me strength, kept me going through the most challenging days and always believed in me.

Chapter 1

Introduction

1.1 Skin structure and biology

The skin is a protective organ that forms a defensive barrier against external threats such as ultraviolet radiation (UVR), microorganisms and mechanical assault. In addition to this, skin prevents water and essential electrolytes within the body from being lost, thus, maintaining homeostasis. However, it goes beyond being a biological and physical barrier to being a multifunctional organ consisting of specialised cells that initiate and regulate sensory and immune response mechanisms (Proksch et al., 2008, Tobin, 2017, Chuong et al., 2002). The skin is a major site for the production and metabolism of bioactive lipids such as ceramides, membrane lipids, and lipid metabolites such as endocannabinoids and eicosanoids (Harding, 2004, Kendall et al., 2015). These bioactive lipids and their metabolites are major signalling molecules involved in inflammatory response mechanisms and regulation of cellular function (Kendall and Nicolaou, 2013). Therefore, the skin is considered a great model to study lipid function and metabolism pathways in health and disease. The three layers of which skin is composed are: the epidermis, the dermis and the hypodermis (**Figure 1.1**).

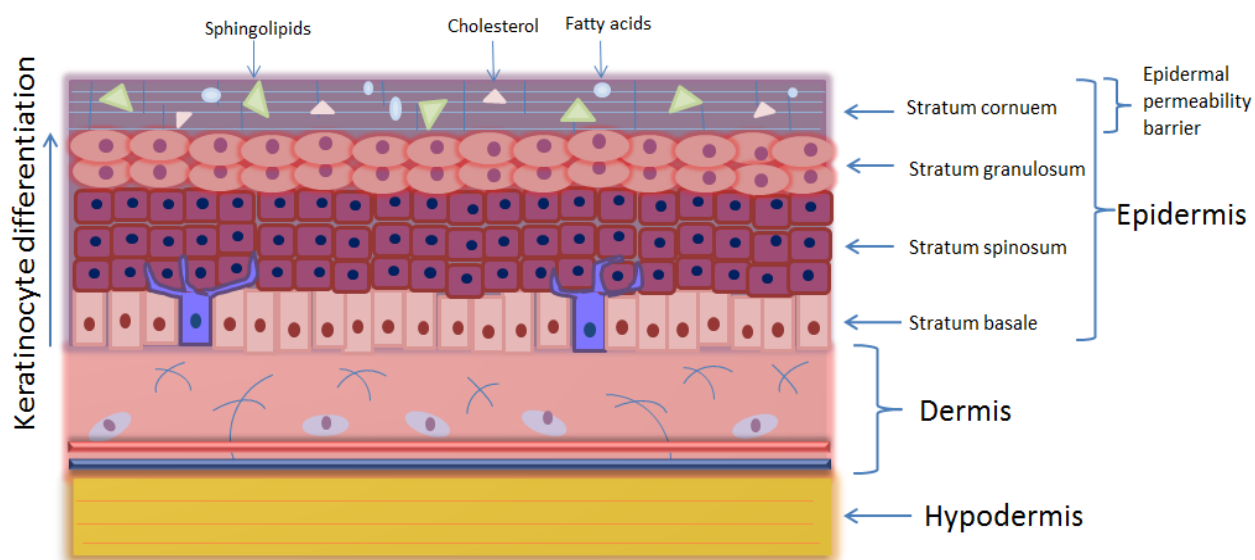


Figure 1.1 Skin structure. The illustration shows the deepest skin layer, the hypodermis; with the overlying dermis that contains dermal cells and fibres. The epidermis is composed of four layers: stratum basale, stratum spinosum, stratum granulosum and stratum corneum where fully differentiated keratinocytes are found. The stratum corneum, together with its lipids form the skin's permeability barrier.

Starting from the innermost layer, the hypodermis is vascularised and is composed of adipose tissue that connects the skin to the underlying muscle tissue. It contains adipocytes that store lipids such as fatty acids, triacylglycerols and lipid mediators, which serve to provide energy, structurally support the skin and trigger inflammatory responses (Iyer et al., 2010, Coelho et al., 2013). Above the hypodermis is the dermis, which contains blood vessels, immune cells, functionally heterogeneous fibroblasts, nerve endings, structural proteins, sweat glands and hair follicles (Lai-Cheong and McGrath, 2013). Dermal bioactive lipids such as ceramides, sterols, FAs, phospholipids, in addition to receptors for lipid mediators are involved in inflammatory mechanisms (Uchida et al., 1988, Kendall and Nicolaou, 2013). Overlying the dermis is the epidermis, which contains nerve endings, keratinocytes, melanocytes, Langerhans cells and Merkel cells that play a role in immune response (Lai-Cheong and McGrath, 2013). It contains a higher lipid content than the dermis, which is mainly produced by keratinocytes, and forms the skin's first line of defense, the permeability barrier (Uchida et al., 1988, Weerheim and Ponc, 2001). The epidermis and dermis communicate by transcellular signalling and support each other through an exchange of nutrients (Yamaguchi et al., 2005, Kendall et al., 2015). The following sections will discuss the biology of the main epidermal and dermal cells, keratinocytes and fibroblasts.

1.1.2 Epidermal keratinocytes

The epidermis is composed of four layers of keratinocytes that undergo a gradual terminal differentiation process starting from the innermost stratum basale, then moving through the overlying stratum spinosum, stratum granulosum and reaching the outermost stratum corneum (SC) (**Figure 1.2**) (Proksch et al., 2008). The outermost layer of the epidermis, SC, contains fully differentiated keratinocytes (corneocytes) and forms the epidermal permeability barrier, which serves as a shield against the environment. The barrier is enriched with an extracellular lipid matrix of ceramides (50%), cholesterol (25%), fatty acids (15%) that are secreted by lamellar bodies from keratinocytes in the underlying granular layers (Harding, 2004, Menon, 2002). Lipids secreted by differentiating keratinocytes are crucial for barrier integrity and homeostasis. Studies on murine keratinocytes, normal human keratinocytes and immortalized human keratinocytes showed a correlation between

their lipid content and their state of differentiation (Calderón et al., 2020). In addition to this, corneocytes provide protection from mechanical and chemical stress due to the cornified envelope structure which surrounds the cells (Matoltsy and Matoltsy, 1966, Sun and Green, 1976). Similarly, the lipid matrix regulates permeability and selective absorption, in addition to corneocyte development (Murphrey et al., 2020). The main barrier lipids are ceramides, which constitute about 50 % of the total permeability barrier lipid content (Breiden and Sandhoff, 2014). Ceramides are highly complex bioactive sphingolipids that have earned great interest in studies on inflammation, diabetes, neurodegenerative disease and cutaneous disorders. Permeability barrier perturbations such as increased water permeability and altered ceramide profile are seen in multiple inflammatory skin disorders such as atopic dermatitis (AD), atopic eczema (AE) and psoriasis (Harding, 2004, Jungersted *et al.*, 2010, Lee and Lee, 2014).

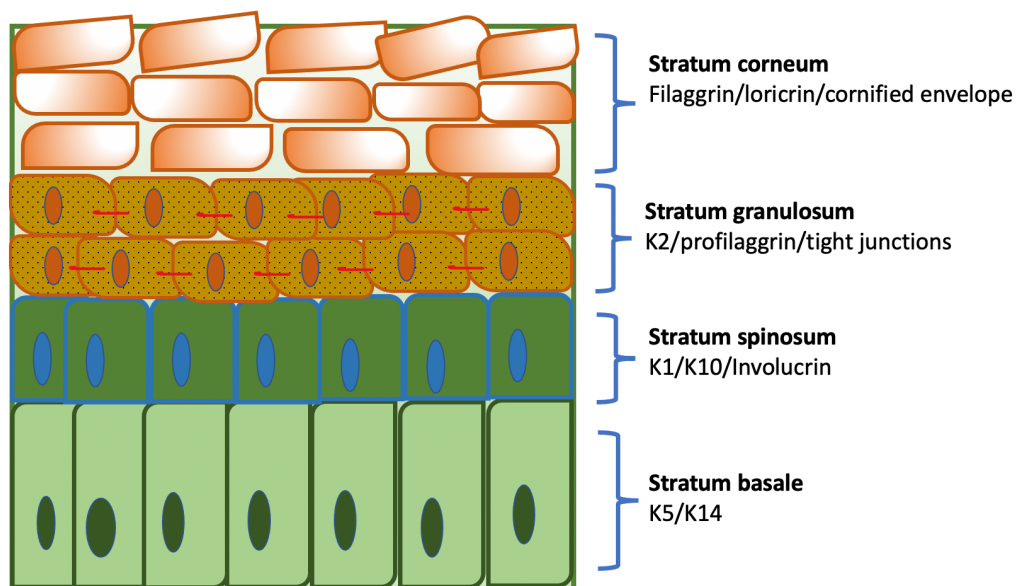


Figure 1.2 The layers of the epidermis. The epidermis consists of four layers: stratum corneum, stratum granulosum, stratum spinosum, and stratum basale. Adapted from (Bikle et al., 2012).

Keratinocyte differentiation is a highly regulated process that aims to form the cornified envelope in the SC and tight junctions in the granular layer (**Figure 1.2**). In addition to this, it occurs under specific conditions such as an epidermal calcium and pH gradient, and temperature (Bikle et al., 2012, Borowiec et al., 2013, Ohman and Vahlquist, 1994). During Keratinocyte differentiation, changes in cellular

morphology and in the expression of proliferation and differentiation markers occur. Firstly, proliferating cells, which originate from stem cells in the stratum basale, form a monolayer of nucleated columnar-shaped cells that attach to the basement membrane underneath (Proksch et al., 2008). Proliferating keratinocytes in the basal layer express proliferation makers such as keratin 5 (K5) and keratin 14 (K14) (Nelson and Sun, 1983). The nucleated cells in the basal layer can synthesize DNA and are therefore in a proliferative mitotic state (Wikramanayake et al., 2014, Fuchs, 1990). Next, the cells exit mitosis and differentiation is initiated, where cells detach from the basement membrane and migrate to the stratum spinosum. Here the morphological changes include the formation of large and flat cells that are connected by structures known as desmosomes. Differentiating cells at this stage express early differentiation markers: keratin 1 (K1), keratin 10 (K10), involucrin and transglutaminases (Yuspa et al., 1989, Rice and Green, 1979).

The cells continue to migrate up through the granular layers where, as the name suggests, the cells contain keratohyalin granules in addition to lamellar bodies (Lavker and Matoltsy, 1971, Ishida-Yamamoto et al., 1993). Here tight junctions form and the cells produce keratin 2 (K2) and profilaggrin (Collin et al., 1992, Matsui and Amagai, 2015). When the cells reach the SC, they are enucleated, and the plasma membrane is replaced with a cornified envelope. Fully differentiated cells in the SC connect with each other by corneodesmosomes and form multiple layers that forms the SC (Blaydon and Kelsell, 2014, Wikramanayake et al., 2014). Markers of the final stage of differentiation include filaggrin and loricrin (Mehrel et al., 1990, Matsui and Amagai, 2015).

1.1.3 Dermal fibroblasts

Fibroblasts are functionally heterogenous cells that are found in different tissues, which produce extracellular matrix (ECM) proteins such as collagen, fibrin, elastin and proteoglycans which play a role in injury repair and support tissue integrity (Muhl et al., 2020). Dermal fibroblast phenotype is based on the dermis layer at which they reside (Sorrell et al., 2007). The dermis consists of two vascular layers: the upper papillary dermis and the lower reticular dermis. The papillary dermis contains blood vessels and nerves that supply the epidermis, in addition to papillary fibroblasts that support epidermal development. Papillary fibroblasts communicate

with keratinocytes via the dermal-epidermal junction (DEJ) to form the basement membrane where the two skin layers attach (Marinkovich et al., 1993). The reticular dermis contains reticular fibroblasts and hair follicles which terminate in the hypodermis (Sorrell and Caplan, 2004). Although the exact function of the different fibroblast types is not fully understood, it has been suggested that papillary and reticular fibroblasts are metabolically distinct. For example, the papillary dermis is thinner and contains a less dense amount of connective tissue fibres than that in the reticular dermis (Woodley, 2017). Similarly, the amount of ECM produced by dermal fibroblasts differ according to the dermal layer in which fibroblasts are found (Sorrell et al., 2007).

Moreover, fibroblasts can differentiate into specialised cells such as myofibroblasts and adipocytes. For example, following injury, endoplasmic reticulum (ER) stress initiates fibroblast differentiation into myofibroblasts that possess fibroblast and smooth muscle cell properties, which is essential for fibrosis (Matsuzaki et al., 2015, Griffin et al., 2020). Additionally, fibroblasts could differentiate into adipocytes via peroxisome proliferator-activated receptor gamma (PPAR- γ) activation (Takeda et al., 2017, Gregoire, 2001). It has been suggested that reticular fibroblasts are the key players in wound healing, whereas papillary fibroblasts are activated at later stages as keratinocytes reepithelialise the injury site (Woodley, 2017).

1.2 Ceramides

Ceramides (CERs) are bioactive lipids that are actively involved in major molecular mechanisms in the body. The term bioactive lipids refers to “lipids derived from components of the cellular membrane that mediate cellular function”, where a decrease or accumulation of these lipids could disturb cellular function and cause disease (Nicolaou and Kokotos, 2004). Advances in lipid research revealed the crucial contributions of CERs in regulating various processes from skin barrier stability, energy production, and signal transduction, to apoptosis, inflammation and insulin-resistance (Hannun and Obeid, 2011, Hannun and Obeid, 2008, Charruyer et al., 2008). However, the mechanisms involved in CER metabolism and function, such as the synthesis and metabolism of 6-hydroxyceramide, and the

specific functions of individual CER species have not been fully explored. Elucidating CER function relies not only on classifying and quantifying CER classes, but on investigating CER production and metabolism as well, which remains a challenge. Although this field has been rapidly developing, studies on the major biochemical pathways and the regulating enzymes involved in cutaneous CER metabolism are limited. The reason for this could be owed to the structural and functional complexity of these bioactive lipids.

1.2.1 Ceramide structure and nomenclature

Ceramides are sphingolipids which contain an amino alcohol sphingoid-base chain such as sphingosine and form the backbone for the more complex sphingolipids such as sphingomyelin (Chakraborty and Jiang, 2013). The complexity of CERs arises from the variation in fatty acid (FA) and sphingoid-chain base combinations that form these significant epidermal sphingolipids. In addition to the numerous possibilities for amide bond coupling of sphingoid bases and FAs, CER heterogeneity is attributed to other factors such as chain length variations, hydroxylation, degree of saturation and the number of double bonds (Coderch et al., 2003, Kihara, 2016). Regarding the sphingoid -base chains, four main sphingoid bases could be found in different CER species including dihydrosphingosine [DS] also known as sphinganine, sphingosine [S], phytosphingosine [P] and 6-hydroxysphingosine [H]. These CER structural units vary according to the number of hydroxyl groups and the presence of double bonds. **Figure 1.3** illustrates the different structural characteristics of the four main sphingoid bases, where dihydrosphingosine and sphingosine share similar structures consisting of a carbon chain, two hydroxyl groups with an additional double bond positioned at carbon 4 in sphingosine. Phytosphingosine is similar to dihydrosphingosine with a third hydroxyl group at position 4, whereas 6-hydroxysphingosine structure includes both a double bond at position 4 and a third hydroxyl group at position 6 as the name suggests.

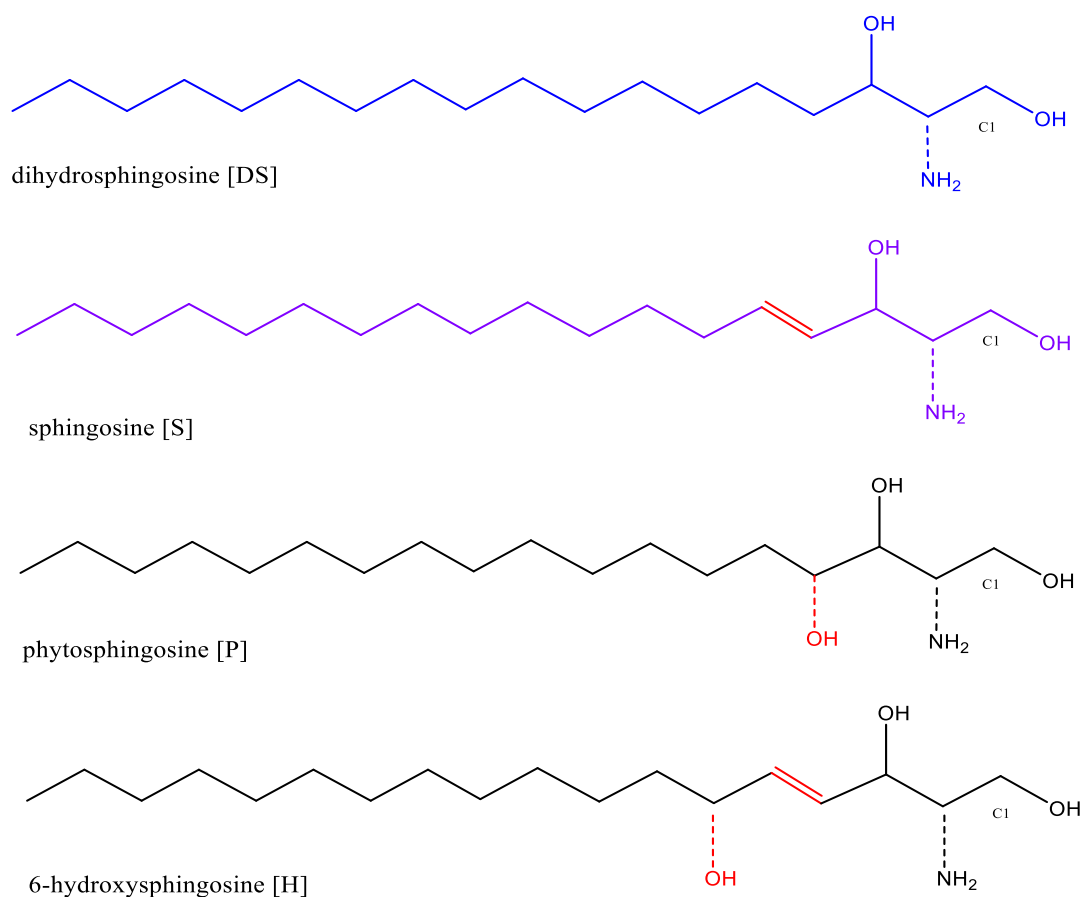
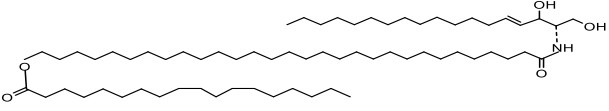
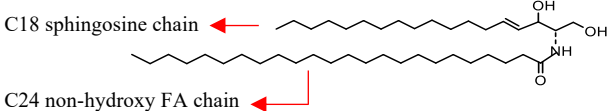
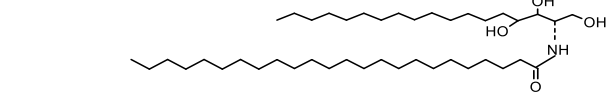
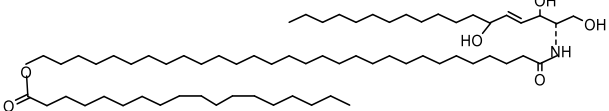
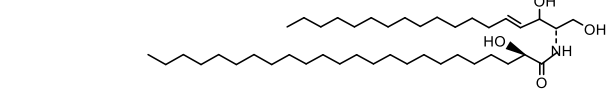
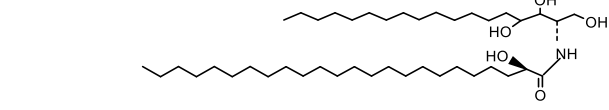
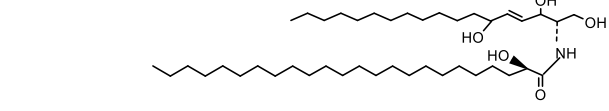


Figure 1.3 Sphingoid base structures. In this figure, examples of the four main long-chain base molecular structures are shown: dihydrosphingosine, sphingosine, phytosphingosine and 6-hydroxysphingosine. Figure shows structural similarities and differences in the the four sphingoid bases in different colours. C1 refers to the the carbon at position 1 in the sphingoid-base chain.

Furthermore, as reviewed by (Kendall and Nicolaou, 2013), FA chains are major constituents that form CER and are found as either non-hydroxy (N), alpha-hydroxy (A), or esterified omega-hydroxy (EO) FAs. Combining the two basic building blocks that generate CER, nomenclature mainly depends on the specific long chain base present and the FA's degree of hydroxylation. For example, CER[NS] represent the most common CER species which contain sphingosine and a simple non-hydroxy FA (**Table 1.1**). 12 CER families have been reported in human SC and are classified according to the two carbon chains (long-chain base and amide-linked FA chain) with varying lengths, and the type of polar head groups attached (van Smeden et al., 2011, Janssens et al., 2012, Kendall and Nicolaou, 2013). **Table 1.1** lists the 12 CER families that have been identified in skin and their nomenclature, where the CER-1 family as previously known, for example, includes

the CER[EOS] species with a sphingosine long-chain base and an ester-linked omega-hydroxy fatty acid (Breiden and Sandhoff, 2014). To name CER, the following notation is used: adding a number after the fatty acid abbreviation (N, A, EOS) represents the FA chain length and the degree of saturation, whereas the number following the sphingoid base indicates the number of carbon atoms present in the sphingoid base chain. For example, CER[NS] described as N(24)S(18) denotes the presence of a C24 non-hydroxy FA chain and a C18 carbon sphingosine chain. An example for this would be *CER-2* in (Table 1.1).

Ceramide class (old notation)	Nomenclature (new notation)	Representative CER structures
<i>CER-1</i>	CER[EOS]	
<i>CER-2</i>	CER[NS]	<p>C18 sphingosine chain ←</p>  <p>C24 non-hydroxy FA chain ←</p>
<i>CER-3</i>	CER[NP]	
<i>CER-4</i>	CER[EOH]	
<i>CER-5</i>	CER[AS]	
<i>CER-6</i>	CER[AP]	
<i>CER-7</i>	CER[AH]	

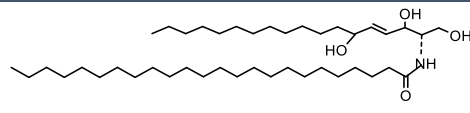
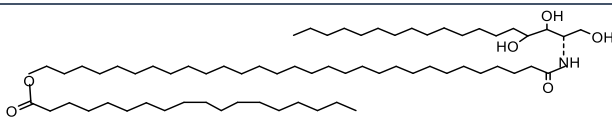
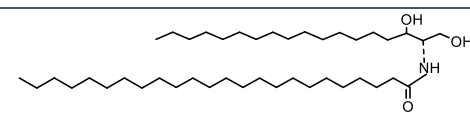
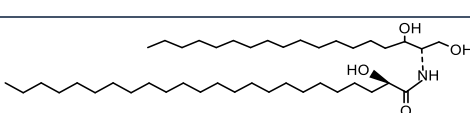
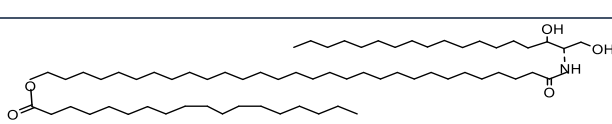
<i>CER-8</i>	CER[NH]	
<i>CER-9</i>	CER[EOP]	
<i>CER-10</i>	CER[NDS]	
<i>CER-11</i>	CER[ADS]	
<i>CER-12</i>	CER[EODS]	

Table 1.1 Ceramide notation systems. EOS: ester-linked omega hydroxy FA + sphingosine, NS: non-hydroxy FA + sphingosine, NP: non-hydroxy FA+ phytosphingosine, EOH: ester-linked omega hydroxy FA + 6-hydroxysphingosine, AS: alpha-hydroxy FA+ sphingosine, AP: alpha-hydroxy FA+ phytosphingosine, AH: alpha-hydroxy FA + 6-hydroxysphingosine, NH: non-hydroxy FA+ 6-hydroxysphingosine, EOP: ester-linked omega hydroxy FA + phytosphingosine, NDS: non-hydroxy FA + dihydrosphingosine, ADS: alpha-hydroxy FA + dihydrosphingosine, EODS: ester-linked omega hydroxyl FA + dihydrosphingosine.

1.2.2 Ceramide metabolism

Ceramide biosynthesis is a dynamic process that involves a group of at least 28 individual enzymes and complex regulatory mechanisms, which altogether lead to the combination of specific sphingoid bases, FAs and headgroups, thus, generating various CER species with unique characteristics and roles (Hannun and Obeid, 2011). A schematic outline of this pathway is shown in **Figure 1.4**.

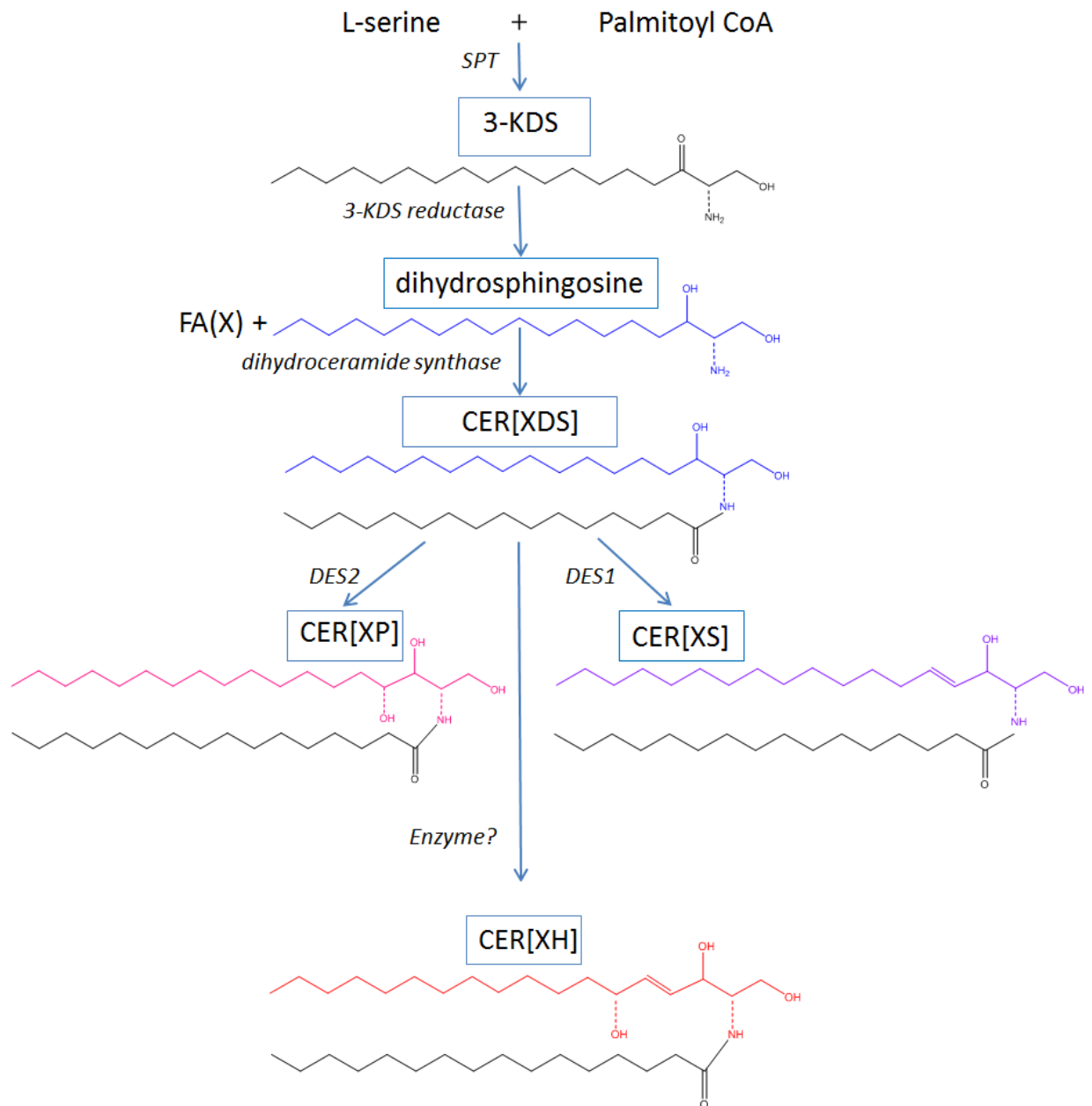
The first and rate limiting step in the CER *de novo* synthesis pathway occurs in the endoplasmic reticulum (ER), and is catalysed by serine palmitoyltransferase (SPT), which is responsible for the production of 3-ketodihydrosphingosine (KDS) by the condensation of an amino acid and a palmitic acid (C16), mainly, L-serine and palmitoyl-CoA respectively (C16) (Yard et al., 2007, Kihara, 2016, Martinez-Montanes et al., 2016).

The second step in the *de novo* synthesis pathway involves the reduction of 3-ketodihydrosphingosine (3-KDS) to form dihydrosphingosine, which is then N-acylated by a ceramide synthase (CerS) which is a group of six enzymes with specific acyl-chain preference. This step generates dihydroceramide (CER[DS]) (Airoola and Hannun, 2013). The degree of saturation for the fatty acid added to generate CER[DS] could either be N, A, EO or O, and is referred to as X in **Figure 1.4**. Dihydrosphingosine is considered an important intermediate in the formation of sphingosine and subsequently, other CER classes (Pruett et al., 2008).

The final step in this pathway generates either sphingosine-based CER (CER[S]) or phytoceramide CER[P], where CER[DS] is either desaturated by using Δ -4 desaturase-1 (Des1) to give CER[S] or hydroxylated by desaturase-2 (Des2) to give CER[P] (Ternes et al., 2002, Kihara, 2016). However, knowledge on 6-hydroxyceramide (CER[H]) is limited, as its synthesis remains unexplored.

Additional structural modifications to the sphingoid base polar headgroup of CER produce more complex sphingolipids such as sphingomyelin (SM) where a phosphocholine group is introduced, and glycosphingolipids such as glucosylceramide (GlcCer) and galactosylceramide (GalCer) where glucose or galactose are added, respectively (**Figure 1.5**) (Kihara et al., 2007, Kihara, 2016). The salvage pathway in CER biosynthesis is responsible for the breakdown of SM and glycosphingolipids in the lysosome or endosome (Wegner et al., 2016). This involves the recycling of SM by sphingomyelinase (SMase) where SM is hydrolysed in the lysosome into CER and the additional headgroup, phosphorylcholine (Goni and Alonso, 2002). Another route for CER production is the recycling of free sphingosine using the CerS family (**Figure 1.4 B**). Sphingosine could be directly released from CER by ceramidases, or from CER resynthesised from SM and glycosphingolipids via SMase and glycosidase (GCase), respectively (Kitatani et al., 2008, Mullen et al., 2012). Following the release of sphingosine, tissue specific CerS1-CerS6 reassemble CER. Moreover, ceramide-1-phosphate (C1P) and sphingosine-1-phosphate (S1P) are produced by phosphorylation of the 1-hydroxy group of sphingosine.

A



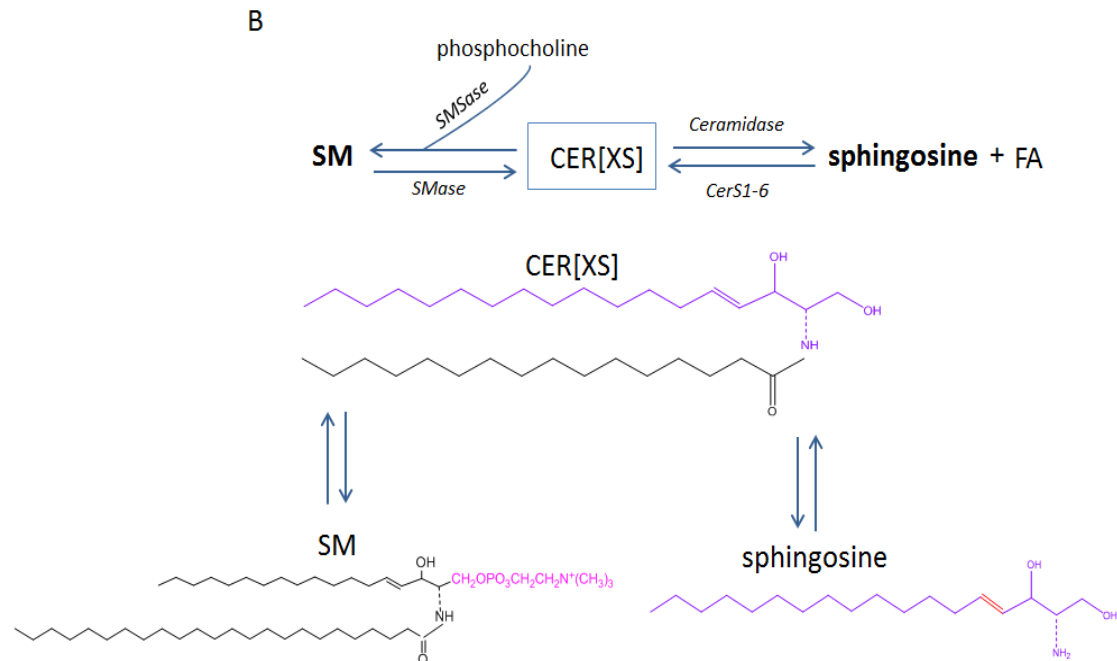


Figure 1.4 Ceramide biosynthesis pathways. (A) shows the main biosynthesis pathway where SPT is the first and rate limiting step that leads to the production of CER[DS] and subsequently CER[S] or CER[P]. (B) shows the possible route which CER is generated from (A): CER[S] could be taken to either generate sphingosine or complex sphingolipids such as SM. X stands for the degree of hydroxylation for the fatty acid incorporated in CER that could be either: N, A, or EO.

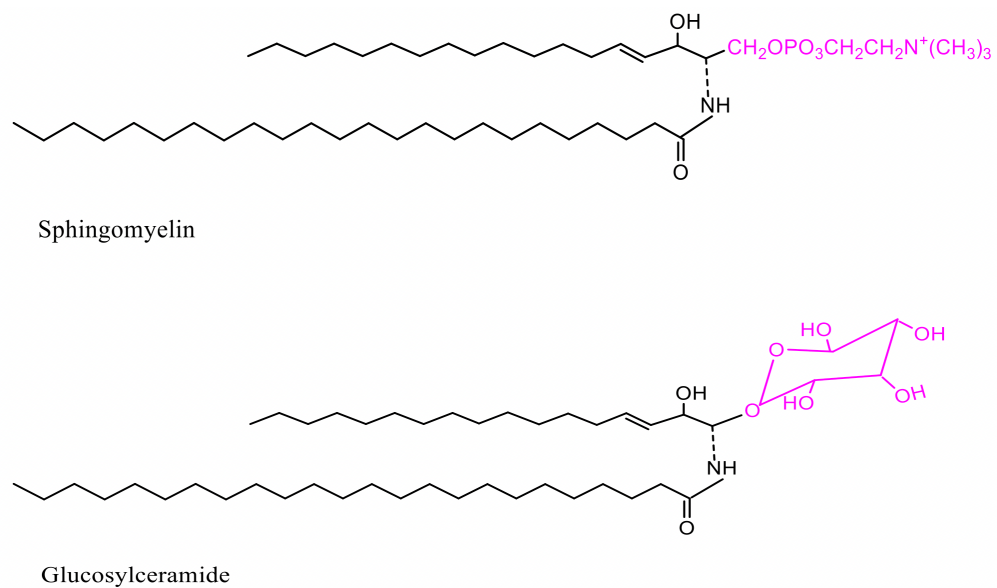


Figure 1.5 Examples of two complex sphingolipids. A sphingomyelin and a glucosylceramide. Both are derivatives of CER with phosphocholine or glucose.

1.2.2.1 Serine palmitoyltransferase

As mentioned above (**Figure 1.5**), SPT catalyses the first step in CER synthesis. This is a membrane bound enzyme that is found in the ER (Bode et al., 2016). It is composed of two main subunits, SPTLC1 and SPTLC2, and is part of a family of enzymes known as pyridoxal 5'-phosphate (PLP)-dependent α -oxoamine synthases (POAS) that require (PLP) as a co-factor, which binds to the SPTLC2 subunit (Yard et al., 2007, Bourquin et al., 2011, Bode et al., 2016). A third subunit has been reported in humans, known as, SPTLC3 (Hornemann et al., 2006). In addition, a subunit known as ssSPT was found to be important for SPT activity and acyl-CoA chain length specificity (Han et al., 2009). SPT activity is subjected to several variables such as tissue type, the developmental stage of the tissue and diet (Hanada, 2003). Studies on skin are limited, however, a study on SPT activity in the hypothalamus of malnourished developing rat showed a marked decrease in SPT activity and L-serine incorporation after one week when compared with normal diet rat (Rotta et al., 1999). Moreover, SPTLC1 and SPTLC2 messenger ribonucleic acid (mRNA) levels were found to be increased in cultured human keratinocytes treated with nicotineamide (Tanno et al., 2000). The preference of SPT for a fatty acid with a C16 carbon chain and the abundance of palmitic acid could explain SPT's preference for palmitoyl CoA among other acyl-CoAs and to the predominance of sphingosine (C18) as the most common sphingoid base found in sphingolipids (Hanada, 2003, Haynes et al., 2008, Hanada et al., 2000). Additionally, SPT was found to be preference for the amino acid L-serine (Hanada et al., 2000).

1.2.2.2 Ceramide synthase

There are six mammalian CerS isoforms that are major regulators of CER synthesis through the regulation of the de novo pathway, recycling free sphingosine and controlling the levels of long-chain bases. Each CerS has a preference for an acyl-chain length (Mullen et al., 2012, Wegner et al., 2016). For example, CerS1 generates ceramides with C18 acyl-chain length, CerS5 and CerS6 are found to induce C16 acyl-chain ceramides and CerS2 and CerS3 are specific for the longer ceramides with C22-C24 acyl-chain lengths (Mizutani et al., 2009). These enzymes are also tissue specific. **Table 1.2** summarises CerS acyl-chain length specificity and tissue distribution, where CerS1 levels are highest in brain, CerS2 is found in

most tissue with highest concentrations in kidney, CerS3 and CerS4 are found in skin at higher concentrations than other CerS subclasses, whereas CerS5 and CerS6 are distributed across all tissue (Mullen et al., 2012, Park et al., 2014).

CerS	Tissue Distribution	Acyl-chain Length
CerS1	Brain, skeletal muscle, lymph node	C18
CerS2	Kidney, liver, other tissue	C22-C26
CerS3	Testis, skin	C18-C24
CerS4	Skin, other tissue	C18-C20
CerS5	Ubiquitous	C14-C16
CerS6	Ubiquitous	C14-C16

Table 1.2 CerS tissue distribution and acyl-chain length specificity. CerS3 and CerS4 are most abundant in skin, whereas CerS5 and CerS6 are distributed across all tissue.

Using mouse models, mutations in each CerS results in a specific abnormality according to the CerS compartmentalisation and acyl-chain length preference (Park et al., 2014). Although the exact function of specific CER species in different tissues remains to be investigated, Jennemann et al. found that CerS3 is responsible for the formation of the C18-C24 acyl-chain CERs in human and mouse skin, and that reduced CerS3 levels in mice lead to absolute loss of these epidermal CERs, abnormal barrier function characterised by increased water loss and subsequently death (Jennemann et al., 2012). In addition, the main synthase expressed in keratinocytes is CerS3 and is increased in differentiated keratinocytes (Mizutani et al., 2008). Acyl-chain length preference of CerS plays a major role in CER biosynthesis regulation, where genetic studies on skin specific CerS3 and CerS4 for

example, showed a preference for C18-C24 carbon chains (Park et al., 2014). It has been found that UVB could activate CerS pro-apoptotic activity in human keratinocytes (Uchida et al., 2003). Although inhibitors for specific CerSs are not available, and studies in skin are limited, Fumonisin B1 is a CerS inhibitor used to study general CerS activity and was found to prevent the production of CER from sphingosine in the de novo pathway in rat hepatocytes (Wang et al., 1991).

1.2.2.3 Dihydroceramide delta 4-desaturase

Desaturases are responsible for the addition of double bonds or hydroxy groups, and eventually produce CER[S] or CER[P]. Des1, also known as dihydroceramide desaturase, introduces a 4,5-*trans*-double bond to its substrate CER[DS] to give CER[S] at ER membranes (Michel et al., 1997). Des2 mRNA is expressed mainly in skin, kidney, intestine, and lung and was found to be the enzyme responsible for CER[P] production (Ternes et al., 2002, Mizutani et al., 2004). Regarding CER[H] synthesis, one suggestion is that it could result from the hydroxylation of CER[DS] by an enzyme similar to Des2 (Kovacik et al., 2014, Masukawa et al., 2008). More investigation on the biosynthesis pathway of CER[H] is still required to fully uncover the enzymes and precursors involved in its generation.

1.2.2.4 Sphingomyelin and glucosylceramide metabolising enzymes

One of the significant complex sphingolipids is SM that SC CERs could be converted to/from. The comparison of the structures of CER in SM from hairless mouse and human epidermis with the structures of CER species in SC, and with CER produced by SMase treatment, showed an epidermal SMs are precursors of CER[NS] and CER[AS] (Uchida et al., 2000). Five classes of SMases are identified and are: acidic (aSMase), secretory (sSMase), Mg²⁺-dependent neutral (nSMase), Mg²⁺-independent nSMase and alkaline SMase (Goni and Alonso, 2002). It was found that aSMase was reduced in human aged skin when compared with young skin enzyme activity, which could contribute to the weakened barrier in aging skin (Yamamura and Tezuka, 1990). Similarly, nSMase also plays a role in skin barrier stability and repair where it was found that mice lacking a protein needed for nSMase activation had impaired barrier repair (Kreder et al., 1999, Goni and Alonso, 2002). Moreover, ceramide transporting protein (CERT), which is a protein required for the transfer of CER from the ER to the trans-Golgi for SM synthesis,

and SM synthase were found to be significantly decreased following UVB irradiation in cultured human keratinocytes, which resulted in down-regulation of SM generation and CER accumulation (Charruyer et al., 2008). This suggests that SMs are an important source of barrier crucial CERs.

In addition to SM, GlcCer is a major sphingolipid and the main source for CER synthesis via the salvage pathway catalysed by β -glucocerebrosidase, in addition to being an intermediate in the synthesis of many glycosphingolipids (Ichikawa and Hirabayashi, 1998, Uchida et al., 2000). In a study on Gaucher mouse epidermis where the enzyme β -glucocerebrosidase is deficient and GlcCer is accumulated, it was found that all SC CER species were decreased except for CER[AS] that is produced by SM as previously discussed, while CER[NS] was said to be produced by either GlcCer or SM (Uchida et al., 2000). In the same study, epidermal SM was not found to contain omega hydroxy CER structures (Uchida et al., 2000). In addition, mice deficient in these long-chain CERs had an increase in GlcCer (Zuo et al., 2008). Taken together, this suggests that GlcCer is the main storage of these CERs and that CER biosynthesis from GlcCer could be an important pathway for the formation and function of the epidermal barrier (Uchida et al., 2000, Holleran et al., 2006).

1.3 Cutaneous ceramide biology

Understanding CER function requires knowledge on the regulation and function of the major biosynthetic enzymes, sphingoid base characteristics, CER product/precursor regulation, in addition to understanding the diverse interconnections between the molecular and biochemical processes involved in phospholipid metabolism and regulation, which have not been fully elucidated. For example, although CerS enzymes play a major role in CER synthesis, there are limitations in CerS research due to the lack of pharmacological inhibitors for individual CerS isoforms (Mullen et al., 2011). CER building blocks sphingosine and dihydrosphingosine are distributed across human tissues, whereas phytosphingosine, as previously mentioned, is found mainly in the brain, skin, liver and kidney. Interestingly, 6-hydroxysphingosine has been reported to be characteristic to the skin (Robson et al., 1994, Kovacik et al., 2014). Additionally, CER pathway enzymes are expressed in various tissues, which correlate with the

diverse functions that related CER species carryout in the body from cell signalling, growth and differentiation to apoptosis and inflammation.

The variety in chain length, degree of saturation, type of hydroxylation and double bond number in long-chain bases and fatty acids contribute to the heterogeneity of CER species, especially in the epidermis (Coderch et al., 2003, Kihara, 2016). It has been estimated that the SC of the skin is composed of 33%wt CER[H] species , 32% CER[P], 24% CER[S] and 11% CER[DS] (Table 1) (Kendall et al., 2017, Skolova et al., 2017). The structure of skin CERs is unique to this site, where FAs with chains longer than those found in other tissue exist such as CERs with the EO hydroxy FAs: CER[EOS], CER[EODS], CER[EOP] and CER[EOH] (Jennemann et al., 2012, t'Kindt et al., 2012). Masukawa et al. have reported 342 CER species in healthy human SC then developed a sensitive method to quantify the levels of individual CER species in an aim to provide a better understanding of CER biosynthesis and function in the skin, where it was suggested that species that contain longer sphingoid bases and FA chains provided the best insight on CER function (Masukawa et al., 2008, Masukawa et al., 2009).

As previously discussed, CER is a major constituent of the epidermal permeability barrier. It has been found that alterations in epidermal CER species, chain length and levels are major factors for impaired epidermal barrier function and transepidermal water loss seen in several dermatologic diseases with barrier disturbance (Coderch et al., 2003, Masukawa et al., 2008). Such disorders associated with disruption in the permeability barrier activity include, but are not limited to: AD, psoriasis, autosomal recessive congenital ichthyosis, Netherton syndrome, Niemann-Pick disease and Gaucher disease (Meckfessel and Brandt, 2014, Borodzicz et al., 2016). For example, in a comparison study between healthy and AD patients, both lesional and non-lesional forearm skin from AD patients showed a significant decrease in CER levels when compared with those of healthy individuals of the same age (Imokawa et al., 1991). Another study on AD reported that among CER species in SC of AD patients, those with phytosphingosine and 6-hydroxysphingosine LCBs were the most decreased CERs in lesional skin, which represent the main CER species found in the epidermal barrier (Macheleidt et al., 2002).

Furthermore, it was found that short-chain CERs were highly increased in skin of AE subjects, with short-chain C34 CERs being the most observed in AE skin in the following classes: CER [NS], [NH], [AS], and [AH], and this correlated with the altered lipid grouping in SC where there was a decrease in barrier lipid packing that is a major cause for disruption in barrier function (Janssens et al., 2012). Regarding psoriasis, it was found that CER[EOS] levels and phytosphingosine-containing CERs were decreased in psoriatic scale when compared with normal SC (Motta et al., 1993). In addition, CER[EOS] was found to significantly effect epidermal barrier characteristics in pig SC (Mojumdar et al., 2014). Although the association of CER[H] levels has been reported in dermatologic diseases, the exact effect of these species on the barrier function have not been fully investigated. In a recent study using model lipid membranes containing the main membrane lipids, the behaviour of CER[H] in lipid membranes and its effect on membrane permeability was analysed. This was done by comparing CER[NH] with CERs of other sphingoid base groups and similar FA chain lengths (N), which included CER[NS], CER[NDS], and CER[NP]. In this study, the 6-hydroxysphingosine group in CER was found to highly affect permeability and lipid organization by decreasing lipid packing and chain order and increasing thermal stability and permeability (Kovacik et al., 2017).

In addition to the role specific CER species with long acyl-chain lengths play in skin, CER pathway enzymes have been found to be major contributors to normal skin structure and function through synthesising these skin CERs and regulating their levels in skin. GlcCer, as an example of the main precursor for the majority of epidermal CER species, plays crucial roles in maintaining normal membrane barrier structure and function (Wertz and van den Bergh, 1998, Holleran et al., 2006, Merrill, 2011). In a study on β -glucocerebrosidase deficient Gaucher mice, epidermal CERs derived from GlcCer were found to be decreased (Doering et al., 1999). Another study on Gaucher mice revealed disrupted barrier function characterized by a significant increase in transepidermal water loss and abnormal SC lipid organization in both Gaucher mice and hairless mice treated with a glucocerebrosidase inhibitor (bromoconduritol B epoxide) (Holleran et al., 1994).

Moreover, epidermal aSMase localised in the outer epidermis has been found to contribute in maintaining barrier homeostasis, whereas that found in the inner

epidermis is involved in repair of injured barrier in hairless mice (Jensen et al., 2005). Regarding autosomal recessive congenital ichthyosis, it has been found that CerS3 was decreased in SC of ichthyosis subjects accompanied by a 50% decrease in very-long chain CERs produced by this enzyme and affected epidermal differentiation (Radner et al., 2013). The involvement of CerS3 in this disorder was also demonstrated in a study on family members with autosomal recessive congenital ichthyosis, where a mutation in the *CERS3* gene was found to be the cause for the inactivation of CerS3 in keratinocytes and, therefore, the decrease in long-chain skin characteristic CERs (Eckl et al., 2013). In addition to CER biosynthesis enzymes, catabolic enzymes such as ceramidases are highly involved in the maintenance of a structurally and functionally competent epidermis as well. Houben et al. suggested the involvement of each of five ceramidase isoforms in human epidermal keratinocytes and in whole human and mouse epidermis with epidermal differentiation, function and membrane barrier homeostasis, such as inhibiting CER mediated apoptosis, producing differentiation signals and preventing the accumulation of CER in tissue (Houben et al., 2006). In this study, ceramidase isoform mRNA expression was analysed in the epidermis and in other tissue, where alkaline ceramidase-1 was found to be the most abundant and active in both human and murine skin samples. CIP has been found to participate in wound healing as a signalling molecule that is required for fibroblast migration and proliferation (Wijesinghe et al., 2016).

The effects of sphingoid bases on skin function have been investigated as well. It has been found that treating normal human epidermal keratinocytes (NHEKs) and mouse skin with phytosphingosine upregulated mRNA level of Peroxisome proliferator-activated receptor-gamma (PPAR- γ) that is highly involved in regulating epidermal barrier function (Kim et al., 2006). In the same study, epidermal differentiation marker proteins were increased in treated cells as well, whereas phytosphingosine treatment in a hairless mouse model with irritant contact dermatitis was found to possess anti-inflammatory effects by preventing oedema and inflammatory cell infiltration (Kim et al., 2006). Furthermore, treating keratinocytes with dihydrosphingosine, sphingosine and phytosphingosine resulted in the following, respectively: cell differentiation and upregulation of all CER species, especially the very long-chain species, increase in CER[NS] and CER[NP]

(Sigruener et al., 2013). It has been found that mice deficient in ceramides with very long chain fatty acids presented with a dysfunctional permeability barrier characterised by an increase in water loss (Li et al., 2007). In addition to this, CER[NP] was found to be significantly reduced in AD skin (Macheleidt et al., 2002). From this, it could be concluded that cutaneous CERs play a crucial role in maintaining the structural and functional stability of the body's primary defence organ. Recent developments in lipidomics have allowed analysis of individual ceramide species for the first time, which will allow for a better understanding of their role in the skin barrier (van Smeden et al., 2014).

1.3.1 Cutaneous ceramides in diabetic dermopathies

Diabetes is a metabolic disease with complications that could present in the skin. A few studies on the functional properties of the permeability barrier in diabetes have reported changes in the profile of SC lipids such as CERs (Sakai et al., 2003, Sakai et al., 2005, Kim et al., 2018). Regarding skin CERs and diabetes, a study using human and murine diabetic uninjured skin reported barrier changes in type-2 diabetes mellitus (DM), where there was a decrease in human and murine SC total CER, and a decrease in epidermal proliferation with an increase in advanced glycation end products (AGEs) epidermal receptors in mice (Kim et al., 2018). Moreover, when examining dysfunctional wound healing in diabetes, the same study reported delayed skin barrier repair after tape stripping, which correlated with a decrease in the gene expression of the CER *de novo* biosynthesis enzyme, SPT. Additionally, abnormalities in sphingosine-1-phosphate (S1P) signaling have been found to compromise wound healing by affecting angiogenesis and skin cell migration to injury site (Francis-Goforth et al., 2010). It has been found that in diabetes, dysfunctional insulin signaling affects the proliferation, differentiation and migration of CER producing keratinocytes, which leads to barrier function impairment and consequently, impaired wound healing (Wertheimer et al., 2000). Insulin treatment has been found to have a weaker effect on muscle tissue CER levels, where only SPT and *CERS1* expression were normalised but not that of *CERS5*, leading to a selective normalisation of CER levels based on the targeted CerS (Zabielski et al., 2014).

Furthermore, available literature on systemic CERs and diabetes mentions that alterations in plasma CER may be associated with the development of diabetes through several pathways involved in two main mechanisms: β -cell dysfunction and insulin signaling (Yaribeygi et al., 2020). For example, it has been found that plasma CER accumulation induces β -cell apoptosis by inhibiting ion channel activity, and leads to downregulation of insulin gene expression in pancreatic β -cells (Zhang et al., 2009, Guo et al., 2010). In addition to this, high circulating and tissue CER levels may induce peripheral insulin resistance through several pathways such as phosphorylation of insulin receptor substrate-1 (IRS-1) and inhibition of Akt pathway, which both impair insulin signaling and glucose metabolism (Hage Hassan et al., 2016, Yaribeygi et al., 2020). Interestingly, not only are CERs considered diabetic factors, but are found to be early biomarkers as well, where dihydroceramides, for example, were found to be elevated in the plasma of two cohorts for up to 9 years before their diagnosis with type-2 DM (Wigger et al., 2017). However, there are questions that remain to be answered around the possibility that the role of CER could be secondary to triggering mechanisms such as hyperglycemia, AGEs, oxidative stress and inflammation, or a direct mediator for inflammatory and cellular stress signaling pathways in diabetes and its complications (Yaribeygi et al., 2020). Although when discussing CER function it is usually the function of CER[NS] and its products that is mentioned, CER[NDS] has been found to have distinct cellular functions. In a recent review, Siddique et al. argue that CER[NDS] and their products such as dihydrosphingomyelin are biologically active species that play unique roles (Siddique et al., 2015). However, it has been mentioned that CER[NS] has a more significant role in cell signalling than CER[NDS] such as in insulin resistance and inflammation (Hannun and Obeid, 2008, Gault et al., 2010).

1.4 Membrane lipid biology

The main cellular lipid families, of which multiple lipid structures are derived from, include: sphingolipids, fatty acids, sterols, glycerolipids, and glycerophospholipids (Fahy et al., 2005). Cells are surrounded by the plasma membrane, which serves as a protective structure that surround the outer cellular boarder and sub-cellular organelles. The plasma membrane separates the intracellular constituents from the

extracellular matrix and is mainly composed of membrane lipids and proteins that perform regulatory and signalling functions within the cell, which maintain biological processes in the body. The amphipathic structures of membrane lipids that consist of hydrophobic tails and hydrophilic heads form the membrane lipid bilayer. The major constituents of the plasma membrane include complex sphingolipids, FAs, sterol lipids, glycerolipids and glycerophospholipids (Head et al., 2014). Cholesterol is distributed equally across the inner and outer leaflets of the bilayer, whereas complex sphingolipids are mainly found facing the outer side of the membrane while phospholipids are mainly facing the cytosol (Bretscher, 1973, Munro, 2003). The structure and synthesis of complex sphingolipids such as SM and GlcCer is explained in (Section 1.2.2).

1.4.2.1 Cholesterol, glycerolipids and glycerophospholipids

Cholesterol is the most important sterol lipid in cellular membranes, which is required for membrane rigidity and is a precursor for steroid hormones (Figure 1.6) (Bach and Wachtel, 2003). It could be obtained through diet and stored in tissue as cholesterol ester (CE) or converted into bile acids (Björkhem, 2013, Meaney, 2014). Additionally, although cholesterol could be synthesised in most nucleated cells, its biosynthesis mainly takes place in the ER of hepatic cells (Alphonse and Jones, 2016).

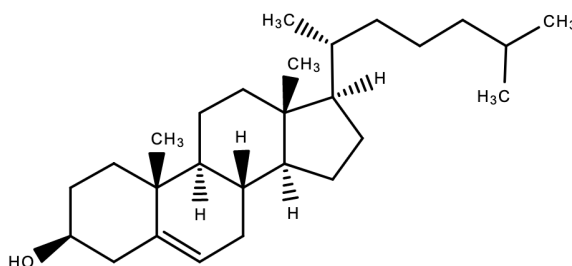


Figure 1.6 The structure of cholesterol.

First, acetyl-CoA and acetoacetyl-CoA form 3-hydroxy-3-methylglutaryl CoA (HMG-CoA) which contains 6 carbon atoms (C6). Then, a reduction reaction takes place where mevalonate is produced. This reaction is considered a main target for statin drugs (Meaney, 2014). After that, isopentenyl pyrophosphate (IPP) is formed through a series of phosphorylation and decarboxylation reactions, which then produces the C10 geranyl pyrophosphate (GPP) (DeBose-Boyd, 2008). A C15

farnesyl pyrophosphate (FPP) is then produced and condensed to form the C30 squalene (Russell, 1992). Squalene then undergoes a complex series of reactions to form a steroid structure (G J Schroepfer, 1982). It had been suggested that this step, which catalyses the first oxygenation reaction in cholesterol biosynthesis, could be a second target to inhibit cholesterol synthesis (Gill et al., 2011). Finally, demethylation reaction produces the C27 cholesterol.

Glycerolipids include lipid structures with a glycerol group which could contain either one, two or three fatty acids (monoacylglycerol, diacylglycerol or triacylglycerol, respectively) (**Figure 1.7**) (Fahy et al., 2005). Triacylglycerol (TG) plays a structural and functional role in cells as it is used for energy production, such as that in adipocytes, is a precursor for lipid mediators, and is essential for a healthy permeability barrier (Radner and Fischer, 2014).

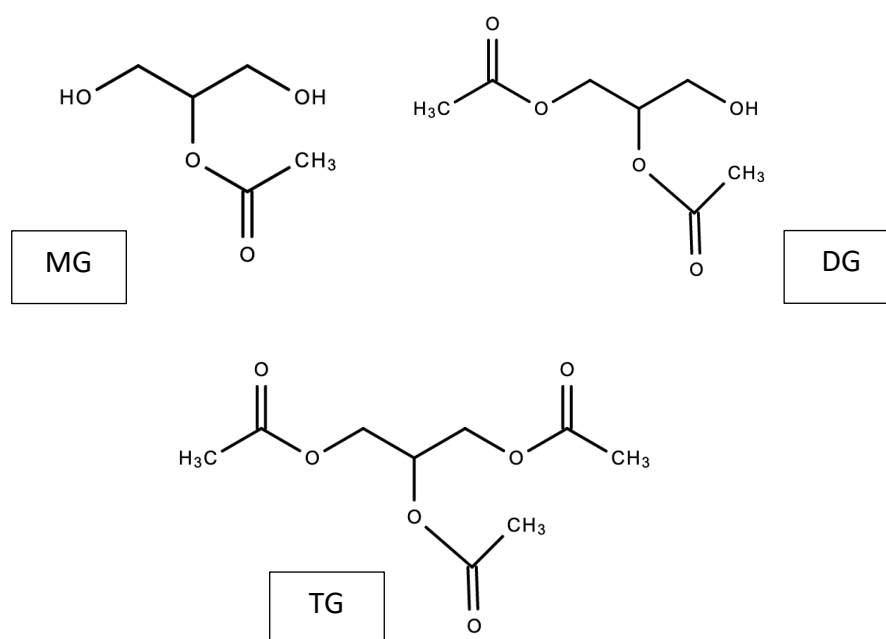


Figure 1.7 The structure of glycerolipids. MG: monoacylglycerol; DG: diacylglycerol; TG: triacylglycerol.

Moreover, glycerophospholipids are the most abundant membrane lipids and are composed of a hydrophobic fatty acid chain and a hydrophilic phosphate-containing glycerol chain (Berg et al., 2002). The most abundant glycerophospholipids in skin are phosphatidylcholine (PC) and phosphatidylethanolamine (PE) (van der Veen et al., 2017) (**Figure 1.8**). Other glycerophospholipid structures include: lysophosphatidylcholine (LPC), lysophosphatidylethanolamine (LPE),

lysophosphatidic acid (LPA), phosphatidic acid (PA) and phosphatidylinositol (PI). In addition to their role in cell membrane formation, glycerophospholipids produce crucial lipid mediators such as endocannabinoids (Wertz, 1992, Aloulou et al., 2012).

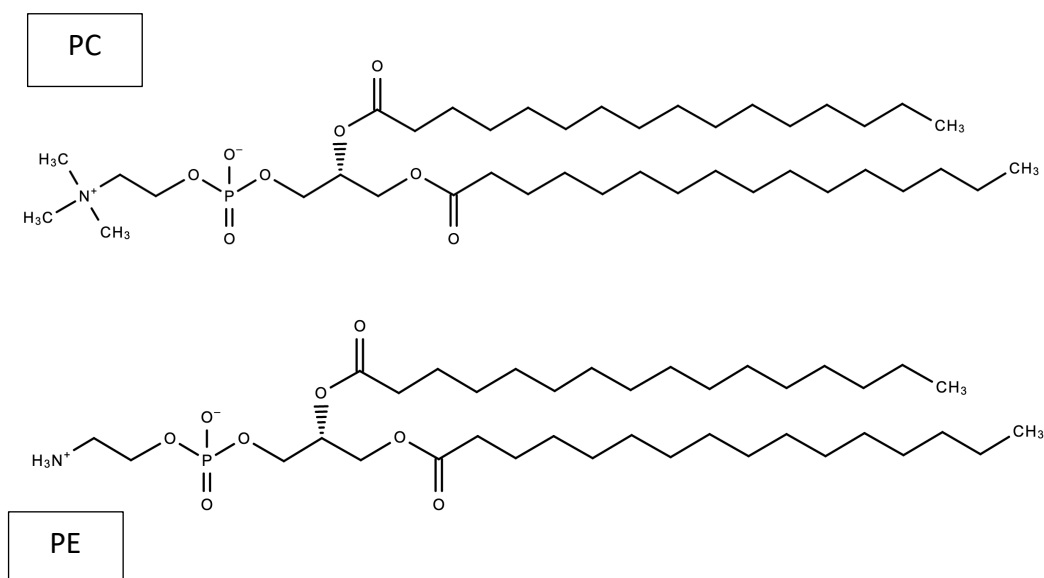


Figure 1.8 The structure of two abundant glycerophospholipids in skin. PC: phosphatidylcholine; PE: phosphatidylethanolamine.

The synthesis of glycerolipids and glycerophospholipids is a complex and interconnected process known as the Kennedy pathway. It starts with an acylation step where LPA is produced by the esterification of glycerol-3-phosphate to an acyl-CoA. LPA is then acetylated to produce PA. Next, diacylglycerol (DG) results from the dephosphorylation of PA, which could either be esterified with an acyl-CoA to produce TG or used to produce PC and PE (Lehner et al., 1996, Kennedy, 1958, Yeagle, 2016). For the synthesis of PC or PE, a choline or ethanolamine group, respectively, is phosphorylated to produce either phosphocholine or phosphoethanolamine. These products undergo several reactions where the final products react with DG to form PC or PE. Dysregulation in the activity of the PC Kennedy pathway has been found to alter TG biosynthesis, which shows that this pathway is essential for maintaining a balanced glycerolipid and glycerophospholipid level (Moessinger et al., 2014).

1.4.2.2 Endocannabinoids and their congeners

Endocannabinoids are bioactive lipid mediators involved in different functions such as pain perception, memory and immune responses to name a few (Marzo et al., 2004). Additionally, cannabinoid receptors (CB1 and CB2) are widely distributed in several tissues such as skin, muscle and the immune cells. In the skin, the endocannabinoid system has been found to regulate keratinocyte growth and differentiation, inflammatory response and sensation (Río et al., 2018). Endocannabinoid synthesis reflects the interconnection between the metabolism of different membrane lipids as it involves several membrane lipids such as FAs, PC, PE, PI and DG. The main endocannabinoids are arachidonoyl ethanolamine (AEA) and monoacylglycerol 2-arachidonoylglycerol (2-AG) (**Figure 1.9**). In addition to this, endocannabinoid congeners which are related molecules with different FA subunits, include N-acyl ethanolamines (NAE), monoacyl glycerols (MAG) and N-acyl amino acids (NAA) (Fontana et al., 1995, Mechoulam et al., 1998, Farrell and Merkler, 2008).

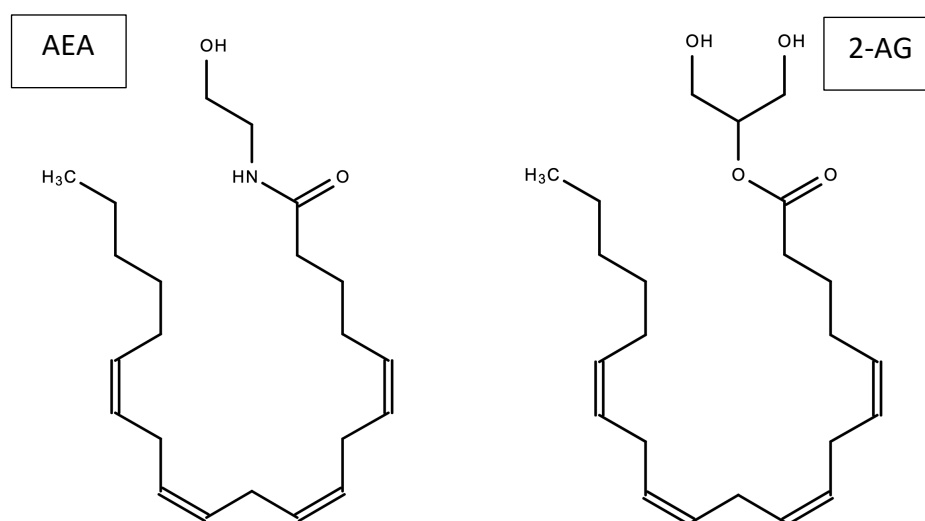


Figure 1.9 The structure of AA-derived endocannabinoids. AEA: anandamide; 2-AG: 2-arachidonoylglycerol .

The biosynthesis of AEA involves membrane lipids PC and PE in addition to PUFA. First, AA is transferred from PC to PE resulting in the N-acyl-phosphatidylethanolamine (NAPE). Next, NAPE is hydrolysed to form AEA (Kendall and Nicolaou, 2013, Devane et al., 1992, Liu et al., 2006) (**Figure 1.10**). The type of fatty acid in PC or PE decides the final endocannabinoid product. For

example, AA produces AEA, whereas palmitic acid produces PEA and oleic acid (OA) produces (OEA) (Di Marzo and Petrosino, 2007, Wang et al., 2006, Wang and Ueda, 2009). Similarly, endocannabinoid congeners eicosapentaenoyl ethanolamine (EPEA) are derived from EPA, whereas docosahexaenoyl ethanolamine (DHEA) are produced from DHA (Watson et al., 2019). The synthesis of 2-AG involves PI and DG. It begins with the hydrolysis of PI to form DG which is then hydrolysed to 2-AG (Di Marzo, 2008, Wang and Ueda, 2009, Kendall and Nicolaou, 2013, Urquhart et al., 2015) (**Figure 1.11**).

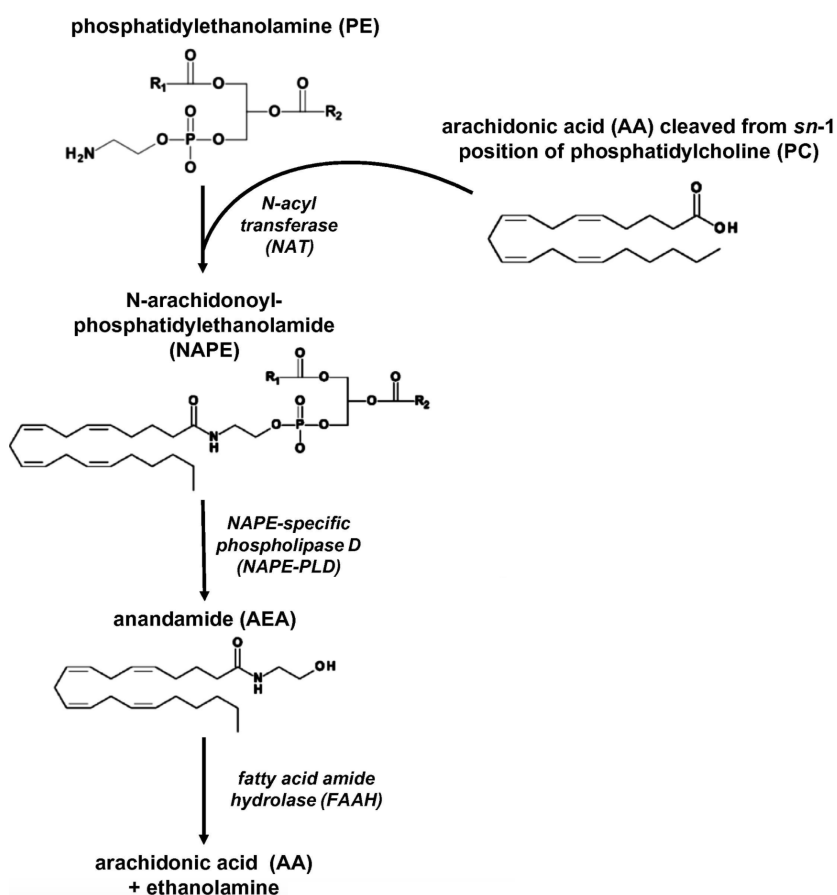


Figure 1.10 The synthesis of anandamide. Anandamide is synthesised from glycerophospholipids: phosphatidylcholine and phosphatidylethanolamine. The illustration is adapted from (Kendall and Nicolaou, 2013).

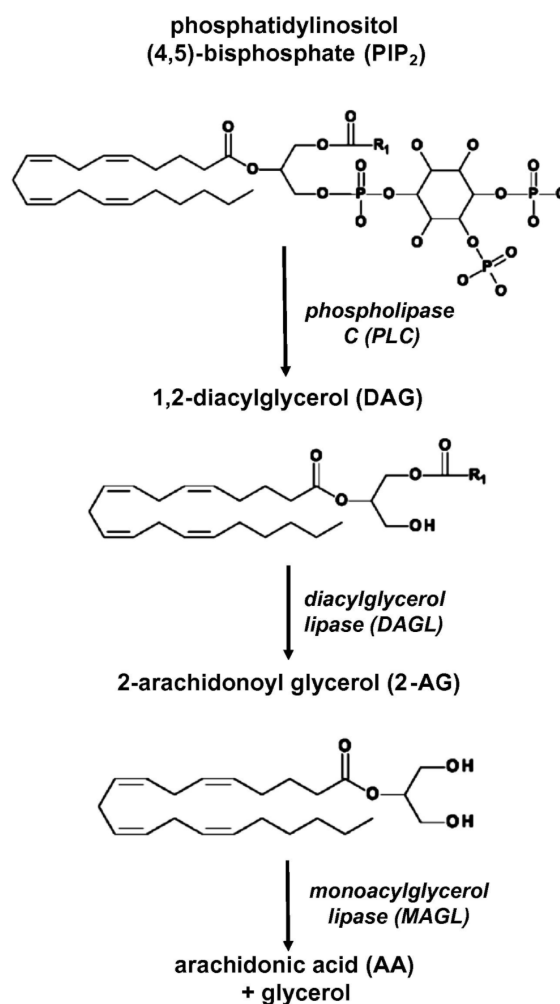


Figure 1.11 The synthesis of 2-arachidonoylglycerol. 2-arachidonoylglycerol synthesis involved diacylglycerol. The illustration is taken from (Kendall and Nicolaou, 2013).

Table 1.3 lists the bioactive lipids and their derivatives, showing the connection in their biosynthesis as discussed above.

Lipid class	Lipid species	Derivatives
Spingolipids	CER	SM, GlcCer
Sterol lipids	Cholesterol	CE
Glycerolipids	MG, TG, DG	PC, PE
Glycerophospholipids	PC, PE, LPC, LPE, PI, PA, LPA	DG, Endocannabinoids
FAs	AA, Palmitic acid, OA, DHA, EPA	Endocannabinoids

Table 1.3 Bioactive lipids and their derivatives. CER: ceramide; SM: sphingomyelin; GlcCer: glucosylceramide; CE: cholesterol ester; MG: monoacylglycerol; TG: triacylglycerol; DG: diacylglycerol; PC: phosphatidylcholine; PE: phosphatidylethanolamine; LPC: lysophosphatidylcholine; LPE:

lysophosphatidylethanolamine; LPA: lysophosphatidic acid; PA: phosphatidic acid; PI: phosphatidylinositol; AA: arachidonic acid; OA: oleic acid; DHA: docosahexaenoic acid; EPA: eicosapentaenoic acid.

1.4.2.3 Fatty acids

Fatty acids are major precursors to most bioactive lipids and lipid mediators. Additionally, they are considered crucial permeability barrier lipids and are an integral moiety in CER structure. They are composed of a hydrocarbon chain with a methyl group and a carboxyl group that binds to other lipids through their alcohol groups to form complex lipid classes (Nicolaou and Kokotos, 2004). Fatty acids are found either saturated or unsaturated. Fatty acids lacking double bonds are known as saturated FAs, whereas those containing one double bond are monounsaturated FAs and those containing more than one double bond are polyunsaturated FAs (PUFAs) (**Figure 1.12**). The nomenclature of PUFAs takes account of the number of double bonds and the position (x) of the last double bond at the end of the acyl chain referred to as the omega (n) carbon, which forms the $n-x$ based nomenclature. For example, docosahexaenoic acid (22:6 $n-3$) has an acyl chain of 22 C with six double bonds the last of which is found on the third last carbon of the methyl end of the chain.

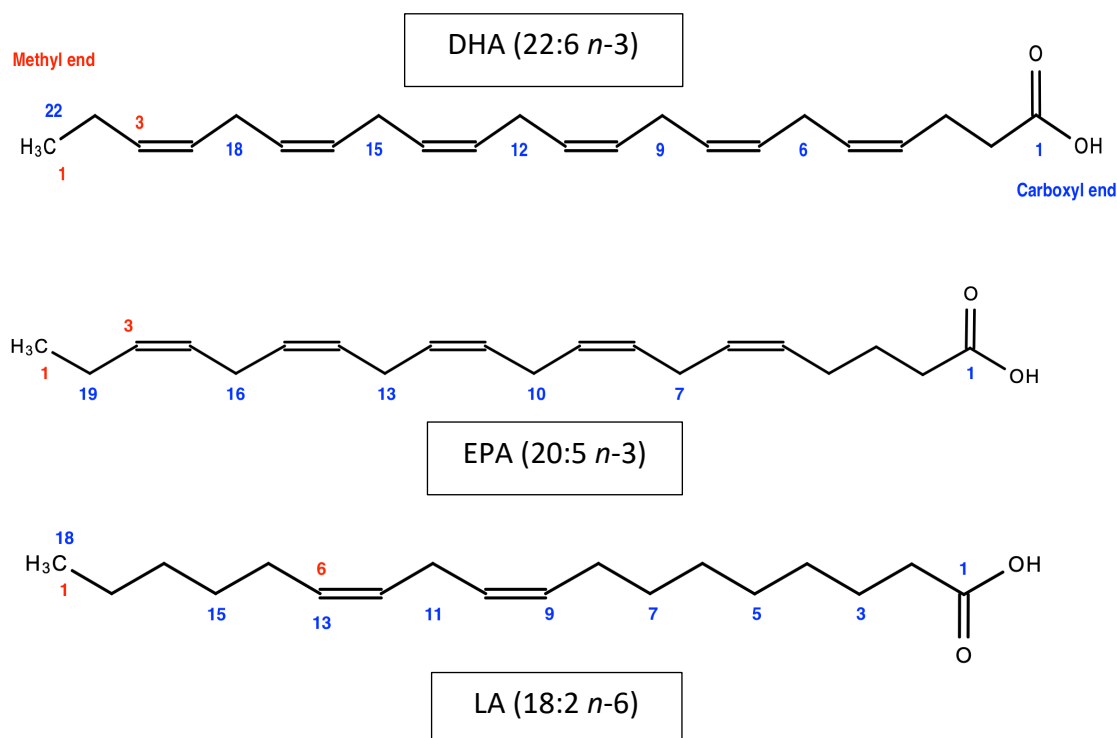


Figure 1.12 The structure of $n-3$ and $n-6$ PUFAs. DHA: docosahexaenoic acid; EPA: eicosapentaenoic acid; LA: linoleic acid .

Although FAs are abundant in human tissue, the linoleic and linolenic acids cannot be synthesised in the body and are, therefore, considered essential nutrients that are acquired externally. The reason for this is the lack of delta (Δ) desaturases that are responsible for the addition of double bonds to the carboxyl carbons beyond position 9 in the acyl chain (Whelan and Rust, 2006). Alpha-linolenic acid (ALA) and linoleic acid (LA) are precursors of the *n*- 3 and *n*- 6 PUFA families, respectively, from which long chain PUFAs are synthesised in the ER through desaturation-elongation reactions (Zhou and Nilsson, 2001). **Figure 1.13** demonstrates the main mammalian desaturation-elongation enzymes and products in PUFA synthesis.

Among the desaturase enzymes, Δ 6 and Δ 5 desaturases catalyze synthesis of LA-derived and ALA-derived long chain PUFAs such as *n*- 6 arachidonic acid (AA) and *n*- 3 eicosapentaenoic acid (EPA) (Nakamura and Nara, 2004). Moreover, in humans, Δ 4 desaturase that is responsible for the synthesis of docosahexaenoic acid (DHA) in lower eukaryotes is absent, whereas production rate of EPA from ALA is low. Therefore, EPA and DHA are acquired through diet. When available, PUFAs are either utilized for phospholipid synthesis or hydrolysed to free fatty acids. They could also undergo degradation by peroxisomal β -oxidation in the mitochondria (Sprecher, 2000). It has been found that 75.5% and 84.9% of dietary LA and ALA, respectively, are β -oxidised (Cunnane and Anderson, 1997). The second group of enzymes involved in PUFA biosynthesis is the elongase group (ELOVL), which includes 7 ELOVLs that catalyse the first and rate limiting step in the elongation cycle of monounsaturated and polyunsaturated fatty acid with ELOVL2, 4 and 5 being specific for PUFA (Jakobsson, Westerberg and Jakobsson, 2006; Ohno *et al.*, 2010).

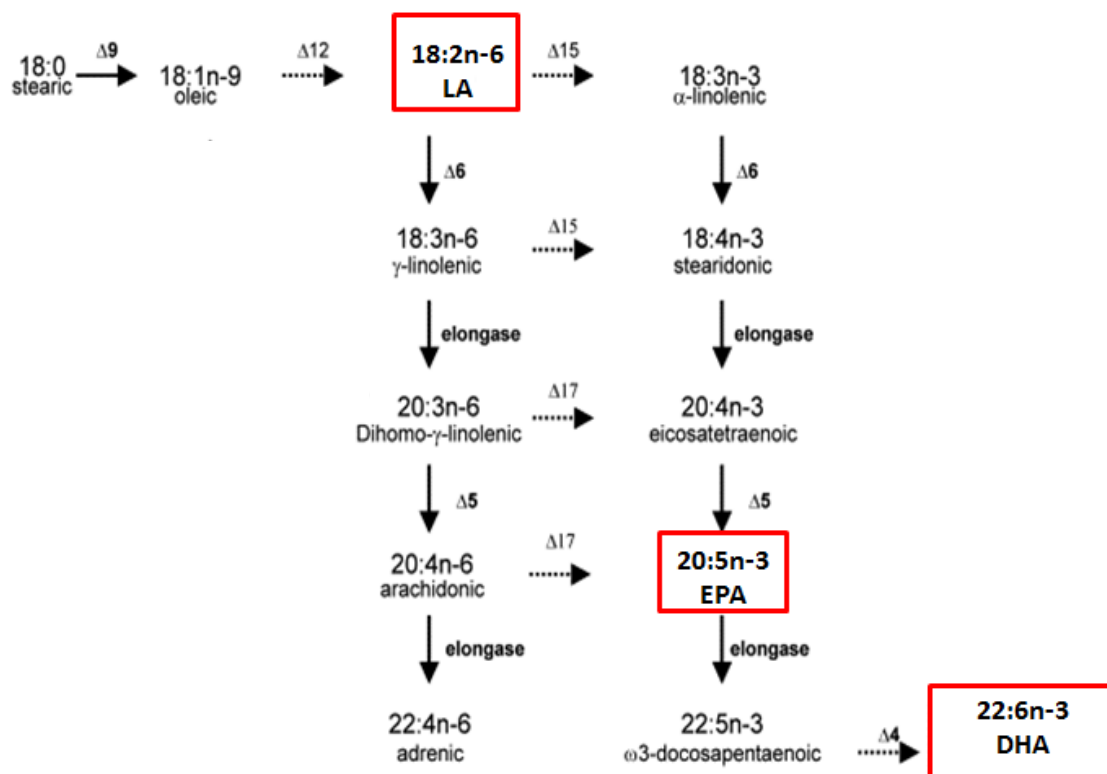


Figure 1.13 Enzymes regulating the biosynthesis of polyunsaturated fatty acids.
Adapted from (Leonard et al., 2004).

1.5 Omega-3 and omega-6 PUFA in skin health and disease

There is an outstanding amount of evidence on PUFA health benefits especially in cardiovascular and skin health, in addition to their involvement in disease prevention (McCusker and Grant-Kels, 2010; Trebatická *et al.*, 2017). However, the exact mechanisms by which these potent bioactive lipids influence physiological processes are not fully understood (Schunck, 2016). Cutaneous *n*-3 PUFA possess profound anti-inflammatory and photoprotective effects mediated by their metabolites, eicosanoids (Nicolaou, Pilkington and Rhodes, 2011). In a study on the effects of a 12-week dietary EPA supplementation on UV-exposed human skin, AA-derived pro-inflammatory mediators: 12-hydroxyeicosatetraenoic acid (12-HETE) and prostaglandin E₂ (PGE₂) were found to be significantly reduced relative to EPA-derived anti-inflammatory PGE₃ and 12-hydroxyeicosapentaenoic acid (12-HEPE) levels (Pilkington *et al.*, 2014). Furthermore, EPA

supplementation was found to increase UVR erythema threshold from 36 mJ/cm² to 49 mJ/cm² (Rhodes *et al.*, 2003). In addition, intravenous administration of 4.2 g of EPA and DHA had a positive effect on scaling and erythema reduction in psoriasis patients (Mayser *et al.*, 1998). With the already existing low $\Delta 5$ and $\Delta 6$ desaturase activity in normal human epidermis, it was found that psoriatic epidermis lacks the ability to convert LA to AA (Chapkin *et al.*, 1986). Although LA has pro-inflammatory effects, it is crucial for barrier function as it constitutes around 12% of total fatty acids in human epidermis and is considered an essential component of the epidermal CER[EOS], CER[EOH] and CER[EOP] species (Zuo *et al.*, 2008; Elias and Wakefield, 2015). It has been found that mice lacking the lipid transporter protein ACBA12, had a significant decrease in LA containing CERs, which led to barrier disruption (Zuo *et al.*, 2008). The distinct effects of each *n*-3 and *n*-6 PUFA are well demonstrated (Di Nunzio, Valli and Bordoni, 2016). With cutaneous CER being a potent bioactive lipid that is involved in a wide range of skin disorders, it would be interesting to examine the effect of PUFA on CER synthesis in the skin to help provide a better understanding of their role in skin health.

1.5.1 PUFA and ceramide synthesis

In a recent study by Kendall *et al.* treatment of human *ex vivo* skin with omega-3 polyunsaturated fatty acids (50 μ M) has been found to upregulate CER species in skin (Kendall *et al.*, 2017). The biomolecular processes, however, by which polyunsaturated fatty acids effect CER synthesis and expression are not clear. In addition to FA being a major moiety in the structure of CER, it has been shown that saturated and unsaturated FA can influence CER levels. Studies on the effect of PUFA on cutaneous CER synthesis are limited as skin CERs are among the most variable and complex in structure. It has been suggested that PUFA upregulation of CER in skin works through the *de novo* synthesis pathway or by the release of CER from the main epidermal precursors, SM and GlcCer as in other tissue (Kendall *et al.*, 2017). In addition, it is suggested that α -hydroxy CER could be produced after α -hydroxylation in the epidermis, where SM synthase and GlcCer synthase are involved and are specific for short-chain and long-chain FAs, respectively (Uchida *et al.*, 2000).

Studies on tissue other than skin have found that treating mouse myotubes with saturated and unsaturated FA augmented CER concentrations in mouse skeletal muscles (Schmitz-Peiffer, Craig and Biden, 1999). Regarding CER biosynthesis in ER, Masukawa et al. (2008) mention that either before or after the production of CER[NDS], non-hydroxy fatty acids are 2-hydroxylated to form α -hydroxy FAs by the enzyme fatty acid 2-hydroxylase (FA2H) (Masukawa *et al.*, 2008). Ohno et al. (2010) reported the specificity of ELOVL1 in humans to C24 CER synthesis and the regulation of ELOVL1 by CerS2, using HeLa cell knockdown analysis. They explain that CerS2 could be required for the release of C24-CoA produced by ELOVL1 and the addition of a sphingoid base to form C24 CER. The molecular mechanisms behind this ELOVL and CerS connection are not fully understood due to several limitations such as restricted techniques and lack of substrates. However, the novel field of study concerning PUFA effects on cutaneous CER synthesis requires more research to examine the possible enzymes and precursors involved in the upregulation of CER species in skin.

1.6 Study aim and objectives

From this, it is shown that ceramides are a dynamic group of bioactive lipids, which are considered a major constituent of the epidermal permeability barrier. Alterations in CER classes and chain-lengths have been reported in several skin disorders with barrier dysfunction. For example, studies have shown that a decrease in CER[NP] and CER[NH] is seen in SC of AD patients (Macheleidt et al., 2002). In addition, it was found that short-chain CERs were highly increased in skin of patients with AE (Janssens et al., 2012). Another study on autosomal recessive congenital ichthyosis, found a decrease in *CERS3* expression and in very-long chain CERs in the SC (Radner et al., 2013). Although reductions in SC lipids and total CERs have been reported in diabetic skin with barrier function impairment, there is a gap in knowledge on the potential changes in cutaneous CER profile and on the role of CERs in the development of diabetic dermopathies (Sakai et al., 2003, Sakai et al., 2005, Kim et al., 2018). In addition to this, the exact roles of individual CER species in health and disease remain unclear. Furthermore, PUFAs have been recently found to influence CER concentrations in human skin (Kendall et al., 2017). The mechanisms, however, by which these fatty acids could regulate CER

metabolism in normal skin requires further investigation. Therefore, investigating CER profile in diabetic skin and exploring CER metabolism pathways that may be targeted by PUFAs, could help to better understand the role of CERs in diabetic dermopathies and to develop therapeutic approaches.

The hypothesis of the thesis was that *n*-3 and *n*-6 PUFAs have a differential effect on the metabolism of CERs and other complex lipids in normal epidermal and dermal cells, and that CER profile is altered in diabetic skin. The general aim of this project was to explore mechanisms involved in the metabolism of cutaneous lipids in normal skin cells treated with PUFAs, and to examine differences in cutaneous and systemic lipid levels in diabetes when compared with control. To study the effect of PUFA supplementation on lipid metabolism in skin cells, proliferating and differentiating NHEK representing the basal and granular epidermis, in addition to human dermal fibroblasts (HDF) were treated with DHA, EPA and LA. The specific objectives were to:

1. Examine the effect of DHA, EPA and LA supplementation on lipid metabolism in proliferating and differentiating NHEK by analysing: the profile of CERs, CER carbon chain lengths, gene expression of the CER *de novo* biosynthesis enzymes, and the profiles of complex membrane lipids (cholesterol, FAs, SM, glycerolipids and glycerophospholipids) (addressed in **Chapter 3**).
2. Study the expression of lipid metabolism genes in differentiating NHEK (without PUFA treatment) compared to proliferating NHEK (without PUFA treatment) using gene sequencing analysis (addressed in **Chapter 3**).
3. Examine the effect of DHA, EPA and LA supplementation on lipid metabolism in proliferating and differentiating NHEK by analysing: the profile of CERs, CER carbon chain lengths, gene expression of the CER *de novo* biosynthesis enzymes, and the profiles of complex membrane lipids (cholesterol, FAs, SM, glycerolipids and glycerophospholipids) in HDF (addressed in **Chapter 4**).

Furthermore, alterations in skin CER levels in DPN have not been previously explored and could indicate a role for cutaneous bioactive lipids in the progression of the complications observed in the skin. For this project, a streptozotocin (STZ) -

diabetic rat model of DPN, which has been found to exhibit structural peripheral nerve damage and neuropathic symptoms, was used as a tool to investigate changes in cutaneous and systemic CER and lipid mediator profiles in diabetes compared with control (Sima and Sugimoto, 1999, Gardiner et al., 2007, Zherebitskaya et al., 2012, Biessels et al., 2014). The specific objectives were to:

4. Examine skin CER profile, CER carbon chain lengths, and endocannabinoids and their congeners, in addition to plasma CER profile, CER carbon chain lengths, and endocannabinoids and their congeners in an STZ-induced type-1 DM rat model of DPN (addressed in **Chapter 5**).

Chapter 2

Materials and Methods

2.1 Cell culture

The following human skin cells were used: human adult low-calcium high-temperature immortalised keratinocytes (HaCaT), immortalised human dermal fibroblast cell line (46BR.1N), primary NHEK, primary HDF. For method validation experiments, primary cells and cell lines were used. Although no major morphological changes have been reported in transformed cell lines such as HaCaTs (Boukamp et al., 1988) and 46BR.1N (Arlett et al., 1988), genetic code alterations during cell transformation could affect cellular growth and function (Segrelles et al., 2011). Therefore, final experiments were performed using primary human skin cells as this could represent biological responses that occur *in vivo* more accurately (Fernandes et al., 2016).

2.1.1 Reagents and consumables

2.1.1.1 Primary cells and cell lines

The epidermal cell line HaCaT, was purchased from CLS Cell Lines Service GmbH (Eppelheim, Germany). The dermal cell line 46BR.1N, was purchased from The European Collection of Authenticated Cell Cultures (ECACC) (Salisbury, UK). Cell lines were between passage 23-47. Juvenile primary NHEK were purchased from PromoCell (Heidelberg, Germany). These cells were isolated from juvenile foreskin (different donors) and seeded in T-25 flasks at passage 2. Primary HDF were generously provided by Dr Suzanne Pilkington and Dr Kieran Mellody. The primary dermal cells were isolated from skin of healthy young (<30 years) donors, cultured for 6 days and pelleted at 100% confluency or seeded in T-75 flasks at passage 2-4. **Figure 2.1** shows proliferating NHEK and HDF used for this project.

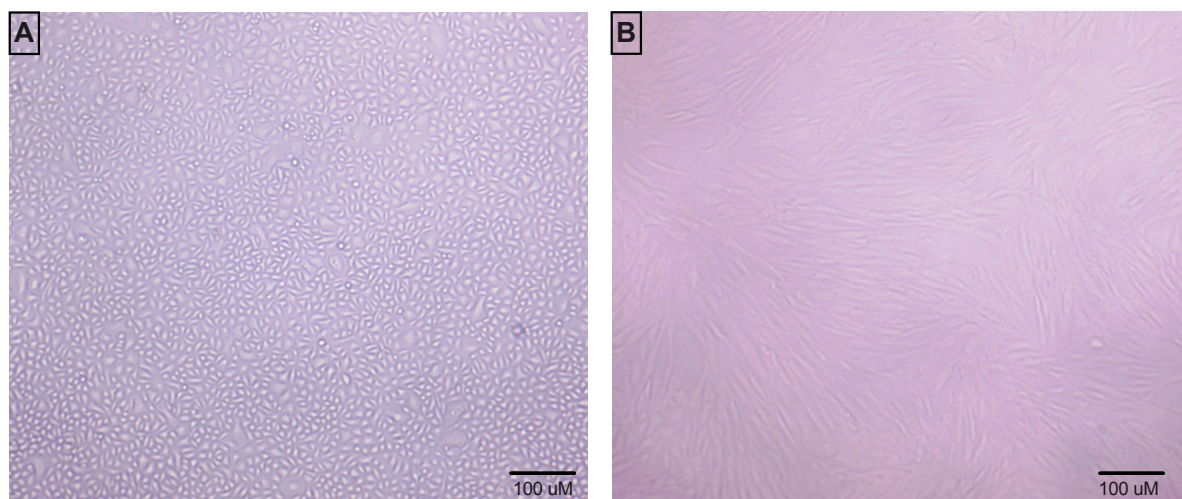


Figure 2.1 Representative figures of primary NHEK and primary HDF. A) primary normal human epidermal keratinocytes; B) primary human dermal fibroblasts. Images were produced using an Optika microscope digital system. Scale bar 100 µm.

2.1.1.2 Reagents

HaCaT human epidermal keratinocytes

Dulbecco's modified Eagle's medium (DMEM, high glucose 4500 mg/l), phosphate buffered saline (PBS), foetal bovine serum (FBS)-heat inactivated and 0.25% trypsin/ethylenediaminetetraacetic acid (EDTA) solution (1 mM), dimethyl sulfoxide (DMSO) (ACS grade; >99.0%), 0.4% trypan blue (Sigma Aldrich, Gillingham, United Kingdom).

46.BR.1N human dermal fibroblasts

Minimum essential medium eagle (MEM), non-essential amino acid solution (including L-alanine, L-asparagine, L-aspartic acid, L-glycine, L-serine, L-proline and L-glutamic acid), sodium pyruvate solution, FBS-heat inactivated, L-glutamine solution and 0.25% trypsin/EDTA solution (1 mM), PBS, DMSO (ACS grade; >99.0%), 0.4% trypan blue. Reagents were purchased from Sigma Aldrich (Gillingham, United Kingdom).

Primary NHEK

Keratinocyte growth medium-2 with supplement mix (0.004 mg/ml bovine pituitary extract, 0.125 ng/ml epidermal growth factor (recombinant human), 5 µg/ml insulin (recombinant human), 0.33 µg/ml hydrocortisone, 0.39 µg/ml epinephrine, 10 µg/ml transferrin (recombinant human), and 0.06 mM calcium chloride (CaCl₂), 4-(2-hydroxyethyl)-1-piperazineethanesulfonic acid (HEPES), 0.04%/0.03% TrypLE

solution and Trypsin Neutralising Solution (TNS) cryo-SFM which were purchased from PromoCell (Heidelberg, Germany) and 0.4% trypan blue (Sigma Aldrich, Gillingham, United Kingdom). For differentiation: Epilife growth medium and Epilife defined growth supplement (EDGS) (Thermo Fisher Scientific, Massachusetts, USA), CaCl₂ (0.5 M) (Promo Cell, Germany).

Primary HDF

DMEM (high glucose 4500 mg/l), FBS-heat inactivated, L-glutamine solution, PBS and 0.25% trypsin/EDTA, DMSO (ACS grade; >99.0%), 0.4% trypan blue (Sigma Aldrich, Gillingham, United Kingdom).

2.1.1.3 Consumables and equipment

All cell culture procedures were performed in sterile Class II MSC cell culture hood (Walkers, Safety Cabinet Ltd., Glossop, United Kingdom). Cells were incubated at the same conditions: 37°C, 5% CO₂ atmosphere, 95% humidity (Hereus CO₂ Cell Culture Incubator BBD 622, Thermo Scientific, Massachusetts, USA). For cell viability using 0.4% trypan blue, an automated cell counter was used (TC20TM automated cell counter, Bio-Rad, Hertfordshire, United Kingdom), in addition to TC20TM cell counting slides (Bio-Rad, Hertfordshire, UK). Cells were centrifuged at 200xg for 3-5 minutes at room temperature (non-refrigerated centrifuge 2-6E, SIGMA Laborzentrifugen GmbH, Osterode am Harz, Germany). All cell and tissue culture flasks used for cell culture, including cell culture well plates (6, 12, and 96 well plate), centrifuge tubes, tissue culture plates, and serological pipettes were purchased from Corning (New York, USA). Other equipment included Eppendorf pipette tips (Eppendorf, Hamburg, Germany), inverted microscope Primovert (Zeiss, Cambridge, United Kingdom), pipette controller (SLS International, Nottingham, UK), multichannel pipette (SLS International, Nottingham, UK). CoolCellTM LX cell freezing container was purchased from Sigma-Aldrich, Dorset, UK. Photographs of cells were taken using a digital microscope system from Optika Microscopes (Ponteranica, Italy).

2.1.2 Maintenance and subculture of cells

Cryopreserved cells were thawed for less than 1 min and then transferred gently to a centrifuge tube containing cell specific warm media. If cells were provided in a

flask, cells were detached by removing the cell culture medium and washing with HEPES (100 μl per cm^2) for primary NHEK or PBS (100 μl per cm^2) for the rest of cells types. Cells and PBS or HEPES was then replaced with TrypLE for NHEK or trypsin- EDTA for other cells (100 μl per cm^2). Cells were then incubated for up to 15 min at 37°C (5% CO_2) until cells were fully detached. TrypLE or Trypsin/EDTA was then neutralized with TNS inhibitor solution (100 μl per cm^2) for NHEK cells or complete medium (100 μl per cm^2) specific for other cell types (DMEM or MEM). The tube containing either thawed or detached cells was then centrifuged (200xg, 5 min). The supernatant was removed and the cell pellet was reconstituted with fresh medium (1 ml) and transferred to a clean culture container; for example: T75 flask containing fresh media (9 ml). Cells were then incubated at 37°C (5% CO_2). After 24 h incubation, cells were checked to make sure the cells were alive and attached to the bottom of the flask, and then cell culture media was changed to dispose of dead or floating cells. Cell culture media was changed every two days and cells were incubated until confluent (more than 80%). Fully confluent cells were then subcultured by removing the cell culture medium and washing with HEPES (100 μl per cm^2) for primary NHEK and PBS (100 μl per cm^2) for the rest of cells types. Cells and PBS or HEPES was then replaced with trypsin-/EDTA (100 μl per cm^2). Cells were then incubated for up to 15 min at 37°C (5% CO_2) until cells were fully detached. Trypsin/EDTA was then neutralized with TNS inhibitor solution (100 μl per cm^2) for NHEK cells or DMEM-FBS (100 μl per cm^2) for other cell types. This cell suspension was then centrifuged (200xg, 5 min) and the supernatant was removed. If the cells were needed for further experiments, the cell pellet was then reconstituted with medium and plated/subcultured into new flasks. If the cells were not needed for further experiments at that time, cells were cryopreserved (**section 2.1.2.1**).

2.1.2.1 Cryopreservation of cells

To freeze cells for later use, cell pellets were collected and centrifuged as above. Supernatant was then removed and the cell pellet was suspended in appropriate freezing medium. For NHEK, (1 ml) of Cryo-SFM was added to the pellet or a 1:10 mixture of 90% v/v FBS (900 μl) and 10% v/v DMSO (100 μl) for other cells. Suspended cells were then transferred to a labelled sterile cryopreservation vial and

lid was tightly closed. Cells were then placed in the CoolCell™ Cell freezing container allowing slow freezing for 24 h (-80°C freezer) before cells were stored in liquid nitrogen storage (-196°C).

2.1.2.2 Cell count and seeding density determination

To calculate viable cells number, a 1:1 dilution of 0.4% trypan blue solution and cell suspension was prepared (10 µl of 0.4% trypan blue solution + 10 µl of cell suspension). 10 µl of this mixture was then added to the cell counting chamber and the number of the cells was counted using a TC20™ Automated cell counter. Trypan blue is a diazo dye which interacts with damaged cell membranes that produces the blue stains seen in counting chambers. Cells that are viable are not coloured blue (Tran et al., 2011).

Seeding density and passage ratio calculation

To calculate passage ratio: seeding NHEK into a T-75 flask for example: flask dimensions: 75 cm², 10ml, target cell count: 2x10⁶ cells when fully confluent. Using a seeding density of 5000 cells/ cm² as recommended by cell provider (PromoCell, Germany).

$$C1 \times V1 = C2 \times V2$$

$$2 \times 10^6 \text{ cells} \times V1 = (5000/\text{cm}^2 \times 75 \text{ cm}^2) \times 10\text{ml}$$

$$2 \times 10^6 \text{ cells} \times V1 = (375000 \text{ cells}/ 10\text{ml}) \times 10 \text{ ml}$$

$$V1 = 375000/2 \times 10^6$$

= 0.1875 ml = 187.5 µl (Use 187.5 µl of the 1ml cell suspension for one T-75 flask).

$$1000/ 187.5 = \sim 5 \text{ (1:5 passage ratio)}$$

2.1.3 Keratinocyte differentiation

To differentiate keratinocytes, when cells were at >80% confluency and a monolayer was formed, differentiation was induced by a calcium (Ca²⁺) switch: cell culture media was removed and cells were washed with Hepes BSS for NHEK (100 µl per cm²). Hepes BSS was then removed and replaced with Epilife medium with high calcium (1.8 mM). High calcium medium was prepared by adding 1.8 ml of 0.5 M CaCl₂ to 500 ml Epilife medium. Cells were incubated at 37°C, 5% CO₂ atmosphere, 95% humidity. Differentiation would start after incubation for 24 hours

with high CaCl_2 treatment. **Figure 2.2** shows the morphological changes in NHEK differentiated for 24 hours compared to proliferating NHEK.

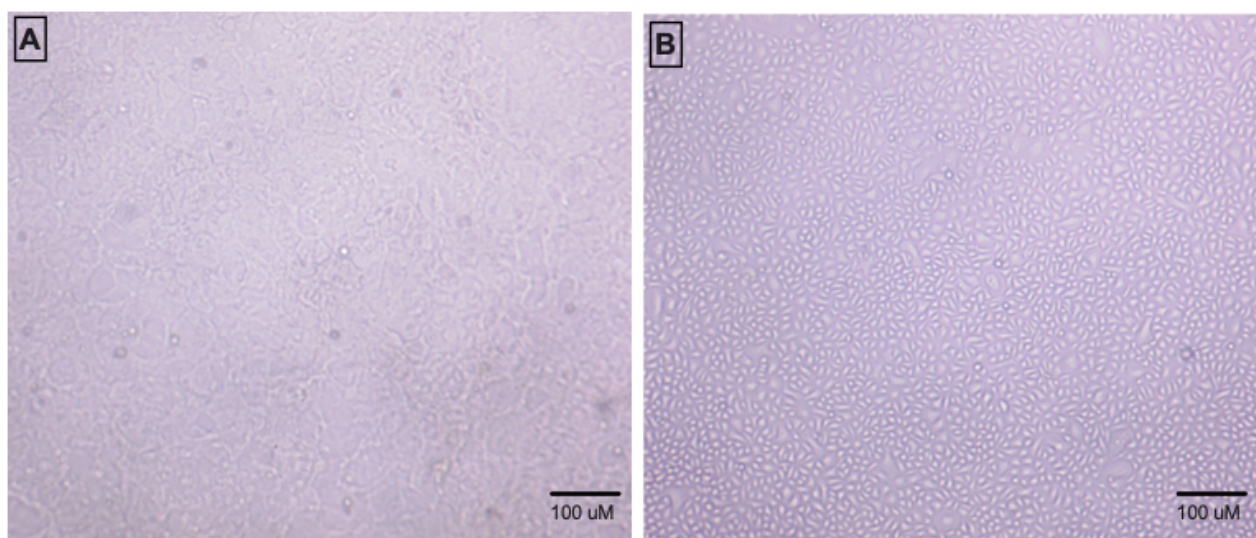


Figure 2.2 Representative figures of differentiated and proliferating NHEK. A) NHEK cultured with high calcium; B) NHEK cultured with low calcium. Images were produced using an Optika microscope digital system. Scale bar 100 μm .

Gene expression of keratinocyte differentiation and proliferation markers was measured using next generation sequencing as described in (**Section 2.3.5**). **Table 2.1** lists the gene expression for differentiation and proliferation markers measured in differentiated NHEK (high Ca^{2+}) compared to proliferating NHEK before the Ca^{2+} switch (low Ca^{2+}). NHEK were differentiated for four days then RNA was extracted for gene sequencing analysis. All differentiation genes were upregulated in differentiated NHEK, whereas proliferating genes were downregulated.

Gene	Description	Log2 Fold change
<i>LCE3E</i>	Late cornified envelope 3E	8.12
<i>LCE3D</i>	Late cornified envelope 3D	7.74
<i>LCE3C</i>	Late cornified envelope 3C	8.46
<i>LCE2B</i>	Late cornified envelope 2B	6.81
<i>LCE2A</i>	Late cornified envelope 2A	7.76

<i>LCE1F</i>	Late cornified envelope 1F	6.62
<i>LCE1D</i>	Late cornified envelope 1D	5.98
<i>LCE1A</i>	Late cornified envelope 1A	6.93
<i>IVL</i>	involucrin	2.1
<i>FLG</i>	Filaggrin	1.4
<i>KRT1</i>	Keratin 1	-1.3
<i>KRT5</i>	Keratin 5	-1.4
<i>KRT10</i>	Keratin 10	-1.1

Table 2.1 The expression of differentiation and proliferation genes in differentiated NHEK. The expression of differentiation markers in differentiated NHEK (High Ca²⁺, n=3) compared to proliferating NHEK (High Ca²⁺, n=3) was analysed by IPA[®] software. IPA[®] statistical analysis settings: p-value < 0.001, log₂ fold change < -1 downregulation, log₂ fold change > 1 upregulation. NHEK: normal human epidermal keratinocytes.

2.2 PUFA cell treatment and toxicity assessment

2.2.1 Preparation of PUFA stock solutions

2.2.1.1 Reagents and materials

The following PUFAs were purchased from Sigma Aldrich (Dorset, UK): cis-4,7,10,13,16,19-docosahexaenoic acid (DHA; ≥98% purity), cis-5,8,11,14,17-eicosapentaenoic acid (EPA; ≥99% purity), 9-cis,12-cis-Linoleic acid (LA; ≥99% purity); DMSO (ACS grade; >99.0%) was purchased from Sigma Aldrich (Dorset, UK). Eppendorf tubes and pipette tips were purchased from (Eppendorf, Hamburg, Germany), and cell culture flasks were from (Corning, New York, USA).

2.2.1.2 PUFA stock solution preparation

Fatty acid stock solutions were prepared by dissolving DHA, EPA, LA in DMSO to prepare a 100 mM stock solution of each fatty acid, as described in (**Table 2.2**). Stock fatty acid solutions were used to prepare the necessary concentrations of diluted fatty acid solutions for the toxicity and PUFA treatment experiments (**Section 2.2.2-2.2.3**). A 15 µl stock solution was aliquoted into Eppendorf tubes and stored at -80°C. Once thawed, the aliquots were only be used once.

PUFA	Stock solution	Dilution
DHA (25 mg)	100 mM	0.76 ml DMSO
EPA (25 mg)	100 mM	0.83 ml DMSO
LA (100 mg)	100 mM	3.6 ml DMSO

Table 2.2 Preparation of PUFA treatment stock solutions. Concentrated PUFA solutions were diluted with DMSO to prepare the stock solutions. DHA: docosahexaenoic acid; EPA: eicosapentaenoic acid; LA: linoleic acid; DMSO: dimethyl sulfoxide.

2.2.2 PUFA toxicity assessment

The viability of keratinocytes following the exposure to DHA, EPA and LA and exposure time was experimentally determined by our group and fatty acid concentrations for cell culture treatment have been reported in previous reports (treatment concentrations ranged from 10-15 μ M)(Yoon et al., 2020, Gallala et al., 2004, Breiden et al., 2007b, Hanley et al., 1998). Toxicity assessment was used to examine the effect of several DHA, EPA and LA concentrations on primary HDF viability. The tetrazolium salt 3-(4, 5-dimethylthiazol-2-yl)-2,5-diphenyltetrazolium bromide (MTT) assay was performed, which is based on a colorimetric reaction that quantitates cell viability (Mosmann, 1983). Living cells are able to reduce yellow MTT to insoluble purple formazan in a reaction catalysed by mitochondrial reductases. The colour intensity of produced formazan can proportionally reflect the metabolic function of cells and proliferation changes.

2.2.2.1 Reagents and consumables

DHA, EPA and LA stock solutions (100 mM) were prepared as explained in (section 2.2.1). Chemicals used in the MTT assay: DMSO, 3-[4,5-dimethylthiazol-2-yl]- 2,5-diphenyl tetrazolium bromide (MTT reagent), and PBS (all purchased from Sigma-Aldrich, Dorset, UK). The equipment used for the MTT assay were pipette tips and tubes (Eppendorf, Hamburg, Germany), nylon syringe filters (0.20 μ m) (Corning, New York, USA), orbital shaker TITRAMAX 100 (Headolph, Stone, United Kingdom), cell culture incubator (Hereus CO2 Incubator BBD 622, Thermo Fisher Scientific, Massachusetts, USA), and multiskan RC plate reader

(Labsystems, Hull, United Kingdom) with Genesis software (version 2.0) were used for assay preparation and absorbance readings.

2.2.2.2 Preparation of PUFA doses for the MTT assay

The following PUFA concentrations were prepared to assess toxicity: 5, 10, 20, and 50 μM . To prepare the 50 μM dose for example, 5 μl of 100 mM PUFA stock solution was diluted with 10 ml of appropriate complete medium, whereas 5 μl of DMSO was added to the medium to prepare the control. Similarly, a 25 μM dose of fatty acids was prepared by adding 2.5 μl of DMSO and 2.5 μl of 100 mM PUFA stock solution to 10 ml of complete medium. The final concentration of DMSO in the cell culture medium did not exceed 0.1% v/v.

2.2.2.3 MTT assay

Cells were seeded into 96 well plates following the seeding density calculation as described in (**section 2.1.2.2**). When subconfluent, cells were treated with vehicle control (DMSO, 0 μM dose), and DHA, EPA, or LA PUFA treatment at 5, 10, 20, 50 μM doses for 72 hours. The MTT stock solution (5 mg/ml) was prepared by dissolving 0.1 g of MTT powder in 20 ml of PBS. The solution was filtered using 0.20 μm syringe filters and aliquoted in microcentrifuge tubes wrapped with aluminium foil and stored at -20°C for further use. A working stock of 0.5 mg/ml was prepared fresh at the beginning of each experiment by diluting 1 ml of MTT solution stock (5 mg/ml) with 9 ml of PBS. After 24 h of cell incubation following treatment according to each time-point, cell culture medium was removed from each well and the cells were washed twice with PBS (200 μl /well for a 96 well-plate). PBS was then removed and MTT reagent was added (100 μl per well for 96 well plate) followed by incubation for 4 h at 37°C (5% CO_2) in a cell culture incubator. After 4 h, the MTT reagent was then removed and replaced with DMSO (100 μl per well for 96-well plate). The plate was covered with aluminium foil and was then gently shaken on a shaker for about 10-15 min to dissolve the formazan crystal. For cells that were directly cultured and treated in a 96 well plate, the absorbance was directly measured at 540 nm and the % cell viability was calculated using the following equation. A dose of 10 μM was chosen as it was not found to affect cell viability (**Figure 2.3**). The 20 μM DHA treatment significantly increased cell viability % ($p= 0.006$), whereas EPA concentration of 20 μM significantly

increased HDF viability % ($p = 0.002$). All LA concentrations stimulated HDF viability; 5 μM ($p = 0.03$), 10 μM ($p = 0.0096$), 20 μM ($p = 0.03$), 50 μM ($p = 0.001$).

$$\text{Viability (\%)} = \frac{\text{Mean absorbance at 540 nm of sample} - \text{Mean absorbance at 540 nm of blank}}{\text{Mean absorbance at 540 nm of control} - \text{Mean absorbance at 540 nm of blank}} \times 100\%$$

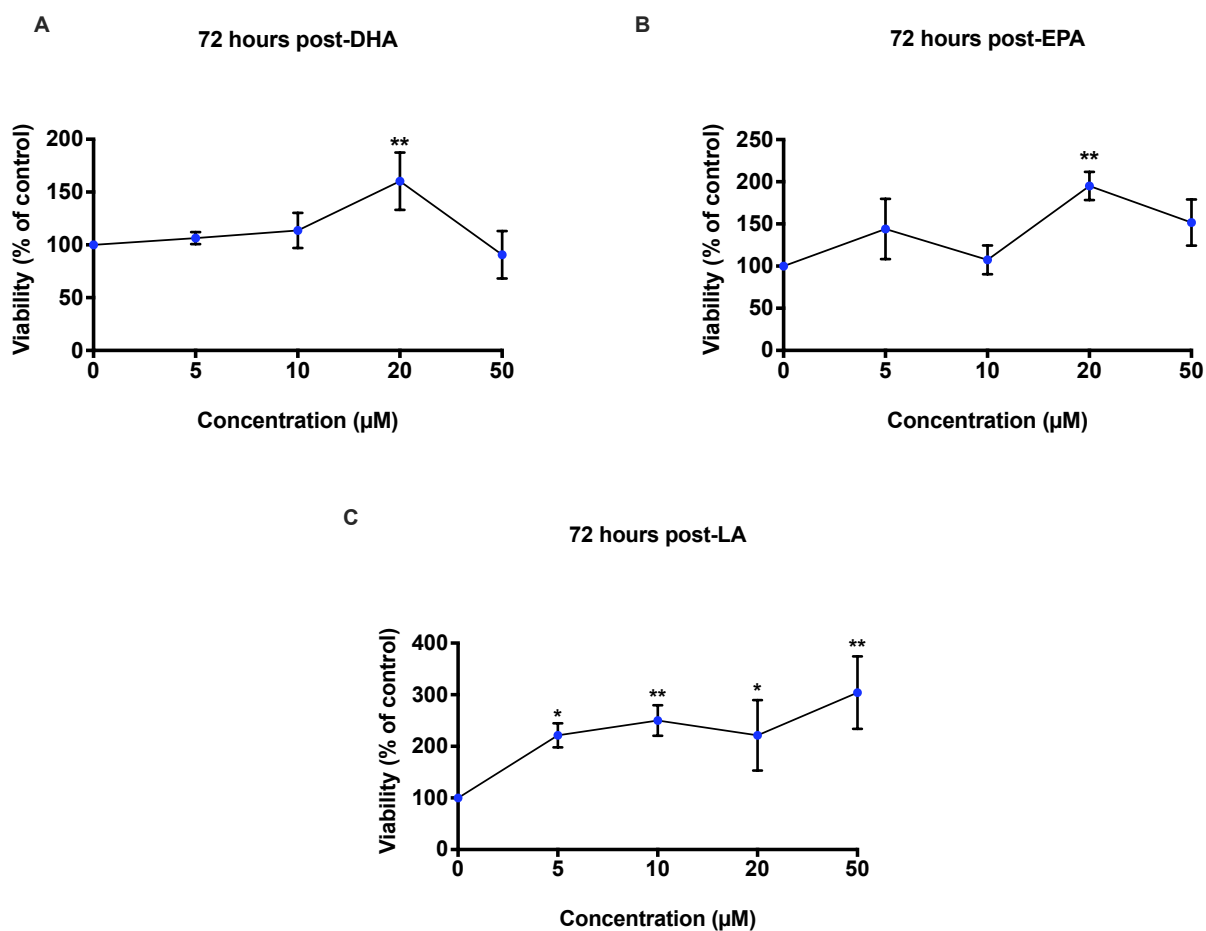


Figure 2.3 PUFA toxicity assessment for HDF treatment. HDF cells ($n = 3$) were treated with 0 (control), 5, 10, 20 and 50 μM of A) DHA, B) EPA and C) LA for 72 hours. Data are presented as mean viability \pm SD. Data were analysed by One-Way ANOVA comparing differences over treatment concentration compared with control; * $p < 0.05$; ** $p < 0.01$. HDF: human dermal fibroblasts; DHA: docosahexaenoic acid; EPA: eicosapentaenoic acid; LA: linoleic acid.

2.2.3 Treatment of cells with PUFAs

A dose of 10 μM was chosen based on previous reports, which used a fatty acid concentration that ranged from 10-15 μM (Yoon et al., 2020, Gallala et al., 2004, Breiden et al., 2007b, Hanley et al., 1998). In addition, the MTT assay showed that

this dose was not found to be toxic and there was low variability between samples as shown in **(Figure 2.3)**. The 10 μM dose was prepared as described above **(section 2.2.2.2)**. When cultured cells reached 70-80% confluency, media was discarded and cells were washed with PBS or HEPES. Fresh medium containing the calculated volume of the PUFA dose was then added and cells were incubated at 37 °C, 5 % CO₂. Media containing fresh treatments was replaced daily.

2.3 Real time quantitative polymerase-chain reaction (RT-qPCR) analysis

Ceramide biosynthesis enzyme gene expression was measured in primary human skin cells using RT-qPCR analysis, in order to examine the effect of PUFA treatments on ceramide biosynthesis in primary NHEK and HDF **(Chapters 3 and 4)**.

2.3.1 Reagents and consumables

Chemicals and reagents used in PCR assay included ethanol (HPLC grade, purity $\geq 99.8\%$) and β -mercaptoethanol (purity $\geq 99\%$) were purchased from Sigma-Aldrich, Dorset, UK. Qiagen Rneasy[®] mini kit, consisting of RNeasy mini elute spin columns, collection tubes, RNase-free water, and wash buffer (Buffer RW1), concentrated wash buffer (Buffer RPE), RNeasy lysis buffer (Buffer RLT), 96-well plates, 384-well plates were purchased from Qiagen (Hilden, Germany). High Capacity RNA-to-cDNA kit was purchased from Thermo Fisher Scientific, UK. TaqMan[™] Fast Universal PCR Master Mix and nuclease-free water were purchased from Thermo Fisher Scientific, Massachusetts, USA. The predesigned primer and probe mix was purchased from TaqMan[™] gene expression assay, Thermo Fisher Scientific (Massachusetts, USA). Details for the primers and probe mix used in the experiments are listed in **(Table 2.3)**. The equipment used in PCR assay were: Nanodrop[™] (Thermo Fisher Scientific, UK), PCR Thermal cycler (Thermo Fisher Scientific, Massachusetts, USA), refrigerated centrifuge (Eppendorf, Stevenage, UK), StepOnePlus Real Time PCR System (Applied Biosystems, Massachusetts, USA), 7900HT Fast Real-Time PCR System (Thermo Fisher Scientific, Massachusetts, USA).

Reagent symbol	Target Species	Details
TaqMan™	NA	TaqMan™ fast universal master mix; Reference dye: ROX(pre-mixed); Detection method: primer-probe detection
<i>GAPDH</i>	Human	Glyceraldehyde-3-phosphate dehydrogenase; Assay ID Hs02758991_g1; Cat.No. 4331182
<i>RPL27</i>	Human	Ribosomal protein L27; Assay ID Hs0044961_g1; Cat.No. 4331182
<i>CERS1</i>	Human	Ceramide synthase 1; Assay ID Hs04195319_s1; Cat.No. 4331182
<i>CERS2</i>	Human	Ceramide synthase 2; Assay ID Hs00371958; Cat. No. 4331182
<i>CERS3</i>	Human	Ceramide synthase 3; Assay ID Hs00698859_m1; Cat.No. 4331182
<i>CERS4</i>	Human	Ceramide synthase 4; Assay ID Hs00226114_m1; Cat.No. 4331182
<i>CERS5</i>	Human	Ceramide synthase 5; Assay ID Hs00382151_m1; Cat. No. 4351372
<i>CERS6</i>	Human	Ceramide synthase 6; Assay ID Hs01372225_m1; Cat.No. 4351372
<i>DES1</i>	Human	Desaturase 1; Assay ID Hs00186447_m1; Cat.No. 4331182
<i>DES2</i>	Human	Desaturase 2; Assay ID Hs01380343_m1; Cat.No. 4331182

Table 2.3 Details for the primers and probe mix used. All reagents were purchased from Thermo Fisher Scientific.

2.3.2 Method optimisation

2.3.2.1 Housekeeping gene assessment

As the housekeeping gene *GAPDH* is widely used in RT-qPCR, additional housekeeping genes were assessed to choose the most reliable one in addition to *GAPDH* as references for gene expression studies (Zainuddin et al., 2008, Bonnet-Duquennoy et al., 2006). Cells were prepared as described in (Section 2.1.2-2.1.3). Samples and cDNA preparation was done as described in (Section 2.3.3). Gene expression quantification and analysis was done as described in (Section 2.3.4). Housekeeping genes *GAPDH* and *RPL27* showed low variability between different cell types and treatments, which is a main characteristic of an ideal housekeeping gene (Jaramillo et al., 2017). This was consistent with previous and recent data that shows *RPL27* to be a stable housekeeping gene (de Jonge et al., 2007, Ho and Patrizi, 2021). **Figure 2.4** shows the mean cycle threshold values for *GAPDH* and

RPL7 measured in HDF (n= 3 individual donors), proliferating NHEK (low Ca²⁺, n= 3 individual donors) and differentiated NHEK (high Ca²⁺, n= 3 individual donors). For the RT-qPCR experiments, cycle threshold values from both housekeeping genes were averaged and used to normalise data.

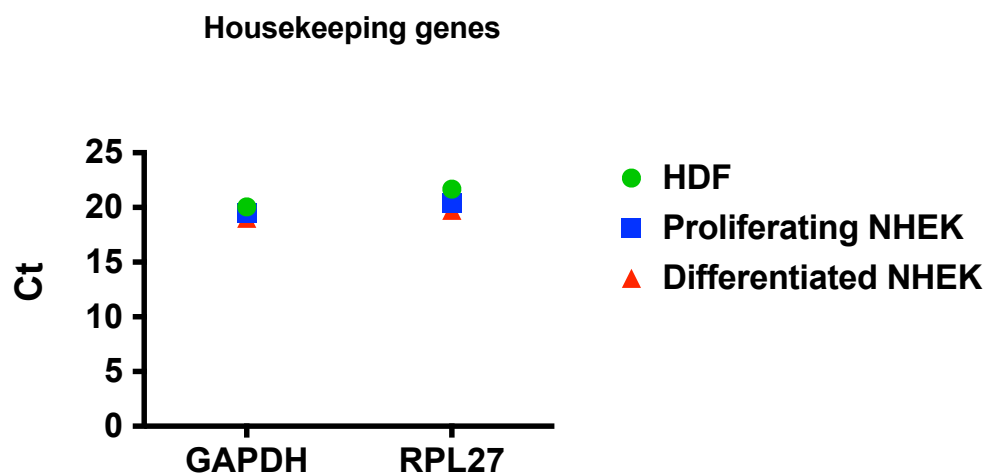


Figure 2.4 Measurement of GAPDH and RPL27 in different cell types and conditions. The graph shows the mean cycle threshold value for *GAPDH* and *RPL27* measured in HDF (n= 3 donors), proliferating NHEK (n= 3 donors) and differentiated NHEK (n= 3 donors). Data are presented as mean Ct (\pm SD). GAPDH: HDF (mean= 20.05 \pm 0.595), proliferating NHEK (mean= 19.54 \pm 0.316), differentiated NHEK (mean= 19.01 \pm 0.531); RPL27: HDF (mean= 21.68 \pm 0.719), proliferating NHEK (mean= 20.4 \pm 0.329), differentiated NHEK (mean= 19.75 \pm 0.346). GAPDH: glyceraldehyde 3-phosphate dehydrogenase; RPL27: ribosomal protein L27; HDF: human dermal fibroblast; NHEK: normal human epidermal keratinocyte; Ct: cycle threshold.

2.3.2.2 Primers target specificity validation

Agarose gel electrophoresis was performed in order to confirm the specificity of the primers to the target genes. Reagents and equipment were kindly provided by Dr Debbie Fischer. Briefly, 4%w/v Agarose gel (Invitrogen, USA) was prepared in 0.5X Tri-borate-EDTA (TBE) buffer (Ambion, USA). First, the solution was heated into a microwave for two minutes, then mixed at 30 sec intervals to completely dissolve of the agarose. After that, 0.1 μ L/ml ethidium bromide (Sigma, Germany) was added to the mixture, after leaving it to cool down for a few minutes. The gel was poured into the tray with the combs and let solidify. After 40 minutes, the combs were removed and the DNA samples (taken out of the PCR plate) were mixed, according to a 4:1 proportion, with Blue/Orange Loading Dye (Promega, USA) and added to the wells. Blue/Orange Loading Dye composed of: 0.03% bromophenol blue, 0.03% xylen cyanol FF, 0.4% orange G, 15% Ficoll® 400,

10mM Tris-HCl (pH 7.5), 50mM EDTA (pH 8.0). After placing the gel in a tank containing 0.5X TBE buffer, 5 μ L of 20 base pairs (bp) DNA ladder (Generon, Slough, United Kingdom) and 18 μ L of the samples were added to the wells. The tank was then attached to the power supply and, the gel was left to run for 75 minutes under a voltage of 120V. When the electrophoresis was completed, the gel was placed into a UV chamber to visualise the migrations (**Figure 2.5**).

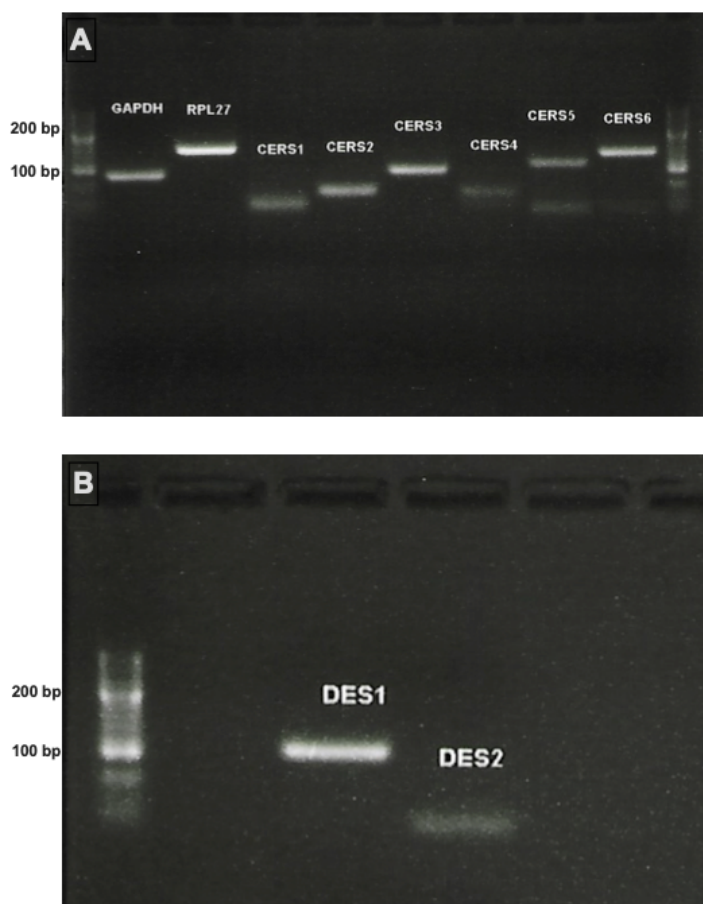


Figure 2.5 Agarose gel electrophoresis for RT-qPCR primers. Bands are visible for all the products. Amplicon length: GAPDH (93 pb);RPL27 (152 bp); CERS1 (64 bp); CERS2 (66 bp); CERS3 (99 bp); CERS4 (65 bp); CERS5 (116 bp); CERS6 (141 bp); DES1 (108 bp); DES2 (50 pb).

2.3.2.3 Determination of reaction volume and cDNA concentration

The concentration of cDNA samples and the reaction volume of the PCR reaction were optimized. Working with a reaction volume of 10 μ l did not affect the cycle threshold of housekeeping and ceramide genes when compared to the standard 20 μ l reaction volume. Therefore, the smaller reaction volume was used. In addition, diluting the cDNA samples to a final volume of 200 μ l did not have an effect on the

cycle threshold values when compared to using the original final volume of 20 μ l (Appendix 1).

2.3.3 Experimental protocol

2.3.3.1 RNA extraction and quantification

Samples were taken out of the incubator, media were discarded and cells were washed with PBS. RNA was isolated from cells using the Qiagen Rneasy[®] Mini Kit as follows. RLT buffer (1 ml) with β -mercaptoethanol (β -ME) (10 μ l) was added to the washed cells and gently shaken until the cells were detached from the 6-well plates as per manufacturer's instructions. In brief, 70% ethanol (350 μ l) was then added to each sample and mixed well by pipetting. 700 μ l of this mixture was then transferred to a Rneasy[®] Mini spin column placed in a 2 ml collection tube and the column was centrifuged for 15 s at 8000 x g. The flow-through liquid was discarded. Buffer RW1 (700 μ l) was then added to the column and centrifuged for 15 s at 8000 x g. The flow-through liquid was also discarded. Buffer RPE (500 μ l) was then added to the column and centrifuged again for 15 s at 8000 x g. The flow-through was again discarded and buffer RPE (500 μ l) was added to the column followed by centrifugation for 2 min at 8000 x g. The 2 ml collection tube at the bottom was also discarded and replaced with a clean 1.5 ml collection tube. RNase-free water (30 μ l) was then added directly to the spin column membrane and the column was centrifuged for 1 min at 8000 x g to elute the RNA. RNA was then stored in -80°C for further analysis. Eluted RNA was then measured using a Nanodrop[™], a UV-Vis spectrophotometer.

RNA quantification

RNA was measured using UV absorbance. Three wavelengths are used: 260 nm to measure the amount of nucleic acid present in the sample, 280 nm to measure the amount of protein in the sample and 230 nm to measure the amounts of other contaminants in the samples, such as DNA or phenols. The concentration of RNA was calculated by taking the 260 nm reading and a conversion factor based on the extinction coefficient for RNA (40 $\mu\text{g/ml}$). Pure RNA has a A_{260}/A_{280} ratio ranging between 1.8-2.2, and A_{260}/A_{230} ratio of more than 1.7 (Desjardins and Conklin, 2010). Before measuring the samples, the Nanodrop[™] sensor was cleaned

by wiping it with a soft tissue followed by measurement of a blank sample (RNase-free water). After measuring the blank, the sensor was wiped again and test sample was measured by adding a small volume of the sample (1 μ l) on the sensor, and the RNA count was then recorded in μ g / μ l. Sample and reagents were always kept on ice during procedures. Samples with a low RNA yield (< 50 ng) were excluded.

2.3.3.2 RNA conversion to cDNA

RNA was transcribed into cDNA by using the High Capacity RNA-to-cDNA kit. To prepare the master mix containing a total RNA concentration of 500 ng, the following equation was followed:

$$500/\text{RNA concentration (ng/ } \mu\text{l)} = X \text{ } \mu\text{l of sample}$$

$$9\mu\text{l} - X = Y \text{ } \mu\text{l of nuclease-free water}$$

For each sample, 11 μ l of a cDNA mix containing 10 μ l buffer enzyme and 1 μ l enzyme mix per sample, was added to each 9 μ l containing sample + nuclease-free water. The mixture was then pipetted into an RNA-free tube. The cDNA transcription process was performed on a Thermo Fisher PCR Thermal Cycler with the following programme: 25°C for 10 min followed by 45°C for 30 min and reaction was terminated by incubating samples at 85°C for 5 min. Once the cycle was complete (after approximately 40 min), the resulting cDNA (20 μ l) was diluted with 180 μ l RNase-free water and used for quantitative RT- qPCR analysis. Sample and reagents were always kept on ice during procedures.

2.3.3.3 RT-qPCR analysis

RT-qPCR analysis was performed in either a 96 or 384 well plates. A master mix consisting of TaqMan™ Fast Universal PCR Master Mix (10 or 5 μ l), primers and probes mix (1 or 0.5 μ l), and RNase-free water (5 or 2.5 μ l) was prepared. The mixture was vortexed and 16 or 8 μ l was loaded into each well in the 96 or 384 well-plate. cDNA (4 or 2 μ l) was then added to the well and RT-PCR was performed using an Applied Biosystems StepOne Plus Real Time PCR instrument when using 96- well plates and the 7900HT Fast Real-Time PCR System for the 384-well plates. Both machines were set up to run 40 cycles. Each cycle consists of 2 stages, the holding stage and the cycling stage. The holding stage has 1 step. This step is the initial denaturing step and was set to run at 95 °C for 20 s. The second stage

consists of 2 steps. The first step is the denaturing step and was set to run at 95 °C for 3 s and the second step was the anneal and elongation step and was set to run at 60 °C for 20 s (**Figure 2.6**).

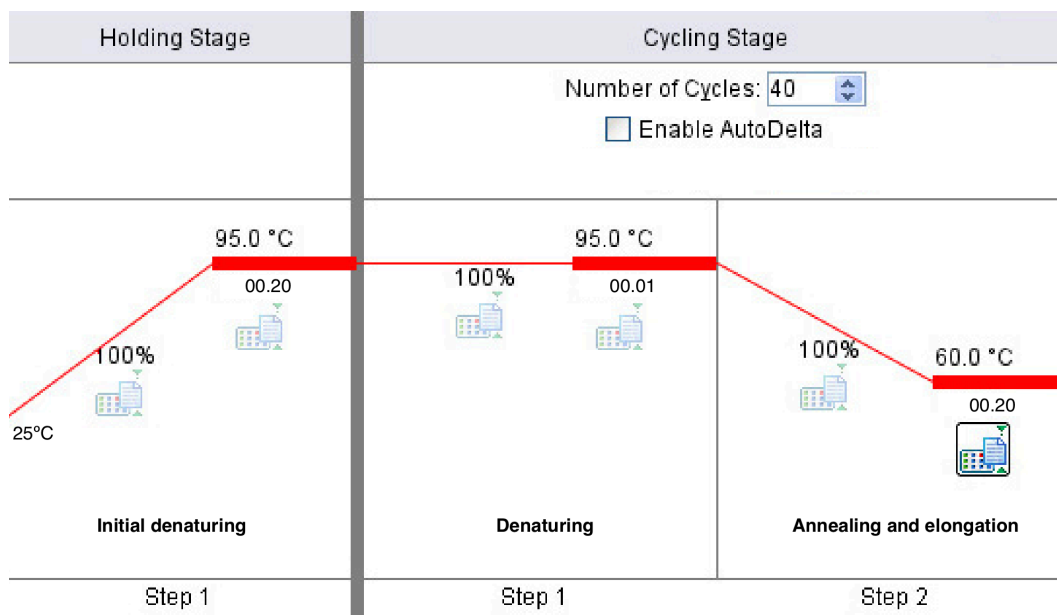


Figure 2.6 Schematic of the RT-qPCR steps. The instrument runs two stages, the holding stage and the cycling stage. There are three steps in total: initial denaturing, denaturing and annealing and elongation. Adapted from (Applied Biosystems StepOne Plus Real Time PCR instrument manual).

2.3.4 Gene expression quantification and analysis

To quantify RT-qPCR data, absolute and relative quantification methods are used. Absolute quantification method uses a standard curve to quantify a PCR signal, whereas relative quantification method compares a threshold cycle (C_t) value of a reference gene with C_t value from a target gene (Livak and Schmittgen, 2001, Valasek and Repa, 2005). As the main purpose of the present study was to see relative changes in gene expression between treatments, data were analysed using the C_t method. The C_t value indicates the number of transcription cycles required to detect the gene and is, therefore, inversely proportional to the expression of the gene in a sample. From this value, a series of calculations are performed to calculate the ΔC_t , $\Delta\Delta C_t$ and the relative fold increase (RFI) (**Table 2.4**). The ΔC_t value represents the C_t value of target genes normalised with mean C_t value of house-keeping genes. The $\Delta\Delta C_t$ value indicates the ΔC_t value of the test sample normalised with ΔC_t value of untreated (control) sample. RFI indicates the gene expression relative to the untreated control.

ΔCt	Ct target gene – Ct reference gene
$\Delta\Delta\text{Ct}$	ΔCt treated sample – ΔCt untreated (control) sample
RFI	$2^{-\Delta\Delta\text{Ct}}$

Table 2.4 ΔCt calculations for RT-qPCR data analysis. The Ct value for the two reference genes was averaged and used to normalise the data and calculate ΔCt values for control and treated samples.

2.3.5 Next-generation sequencing analysis

The gene sequencing analysis was performed in collaboration with Prof. Christian Wolfrum and Dr Sun Wenei (ETH, Zürich), and Maya Haaker (Utrecht University, Netherlands). Differentiated and proliferating primary NHEK were prepared as described in (Section 2.1.2, 2.1.3). Cells were collected in RLT buffer (1 ml) with β -mercaptoethanol (β -ME) (10 μl) in vials and sent to Maya Haaker for RNA extraction; the RNA extraction protocol followed was the same as described in (Section 2.3.3). Extracted RNA was then sent to Dr Sun Wenfei for gene sequencing. Gene sequencing was performed using Deseq2 following the standard workflow: polyA RNA extraction-> cDNA transcription-> cDNA tagging with barcodes -> loading samples to Novaseq-> acquire raw reads-> map raw reads to the genome-> obtain gene expression matrix-> statistically analyse gene expression profiles. The data were then sent to me for analysis using the Ingenuity Pathway Analysis software (IPA). Gene expression in differentiated NHEK was compared to that in proliferating NHEK. Core analysis was performed and a p value of 0.001 was set to narrow down the list of genes from 21695 genes to 3011 genes. Log2 fold change of < -1 was considered downregulated, whereas a log2 fold change of > 1 was considered upregulated. Enriched pathways were explored using canonical pathways analysis. Pathway enrichment shows if a certain pathway in IPA[®] database is highly represented in the list of genes tested. It uses a series of statistical analyses which relate the activation state of a pathway to the p value of the analysed genes in the samples. For example, if most genes found to be involved in a specific pathway were significantly upregulated/downregulated, then the pathway is

considered in an activation/inhibition state, depending on the pathway and related biological functions.

2.4 Lipidomic analysis using UPLC/ESI-MS/MS

Ceramides were measured in primary human skin cells in order to examine the effect of PUFA treatments on ceramide biosynthesis in primary NHEK and HDF (**Chapters 3 and 4**). Ceramides, endocannabinoids, N-acyl ethanolamines and monoacylglycerols were measured in rat skin tissue and plasma to study changes in lipid profile with diabetes in an animal model of diabetic peripheral neuropathy (DPN) (**Chapter 5**). Lipidomic analysis was performed using ultraperformance liquid chromatography coupled to electrospray ionisation with triple quadrupole tandem mass spectrometry (UPLC/ESI-MS/MS) using previously published protocols (Kendall et al., 2017, Felton et al., 2017, Kendall et al., 2015, Kendall et al., 2016, Poolman et al., 2019, Pappas et al., 2018). Analysis using the highly sensitive targeted UPLC/ESI-MS/MS involves the following main steps: lipid extraction, liquid chromatography (LC) followed by separation and Ionisation, MS/MS fragmentation and finally lipid detection and quantification (**Figure 2.7**).

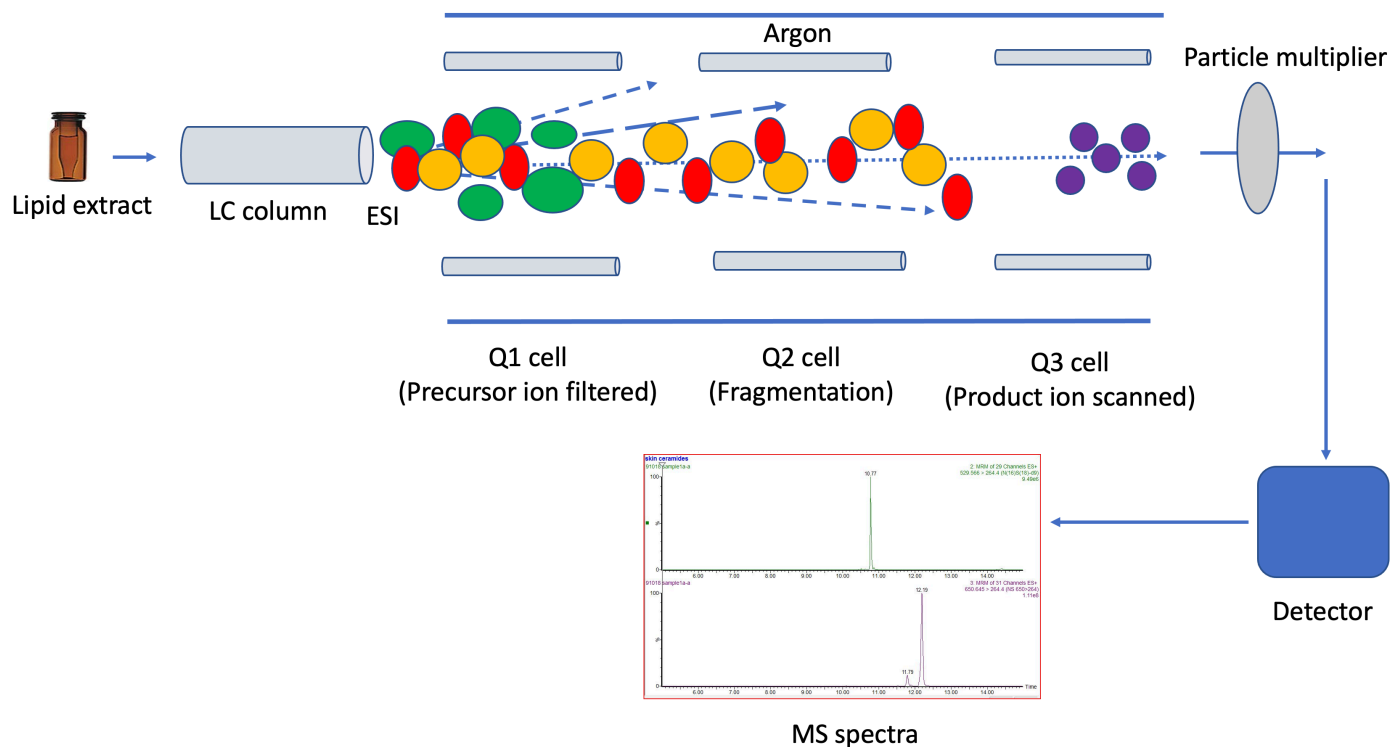


Figure 2.7 Schematic diagram of the UPLC-ESI-MS/MS principle. First, the lipid extract is separated by liquid chromatography (LC), which is then vapourised and ionised (charged droplets) by electrospray ionization (ESI). Ions are separated based on their mass-to-charge ratio (m/z). The first quadrupole (Q1) is where charged droplets (ions) pass through and selects specific ion masses. The second quadrupole (Q2) is where collision-induced occurs. The third quadrupole (Q3) is the mass filter cell where the ions are filtered and the product ions are scanned. The product ions then pass to the particle multiplier for signal amplification. The molecules then hit the detector and the system, which generates spectra that are used for lipid analysis.

2.4.1 Reagents and consumables

2.4.1.1 Reagents

Methanol and chloroform (both LC-MS grade, $\geq 99.9\%$) were purchased from Fisher Scientific (Loughborough, UK). Ethanol (HPLC grade; $>99.8\%$), formic acid (HPLC grade; $>99.8\%$), acetic acid (HPLC grade; $>99.8\%$), hexane (HPLC grade; $\geq 97.0\%$), acetonitrile (LC-MS grade, $\geq 99.9\%$), isopropanol (LC-MS grade, $\geq 99.9\%$) were acquired from Sigma (Gillingham, UK).

The following ceramide deuterated internal standards (CER IS-*d*) were obtained from Avanti Polar Lipids (Alabaster, Alabama, US): CER[N(16)S(18)]-*d*₉, CER[N(16)DS(18)]-*d*₉, CER[N(16)H(18)]-*d*₉, CER[N(16)P(18)]-*d*₉, CER[A(16)S(18)]-*d*₉, CER[A(16)DS(18)]-*d*₉, CER[A(16)H(18)]-*d*₉, CER[A(16)P(18)]-*d*₉, CER[E(26)O(18:1)S(18)]-*d*₉, CER[E(26)O(18:1)P(18)]-*d*₉. All lipid standards were in powder form and stock solutions in ethanol were prepared at concentrations 1 mg/ml (CER[N(16)H(18)]-*d*₉, CER[A(16)S(18)]-*d*₉, CER[A(16)DS(18)]-*d*₉, CER[A(16)H(18)]-*d*₉, CER[A(16)P(18)]-*d*₉, CER[E(26)O(18:1)S(18)]-*d*₉, CER[E(26)O(18:1)P(18)]-*d*₉) or 5 mg/ml (CER[N(16)S(18)]-*d*₉, CER[N(16)DS(18)]-*d*₉, CER[N(16)P(18)]-*d*₉).

The following standards for endocannabinoids and bioactive lipid mediators were obtained from Cayman Chemicals (Ann Arbor, MI, USA): 2-AG, AEA, myristoyl ethanolamide (MEA), palmitoleoyl EA (POEA), pentadecanoyl EA (PDEA), palmitoyl EA (PEA), heptadecanoyl EA (HEA), stearoyl EA (STEA), oleoyl EA (OEA), vaccenoyl EA (VEA), lineoleoyl EA (LEA), α -linolenoyl EA (ALEA), dihomo- γ -linolenoyl EA (DGLEA), eicosapentaenoyl EA (EPEA), docosapentaenoyl EA (DPEA), docosahexaenoyl EA (DHEA), docosanoyl EA (DEA), nervonoyl EA (NEA), lignoceroyl EA (LGEA) and N-arachidonoyl taurine (NAT), PGF₂ α -EA, PGE₂-EA, PGD₂-EA, 15-HETE-EA, 5,(6)-EET-EA, 8,(9)-EET-EA, 11,(12)-EET-EA, 14,(15)-EET-EA, 2-palmitoyl glycerol (2-PG), 2-lineoleoyl glycerol (2-LG). All lipid standards were delivered in solution in methyl acetate or ethanol at various concentrations. The following endocannabinoid and NAE deuterated internal standards were obtained from Cayman Chemicals (Ann Arbor, MI, USA): AEA-*d*₈ (solution in methyl acetate) and 2-AG-*d*₈ (solution in acetonitrile).

2.4.1.2 Consumables and equipment

Deionised ultrapure water was provided by Elga Water Purelab flex purification system (High Wycombe, UK). A Dounce homogeniser was used for skin cells homogenisation (Ystral, Ballrechten- Dottingen, Germany). A Sorvall refrigerated centrifuge (Dupont Stevenage, Herts, UK), whirlmixer (Fisher Scientific, Loughborough, UK), SPE vacuum manifold (Phenomenex) equipped with vacuum pump (1c Vacuumbrand, Wertheim, Germany), and custom-made solvent drying apparatus with gaseous nitrogen supply were used for the lipid extractions. STRATA™ SPE cartridges were bought from Phenomenex (Macclesfield, UK). Hamilton glass syringes (volumes: 10 µl, 50 µl, 100 µl, 250 µl) were purchased from SGE (Melbourne, Australia), Gilson Pipetman pipettes (different volume ranges), dissecting equipment (tweezers and scissors) and 50 mm length glass transfer Pasteur Pipettes (Fisher Scientific, Loughborough, UK). Flat- and round-bottomed 10 mL wide-neck glass extraction tubes with lids, amber glass vials (2 ml) with conical glass inserts (200 µl) and screw caps (8 mm) with PTFE septa were obtained from Phenomenex (Macclesfield, UK), Parafilm® , Septa and cryogenic storage boxes for 2 ml glass vials (Fisher Scientific, Loughborough, UK).

Ceramide analysis was performed using an Acquity UPLC system fitted with a pre-column filter and C8 column (Acquity UPLC BEH, 1.7 µm, 2.1 x 100 mm). Endocannabinoids and other bioactive lipids analysis was performed using an Acquity UPLC system fitted with the pre-column filter and a C18 column (Acquity UPLC BEH, 1.7 µm, 2.1 x 50 mm). UPLC was coupled to an ESI tandem quadrupole Xevo TQ-S mass spectrometer (Waters, UK).

2.4.2 Preparation of internal standards and calibration samples

2.4.2.1 Ceramide internal standards

Due to the unavailability of commercially developed ceramide internal standards for every CER species, relative quantitation against CER IS-*d* for the different CER classes is performed (Kendall et al., 2018). The master stock cocktail contains each lipid standard mentioned above at a concentration of 100 µg/ml. This was prepared by mixing 100 µl of the 1 mg/ml CER IS-*d*: CER[N(16)H(18)]-*d*₉, CER[A(16)S(18)]-*d*₉, CER[A(16)DS(18)]-*d*₉, CER[A(16)H(18)]-*d*₉,

CER[A(16)P(18)]-*d*₉, CER[E(26)O(18:1)S(18)]-*d*₉, CER[E(26)O(18:1)P(18)]-*d*₉ and 20 µl of the 5 mg/mL CER IS-*d*: CER[N(16)S(18)]-*d*₉, CER[N(16)DS(18)]-*d*₉, CER[N(16)P(18)]-*d*₉, then adding ethanol to prepare (1 ml). CER IS-*d* cocktail was stored at -80°C for up to six months and was diluted to prepare working solutions. This was prepared by adding 10 µl of the (100 µg/ml) master stock cocktail to 990 µl of ethanol to give a 1 µg/ml CER IS-*d* working solution which was then further diluted by adding 100 µl of (1 µg/ml) to 900 µl ethanol. This final concentration of 100 ng/ml was used for all further experiments. CER IS-*d* solutions were sealed with an 8 mm screw cap and Parafilm and stored at -20°C for up to 3 months.

2.4.2.2 Internal standards and quantitative calibration samples for endocannabinoids, N-acyl ethanolamines and monoacylglycerols

Unlike ceramides, internal standards for lipid mediator compounds are commercially available, allowing for accurate quantification using calibration lines. Additionally, deuterated internal standards are added to samples for added accuracy by normalising peak integrals (Kendall et al., 2018, Kendall et al., 2016). The lipid standards were dissolved in ethanol to prepare 10 ng/µL of: 2-AG, AEA, ALEA, DHEA, EPEA, OEA, SEA, PEA, LEA, MEA, PDEA, HEA, POEA, DGLEA, DPEA, DEA, NEA, LGEA, NAT, PGF2 α -EA, PGE2-EA, PGD2-EA, 15-HETE-EA, 5,(6)-EET-EA, 8,(9)-EET-EA, 11,(12)-EET-EA, 14,(15)- EET-EA, 2-PG, 2-LG. These were stored at -80°C for up to a year. Lipid cocktail (100 pg/µl) was prepared by adding 10 µl of each stock solution (10 ng/µl) to 760 µl ethanol. To prepare the deuterated internal standards, 100 µl of AEA-*d*₈ (10 ng/µl) and 200 µl of 2-AG-*d*₈ (10 ng/µl) were mixed with 700 µl ethanol to prepare 1 ng/µl AEA-*d*₈ and 2 ng/µl 2-AG-*d*₈. Freshly made internal standard solutions were sealed with an 8 mm screw cap and Parafilm and stored at -20°C for up to 3 months.

Quantitative calibration standards were prepared by serial dilutions of the lipid cocktail (100 pg/µl) to achieve the following concentrations: 20.0 pg/µl, 10.0 pg/µl, 5.00 pg/µl, 2.50 pg/µl, 1.30 pg/µl, 0.60 pg/µl, 0.30 pg/µl, 0.20 pg/µl, 0.10 pg/µl, and 0.04 pg/µl. First, 20µl of lipid cocktail (100 pg/µl) and 180 µl ethanol was added to a clean vial. Then, 100 µl of this solution and 100 µl ethanol was added to

another vial. The rest of the serial dilutions were prepared in the same manner until the lowest concentration was prepared. Finally, deuterated internal standard cocktail (1 ng/ μ l AEA, 2 ng/ μ l 2AG) was added to each vial, and the solvent was evaporated under gaseous nitrogen. The mixture was then reconstituted in ethanol (100 μ l). Vials were sealed with an 8 mm screw cap and Parafilm before storing at -20°C prior to UPLC-MS/MS analysis but they were not kept longer than a week.

2.4.3 Lipid extraction from skin and plasma samples

Lipids were extracted using the Bligh and Dyer method (Bligh and Dyer, 1959). Ceramides and endocannabinoids were extracted from primary human skin cells, and from rat skin and plasma, using a combined extraction procedure for each sample. This is due to the small amount of skin tissue/cells and plasma available, which allowed the measurement of ceramides and endocannabinoids and related lipid mediators in one extract. Preliminary experiments which were conducted to optimise the extraction protocol are presented in (**Appendix 2**). The optimisation experiments aimed to test several extraction methods to examine matrix effect and process efficiency (PE) described in (Matuszewski et al., 2003). The extraction protocol was then further developed by Dr Alexandra Kendall and Dr Maria Dolores Camacho-Munoz.

Briefly, cell pellets were homogenised using a Dounce homogeniser, whereas skin tissue was minced with dissecting scissors. Homogenised cells/tissue or 50 μ l of plasma was added to flat-bottomed glass tubes containing 4 ml ice cold chloroform. 2 ml of ice-cold methanol was then added to the tubes and spiked with 40 μ l CER IS-*d* (100 ng/mL) and 20 μ l (1 ng/ μ l AEA-*d*8 and 2 ng/ μ l 2AG-*d*8) cocktail if analysing endocannabinoids and lipid mediators. Samples were then vortexed and 1.5 ml ice-cold water was added then vortexed again. Samples were incubated on ice in the dark for 30-40 minutes, and vortexed every 10 minutes. After that, samples were centrifuged (1500 x g, 5 min, 4 °C). Using a glass pipette, the bottom organic layer was transferred to a clean round-bottomed tube. For skin tissue, at this stage the remaining minced skin tissue was stored at -20 °C for protein content analysis (**Section 2.4.4.3**). Samples were then completely dried under nitrogen. Then, using a Hamilton syringe, samples were reconstituted in 200 μ l ice-cold chloroform and vortexed then pulse centrifuged.

The next step was to semi-purify the extract using SPE cartridges. After conditioning 100 mg silica cartridges with 2 x 1 ml ice-cold hexane, samples were loaded onto the SPE cartridges using Hamilton syringe. Cartridges were washed twice with 0.75 ml ice-cold chloroform, then new round-bottom tubes were used to collect the eluate. Lipids were eluted with 2 x 0.75 ml 2:1 chloroform:methanol, then 2 x 0.75 ml 2:1 chloroform:methanol + 0.1 % formic acid. Samples were dried again under nitrogen then reconstituted in 150 µl methanol + 0.1 % formic acid for ceramides and stored at -20 °C until analysis. The same extract was used if measuring endocannabinoids and lipid mediators.

2.4.4 Targeted UPLC/ESI-MS/MS lipid analysis

2.4.4.1 Analysis of skin and plasma ceramides

The targeted mass spectrometry assays used in this study, which investigate specific lipid classes and compounds in different types of biological samples, have been developed by our group (Kendall et al., 2017, Kendall et al., 2015, Kendall et al., 2016). Analysis was performed using UPLC coupled to a triple quadrupole mass spectrometer with ESI. Chromatographic separation was done using a C8 column (1.7 µm, 2.1 x 100 mm). The MS was operated in the positive ionisation mode using the MS/MS mode. The skin and plasma CER methods differed slightly depending on the type of sample due to the higher number of CERs found in skin; skin CER protocol used the following conditions: sample manager temperature 8 °C; mobile phase A solvent (purified water with 0.1% formic acid) in addition to mobile phase B solvent (methanol with 0.1% formic acid) at a flow rate of 0.3 ml/min; injection volume 3 µl, and column temperature 30 °C. The seal wash was MeOH:H₂O (1:1, v/v); weak needle wash was MeOH:H₂O (60:40) and strong needle wash was H₂O:ACN:MeOH:IPA (1:1:1:1, v/v/v/v).

One method was used for plasma CERs, where samples were injected once (in duplicate), whereas five methods (one injection per method) were needed for the skin CER assay to allow for the analysis of around 340 CER species as previously identified in skin (Masukawa et al., 2008, t'Kindt et al., 2012). Blanks consisting of (MeOH with 0.1% formic acid) were injected after each sample. Analytes were fragmented using argon as a collision gas (collision cell pressure approx. 8.03×10^{-5} Torr).

⁵ mbar) and monitored in the positive ion mode by multiple reaction monitoring (MRM). MRM transitions and indicative retention times for CER assay were previously optimised by our group (Kendall et al., 2017, Kendall et al., 2015, Kendall et al., 2016) (**Appendix 3**). The MS tuning parameters for the analysis were: capillary voltage 3.5 kV, source temperature 100 °C; desolvation temperature 450 °C; Instrument used was MassLynx (version: 4.1) as an operating software. Relative quantification of analytes was performed using the class-specific internal standards as previously mentioned. A representative UPLC-ESI-MS/MS chromatogram for CER assay is shown in (**Figure 2.8**).

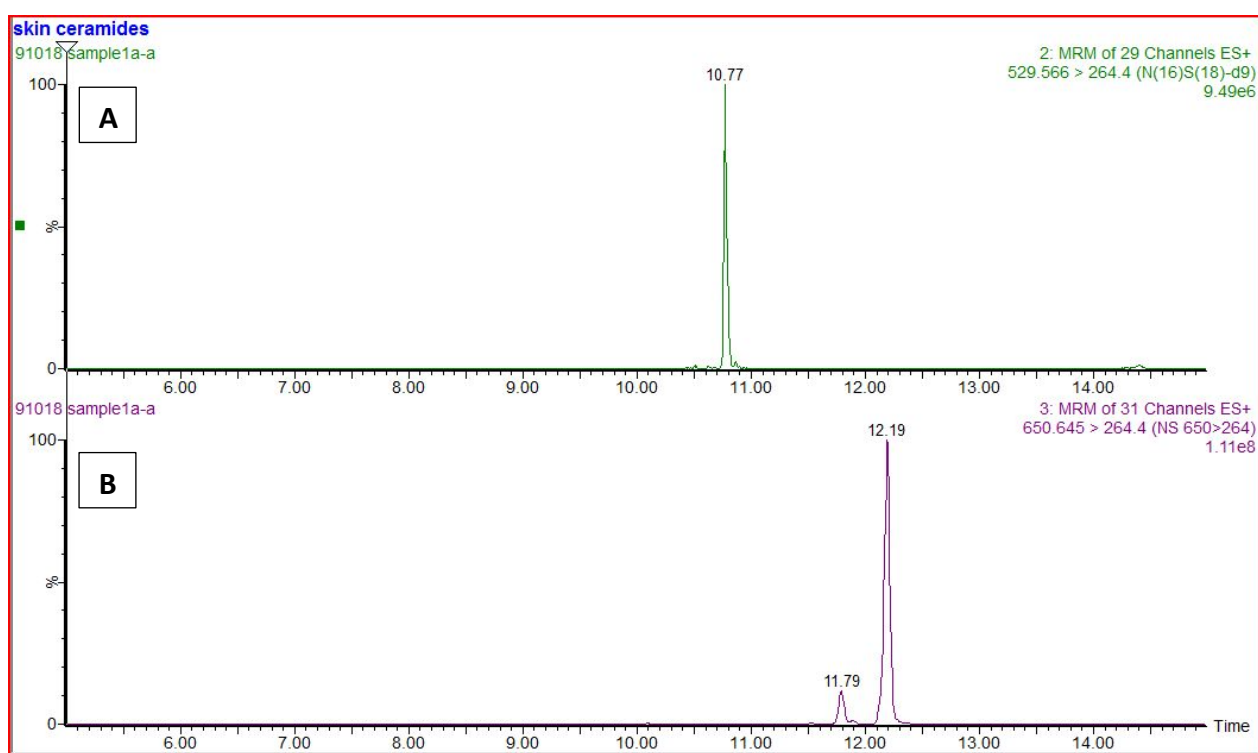


Figure 2.8 Representative UPLC/ESI-MS/MS chromatogram of ceramide internal standard and species. A) CER internal standard: N(16)S(18)-*d9*; B) CER[NS] species: N(24)S(18) identified in rat hind-paw skin. CER: ceramide; CER[NS]: non-hydroxy ceramide.

2.4.4.2 Analysis of skin and plasma endocannabinoids, *N*-acyl ethanolamines and monoacylglycerols

Chromatographic separation was done using UPLC fitted with pre-column filter and a C18 column (1.7 μm , 2.1 x 50 mm) coupled to an ESI triple quadrupole Xevo TQ-S MS. ESI was operated in positive ionisation mode. The method for the

endocannabinoid analysis used the following conditions: sample manager temperature 8 °C; mobile phase A (ultrapure water with 0.02% acetic acid) and mobile phase B (acetonitrile with 0.02% acetic acid) at a flow rate 0.6 ml/min; injection volume 3 µl, and column temperature 25 °C. Each sample was injected in duplicate for plasma and skin. Blanks consisting of (ethanol) for plasma or (MeOH with 0.1% formic acid) for skin were injected after each sample. The seal wash was MeOH:H₂O (1:1, v/v); weak needle wash was MeOH:H₂O (60:40) and strong needle wash was H₂O:ACN:MeOH:IPA (1:1:1:1, v/v/v/v). Analytes were fragmented using argon as a collision gas (collision cell pressure approx. 8.03×10^{-5} mbar) and monitored in the positive ion mode by MRM. MRM transitions and indicative retention times for the endocannabinoid assay were optimised by our group and are listed in **(Appendix 4)**. The MS tuning parameters for the analysis were: capillary voltage 1.8 kV, source temperature 150°C, desolvation temperature 400°C. The instrument used MassLynx (version: 4.1) as an operating software.

2.4.4.3 Protein content determination

In order to determine the concentration of lipids extracted from skin tissue samples, lipid quantities were normalised to protein content. Semi-quantitative analysis was performed using TargetLynx (**section 2.4.5**), which is then normalised against sample volume, cell number, or protein content. For rat foot pad skin, protein content analysis was performed using a standard Bradford protein assay kit (Bio-Rad Protein Assay, Bio-Rad, Hemel Hempstead, U.K.) following the (Bradford, 1976) protein content estimation assay.

Reagents and equipment

Sodium hydroxide (NaOH) (pellets, ≥98%; Sigma-Aldrich, Poole, UK) was used to prepare a solution of 1 M in ultra-pure water. DC Protein Assay Kit II was bought from Bio-Rad (Hercules, California, US). Bovine serum albumin (BSA) (Bio-Rad, Hercules, California, US) (1.5 mg/ml) was used as a standard. Water bath SBS40 (Stuart Equipment, Stone, UK) was used to prepare samples for the protein content measurement. All measurements were performed using MultiskanTM FC plate reader with internal shaker at 650 nm wavelength. Corning[®] Costar[®] flat bottom 96-well plates were bought from Sigma-Aldrich (St. Louis, MO, USA).

Protocol

To prepare the BSA 6-point calibration line series, the following dilutions were made (**Table 2.5**). All rat foot-pad skin samples were retained after lipid extraction as described in (**section 2.4.3**). Samples were allowed to stand at room temperature and any remaining extraction solvent was removed using a glass Pasteur pipette. Then, NaOH (1 ml, 1 M) was added to each sample and the samples were heated at 60°C for 90 min in a water bath to solubilise the protein. The solutions were diluted 1:10 with NaOH (1 M). Diluted samples (5 µl) and BSA solutions (5 µl) were placed into 96-well plate in triplicate. Next, 25 µl of Protein Assay Reagent A (alkaline copper tartrate solution) and 200 µl of Protein Assay Reagent B (folin reagent) were added to each well. The plate was then incubated in the dark for 15 min at room temperature. The absorbance was then measured at 650 nm.

Solution	BSA (mg/ml)	Series dilution
A	1.5	400 µl BSA stock
B	0.75	200 µl of A + 200 µl 1M NaOH
C	0.375	200 µl of B + 200 µl 1M NaOH
D	0.188	200 µl of C + 200 µl 1M NaOH
E	0.094	200 µl of D + 200 µl 1M NaOH
F	0	200 µl 1M NaOH

Table 2.5 BSA standard preparation.

Protein content was estimated based on BSA calibration line (**Figure 2.9**). BSA calibration line is prepared by calculating the mean absorbance of three BSA replicates per BSA concentration (x axis).

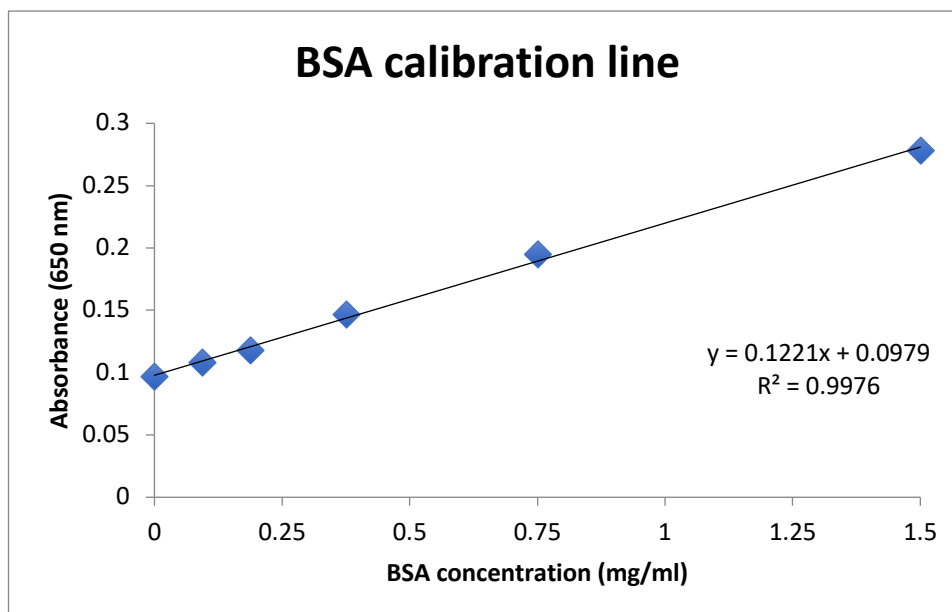


Figure 2.9 BSA standard calibration line.

Data were expressed as mg of protein/sample. To calculate protein content using the above calibration line, the absorbance of three sample replicates is averaged, then subtracted from (0.0979). The value is then divided by the intercept/slope factor (0.1221). The result is then multiplied by the dilution factor.

2.4.5 Data processing and quantitation

2.4.5.1 Ceramide data processing and semi-quantitation

TargetLynx (version: 4.1) was used for peak detection and semi-quantitation of compounds of interest. After integration of the chromatograms, concentration of the lipid “response” was calculated relative to relevant CER IS-d based on the lipid/deuterated internal standard peak area ratio. Based on our CER assay, a total of 4 ng of each ceramide standard were added during the extraction process (**section 2.4.3**). The TargetLynx method was programmed to calculate the absolute concentration of each ceramide relative to the amount of standard (4 ng), which is then normalised against sample size: ng/mL of plasma, ng/cell count or ng/mg of protein.

2.4.5.2 Endocannabinoids, N-acyl ethanolamines and monoacylglycerols data processing and quantitation

TargetLynx (version: 4.1) was used for peak detection and semi-quantification of compounds of interest. The instrumental limit of detection (ILOD) was set to signal-

to-noise ratio of 3; the instrumental limit of quantification (ILOQ) was set to signal-to-noise ratio of 10. As explained above, TargetLynx normalised the peak area for each compound against the relevant internal standard, which results in the concentration of the lipid (the response). TargetLynx will then calculate a concentration for each compound in each sample based on the generated calibration line equations and the responses (pg/ μ l of injected extract). This is then multiplied by the reconstitution volume (150 μ l). The calculated total amount of lipid per samples are then normalised against sample size: pg/ml of plasma or pg/mg of protein.

2.5 Analysis of membrane lipids using UHPSFC-MS^E

Membrane lipids were measured in skin cells in order to examine the effect of PUFA treatments on lipid biosynthesis in primary NHEK and HDF (**Chapters 4 and 5**). Extracted lipids were analysed by Dr Marta Koszyczarek using ultrahigh performance supercritical fluid chromatography coupled to electrospray ionisation and quadrupole time-of-flight mass spectrometry (UHPSFC/ESI-MS) using MS^E data acquisition mode.

2.5.1 Reagents and consumables

2.5.1.1 Reagents

MeOH, IPA, and CHCl₃ (all HPLC grade, $\geq 99.0\%$), ammonium acetate ($>98\%$), and acetic acid (HPLC grade; $\geq 99.7\%$) were purchased from Sigma-Aldrich (Poole, UK). CO₂ was liquid CO₂ CP grade supplied by BOC (Guildford, UK). Membrane lipids deuterated internal standards (ML IS-*d*) were obtained from Avanti Polar Lipids in a powder form (Alabaster, Alabama, US): CE 15:0-*d*₇, CHL-*d*₇, SM 16:0-*d*₃₁, PC 16:0-*d*₃₁-18:1, LPC 26:0-*d*₄, PE 16:0-*d*₃₁, TG 17:0-17:1-17:0-*d*₅, DG 18:1-*d*₅, PG 16:0-*d*₃₁-18:1, LPE 18:1-*d*₇, and PALM-*d*₃₁. The internal standard cocktail contained the following deuterated lipid standards dissolved in MeOH: PC 15:0-18:1-*d*₇ (160.7 μ g/ml), PE 15:0-18:1-*d*₇ (5.7 μ g/ml), PS 15:0-18:1-*d*₇ (4.2 μ g/ml), PG 15:0-18:1-*d*₇ (29.1 μ g/ml), PI 15:0-18:1-*d*₇ (9.1 μ g/ml), PA 15:0-18:1-*d*₇ (7.4 μ g/ml), LPC 18:1-*d*₇ (25.5 μ g/ml), LPE 18:1-*d*₇ (5.3 μ g/ml), CE 18:1-*d*₇ (356.1 μ g/ml), MG 18:1-*d*₇ (2.0 μ g/ml), DG 15:0-18:1-*d*₇ (9.4 μ g/ml), TG 15:0-18:1-*d*₇-15:0 (57.3 μ g/ml), SM 18:1-*d*₉ (30.9 μ g/ml), and CHL-*d*₇ (98.4 μ g/ml).

2.5.1.2 Consumables and equipment

The equipment used is described in (Section 2.4.1.2). Lipid analysis was performed using an Acquity UPC² UHPSFC system equipped with HPLC 515 pump and fitted with the pre-column filter and column (Torus 2-PIC column, 100mm x 2.1mm x 1.7µm). UHPSFC was coupled to an electrospray ionisation quadrupole time-of-flight MS Synapt G2 (all from Waters, UK).

2.5.2 Preparation of deuterated internal standards

Similar to ceramides, internal standards for all membrane lipid species are unavailable commercially. Therefore, a known amount of a ML IS-*d* representing each lipid class is added to perform semi-quantitation. A specific volume of each individual ML IS-*d* powder was mixed with chloroform or ethanol to prepare master stock solutions (10 mg/ml). To prepare the ML IS-*d* cocktail working solution, specific volumes of the individual ML IS-*d* stock solutions were mixed together and dried under gaseous nitrogen, then reconstituted in CHCl₃:IPA (2 mL; 1:1, v/v) and stored at -20°C for up to 3 months. The cocktail contained the following final lipid concentrations: 100 µg/ml (PALM-*d*31, CE-*d*7, PC 16:0-*d*31-18:1, PE 16:0-*d*31-18:1, LPC 26:0-*d*4, SM 16:0-*d*31, TG 17:0-17:1-17:0-*d*5, DG 18:1-*d*5, LPE 18:1-*d*7); 200µg/ml (CHL-*d*7), or 300µg/ml (PG 16:0-*d*31-18:1).

2.5.3 Lipid extraction from skin cells

Lipids were extracted from primary NHEK and HDF as described in (section 2.4.3). After adding 4 ml of chloroform to the homogenised samples, 40 µl of the ML IS-*d* cocktail was added using a Hamilton syringe. After drying the extract under a stream of nitrogen, 200 µl of CHCl₃:IPA (1:1, v/v) was added. Lipid extracts were then split into two 100 µl aliquots (one for positive mode and one for negative mode). Samples were stored for up to a week at -20°C prior to analysis.

2.5.4 Untargeted membrane lipid analysis

Analysis of the extracted lipids using UHPSFC-MS^E was done by Dr Marta Koszyczarek. The method for complex lipid analysis was optimised by Dr Marta Koszyczarek as part of her PhD project. Chromatographic separation was

performed using an Acquity UPC² system fitted with pre-column and Acquity UPC² Torus 2-PIC column (100 mm x 3 mm x 1.7 μ m), coupled to Synapt G2 ToF MS.

The following conditions were used: sample manager temperature 8°C, mobile phase flow rate 1.5 ml/min, injection volume 2 μ l in the positive ionisation mode and 7 μ l in the negative ionisation mode, column temperature 60°C, ABPR 1800 psi, and injector needle wash was 100% MeOH (used after every injection). Mobile phase A was CO₂ and mobile phase B was a gradient of MeOH:H₂O mixture (99:1, v/v) containing 30 mM ammonium acetate at a flow rate of 0.25 ml/min. The seal wash used was MeOH:H₂O (1:1, v/v); both weak needle wash and strong needle wash were MeOH. Samples were injected in triplicate. CHCl₃:IPA (1:1, v/v) blanks were injected after each sample. For the data acquisition the Q-ToF-MS was set to high-sensitivity in both positive and negative ionisation modes using ESI probe. Recorded mass ranges were m/z 183-950 (positive mode) and m/z 229-950 (negative mode). The collision gas used was argon (collision cell pressure approx. 8.25×10^{-3} mbar). The MS tuning parameters were: capillary voltage 3.0 kV and 2.75 kV, in positive and negative mode, respectively; the sampling cone 40 V, source offset 90 V, source temperature 150°C, desolvation temperature 500°C, desolvation gas flow 750 L/h, drying gas flow 1 L/min, and the nebulizer gas flow 4 bar. Leucine enkephaline at m/z 556.6 (positive mode) and m/z 554.6 (negative mode) was used as the lockspray: lockspray infusion flow rate 20 μ l/min, lockspray capillary voltage 3.0 kV; sodium formate was used as a reference for the MS calibration.

2.5.5 Data processing and semi-quantitation

Data processing using Progenesis QI software (v 2.3, NonLinear Dynamics, Newcastle, UK) was carried out by Dr Marta Koszyczarek. In-house data base and LIPID MAPS database was used to semi-quantitate lipids, which were then normalised against cell number (Fahy et al., 2009, Lísá and Holčápek, 2015, Lísá et al., 2017). Precursor and corresponding fragment masses were determined from the UHPSFC-MS^E files by combining low and high collision energy data.

After data processing, detected lipids were semi-quantified based on the provided lipid/deuterated internal standard ratio. Data were reported as amount of lipid/ number of cells. The amount of lipid/ number of cells was calculated as follows:

$$\text{Amount of lipid } (\mu\text{g}/\mu\text{l}) = \frac{\text{Peak area of lipid} \times \text{Concentration of ML IS-}d \text{ in the extract}}{\text{Peak area of ML IS-}d}$$

The value was then normalised to cell number ($\mu\text{g}/ 10^6$ cells). To get the concentration of each ML IS-*d* in the extract: the final concentration of each standard in the ML IS-*d* cocktail was multiplied by the total amount of ML IS-*d* cocktail added to each sample during the extraction (40 μl) (**Table 2.6**).

Standard	Concentration (mg/ml)
FFA-d31	0.1
15:0 CE-d7	0.1
16:0-d31-18:1 PC	0.1
16:0-d31-18:1 PE	0.1
17:0-17:1-17:0 D5 TG	0.1
26:0-d4 Lyso PC	0.1
16:0-d31 SM	0.1
18:1 DAG d5	0.1
18:1 LysoPE d7	0.1
cholesterol-d7	0.2

Table 2.6 The final concentration of standards in the ML IS-*d* cocktail. FFA-D31: Free fatty acids standard; 15:0 CE-d7: cholesterol ester standard; 16:0-d31-18:1 PC: phosphatidylcholine standard; 16:0-d31-18:1 PE: phosphatidylethanolamine standard; 17:0-17:1-17:0 D5 TG: triacylglycerol standard; 26:0-d4 Lyso PC: lysophosphatidylcholine standard; 16:0-d31 SM: sphingomyelin standard; 18:1 DAG d5 diacylglycerol standard ; 18:1 LysoPE d7: lysophosphatidylethanolamine standard; cholesterol-d7: cholesterol standard.

2.6 Statistical analysis

Data distribution were assessed for normality using the Shapiro-Wilk test. Statistical analysis for the skin cells lipidomics data was performed using three independent biological replicates (n=3). Data were mainly parametric and a one-way ANOVA comparing treatments with controls, with corrections for multiple analyses using the Dunnett method was chosen. The skin tissue and plasma lipidomics data (n > 3 independent donors) were not normally distributed.

Therefore, data were analysed using non-parametric tests and performed tests in the raw and log transformed data. Statistical analysis was performed using t-tests comparing diabetes with control, with corrections for multiple analyses using the Holm-Sidak method. Gene expression statistical analysis (n= 4 biological replicates for NHEK; n=3 biological replicates for HDF) was performed using two-way ANOVA comparing changes over treatment and time, with corrections for multiple analyses using the Dunnett method; details are provided in the relevant chapters (**Chapter 3-5**). For all experiments, data were presented as mean of biological replicates \pm SD; $p < 0.05$ was considered statistically significant (GraphPad Prism software). The small sample number (for example, n= 3 biological replicates) could affect statistical significance. Therefore, p values that were not statistically significant but close to 0.05 were reported.

Chapter 3

**The effect of PUFA supplementation on
ceramide biosynthesis in primary human
epidermal keratinocytes**

3.1 Introduction

The epidermis consists of four layers with different cellular developmental stages starting from the stratum basale where proliferating keratinocytes, in the presence of a Ca^{2+} gradient, terminally differentiate towards the SC. Fully differentiated keratinocytes in the uppermost layer of the epidermis release CERs, which along with the intercellular membrane lipids, cholesterol and FFAs, form the permeability barrier (Weerheim and Ponc, 2001). Alterations in CER levels contribute to structural and functional impairment of the barrier seen in several skin disorders such as AD, psoriasis and acne vulgaris, to name a few (Kendall and Nicolaou, 2013). *De novo* biosynthesis of CERs is a dynamic process that involves a group of tissue and FA-specific CER synthases, in addition to sphingoid base-specific desaturases, which lead to the combination of specific sphingoid bases, FA chains and headgroups, generating various CER species with unique characteristics (**Table 1.1**) (Hannun and Obeid, 2011). For example, in the epidermis, CERs with long-chain FAs and phytosphingosine, which are characteristic of the skin, are produced by skin-active CerS3 and Des2 (Choi et al., 2018).

Although the role of skin CERs in barrier health and disease is well established, the exact mechanisms involved in regulating CER synthesis are not fully understood. To interrogate the CER biosynthetic pathways we can utilise agents such as PUFAs which serve principal roles in maintaining the barrier's structure and function (McCusker and Grant-Kels, 2010). For example, *n*-3 PUFAs, DHA and EPA, are known for their diverse roles in protecting the skin from inflammatory insults such UVR (Pilkington et al., 2011), and have been found to alter CER levels in cultured skin explants (Kendall et al., 2017). In addition, the *n*-6 PUFA, LA, is essential for barrier homeostasis and the production of the crucial SC acylceramides (Fujii et al., 2013, Wertz et al., 1983). In addition to this, both EPA and LA were found to increase CER levels and glucosylceramide synthase mRNA expression in canine keratinocytes (Yoon et al., 2020). Moreover, oral administration of EPA ethyl ester was found to increase specific SC CER levels in AD mice in a dose-dependent manner (Fujii et al., 2018). However, studies exploring the effect of PUFAs on skin CER metabolism and the subsequent impact on skin health are limited, and the

mechanisms by which PUFA alters CER concentrations in human keratinocytes are not fully understood.

Other structural and functional lipids that support the skin's integrity include membrane lipids such as sterols, glycerolipids, glycerophospholipids and complex sphingolipids (van der Veen et al., 2017). Membrane lipid metabolism is a dynamic and interconnected process that generates lipid mediators which regulate inflammatory responses and cellular function. In addition to their role in regulating inflammatory responses, *n*-3 DHA and *n*-6 LA are peroxisome proliferator-activated receptor alpha (PPAR- α) agonists, which act in the nucleus to regulate keratinocyte differentiation and epidermal lipid synthesis (Rivier et al., 1998, Rivier et al., 2000). For example, specific activation of PPAR- α with Wy 14,643, was found to stimulate SPLTC2 expression and CER synthesis, and increased CE, and cholesterol sulfate in a skin equivalent model (Rivier et al., 2000). In addition, activating PPAR- α using LA was found to stimulate keratinocyte differentiation and the expression of CER generating enzymes, glucosylceramide synthase, aSMase and SPLTC2 (Gallala et al., 2004). Similarly, PPAR- α agonist, DHA, was found to increase filaggrin expression and normalised SC lipid ratio (FFA:CER:cholesterol) in a filaggrin deficient skin model (Wallmeyer et al., 2015). Therefore, *n*-3 and *n*-6 PUFAs act as gene regulators influencing epidermal differentiation, immune responses and CER and membrane lipid metabolism. Therefore, in order to better understand the role of PUFAs in modifying lipid synthesis and specifically the metabolism of CER at different stages of epidermal development, we examined the effects of *n*-3 (DHA, EPA) and *n*-6 (LA) PUFA supplementation on cutaneous CER and membrane lipids synthesis, and on CER biosynthesis gene expression in proliferating and differentiating NHEK.

Specific objectives:

To determine the effects of DHA, EPA and LA treatment on:

- 1) NHEK CER profile and concentrations,
- 2) gene expression of CER *de novo* biosynthesis enzymes,

- 3) the profiles of complex membrane lipids (cholesterol, FAs, SM, glycerolipids and glycerophospholipids) in proliferating and differentiating NHEK.

3.2 Materials and methods

3.2.1 Analysis of keratinocyte ceramides using UPLC/ESI-MS/MS

Keratinocyte CER analysis was performed using ultraperformance liquid chromatography coupled to electrospray ionisation with triple quadrupole tandem mass spectrometry (UPLC/ESI-MS/MS) (**Section 2.4**). Proliferating (low Ca^{2+}) and differentiated (high Ca^{2+}) primary NHEK were treated with 10 μM DHA, EPA or LA, for 72 hrs. Media were replaced daily with fresh media containing the PUFA treatments. CaCl_2 and PUFA treatments were prepared as described in (Section 2.1, 2.2). Cells were pelleted at 72 hrs post-PUFA treatment and CERs were extracted then analysed. CER concentrations in treated cells were compared to those in DMSO vehicle controls with the same Ca^{2+} conditions; proliferating NHEK (n=3 individual donors), differentiated NHEK (n=3 individual donors). Appendix 3 lists the MRM transitions and indicative retention times for skin CER assay. Data were processed using MassLynx software (Waters). Semi-quantitation using class-specific deuterated internal standards was used for ceramides. Ceramide quantities were normalised to cell number ($\text{ng}/10^6$ cells). Statistical analysis was performed using one-way ANOVA comparing treatments with controls of the same time-point, with corrections for multiple analyses using the Dunnett method. Data were presented as mean \pm SD; $p < 0.05$ was considered statistically significant (GraphPad Prism software). The small sample number (n= 3 biological replicates) could affect statistical significance. Therefore, p values that were not statistically significant but close to 0.05 were reported.

3.2.2 Measurement of ceramide biosynthesis enzyme mRNA levels

Gene expression was measured by RT-qPCR analysis as described in section 2.3. Proliferating (low Ca^{2+}) and differentiated (high Ca^{2+}) primary NHEK were treated with 10 μM DHA, EPA or LA. CaCl_2 and PUFA treatments were prepared as described in (**Section 2.1, 2.2**). Media were replaced daily with fresh media containing 10 μM DHA, EPA or LA, and cells were pelleted at six, 24 and 48 hrs post PUFA-supplementation. Data were presented as individual ΔCt values, which

are inversely proportional to the expression of the gene in a sample (smaller ΔCt value = higher gene expression) and relative fold increase (RFI), which compares CER biosynthesis enzyme gene expression in treated cells to that in controls of the same time-point where RFI of 1 = no change, <1 = downregulated, >1 = upregulated; Proliferating NHEK: (n=4 individual donors); Differentiated NHEK: (n=4 individual donors). The individual ΔCt values for all genes analysed are presented in (**Appendix 5**). Statistical analysis was performed using two-way ANOVA comparing changes over treatment and time. Corrections for multiple analyses was performed using the Dunnett method. Data were presented as mean \pm SD; $p < 0.05$ was considered statistically significant (GraphPad Prism software).

3.2.3 Analysis of membrane lipids using UHPSFC-MS^E

Membrane lipids were analysed using UHPSFC-MS^E system by Dr Marta Koszyczarek (**Section 2.5**). Samples and PUFA treatments were prepared as mentioned above (**3.2.1**). Membrane lipid concentrations in treated cells were compared to those in controls with the same Ca²⁺ conditions; proliferating NHEK (n=3 individual donors), differentiated NHEK (n=3 individual donors). Data were processed using Progenesis QI software (v 2.3, NonLinear Dynamics, Newcastle, UK). Lipid quantities were normalised to cell number ($\mu\text{g}/10^6$ cells). Statistical analysis was performed using repeated measures One-Way ANOVA comparing differences over treatment compared with control of the same time-point, with corrections for multiple analyses using the Dunnett method. Data were presented as mean \pm SD; $p < 0.05$ was considered statistically significant (GraphPad Prism software).

3.2.4 Gene sequencing analysis

The gene sequencing analysis was in collaboration with Prof. Christian Wolfrum and Dr Sun Wenfei (ETH, Zürich) and Maya Haaker (Utrecht University, Netherlands). Differentiated (High Ca²⁺, n=3) and proliferating (Low Ca²⁺, n=3) primary NHEK were prepared as described in (**Section 2.1.2, 2.1.3**). Dr Sun Wenfei performed gene sequencing using Deseq2 software as described in (**Section 2.3.5**). The data were then sent to me for analysis using the Ingenuity Pathway Analysis software (IPA[®], Qiagen) as described in (**Section 2.3.5**).

3.3 Results

3.3.1 Effect of PUFA supplementation on ceramide levels

The effect of *n*-3 PUFAs (DHA, EPA) and *n*-6 PUFA (LA) on CER concentration was analysed using UPLC/ESI-MS/MS. Proliferating NHEK representing the basal epidermal layers, and Ca²⁺ differentiated NHEK representing the granular cells were used to explore CER synthesis at the two developmental stages of the epidermis under the influence of PUFA supplementation. For each sample analysed, concentrations of detected CER species were reported as absolute values in ng/10⁶ cells (mean ± SD). Data were categorised based on ceramide class and carbon chain numbers to help identify possible trends.

3.3.1.1 Total ceramide levels were higher in differentiated NHEK

The amounts of individual ceramide species were quantitated and totalled. **Figure 3.1** shows the concentrations (ng/10⁶ cells) for total CER measured in proliferating and differentiated NHEK. Differentiated NHEK produced more CERs than proliferating controls, with a total CER concentration of (mean= 852.6 ng/10⁶ cells) in differentiated cells and (mean= 29.37 ng/10⁶ cells) in proliferating cells.

3.3.1.2 Ceramide levels in proliferating NHEK were significantly increased with DHA treatment

Changes in total ceramides per class were analysed to investigate the effect of PUFA supplementation on the different classes of ceramides that are produced using specific enzymes in the *de novo* biosynthesis pathway. Six CER classes were detected in proliferating NHEK: CER[NS], CER[NDS], CER[NH], CER[NP], CER[AH], CER[AS], whereas an additional class, CER[AP] was detected in differentiated NHEK. The most abundant ceramides in both cell types were the CER[NS] (Proliferating NHEK: mean= 19.74 ng/10⁶ cells, Differentiated NHEK: mean= 396.5 ng/10⁶ cells).

Examining individual CER classes revealed a significant increase in total CER[NS] (*p* <0.0001) in proliferating NHEK with DHA supplementation compared with control. In differentiated NHEK, DHA significantly increased total CER[NS]

concentration ($p= 0.006$) and seemed to increase total CER[NDS] concentration ($p= 0.08$) (**Figure 3.2**).

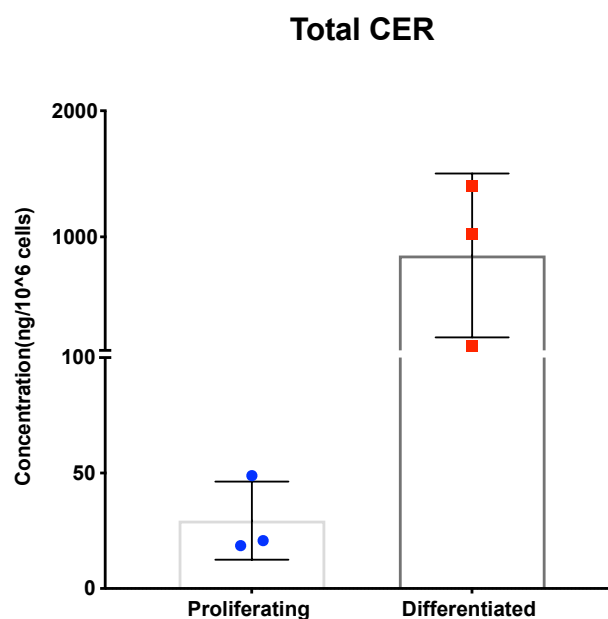
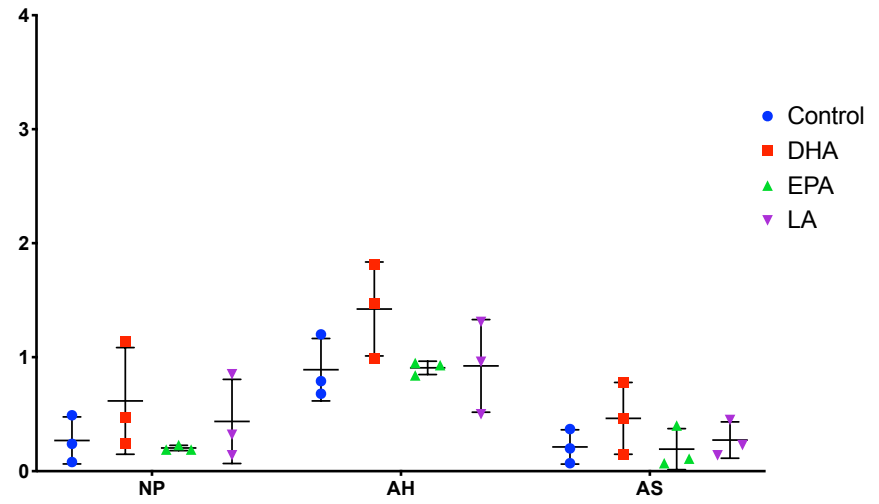
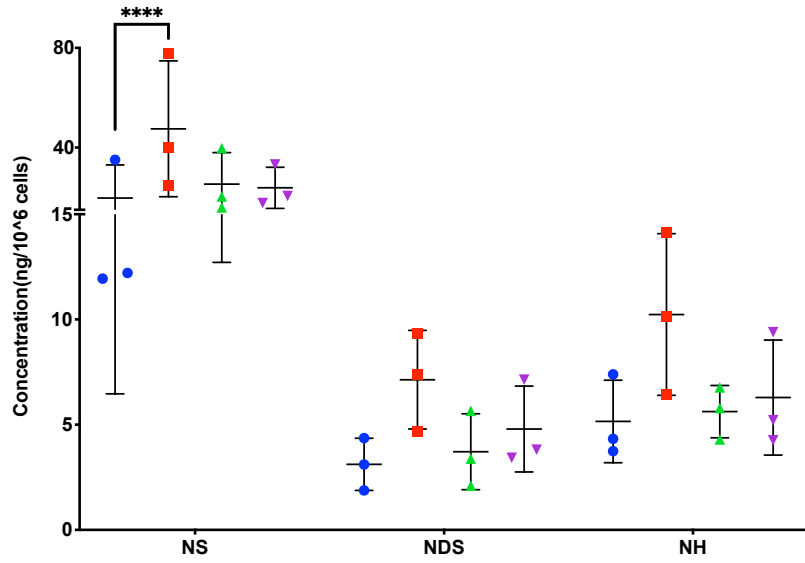


Figure 3.1 Total ceramide concentration in control proliferating and differentiated NHEK. Ceramides were measured using UPLC/ESI-MS/MS in proliferating and differentiated NHEK at 72 hours, then concentrations were totaled. Data are presented as absolute concentration in ng/10⁶ cells (mean \pm SD). Comparisons were performed between proliferating NHEK (Low Ca²⁺, n=3 donors) and differentiated NHEK (High Ca²⁺, n=3 donors). Data were analysed by Student's t-test. CER: ceramide; NHEK: normal human epidermal keratinocytes; Ca²⁺: Calcium.

Proliferating NHEK



Differentiated NHEK

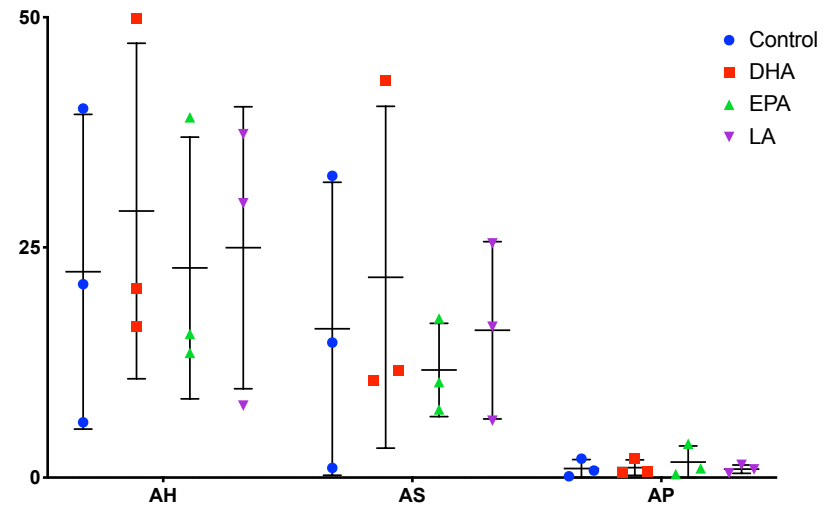
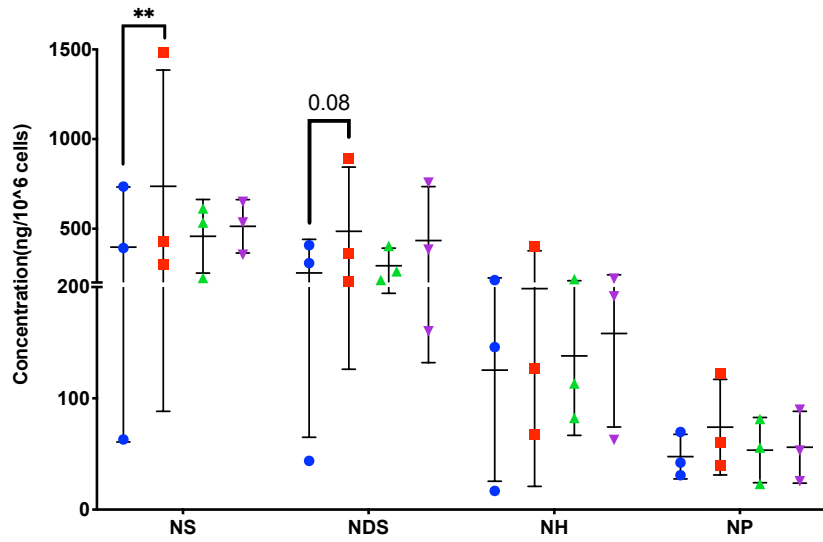


Figure 3.2 The effect of PUFA supplementation on total ceramide levels per class in proliferating and differentiated NHEK. Total ceramide classes were measured using UPLC/ESI-MS/MS in proliferating and differentiated NHEK at 72 hours post DHA, EPA and LA supplementation. Data are presented as absolute concentration in ng/10⁶ cells (mean ± SD). Comparisons were performed between the control and PUFA treated cells of the same Ca²⁺ condition; proliferating NHEK (n=3 donors), differentiated NHEK (n=3 donors). Data were analysed by One-Way ANOVA comparing differences over treatment compared with control; **p <0.01; ***p <0.0001. NHEK: normal human epidermal keratinocytes; PUFA: polyunsaturated fatty acid; DHA: docosahexaenoic acid; EPA: eicosapentaenoic acid; LA: linoleic acid; CER: ceramide; NS: non-hydroxy ceramide; NDS: non-hydroxy dihydroceramide; NH: non-hydroxy 6-hydroxyceramide; NP: non-hydroxy phytoceramide; AH: alpha-hydroxy 6-hydroxyceramide; AS: alpha-hydroxy ceramide; AP: alpha-hydroxy phytoceramide.

3.3.1.3 Treatment with DHA significantly enhanced the concentration of most ceramide classes in both cell types, whereas LA significantly increased CER[NDS] levels in differentiated NHEK

Individual species were analysed to observe possible trends in skin CER metabolism with PUFA treatment. In general, more CER species were detected in differentiated cells. DHA increased CER concentrations in both cell types, whereas LA mainly affected CER levels in differentiated cells. The following subsections explain changes in each CER class: CER[NS], CER[NDS], CER[NH], CER[NP], and alpha-hydroxy CERs.

Several CER[NS] species were elevated with DHA treatment in both cell types

A total of 20 CER[NS] species were detected in proliferating cells, whereas 31 CER[NS] species were found in differentiated NHEK (**Figure 3.3, 3.4**). In proliferating NHEK, DHA significantly increased the levels of N(24)S(16), N(24)S(18) and N(26)S(18) ($p= 0.0002$, $p= <0.0001$, $p <0.0001$, respectively). In differentiated NHEK, DHA significantly increased N(22)S(18), N(24)S(18) and N(26) S(18) ($p= 0.003$, $p <0.0001$, $p <0.001$, respectively). LA increased the levels of the most abundant CER[NS] species, N(24)S(18) and N(26)S(18), in differentiated NHEK ($p= 0.007$, $p= 0.07$, respectively).

CER[NS] species in proliferating NHEK

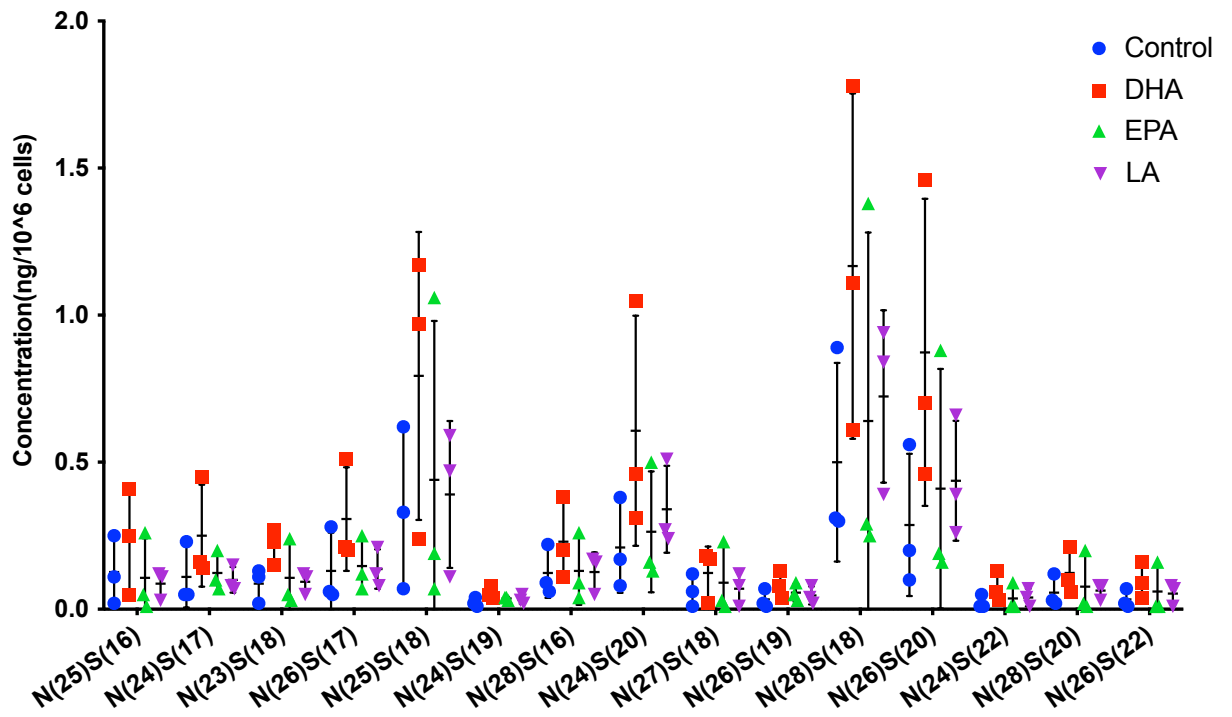
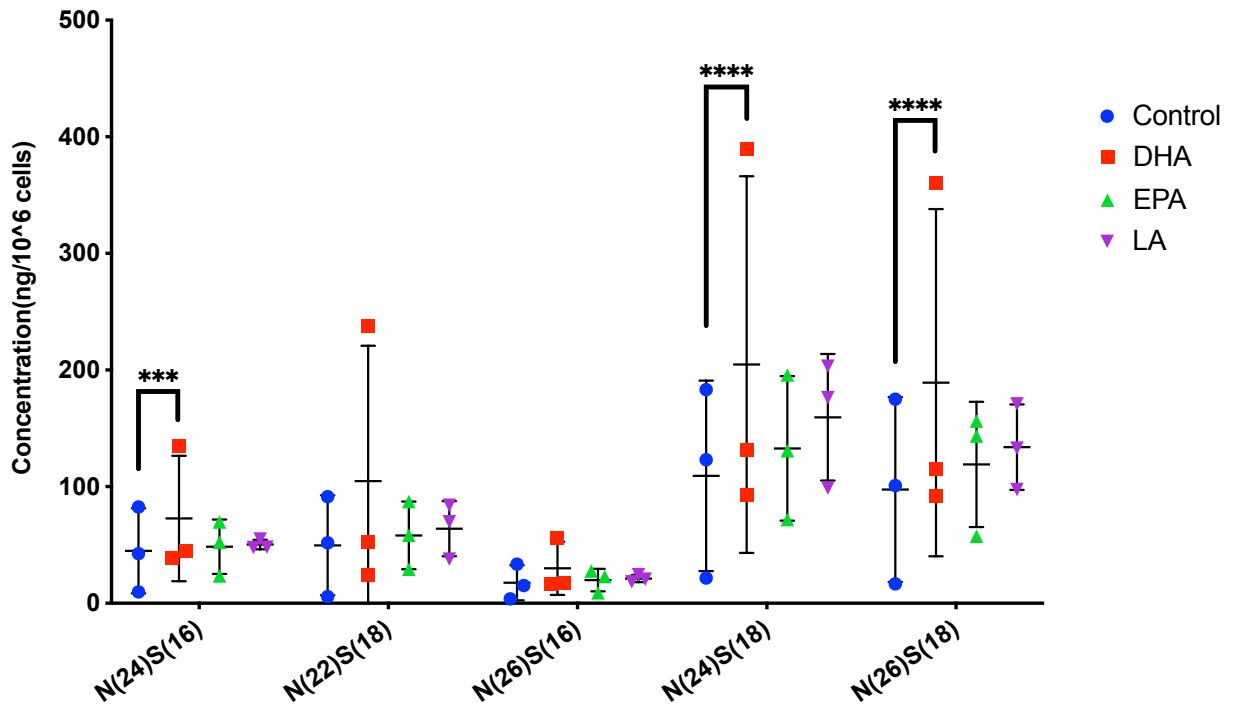
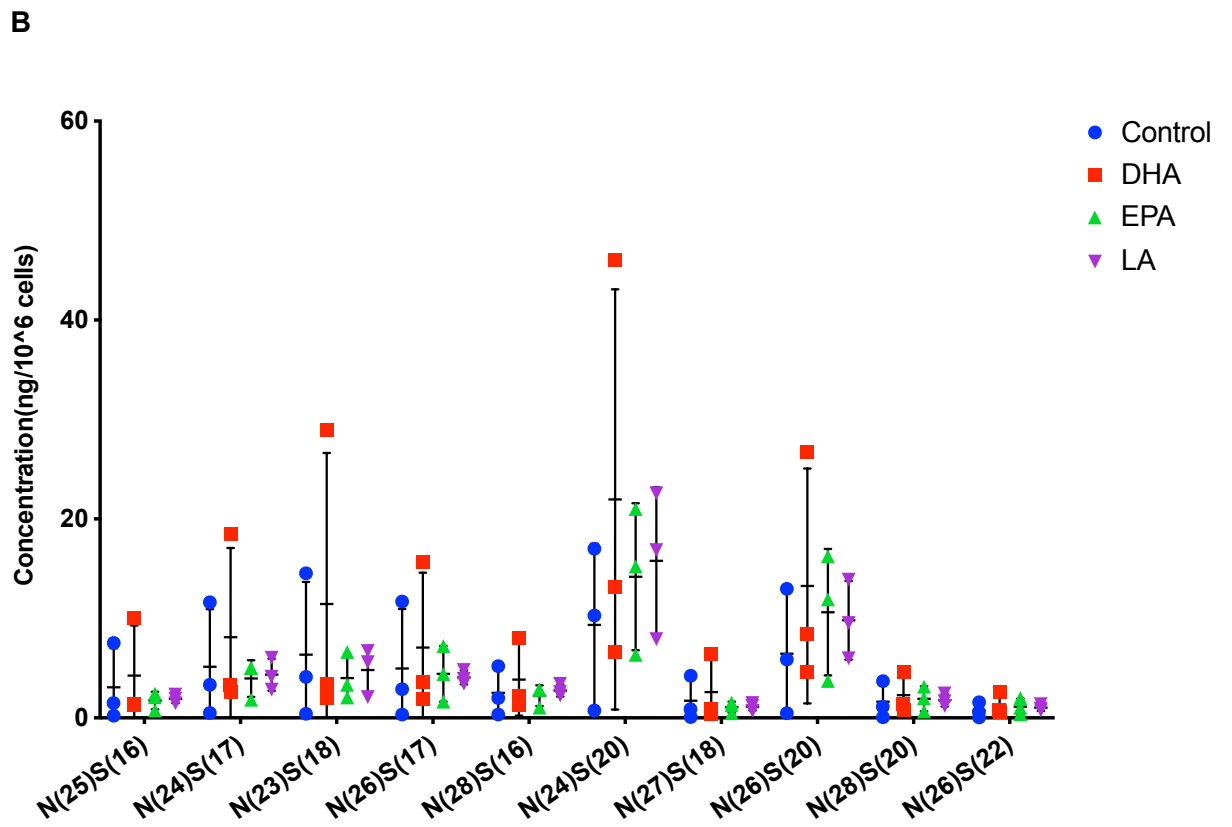
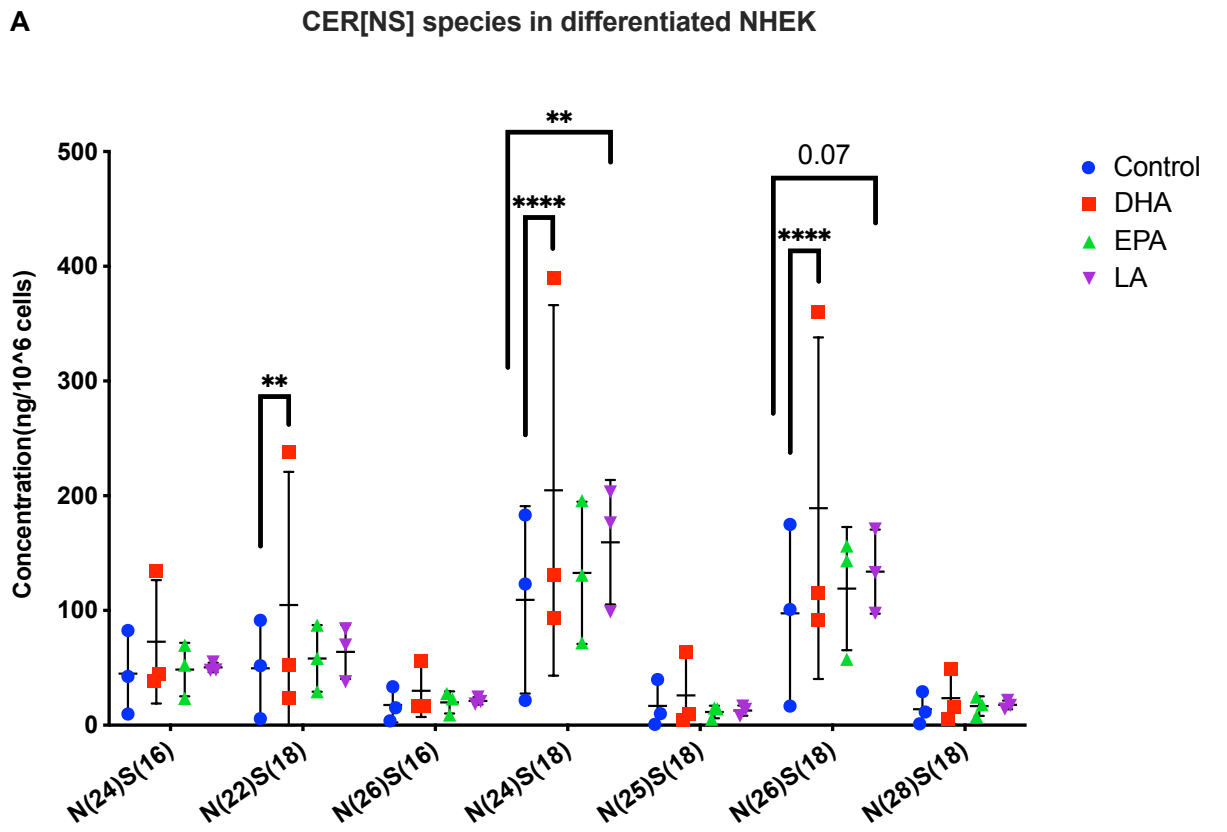


Figure 3.3 The effect of PUFA supplementation on CER[NS] species levels measured in proliferating NHEK. Ceramides were measured using UPLC/ESI-MS/MS in proliferating NHEK at 72 hours post DHA, EPA and LA supplementation. Data are presented as absolute concentration in ng/10⁶ cells (mean ± SD). Comparisons were performed between the control and PUFA treated cells; proliferating NHEK (n=3 donors). Data were analysed by One-Way ANOVA comparing differences over treatment compared with control; ***p <0.001; ****p <0.0001. NHEK: normal human epidermal keratinocytes; PUFA: polyunsaturated fatty acid; DHA: docosahexaenoic acid; EPA: eicosapentaenoic acid; LA: linoleic acid; CER: ceramide; NS: non-hydroxy ceramide.



C

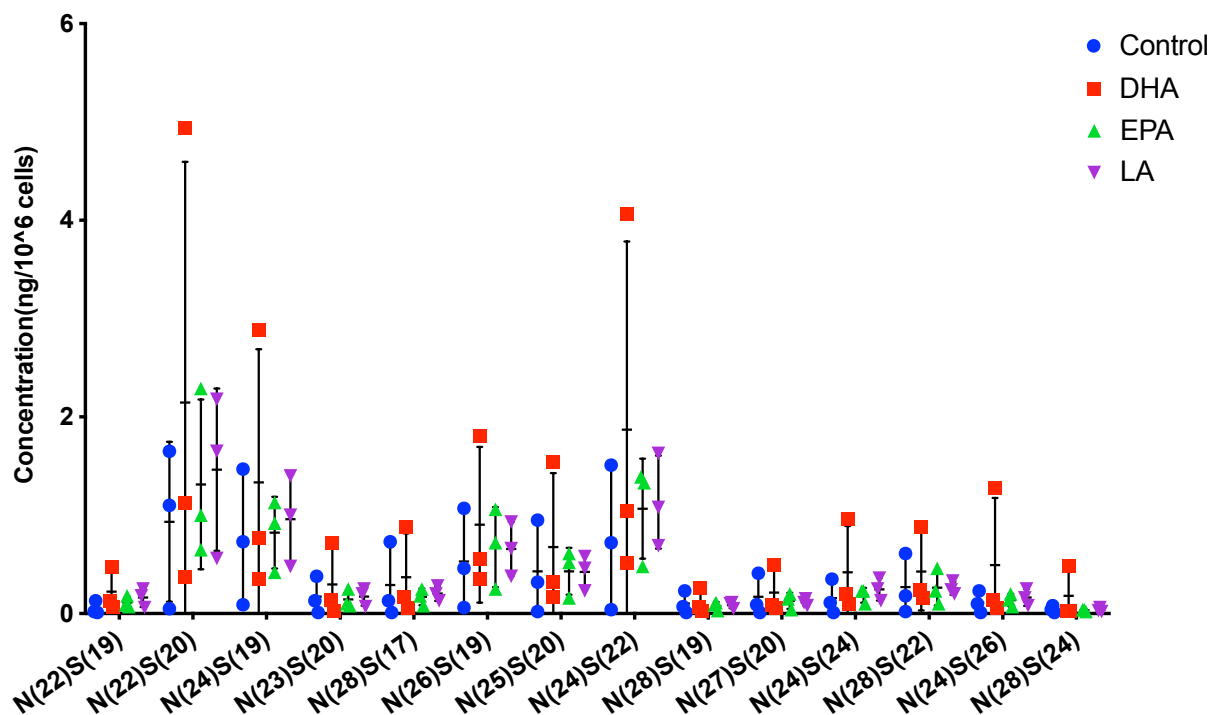


Figure 3.4 The effect of PUFA supplementation on CER[NS] species levels measured in differentiated NHEK. A-C) CER[NS] species were measured using UPLC/ESI-MS/MS in differentiated NHEK at 72 hours post DHA, EPA and LA supplementation. Data are presented as absolute concentration in ng/10⁶ cells (mean \pm SD). Comparisons were performed between the control and PUFA treated cells; differentiated NHEK (n=3 donors). Data were analysed by One-Way ANOVA comparing differences over treatment compared with control; **p <0.01; ****p <0.0001. NHEK: normal human epidermal keratinocytes; PUFA: polyunsaturated fatty acid; DHA: docosahexaenoic acid; EPA: eicosapentaenoic acid; LA: linoleic acid; CER: ceramide; NS: non-hydroxy ceramide.

Several CER[NDS] species were increased in both cell types with DHA treatment and in differentiated NHEK with LA treatment

Figure 3.5 shows the 12 CER[NDS] species measured in proliferating NHEK. DHA significantly increased N(24)DS(16), N(22)DS(18), N(24)DS(18), N(18)DS(24) and N(26)DS(18) levels in proliferating NHEK ($p=0.04$, $p=0.02$, $p<0.0001$, $p=0.002$, $p<0.0001$, respectively), whereas LA only increased the most abundant CER[NDS] species, N(24)DS(18) ($p=0.003$).

Figure 3.6 shows the 38 CER[NDS] species detected in differentiated NHEK. DHA significantly increased N(22)DS(18), N(18)DS(22), N(24)DS(18), N(18)DS(24) and N(26)DS(18) ($p=0.001$, $p=0.004$, $p<0.0001$, $p<0.0001$, $p=0.04$, respectively). LA increased the concentration of the following CER[NDS] species in differentiated NHEK: N(22)DS(18) ($p=0.01$), N(24)DS(18) ($p<0.0001$) and N(18)DS(24) ($p=0.002$).

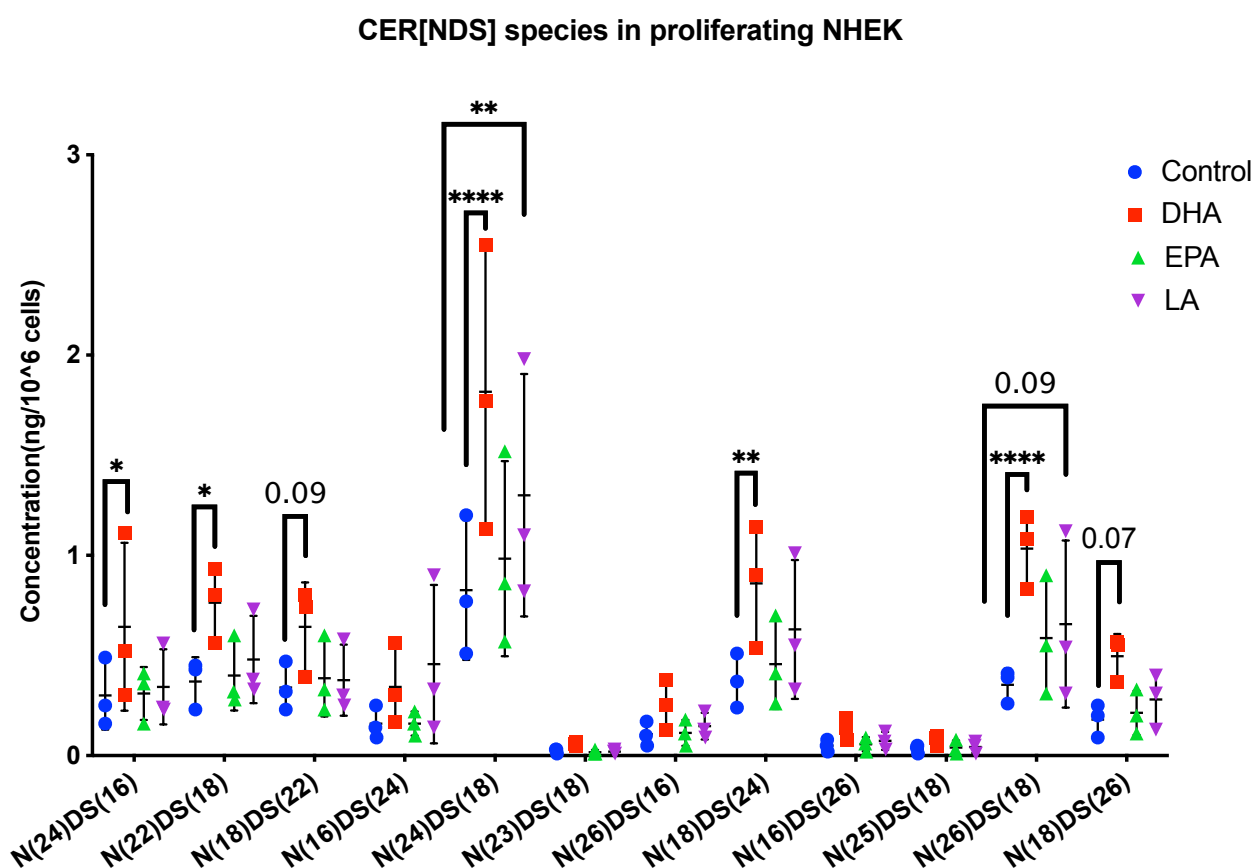
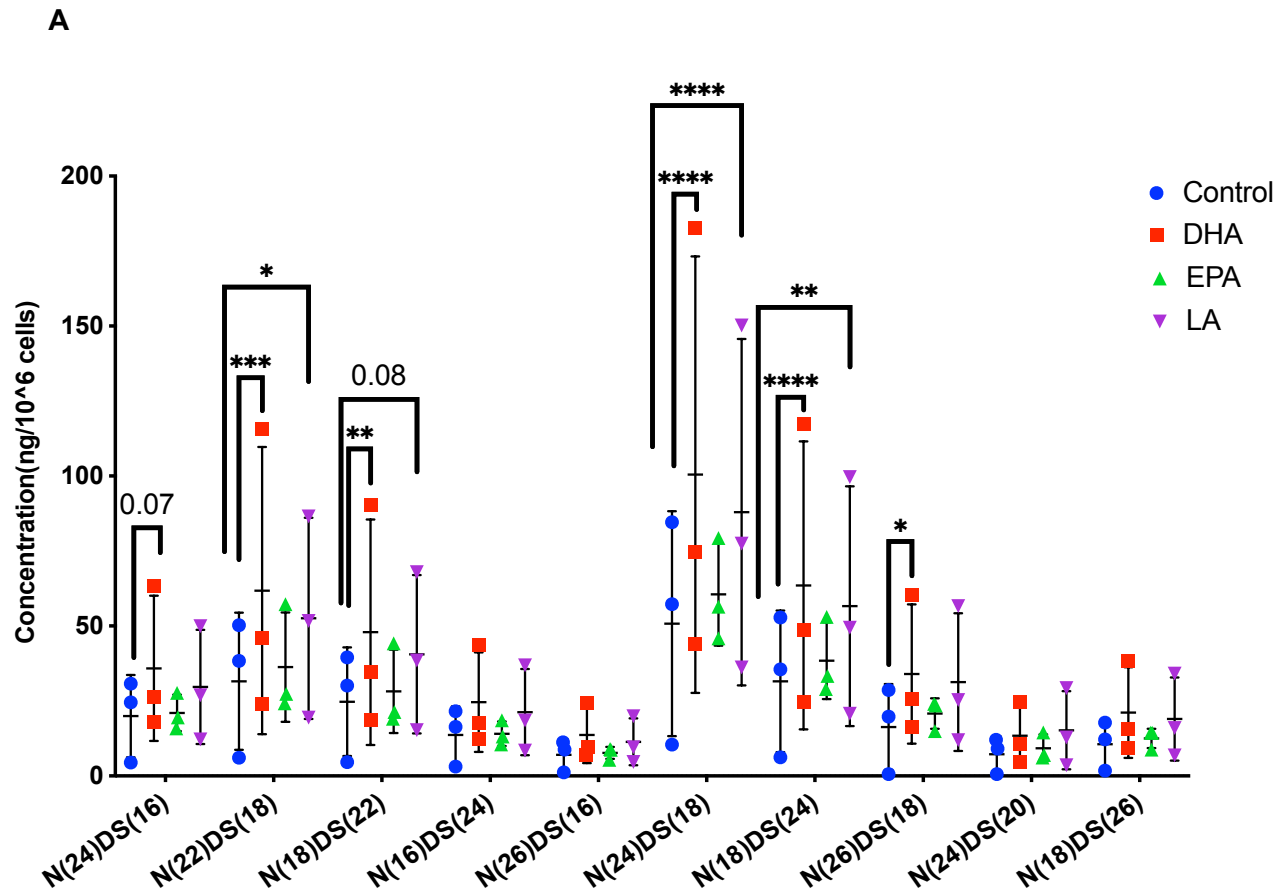


Figure 3.5 The effect of PUFA supplementation on CER[NDS] species levels measured in proliferating NHEK. Ceramides were measured using UPLC/ESI-MS/MS in proliferating NHEK at 72 hours post DHA, EPA and LA supplementation. Data are

presented as absolute concentration in $\text{ng}/10^6$ cells (mean \pm SD). Comparisons were performed between the control and PUFA treated cells; proliferating NHEK (n=3 donors). Data were analysed by One-Way ANOVA comparing differences over treatment compared with control; *p <0.05; **p <0.01; ****p <0.0001. NHEK: normal human epidermal keratinocytes; PUFA: polyunsaturated fatty acid; DHA: docosahexaenoic acid; EPA: eicosapentaenoic acid; LA: linoleic acid; CER: ceramide; NDS: non-hydroxy dihydroceramide.

CER[NDS] species in differentiated NHEK



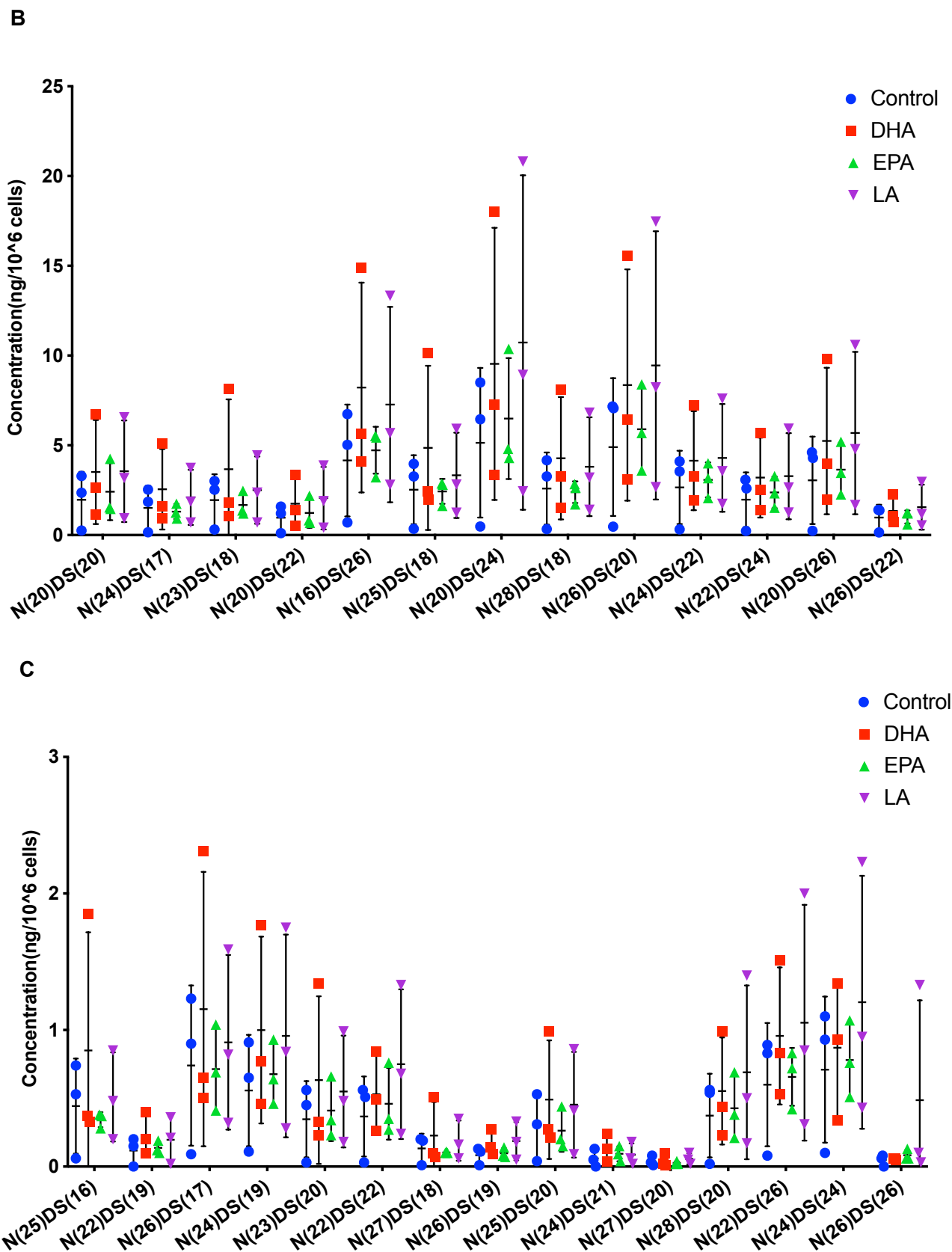


Figure 3.6 The effect of PUFA supplementation on CER[NDS] species levels measured in differentiated NHEK. Ceramides were measured using UPLC/ESI-MS/MS in differentiated NHEK at 72 hours post DHA, EPA and LA supplementation. Data are

presented as absolute concentration in ng/10⁶ cells (mean ± SD). Comparisons were performed between the control and PUFA treated cells; differentiated NHEK (n=3 donors). Data were analysed by One-Way ANOVA comparing differences over treatment compared with control; *p <0.05; **p <0.01; ***p <0.001; ****p <0.0001. NHEK: normal human epidermal keratinocytes; PUFA: polyunsaturated fatty acid; DHA: docosahexaenoic acid; EPA: eicosapentaenoic acid; LA: linoleic acid; CER: ceramide; NDS: non-hydroxy dihydroceramide.

DHA significantly increased CER[NH] species in both cell types

There were five CER[NH] species detected in proliferating NHEK and nine species in differentiated NHEK (**Figure 3.7, 3.8**). In proliferating NHEK, DHA increased the concentration of the two most abundant CER[NH] species, N(26)H(16) and N(28)H(16) ($p < 0.0001$, $p < 0.0001$). In differentiated NHEK, DHA increased the levels of N(26)H(16) ($p = 0.002$).

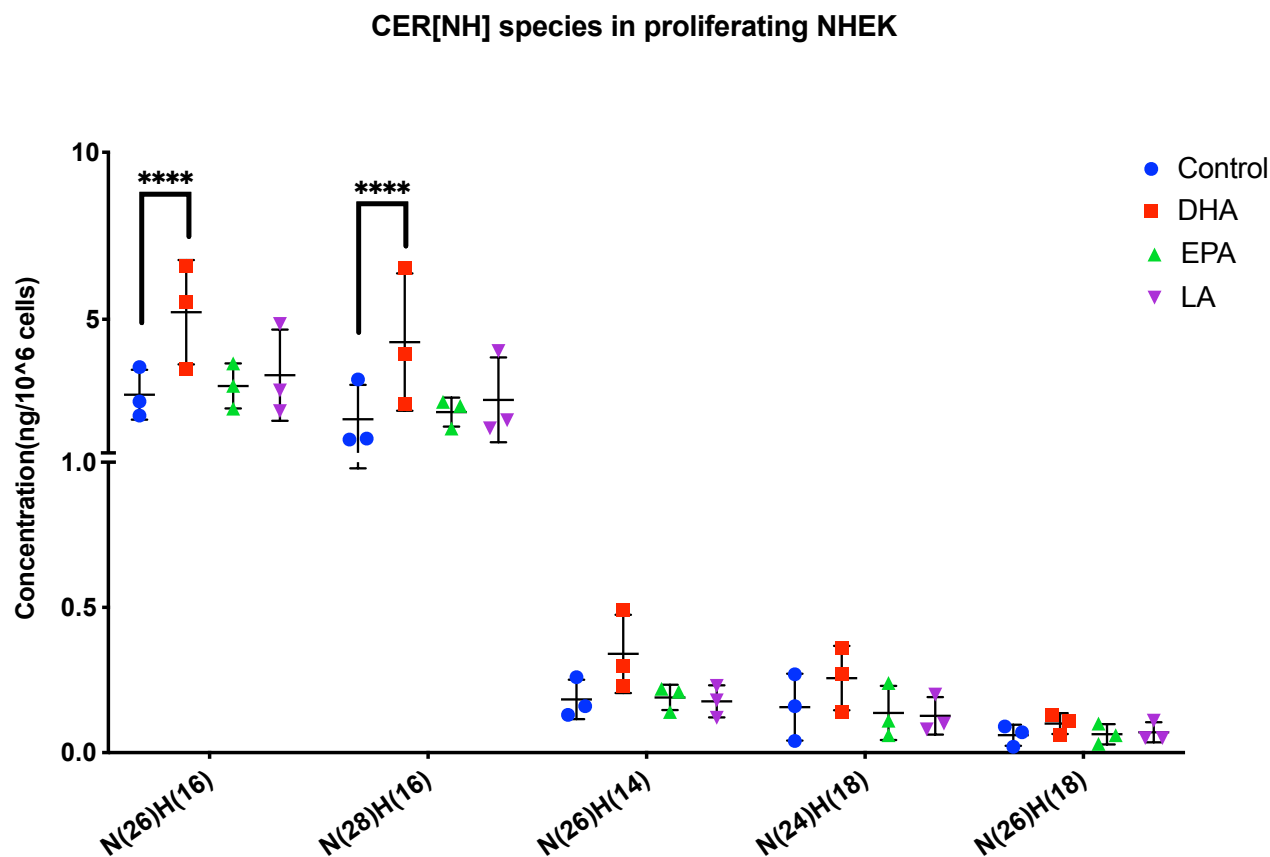


Figure 3.7 The effect of PUFA supplementation on CER[NH] species levels measured in proliferating NHEK. Ceramides were measured using UPLC/ESI-MS/MS in proliferating NHEK at 72 hours post DHA, EPA and LA supplementation. Data are presented as absolute concentration in ng/10⁶ cells (mean \pm SD). Comparisons were performed between the control and PUFA treated cells; proliferating NHEK (n=3 donors). Data were analysed by One-Way ANOVA comparing differences over treatment compared with control; **** $p < 0.0001$. NHEK: normal human epidermal keratinocytes; PUFA: polyunsaturated fatty acid; DHA: docosahexaenoic acid; EPA: eicosapentaenoic acid; LA: linoleic acid; CER: ceramide; NH: non-hydroxy 6-hydroxyceramide.

CER[NH] species in differentiated NHEK

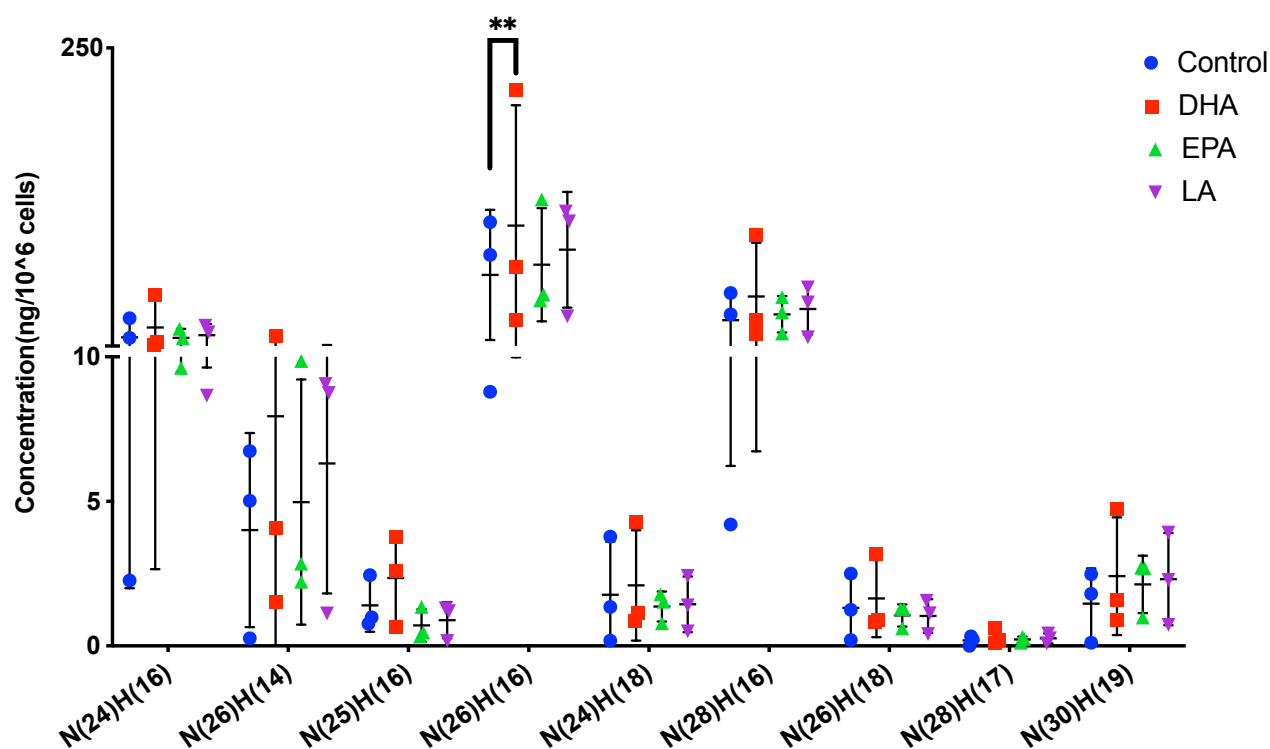


Figure 3.8 The effect of PUFA supplementation on CER[NH] species levels measured in differentiated NHEK. Ceramides were measured using UPLC/ESI-MS/MS in differentiated NHEK at 72 hours post DHA, EPA and LA supplementation. Data are presented as absolute concentration in ng/10⁶ cells (mean \pm SD). Comparisons were performed between the control and PUFA treated cells; differentiated NHEK (n=3 donors). Data were analysed by One-Way ANOVA comparing differences over treatment compared with control; **p < 0.01. NHEK: normal human epidermal keratinocytes; PUFA: polyunsaturated fatty acid; DHA: docosahexaenoic acid; EPA: eicosapentaenoic acid; LA: linoleic acid; CER: ceramide; NH: non-hydroxy 6-hydroxyceramide.

DHA increased CER[NP] species in both cell types

Phytoceramides were mainly found in differentiated cells. A total of 16 CER[NP] species were measured in differentiated NHEK, whereas only three species were detected in proliferating NHEK (**Figure 3.9, 3.10**). All PUFA treatments significantly increased N(24)P(18) levels in differentiated cells. A close to significant increase in N(24)P(18) was also found in proliferating NHEK with DHA treatment (p= 0.06).

CER[NP] species in proliferating NHEK

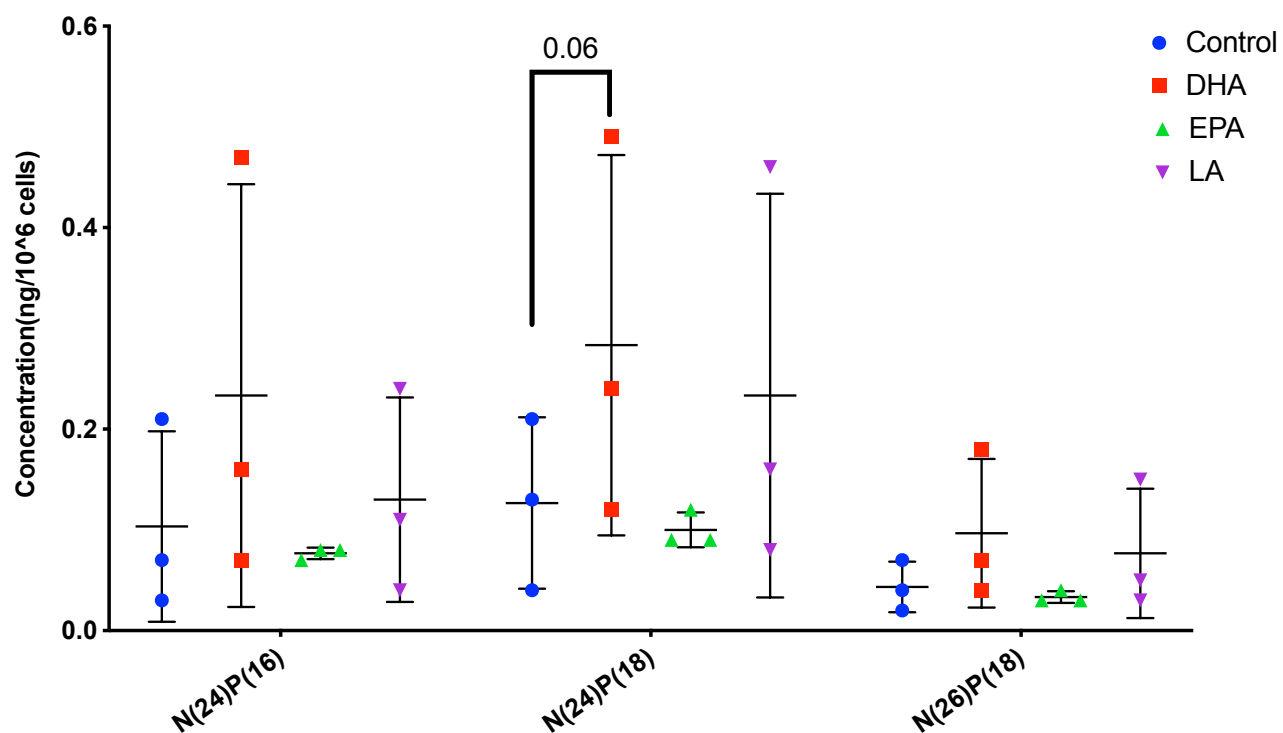


Figure 3.9 The effect of PUFA supplementation on CER[NP] species levels measured in proliferating NHEK. Ceramides were measured using UPLC/ESI-MS/MS in proliferating NHEK at 72 hours post DHA, EPA and LA supplementation. Data are presented as absolute concentration in ng/10⁶ cells (mean ± SD). Comparisons were performed between the control and PUFA treated cells; proliferating NHEK (n=3 donors). Data were analysed by One-Way ANOVA comparing differences over treatment compared with control. NHEK: normal human epidermal keratinocytes; PUFA: polyunsaturated fatty acid; DHA: docosahexaenoic acid; EPA: eicosapentaenoic acid; LA: linoleic acid; CER: ceramide; NP: non-hydroxy phytoceramide.

CER[NP] species in differentiated NHEK

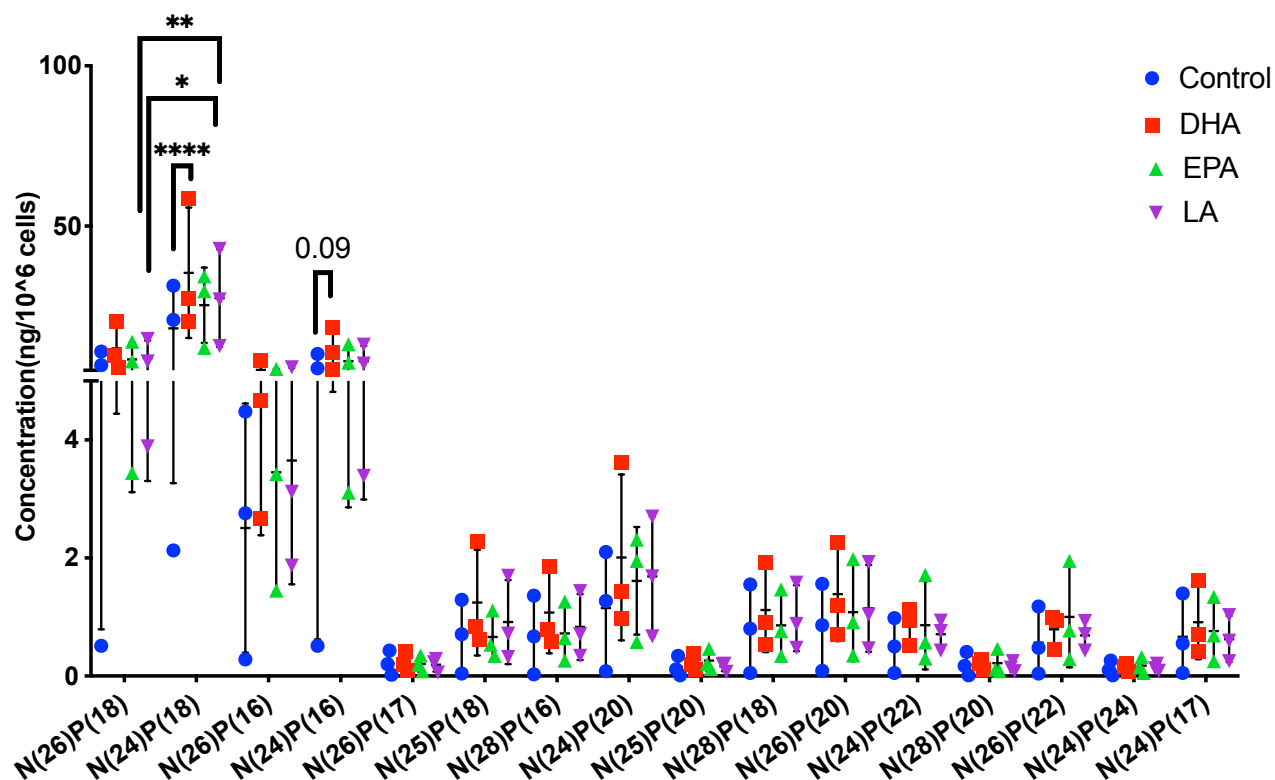


Figure 3.10 The effect of PUFA supplementation on CER[NP] species levels measured in differentiated NHEK. Ceramides were measured using UPLC/ESI-MS/MS in differentiated NHEK at 72 hours post DHA, EPA and LA supplementation. Data are presented as absolute concentration in $\text{ng}/10^6$ cells (mean \pm SD). Comparisons were performed between the control and PUFA treated cells; differentiated NHEK (n=3 donors). Data were analysed by One-Way ANOVA comparing differences over treatment compared with control; *p < 0.05; **p < 0.01; ****p < 0.0001. NHEK: normal human epidermal keratinocytes; PUFA: polyunsaturated fatty acid; DHA: docosahexaenoic acid; EPA: eicosapentaenoic acid; LA: linoleic acid; CER: ceramide; NP: non-hydroxy phytoceramide.

DHA increased alpha-hydroxy CER concentrations in both cell types

There were more alpha-hydroxy CER species, CER[AS] and CER[AH] in differentiated NHEK than in proliferating cells, and CER[AP] was only detected in differentiated cells (**Figures 3.11-3.15**). In proliferating NHEK, a close to significant increase was found in A(24)S(18) with DHA (p= 0.05), whereas in differentiated NHEK, DHA significantly increased A(24)S(18) (p= 0.001). DHA significantly increased A(25)H(16) in proliferating NHEK (p= 0.003), and A(26)H(16) and A(30)H(18) in differentiated NHEK (p= 0.049, p= 0.04, respectively).

CER[AH] species in proliferating NHEK

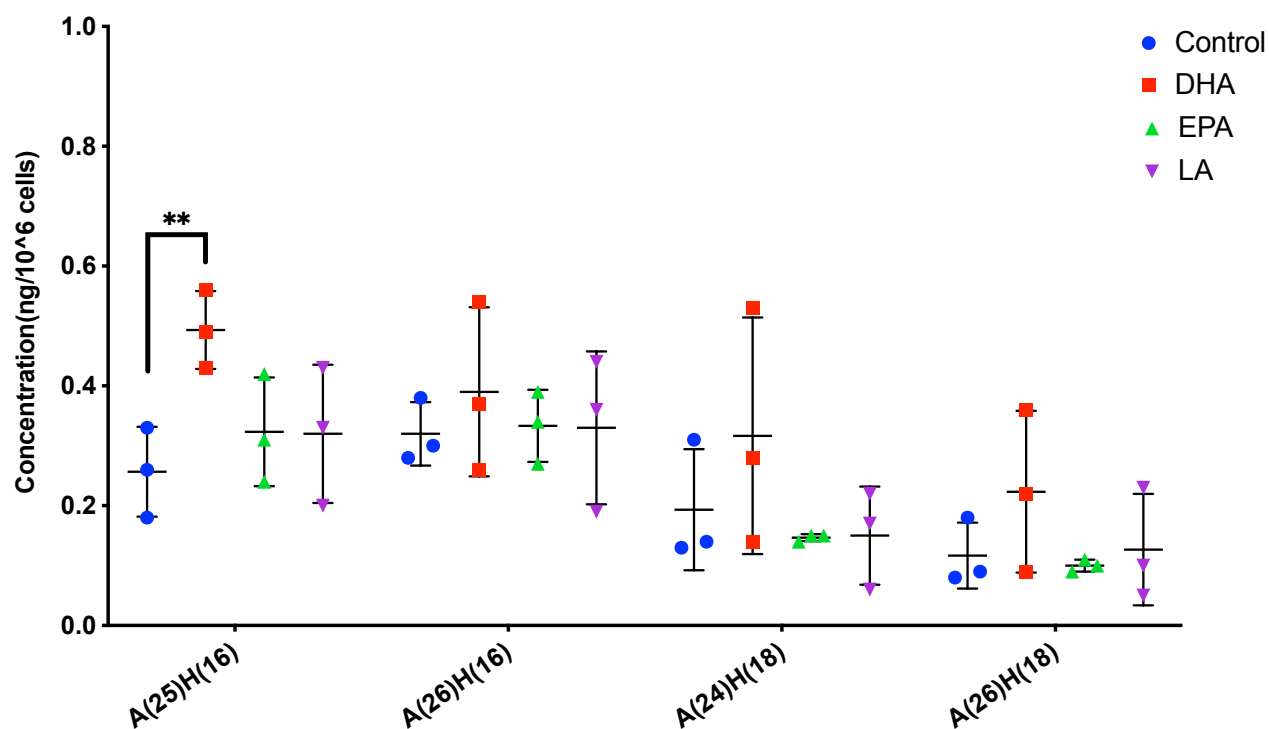


Figure 3.11 The effect of PUFA supplementation on CER[AH] species levels measured in proliferating NHEK. Ceramides were measured using UPLC/ESI-MS/MS in proliferating NHEK at 72 hours post DHA, EPA and LA supplementation. Data are presented as absolute concentration in ng/10⁶ cells (mean \pm SD). Comparisons were performed between the control and PUFA treated cells; proliferating NHEK (n=3 donors). Data were analysed by One-Way ANOVA comparing differences over treatment compared with control; **p < 0.01. NHEK: normal human epidermal keratinocytes; PUFA: polyunsaturated fatty acid; DHA: docosahexaenoic acid; EPA: eicosapentaenoic acid; LA: linoleic acid; CER: ceramide; AH: alpha-hydroxy 6-hydroxyceramide.

CER[AH] species in differentiated NHEK

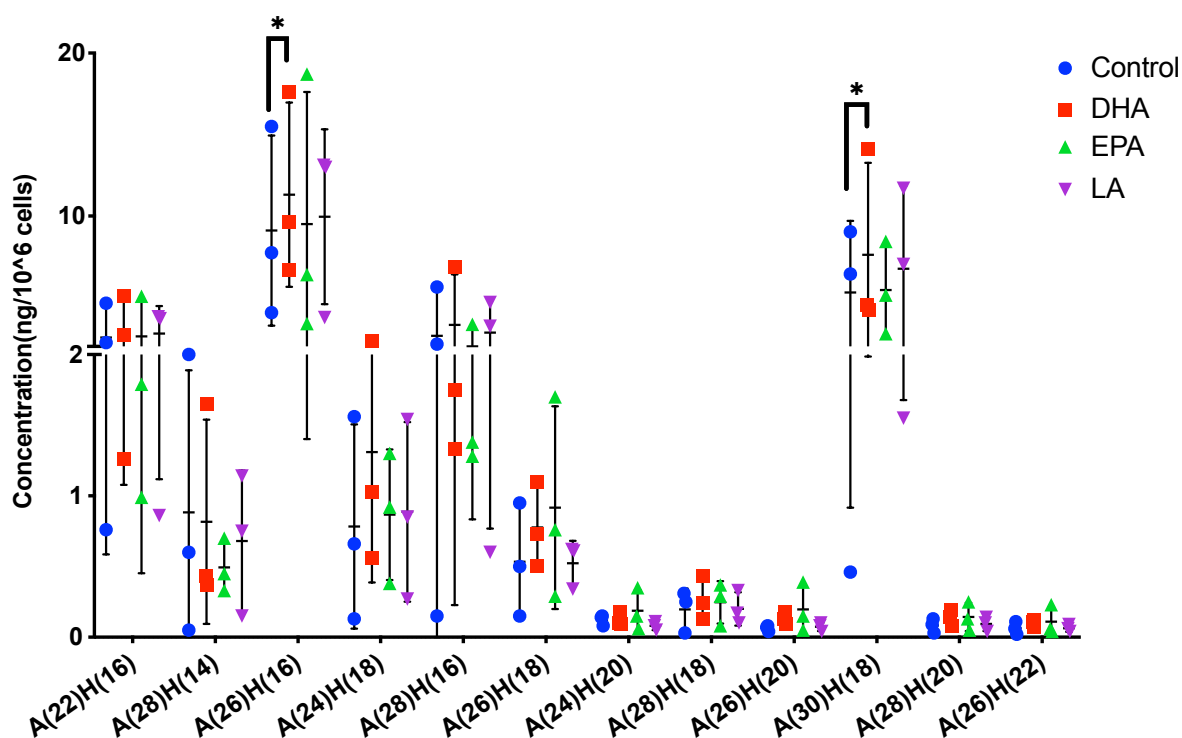


Figure 3.12 The effect of PUFA supplementation on CER[AH] species levels measured in differentiating NHEK. Ceramides were measured using UPLC/ESI-MS/MS in differentiated NHEK at 72 hours post DHA, EPA and LA supplementation. Data are presented as absolute concentration in $\text{ng}/10^6$ cells (mean \pm SD). Comparisons were performed between the control and PUFA treated cells; differentiated NHEK ($n=3$ donors). Data were analysed by One-Way ANOVA comparing differences over treatment compared with control; * $p < 0.05$. NHEK: normal human epidermal keratinocytes; PUFA: polyunsaturated fatty acid; DHA: docosahexaenoic acid; EPA: eicosapentaenoic acid; LA: linoleic acid; CER: ceramide; AH: alpha-hydroxy 6-hydroxyceramide.

CER[AS] species in proliferating NHEK

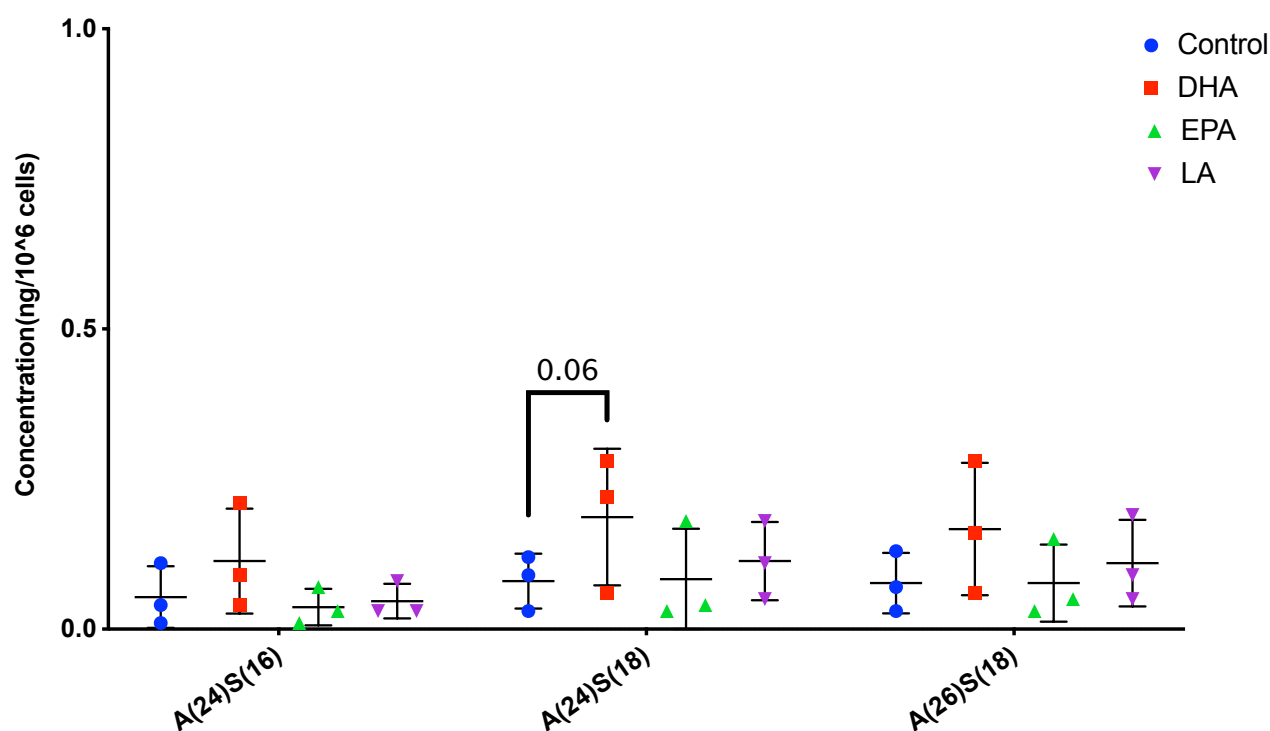


Figure 3.13 The effect of PUFA supplementation on CER[AS] species levels measured in proliferating NHEK. Ceramides were measured using UPLC/ESI-MS/MS in proliferating NHEK at 72 hours post DHA, EPA and LA supplementation. Data are presented as absolute concentration in ng/10⁶ cells (mean \pm SD). Comparisons were performed between the control and PUFA treated cells; proliferating NHEK (n=3 donors). Data were analysed by One-Way ANOVA comparing differences over treatment compared with control. NHEK: normal human epidermal keratinocytes; PUFA: polyunsaturated fatty acid; DHA: docosahexaenoic acid; EPA: eicosapentaenoic acid; LA: linoleic acid; CER: ceramide; AS: alpha-hydroxy ceramide.

CER[AS] species in differentiated NHEK

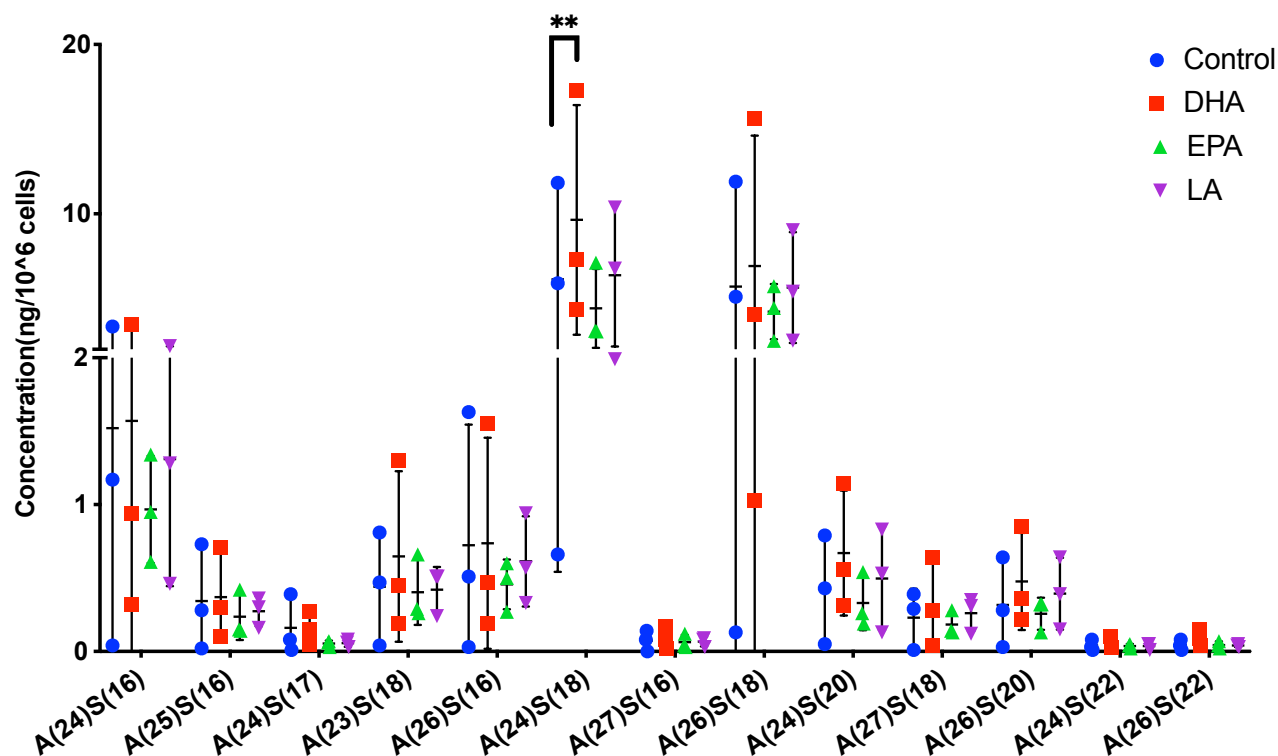


Figure 3.14 The effect of PUFA supplementation on CER[AS] species levels measured in differentiated NHEK. Ceramides were measured using UPLC/ESI-MS/MS in differentiated NHEK at 72 hours post DHA, EPA and LA supplementation. Data are presented as absolute concentration in ng/10⁶ cells (mean \pm SD). Comparisons were performed between the control and PUFA treated cells; differentiated NHEK (n=3 donors). Data were analysed by One-Way ANOVA comparing differences over treatment compared with control; **p < 0.01. NHEK: normal human epidermal keratinocytes; PUFA: polyunsaturated fatty acid; DHA: docosahexaenoic acid; EPA: eicosapentaenoic acid; LA: linoleic acid; CER: ceramide; AS: alpha-hydroxy ceramide.

CER[AP] species in differentiated NHEK

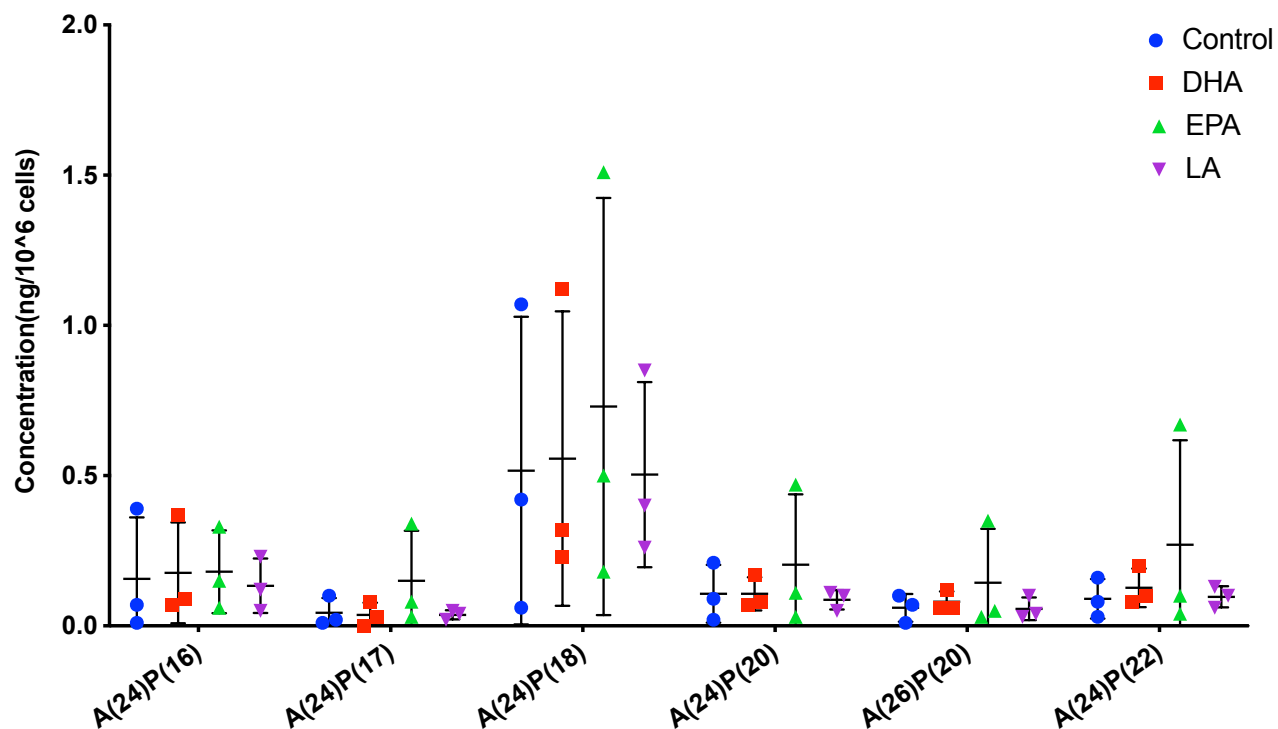


Figure 3.15 The effect of PUFA supplementation on CER[AP] species levels measured in differentiated NHEK. Ceramides were measured using UPLC/ESI-MS/MS in differentiated NHEK at 72 hours post DHA, EPA and LA supplementation. Data are presented as absolute concentration in ng/10⁶ cells (mean \pm SD). Comparisons were performed between the control and PUFA treated cells; differentiated NHEK (n=3 donors). Data were analysed by One-Way ANOVA comparing differences over treatment compared with control. NHEK: normal human epidermal keratinocytes; PUFA: polyunsaturated fatty acid; DHA: docosahexaenoic acid; EPA: eicosapentaenoic acid; LA: linoleic acid; CER: ceramide; AP: alpha-hydroxy phytoceramide.

3.3.1.4 DHA significantly altered total carbon number in both cell types

Total carbon number (carbon number of the fatty acyl-chain + carbon number of the sphingoid base-chain) shows the ceramide chain length. Alterations in total carbon number have been reported in several skin disorders, where when long-chain CERs were reduced, abnormalities in barrier structure and function were reported. Total CER carbon chains were longer in the differentiated cells where they ranged from C38-C52, whereas the C48 chain was the longest in proliferating cells. Analysing ceramide total chain lengths showed a significant increase in the C41 (p= 0.049) and C38 (p= 0.002) CERs with DHA in proliferating and differentiated NHEK, respectively (**Figure 3.16**).

Total carbon number

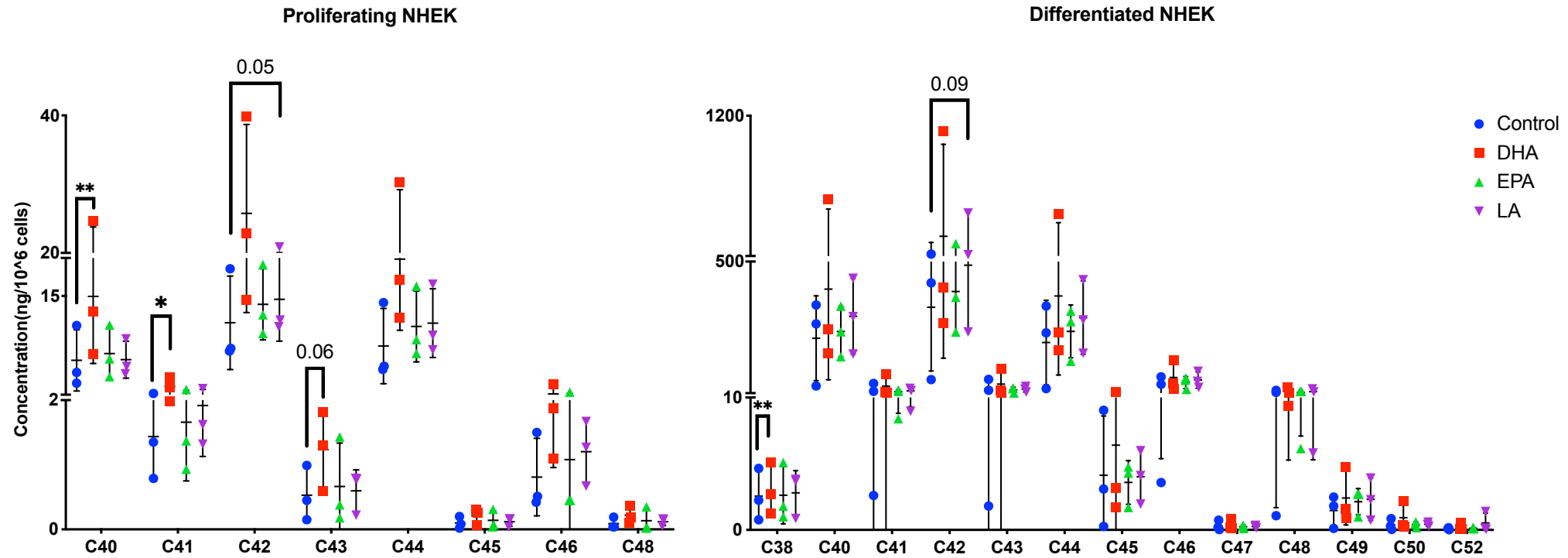


Figure 3.16 The effect of PUFA supplementation on CER total carbon chain number in proliferating and differentiated NHEK. Ceramides were measured using UPLC/ESI-MS/MS in proliferating and differentiated NHEK at 72 hours post DHA, EPA and LA supplementation. Total carbon chain was calculated (sphingoid base-chain carbon number + fatty-acyl chain carbon number) then totaled. Data are presented as absolute concentration in ng/10⁶ cells

(mean \pm SD). Comparisons were performed between the control and PUFA treated cells of the same Ca^{2+} condition; proliferating NHEK (n=3 donors), differentiated NHEK (n=3 donors). Data were analysed by One-Way ANOVA comparing differences over treatment compared with control, with corrections for multiple analyses using the Dunnett method; *p <0.05; **p <0.01. NHEK: normal human epidermal keratinocytes; PUFA: polyunsaturated fatty acid; DHA: docosahexaenoic acid; EPA: eicosapentaenoic acid; LA: linoleic acid; CER: ceramide; C: carbon number.

3.3.1.5 DHA and LA significantly affected total sphingoid base-chain carbon number in proliferating NHEK

The increase in total carbon number could be due to alterations in the sphingoid base-chain, acyl-chain or a combination of both. Therefore, examining where this increase was from could indicate where in the CER biosynthesis pathway PUFA is having an effect. Analysing the data according to the total carbon number of the sphingoid base-chain could reveal effects on the *de novo* biosynthesis pathway regulated by SPT. DHA increased base-chains with a C19 and C26 carbon chain ($p= 0.04$, $p= 0.01$, respectively), whereas LA had an effect on C19 levels ($p= 0.04$) in proliferating NHEK (**Figure 3.17**).

Total base-chain carbon number

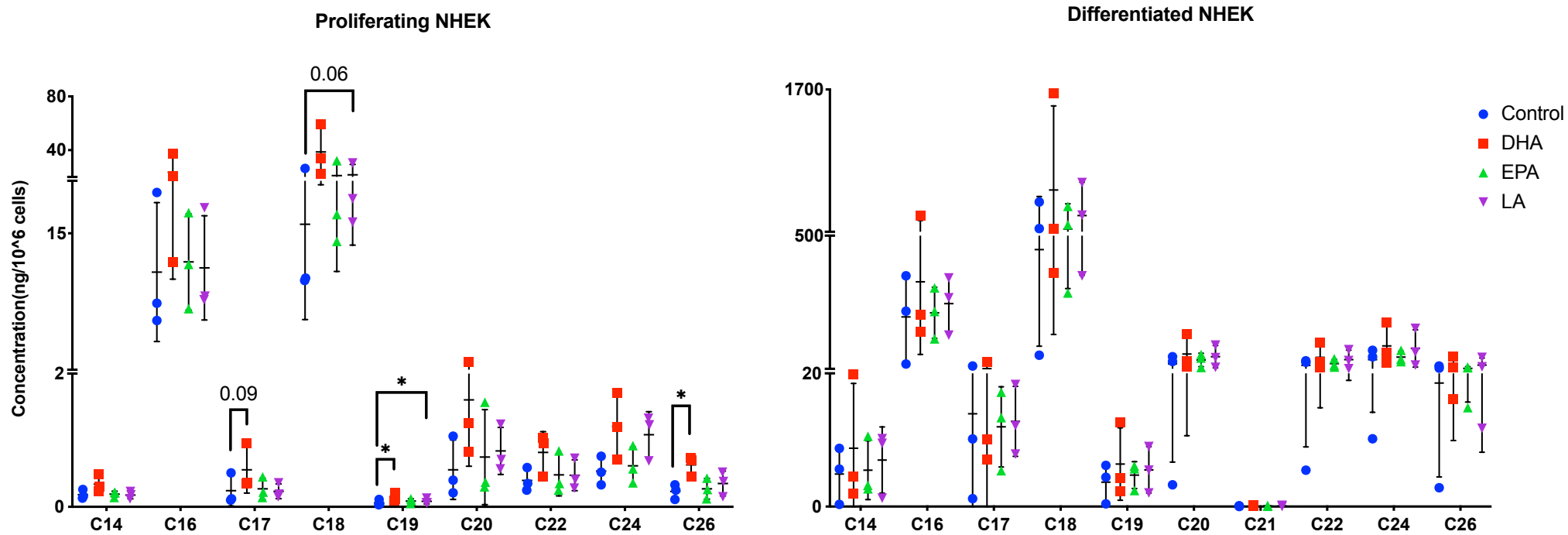


Figure 3.17 The effect of PUFA supplementation on CER total sphingoid base-chain length in proliferating and differentiated NHEK. Ceramides were measured using UPLC/ESI-MS/MS in proliferating and differentiated NHEK at 72 hours post DHA, EPA and LA supplementation. Sphingoid-base carbon chains were totaled (example: C14 = total of all ceramides with C14 sphingoid base-chain). Data are presented as absolute concentration in ng/10⁶ cells (mean \pm SD). Comparisons were performed between the control and PUFA treated cells of the same Ca²⁺ condition; proliferating NHEK (n=3 donors), differentiated NHEK (n=3 donors). Data were analysed by One-Way ANOVA comparing differences over treatment compared with control, with corrections for multiple

analyses using the Dunnett method; * $p < 0.05$. NHEK: normal human epidermal keratinocytes; PUFA: polyunsaturated fatty acid; DHA: docosahexaenoic acid; EPA: eicosapentaenoic acid; LA: linoleic acid; C: carbon number.

3.3.1.6 DHA and LA altered total fatty acyl-chain carbon number in proliferating NHEK

Data were categorised according to fatty-acyl chain length to further examine the increase found in CERs with PUFA treatment. This informs on the contribution of changes to the *de novo* fatty-acyl specific CerS enzymes. Changes were mainly observed in proliferating NHEK where DHA increased the concentration of CERs with a C18, C23 and C25 FA-chains ($p= 0.049$, $p= 0.02$, $p= 0.06$, respectively). LA only affected the longer chain C28 CERs ($p= 0.03$) in proliferating NHEK (**Figure 3.18**).

Total FA-chain carbon number

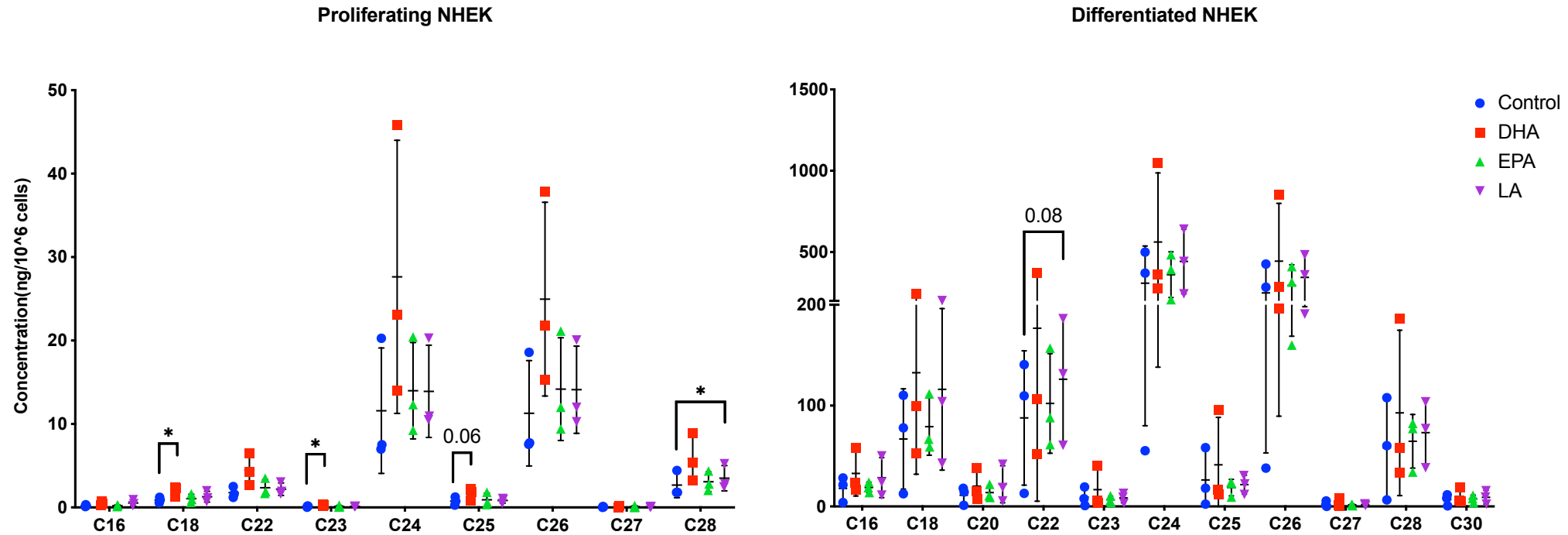


Figure 3.18 The effect of PUFA supplementation on CER total fatty acyl-chain length in proliferating and differentiated NHEK. Ceramides were measured using UPLC/ESI-MS/MS in proliferating and differentiated NHEK at 72 hours post DHA, EPA and LA supplementation. Fatty-acyl carbon chains were totaled (example: C16 = total of all ceramides with C16 fatty-acyl chain). Data are presented as absolute concentration in ng/10⁶ cells (mean ± SD). Comparisons were performed between the control and PUFA treated cells of the same Ca²⁺ condition; proliferating NHEK (n=3 donors), differentiated NHEK

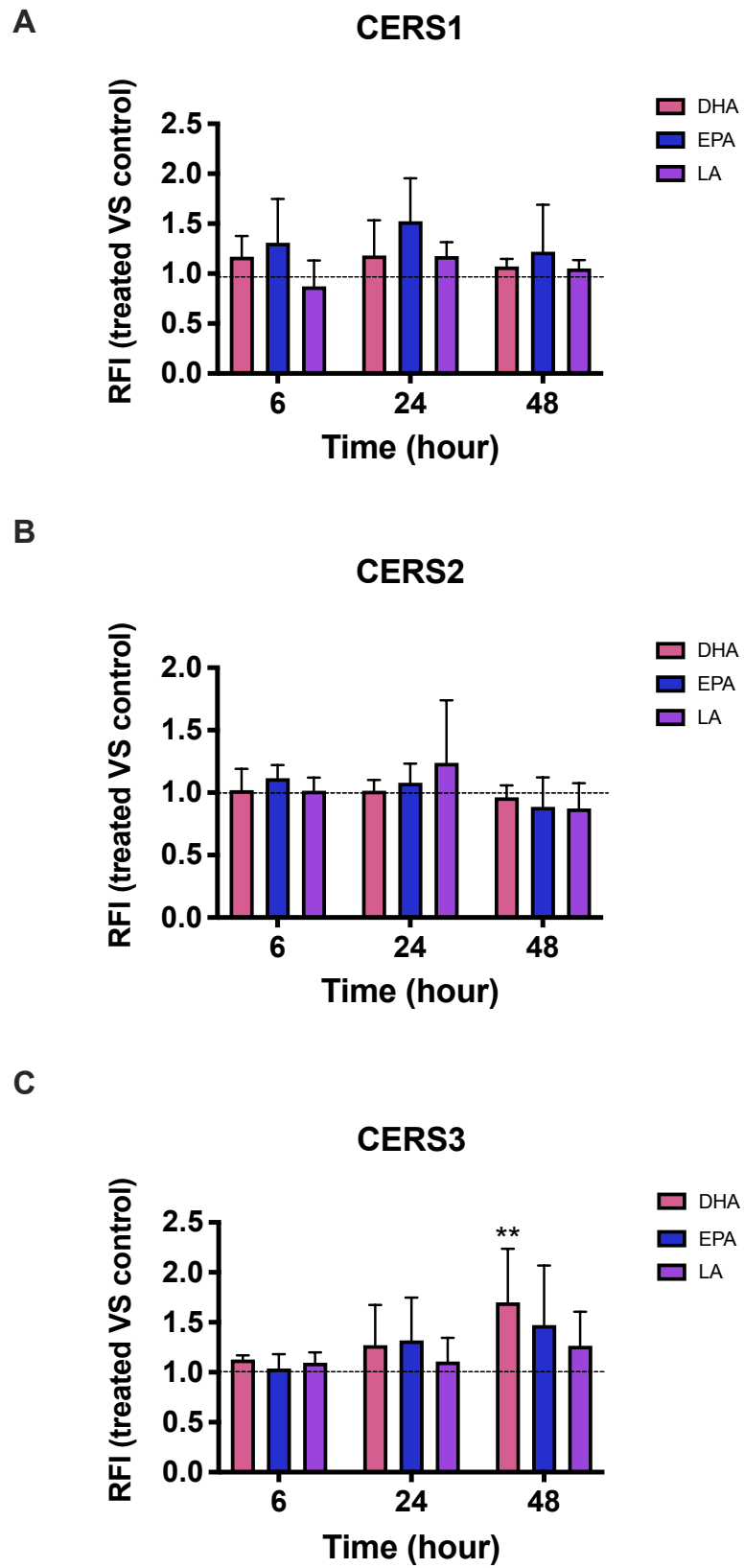
(n=3 donors). Data were analysed by One-Way ANOVA comparing differences over treatment compared with control, with corrections for multiple analyses using the Dunnett method; *p <0.05. NHEK: normal human epidermal keratinocytes; PUFA: polyunsaturated fatty acid; DHA: docosahexaenoic acid; EPA: eicosapentaenoic acid; LA: linoleic acid; C: carbon number; FA: fatty-acyl.

3.3.2 *n*-3 PUFA significantly upregulated *CERS3* and *DES2* expression in proliferating NHEK

CER biosynthesis enzyme mRNA levels were quantitated by RT-qPCR analysis to investigate how PUFA regulates ceramide metabolism in the epidermis via changes in gene expression. The effect of DHA, EPA and LA on the expression of the fatty acyl-specific *CERS1-6* and *DES1,2* that generate the sphingosine and phytosphingosine ceramides, respectively, was analysed at 6, 24 and 48 hours post-PUFA supplementation. Data are presented as relative fold increase (RFI) which compares CER biosynthesis enzyme gene expression in treated cells to that in DMSO controls of the same time-point and Ca²⁺ condition, where RFI of 1 = no change, <1 = downregulated, >1 = upregulated.

3.3.2.1 DHA significantly upregulated *CERS3* expression in proliferating NHEK at 48 hours post supplementation

DHA significantly upregulated *CERS3* expression in proliferating cells at 48 hours post-DHA supplementation (p= 0.003) (**Figure 3.19**). No change in other *CERS* in proliferating NHEK was found.

CERS1-6 expression in proliferating NHEK

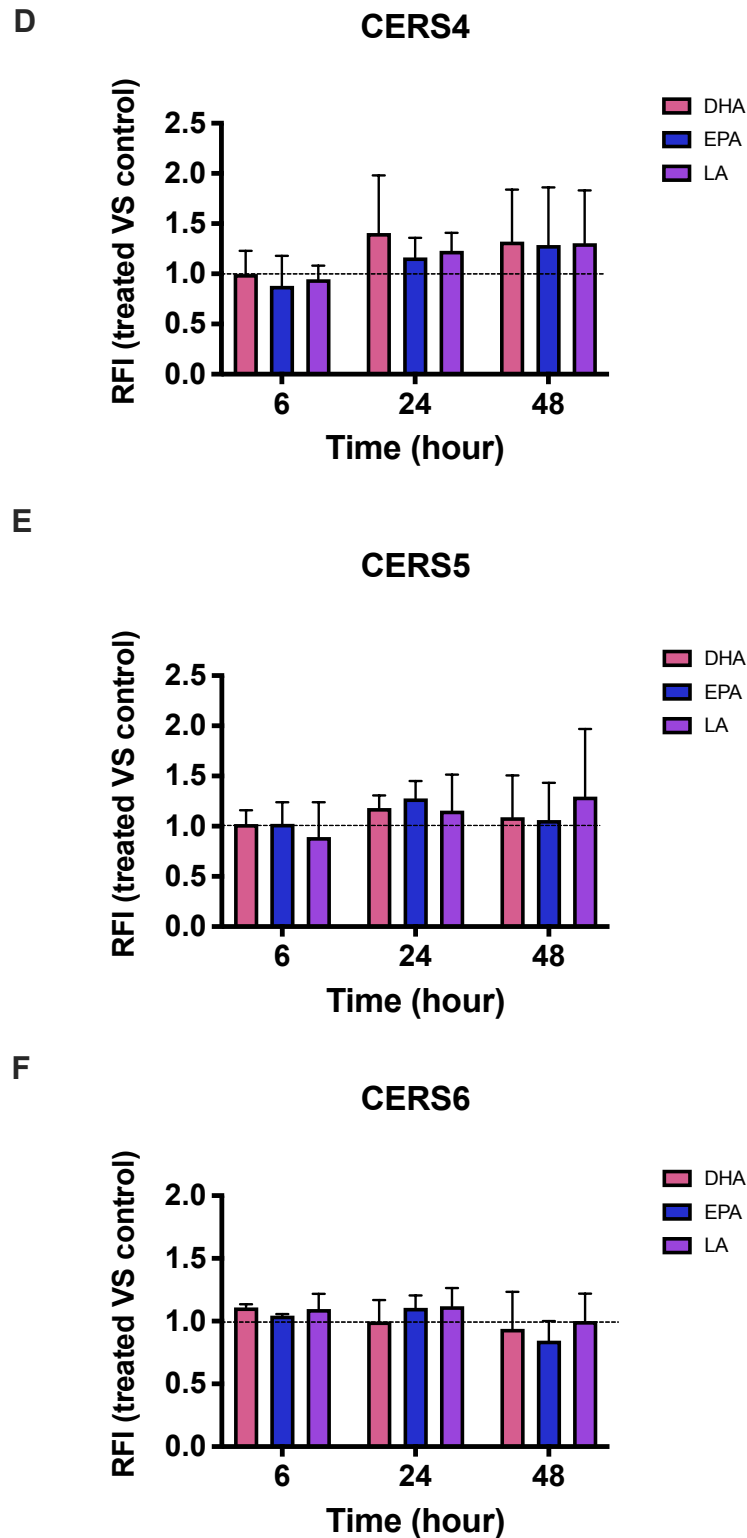


Figure 3.19 The effect of PUFA supplementation on CERS1-6 expression in proliferating NHEK. A-F) Ceramide synthase 1, 2, 3, 4, 5 and 6 mRNA expression were measured using RT-qPCR analysis in proliferating NHEK treated with 10 μ M DHA, EPA and LA for six, 24 and 48 hours. Data are presented as relative fold increase (mean \pm SD). Comparisons were performed between the control and PUFA treated cells of the same time point; (n=4 donors). RFI =1: no change; RFI <1: downregulation; RFI >1: upregulation.

Statistical analysis was performed using Two-Way ANOVA comparing changes with treatment and time. Corrections for multiple analyses was performed using the Dunnett method; ** $p < 0.01$. PUFA: polyunsaturated fatty acid; NHEK: normal human epidermal keratinocytes; DHA: docosahexaenoic acid; EPA: eicosapentaenoic acid; LA: linoleic acid; RFI: relative fold increase; CERS1-6: ceramide synthase 1-6.

3.3.2.2 n-3 PUFA significantly upregulated DES2 expression in proliferating NHEK

Both *n-3* PUFAs, DHA and EPA, significantly upregulated *DES2* expression in proliferating NHEK at 24 ($p = 0.003$, $p = 0.003$, respectively) and 48 hours ($p = 0.0003$, $p = 0.0003$, respectively) (**Figure 3.20**).

DES1 and DES2 expression in proliferating NHEK

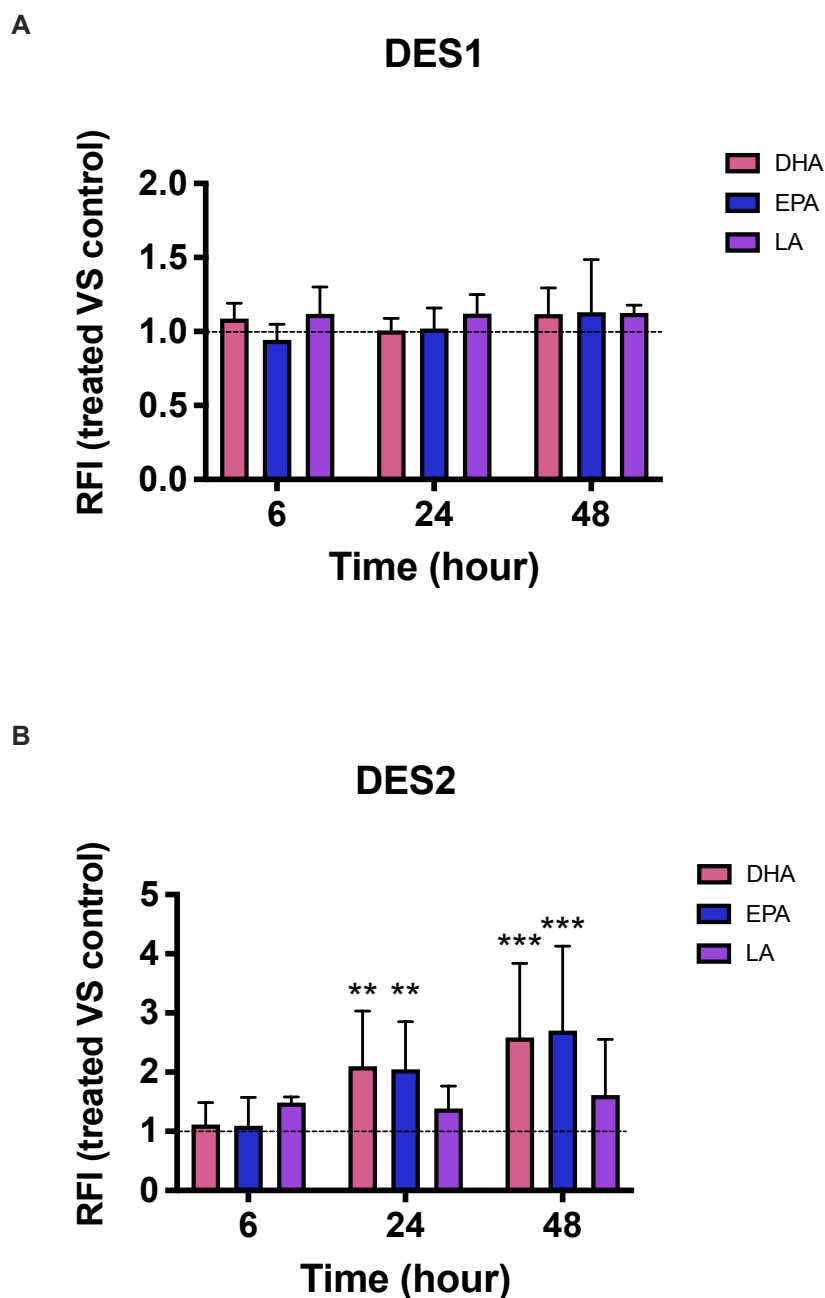


Figure 3.20 The effect of PUFA supplementation on DES1-2 expression in proliferating NHEK. A, B) Desaturase 1, 2 gene expression were measured using RT-qPCR analysis in proliferating NHEK treated with 10 μ M DHA, EPA and LA for six, 24 and 48 hours. Data are presented as relative fold increase (mean \pm SD). Comparisons were performed between the control and PUFA treated cells of the same time point; (n=4 donors). RFI =1: no change; RFI <1: downregulation; RFI >1: upregulation. Statistical analysis was performed using Two-Way ANOVA comparing changes with treatment and time; **p <0.01; ***p <0.001. PUFA: polyunsaturated fatty acid; NHEK: normal human epidermal keratinocytes; DHA: docosahexaenoic acid; EPA: eicosapentaenoic acid; LA: linoleic acid; RFI: relative fold increase; DES1, 2: desaturase1, 2.

3.3.2.3 No change in CER biosynthesis enzyme gene expression was found in differentiated NHEK with PUFA

No change was found in *CERS1*, 2, 3 and 4 expression in differentiated NHEK with PUFA treatment (**Figure 3.21**). There was a short-lived upregulation in *DES2* expression at the earliest stage of NHEK differentiation at 6 hours post-DHA treatment ($p= 0.04$) but this disappeared by 24 hours (**Figure 3.22**).

CERS1-4 expression in differentiating NHEK

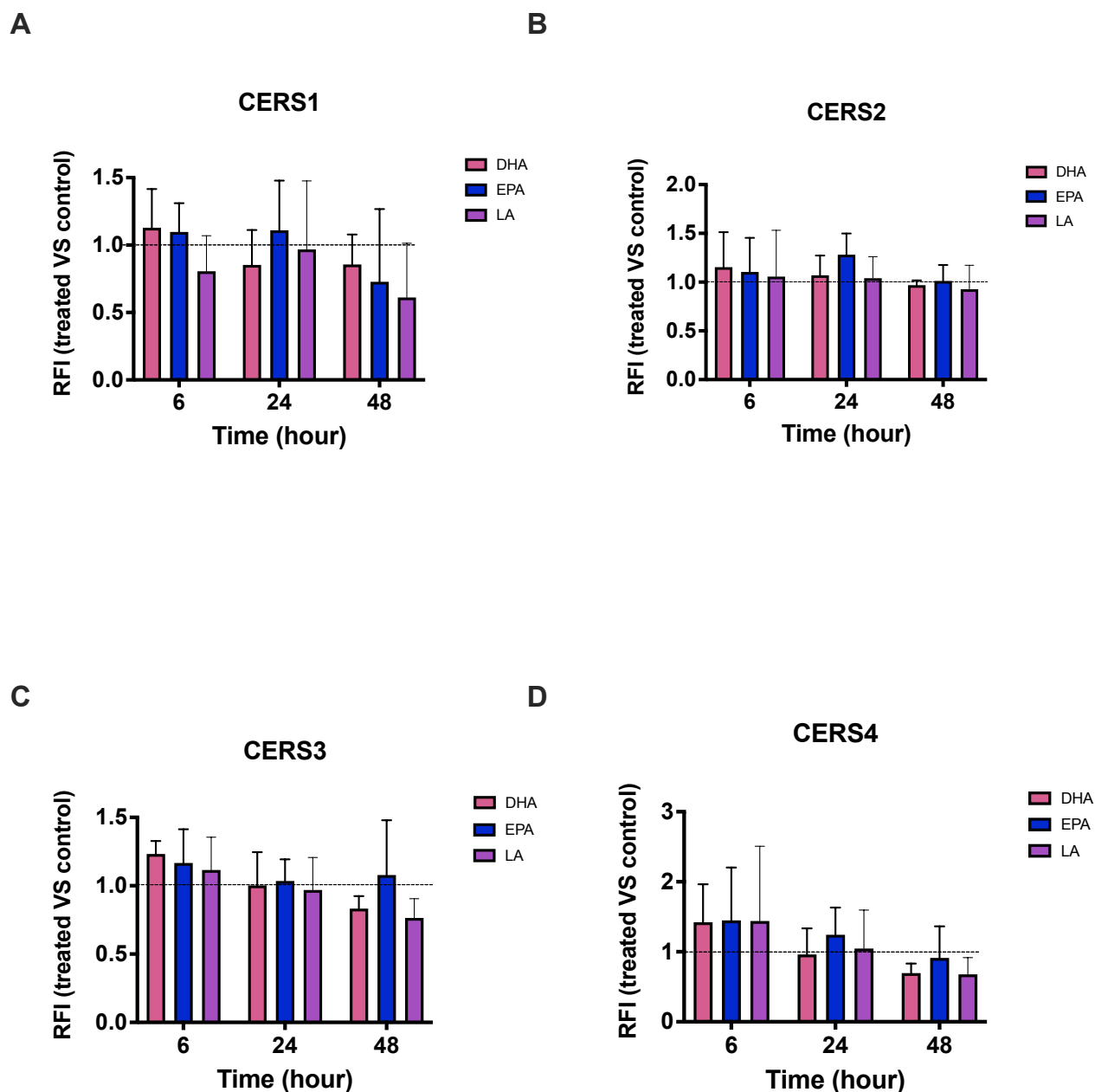


Figure 3.21 The effect of PUFA supplementation on CERS1-4 expression in differentiated NHEK A-D) Ceramide synthase 1, 2, 3 and 4 mRNA expression were measured using RT-qPCR analysis in differentiating NHEK treated with 10 μ M DHA, EPA and LA for six, 24 and 48 hours. Data are presented as relative fold increase (mean \pm SD). Comparisons were performed between the control and PUFA treated cells of the same time point; (n=4 donors). RFI =1: no change; RFI <1: downregulation; RFI >1: upregulation. Statistical analysis was performed using Two-Way ANOVA comparing changes with treatment and time. PUFA: polyunsaturated fatty acid; NHEK: normal human epidermal keratinocytes; DHA: docosahexaenoic acid; EPA: eicosapentaenoic acid; LA: linoleic acid; RFI: relative fold increase; CERS1-4: ceramide synthase 1-4.

DES1 and DES2 expression in differentiating NHEK

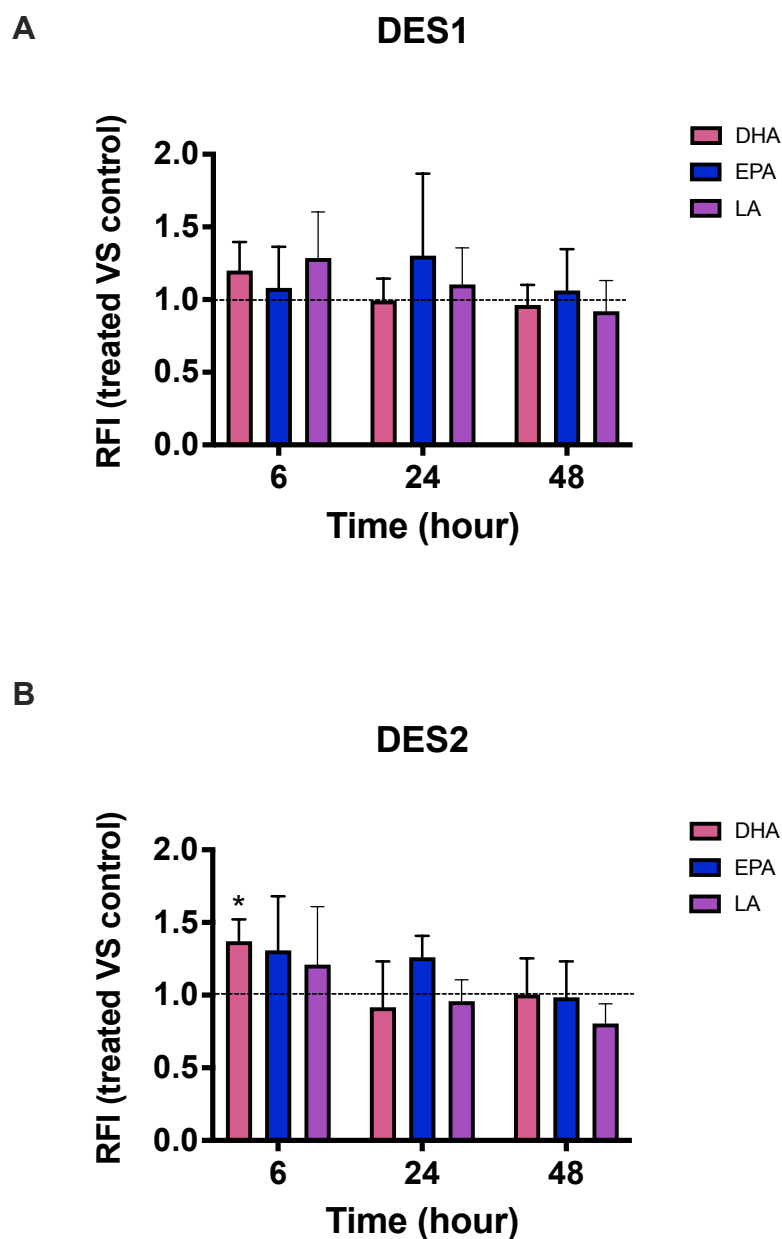


Figure 3.22 The effect of PUFA supplementation on DES1-2 expression in differentiated NHEK. A, B) Desaturase 1, 2 gene expression were measured using RT-qPCR analysis in differentiating NHEK treated with 10 μ M DHA, EPA and LA for six, 24 and 48 hours. Data are presented as relative fold increase (mean \pm SD). Comparisons were performed between the control and PUFA treated cells of the same time point; (n=4 donors). RFI =1: no change; RFI <1: downregulation; RFI >1: upregulation. Statistical analysis was performed using Two-Way ANOVA comparing changes with treatment and time; *p <0.5. PUFA: polyunsaturated fatty acid; NHEK: normal human epidermal keratinocytes; DHA: docosahexaenoic acid; EPA: eicosapentaenoic acid; LA: linoleic acid; RFI: relative fold increase; DES1, 2: desaturase 1, 2.

3.3.3 n-3 PUFA significantly reduced membrane lipid levels in proliferating NHEK, whereas LA significantly increased lipid levels in differentiated NHEK

To further investigate lipid metabolism in proliferating and differentiated NHEK that could be affected by PUFA supplementation, structural and functional membrane lipids that include sterols, FFAs, glycerolipids, glycerophospholipids and complex sphingolipids were analysed using UHPSFC-MS^E system. Data were categorised according to the functional class of membrane lipids. For each sample analysed, concentrations of detected membrane lipid species were reported as absolute values in $\mu\text{g}/10^6$ cells (mean \pm SD).

Generally, concentrations of membrane lipids were higher in differentiated NHEK. DHA mainly affected proliferating cells where it reduced most membrane lipid classes, although not all changes reached statistical significance. LA had an effect on differentiated NHEK where it increased FFA and LPC levels.

3.3.3.1 EPA significantly reduced FFA 24:1 in proliferating NHEK, whereas LA significantly increased FFA 18:2 in differentiated NHEK

In addition to CERs, major barrier structural lipid classes include cholesterol and FFAs. Sterol lipids including total cholesterol and five CE species were detected in proliferating and differentiated NHEK (**Figure 3.23-3.25**). Although changes did not reach statistical significance, DHA reduced CE 16:1 and CE 18:1 concentration in proliferating NHEK ($p=0.07$, $p=0.08$, respectively) (**Figure 3.24**). No change in cholesterol was found (**Figure 3.25**).

In addition to this, 10 FFA species were found in proliferating NHEK, whereas in differentiated NHEK a total of 15 FFAs were detected (**Figure 3.26-3.28**). The most abundant FFAs were the C18:1 in both cell types (mean= $2.8 \mu\text{g}/10^6$ cells, mean= $4.4 \mu\text{g}/10^6$ cells, respectively). In proliferating cells, EPA significantly reduced FFA 24:1 concentration when compared with DMSO control ($p=0.02$) (**Figure 3.27**), whereas in differentiating NHEK, LA significantly increased FFA 18:2 ($p=0.002$) (**Figure 3.28**).

Total CE in NHEK

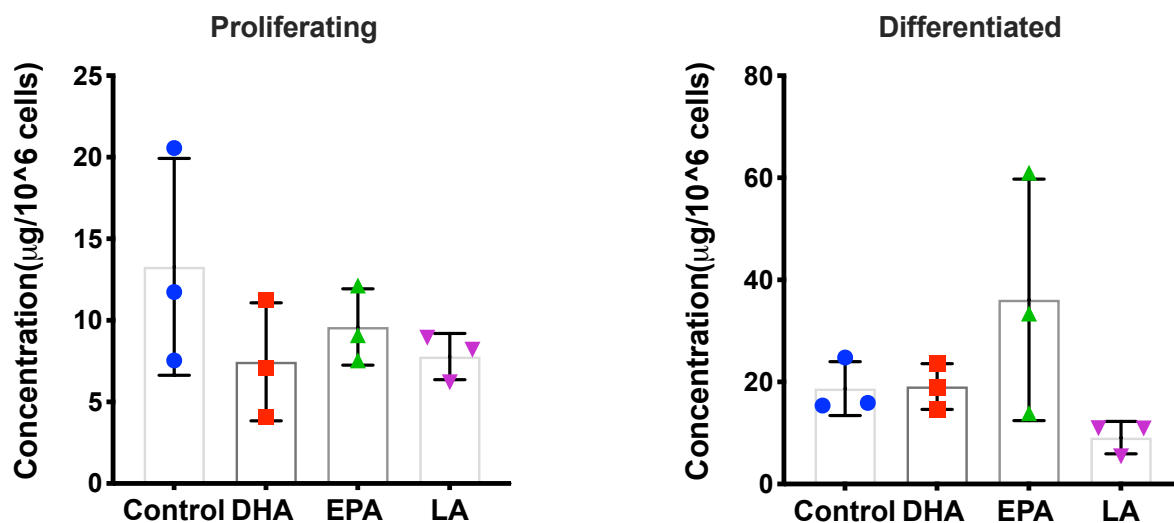


Figure 3.23 The effect of PUFA supplementation on total CE levels in proliferating and differentiated NHEK. Total CE was measured using UHPSFC-MS^E in proliferating and differentiating NHEK treated with 10 μM DHA, EPA and LA for 72 hours. Data are presented as absolute concentration in $\mu\text{g}/10^6$ cells (mean \pm SD). Comparisons were performed between the control and PUFA treated cells of the same Ca^{+2} condition; (n=3 donors) per condition. Statistical analysis was performed using One-Way ANOVA comparing differences over treatment compared with control, with corrections for multiple analyses using the Dunnett method. PUFA: polyunsaturated fatty acid; NHEK: normal human epidermal keratinocytes; DHA: docosahexaenoic acid; EPA: eicosapentaenoic acid; LA: linoleic acid; CE: cholesterol ester.

CE species in NHEK

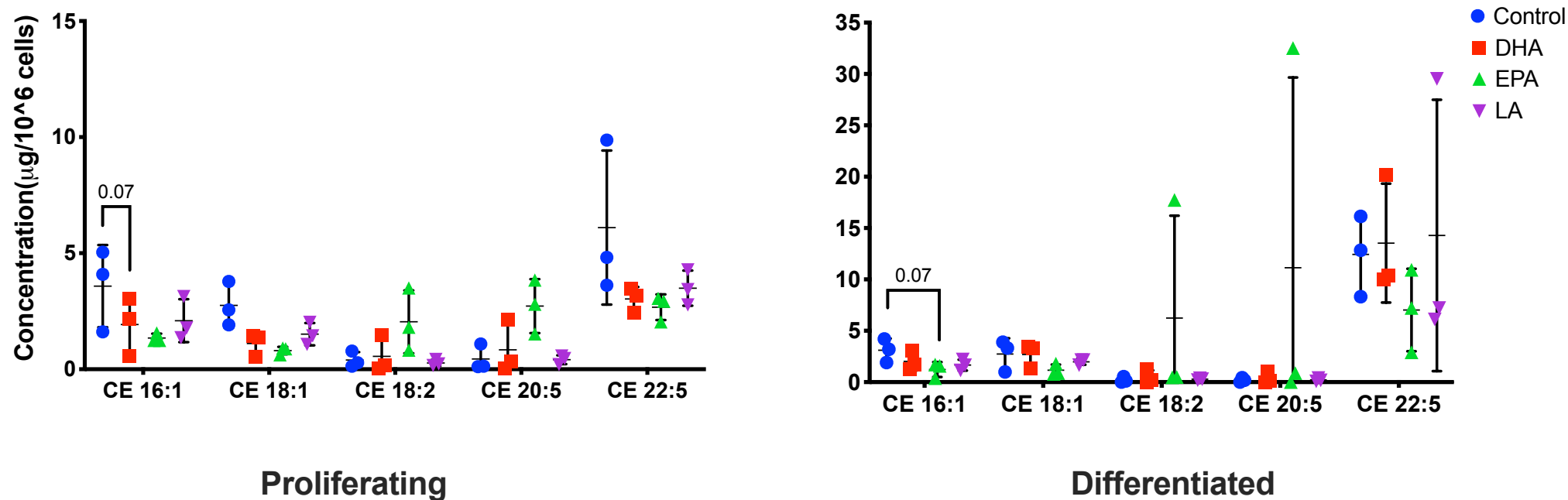


Figure 3.24 The effect of PUFA supplementation on CE species levels measured in proliferating and differentiated NHEK. CE species were measured using UHPSFC-MS^E in proliferating and differentiating NHEK treated with 10 μM DHA, EPA and LA for 72 hours. Data are presented as absolute concentration in μg/10⁶ cells (mean ± SD). Comparisons were performed between the control and PUFA treated cells of the same Ca⁺² condition; (n=3 donors) per condition. Statistical analysis was performed using One-Way ANOVA comparing differences over treatment compared with control, with corrections for

multiple analyses using the Dunnett method. PUFA: polyunsaturated fatty acid; NHEK: normal human epidermal keratinocytes; DHA: docosahexaenoic acid; EPA: eicosapentaenoic acid; LA: linoleic acid; CE: cholesterol ester.

Total cholesterol in NHEK

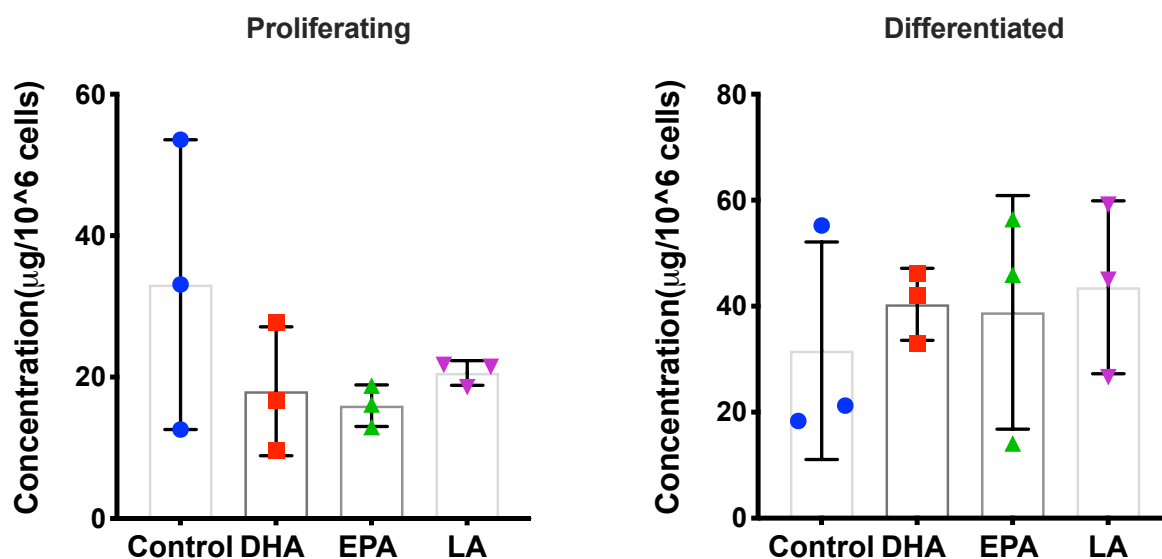


Figure 3.25 The effect of PUFA supplementation on total cholesterol levels in proliferating and differentiated NHEK. Total cholesterol was measured using UHPSFC-MS^E in proliferating and differentiating NHEK treated with 10 μM DHA, EPA and LA for 72 hours. Data are presented as absolute concentration in $\mu\text{g}/10^6$ cells (mean \pm SD). Comparisons were performed between the control and PUFA treated cells of the same Ca⁺ condition; (n=3 donors) per condition. Statistical analysis was performed using One-Way ANOVA comparing differences over treatment compared with control, with corrections for multiple analyses using the Dunnett method. PUFA: polyunsaturated fatty acid; NHEK: normal human epidermal keratinocytes; DHA: docosahexaenoic acid; EPA: eicosapentaenoic acid; LA: linoleic acid.

Total FFA in NHEK

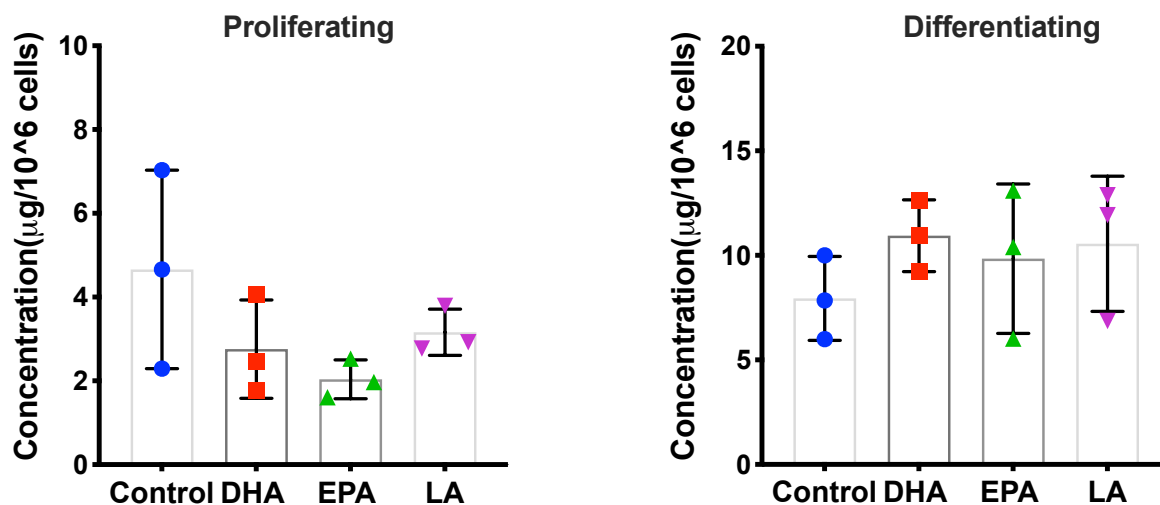


Figure 3.26 The effect of PUFA supplementation on total FFA levels in proliferating and differentiated NHEK. Total FFA were measured using UHPSFC-MS^E in proliferating and differentiating NHEK treated with 10 μM DHA, EPA and LA for 72 hours. Data are presented as absolute concentration in $\mu\text{g}/10^6$ cells (mean \pm SD). Comparisons were performed between the control and PUFA treated cells of the same Ca^{+2} condition; (n=3 donors) per condition. Statistical analysis was performed using One-Way ANOVA comparing differences over treatment compared with control, with corrections for multiple analyses using the Dunnett method. PUFA: polyunsaturated fatty acid; NHEK: normal human epidermal keratinocytes; DHA: docosahexaenoic acid; EPA: eicosapentaenoic acid; LA: linoleic acid; FFA: free fatty acids.

FFA species (Proliferating NHEK)

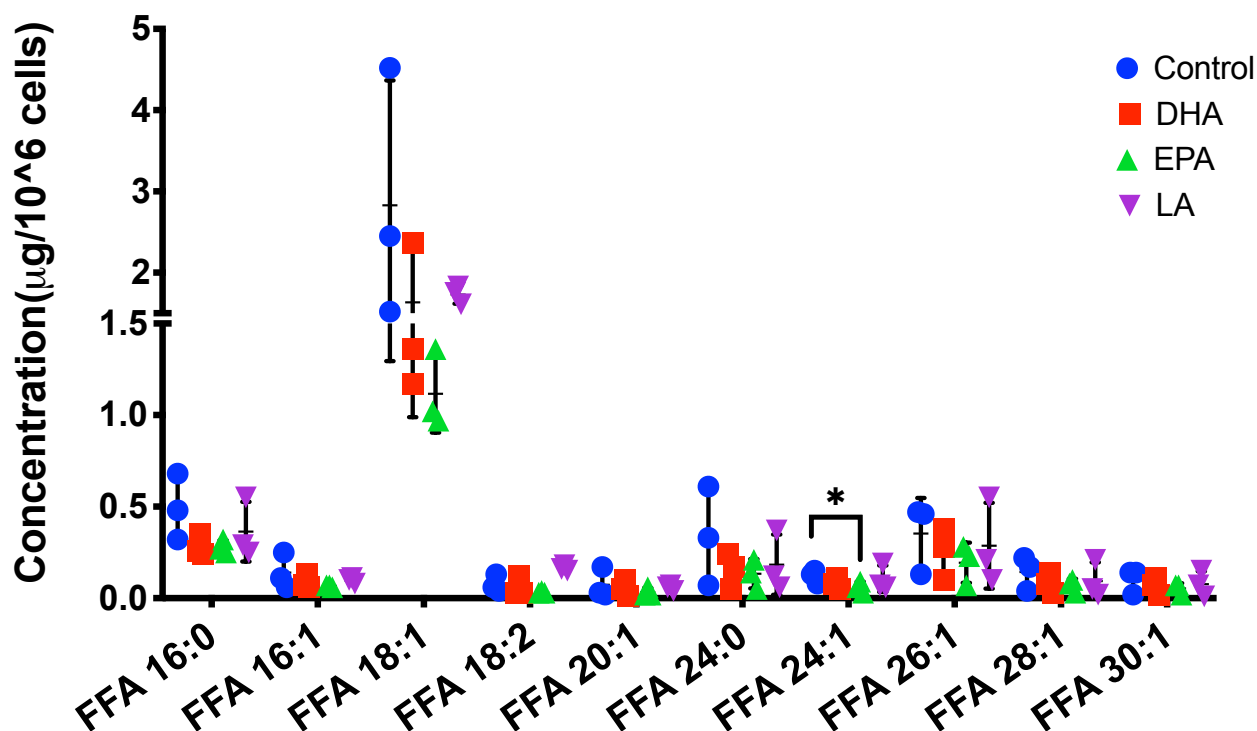


Figure 3.27 The effect of PUFA supplementation on FFA species levels measured in proliferating NHEK. FFA species were measured using UHPSFC-MS^E in proliferating NHEK treated with 10 µM DHA, EPA and LA for 72 hours. Data are presented as absolute concentration in µg/10⁶ cells (mean ± SD). Comparisons were performed between the control and PUFA treated cells; (n=3 donors). Statistical analysis was performed using One-Way ANOVA comparing differences over treatment compared with control, with corrections for multiple analyses using the Dunnett method; *p <0.05. PUFA: polyunsaturated fatty acid; NHEK: normal human epidermal keratinocytes; DHA: docosahexaenoic acid; EPA: eicosapentaenoic acid; LA: linoleic acid; FFA: free fatty acids.

FFA speceis (Differentiating NHEK)

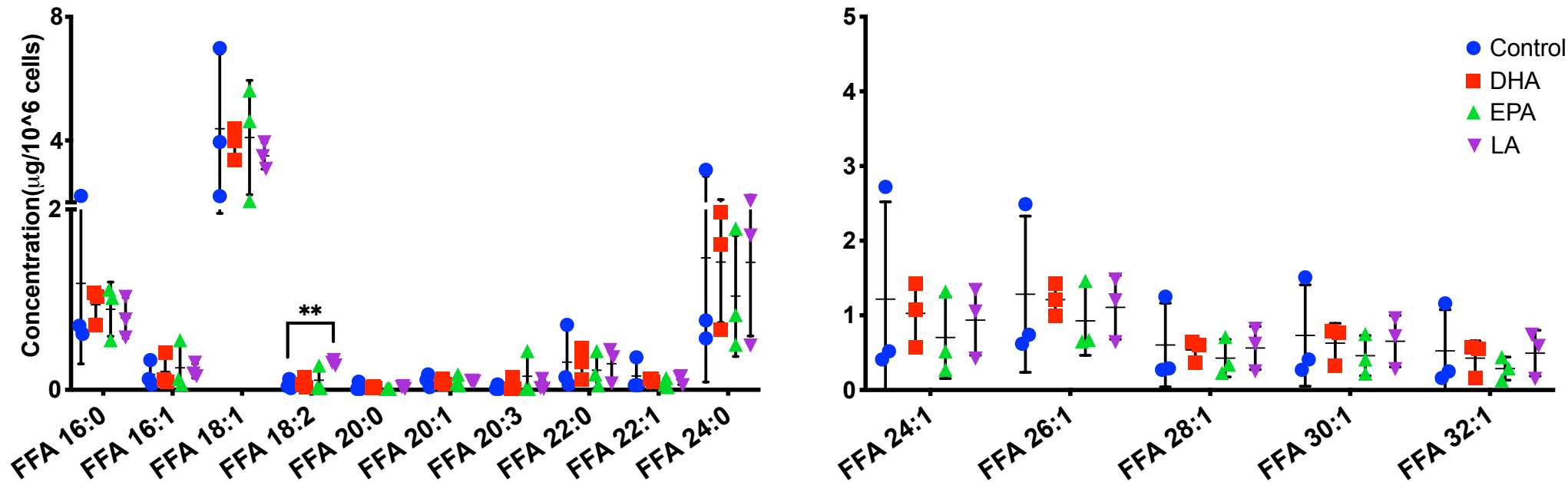


Figure 3.28 The effect of PUFA supplementation on FFA species levels measured in differentiated NHEK. FFA species were measured using UHPSFC-MS^E in differentiated NHEK treated with 10 μM DHA, EPA and LA for 72 hours. Data are presented as absolute concentration in $\mu\text{g}/10^6$ cells (mean \pm SD). Comparisons were performed between the control and PUFA treated cells; (n=3 donors). Statistical analysis was performed using One-Way ANOVA comparing differences over treatment compared with control, with corrections for multiple analyses using the Dunnett method; **p < 0.01. PUFA: polyunsaturated fatty acid; NHEK: normal human epidermal keratinocytes; DHA: docosahexaenoic acid; EPA: eicosapentaenoic acid; LA: linoleic acid; FFA: free fatty acids.

3.3.3.2 DHA significantly reduced SM levels in proliferating NHEK

To further interrogate the changes seen in CER levels with PUFA, the complex sphingolipids, SMs, that form the majority of SC CERs along with glucosylceramides were analysed. We detected 24 and 26 SM species in proliferating and differentiated NHEK, respectively (**Figure 3.29**). In proliferating NHEK, DHA significantly reduced SM 42:2 ($p=0.03$), and there was a close to significant decrease in SM 44:2, SM 44:4 and SM 40:2 ($p=0.06$, $p=0.06$, $p=0.07$, respectively) (**Figure 3.30**). No change was found in SM levels in differentiated NHEK with PUFA supplementation (**Figure 3.31**).

Total SM in NHEK

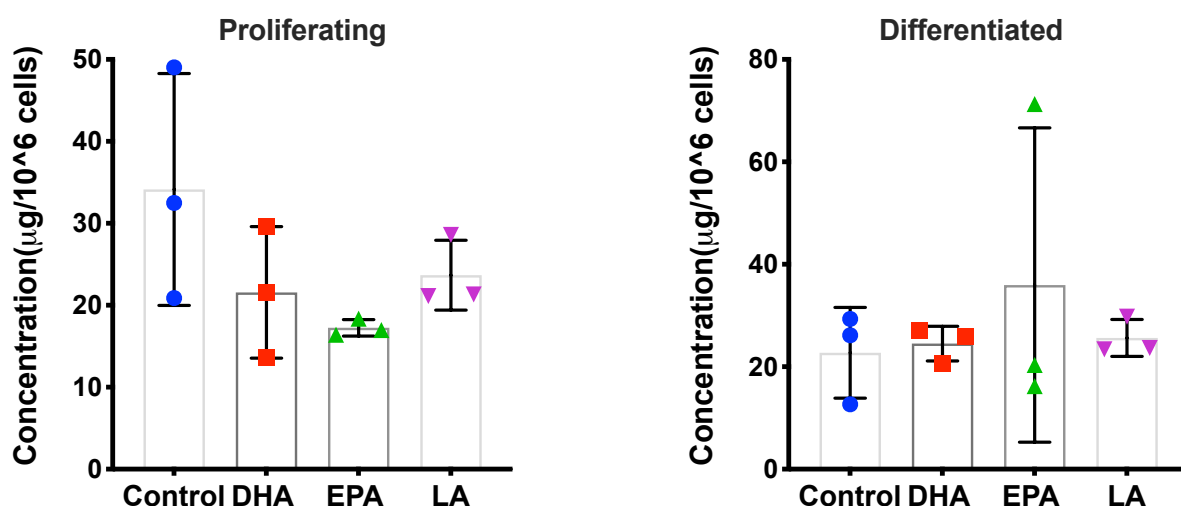


Figure 3.29 The effect of PUFA supplementation on total SM levels measured in proliferating and differentiated NHEK. Total SM was measured using UHPSFC-MS^E in proliferating and differentiated NHEK treated with 10 μM DHA, EPA and LA for 72 hours. Data are presented as absolute concentration in $\mu\text{g}/10^6$ cells (mean \pm SD). Comparisons were performed between the control and PUFA treated cells of the same Ca^{+2} condition; ($n=3$ donors) per condition. Statistical analysis was performed using One-Way ANOVA comparing differences over treatment compared with control, with corrections for multiple analyses using the Dunnett method; $**p < 0.01$. PUFA: polyunsaturated fatty acid; NHEK: normal human epidermal keratinocytes; DHA: docosahexaenoic acid; EPA: eicosapentaenoic acid; LA: linoleic acid; SM: sphingomyelin.

SM species (Proliferating NHEK)

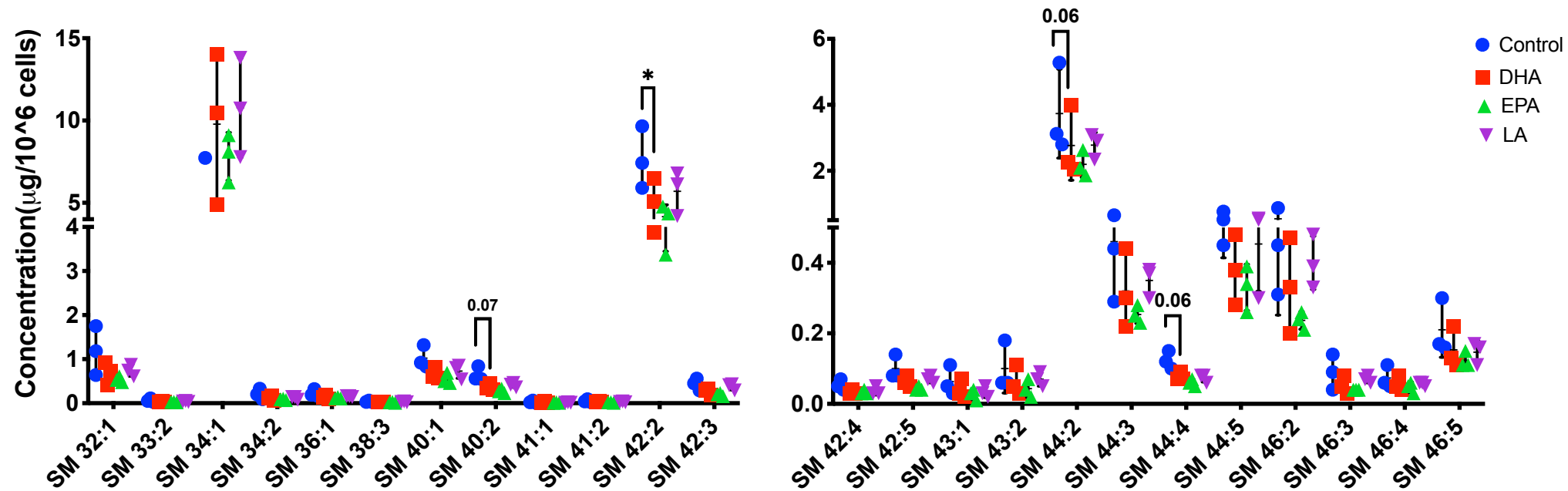


Figure 3.30 The effect of PUFA supplementation on SM species levels measured in proliferating NHEK. SM species were measured using UHPSFC-MS^E in proliferating NHEK treated with 10 μM DHA, EPA and LA for 72 hours. Data are presented as absolute concentration in $\mu\text{g}/10^6$ cells (mean \pm SD). Comparisons were performed between the control and PUFA treated cells; (n=3 donors). Statistical analysis was performed using One-Way ANOVA comparing differences over treatment compared with control of the same time-point, with corrections for multiple analyses using the Dunnett method; *p < 0.05. PUFA:

polyunsaturated fatty acid; NHEK: normal human epidermal keratinocytes; DHA: docosahexaenoic acid; EPA: eicosapentaenoic acid; LA: linoleic acid; SM: sphingomyelin.

SM species (Differentiating NHEK)

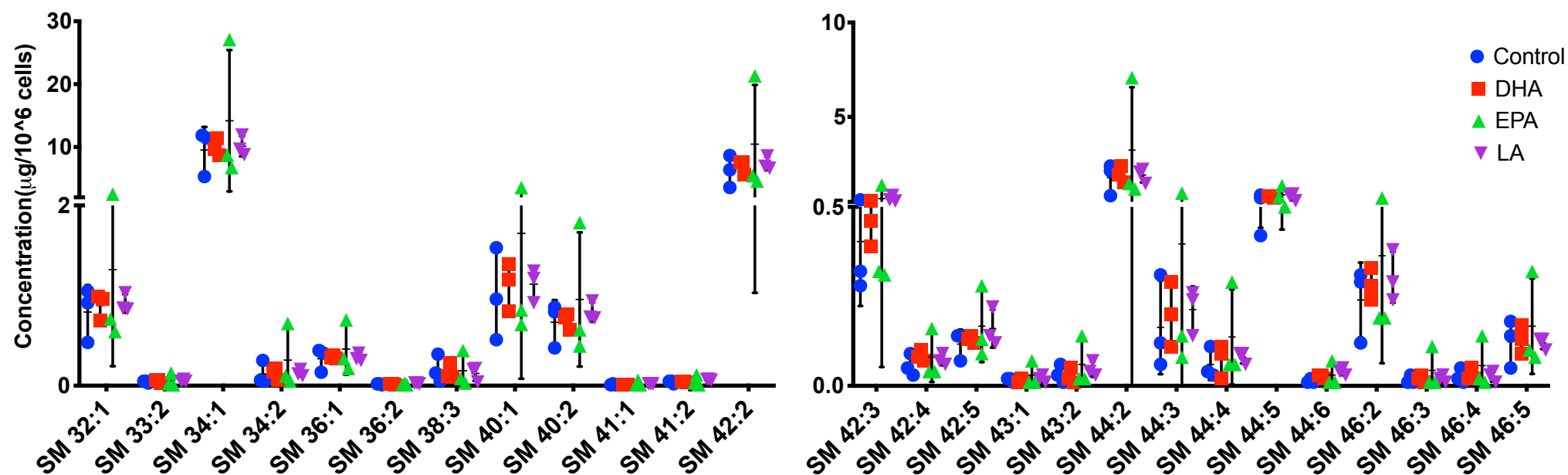


Figure 3.31 The effect of PUFA supplementation on SM species levels measured in differentiated NHEK. SM species were measured using UHPSFC-MS^E in differentiating NHEK treated with 10 µM DHA, EPA and LA for 72 hours. Data are presented as absolute concentration in µg/10⁶ cells (mean ± SD). Comparisons were performed between the control and PUFA treated cells; (n=3 donors). Statistical analysis was performed using One-Way ANOVA comparing

differences over treatment compared with control of the same time-point, with corrections for multiple analyses using the Dunnett method. PUFA: polyunsaturated fatty acid; NHEK: normal human epidermal keratinocytes; DHA: docosahexaenoic acid; EPA: eicosapentaenoic acid; LA: linoleic acid; SM: sphingomyelin.

3.3.3.3 DHA significantly reduced several TG species levels in proliferating NHEK

Glycerolipids are both structural and functional membrane lipids that are utilised for energy production during cellular growth and to generate inflammatory mediators. There were five DG species detected in both cell types (**Figure 3.32**). No significant changes in DG species levels were observed (**Figure 3.32-3.33**). In proliferating NHEK, 32 TG species were detected, whereas in differentiated NHEK a total of 46 TG species were measured (**Figure 3.35-3.36**). DHA significantly decreased total TG concentration in proliferating NHEK ($p=0.04$) (**Figure 3.35**). DHA significantly reduced TG 44:2, TG 46:3, TG 47:1, TG 48:3, TG 48:4, TG 49:2, TG 50:2, TG 50:3, TG 50:4 and TG 56:5 ($p=0.04$, $p=0.03$, $p=0.04$, $p=0.01$, $p<0.0001$, $p=0.009$, $p=0.02$, $p=0.03$, $p=0.03$, $p=0.03$, respectively). No effect on TG concentrations was found in differentiated NHEK with PUFA supplementation (**Figure 3.36**).

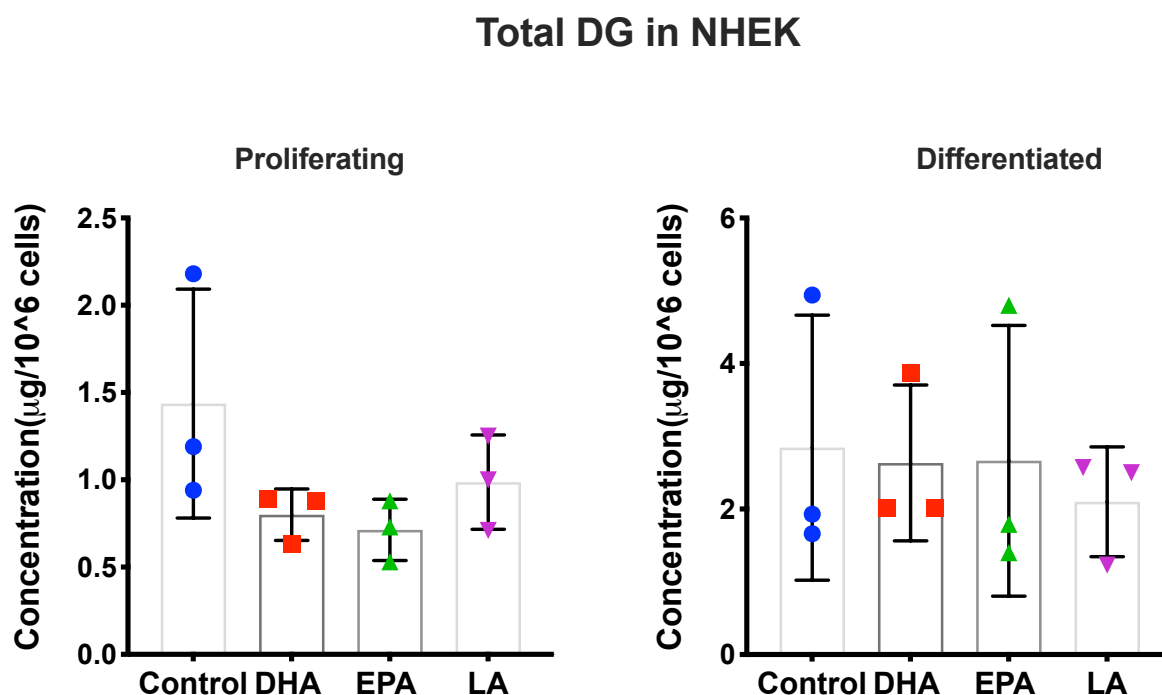


Figure 3.32 The effect of PUFA supplementation on total DG levels measured in proliferating and differentiated NHEK. Total DG was measured using UHPSFC-MS^E in proliferating and differentiating NHEK treated with 10 µM DHA, EPA and LA for 72 hours. Data are presented as absolute concentration in µg/10⁶ cells (mean ± SD). Comparisons were performed between the control and PUFA treated cells of the same Ca⁺ condition; (n=3 donors) per condition. Statistical analysis was performed using One-Way

ANOVA comparing differences over treatment compared with control of the same time-point, with corrections for multiple analyses using the Dunnett method. PUFA: polyunsaturated fatty acid; NHEK: normal human epidermal keratinocytes; DHA: docosahexaenoic acid; EPA: eicosapentaenoic acid; LA: linoleic acid; DG: diacylglycerol.

DG species in NHEK

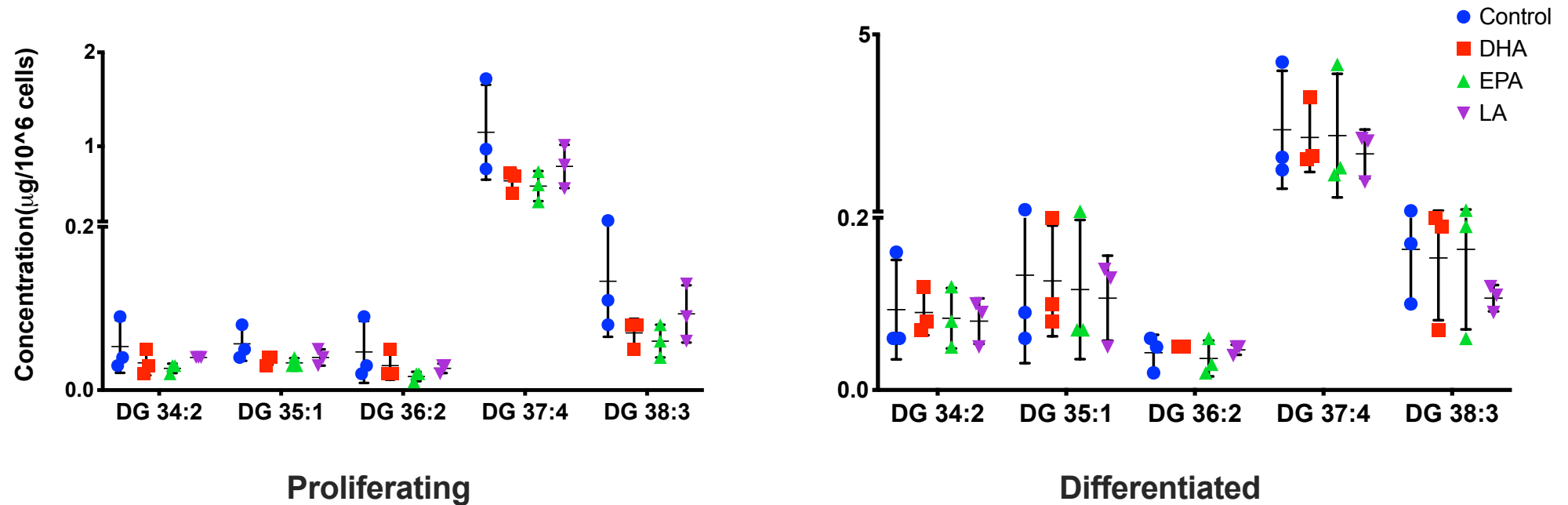


Figure 3.33 The effect of PUFA supplementation on DG species levels measured in proliferating and differentiated NHEK. DG species were measured using UHPSFC-MS^E in proliferating and differentiating NHEK treated with 10 µM DHA, EPA and LA for 72 hours. Data are presented as absolute concentration in µg/10⁶ cells (mean ± SD). Comparisons were performed between the control and PUFA treated cells of the same Ca⁺² condition; (n=3 donors) per condition. Statistical analysis was performed using One-Way ANOVA comparing differences over treatment compared with control of the same time-point,

with corrections for multiple analyses using the Dunnett method; ** $p < 0.01$. PUFA: polyunsaturated fatty acid; NHEK: normal human epidermal keratinocytes; DHA: docosahexaenoic acid; EPA: eicosapentaenoic acid; LA: linoleic acid; DG: diacylglycerol.

Total TG in NHEK

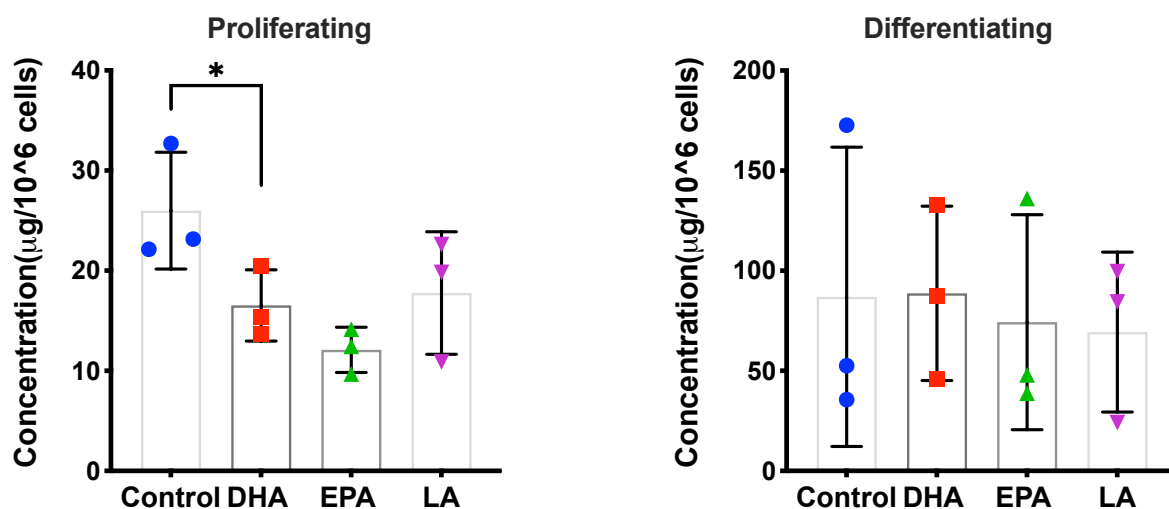


Figure 3.34 The effect of PUFA supplementation on total TG levels measured in proliferating and differentiated NHEK. Total TG was measured using UHPSFC-MS^E in proliferating and differentiating NHEK treated with 10 µM DHA, EPA and LA for 72 hours. Data are presented as absolute concentration in µg/10⁶ cells (mean ± SD). Comparisons were performed between the control and PUFA treated cells of the same Ca⁺ condition; (n=3 donors) per condition. Statistical analysis was performed using One-Way ANOVA comparing differences over treatment compared with control of the same time-point, with corrections for multiple analyses using the Dunnett method; *p < 0.05. PUFA: polyunsaturated fatty acid; NHEK: normal human epidermal keratinocytes; DHA: docosahexaenoic acid; EPA: eicosapentaenoic acid; LA: linoleic acid; TG: triacylglycerol.

TG species (Proliferating NHEK)

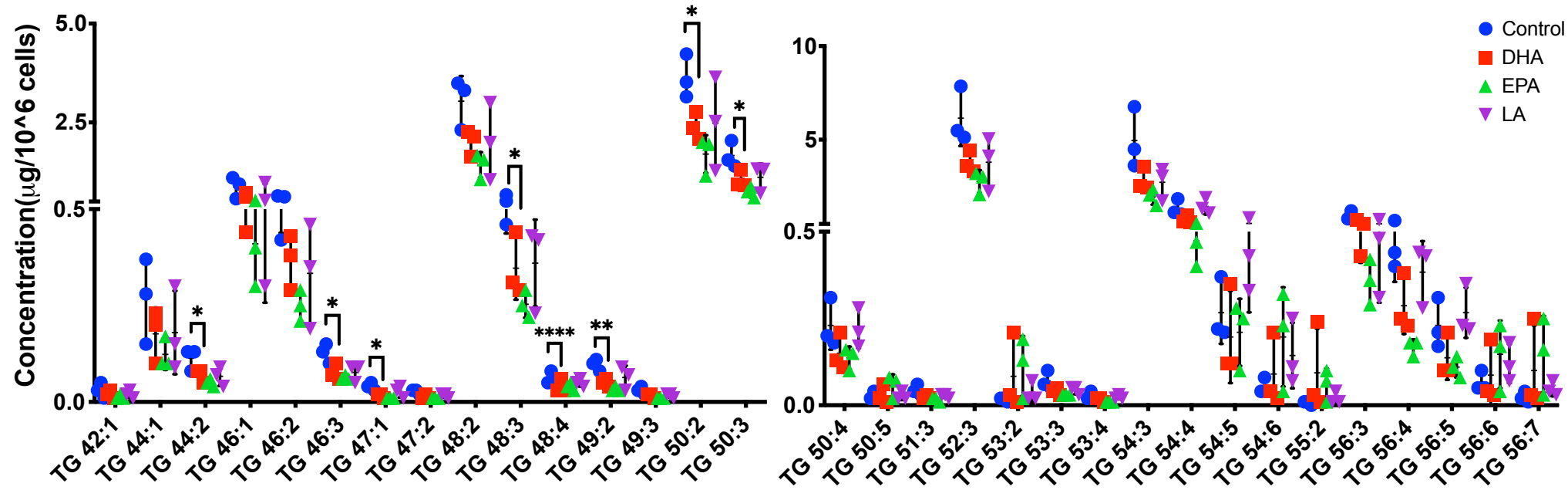


Figure 3.35 The effect of PUFA supplementation on TG species levels measured in proliferating NHEK. TG species were measured using UHPSFC-MS^E in proliferating NHEK treated with 10 µM DHA, EPA and LA for 72 hours. Data are presented as absolute concentration in µg/10⁶ cells (mean ± SD). Comparisons were performed between the control and PUFA treated cells; (n=3 donors). Statistical analysis was performed using One-Way ANOVA comparing differences over treatment compared with control of the same time-point, with corrections for multiple analyses using the Dunnett method; *p < 0.05; **p < 0.01;

*** $p < 0.0001$. PUFA: polyunsaturated fatty acid; NHEK: normal human epidermal keratinocytes; DHA: docosahexaenoic acid; EPA: eicosapentaenoic acid; LA: linoleic acid; TG: triacylglycerol.

TG species (Differentiating NHEK)

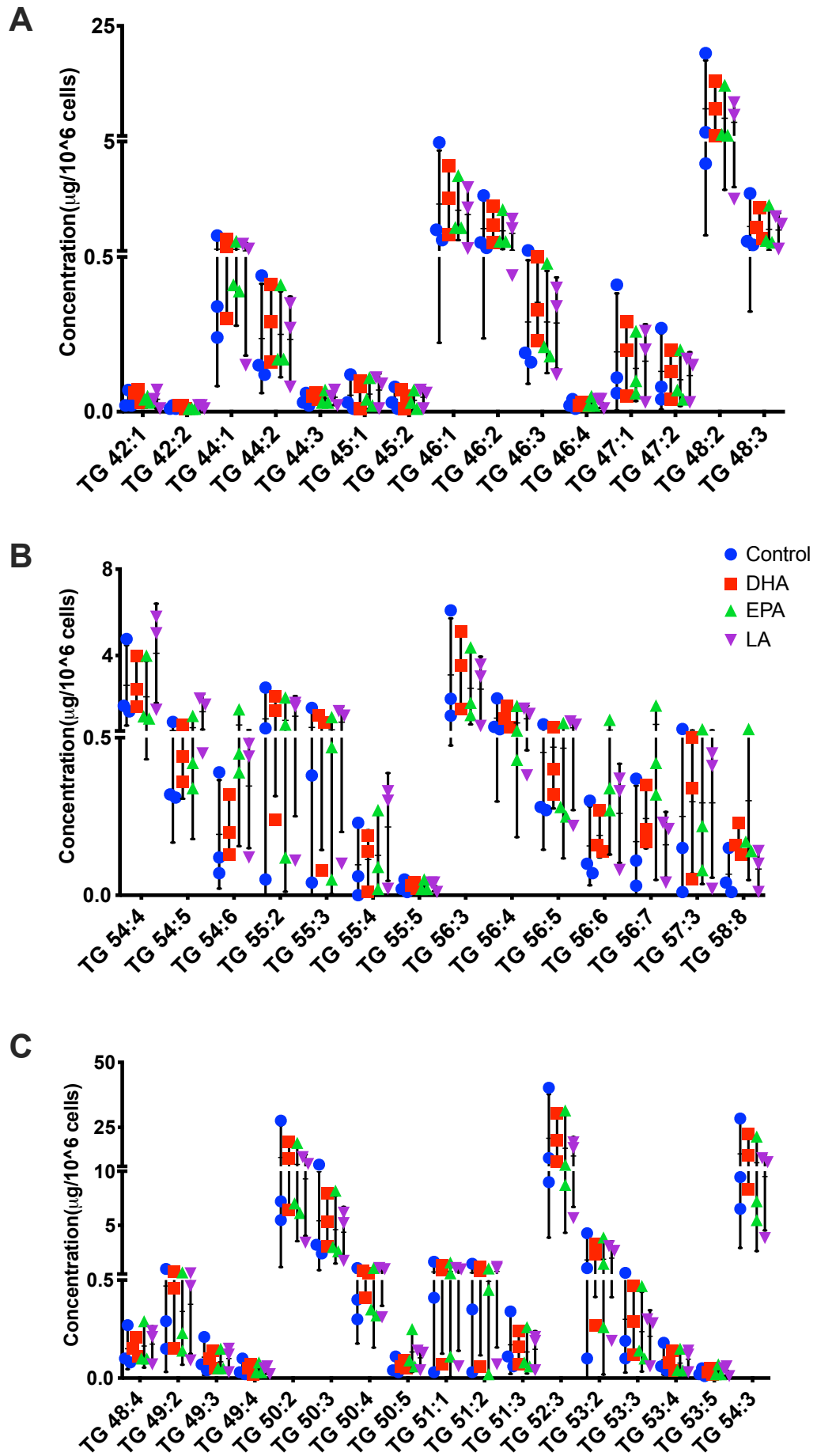


Figure 3.36 The effect of PUFA supplementation on TG species levels measured in differentiated NHEK. TG species were measured using UHPSFC-MS^E in differentiating NHEK treated with 10 μ M DHA, EPA and LA for 72 hours. Data are presented as absolute concentration in μ g/ 10^6 cells (mean \pm SD). Comparisons were performed between the control and PUFA treated cells; (n=3 donors). Statistical analysis was performed using One-Way ANOVA comparing differences over treatment compared with control of the same time-point, with corrections for multiple analyses using the Dunnett method. PUFA: polyunsaturated fatty acid; NHEK: normal human epidermal keratinocytes; DHA: docosahexaenoic acid; EPA: eicosapentaenoic acid; LA: linoleic acid; TG: triacylglycerol.

3.3.3.4 DHA reduced PC and LPC levels in proliferating NHEK, whereas LA significantly increased LPC 16:0 levels in differentiated NHEK

PCs and LPCs are involved in cellular apoptosis and inflammatory responses. In proliferating NHEK, a total of 30 PC species were detected and 29 species in differentiated NHEK (**Figure 3.37**). Although not statistically significant, DHA reduced PC 32:1p/PC 32:2e, PC 36:5, PC 44:2/46:8p/46:9e levels in proliferating NHEK (p= 0.07, p= 0.06, p= 0.07, respectively) (**Figure 3.38**). No changes in PC levels were found in differentiated NHEK with PUFA treatments (**Figure 3.39**).

There were 5 LPC species measured in proliferating and differentiating NHEK. In proliferating NHEK, DHA reduced LPC 16:0 and LPC 16:1, but changes did not reach statistical significance (p= 0.07, p= 0.07) (**Figure 3.40**). In differentiated NHEK, LA significantly increased LPC 16:0 (p= 0.040) (**Figure 3.41**).

Total PC in NHEK

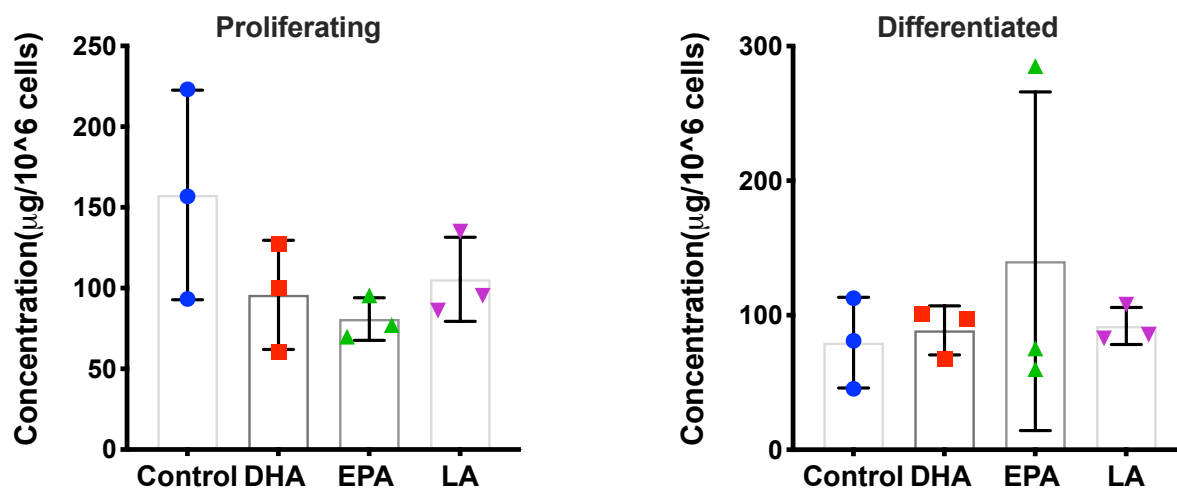


Figure 3.37 The effect of PUFA supplementation on total PC levels measured in proliferating and differentiating NHEK. Total PC was measured using UHPSFC-MS^E in proliferating and differentiating NHEK treated with 10 μM DHA, EPA and LA for 72 hours. Data are presented as absolute concentration in $\mu\text{g}/10^6$ cells (mean \pm SD). Comparisons were performed between the control and PUFA treated cells of the same Ca^{2+} condition; (n=3 donors) per condition. Statistical analysis was performed using One-Way ANOVA comparing differences over treatment compared with control of the same time-point, with corrections for multiple analyses using the Dunnett method. PUFA: polyunsaturated fatty acid; NHEK: normal human epidermal keratinocytes; DHA: docosahexaenoic acid; EPA: eicosapentaenoic acid; LA: linoleic acid; PC: phosphatidylcholine.

PC species (Proliferating NHEK)

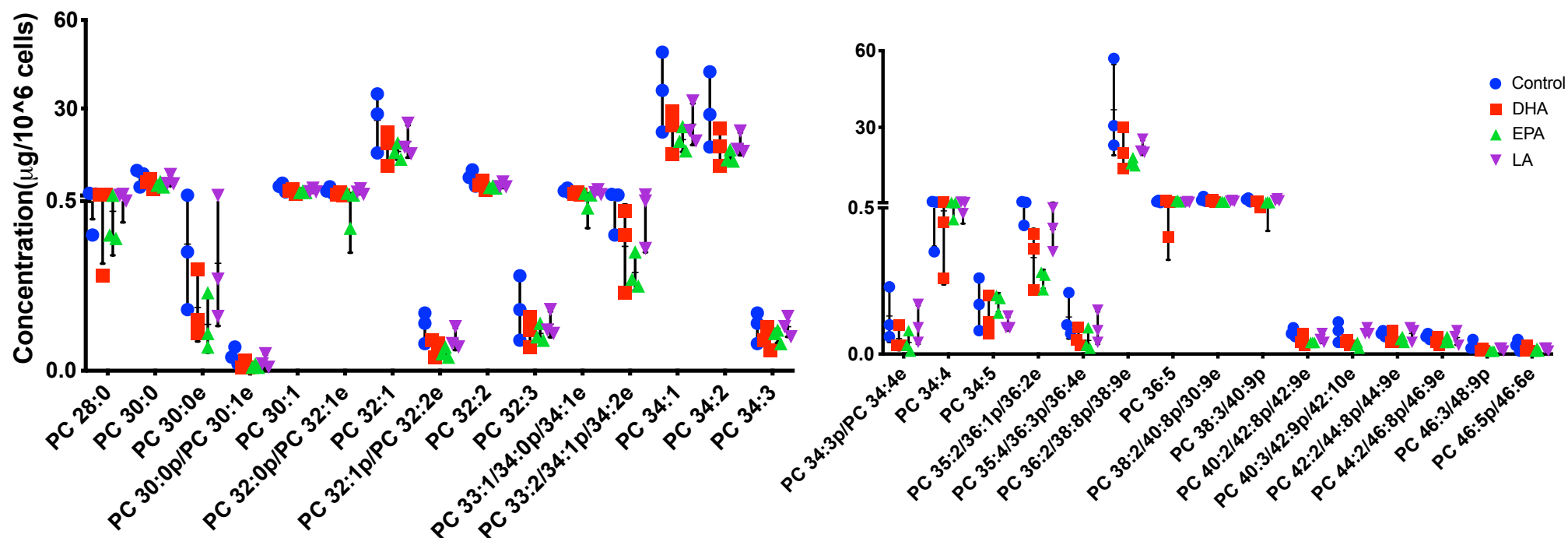


Figure 3.38 The effect of PUFA supplementation on PC species levels measured in proliferating NHEK. PC species were measured using UHPSFC-MS^E in proliferating NHEK treated with 10 µM DHA, EPA and LA for 72 hours. Data are presented as absolute concentration in µg/10⁶ cells (mean ± SD). Comparisons were performed between the control and PUFA treated cells; (n=3 donors). Statistical analysis was performed using One-Way ANOVA comparing differences over treatment compared with control of the same time-point, with corrections for multiple analyses using the Dunnnett method. PUFA:

polyunsaturated fatty acid; NHEK: normal human epidermal keratinocytes; DHA: docosahexaenoic acid; EPA: eicosapentaenoic acid; LA: linoleic acid; PC: phosphatidylcholine.

PC species (Differentiating NHEK)

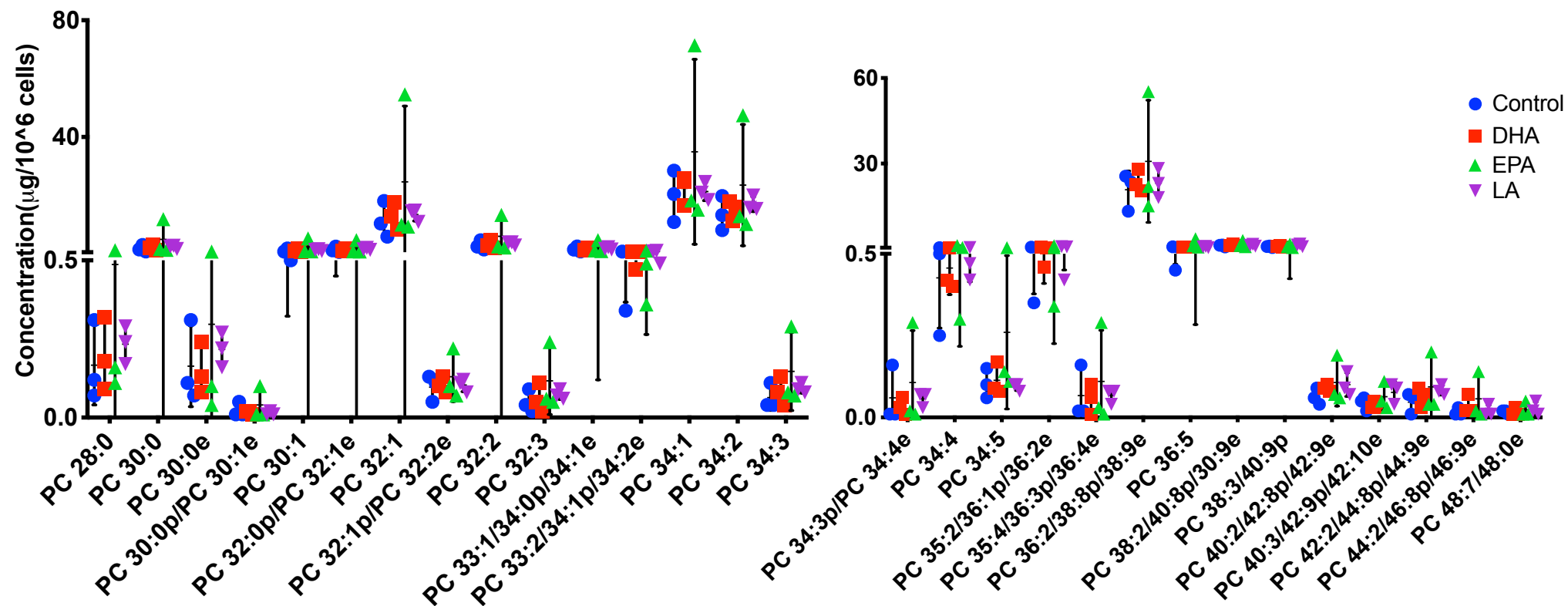


Figure 3.39 The effect of PUFA supplementation on PC species levels measured in differentiated NHEK. PC species were measured using UHPSFC-MS^E in differentiated NHEK treated with 10 μ M DHA, EPA and LA for 72 hours. Data are presented as absolute concentration in μ g/ 10^6 cells (mean \pm SD). Comparisons were performed between the control and PUFA treated cells; (n=3 donors). Statistical analysis was performed using One-Way ANOVA comparing differences over treatment compared with control of the same time-point, with corrections for multiple analyses using the Dunnett method. PUFA: polyunsaturated fatty acid; NHEK: normal human epidermal keratinocytes; DHA: docosahexaenoic acid; EPA: eicosapentaenoic acid; LA: linoleic acid; PC: phosphatidylcholine.

Total PC in NHEK

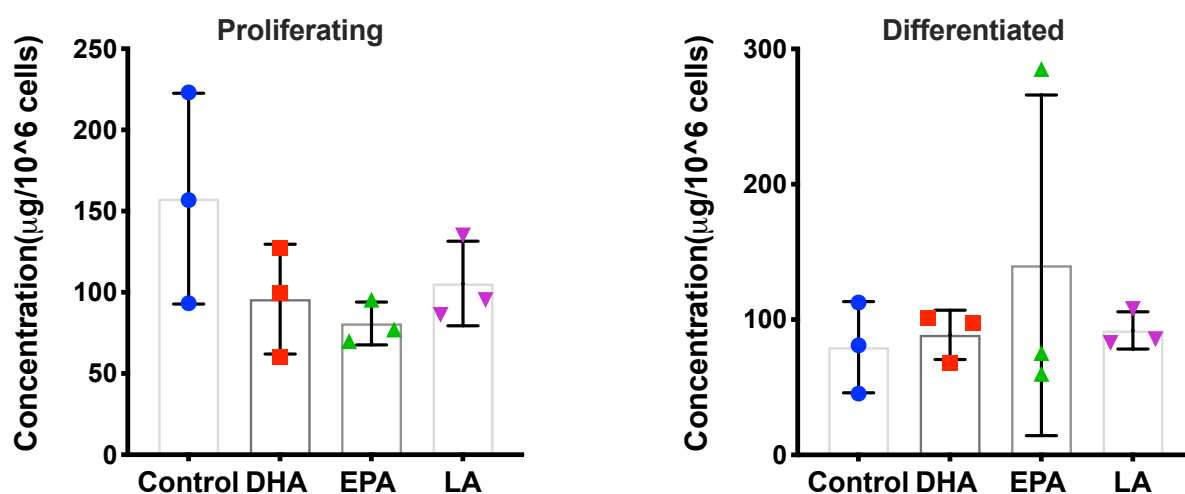


Figure 3.40 The effect of PUFA supplementation on total LPC levels in proliferating and differentiated NHEK. Total LPC was measured using UHPSFC-MSE in proliferating and differentiated NHEK treated with 10 μ M DHA, EPA and LA for 72 hours. Data are presented as absolute concentration in μ g/10⁶ cells (mean \pm SD). Comparisons were performed between the control and PUFA treated cells of the same Ca²⁺ condition; (n=3 donors) per condition. Statistical analysis was performed using One-Way ANOVA comparing differences over treatment compared with control of the same time-point, with corrections for multiple analyses using the Dunnett method. PUFA: polyunsaturated fatty acid; NHEK: normal human epidermal keratinocytes; DHA: docosahexaenoic acid; EPA: eicosapentaenoic acid; LA: linoleic acid; LPC: lysophosphatidylcholine.

LPC species in NHEK

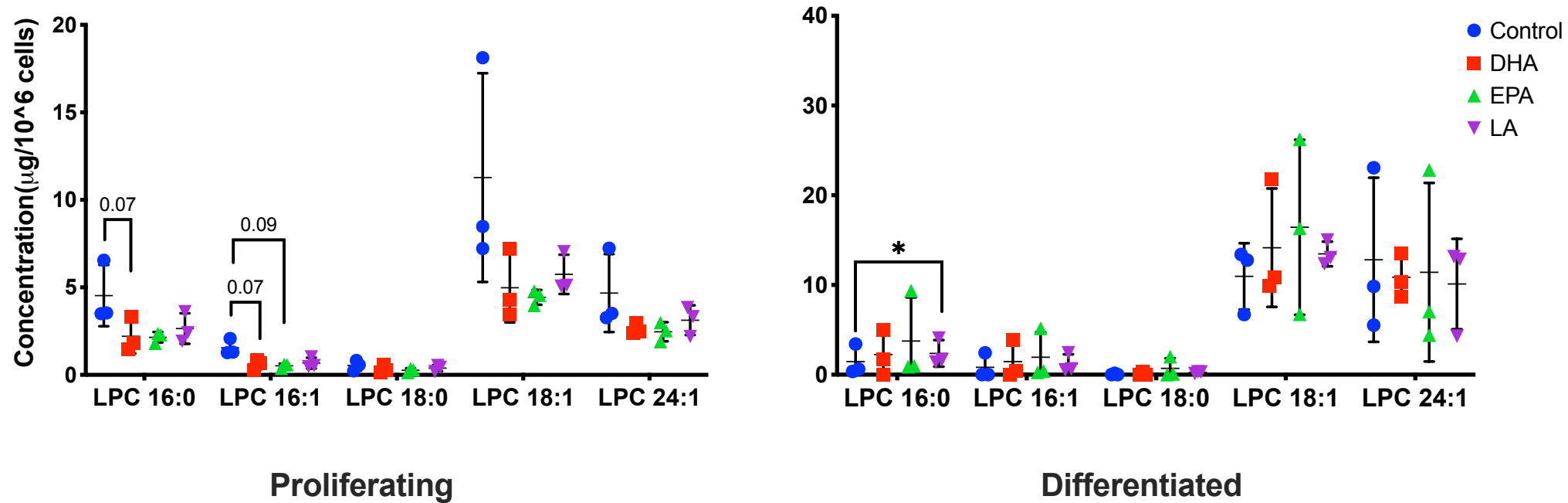


Figure 3.41 The effect of PUFA supplementation on LPC species levels measured in proliferating and differentiated NHEK. LPC species were measured using UHPSFC-MS^E in proliferating and differentiated NHEK treated with 10 µM DHA, EPA and LA for 72 hours. Data are presented as absolute concentration in µg/10⁶ cells (mean ± SD). Comparisons were performed between the control and PUFA treated cells of the same Ca⁺² condition; (n=3 donors) per condition.

Statistical analysis was performed using One-Way ANOVA comparing differences over treatment compared with control of the same time-point, with corrections for multiple analyses using the Dunnett method; * $p < 0.05$. PUFA: polyunsaturated fatty acid; NHEK: normal human epidermal keratinocytes; DHA: docosahexaenoic acid; EPA: eicosapentaenoic acid; LA: linoleic acid; LPC: lysophosphatidylcholine.

3.3.4 Ceramide metabolism pathways were enriched in differentiated NHEK

Bioactive lipid synthesis by differentiating keratinocytes is essential for the formation of the permeability barrier. Therefore, lipid metabolism pathways and keratinocyte differentiation gene expression were analysed using IPA[®] software. Core analysis was performed to filter the data based on a p value of 0.001. Canonical pathway analysis was then performed for a total of 3011 genes. Differentiated NHEK (High Ca²⁺, n=3) were compared to control (undifferentiated/proliferating) NHEK (Low Ca²⁺, n=3). Data were presented as log₂ fold change. Log₂ fold change of < -1 is considered downregulated, whereas a log₂ fold change of >1 is considered upregulated. The analysis is colour coded; genes in red shading are upregulated; genes in green shading are downregulated. The intensity of the shading reflects how high or low was the log₂ fold change is; example: darker shade red= higher log₂ fold change and upregulation. Grey shading= no change (-1 – 1).

3.3.4.1 Ceramide metabolism pathways and differentiation-regulating genes were enriched in differentiated NHEK

Figure 3.42 shows the pathways identified as being enriched (highly represented in the list of genes analysed) in differentiated NHEK when compared to proliferating NHEK. CER metabolism pathways were enriched and these include A) sphingosine and S1P metabolism, B) CER degradation and biosynthesis and C) SM metabolism. The pathways identified include genes involved in CER metabolism and keratinocyte differentiation. The function apoptosis was identified by IPA[®] as it is one of the most studied cellular processes regulated by CER signaling. However, the samples used (NHEK) and the genes included in these pathways, indicate keratinocyte differentiation as a cellular function regulated by CER as well.

Table 3.1 lists the genes included in the pathways identified and their description. All genes analysed were statistically significant with a corrected p value, also known as false discovery rate (FDR), of < 0.0001. The expression of the following genes was upregulated in differentiated NHEK when compared to proliferating NHEK (Log₂ fold change >1): EDG members *SIPR3* (1.5) and *SIPR4* (1.9); SPHK member *SPHK1* (2.4); RAS members: *MRAS* (1.6), *RAP1A* (1.2), *RASD2* (1.6),

RRAS2 (2.6); *ERK1* (1.2); P1K3 catalytic subunit B *PIK3CB* (1.3); PP2A catalytic subunits *PPP2CA* (2.3), *PPP2CB* (1.3), and regulatory subunits *PPP2R2B* (4.2), *PPP2R5B* (1.2); *JNK1/MAPK8* (1.13); *SMPD3* (4.6); TNF receptor subunits *TNFRSF1B* (3.9) and *TNFRSF6B* (2.0). The expression of the following genes was significantly downregulated in differentiated NHEK when compared to proliferating NHEK (Log2 fold change < -1): EDG member, *SIPR5* (-2.2); KSR members *KSRI* (-1.9) and *KSR2* (-1.3); *AP-1* (-2.6); PI3K members *PIK3C2G* (-3.0) and *PIK3RI* (-2.6); PP2A members *PPMIL* (-1.5) and *PPP2R2C* (-1.3).

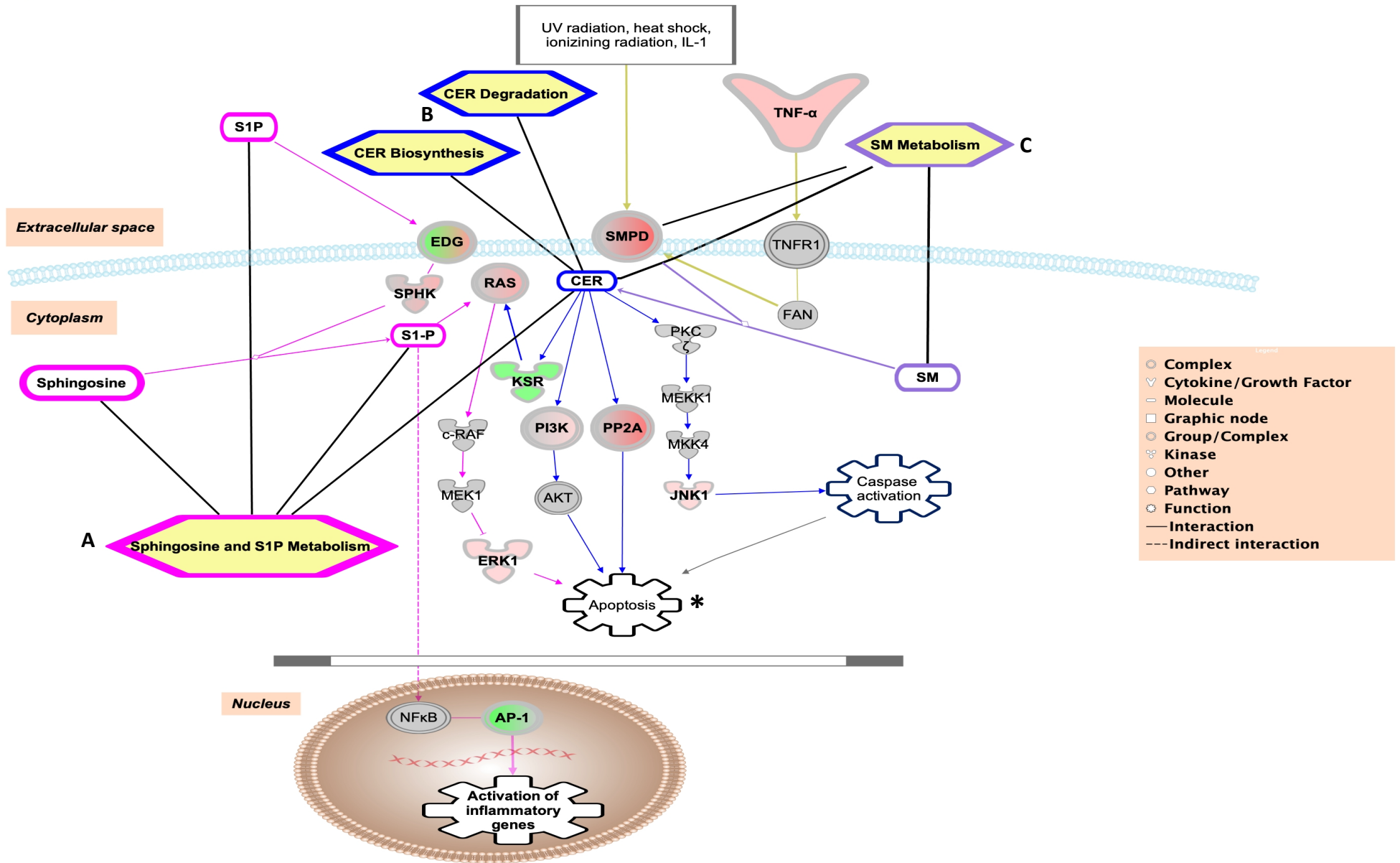


Figure 3.42 Ceramide metabolism pathways regulating keratinocyte differentiation were enriched in differentiated NHEK. Canonical pathway analysis was performed using IPA[®] software to identify enriched pathways in differentiated NHEK (High Ca²⁺, n=3) compared to proliferating NHEK (Low Ca²⁺, n=3). Statistical analysis was performed by IPA[®] software based on a p value and FDR of < 0.001, and a log2 fold change of < -1 for downregulated genes or >1 for upregulated genes. A) Sphingosine and S1P metabolism: This pathway involves CER, S1P and sphingosine. It regulates the following genes in NHEK: EDG complex, SPHK, NFkB, AP-1, KSR, RAS complex, c-RAF, MEK1, ERK1; B) Ceramide metabolism pathway which includes CER synthesis and degradation. CER signaling regulates the following genes in NHEK: PKC ζ, MEKK1, MKK4, JNK1, PP2A complex, PI3K complex, AKT, KSR; C) Sphingomyelin metabolism: This pathway produces SM and CER and is affected by TNF-α, SMPD complex. NHEK: normal human epidermal keratinocytes; CER: ceramide; SM: sphingomyelin; S1P: sphingosine 1 phosphate; EDG: endothelial cell differentiation gene; SPKH: Sphingosine kinase (human); RAS: Rat sarcoma gene group; c-RAF: RAF1-proto-oncogene, serine/threonine kinase; MEK1: Mitogen-activated protein kinase kinase 1; ERK1: Extracellular signal-regulated kinase; NFkB: Nuclear factor kappa B; AP-1: Activator protein-1 transcription factor; KSR: Kinase suppressor of Ras; PI3K: 1-phosphatidylinositol 3-kinase; AKT: Serine/Threonine Kinase 1; PP2A: Protein phosphatase 2; PKC ζ: Protein kinase C zeta; MEKK1: Mitogen-activated protein kinase kinase kinase 1; MKK4: Mitogen-activated protein kinase kinase 4; JNK1: c-Jun N-terminal kinase 1; SMPD: Sphingomyelin cholinephosphohydrolase; TNF-α: Tumor necrosis factor alpha; TNFR1: Tumor necrosis factor alpha receptor; FAN: Neutral sphingomyelinase activation associated factor; IL-1: Interleukin 1; UV: ultraviolet radiation; FDR: false discovery rate. *Cellular functions regulated by CER signaling include apoptosis and keratinocyte differentiation. Red shading: upregulation; Green shading: downregulation; Grey shading: no change.

Gene/group	Description	Members
<i>EDG</i>	Endothelial cell differentiation gene: S1P receptors	<i>SIPR2</i> , <i>SIPR3</i> , <i>SIPR4</i> , <i>SIPR5</i>
<i>SPHK</i>	Sphingosine kinase (human)	<i>SPHK1</i> , <i>SPHK2</i>
<i>RAS</i>	Rat sarcoma gene group	<i>KRAS</i> , <i>MRAS</i> , <i>NRAS</i> , <i>RALB</i> , <i>RAP1A</i> , <i>RAP1B</i> , <i>RAP2A</i> , <i>RAP2B</i> , <i>RASD1</i> , <i>RASD2</i> , <i>RRAS</i> , <i>RRAS2</i>
<i>c-RAF</i>	RAF1-proto-oncogene, serine/threonine kinase	<i>RAF1</i>
<i>MEK1</i>	Mitogen-activated protein kinase kinase 1	<i>MEK1</i> also known as (<i>MAPK1</i> , <i>MAP2K1</i> , <i>ERK2</i>)
<i>ERK1</i>	Extracellular signal-regulated kinase	<i>ERK1</i> (<i>MAPK3</i>)
<i>NFkB</i>	Nuclear factor kappa B	<i>NFkB</i> complex: <i>NFkB</i> subunit 1, <i>NFkB</i> subunit 2, <i>NFkB inhibitor zeta</i> , <i>NFkB activating protein like</i>
<i>AP-1</i>	Activator protein-1 transcription factor	<i>FOS</i> and <i>JUN</i> family
<i>KSR</i>	Kinase suppressor of Ras	<i>KSRI</i> , <i>KSR2</i> , <i>CNKSR</i>
<i>PI3K</i>	1-phosphatidylinositol 3-kinase	Catalytic and regulatory: <i>P110</i> , <i>p85</i> , <i>PI3K</i> , <i>PIK3C2A</i> , <i>PIK3C2B</i> , <i>PIK3C2G</i> , <i>PIKC3</i> , <i>PIK3CA</i> ,

		<i>PIK3CB</i> , <i>PIKECD</i> , <i>PIK3CG</i> , <i>PIK3R1</i> , <i>PIK3R2</i> , <i>PIK3R3</i> , <i>PIK3R4</i> , <i>PIK3R5</i> , <i>PIK3R6</i>
<i>AKT</i>	Serine/Threonine Kinase 1, protein kinase B	<i>AKT1</i> , <i>AKT2</i> , <i>AKT3</i>
<i>PP2A</i>	Protein phosphatase 2	<i>PPM1J</i> , <i>PPM1L</i> , <i>PPP2CA</i> , <i>PPP2CB</i> , <i>PPP2R1A</i> , <i>PPP2R1B</i> , <i>PPP2R2A</i> , <i>PPP2R2B</i> , <i>PPP2R2C</i> , <i>PPP2R3A</i> , <i>PPP2R5A</i> , <i>PPP2R5B</i> , <i>PPP2R5C</i> , <i>PPP2R5D</i> , <i>PPP2R5E</i> , <i>PTPA</i>
<i>PKC ζ</i>	Protein kinase C zeta	<i>PKC</i>
<i>MEKK1</i>	Mitogen-activated protein kinase kinase kinase 1	<i>MEKK1 (MAP3K1)</i>
<i>MKK4</i>	Mitogen-activated protein kinase kinase 4	<i>MKK4 (MAP2K4)</i>
<i>JNK1</i>	c-Jun N-terminal kinase 1	<i>JNK1 (MAPK8)</i>
<i>SMPD</i>	Sphingomyelin cholinephosphohydrolase	<i>SMPD1</i> , <i>SMPD2</i> , <i>SMPD3</i> , <i>SMPD4</i>
<i>TNF- α / TNFRI</i>	Tumor necrosis factor alpha/receptor 1	<i>TNFR</i> superfamily: <i>NGFR</i> , <i>TNFRSF11B</i> , <i>TNFRSF1A</i> , <i>TNFRSF1B</i> , <i>TNFRSF6B</i>
<i>FAN</i>	Neutral sphingomyelinase activation associated factor	<i>NSMAF</i>

Table 3.1 Genes involved in CER signaling pathways controlling differentiation and apoptosis. Genes involved in keratinocyte differentiation were upregulated in differentiated NHEK when compared to proliferating NHEK. NHEK: normal human epidermal keratinocytes; CER: ceramide. RED: upregulated; GREEN: downregulated.

3.3.5 The expression of ceramide, membrane lipids and fatty acid metabolism genes was altered with differentiation

Lipid metabolism gene expression was analysed in differentiated NHEK (High Ca²⁺, n=3) compared to proliferating NHEK (Low Ca²⁺, n=3) using IPA[®] software. Data are presented as log₂ fold change. Analysis of differentially expressed genes was based on a p value and FDR of < 0.001, and log₂ fold change of < -1 for downregulation and > 1 for upregulation. The genes included in the results graphs (3.43-3.45) were significantly changed (FDR < 0.0001).

3.3.5.1 Genes involved in S1P signalling, SPT activity and glucosylceramide metabolism were upregulated upon NHEK differentiation

Figure 3.43 shows the expression of CER metabolism genes in differentiated NHEK when compared to proliferating NHEK. Protein coding genes involved in S1P signaling and SPT activity were significantly upregulated in differentiated

NHEK when compared with proliferating NHEK. The most upregulated gene in differentiated NHEK was *S1PR1* (log₂ fold change 3.1) followed by SPT regulating-*SPTSSB* (log₂ fold change 2.6). Regarding the CER *de novo* biosynthesis pathway, genes encoding the SPT subunits 2 and 3 were upregulated with differentiation (*SPTLC2*, *SPTLC3*), whereas *CERS1* was downregulated. Glucosylceramide metabolism was stimulated in differentiated NHEK where glucosylceramide degradation gene *GBA* was significantly upregulated (log₂ fold change 2.4), followed by *GBA2* (log₂ fold change 2.2) and glucosylceramide synthesis *UGCG* (log₂ fold change 2.1). The expression of S1P receptor, *S1PR5*, was significantly downregulated in differentiated NHEK compared to proliferating NHEK (log₂ fold change -2.2). Additionally, the following S1P and CER degradation genes were downregulated in differentiated NHEK (*SGPP2*, log₂ fold change -1.7; *ACER1*, log₂ fold change -1.7, respectively). Genes not included in the figure were not significantly up/downregulated (log₂ fold change from -1 to 1).

CER metabolism gene expression

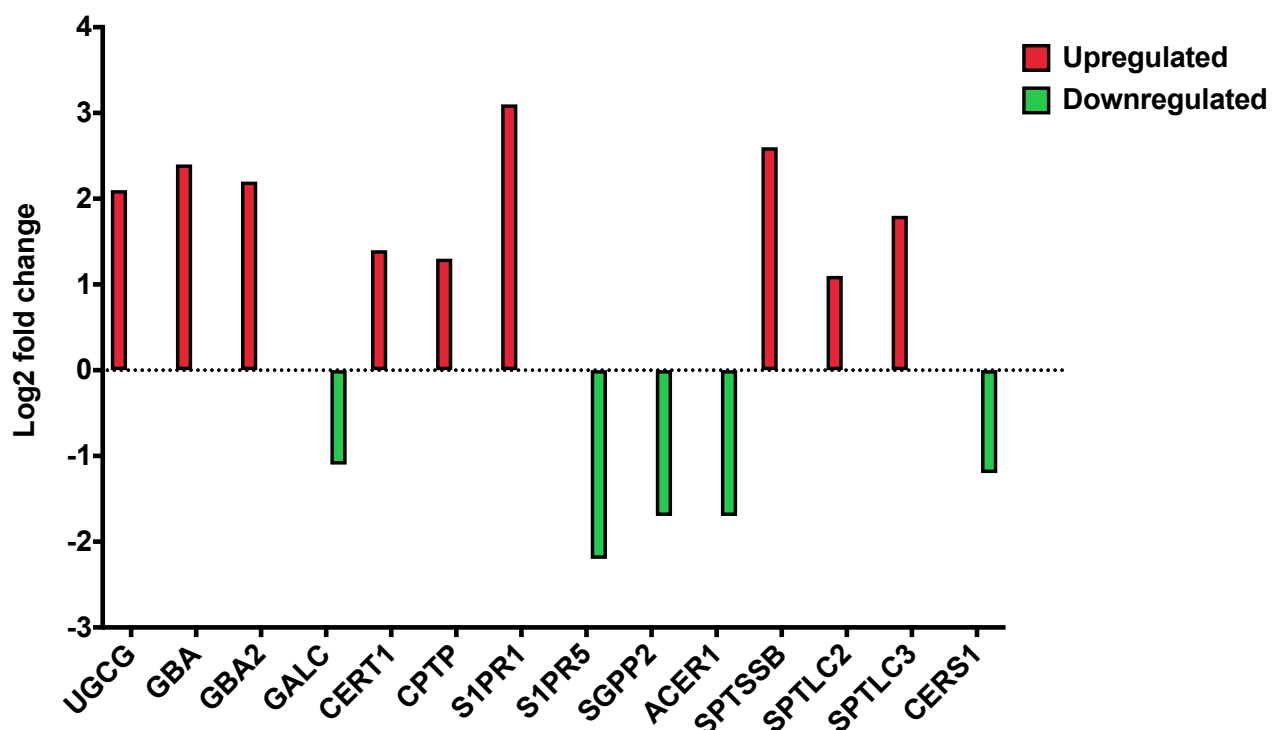


Figure 3.43 Ceramide metabolism gene expression in differentiated NHEK compared to proliferating NHEK. The expression of ceramide metabolism genes in differentiated NHEK (High Ca²⁺, n=3) and proliferating NHEK (Low Ca²⁺, n=3) were analysed by IPA[®] software. IPA[®] statistical analysis settings: p-value < 0.001, log₂ fold change < -1

downregulation, log₂ fold change > 1 upregulation. RED: upregulated; GREEN: downregulated. CER: ceramide; NHEK: normal human epidermal keratinocytes; UGCG: UDP-glucose ceramide glucosyltransferase; GBA: Glucosylceramidase beta; GBA2: Glucosylceramidase beta 2; GALC: Galactosylceramidase; CERT1: Ceramide transporter 1; CPTP: Ceramide-1-phosphate transfer protein; S1PR1, 5: Sphingosine-1-phosphate receptor 1, 5; SGPP2: Sphingosine-1-phosphate phosphatase 2; ACER1: Alkaline ceramidase 1; SPTSSB: Serine palmitoyltransferase small subunit B; SPTLC2, 3: Serine palmitoyltransferase long chain base subunit 2, 3; CERS1: Ceramide synthase 1.

3.3.5.2 DG and TG biosynthesis genes were highly expressed in differentiated NHEK whereas cholesterol degradation genes were downregulated

Figure 3.44 shows the expression of lipid metabolism genes in differentiated NHEK when compared to proliferating NHEK. The TG synthesis gene, *GPAT3*, was highly upregulated in differentiated NHEK (log₂ fold change 8.0). Other protein coding genes related to DG and TG synthesis were upregulated as well, and these include: *DGKB*, *DGKG* and *CDS1* (log₂ fold change 1.5, 1.3, 1.2, respectively). Protein coding *LPCAT1* which is involved in PC synthesis was upregulated in differentiated NHEK (log₂ fold change 1.5), whereas the expression of the isoform, *LPCAT2*, was downregulated (log₂ fold change -1.2). Regarding cholesterol metabolism, cholesterol degradation gene, *CH25H*, was significantly downregulated in differentiated NHEK compared to proliferating NHEK (log₃ fold change -3.5). Additionally, the expression of *DHCR24* and *CETP*, which are involved in cholesterol synthesis and lipid transport was low in differentiated NHEK. Genes not included in the figure were not significantly up/downregulated (log₂ fold change from -1 to 1).

Lipid metabolism gene expression

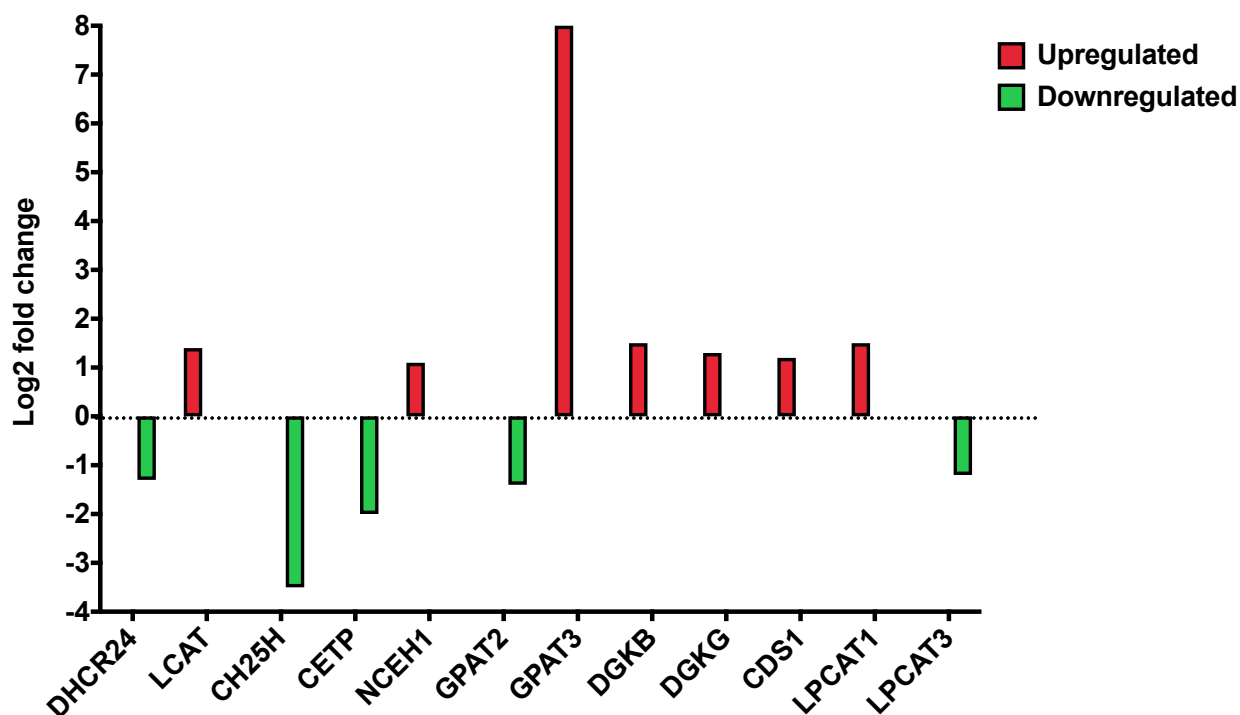


Figure 3.44 Sterol lipids, glycerolipid and glycerophospholipid metabolism gene expression in differentiated NHEK compared to proliferating NHEK. The expression of membrane lipid metabolism genes in differentiated NHEK (High Ca^{2+} , n=3) and proliferating NHEK (Low Ca^{2+} , n=3) were analysed by IPA[®] software. IPA[®] statistical analysis settings: p-value < 0.001, log2 fold change < -1 downregulation, log2 fold change > 1 upregulation. RED: upregulated; GREEN downregulated. CER: ceramide; NHEK: normal human epidermal keratinocytes; DHCR24: 24-dehydrocholesterol reductase; LCAT: Lecithin-cholesterol acyltransferase; CH25H: Cholesterol 25-hydroxylase; CETP: Cholesteryl ester transfer protein; NCEH1: Neutral cholesterol ester hydrolase 1; GPAT2: Glycerol-3-phosphate acyltransferase 2, mitochondrial; GPAT3: Glycerol-3-phosphate acyltransferase 3; DGKB: Diacylglycerol kinase beta; DGKG: Diacylglycerol kinase gamma; CDS1: CDP-diacylglycerol synthase 1; LPCAT1, 3: Lysophosphatidylcholine acyltransferase 1, 3.

3.3.5.3 Fatty acid biosynthesis genes were upregulated upon NHEK differentiation

Figure 3.45 shows the expression FA metabolism genes in differentiated NHEK when compared to proliferating NHEK. Genes encoding fatty acid elongation, desaturation and hydroxylation enzymes were upregulated in differentiated NHEK, except for the fatty acid elongase isoform, *ELOVL3* (log2 fold change -1.8). The expression of *ELOVL4* was the highest in differentiating NHEK (log2 fold change

3.1), followed by FA hydroxylase *FA2H* (log₂ fold change 2.7) and FA desaturase *FADS3* (log₂ fold change 2.1). *FABP7*, which encodes FA binding protein 7 was highly downregulated in differentiated NHEK (log₂ fold change -7.0). Genes not included in the figure were not significantly up/downregulated (log₂ fold change from -1 to 1).

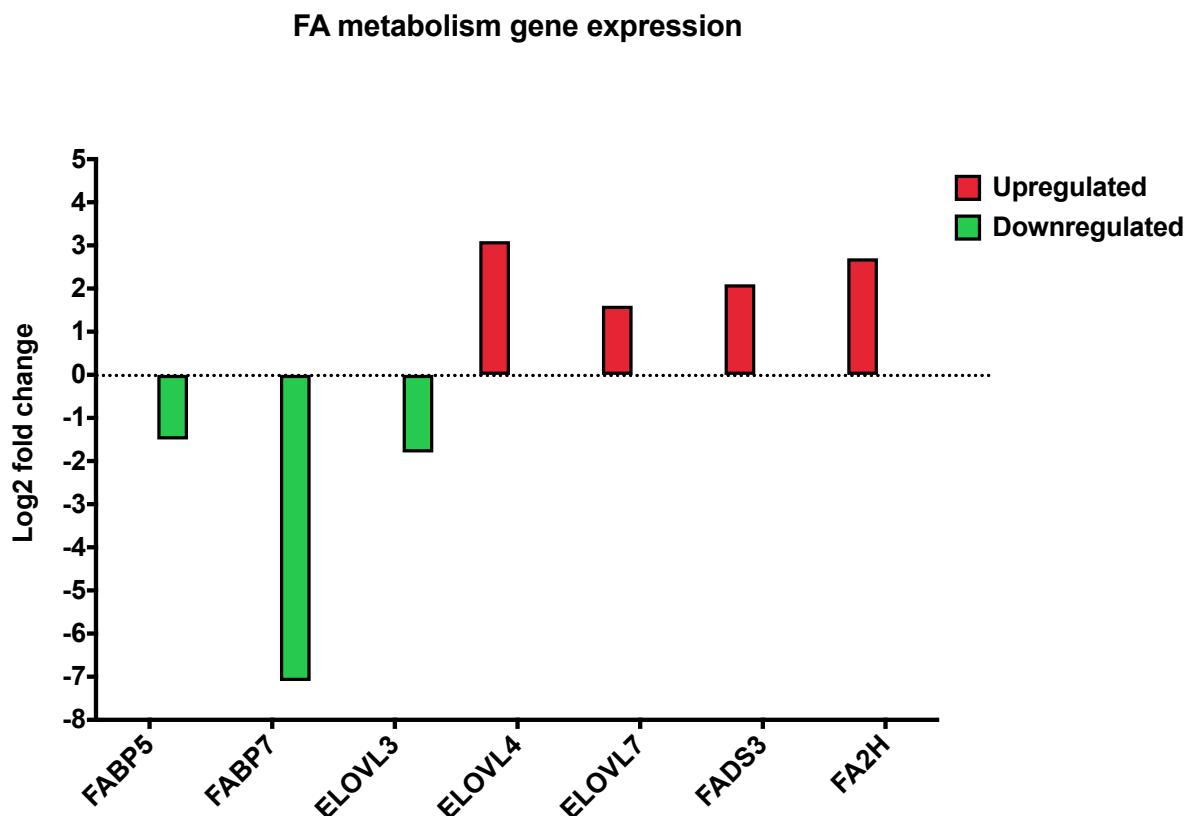


Figure 3.45 Fatty acid metabolism gene expression in differentiated NHEK compared to proliferating NHEK. The expression of fatty acid metabolism genes in differentiated NHEK (High Ca²⁺, n=3) and proliferating NHEK (Low Ca²⁺, n=3) were analysed by IPA[®] software. IPA[®] statistical analysis settings: p-value < 0.001, log₂ fold change < -1 downregulation, log₂ fold change > 1 upregulation. RED: upregulated; GREEN: downregulated. CER: ceramide; NHEK: normal human epidermal keratinocytes; FABP5, 7: Fatty acid binding protein 5, 7; ELOVL 3, 4, 7: Fatty acid elongase 3, 4, 7; FADS3: Fatty acid desaturase 3; FA2H: Fatty acid 2-hydroxylase.

3.4 Discussion

The study's objective was to investigate the pathways mediating PUFA regulation of CER synthesis in the epidermis, aiming to understand the mechanisms by which the *n*-3 and *n*-6 PUFAs can alter ceramide concentrations in normal human epidermal keratinocytes. During the differentiation process, proliferating keratinocytes migrate from the basal epidermal layers towards the SC, where they fully differentiate and release intracellular CERs that form the permeability barrier

together with cholesterol and FFAs (Lampe et al., 1983). Therefore, we aimed to investigate the effect of PUFA supplementation on CER levels at different stages of epidermal cell growth (proliferating vs differentiated). Exploring the barrier lipid profile using an *in vitro* cell culture system is a useful investigative tool as it can be manipulated to reflect the stages of keratinocyte differentiation using different concentrations of Ca^{2+} (Breiden et al., 2007b). Initiating NHEK differentiation *in vitro* with Ca^{2+} has been found to increase CER levels when compared to CER levels in undifferentiated cells (Breiden et al., 2007b). In agreement with this study, more CER species were detected and higher CER concentrations were measured in differentiated NHEK compared to proliferating NHEK (**Figure 3.1**). The alterations in CER[NP] and CER[AP], that were detected were consistent with previous observations regarding changes in CER production with keratinocyte differentiation (Mizutani et al., 2004). More CER[NP] species were detected with differentiation, and CER[AP] was only detected in differentiated NHEK (**Figure 3.9, 3.10, 3.15**). In addition to this, CER *de novo* synthesis enzymes were highly expressed in differentiated NHEK, where SPT catalytic subunits, *SPTLC2* and *SPTLC1*, were highly expressed in differentiated cells in addition to SPTSSB, which is involved in SPT activity and acyl-CoA preference (**Figure 3.43**). These findings demonstrate the abundance of CERs with the gradual increase in the Ca^{2+} gradient in the skin reaching the CER-rich SC where keratinocytes are fully differentiated.

The production of CER is stimulated with keratinocyte differentiation and CER signaling regulates differentiation (Uchida, 2014). Additionally, differentiating keratinocytes with Ca^{2+} has been found to activate differentiation pathways such as c-Raf/ ERK1/2 (Schmidt et al., 2000). Gene sequencing analysis showed CER signaling pathways which regulate differentiation to be highly represented in Ca^{2+} -differentiated NHEK (**Figure 3.42**). This study showed the regulation of genes involved in keratinocyte differentiation pathways such as ERK1/2 MAPK pathway, JNK signaling pathway and p38 MAPK pathway by S1P, CER and SM signaling (Meng et al., 2018). For example, S1P was found to activate keratinocyte differentiation by binding to S1P receptors (Igawa et al., 2019). The signaling pathways activated depend on the S1P receptor isoform and cell type. In the current study, S1P was found to be involved in the RAS/ERK1/2 pathway (**Figure 3.42 A**).

Additionally, *KSR* which inhibits the RAS/ERK1/2 pathways was downregulated. CER could produce S1P and was involved in the PI3K pathway as well (**Figure 3.42 B**). The S1P receptor, *SIPRI*, was highly expressed in differentiated NHEK (**Figure 3.43**). In endothelial cells, *SIPRI* was found to be associated with regulating the PI3K pathway (Igawa et al., 2019). *PPA2* was another gene that were upregulated in differentiated NHEK and associated with CER signaling. This gene plays a major role in filaggrin production and was found to be blocked in cultured keratinocytes from harlequin ichthyosis patients (KAM et al., 1997). Similarly, pathway analysis showed that CER was associated with the upregulation in *JNK1* which is involved in the expression of cornified envelope protein, cystatin A (Takahashi et al., 2001). From this, the involvement of CER signaling in regulating NHEK differentiation is clear.

In addition to demonstrating the difference in CER profile seen at different stages of epidermal cell growth, analysis of the individual effects of DHA, EPA and LA supplementation on CER concentration in the two epidermal cell types was performed. **Figure 3.46** summarises the main findings. Interestingly, we found that LA supplementation significantly affected differentiated NHEK where CER[NDS], CER[NS] and CER[NP] levels were increased. On the other hand, DHA supplementation had the same effect on both developmental stages of epidermal cells, where it significantly increased the concentrations of CER species from most CER classes. DHA significantly enhanced the levels of the most abundant CERs where total CER[NS] was significantly increased in both proliferating and differentiated NHEK, in addition to several CER[NS] species (**Figure 3.2-3.4**). The physiological significance of the CER species that were affected by DHA and LA is not understood as the role of specific CER species has not been fully explored (Kendall et al., 2017, Takeda et al., 2018). However, one way to interrogate this further is by grouping CERs based on total carbon-chain length, as skin CERs with long chains are crucial for a healthy barrier (Jennemann et al., 2012, Janssens et al., 2012). Interestingly, longer-chain CERs were found in the differentiated cells where they ranged from C38-C52, whereas the C48 chain was the longest in proliferating cells. Moreover, DHA had a stronger effect on proliferating cells where it increased C41 ($p=0.05$) and C43 ($p=0.06$) levels. In differentiated cells,

DHA only increased C38 CERs ($p=0.002$), whereas LA did not have a significant effect CER total chain length in both cell types (**Figure 3.16**).

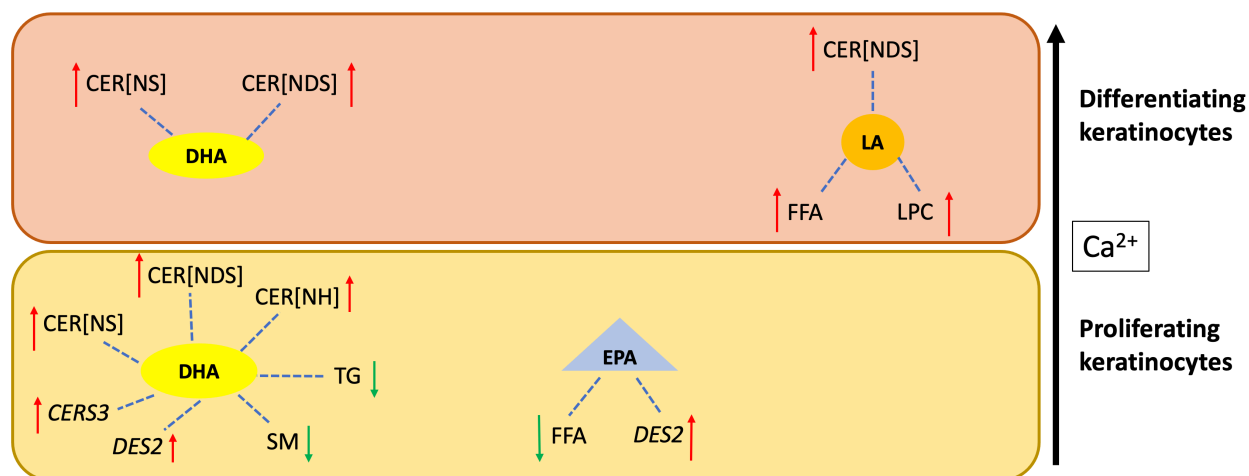


Figure 3.46 Summary of PUFA treatment effects on lipid metabolism in NHEK. The figure summarises the main increases and decreases found in CER and membrane lipid levels, in addition to CER biosynthesis mRNA expression measured in differentiating NHEK (High Ca²⁺, n= 3 donors), and proliferating NHEK (Low Ca²⁺, n= 3 donors) treated with DHA, EPA and LA (10 μ M) compared to control. Ceramides and membrane lipids were measured using UPLC-MS/MS; CER biosynthesis enzyme gene expression was measured by RT-qPCR. NHEK: normal human epidermal keratinocytes; Ca²⁺: calcium; PUFA: polyunsaturated fatty acid; DHA: docosahexaenoic acid; EPA: eicosapentaenoic acid; LA: linoleic acid; CER: ceramide; CER[NS]: non-hydroxy ceramide; CER[NDS]: non-hydroxy dihydroceramide; CER[NH]: non-hydroxy 6-hydroxyceramide; *CERS3*: ceramide synthase 3; *DES2*: dihydroceramide desaturase 2; FFA: free fatty acids; SM: sphingomyelin; TG: triacylglycerol; LPC: lysophosphatidylcholine.

To better understand where in the CER biosynthesis pathway PUFAs are having an effect on CER levels, alterations in the two chains that form CERs (the FA and sphingoid base-chains) were investigated along with changes in CER *de novo* biosynthesis enzyme gene expression. As previously explained in (**Chapter 1**), newly synthesised CERs are produced through the *de novo* pathway from CER[NDS]. The rate-limiting enzyme, SPT, produces dihydrosphingosine, then CerS1-6 acylate FA-chains with specific carbon numbers to produce the CER precursor, CER[NDS] (**Figure 1.4**) (Mullen et al., 2012). DHA altered base-chain length in proliferating cells, which reflects dihydrosphingosine production and SPT activity (**Figure 3.17**). Additionally, alterations in FA-chains were observed in proliferating cells with DHA supplementation, and included those ranging from C18-C25 (**Figure 3.18**). Interestingly, we found a significant upregulation in gene expression of epidermis-specific CerSase, *CERS3*, ($p=0.003$) in proliferating

NHEK with DHA (**Figure 3.19**). The FA preference of CerS3 includes chains with medium (C18-C21) and long (C22-C25) carbon chains (Mizutani et al., 2004). Moreover, both n-3 PUFAs (DHA and EPA) significantly upregulated DES2 expression in proliferating cells (**Figure 3.20**). In addition, it has been suggested that CER[NH] is potentially synthesised by a desaturase similar to *DES2* (Kovacic et al., 2014). Consistent with this, DHA supplementation had a significant effect on CER[NH] concentration, and led to a close to significant increase in N(24)P(18) ($p=0.06$) in proliferating NHEK. (**Figure 3.7, 3.9**). These initial observations show that proliferating NHEK are more responsive to the n-3 PUFA, DHA, and the effect of DHA on CER metabolism in these cells are likely mediated through activation of the *de novo* biosynthesis pathway.

Dysregulation in membrane lipid metabolism has been reported in inflammatory skin disorders such as AD and psoriasis (Schäfer and Kragballe, 1991, Gerstein, 1963). Gene sequencing analysis showed an upregulation in the expression of TG biosynthesis gene, *GPAT3* in differentiated NHEK (**Figure 3.44**). *GPAT3* is expressed in the epidermis and in keratinocytes and was found to be upregulated with treatment with PPAR γ activators (Lu et al., 2010). Furthermore, treating immortalised keratinocytes with betulin, an anti-inflammatory and epidermal differentiating agent, has been found to alter membrane lipid profile where CEs and TGs were significantly downregulated, whereas glycerophospholipids, diacylglycerides and CER were upregulated in betulin treated cells (Calderón et al., 2020). Similarly, reducing dietary EPA and DHA was found to alter epidermal phospholipid and sphingolipid profile in salmon skin (Cheng et al., 2018). Therefore, examining changes in epidermal membrane lipids could help further explain how PUFAs could modulate cutaneous lipid metabolism. Interestingly, consistent with the CER data, DHA mainly affected membrane lipids in proliferating cells, whereas LA mainly affected those in differentiated cells.

In proliferating NHEK, there was a decrease in SM 42:2 ($p=0.03$) as well as in total TG ($p=0.04$) and in most TG species levels with DHA treatment (**Figure 3.30, 3.35**). DHA supplementation also decrease CE and proapoptotic PC and LPC levels in proliferating cells, but the changes did not reach statistical significance. In addition to the role of CerSases in the CER *de novo* biosynthesis pathway, these

enzymes are involved in generating CERs via the salvage pathway by utilising free sphingoid bases (**Figure 1.4**). CERs could also be released from SM or glucosylceramide degradation. Therefore, the decrease in SM together with the upregulation in *CERS3* in proliferating cells with DHA supplementation could be an indication for a mechanism by which DHA targets CER synthesis in the basal epidermis by utilizing SM. Additionally, SM contains CER[NS] and CER[AS] species (Holleran et al., 1993), which we found to be increased in proliferating NHEK with DHA treatment. Taken together, this could suggest an upregulation in CER levels in proliferating NHEKs with DHA through the breakdown of SM. In addition to this, the decrease in proapoptotic glycerophospholipids and energy producing glycerolipids in proliferating cells with DHA could reflect the anti-inflammatory effect of *n*-3 PUFA, and suggest a proliferative effect on the basal layers of the epidermis where these membrane lipids are utilized for cellular growth. It has been found that CER synthesis and the activity of CER-related enzymes depend on the type of tissue and its stage of development (Mullen et al., 2012).

Although DHA stimulated CER synthesis in differentiated NHEK, no effect on *CERS de novo* biosynthesis enzymes, FA-chain and base-chain length was observed. Additionally, the significant increase in CER[NS] and CER[AS] in differentiated cells with DHA was not accompanied with changes in SM or other membrane lipids. Furthermore, an increase in the concentration of CERs from most classes with alterations in the sphingoid-base chains could suggest a role for SPT. However, we did not observe changes in the sphingoid-base chains in differentiated NHEK with DHA. Therefore, in differentiated cells, DHA could be targeting alternative pathways to those of the *CER de novo* and SM recycling pathways. Similarly, LA mainly enhanced non-hydroxy CER levels in differentiated cells, with no changes in CER carbon-chains. Interestingly, LA supplementation showed a trend for a gradual mRNA downregulation of the epidermal *de novo* biosynthesis enzymes, *CerS3* and *Des2*, with time in differentiated NHEK (**Figure 3.21, 3.22**). In addition to this, LA did not have a significant effect on CER[AS] levels in differentiated NHEK and no change was found in SM levels. The precursors for the majority of SC CERs are SMs and glucosylceramides, which are converted back to CER by SMase and GBA, respectively (Uchida et al., 2000, Holleran et al., 1994). SM produces CER[NS] and CER[AS] species, whereas LA-containing omega-

hydroxy CERs are produced from glucosylceramides (Holleran et al., 1993, Uchida et al., 2000). Therefore, glucosylceramide degradation could be activated with LA treatment during keratinocyte differentiation.

Moreover, previous studies and the present study showed that glucosylceramide synthesis is stimulated during differentiation of keratinocytes (Sando et al., 1996). The present study showed *UGCG*, a protein coding gene involved in glucosylceramide synthesis, to be upregulated in differentiated NHEK (**Figure 3.43**). Additionally, ceramide synthesis from glucosylceramide was found to be stimulated in differentiated NHEK where *GBA* was significantly upregulated (Lu et al., 2010). In agreement with this, glucosylceramide degradation genes *GBA* and *GBA2* were highly expressed in differentiating NHEK (**Figure 3.43**). LA is used to differentiate keratinocytes; administration of a high dose of LA (15 μ M) to NHEKs cultured in low CaCl_2 (0.03 mM) media upregulates involucrin and transglutaminase gene and protein expression (Hanley et al., 1998). Similarly, the addition of LA (10 μ M) to high- Ca^{2+} medium resulted in a significant increase in differentiation markers and *GBA*, whereas *SPTLC2* was not affected (Breiden et al., 2007b). Breiden et al. also reported that administration of PPAR- α activator, LA, to the differentiation media led to a further increase in CER synthesis when compared to CER levels in differentiated NHEK without LA (Breiden et al., 2007b). Moreover, we found that LA significantly increased proapoptotic, LPC 16:0, and FFA18:2 species in differentiated cells ($p=0.04$, $p=0.008$, respectively). Similarly, gene sequencing analysis showed an increase in the expression of *LPCAT1* which catalyses the breakdown of LPC to PC, and fatty acid metabolism genes *ELOVL4*, *ELOVL7*, *FADS3* and *FA2H* in differentiated NHEK (**Figure 3.44, 3.45**). This could indicate a role for LA in epidermal growth and differentiation by stimulating FA and membrane lipid synthesis, in addition to SC CER production from glucosylceramide.

In addition to the role of *n*-6 PUFA LA in the differentiation process, activation of PPAR- α with DHA treatment was found to upregulate filaggrin expression, but not that of involucrin or loricrin, and to normalise SC lipid ratio (FFA:CER:cholesterol) in a filaggrin deficient mouse skin model, indicating a role for DHA in inducing

keratinocyte differentiation (Wallmeyer et al., 2015). Another study mentioned that activating PPAR- α using strawberry seed extract (SSE) upregulated *SPTLC2*, *CERS3*, and *GBA*, but not SM metabolism related genes in SC of skin equivalents (Takeda et al., 2018). The studies on the effect of DHA on keratinocyte differentiation and CER production are limited. However, it could be concluded that alterations in CER synthesis reported in differentiation studies depend on the PPAR- α activator and sample type. In our study, since DHA had a broad effect on CER concentration in differentiated NHEK, without affecting *CERS3* expression, CER carbon-chains and membrane lipid metabolism, alteration in CER synthesis could be due to activation of *GBA* through PPAR- α . From this, it could be shown that *n*-3 and *n*-6 PUFA play a crucial role in modulating the epidermal differentiation process, and ultimately the biosynthesis of permeability barrier CERs.

3.5 Conclusion

This study examined potential PUFA-CER mechanisms involving the CER *de novo* biosynthesis pathway in primary human epidermal skin cells. The individual effects of *n*-3 (DHA, EPA) and *n*-6 (LA) PUFA supplementation on CER biosynthesis in different layers of epidermal growth have been demonstrated independently. In proliferating NHEK, which represent the basal layers, DHA increased the concentration of most CER classes, and was paralleled by an upregulation in *CERS3* and *DES2* gene expression and a reduction in SM and membrane lipid levels. This could suggest that DHA stimulates CER synthesis in proliferating NHEK through activating the CER *de novo* biosynthesis and SM recycling pathways. In differentiated NHEK, which represents the granular layer, gene sequencing analysis demonstrated the role of CER signaling in keratinocyte differentiation. Additionally, genes involved in CER biosynthesis through SPT and glucosylceramide metabolism were highly expressed in differentiated NHEK, in addition to FA and TG synthesis genes. DHA might affect CER metabolism in differentiated NHEK through pathways linked to differentiation which activate *GBA*, as the increase in CER levels was not accompanied by changes in *CERS* gene expression, SM and membrane lipid metabolism. This shows that the biomolecular mechanisms by which DHA modulates CER synthesis differs according to the

developmental stage of the epidermis. On the other hand, supplementation with LA mainly affected the differentiated cells, by increasing non-hydroxy CER concentrations, without affecting CER *de novo* biosynthesis enzymes or SM levels, suggesting a specific role for *n*-6 LA in pathways involved in SC glucosylceramide and differentiation. From this, it could be shown that DHA and LA mainly target the CER generating pathways. In addition, LA is essential for improving skin barrier function, whereas DHA may have a broader therapeutic benefit in the epidermis as it could affect CER metabolism at basal and differentiated epidermal layers. Future studies could focus on exploring the effect of DHA on the SM degradation pathways in proliferating keratinocytes, and on the effect of DHA and LA supplementation on glucosylceramide metabolism in differentiated NHEK. In addition, the role of DHA in keratinocyte differentiation requires further investigation.

Chapter 4

**The effect of DHA, EPA and LA
supplementation on ceramide biosynthesis in
primary human dermal fibroblasts**

4.1 Introduction

The intermediate layer of the skin, the dermis, contains heterogeneous fibroblast populations that produce ECM proteins, nerve endings, immune cells and a vascular network, which support the integrity of the skin and keratinocyte growth (Russo et al., 2020). Reticular fibroblasts are mainly involved in wound healing, where they migrate towards the wound site and differentiate into myofibroblasts, followed by a second migration to release collagen, which leads to the formation of scars (Sorrell and Caplan, 2004). In addition to their role in supporting the epidermis and keratinocyte growth, it has been suggested that papillary fibroblasts are involved in the later stages of wound healing (Sorrell et al., 2004, Woodley, 2017, Griffin et al., 2020). Additionally, dermal immune cells and lipid mediators are tightly involved in the cutaneous inflammatory response and resolution (Hawkshaw et al., 2020). As in the epidermis, the dermis contains lipids such as sterols, FAs, CERs and phospholipids, but are found in lower concentrations than those in the epidermis (Uchida et al., 1988). The lower lipid content in the dermis is reflected by the limited number of studies on the role of dermal lipids and their metabolites in skin health and disease, (Kendall et al., 2015). Moreover, although the involvement of cutaneous lipids and their mediators in wound healing (Shakespeare and Strange, 1982, Balazs et al., 2001) and skin inflammation (Nicolaou et al., 2011) has been reported in several studies, results primarily depended on the presence of the lipid-rich epidermis and epidermal-dermal interaction. Therefore, little is known about the individual pathophysiological mechanisms which dermal lipids may be involved in.

Two of the main lipid classes involved in skin inflammation are CERs and PUFA. Ceramides are one of most crucial bioactive lipids implicated in cutaneous homeostasis and disease as discussed in (**Section 1.3**). The role of *n*-3 and *n*-6 PUFA and their mediators in inflammation and wound healing has also been extensively reviewed (Pilkington et al., 2011, Kendall and Nicolaou, 2013). Research on dermal lipids in the absence of the epidermis has gained more interest to elucidate the role of the dermis in skin health and disease. It was found that treating HDF with DHA reduced the mRNA expression of profibrotic factors after stimulating inflammation by lipopolysaccharide treatment (LPS) (Maeshige et al.,

2019). In a study on hypertrophic scar (HS) formation using deepithelialised normal and HS dermis, it was found that *n*-6 AA, which produces inflammatory mediators, was significantly higher in whole tissue and cell membrane of HS dermis, suggesting its role in the formation and maintenance of HS (Nomura et al., 2007). Our laboratory group previously found that *n*-3 EPA altered CER profile in human skin explants, where CER[NS] and CER[NDS] levels were increased in the dermis but not in the separated epidermis (Kendall et al., 2017). Our aim from the present study was to further examine the potential mechanisms involved in lipid metabolism in the dermis independently, showing the individual effects of *n*-3 (DHA, EPA) and *n*-6 (LA) PUFA supplementation on CER concentrations, CER *de novo* biosynthesis gene expression and membrane lipid levels in cultured HDF.

Specific objectives:

To determine the effects of DHA, EPA and LA treatment on:

1. Fibroblast CER profile and concentrations,
2. gene expression of CER *de novo* biosynthesis enzymes,
3. the profiles of complex membrane lipids (cholesterol, FAs, SM, glycerolipids and glycerophospholipids) in HDF.

4.2 Materials and methods

4.2.1 Analysis of fibroblast ceramides using UPLC/ESI-MS/MS

Fibroblast CER analysis was performed using ultraperformance liquid chromatography coupled to electrospray ionisation with triple quadrupole tandem mass spectrometry (UPLC/ESI-MS/MS) (**Section 2.4**). HDF were treated with 10 μ M DHA, EPA or LA, for three and seven days. Media were replaced daily with fresh media containing 10 μ M DHA, EPA or LA. PUFA treatments were prepared as described in (**Section 2.2.3**). Cells were pelleted at three and seven days post-PUFA treatment and CERs were extracted then analysed. CER concentrations in treated cells were compared to those in DMSO vehicle controls from the same time-point (n=3 individual donors) per time-point. **Appendix 3** lists the MRM transitions and indicative retention times for skin CER assay. Data were processed using MassLynx software (Waters). Semi-quantitation using internal standards was used for ceramides. Ceramide quantities were normalised to cell number (ng/ 10^6 cells).

Statistical analysis was performed using repeated measures One-Way ANOVA comparing differences over treatment compared with control of the same time-point, with corrections for multiple analyses using the Dunnett method. Data were presented as mean \pm SD; $p < 0.05$ was considered statistically significant (GraphPad Prism software). The small sample number ($n = 3$ biological replicates) could affect statistical significance. Therefore, p values that were not statistically significant but close to 0.05 were reported.

4.2.2 Measurement of ceramide biosynthesis enzyme mRNA levels

Gene expression was measured by RT-qPCR analysis as described in (section 2.3). Primary HDF were treated with 10 μ M DHA, EPA or LA. PUFA treatments were prepared as described in (Section 2.2.3). Media were replaced daily with fresh media containing 10 μ M DHA, EPA or LA, and cells were pelleted at six, 24 and 48 hours post PUFA-supplementation. Data were presented as individual Δ Ct values (Appendix 5) and relative fold increase (RFI) which compares CER biosynthesis enzyme gene expression in treated cells to that in DMSO vehicle controls of the same time-point where RFI of (1) is no change; ($n = 3$ individual donors). Statistical analysis was performed using repeated measures Two-Way ANOVA comparing changes with treatment and time. Corrections for multiple analyses was performed using the Dunnett method. Data were presented as mean \pm SD; $p < 0.05$ was considered statistically significant (GraphPad Prism software).

4.2.3 Analysis of complex membrane lipids using UHPSFC-MS^E

Complex lipids were analysed using UHPSFC-MS^E system by Dr Marta Koszyczarek (Section 2.5). Samples and PUFA treatments were prepared as described above (4.2.1). Complex lipid concentrations in treated cells were compared to those in DMSO vehicle controls of the same time-point; ($n = 3$ individual donors) for each time-point. Data were processed using Progenesis QI software (v 2.3, NonLinear Dynamics, Newcastle, UK). Lipid quantities were normalised to cell number (μ g/ 10^6 cells). Statistical analysis was performed using repeated measures One-Way ANOVA comparing differences over treatment compared with control of the same time-point, with corrections for multiple

analyses using the Dunnett method. Data were presented as mean \pm SD; $p < 0.05$ was considered statistically significant (GraphPad Prism software).

4.3 Results

4.3.1 Supplementation with DHA and EPA for seven days significantly increased ceramide concentrations in primary HDF

The effect of *n*-3 PUFAs (DHA, EPA) and *n*-6 PUFA (LA) on CER levels was analysed using UPLC/ESI-MS/MS. Primary HDF were treated with PUFA for three or seven days. For each sample analysed, concentrations of detected CER species were reported as absolute values in ng/10⁶ cells (mean \pm SD). Data were categorised based on ceramide class and carbon chain numbers to help identify possible trends.

4.3.1.1 Total ceramide levels were increased in HDF cultured for seven days

The amounts of individual ceramide species were quantitated and totalled. **Figure 4.1** shows the concentrations (ng/10⁶ cells) for total CER measured in HDF cultured for three and seven days. Control cells cultured for seven days produced more CERs than those cultured for three days ($p = 0.03$), with a total CER concentration of (mean = 24.36 ng/10⁶ cells) in the 7-day group and (mean = 8.78 ng/10⁶ cells) in the 3-day group.

4.3.1.2 Total CER[NS] levels were increased with DHA treatment for three days

Changes in total ceramides per class were analysed to investigate the effect of PUFA supplementation on the different classes of ceramides that are produced using specific enzymes in the *de novo* biosynthesis pathway. Five CER classes were detected in HDF: CER[NS], CER[NDS], CER[NH], CER[NP] CER[AH]. The most abundant ceramides in both groups were the CER[NS] (3-days: mean = 4.36 ng/10⁶ cells, 7-days: mean = 13.09 ng/10⁶ cells).

Although no significant change was found in total CER levels, examining individual CER classes revealed a trend for an increase in total CER[NS] 7-days post DHA and LA treatment compared with control ($p = 0.05$, $p = 0.08$, respectively) (**Figure 4.2**).

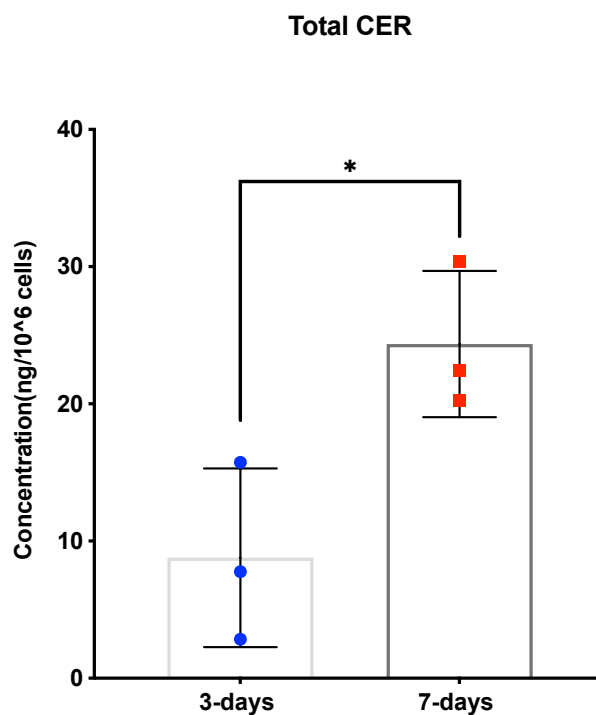


Figure 4.1 Total ceramide concentration in control HDF cultured for three and seven days. Total ceramide was measured using UPLC/ESI-MS/MS in HDF cultured for three or seven days. Data are presented as absolute concentration in ng/10⁶ cells (mean \pm SD). Comparisons were performed between HDF cultured for three days (n=3 donors) and HDF cultured for seven days (n=3 donors). Data were analysed by Student's t-test. CER: ceramide; HDF: human dermal fibroblast.

Total ceramide per class

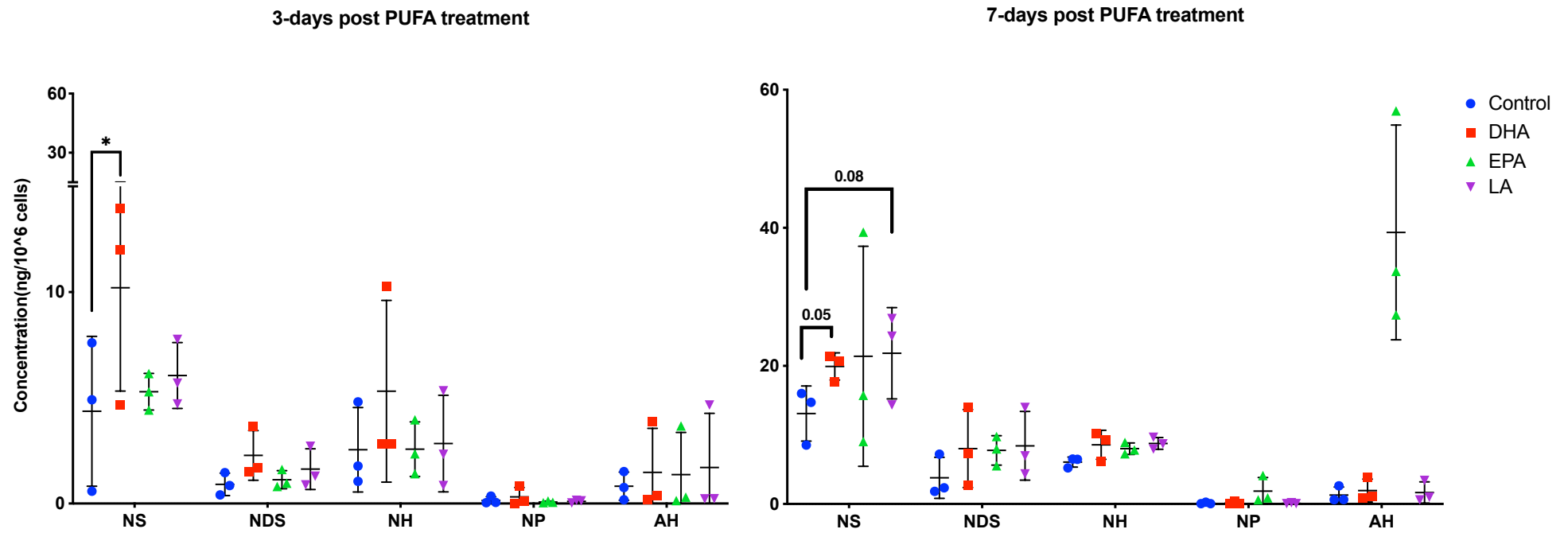


Figure 4.2 The effect of PUFA supplementation on total ceramide levels per class in HDF. Total ceramide classes were measured using UPLC/ESI-MS/MS in HDF treated with 10 μ M DHA, EPA and LA for three or seven days. Data are presented as absolute concentration in ng/10⁶ cells (mean \pm SD). Comparisons were performed between the control and PUFA treated cells of the same time point; (n=3 donors) per time-point. Data were analysed by One-Way ANOVA

comparing differences over treatment compared with control, with corrections for multiple analyses using the Dunnett method; *p <0.05. PUFA: polyunsaturated fatty acid; HDF: human dermal fibroblast; DHA: docosahexaenoic acid; EPA: eicosapentaenoic acid; LA: linoleic acid; NS: non-hydroxy ceramide; NDS: non-hydroxy dihydroceramide; NH: non-hydroxy 6-hydroxyceramide; NP: non-hydroxy phytoceramide; AH: alpha-hydroxy 6-hydroxyceramide.

4.3.1.3 Treatment with DHA or EPA for seven days significantly increased the concentration of several CER[NS], CER[NH] and CER[AH] species

Class specific species were analysed to observe possible trends in skin CER metabolism in HDF. Generally, *n*-3 PUFA significantly increased CER levels with the longer treatment period of seven days when compared with controls. Increases with *n*-6 LA did not reach statistical significance.

Most CER[NS] species were significantly increased with DHA treatment for seven days

A total of eight CER[NS] species were detected in HDF (**Figure 4.3**). The small sample number ($n = 3$ biological replicates) could affect statistical significance. Therefore, *p* values that were not statistically significant but close to 0.05 were reported. DHA significantly increased N(24)S(17) ($p = 0.02$), N(23)S(18) ($P = 0.04$), N(24)S(18) ($p = 0.047$), N(24)S(19) ($p = 0.004$) when compared with control, whereas the increase in N(24)S(16) and N(25)S(18) was close to significant ($p = 0.06$, $p = 0.07$, respectively). At three days post DHA, the most abundant CER[NS] species, N(24)S(18), were significantly increased ($p = 0.03$). LA increased the concentrations of N(22)S(18), N(23)S(18) and N(24)S(18) without reaching statistical significance ($p = 0.08$, $p = 0.08$, $p = 0.05$, respectively).

No significant changes were found in CER[NDS] species levels with PUFA

Figure 4.4 shows the eight CER[NDS] species detected in HDF. Although no significant changes were detected with PUFA treatment, DHA seemed to increase N(22)DS(18) ($p = 0.06$) after three days of treatment, whereas there was a trend for an increase in N(22)DS(18) and N(18)DS(22) ($p = 0.09$, $p = 0.06$) at seven days post EPA-supplementation when compared with control.

CER[NS] species

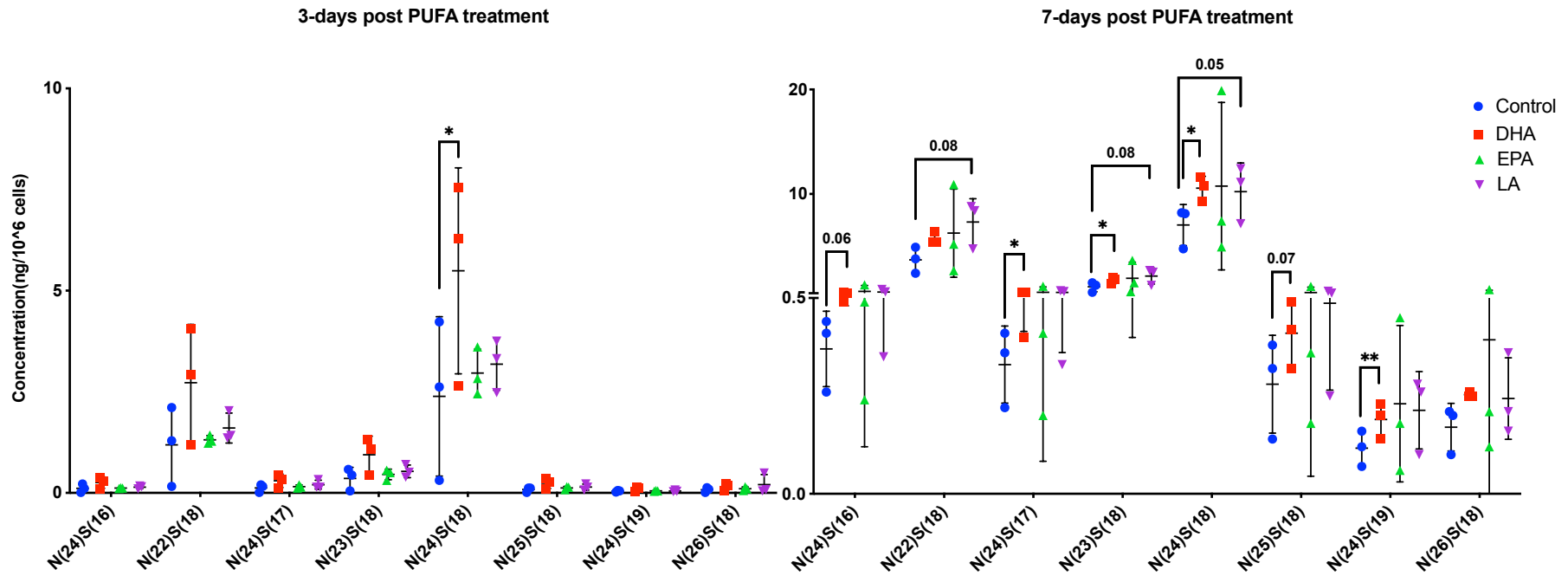


Figure 4.3 The effect of PUFA supplementation on CER[NS] species levels measured in HDF. Ceramides were measured using UPLC/ESI-MS/MS in HDF treated with 10 μ M DHA, EPA and LA for three or seven days. Data are presented as absolute concentration in ng/10⁶ cells (mean \pm SD). Comparisons

were performed between the control and PUFA treated cells of the same time point; (n=3 donors) per time-point. Data were analysed by One-Way ANOVA comparing differences over treatment compared with control, with corrections for multiple analyses using the Dunnett method; *p <0.05; **p <0.01. PUFA: polyunsaturated fatty acid; HDF: human dermal fibroblast; DHA: docosahexaenoic acid; EPA: eicosapentaenoic acid; LA: linoleic acid; CER: ceramide; NS: non-hydroxy ceramide.

CER[NDS] species

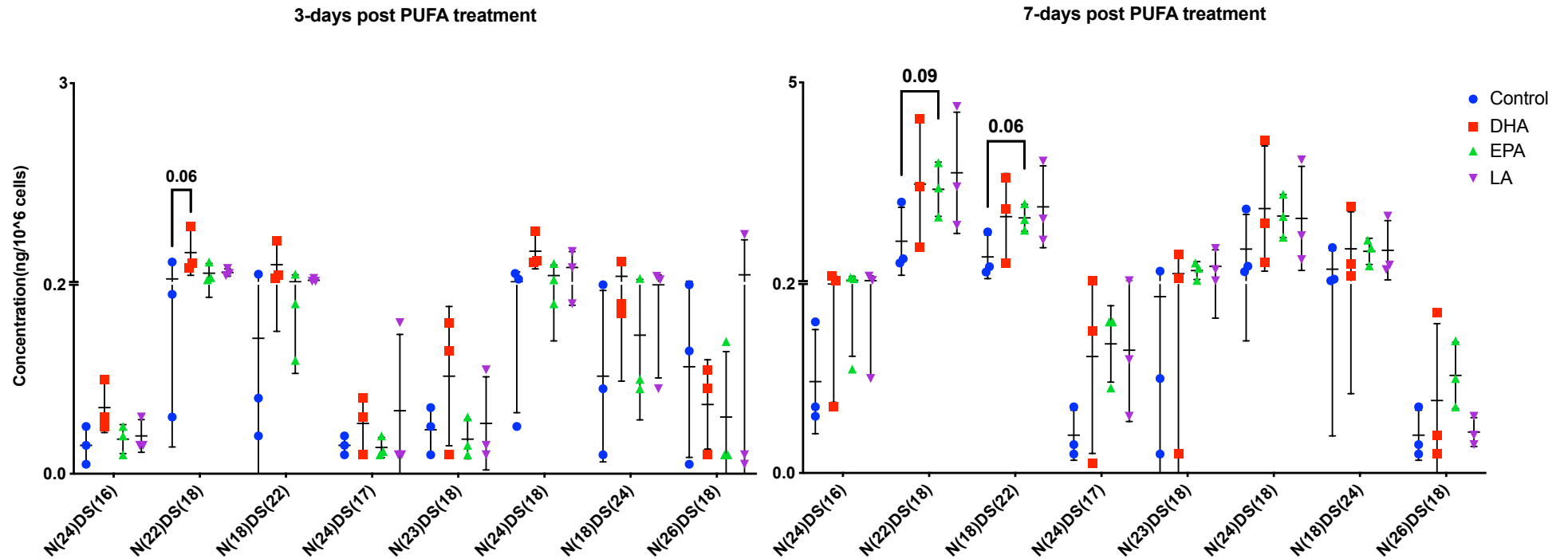


Figure 4.4 The effect of PUFA supplementation on CER[NDS] species levels measured in HDF. Ceramides were measured using UPLC/ESI-MS/MS in HDF treated with 10 μ M DHA, EPA and LA for three or seven days. Data are presented as absolute concentration in ng/10⁶ cells (mean \pm SD). Comparisons were performed between the control and PUFA treated cells of the same time point; (n=3 donors) per time-point. Data were analysed by repeated measures One-Way ANOVA comparing differences over treatment compared with control, with corrections for multiple analyses using the Dunnett method. PUFA:

polyunsaturated fatty acid; HDF: human dermal fibroblast; DHA: docosahexaenoic acid; EPA: eicosapentaenoic acid; LA: linoleic acid; CER: ceramide; NDS: non-hydroxy dihydroceramide.

n-3 PUFA significantly increased CER[NH] and CER[AH] species levels at seven days post supplementation

A total of four CER[NH] species were measured in HDF, whereas two CER[NP] and three CER[AH] were measured (**Figure 4.5**). *n-3* PUFA had an effect on the 6-hydroxyceramides where EPA significantly increased N(25)H(16) concentration when compared with control ($p= 0.007$), and DHA significantly increased A(24)H(18) ($p= <0.0001$).

CER[NH], CER[NP] and CER[AH] species

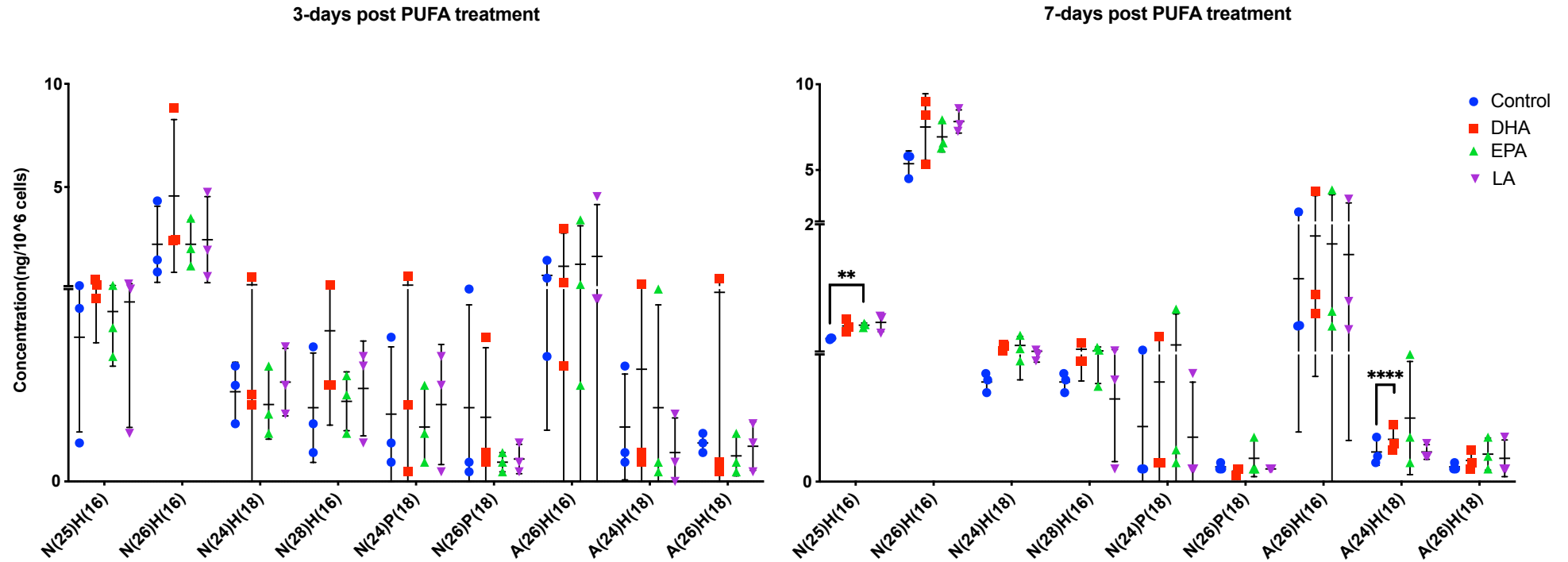


Figure 4.5 The effect of PUFA supplementation on CER[NH], CER[NP] and CER[AH] species measured in HDF. Ceramides were measured using UPLC/ESI-MS/MS in HDF treated with 10 μ M DHA, EPA and LA for three or seven days. Data are presented as absolute concentration in ng/10⁶ cells (mean

± SD). Comparisons were performed between the control and PUFA treated cells of the same time point; (PUFA-treated n=3 each, control n=3) per time-point. Data were analysed One-Way ANOVA with comparing differences over treatment compared with control, with corrections for multiple analyses using the Dunnett method; **p <0.01; ***p <0.0001. PUFA: polyunsaturated fatty acid; HDF: human dermal fibroblast; DHA: docosahexaenoic acid; EPA: eicosapentaenoic acid; LA: linoleic acid; CER: ceramide; NH: non-hydroxy 6-hydroxyceramide; NP: non-hydroxy phytoceramide; AH: alpha-hydroxy 6-hydroxyceramide.

4.3.1.4 DHA altered total carbon number of ceramides in HDF

Total carbon number (carbon number of the fatty acyl-chain + carbon number of the sphingoid base-chain) shows the ceramide chain length which is important in skin studies as alterations in total carbon number in the epidermis has been reported in several skin disorders. Analysing ceramide total chain lengths in HDF showed a significant increase in C42 ceramides at three days post DHA-supplementation ($p=0.04$). In addition, DHA treatment for seven days increased C43 ceramides with ($p=0.03$), whereas C41, C42 were increased but did not reach statistical significance ($p=0.06$, $p=0.09$, respectively) (**Figure 4.6**).

Total carbon number

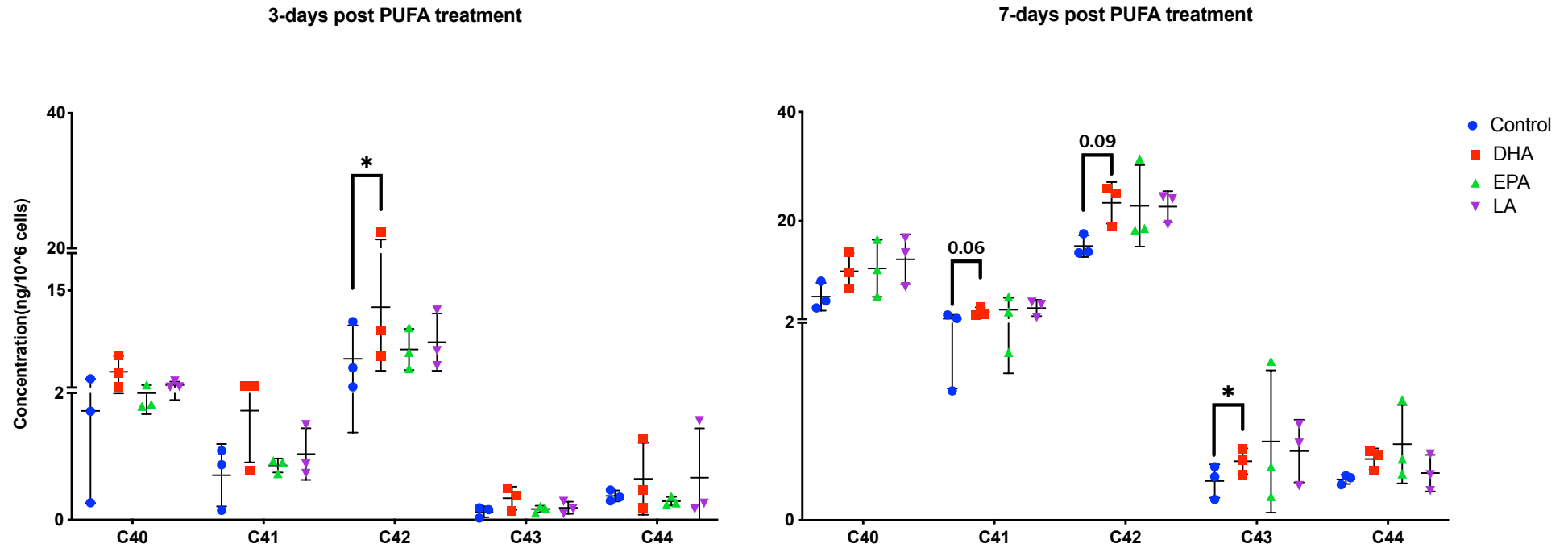


Figure 4.6 The effect of PUFA supplementation on CER total carbon chain number in HDF. Ceramides measured using UPLC/ESI-MS/MS in HDF treated with 10 μ M DHA, EPA and LA for three or seven days. Total carbon chain was calculated (sphingoid base-chain carbon number + fatty-acyl chain carbon number) then totaled. Data are presented as absolute concentration in ng/10⁶ cells (mean \pm SD). Comparisons were performed between the control and PUFA treated cells of the same time point; (n=3 donors) per time-point. Data were analysed by One-Way ANOVA comparing differences over treatment

compared with control, with corrections for multiple analyses using the Dunnett method; * $p < 0.05$. PUFA: polyunsaturated fatty acid; HDF: human dermal fibroblast; DHA: docosahexaenoic acid; EPA: eicosapentaenoic acid; LA: linoleic acid; CER: ceramide; C: carbon number.

4.3.1.5 DHA significantly affected total sphingoid base-chain carbon number at seven days post supplementation

Analysing the data according to the total carbon number of the sphingoid base-chain could reveal effects on the *de novo* biosynthesis pathway regulated by SPT. DHA significantly elevated ceramides with a C19 base chain ($p= 0.004$), whereas the increase in C18 was close to significant ($p= 0.06$) (**Figure 4.7**). In addition, EPA seemed to increase the C22 CERs ($p= 0.06$).

Total base-chain carbon number

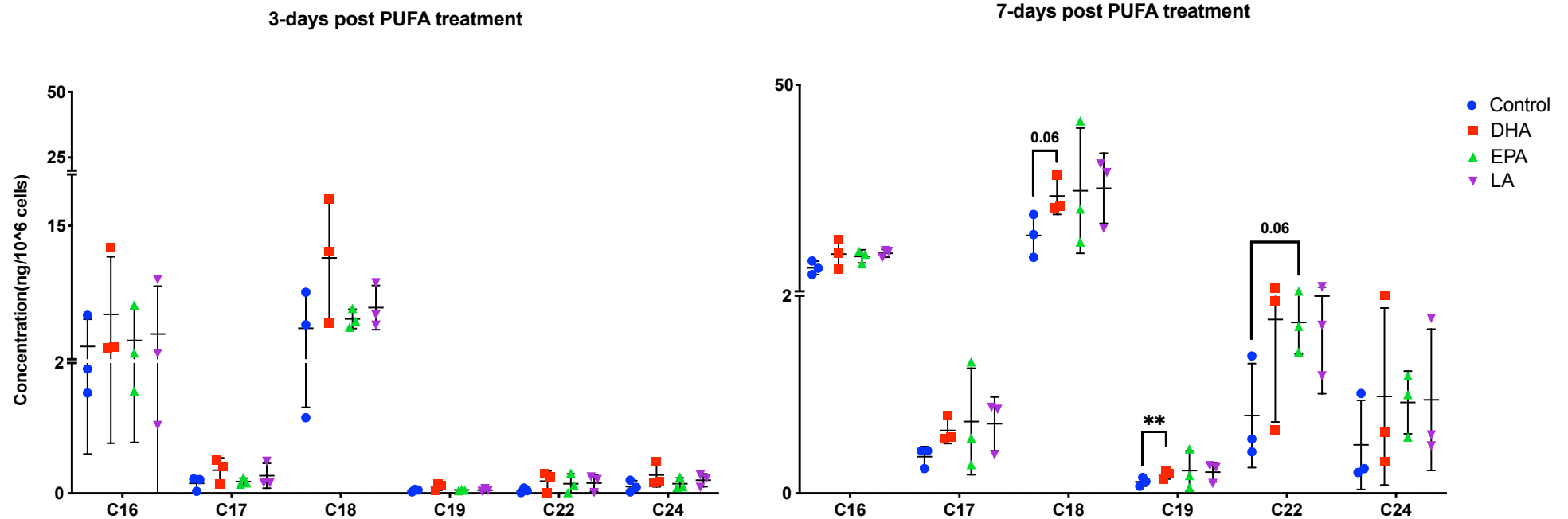


Figure 4.7 The effect of PUFA supplementation on CER total spingoid base-chain length in HDF. Ceramides were measured using UPLC/ESI-MS/MS in HDF treated with 10 μ M DHA, EPA and LA for three or seven days. Spingoid-base carbon chains were totaled (example: C16 = total of all ceramides with C16 spingoid base-chain). Data are presented as absolute concentration in ng/10⁶ cells (mean \pm SD). Comparisons were performed between the control and

PUFA treated cells of the same time point; (n=3 donors) per time-point. Data were analysed by One-Way ANOVA comparing differences over treatment compared with control, with corrections for multiple analyses using the Dunnett method; **p <0.01. PUFA: polyunsaturated fatty acid; HDF: human dermal fibroblast; DHA: docosahexaenoic acid; EPA: eicosapentaenoic acid; LA: linoleic acid; CER: ceramide; C: carbon number.

4.3.1.6 DHA had a significant effect on total fatty acyl-chain carbon number

Data were also categorised according to fatty-acyl chain length. This informs on the contribution of changes to the fatty-acyl specific CerS enzymes. DHA increased the concentration of C22 CERs at 3-days post treatment ($p= 0.047$). After seven days of DHA treatment, long-chain CERs with a C23 and C24 FA-chains were significantly increased ($p= 0.04$, $p= 0.04$). Ceramides with C25 FA-chain were increased with DHA supplementation for seven days but did not reach statistical significance ($p= 0.08$) (**Figure 4.8**)

Total FA-chain carbon number

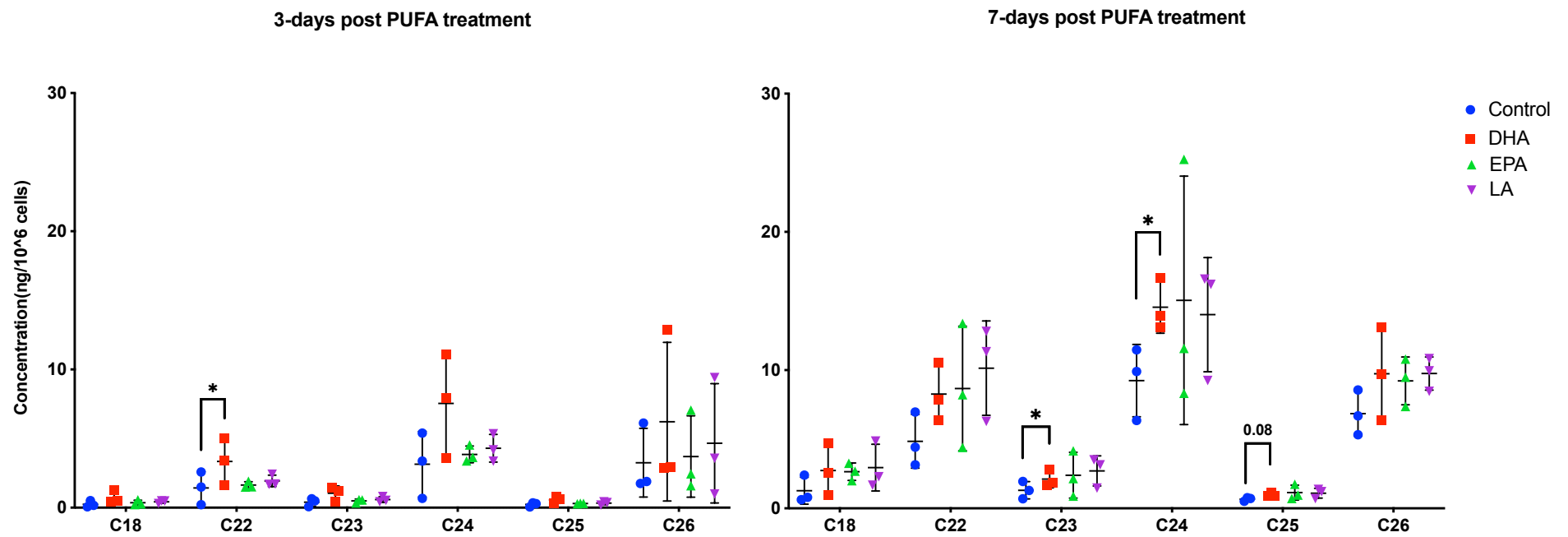


Figure 4.8 The effect of PUFA supplementation on CER total fatty acyl-chain length in HDF. Ceramides were measured using UPLC/ESI-MS/MS in HDF treated with 10 μ M DHA, EPA and LA for three or seven days. Fatty-acyl carbon chains were totaled (example: C18 = total of all ceramides with C18

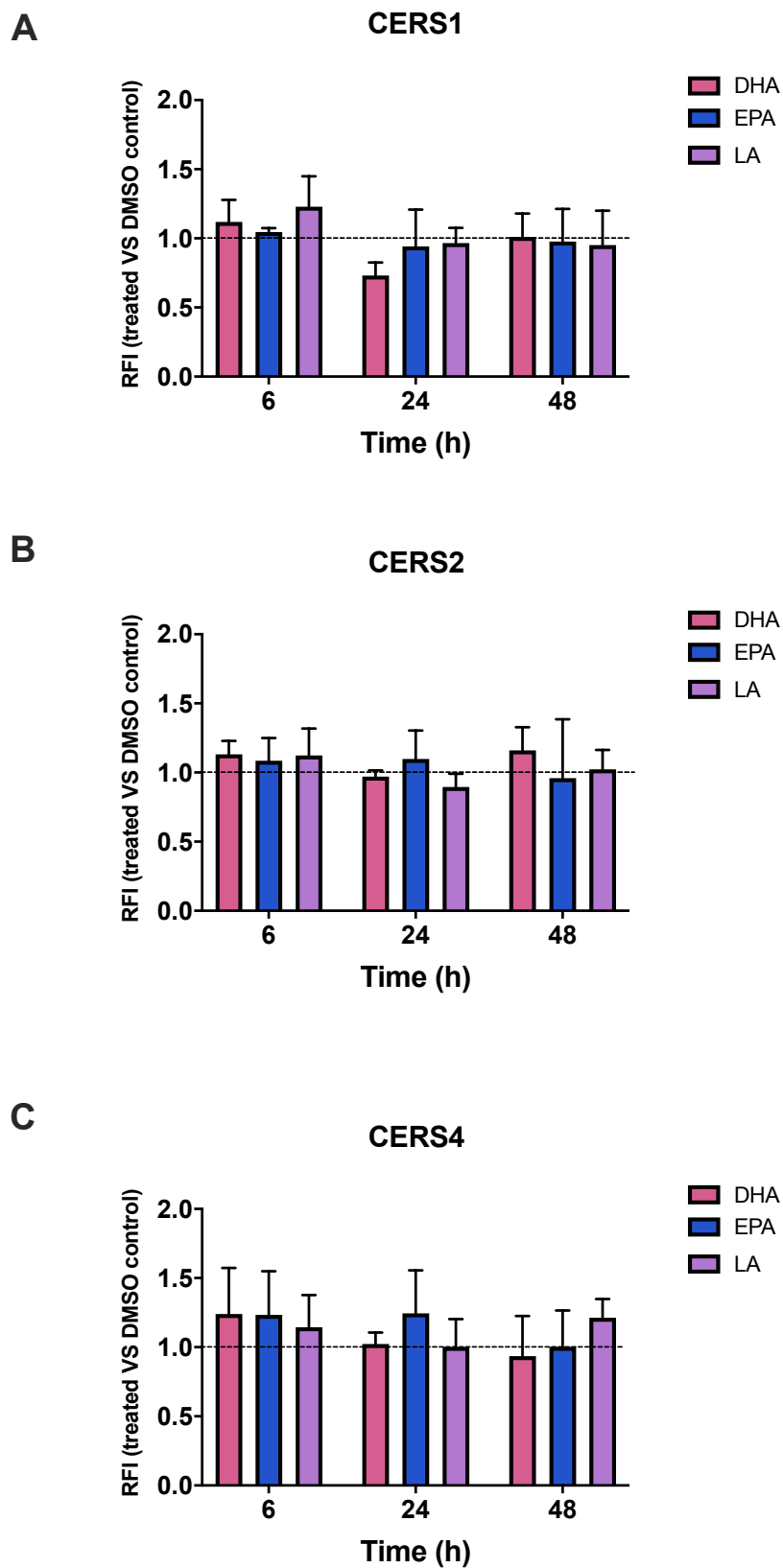
fatty-acyl chain). Data are presented as absolute concentration in $\text{ng}/10^6$ cells (mean \pm SD). Comparisons were performed between the control and PUFA treated cells of the same time point; (n=3 donors) per time-point. Data were analysed by One-Way ANOVA comparing differences over treatment compared with control, with corrections for multiple analyses using the Dunnett method; *p <0.05. PUFA: polyunsaturated fatty acid; HDF: human dermal fibroblast; DHA: docosahexaenoic acid; EPA: eicosapentaenoic acid; LA: linoleic acid; FA: fatty acyl; CER: ceramide; C: carbon number.

4.3.2 *n*-3 PUFA downregulated *CERS5* and *CERS6* expression in HDF

CER biosynthesis enzyme mRNA levels were quantitated by RT-qPCR analysis to investigate how PUFA regulates ceramide metabolism in the dermis via changes in gene expression. The effect of DHA, EPA and LA on the expression of the fatty acyl-specific *CERS1-6* and *DESI,2* that generate the sphingosine and phytosphingosine ceramides, respectively, were analysed at six, 24 and 48 hours post-PUFA supplementation. Data were presented as RFI, which compares CER biosynthesis enzyme gene expression in treated cells to that in untreated controls of the same time-point (n=3 donors).

4.3.2.1 *DHA and EPA significantly downregulated CERS5 and CERS6 expression at 24 and 48 hours post supplementation*

Figure 4.9 shows the RFI of CERS genes that were measured in HDF treated with DHA, EPA and LA compared with control. The epidermis-specific *CERS3* was not detected in HDF. No change was found in the expression of *CERS1-4* (**Figure 4.9 A-C**). The expression of *CERS5* was significantly downregulated at 24 hours post-DHA supplementation compared with control ($p= 0.008$). There was a close to significant downregulation of *CERS5* and a significant downregulation of *CERS6* at 48 hours post-EPA supplementation compared with control ($p= 0.06$, $p= 0.049$, respectively) (**Figure 4.9 D,E**).



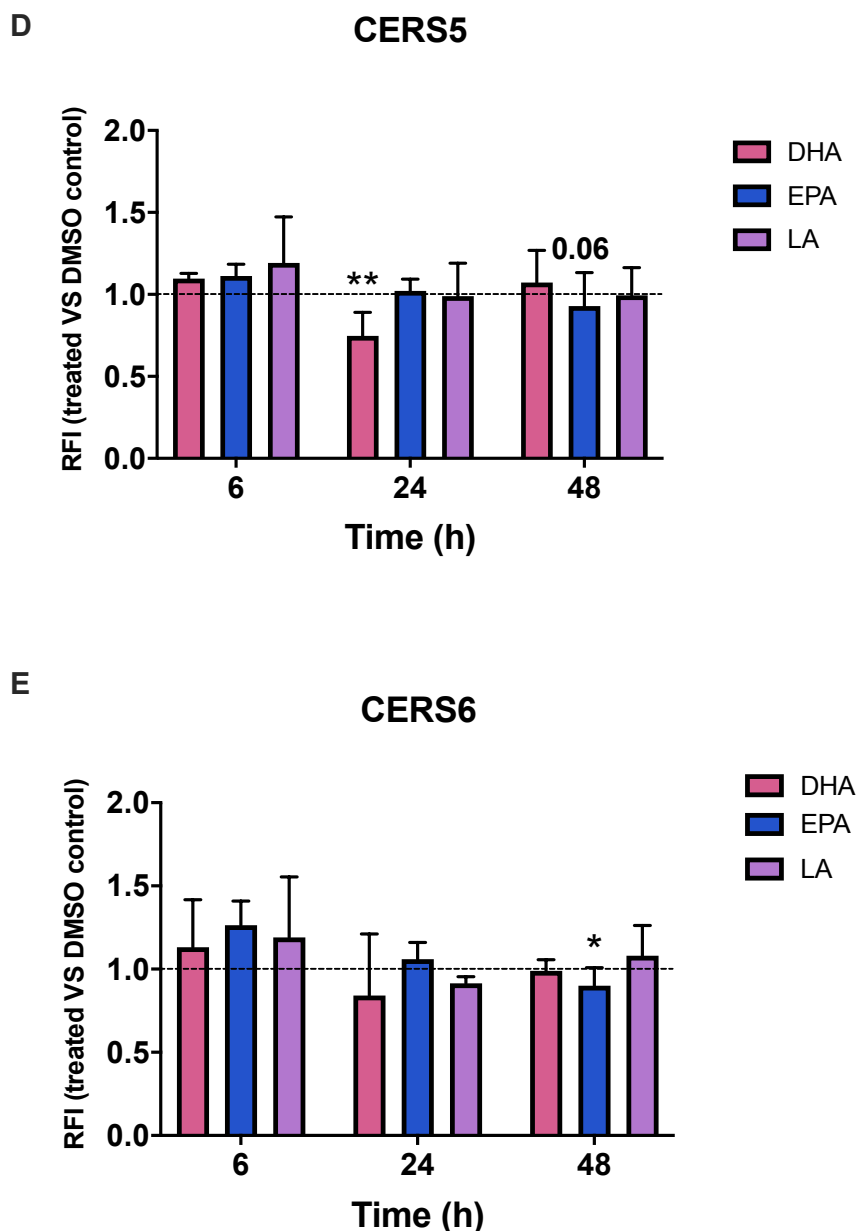


Figure 4.9 The effect of PUFA supplementation on CERS1-6 expression in HDF. A-E) Ceramide synthase 1, 2, 4, 5 and 6 gene expression were measured using RT-qPCR analysis in HDF treated with 10 μ M DHA, EPA and LA for six, 24 and 48 hours. Data are presented as relative fold increase (mean \pm SD). Comparisons were performed between the control (vehicle DMSO) and PUFA treated cells of the same time point; (n=3 donors). RFI =1: no change; RFI <1: downregulation; RFI >1: upregulation. Statistical analysis was performed using repeated measures Two-Way ANOVA comparing changes with treatment and time. Corrections for multiple analyses was performed using the Dunnett method; *p <0.05; **p <0.01. PUFA: polyunsaturated fatty acid; HDF: human dermal fibroblast; DHA: docosahexaenoic acid; EPA: eicosapentaenoic acid; LA: linoleic acid; h: hour; RFI: relative fold increase; CERS1-6: ceramide synthase 1-6.

4.3.2.2 No change was found in the expression of *DES1* and *DES2* expression in PUFA treated HDF

Figure 4.10 shows the RFI of *DES1* and *DES2* that were measured in HDF treated with DHA, EPA and LA compared with control. No significant change was observed in the expression of *DES1* and *DES2*.

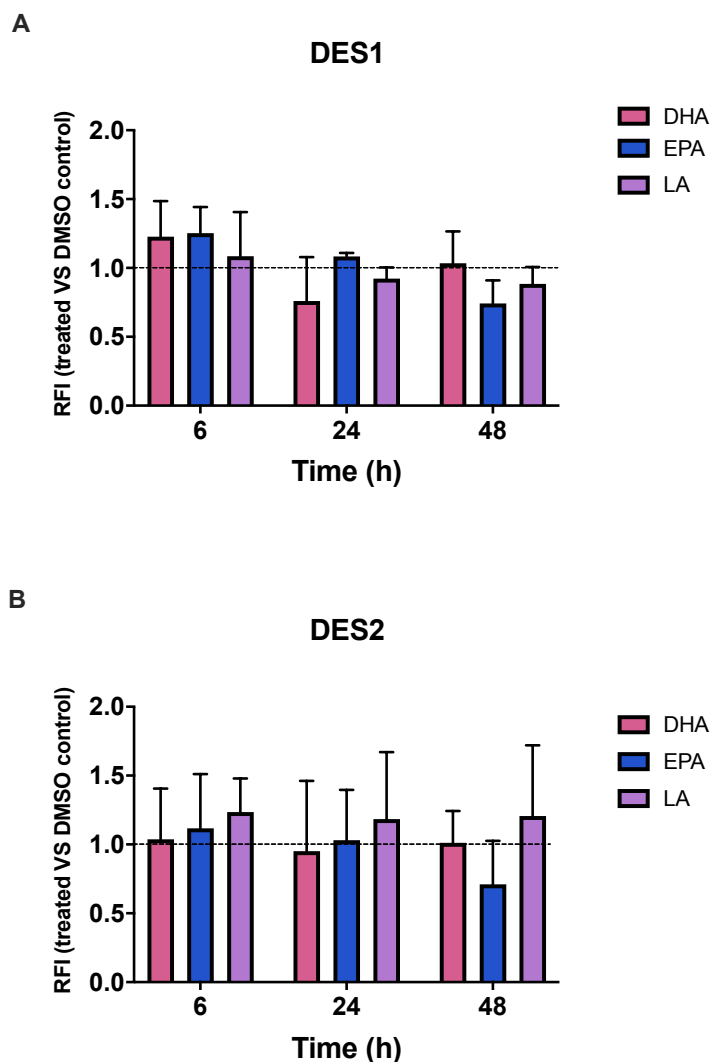


Figure 4.10 The effect of PUFA supplementation on *DES1-2* expression in HDF. A-B) Desaturase 1, 2 gene expression were measured using RT-qPCR analysis in HDF treated with 10 μ M DHA, EPA and LA for six, 24 and 48 hours. Data are presented as relative fold increase (mean \pm SD). Comparisons were performed between the control (vehicle DMSO) and PUFA treated cells of the same time point; (n=3 donors). RFI =1: no change; RFI <1: downregulation; RFI >1: upregulation. Statistical analysis was performed using repeated measures Two-Way ANOVA comparing changes with treatment and time. Corrections for multiple analyses was performed using the Dunnett method. PUFA: polyunsaturated fatty acid; HDF: human dermal fibroblast; DMSO: dimethyl sulfoxide; DHA: docosahexaenoic acid; EPA: eicosapentaenoic acid; LA: linoleic acid; h: hour; RFI: relative fold increase; DES1, 2: desaturase1, 2.

4.3.3 *n*-3 and *n*-6 PUFA supplementation altered membrane lipid metabolism in HDF

To further investigate lipid metabolism in HDF that could be affected by PUFA supplementation, structural and functional membrane lipids that include sterols, FFAs, glycerolipids, glycerophospholipids and complex sphingolipids were analysed using UHPSFC-MS^E system. Primary HDF were treated with DHA, EPA and LA for three or seven days and grouped according to time post-PUFA supplementation. For each sample analysed, concentrations of detected lipid species were reported as absolute values in $\mu\text{g}/10^6$ cells (mean \pm SD).

4.3.3.1 LA significantly reduced CE and TG levels, whereas DHA altered SM levels

Sterol lipids including total cholesterol and six CE species were detected in cultured HDF (**Figure 4.11-4.13**). In addition to this, two FFA species and 17 SM species were measured (**Figure 4.14-4.17**). Among the two glycerolipids measured, a total of three DG species and 11 TG species were detected in cultured HDF (**Figure 4.18-4.21**).

Although no change was found in total CE levels, LA significantly decreased CE 22:6 concentrations at seven days post supplementation ($p=0.03$) (**Figure 4.12**). No change was found in total cholesterol, total SM, total FFA and species levels. DHA significantly increased SM 40:1 and reduced SM 40:2 at seven days post supplementation ($p=0.04$, $p<0.0001$, respectively) (**Figure 4.18**). LA significantly decreased TG 48:1, TG 50:1 and TG 50:2 at seven days post supplementation ($p=0.03$, $p=0.003$, $p<0.0001$, respectively) (**Figure 4.23**).

Total CE in HDF

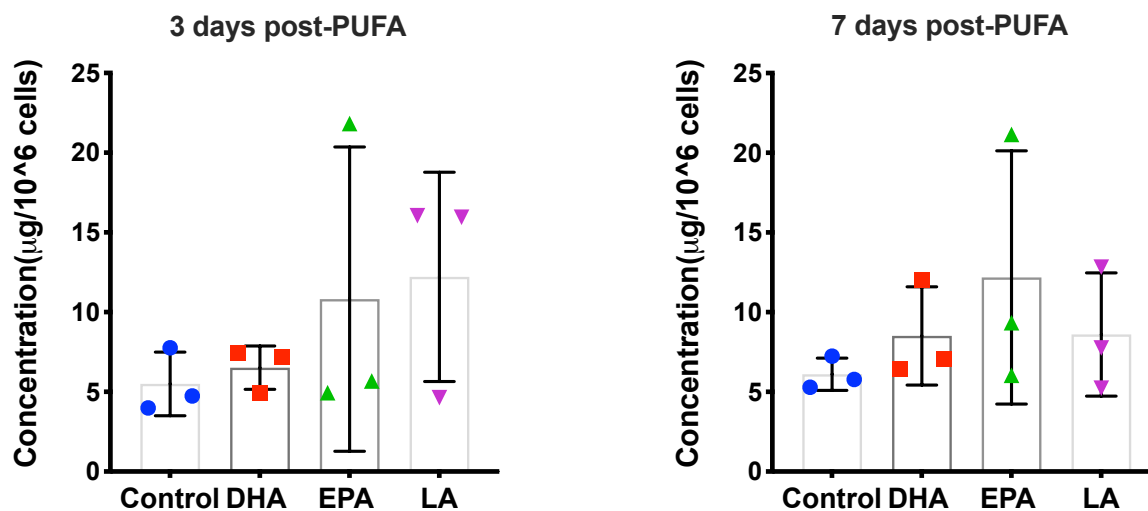


Figure 4.11 The effect of PUFA supplementation on total CE levels in HDF. Total CE was measured using UHPSFC-MS^E in HDF treated with 10 µM DHA, EPA and LA for three or seven days. Data are presented as absolute concentration in µg/10⁶ cells (mean ± SD). Comparisons were performed between the control and PUFA treated cells of the same time point; (n=3 donors) per time-point. Statistical analysis was performed using One-Way ANOVA comparing differences over treatment compared with control, with corrections for multiple analyses using the Dunnett method. PUFA: polyunsaturated fatty acid; HDF: human dermal fibroblast; DHA: docosahexaenoic acid; EPA: eicosapentaenoic acid; LA: linoleic acid; CE: cholesterol ester.

CE species in HDF

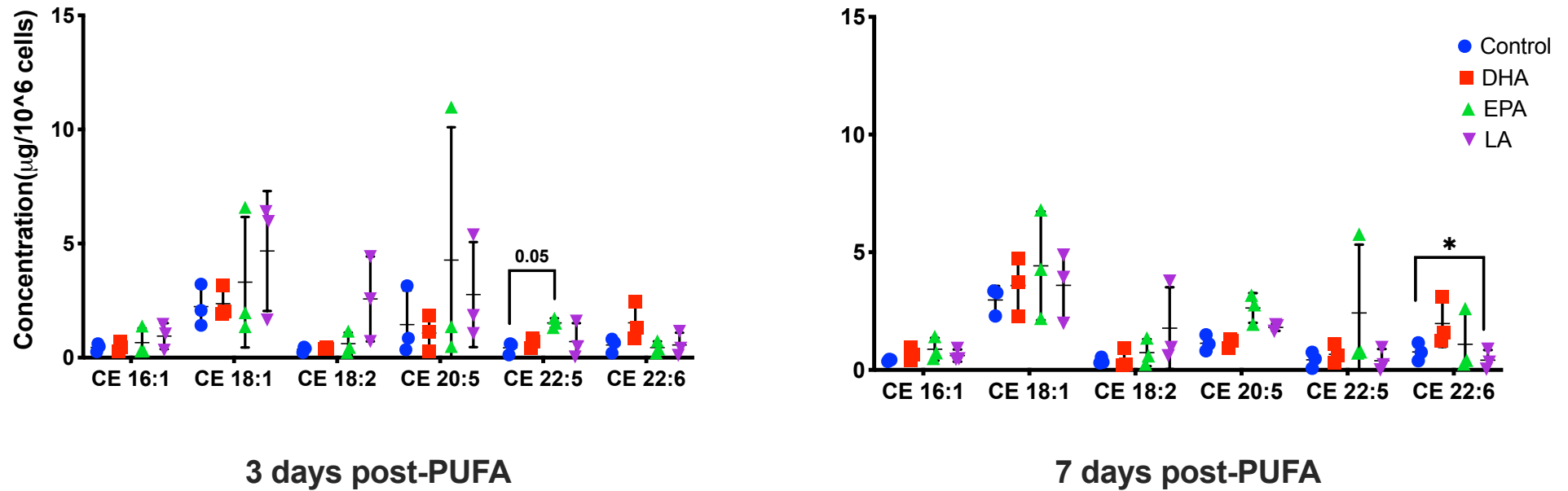


Figure 4.12 The effect of PUFA supplementation on CE species levels measured in HDF. CE species were measured using UHPSFC-MS^E in HDF treated with 10 μM DHA, EPA and LA for three or seven days. Data are presented as absolute concentration in $\mu\text{g}/10^6$ cells (mean \pm SD). Comparisons were performed between the control and PUFA treated cells of the same time point; (n=3 donors) per time-point. One-Way ANOVA comparing differences over treatment

compared with control, with corrections for multiple analyses using the Dunnett method; * $p < 0.05$. PUFA: polyunsaturated fatty acid; HDF: human dermal fibroblast; DHA: docosahexaenoic acid; EPA: eicosapentaenoic acid; LA: linoleic acid; CE: cholesterol ester.

Total cholesterol in HDF

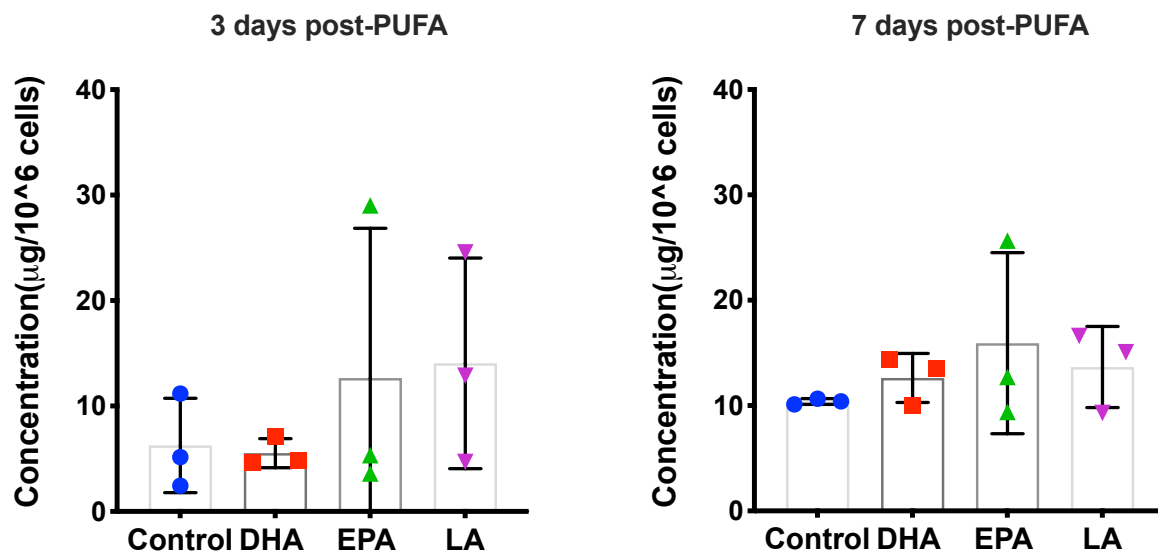


Figure 4.13 The effect of PUFA supplementation on total cholesterol levels in HDF. Total cholesterol was measured using UHPSFC-MS^E in HDF treated with 10 µM DHA, EPA and LA for three or seven days. Data are presented as absolute concentration in µg/10⁶ cells (mean ± SD). Comparisons were performed between the control and PUFA treated cells of the same time point; (n=3 donors) per time-point. Statistical analysis was performed using One-Way ANOVA comparing differences over treatment compared with control, with corrections for multiple analyses using the Dunnett method. PUFA: polyunsaturated fatty acid; HDF: human dermal fibroblast; DHA: docosahexaenoic acid; EPA: eicosapentaenoic acid; LA: linoleic acid.

Total FFA in HDF

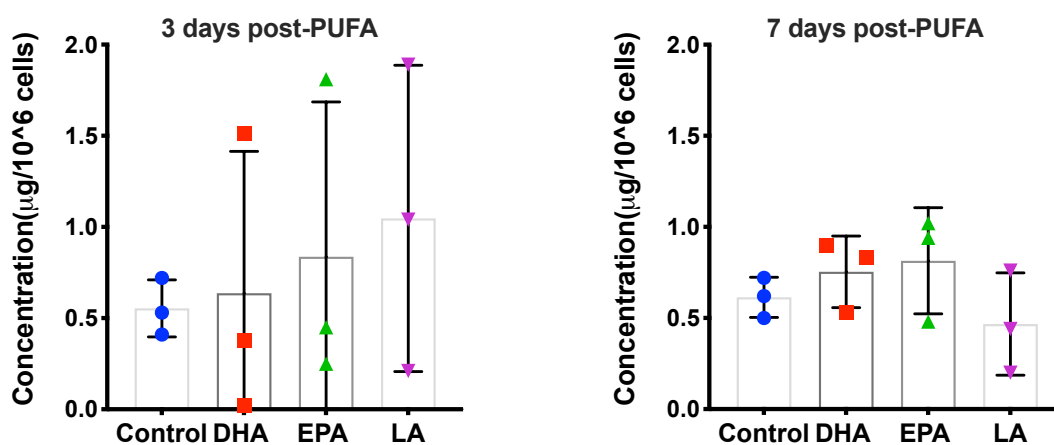


Figure 4.14 The effect of PUFA supplementation on total FFA levels in HDF. Total FFA were measured using UHPSFC-MS^E in HDF treated with 10 µM DHA, EPA and LA

for three or seven days. Data are presented as absolute concentration in $\mu\text{g}/10^6$ cells (mean \pm SD). Comparisons were performed between the control and PUFA treated cells of the same time point; (n=3 donors) per time-point. Statistical analysis was performed using One-Way ANOVA comparing differences over treatment compared with control, with corrections for multiple analyses using the Dunnett method. PUFA: polyunsaturated fatty acid; HDF: human dermal fibroblast; DHA: docosahexaenoic acid; EPA: eicosapentaenoic acid; LA: linoleic acid. FFA: free fatty acids.

FFA species in HDF

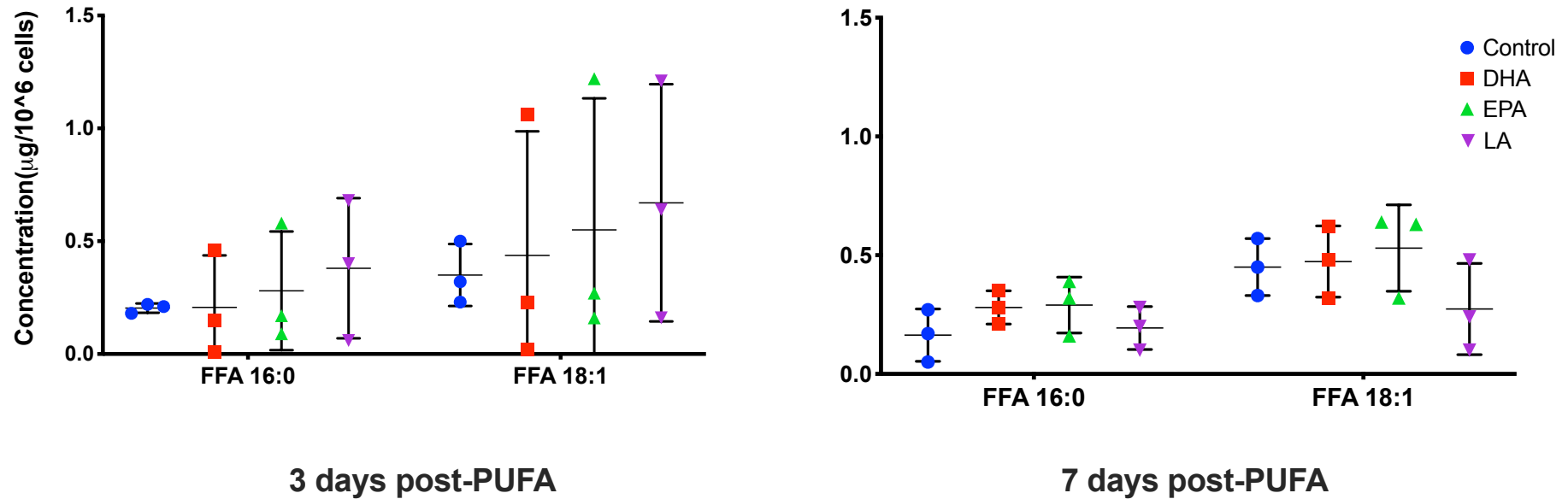


Figure 4.15 The effect of PUFA supplementation on FFA species levels measured in HDF. FFA species were measured using UHPSFC-MS^E in HDF treated with 10 µM DHA, EPA and LA for three or seven days. Data are presented as absolute concentration in µg/10⁶ cells (mean ± SD). Comparisons were performed between the control and PUFA treated cells of the same time point; (PUFA-treated n=3 each, control n=3) per time-point. Statistical analysis was performed using One-Way ANOVA comparing differences over treatment compared with control, with corrections for multiple analyses using the Dunnett method. PUFA: polyunsaturated fatty acid; HDF: human dermal fibroblast; DHA: docosahexaenoic acid; EPA: eicosapentaenoic acid; LA: linoleic acid. FFA: free fatty acids.

Total SM in HDF

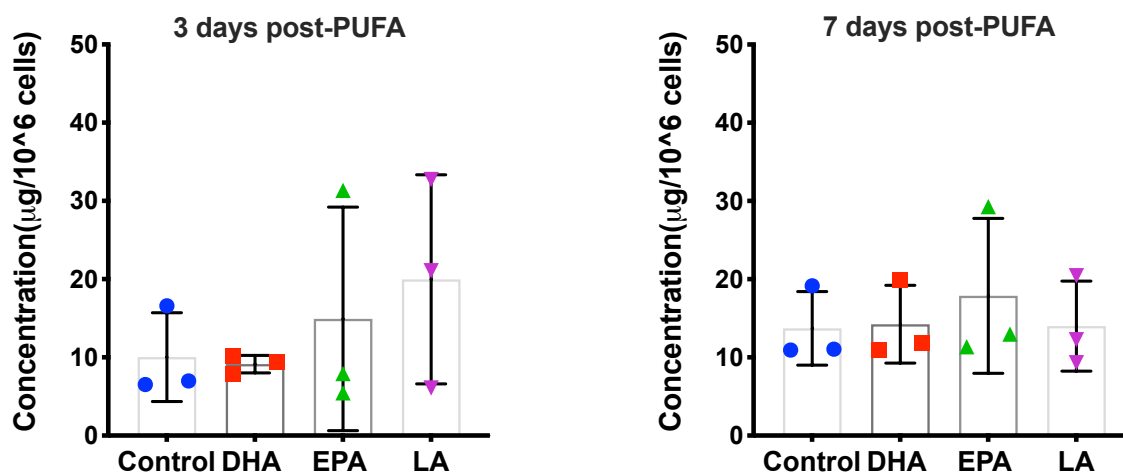


Figure 4.16 The effect of PUFA supplementation on total SM levels measured in HDF.

Total SM was measured using UHPSFC-MS^E in HDF treated with 10 µM DHA, EPA and LA for three or seven days. Data are presented as absolute concentration in µg/10⁶ cells (mean ± SD). Comparisons were performed between the control and PUFA treated cells of the same time point; (n=3 donors) per time-point. Statistical analysis was performed using One-Way ANOVA comparing differences over treatment compared with control, with corrections for multiple analyses using the Dunnett method. PUFA: polyunsaturated fatty acid; HDF: human dermal fibroblast; DHA: docosahexaenoic acid; EPA: eicosapentaenoic acid; LA: linoleic acid. SM: sphingomyelin.

SM species (3 days post-PUFA)

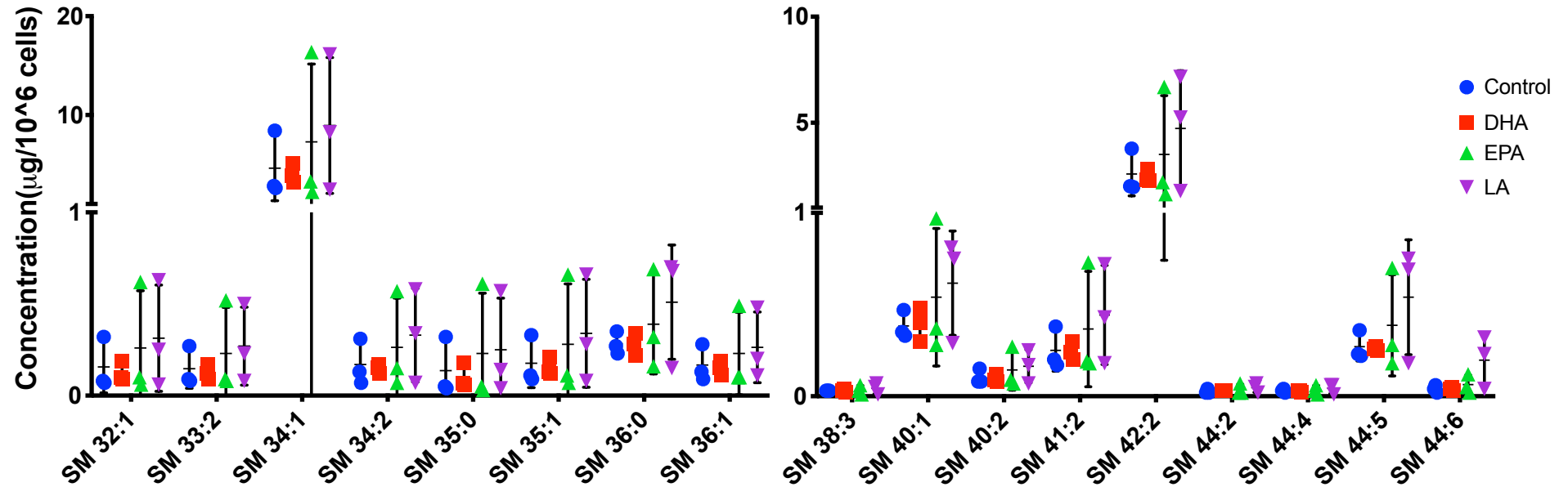


Figure 4.17 SM species levels measured in HDF after three days of PUFA supplementation. SM species were measured using UHPSFC-MS^E in HDF treated with 10 μM DHA, EPA and LA for three days. Data are presented as absolute concentration in $\mu\text{g}/10^6$ cells (mean \pm SD). Comparisons were performed between the control and PUFA treated cells; (n=3 donors). Statistical analysis was performed using One-Way ANOVA comparing differences over treatment compared with control, with corrections for multiple analyses using the Dunnett method. PUFA: polyunsaturated fatty acid; HDF: human dermal fibroblast; DHA: docosahexaenoic acid; EPA: eicosapentaenoic acid; LA: linoleic acid. SM: sphingomyelin.

SM species (7 days post-PUFA)

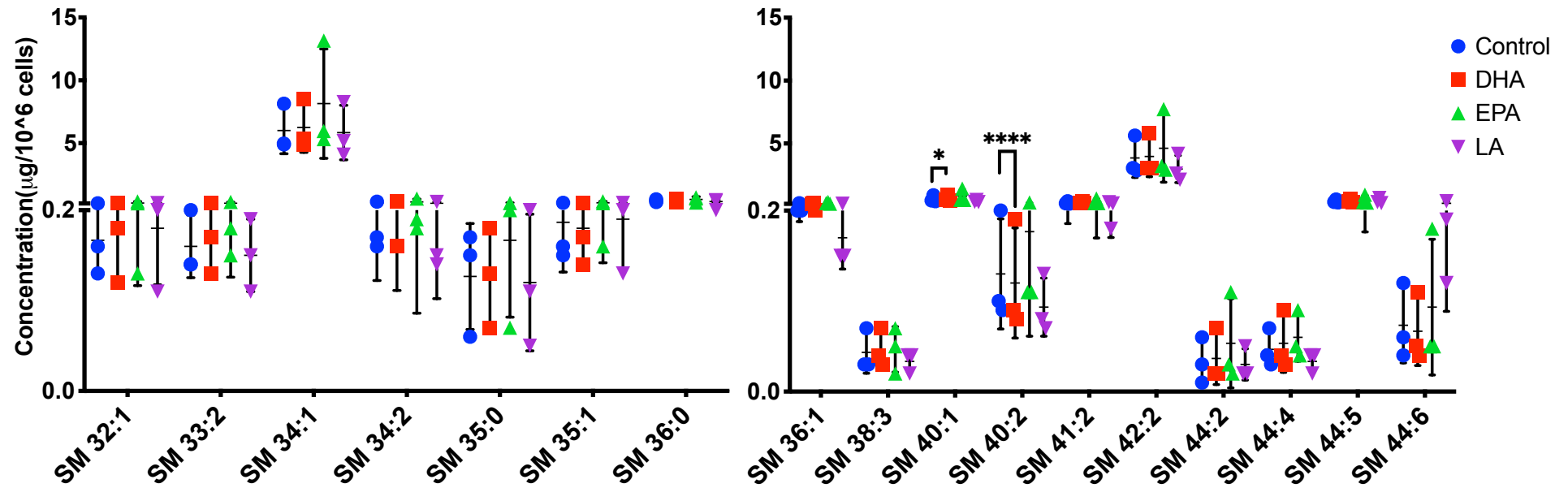


Figure 4.18 SM species levels measured in HDF after seven days of PUFA supplementation. SM species were measured using UHPSFC-MS^E in HDF treated with 10 µM DHA, EPA and LA for seven days. Data are presented as absolute concentration in µg/10⁶ cells (mean ± SD). Comparisons were performed between the control and PUFA treated cells; (n=3 donors). Statistical analysis was performed using One-Way ANOVA comparing differences over treatment compared with control, with corrections for multiple analyses using the Dunnett method; *p < 0.05; ****p < 0.0001. PUFA: polyunsaturated fatty acid; HDF: human dermal fibroblast; DHA: docosahexaenoic acid; EPA: eicosapentaenoic acid; LA: linoleic acid. SM: sphingomyelin.

Total DG in HDF

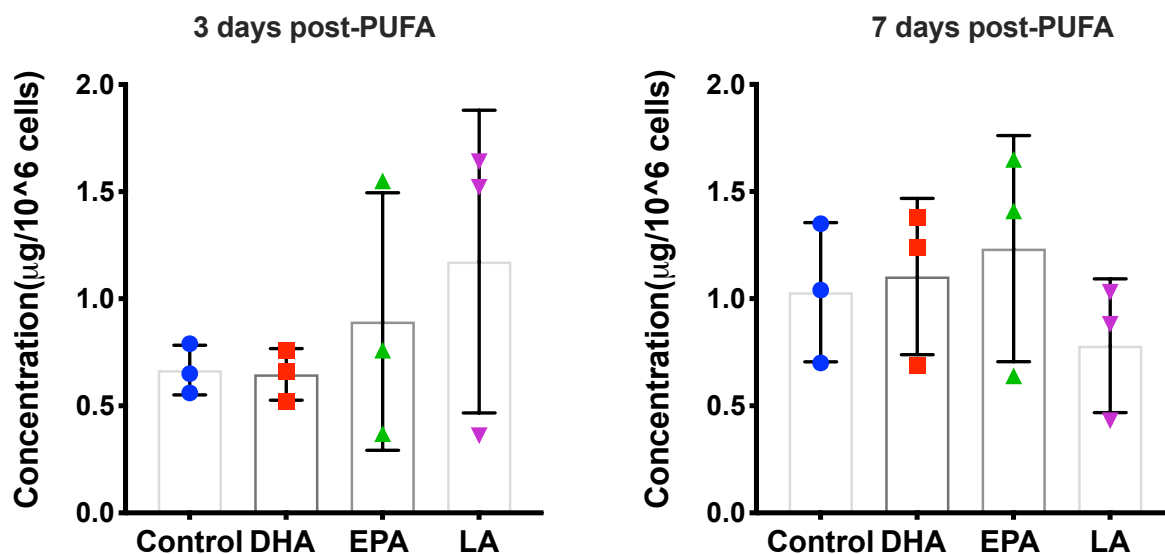


Figure 4.19 The effect of PUFA supplementation on total DG levels measured in HDF. Total DG was measured using UHPSFC-MS^E in HDF treated with 10 µM DHA, EPA and LA for three and seven days. Data are presented as absolute concentration in µg/10⁶ cells (mean ± SD). Comparisons were performed between the control and PUFA treated cells of the same time-point; (n=3 donors). Statistical analysis was performed using One-Way ANOVA comparing differences over treatment compared with control, with corrections for multiple analyses using the Dunnett method. PUFA: polyunsaturated fatty acid; HDF: human dermal fibroblast; DHA: docosahexaenoic acid; EPA: eicosapentaenoic acid; LA: linoleic acid. DG: diacylglycerol.

DG species in HDF

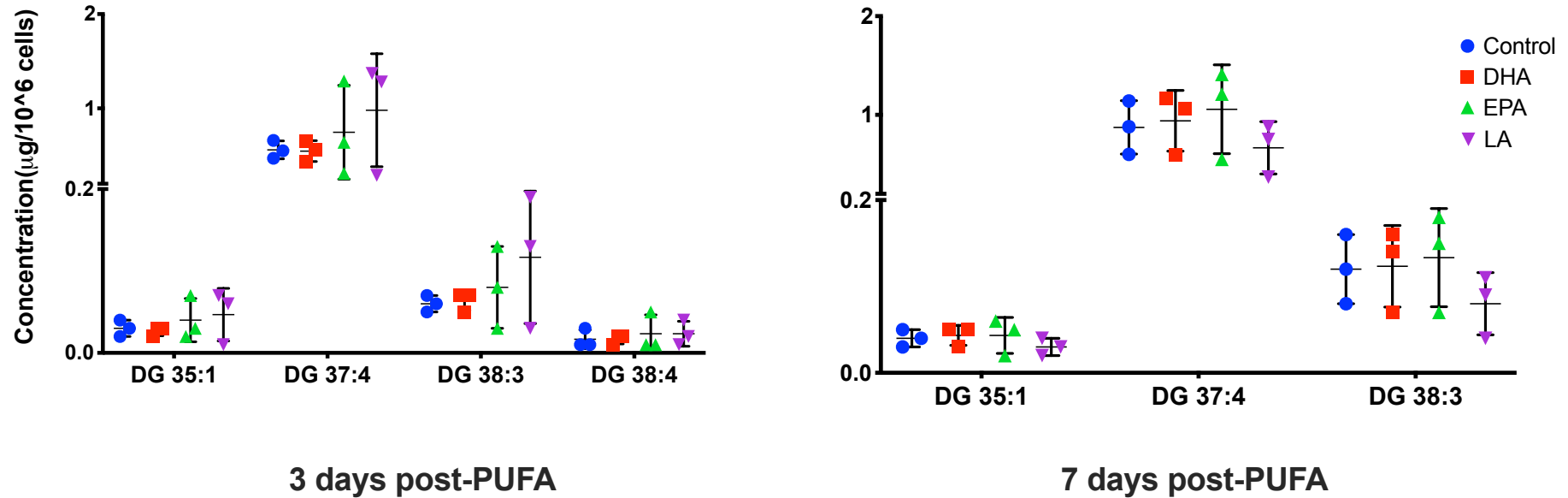


Figure 4.20 The effect of PUFA supplementation on DG species levels measured in HDF. DG species were measured using UHPSFC-MS^E in HDF treated with 10 μM DHA, EPA and LA for three and seven days. Data are presented as absolute concentration in $\mu\text{g}/10^6$ cells (mean \pm SD). Comparisons were performed between the control and PUFA treated cells of the same time-point; (n=3 donors). Statistical analysis was performed using One-Way ANOVA comparing differences over treatment compared with control, with corrections for multiple analyses using the Dunnett method. PUFA: polyunsaturated fatty acid; HDF: human dermal fibroblast; DHA: docosahexaenoic acid; EPA: eicosapentaenoic acid; LA: linoleic acid. DG: diacylglycerol.

Total TG in HDF

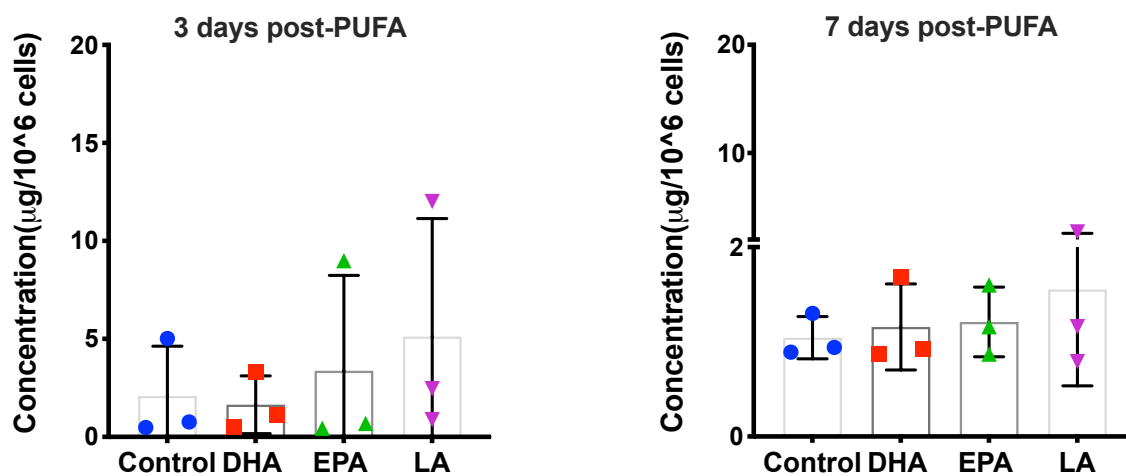


Figure 4.21 The effect of PUFA supplementation on total TG levels measured in HDF. Total TG was measured using UHPSFC-MS^E in HDF treated with 10 μM DHA, EPA and LA for three and seven days. Data are presented as absolute concentration in $\mu\text{g}/10^6$ cells (mean \pm SD). Comparisons were performed between the control and PUFA treated cells of the same time-point; (n=3 donors). Statistical analysis was performed using One-Way ANOVA comparing differences over treatment compared with control, with corrections for multiple analyses using the Dunnett method. PUFA: polyunsaturated fatty acid; HDF: human dermal fibroblast; DHA: docosahexaenoic acid; EPA: eicosapentaenoic acid; LA: linoleic acid. TG: triacylglycerol.

TG species (3 days post-PUFA)

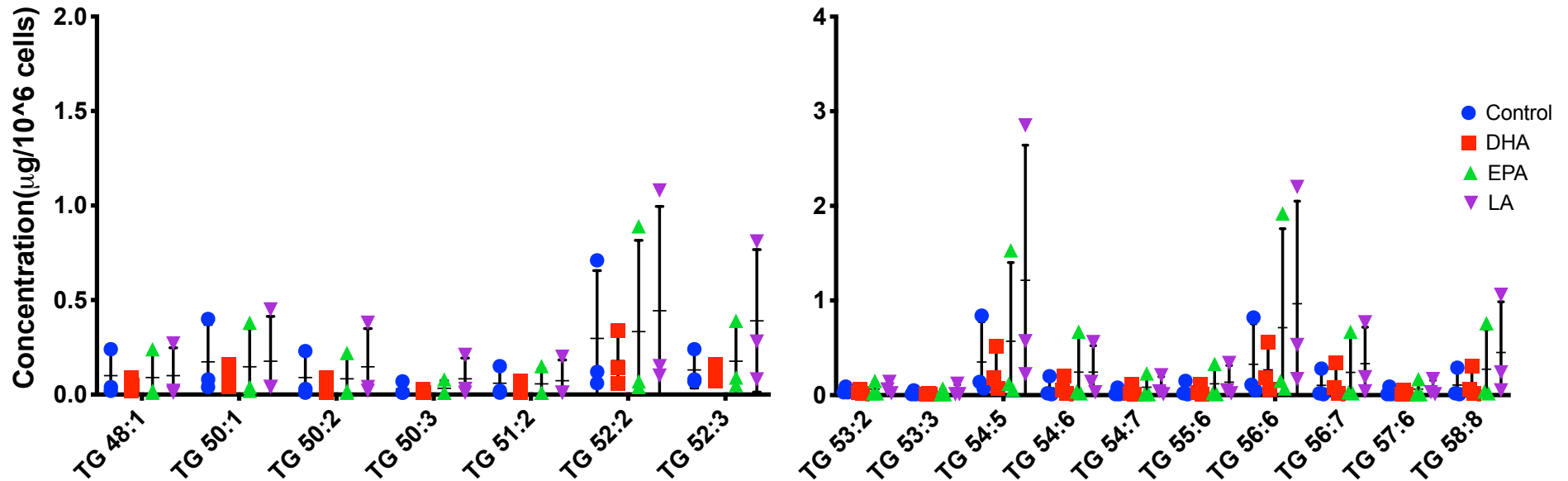


Figure 4.22 TG species levels measured in HDF after three days of PUFA supplementation. TG species was measured using UHPSFC-MS^E in HDF treated with 10 μM DHA, EPA and LA for three days. Data are presented as absolute concentration in $\mu\text{g}/10^6$ cells (mean \pm SD). Comparisons were performed between the control and PUFA treated cells; (n= 3 donors). Statistical analysis was performed using One-Way ANOVA comparing differences over treatment compared with control, with corrections for multiple analyses using the Dunnett method. PUFA: polyunsaturated fatty acid; HDF: human dermal fibroblast; DHA: docosahexaenoic acid; EPA: eicosapentaenoic acid; LA: linoleic acid. TG: triacylglycerol.

TG species (7 days post-PUFA)

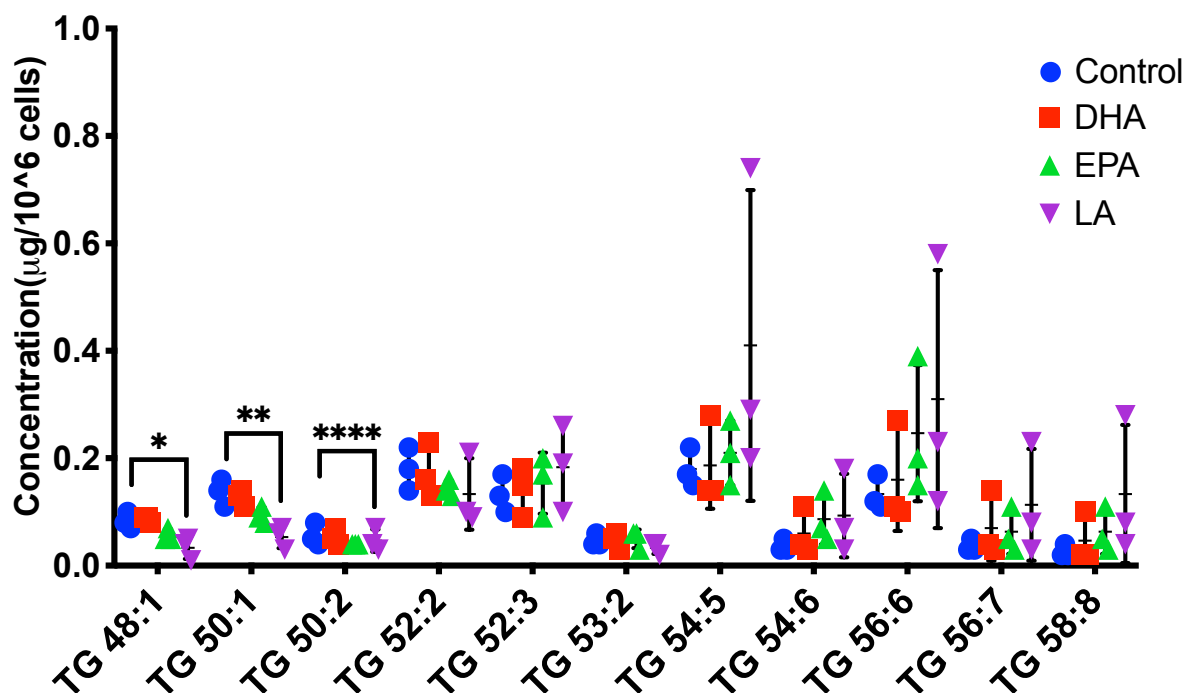


Figure 4.23 TG species levels measured in HDF after seven days of PUFA supplementation. TG species was measured using UHPSFC-MS^E in HDF treated with 10 μ M DHA, EPA and LA for seven days. Data are presented as absolute concentration in μ g/ 10^6 cells (mean \pm SD). Comparisons were performed between the control and PUFA treated cells; (n=3 donors). Statistical analysis was performed using One-Way ANOVA comparing differences over treatment compared with control, with corrections for multiple analyses using the Dunnett method; *p < 0.05; **p < 0.01; ****p < 0.0001. PUFA: polyunsaturated fatty acid; HDF: human dermal fibroblast; DHA: docosahexaenoic acid; EPA: eicosapentaenoic acid; LA: linoleic acid. TG: triacylglycerol.

4.3.3.2 DHA significantly reduced PE levels and increased PC levels, whereas LA significantly reduced PC and LPC levels in HDF

The most abundant glycerophospholipids in HDF were the PCs with 48 species detected, followed by 15 PE species and five LPC species. DHA significantly reduced PE 36:4p/36:5e at 3 days post supplementation (p= 0.02), and a close to significant decrease was also found three days-post DHA treatment in the following species: PE 36:3, PE 36:4, PE 36:5 (p= 0.05, p= 0.09, p= 0.07, respectively) (**Figure 4.24**).

Both DHA and LA altered PC concentrations at seven days post PUFA treatment. *n*-3 DHA significantly increased PC 32:1, PC 34:5 and PC 36:5 (p= 0.04, p=

<0.0001, $p=0.04$, respectively) (**Figure 4.28**). DHA also increased the levels of the following PC species, although changes did not reach statistical significance: PC 32:2, PC 34:1, PC 34:2, PC 36:2/38:8p/38:9e, PC 38:6 ($p=0.09$, $p=0.06$, $p=0.07$, $p=0.08$, $p=0.09$, respectively). On the other hand, LA significantly reduced PC 32:1, PC 33:1/34:0p/34:1e, PC 34:1 ($p=0.048$, $p=0.02$, $p=0.03$, respectively) (**Figure 4.28**). LA also reduced PC 30:1 and PC 40:4p/40:6e, but changes did not reach statistical significance ($p=0.07$, $p=0.06$, respectively).

In addition, the seven-day supplementation with LA significantly decreased total LPC levels in HDF ($p=0.009$) (**Figure 4.29**). LPC 16:0 and LPC 18:1 species were reduced at seven days post-LA ($p=0.02$, $p=0.007$, respectively) (**Figure 4.30**).

Total PE in HDF

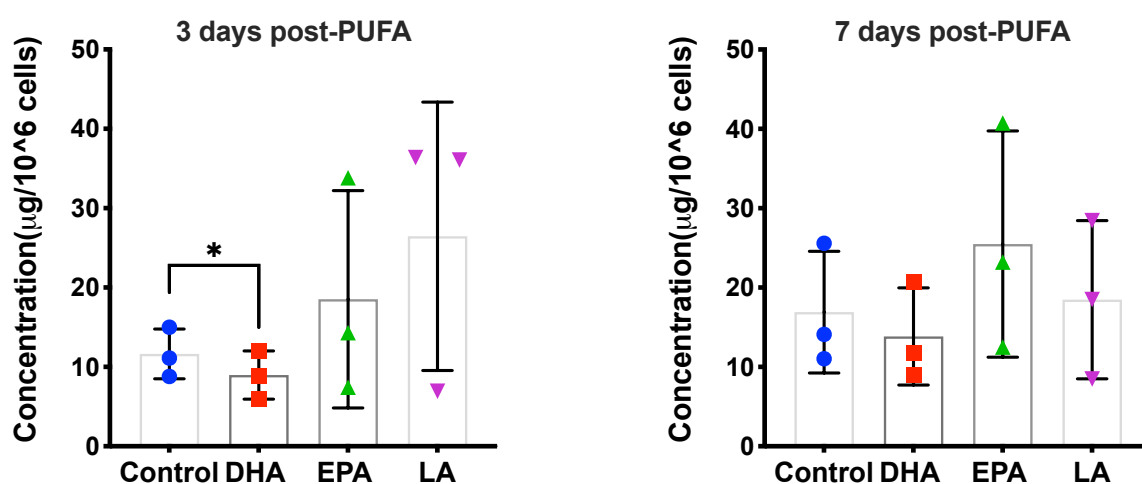


Figure 4.24 The effect of PUFA supplementation on total PE levels measured in HDF. Total PE was measured using UHPSFC-MS^E in HDF treated with 10 µM DHA, EPA and LA for three and seven days. Data are presented as absolute concentration in µg/10⁶ cells (mean ± SD). Comparisons were performed between the control and PUFA treated cells of the same time-point; (n=3 donors). Statistical analysis was performed using One-Way ANOVA comparing differences over treatment compared with control, with corrections for multiple analyses using the Dunnett method; * $p < 0.05$. PUFA: polyunsaturated fatty acid; HDF: human dermal fibroblast; DHA: docosahexaenoic acid; EPA: eicosapentaenoic acid; LA: linoleic acid. PE: phosphatidylethanolamine.

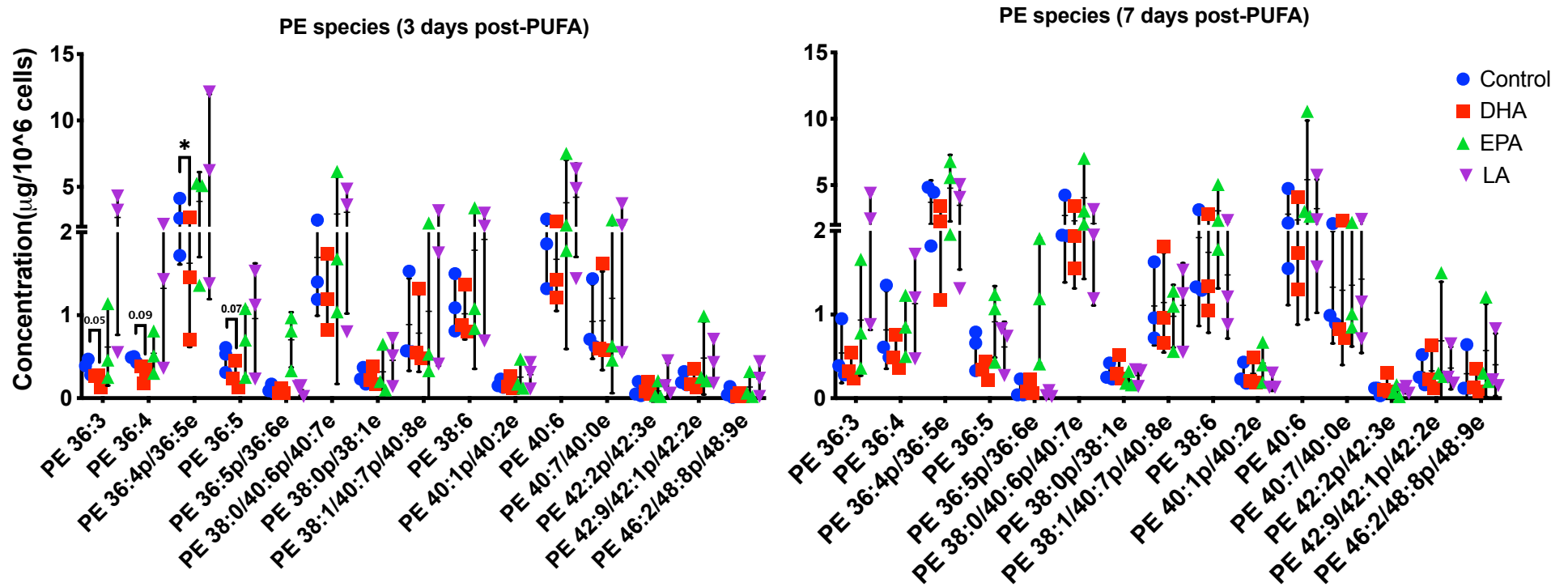


Figure 4.25 The effect of PUFA supplementation on PE species levels measured in HDF. PE species were measured using UHPSFC-MS^E in HDF treated with 10 µM DHA, EPA and LA for three and seven days. Data are presented as absolute concentration in µg/10⁶ cells (mean ± SD). Comparisons were performed between the control and PUFA treated cells of the same time-point; (n=3 donors). Statistical analysis was performed using One-Way ANOVA comparing differences over treatment compared with control, with corrections for multiple analyses using the Dunnett method; *p < 0.05. PUFA: polyunsaturated fatty acid; HDF: human dermal fibroblast; DHA: docosahexaenoic acid; EPA: eicosapentaenoic acid; LA: linoleic acid. PE: phosphatidylethanolamine.

Total PC in HDF

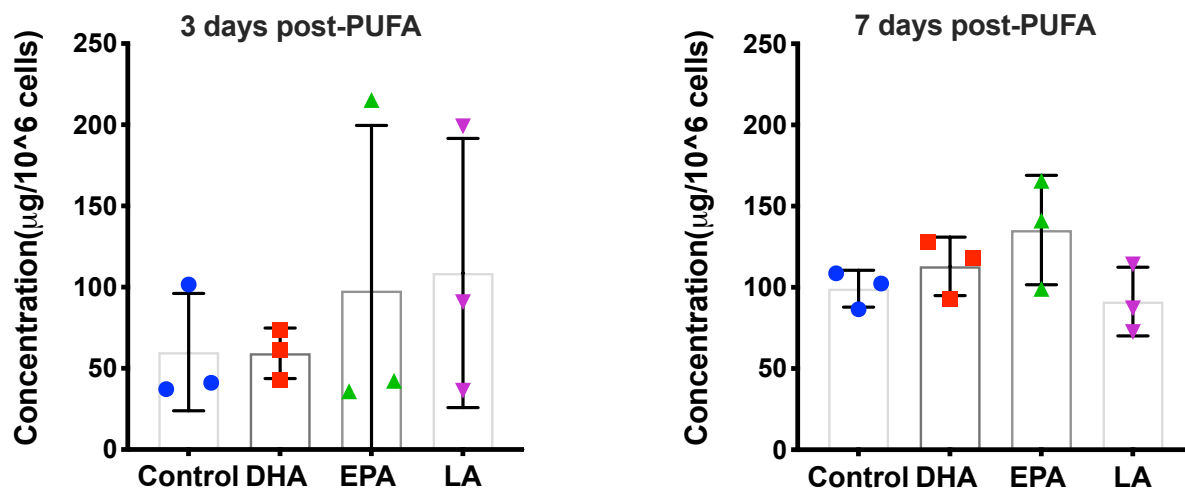


Figure 4.26 The effect of PUFA supplementation on total PC levels measured in HDF. Total PC was measured using UHPSFC-MS^E in HDF treated with 10 µM DHA, EPA and LA for three and seven days. Data are presented as absolute concentration in µg/10⁶ cells (mean ± SD). Comparisons were performed between the control and PUFA treated cells of the same time-point; (n=3 donors). Statistical analysis was performed using One-Way ANOVA comparing differences over treatment compared with control, with corrections for multiple analyses using the Dunnett method. PUFA: polyunsaturated fatty acid; HDF: human dermal fibroblast; DHA: docosahexaenoic acid; EPA: eicosapentaenoic acid; LA: linoleic acid. PC: phosphatidylcholine.

PC species (3 days post-PUFA)

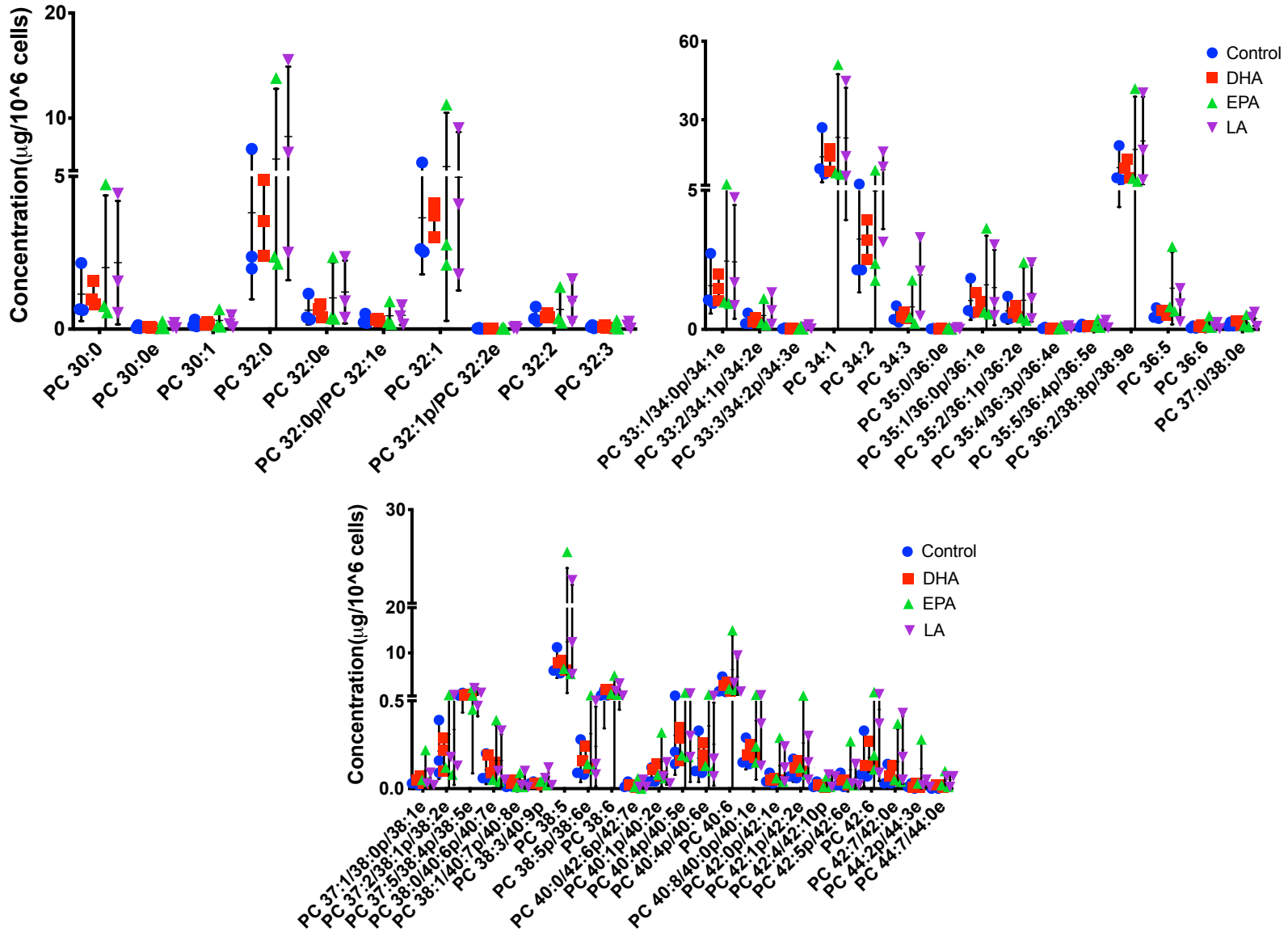


Figure 4.27 PC species levels measured in HDF after three days of PUFA supplementation. PC species were measured using UHPSFC-MS^E in HDF treated with 10 μ M DHA, EPA and LA for three days. Data are presented as absolute concentration in $\mu\text{g}/10^6$ cells (mean \pm SD). Comparisons were performed between the control and PUFA treated cells; (n=3 donors). Statistical analysis was performed using One-Way ANOVA comparing differences over treatment compared with control, with corrections for multiple analyses using the Dunnett method. PUFA: polyunsaturated fatty acid; HDF: human dermal fibroblast; DHA: docosahexaenoic acid; EPA: eicosapentaenoic acid; LA: linoleic acid. PC: phosphatidylcholine.

PC species (7 days post-PUFA)

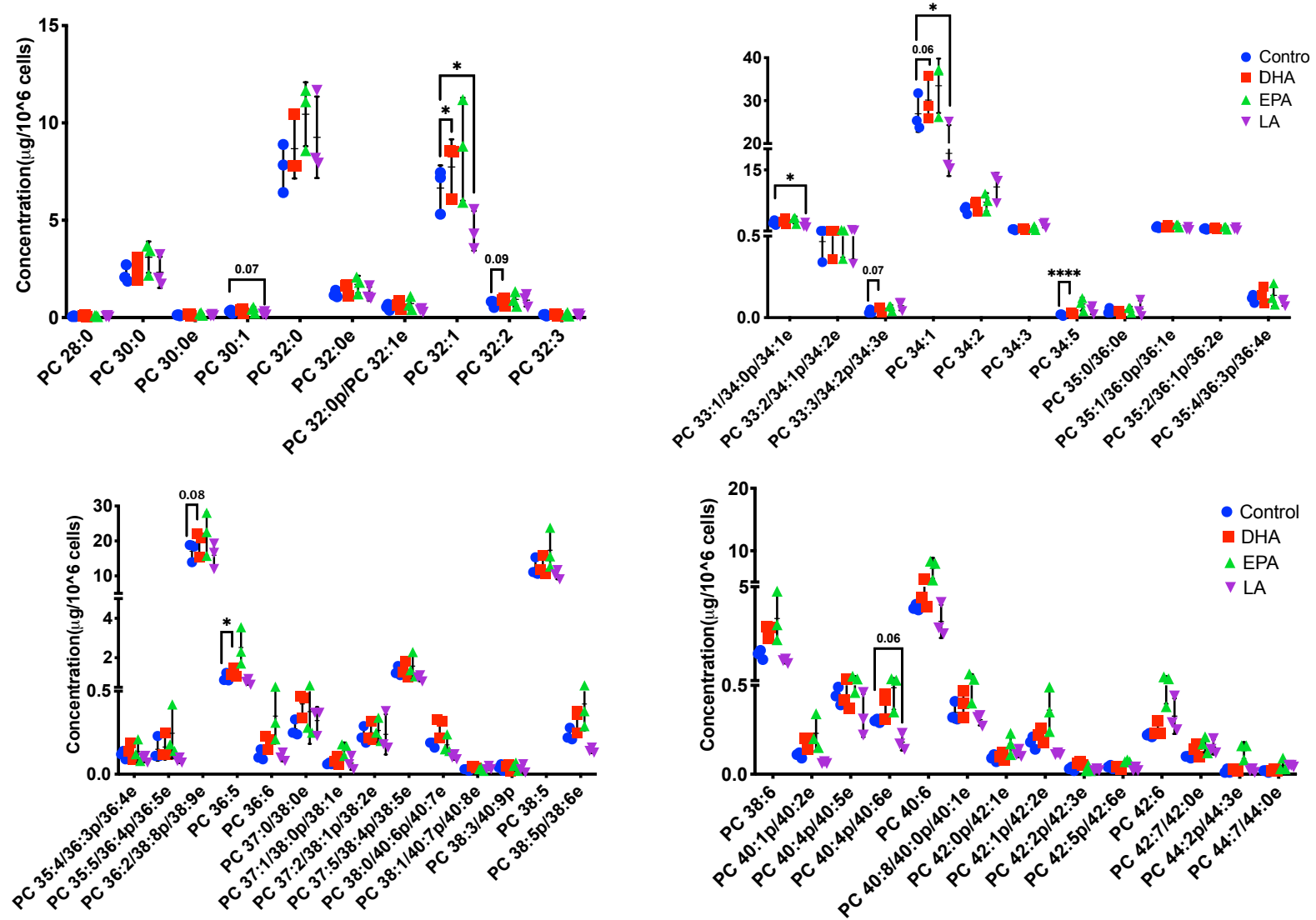


Figure 4.28 PC species levels measured in HDF after seven days of PUFA supplementation. PC species were measured using UHPSFC-MS^E in HDF treated with 10 μ M DHA, EPA and LA for seven days. Data are presented as absolute concentration in $\mu\text{g}/10^6$ cells (mean \pm SD). Comparisons were performed between the control and PUFA treated cells; (n=3 donors). Statistical analysis was performed using One-Way ANOVA comparing differences over treatment compared with control, with corrections for multiple analyses using the Dunnett method; *p < 0.05; ****p < 0.0001. PUFA: polyunsaturated fatty acid; HDF: human dermal fibroblast; DHA: docosahexaenoic acid; EPA: eicosapentaenoic acid; LA: linoleic acid. PC: phosphatidylcholine.

Total LPC in HDF

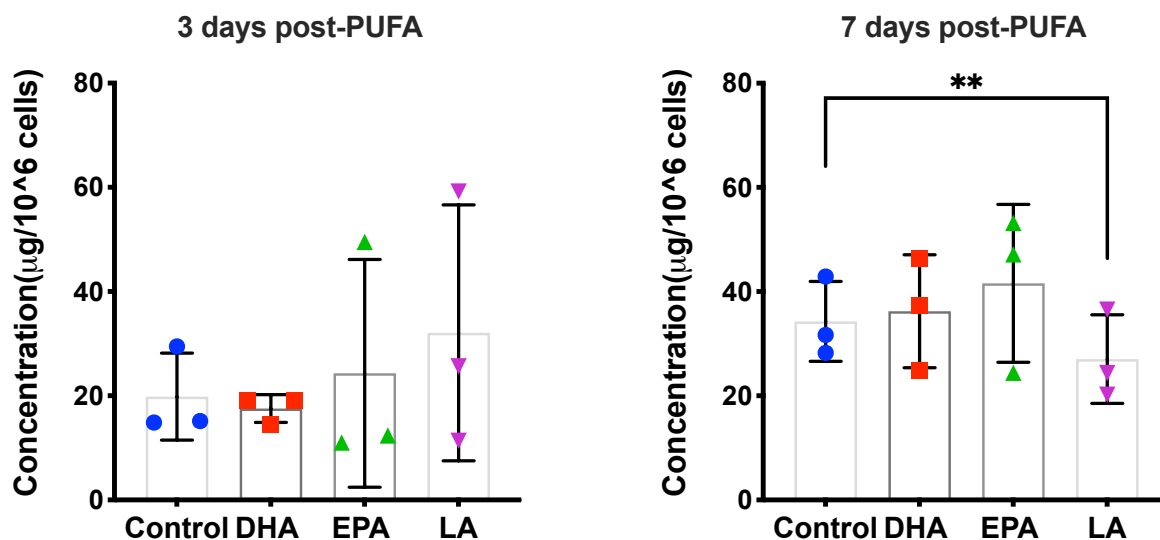


Figure 4.29 The effect of PUFA supplementation on total LPC levels measured in HDF. Total LPC was measured using UHPSFC-MS^E in HDF treated with 10 µM DHA, EPA and LA for three and seven days. Data are presented as absolute concentration in µg/10⁶ cells (mean ± SD). Comparisons were performed between the control and PUFA treated cells of the same time-point; (n=3 donors). Statistical analysis was performed using One-Way ANOVA comparing differences over treatment compared with control, with corrections for multiple analyses using the Dunnett method; **p <0.01. PUFA: polyunsaturated fatty acid; HDF: human dermal fibroblast; DHA: docosahexaenoic acid; EPA: eicosapentaenoic acid; LA: linoleic acid. LPC: lysophosphatidylcholine.

LPC species in HDF

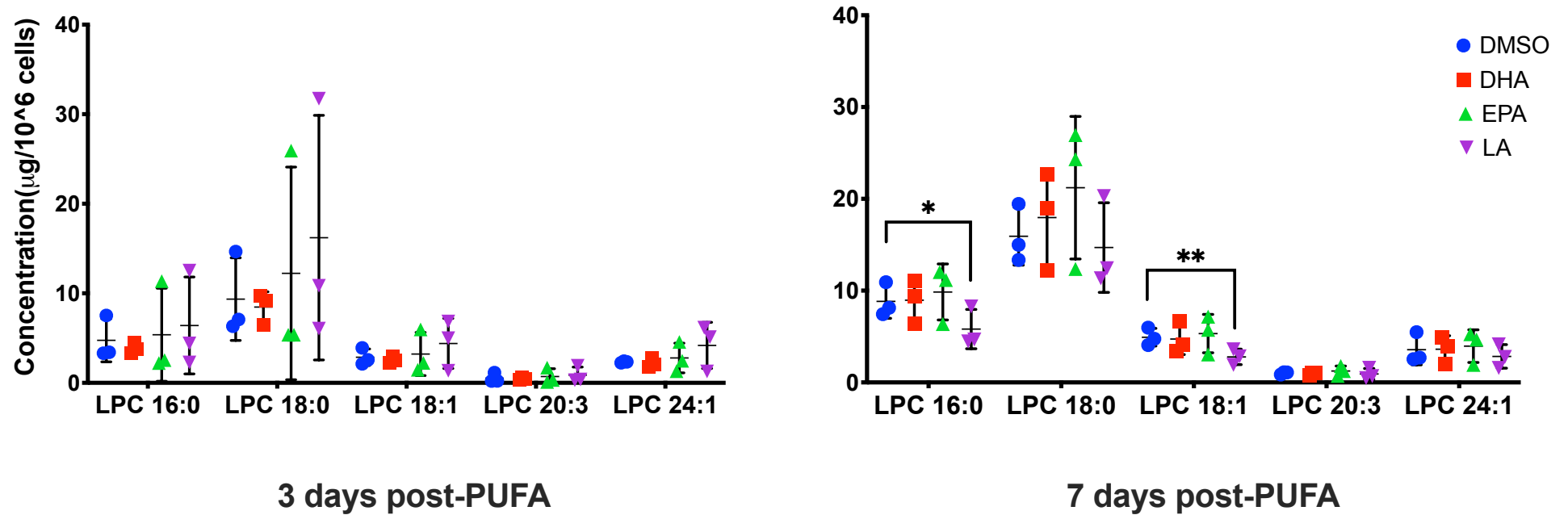


Figure 4.30 The effect of PUFA supplementation on total LPC species levels measured in HDF. LPC species were measured using UHPSFC-MS^E in HDF treated with 10 μ M DHA, EPA and LA for three and seven days. Data are presented as absolute concentration in μ g/ 10^6 cells (mean \pm SD). Comparisons were performed between the control and PUFA treated cells of the same time-point; (n=3 donors). Statistical analysis was performed using One-Way ANOVA

comparing differences over treatment compared with control, with corrections for multiple analyses using the Dunnett method; *p <0.05; **p <0.01. PUFA: polyunsaturated fatty acid; HDF: human dermal fibroblast; DHA: docosahexaenoic acid; EPA: eicosapentaenoic acid; LA: linoleic acid. LPC: lysophosphatidylcholine.

4.4 Discussion

PUFAs are major bioactive lipids involved in skin health, which demonstrate healing properties. However, there is a lack of research on the molecular mechanisms by which PUFAs target dermal lipids and protect the skin. Therefore, a lipidomic analysis of skin CERs and membrane lipids in HDF was performed to monitor alterations in the dermal lipid profiles in response to *n*-3 and *n*-6 PUFA supplementation. Generally, CER levels increased in a time-dependent manner where concentrations were higher in control HDF cultured for seven days when compared with cells cultured for three days. The reason for this could be that fibroblasts are characterised by a steady and slow growth rate during homeostasis, and proliferation is stimulated during skin injury such as in wound healing (Ejiri et al., 2015). Kendall et al. previously demonstrated a significant increase in CER[NS] and CER[NDS] species in isolated dermis tissue with EPA supplementation, whereas DHA also had an effect on these dermal CERs but changes did not reach statistical significance (Kendall et al., 2017). In agreement with this, we found a significant increase in CER levels with *n*-3 PUFA supplementation in HDF. DHA significantly enhanced the concentration of several CER[NS] species (**Figure 4.3**) in addition to A(24)H(18) ($p = <0.0001$), whereas EPA supplementation significantly increased N(25)H(16) ($p = 0.007$). Other than our group's previous study, no information is available on the effect of *n*-3 PUFA supplementation on CER synthesis in the dermis. However, increasing the concentration of CER[NS] and the two 6-hydroxyceramides in HDF with *n*-3 PUFAs could indicate their signaling and protective roles in the skin, respectively.

To elucidate the main increases seen in CER[NS] species with DHA, alterations in carbon chain lengths were examined. DHA mainly increased the concentration of long-chain CERs with a fatty-acyl chain length of C23-C25 (**Figure 4.8**). This could support the explanation suggesting the protective role of DHA in the dermis by increasing the levels of long-chain CERs, which are crucial for skin health as discussed in **Chapter 1**. Interestingly, DHA and EPA downregulated the expression of *CERS5* ($p = 0.008$) and *CERS6* ($p = 0.049$), respectively (**Figure 4.9 D,E**). Both *CERS5* and *CERS6* are expressed ubiquitously and have a fatty-acyl preference for the short-chain C14-C16 FAs (**Table 1.2**). Further investigation of membrane lipid

metabolism in HDF showed an effect of DHA on SM levels where DHA significantly increased SM 40:1 and reduced SM 40:2 at 7 days post supplementation ($p=0.04$, $p<0.0001$, respectively) (**Figure 4.18**). Taken together, this could be an indication for a mechanism by which DHA targets CER synthesis in the dermis by utilizing SM. Although SM usually generates both CER[NS] and CER[AS] in the SC, we did not detect CER[AS] in HDF (Uchida et al., 2000). Additionally, Kendall et al. did not find any changes in CER[AS] with *n*-3 PUFA supplementation in the dermis (Kendall et al., 2017). Furthermore, DHA significantly increased the long-chain PC 32:1, PC 34:5 and PC 36:5 ($p=0.04$, $p<0.0001$, $p=0.04$, respectively), which could reflect the alteration in CER and SM levels seen with DHA as SM is broken down to CER and choline, which then generates PC. The reduction in PE species, was observed with the 3-day DHA supplementation, whereas no significant changes were found at 7-days post-DHA (**Figure 4.25**). The metabolism of membrane lipids is tightly regulated and interconnected. PE, for example, could generate PC, which are both found to be the most abundant glycerophospholipids in the skin (van der Veen et al., 2017). Therefore, the early reduction in PE could reflect the increase in PC observed at 7-days post DHA supplementation. Additionally, PE and PC are structural and functional membrane lipids involved in signaling process in the production of lipid mediators and inflammation (Wertz, 1992).

With regard to the effect of *n*-6 PUFAs on fibroblast lipids, LA supplementation mainly altered membrane lipid levels, whereas no significant effect was observed in CER concentration or biosynthesis enzyme mRNA levels. However, one possible explanation there seemed to be an increase in CER levels with LA but did not reach statistical significance, could be that the increase in CER levels is due to increased cell growth. Additionally, when performing MTT assay to assess LA toxicity on HDF, there was a dose and time-dependent increase in HDF growth with LA supplementation (**Appendix 6**). Treating HDF with AA and LA has been found to stimulate fibroblast growth and proliferation when added to DMEM supplemented with serum (Ejiri et al., 2015). Moreover, LA suppressed most long-chain membrane lipids at 7 days post supplementation. There was a significant reduction in membrane lipids used for energy production, inflammatory response and apoptosis, suggesting a proliferative effect of LA on HDF. CE 22:6 concentration

was significantly decreased ($p= 0.03$), and several long-chain TG species as well: TG 48:1, TG 50:1 and TG 50:2 ($p= 0.03$, $p= 0.003$, $p= <0.0001$, respectively) (**Figure 4.23**). In addition to being a source of energy, TG is used to produce inflammatory lipid mediators (Lass et al., 2011). Therefore, the alteration in CE and TG levels could be a sign of cellular growth. Interestingly, *n*-6 PUFA seemed to have the opposite effect on PC metabolism in HDF to that of *n*-3 PUFA, where it significantly reduced PC 32:1, PC 33:1/34:0p/34:1e and PC 34:1 level ($p= 0.048$, $p= 0.02$, $p= 0.03$, respectively). This could explain the significant reduction in total proapoptotic LPC levels ($p= 0.009$), and two LPC species: LPC 16:0 and LPC 18:1 ($p= 0.02$, $p= 0.007$, respectively) (**Figure 4.30**). In agreement with our observations, *n*-6 PUFA was found to enhance wound closure at early stages of injury in mouse skin, whereas DHA was associated with delayed wound closure and increased inflammatory cells, suggesting a distinctive effect of *n*-6 and *n*-3 PUFA on the dermis in wound healing (Cardoso et al., 2004).

4.5 Conclusion

This study demonstrates the differential effect of *n*-3 and *n*-6 PUFA supplementation on lipid metabolism in HDF. While DHA and EPA stimulated CER synthesis by altering membrane lipid levels, LA significantly reduced membrane lipid concentrations without affecting CER synthesis. DHA seemed to utilize membrane SM in favor of CER and PC generation in HDF, which could indicate its involvement in inflammatory and signaling pathways in the dermis. On the other hand, LA reduced CE, TG, PC and LPC levels, suggesting a role for *n*-6 PUFAs in prevention of apoptosis and stimulation of fibroblast growth. The reason for this differential response of HDF to PUFAs requires further investigation, as most studies on skin CERs are on the epidermis. However, this project could show possible mechanisms by which *n*-3 and *n*-6 PUFAs could affect lipid metabolism in the dermis.

Chapter 5

Skin and plasma analysis of ceramides, endocannabinoids, monoacylglycerols and N-acylethanolamines in a streptozotocin-diabetic rat model of peripheral neuropathy

5.1 Introduction

A few studies on the functional properties of the permeability barrier in diabetes reported barrier dysfunction and changes in SC lipids including CERs (Sakai et al., 2003, Sakai et al., 2005, Kim et al., 2018). Additionally, diabetic peripheral neuropathy (DPN), also known as distal symmetric polyneuropathy, is a serious diabetic complication with skin manifestations, which have severe impact on patient morbidity and healthcare costs (Callaghan et al., 2012a, Pop-Busui et al., 2017). However, the specific mechanisms that are involved in DPN pathogenesis are not fully understood (Alam et al., 2020, England et al., 2005). As the name suggests, DPN is the dysfunction of the peripheral nerves in diabetic patients, which initially affects sensory neurons that connect distal tissues such as the limbs, to the central nervous system (CNS) (Callaghan et al., 2012a). In DPN, distal symmetric sensory manifestations start in the feet with a “stocking and glove distribution” and early painful symptoms include allodynia (pain due to non-painful stimulus), paraesthesia (burning or prickling sensation) and hyperalgesia (hypersensitivity) (Bansal et al., 2006). Advanced DPN leads to peripheral nerve fiber degeneration and consequently, loss of sensation (Said, 2007). This loss of sensation, along with angiopathy, puts the patient at an increased risk for unnoticed injury and impaired wound healing, which could develop into diabetic foot syndrome (Volmer-Thole and Lobmann, 2016, Brem and Tomic-Canic, 2007).

Globally, there are around one million amputations annually due to diabetic foot ulcers (Singh et al., 2020). In the UK, foot ulcer care resulting from DPN and poor wound healing costs about £1 billion (Jeffcoate et al., 2018). However, the International Diabetes Federation mention in their latest Diabetes Atlas edition that these costs could be significantly reduced with proper management of diabetes complications (Williams et al., 2020). There is an urgent need for updated early screening techniques and novel research that looks into alternative pathological mechanisms to the classical pathways associated with hyperglycemia; such as dyslipidemia related mechanisms, and potential new therapeutic targets such as ceramides (Perez-Matos et al., 2017). Since DPN is a complication of diabetes with manifestations in the skin, it is important to consider exploring the tissue at which these debilitating symptoms occur (Callaghan et al., 2012b).

As previously discussed in (**Chapter 1**), the skin is a multifunctional sensory organ that contains a highly interconnected immuno- and neurobiological network of specialised cells which include CER producing keratinocytes and fibroblasts, immune cells, in addition to sensory afferents and receptors (Chi et al., 2013, Kendall and Nicolaou, 2013). Skin CERs are major constituents of the skin permeability barrier, that enforce the barrier structurally and functionally to maintain skin homeostasis. Additionally, studies on diabetic and non- diabetic dermopathies have reported alterations in SC CER to be major contributors in barrier disruption (Jungersted et al., 2010, Kim et al., 2018).

There is a lack of research that points out the potential role of cutaneous CERs in the development of DPN related dermopathies. In addition to this, evidence linking systemic CERs and DPN is scarce. It has been suggested that mutations in the rate-limiting CER synthesis enzyme, SPT, might be a common factor for the development of neuropathy in diabetes. For example, it has been found that mutations in SPT subunit-1 lead to the production of the neurotoxic deoxy-CERs, that have been first reported in the hereditary sensory autonomic neuropathy (HSAN), HSAN1, which closely resembles DPN, and in type-2 diabetes (Bertea et al., 2010, Dawkins et al., 2001). Additionally, a study on plasma sphingolipid profile in DPN, showed that deoxy-CER[NS] were increased in the plasma of type-2 diabetic patients with DPN but not in that of patients with non-diabetic sensory neuropathies (Dohrn et al., 2015). Another pilot study showed that increased very long chain plasma deoxy-CER[NS] and alterations in biological CER species were diagnostic factors in DPN patients, as they were elevated in the plasma of type-1 diabetic patients with DPN but not in diabetics without neuropathy symptoms (Hammad et al., 2017). In addition, the precursor of dihydroceramides, palmitate, has been found have a pro- apoptotic effect in immortalized mouse Schwann cells and rat primary Schwann cells (Suzuki et al., 2011). These findings could show that alterations in circulating CERs may be a predisposing factor for DPN development in diabetic patients. However, studies on the role of CER in diabetes and DPN development are limited; more studies are therefore required to confirm the underlying pathogenetic mechanisms involved.

In addition to CERs, the endocannabinoid system plays a significant role in regulating physiological and pathological processes by mediating mechanisms such as lipogenesis, energy metabolism, immune and inflammatory response (Argenziano et al., 2019, Vettor and Pagano, 2009). Endocannabinoids, along with their receptors (CB₁, CB₂) and bioactive analogues, have been implicated in systemic and peripheral bioactivities associated with diabetes and its complications such as DPN (Gruden et al., 2016). For example, activation of CB₁ receptors in pancreatic β -cells has been found to negatively affect the glucose-mediated release of insulin and glucose homeostasis (Juan-Picó et al., 2006). Similarly, CB₁ receptor activation by ANA was found to cause glucose intolerance, whereas CB₁ receptor antagonists were suggested as therapeutic drugs in obesity-related diabetes (Bermúdez-Siva et al., 2006). In addition, alterations in endocannabinoids and the activity of CB₁ receptor have been reported in obese patients with type-2 DM, and were found to be associated with metabolic dysfunction and impaired insulin sensitivity (Annuzzi et al., 2010). On the other hand, CB₂ receptor agonists have been shown to ameliorate inflammatory responses and tissue injury, and to improve diabetes-related complications such as neuropathic pain (Kumawat and Kaur, 2019, Soethoudt et al., 2017). Moreover, endocannabinoids play a crucial role in mediating skin inflammatory and immune response and have been implicated in various skin diseases and wound healing (Kendall and Nicolaou, 2013, Tóth et al., 2019). Endocannabinoid receptors have been found to be highly expressed in cutaneous nerve endings (Ständer et al., 2005). In addition, it has been found that AEA and its CB₁ receptor negatively affect keratinocyte differentiation (Maccarrone et al., 2003). Most studies on the endocannabinoid system in DPN, however, are around therapeutic strategies that target neuropathic pain. Keratinocyte CB₂ receptors in the epidermis of rat hind paws, were found to be involved in antinociceptive mechanisms (Ibrahim et al., 2005). Additionally, in STZ-diabetic rats, blocking endocannabinoid transport was found to improve DPN-related pain (Hasanein and Soltani, 2009).

From this, it could be shown that studies on systemic CERs and endocannabinoids in non-obesity related type-1 diabetes and DPN are limited. Similarly, there are currently no studies on the involvement of skin CERs and endocannabinoids in the development of DPN. In the present study, we aim to investigate changes in the

levels of skin and systemic CERs and bioactive lipid mediators in an animal model of type-1 diabetes with DPN. In addition to the main initial hyperglycemia related pathways in DPN, we hypothesize that potential changes in skin bioactive lipids profile are involved in the local neuropathy and could be reflected by alterations in systemic bioactive lipids levels.

Specific objectives:

To examine differences in cutaneous and systemic lipid levels in DPN when compared with control by analysing:

- 1) skin CERs and endocannabinoids and their congeners, in addition to,
- 2) plasma CERs and endocannabinoids and their congeners in an STZ-induced type-1 DM rat model of DPN.

5.2 Materials and methods

5.2.1 Animal model and tissue samples

The animal model was prepared, and samples were provided by Louisa Zolkiewski, Dr Natalie Gardiner and Dr Richard Unwin (University of Manchester). All experiments were conducted using adult male Wistar rats (start weight 300-400g; Charles River, UK) in accordance with the UK Animals (Scientific Procedures) Act 1986, EU-201063 and ethical approval (University of Manchester AWERB). When rats weighed around 300gm (8-10 weeks old) diabetes was induced by an intraperitoneal STZ injection as described in (Freeman et al., 2016, Newton et al., 2017, Zhang et al., 2019, Karamoysoyli et al., 2008). STZ (Sigma, UK:Cat No. S0130); 55 mg/kg diluted in 0.9% w/v sterile saline was administered the morning after an overnight fast. After three days, blood glucose levels were measured using a strip-operated reflector photometer (Aviva Blood Glucose Meter System (Accuchek®)). Animals with blood glucose less than 15mmol/L were excluded from the study. The required duration of STZ-induced diabetes to initiate peripheral nerve damage is from 8 to 16 weeks (Biessels et al., 2014, Freeman et al., 2016). Therefore, plasma and hind foot pad skin samples from diabetic and age-matched naïve controls were collected at 8, 12 and 16 weeks post STZ-induced diabetes. For long-term maintenance, diabetic rats of the 16 week group were treated with a subcutaneous slow-release insulin pellet (~1 U insulin/day; Linshin, Canada; inserted under isoflurane anaesthesia (induced at 4% isoflurane and maintained at

2% oxygen flow rate approximately 1L/min) with post-operative analgesia (buprenorphine 0.001mg/kg) on week 12. This dose of insulin was sufficient to maintain condition, but did correct hyperglycaemia (details and blood glucose levels found in [https://www.research.manchester.ac.uk/portal/en/theses/investigating-the-pathogenesis-of-urinary-bladder-dysfunction-in-experimental-diabetes-mellitus\(de49d2cd-ba56-4b74-8022-84458d95c4e7\).html](https://www.research.manchester.ac.uk/portal/en/theses/investigating-the-pathogenesis-of-urinary-bladder-dysfunction-in-experimental-diabetes-mellitus(de49d2cd-ba56-4b74-8022-84458d95c4e7).html)). All tissue samples were stored at -80°C awaiting analysis.

5.2.2 Analysis of skin and plasma ceramides, endocannabinoids and their related mediators using UPLC/ESI-MS/MS

Skin and plasma sample lipid extraction was performed as described in (Section 2.5.3). Lipidomic analysis was performed using ultraperformance liquid chromatography coupled to electrospray ionisation with triple quadrupole tandem mass spectrometry (UPLC/ESI-MS/MS) (Section 2.5.4). Appendix 3, 4 lists the MRM transitions and indicative retention times for skin and plasma lipidomic analysis. Data were processed using MassLynx software (Waters). Semi-quantitation using internal standards was used for ceramides, while endocannabinoids and NAE were quantitated against calibration lines constructed using commercially available standards. Finally, lipid quantities were normalised to protein content for skin, or sample volume for plasma. Protein content determination is described in (Section 2.4.4.3). Data from different time-points were not compared in order to eliminate intra-batch variability due to age difference as it was not the aim of this study. Statistical analysis was performed using t-tests with corrections for multiple analyses using the Holm-Sidak method. Data were presented as mean \pm SD; $p < 0.05$ was considered statistically significant (GraphPad Prism software).

5.3 Results

5.3.1 There was a significant decrease in CER[NH] levels in STZ-diabetic skin

Differences in skin CER levels between control and diabetes were analysed by UPLC/ESI-MS/MS (Section 2.5.4). Skin from STZ-diabetic and age-matched control rats was arranged into three groups based on time of sample collection post-

STZ injection. Skin was sampled at 8 weeks (diabetic n=8, control n=9), 12 weeks (diabetic n=4, control n=4) and 16 weeks (diabetic n=6, control n=6) post-STZ. The 16 weeks diabetic group received insulin. For each sample analysed, concentrations of detected CER species were reported as absolute values in ng/mg protein (mean \pm SD). All ceramides detected in the diabetic skin samples were detected in and compared to their representative control samples. Data were categorised based on ceramide class and carbon chain numbers to help identify possible trends.

5.3.1.1 No differences were found in total ceramide levels between control and STZ-diabetic animals

The amounts of individual ceramide species were quantitated and totalled. **Figure 5.1** shows the concentrations (ng/mg protein) for total CER measured in control and diabetic skin. No significant change was found in total CER levels between control and diabetes.

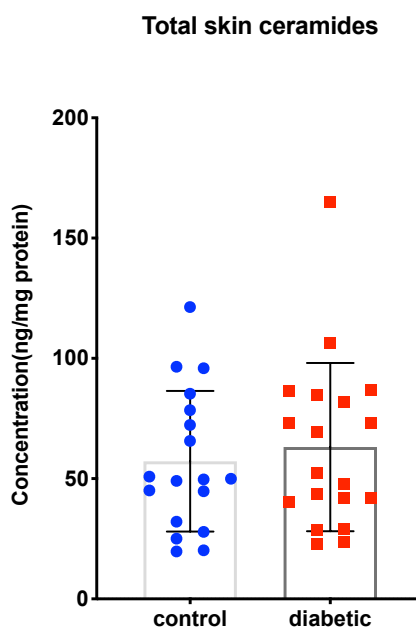


Figure 5.1 Total ceramide concentration in control and STZ- diabetic rat skin. Total ceramide concentration was measured using UPLC/ESI-MS/MS in control and diabetic skin collected at 8, 12 and 16 weeks post-STZ. Comparisons were performed between the control and diabetic group of the same time point; 8 weeks post-STZ control n=8, diabetic n=9; 12 weeks post-STZ control n=4, diabetic n=4; 16 weeks post-STZ control n=6, diabetic n=6. Results are expressed as absolute concentration in ng/mg protein (mean \pm SD). Log transformed data were analysed by t-tests with corrections for multiple analyses using the Holm-Sidak method. STZ: streptozotocin.

5.3.1.2 Total CER[NH] levels were reduced with diabetes

Six CER classes were detected in rat skin: CER[NDS], CER[NS], CER[NH], CER[AS] CER[AP], CER[EOH]. Although no difference was found in total CER levels, examining individual CER classes revealed a close to significant decrease in total CER[NH] at 16 weeks post-STZ ($p=0.05$) (**Figure 5.2**).

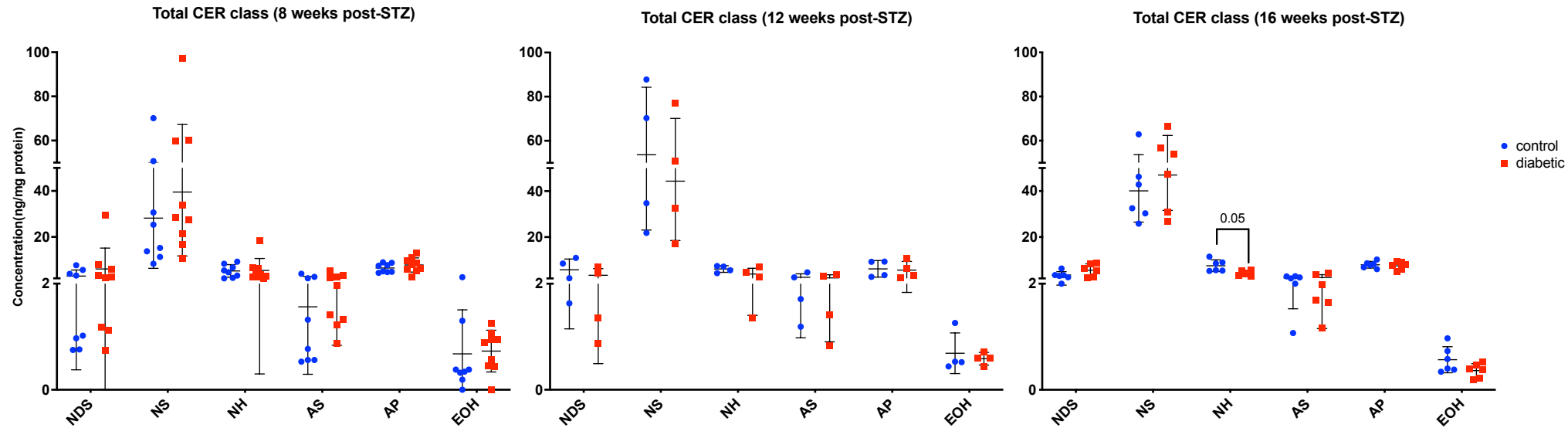


Figure 5.2 Total CER classes measured in control and STZ-diabetic rat skin. Ceramide class totals measured using UPLC/ESI-MS/MS in control and diabetic skin collected at 8,12 and 16 weeks post-STZ; data presented as absolute concentration in ng/mg protein (mean \pm SD); Comparisons were performed between the control and diabetic group of the same time point; 8 weeks post-STZ control n=8, diabetic n=9; 12 weeks post-STZ control n=4, diabetic n=4; 16 weeks post-STZ control n=6, diabetic n=6. Log transformed data were analysed by t-tests with corrections for multiple analyses using the Holm-Sidak method; *p < 0.05. STZ: streptozotocin; CER: ceramide; NDS: non-hydroxy dihydroceramide; NS: non-hydroxyceramide; NH: non-hydroxy 6-hydroxyceramide; AS: alpha-hydroxyceramide; AP: alpha-hydroxy phytoceramide; EOH: ester-linked omega 6-hydroxyceramide.

5.3.1.3 Several CER[NH] species were decreased with diabetes

Individual species were analysed to observe possible trends in skin CER metabolism between control and diabetes. **Figure 5.3-5.6** shows the CER species that were detected in each class: CER[NDS] (six species), CER[NS] (14 species), CER[NH] (10 species), CER[AS] (four species), CER[AP] (10 species) and CER[EOH] (two species). There was a significant difference between control and diabetes in several CER[NH] species at 16 weeks post-STZ; this group received insulin. The decrease was most significant in the following species: N(24)H(17) ($p=0.01$), N(23)H(18) ($p=0.0003$), N(24)H(18) ($p=0.02$), N(25)H(18) ($p=0.001$), N(26)H(18) ($p=0.02$) (**Figure 5.4**). No significant differences between control and diabetes were observed in individual species from other classes.

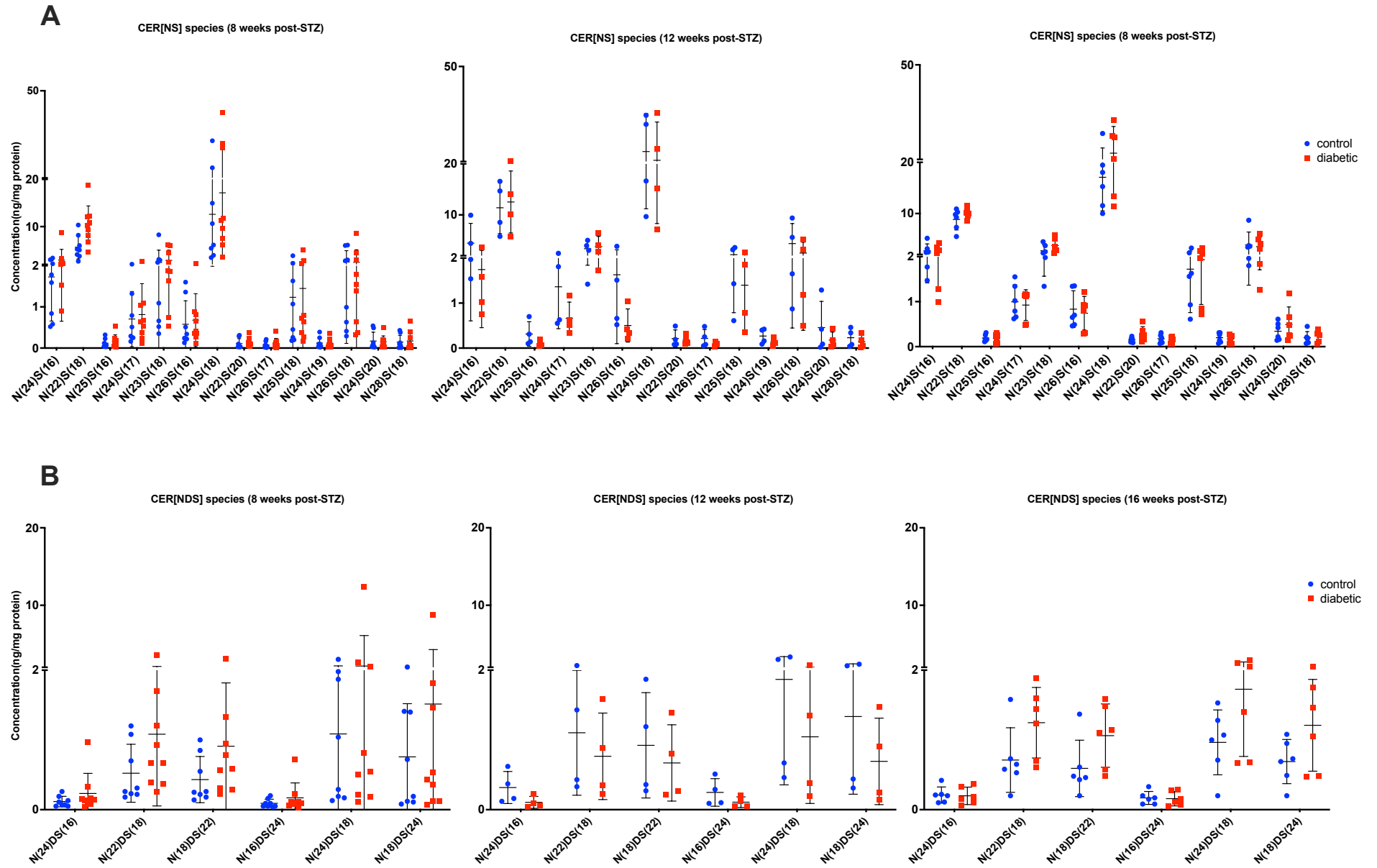


Figure 5.3 CER[NDS] and CER[NS] species measured in control and STZ-diabetic rat skin. A) CER[NS] species totals measured using UPLC/ESI-MS/MS in control and diabetic skin collected at 8,12 and 16 weeks post-STZ; data presented as absolute concentration in ng/mg protein (mean \pm SD); B) CER[NDS] species totals measured using UPLC/ESI-MS/MS in control and diabetic skin collected at 8,12 and 16 weeks post-STZ; data presented as absolute concentration in ng/mg protein (mean \pm SD). Comparisons were performed between the control and diabetic group of the same time point; 8 weeks post-STZ control n=8, diabetic n=9; 12 weeks post-STZ control n=4, diabetic n=4; 16 weeks post-STZ control n=6, diabetic n=6. Log transformed data were analysed by t-tests with corrections for multiple analyses using the Holm-Sidak method. STZ: streptozotocin; CER[NDS]: non-hydroxy dihydroceramide; CER[NS]: non-hydroxyceramide.

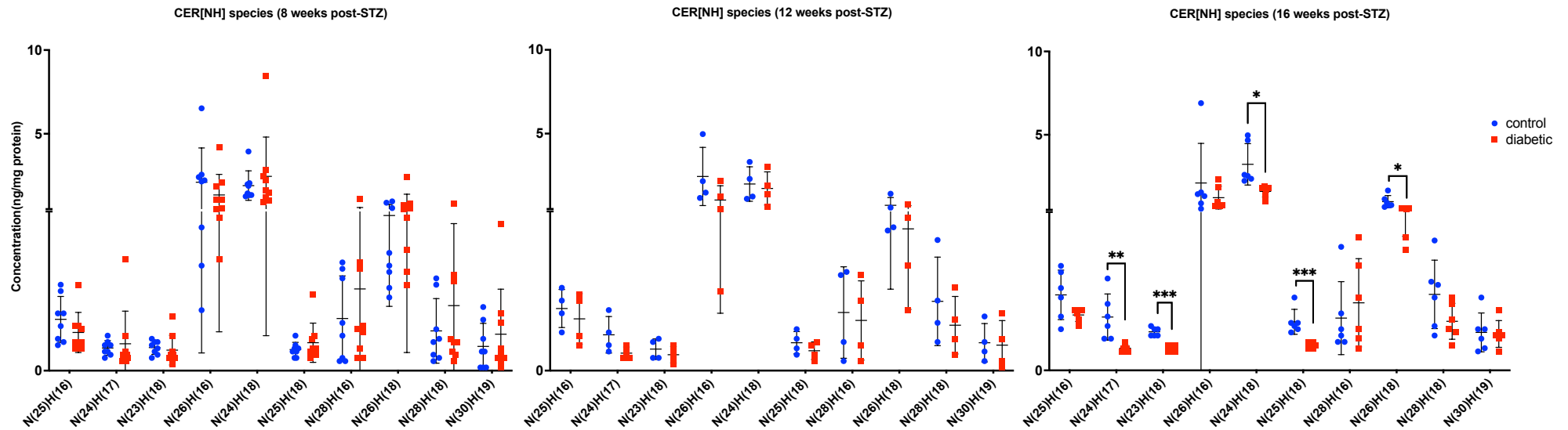


Figure 5.4 CER[NH] species measured in control and STZ-diabetic rat skin. CER[NH] species totals measured using UPLC/ESI-MS/MS in control and diabetic skin collected at 8,12 and 16 weeks post-STZ; data presented as absolute concentration in ng/mg protein (mean \pm SD). Comparisons were performed between the control and diabetic group of the same time point; 8 weeks post-STZ control n=8, diabetic n=9; 12 weeks post-STZ control n=4, diabetic n=4; 16 weeks post-STZ control n=6, diabetic n=6. Log transformed data were analysed by t-tests with corrections for multiple analyses using the Holm-Sidak method; *p <0.05; **p<0.01; *** p<0.001. STZ: streptozotocin; CER[NH]: non-hydroxy 6-hydroxyceramide.

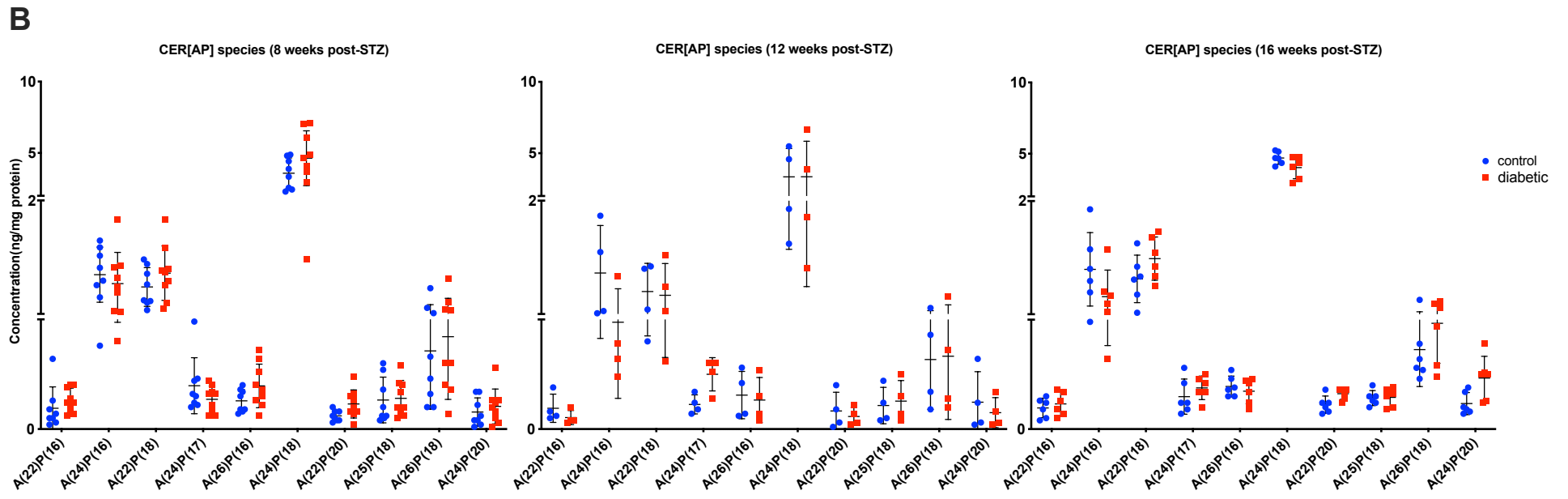
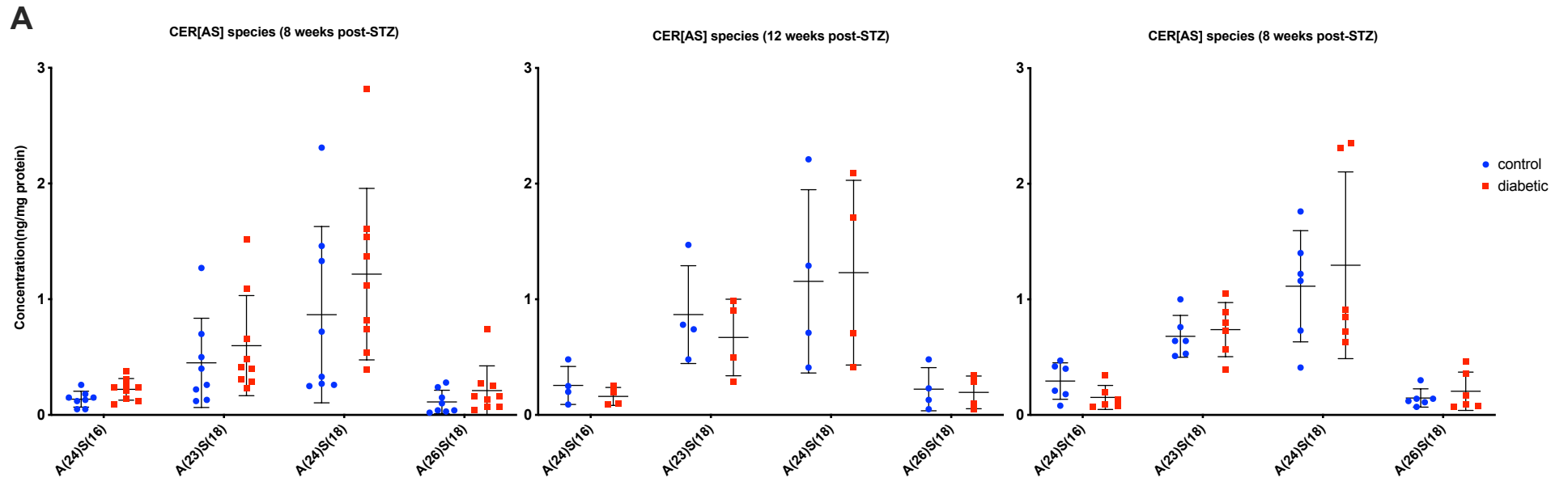


Figure 5.5 CER[AS] and CER[AP] species measured in control and STZ-diabetic rat skin. A) CER[AS] species detected in control and diabetic skin measured using UPLC/ESI-MS/MS in control and diabetic skin collected at 8,12 and 16 weeks post-STZ; data presented as absolute concentration in ng/mg protein (mean \pm SD); B) CER[AP] species measured using UPLC/ESI-MS/MS in control and diabetic skin collected at 8,12 and 16 weeks post-STZ; data presented as absolute concentration in ng/mg protein (mean \pm SD). Comparisons were performed between the control and diabetic group of the same time point; 8 weeks post-STZ control n=8, diabetic n=9; 12 weeks post-STZ control n=4, diabetic n=4; 16 weeks post-STZ control n=6, diabetic n=6. Log transformed data were analysed by t-tests with corrections for multiple analyses using the Holm-Sidak method. STZ: streptozotocin; CER[AS]: alpha-hydroxyceramide; CER[AP]: alpha-hydroxy phytoceramide.

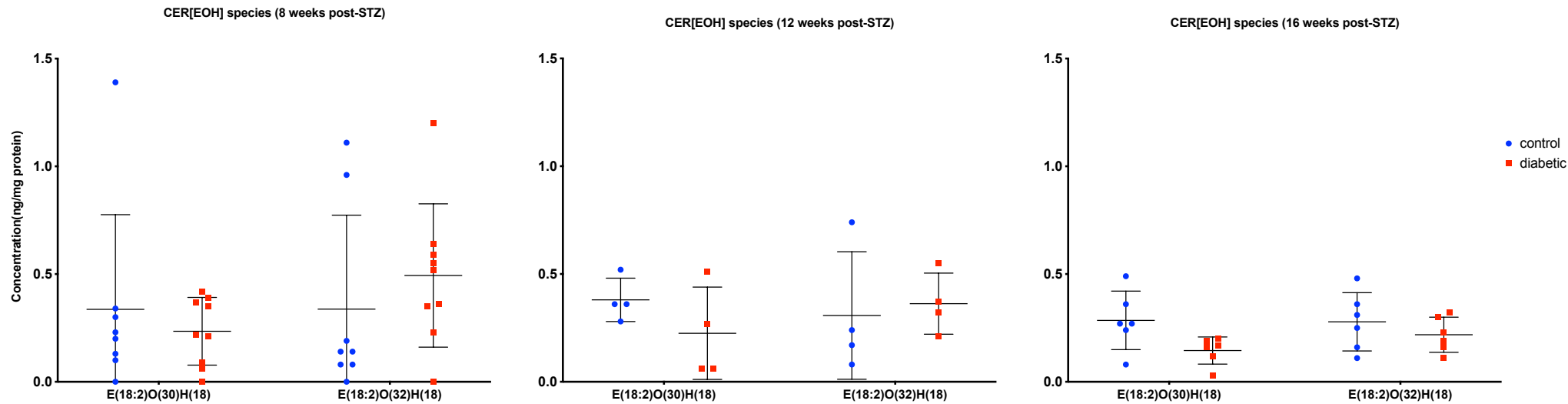


Figure 5.6 CER[E(OH)] measured in control and STZ-diabetic rat skin. CER[E(OH)] species detected in control and diabetic skin collected at 8,12 and 16 weeks post-STZ, data presented as absolute concentration in ng/mg protein (mean \pm SD). Comparisons were performed between the control and diabetic group of the same time point; 8 weeks post-STZ control n=8, diabetic n=9; 12 weeks post-STZ control n=4, diabetic n=4; 16 weeks post-STZ control n=6, diabetic n=6.

n=6. Log transformed data were analysed by t-tests with corrections for multiple analyses using the Holm-Sidak method. STZ: streptozotocin; CER[EOH]: ester-linked omega 6-hydroxyceramide.

5.3.1.4 No difference in total carbon number was found

The measured ceramides had a total carbon number that ranged from C38-C68 (**Figure 5.7**). Analysing ceramide total chain lengths (Total carbon number of the fatty acyl-chain + the sphingoid base-chain) did not show a significant difference between control and diabetes.

5.3.1.5 No difference in total sphingoid-base chains was observed

Ceramides measured had either a dihydrosphingosine, sphingosine, or 6-hydroxysphingosine base chain that ranged from C16-C24. No difference was found in total sphingoid-base chains between control and diabetes (**Figure 5.8**).

5.3.1.6 No difference in total fatty acyl-chain levels was observed

The fatty acyl-chains that were detected were either non-hydroxy acyl-chains or α -hydroxy acyl-chains and ranged from C16-C32 (**Figure 5.9**). Presenting the data according to fatty-acyl chain length, did not show any significant differences with diabetes.

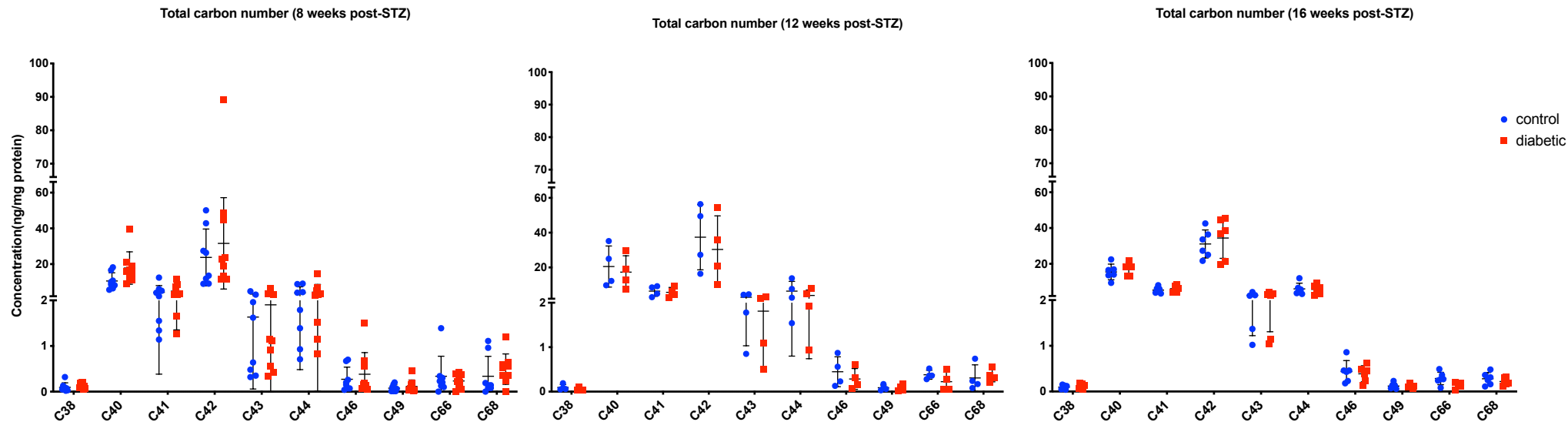


Figure 5.7 Total carbon chain number in control and STZ-diabetic rat skin. Total carbon number in skin ceramides measured using UPLC/ESI-MS/MS in control and diabetic skin collected at 8,12 and 16 weeks post-STZ; data presented as absolute concentration in ng/mg protein (mean \pm SD); Total carbon chain was calculated (sphingoid base-chain carbon number + fatty-acyl chain carbon number) then totaled. Comparisons were performed between the control and diabetic group of the same time point; 8 weeks post-STZ control n=8, diabetic n=9; 12 weeks post-STZ control n=4, diabetic n=4; 16 weeks post-STZ control n=6, diabetic n=6. Log transformed data were analysed by t-tests with corrections for multiple analyses using the Holm-Sidak method. STZ: streptozotocin; CER: ceramide; C: carbon number.

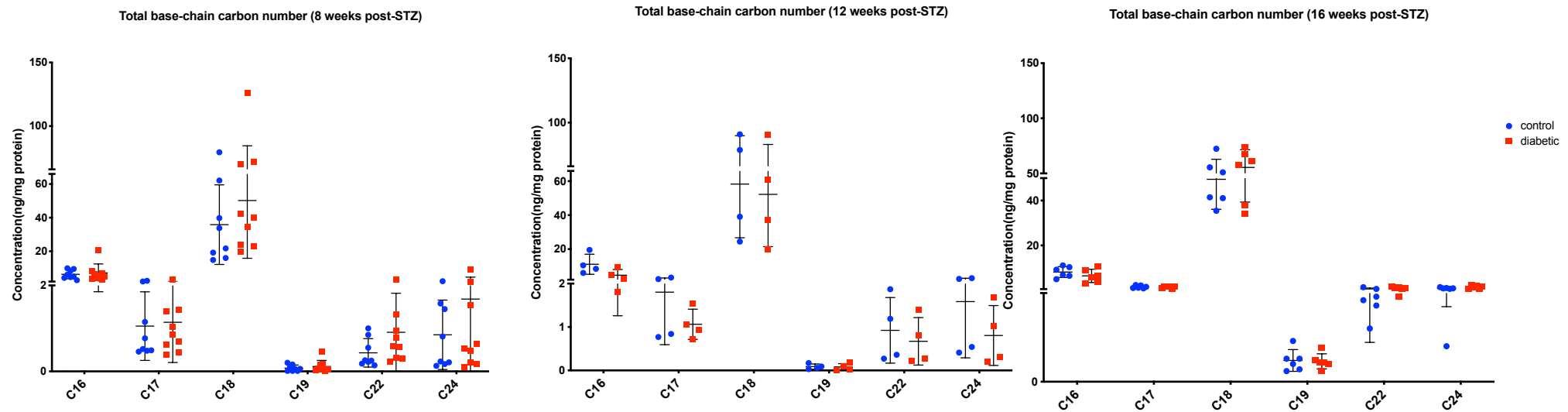


Figure 5.8 Total sphingoid base-chain length in control and STZ-diabetic rat skin. Total sphingoid base-chain length in skin ceramides measured using UPLC/ESI-MS/MS in control and diabetic skin collected at 8,12 and 16 weeks post-STZ; data presented as absolute concentration in ng/mg protein (mean \pm SD); Sphingoid-base carbon chains were totaled (example: C16 = total of all ceramides with C16 sphingoid base-chain). Comparisons were performed between the control and diabetic group of the same time point; 8 weeks post-STZ control n=8, diabetic n=9; 12 weeks post-STZ control n=4, diabetic n=4; 16 weeks post-STZ control n=6, diabetic n=6. Log transformed data were analysed by t-tests with corrections for multiple analyses using the Holm-Sidak method. STZ: streptozotocin; CER: ceramide; C: carbon number.

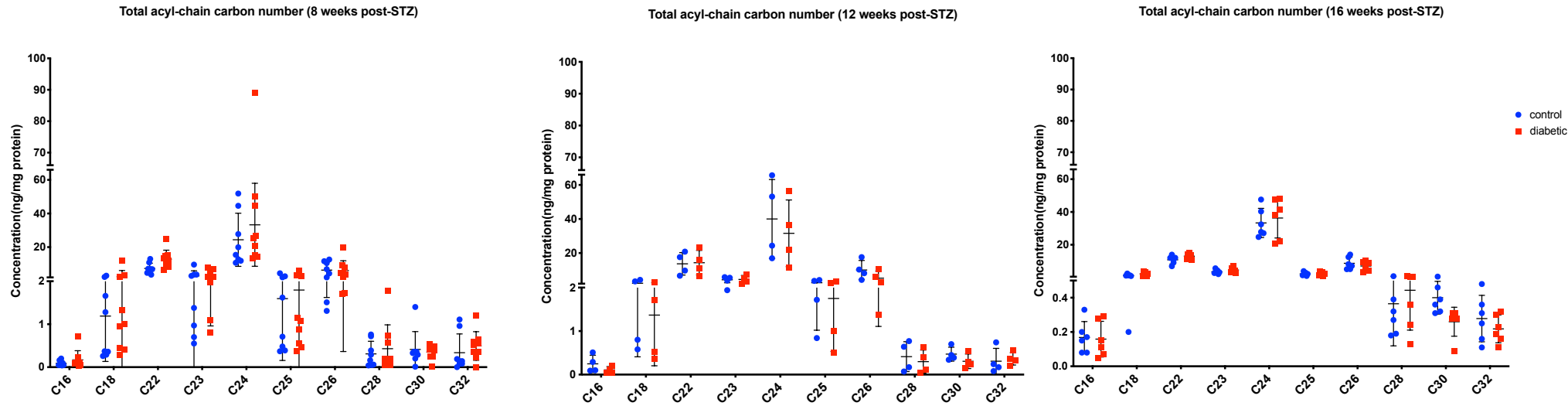


Figure 5.9 Total fatty acyl-chain length in control and STZ-diabetic rat skin. Total fatty acyl-chain length in skin ceramides measured using UPLC/ESI-MS/MS in control and diabetic skin collected at 8,12 and 16 weeks post-STZ; data presented as absolute concentration in ng/mg protein (mean \pm SD); Fatty-acyl carbon chains were totaled (example: C16 = total of all ceramides with C16 fatty-acyl chain). Comparisons were performed between the control and diabetic group of the same time point; 8 weeks post-STZ control n=8, diabetic n=9; 12 weeks post-STZ control n=4, diabetic n=4; 16 weeks post-STZ control n=6, diabetic n=6. Log transformed data were analysed by t-tests with corrections for multiple analyses using the Holm-Sidak method. STZ: streptozotocin; CER: ceramide; C: carbon number.

5.3.2 There was a significant increase in CER[NDS] and CER[NS] levels in diabetic plasma compared with control

Differences in plasma CER levels between control and diabetes was analysed by UPLC/ESI-MS/MS (Section 2.5.4). Plasma from STZ-diabetic and age-matched control rats was arranged into three groups based on time of sample collection post-STZ injection. Plasma was sampled at 8 weeks (diabetic n=9, control n=9), 12 weeks (diabetic n=7, control n=7) and 16 weeks (diabetic n=6, control n=6) post-STZ. The 16 weeks diabetic group received insulin. For each sample analysed, concentrations of detected CER species were reported as absolute values in ng/ml plasma (mean \pm SD). All ceramides detected in the diabetic plasma samples were detected in and compared to their representative control samples. Data were categorised based on ceramide class and carbon chain numbers to help identify possible trends.

5.3.2.1 No significant difference was found in total ceramide levels

The amounts of individual ceramide species were quantitated and totalled. **Figure 5.10** shows the concentrations (ng/ml plasma) for total CER measured in control and diabetic plasma. No significant difference was found in total CER levels between control and diabetes.

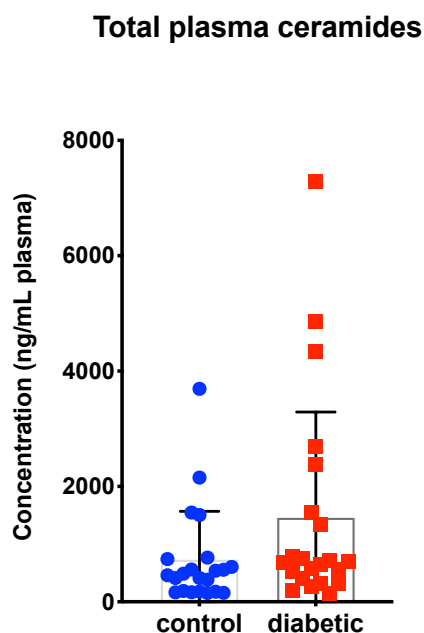


Figure 5.10 Total ceramide levels in control and STZ-diabetic rat plasma. Total ceramide concentration was measured using UPLC/ESI-MS/MS in control and diabetic plasma collected at 8,12 and 16 weeks post-STZ. Comparisons were performed between

the control and diabetic group of the same time point; 8 weeks post-STZ control n=9, diabetic n=9; 12 weeks post-STZ control n=7, diabetic n=7; 16 weeks post-STZ control n=6, diabetic n=6. Results are expressed as absolute concentration in ng/mL plasma (mean \pm SD). Log transformed data were analysed by t-tests with corrections for multiple analyses using the Holm-Sidak method. STZ: streptozotocin.

5.3.2.2 There was a significant increase in total CER[NDS] with diabetes

Presenting the data according to CER class totals could help monitor effects on the ceramide *de novo* biosynthesis enzymes that produce ceramides with a specific sphingoid base-chain; dihydrosphingosine (SPT), sphingosine (Des1) or 6-hydroxysphingosine (unidentified). Four CER classes were detected in rat plasma: CER[NDS], CER[NS], CER[AS], CER[AH]. Although no difference was found in total CER levels, examining individual CER classes revealed a significant increase in CER[NDS] ($p= 0.03$) and a close to significant increase in CER[NS] ($p= 0.05$) at 12 weeks post-STZ. No significant change was found in other CER classes or at the other time-points (**Figure 5.11**).

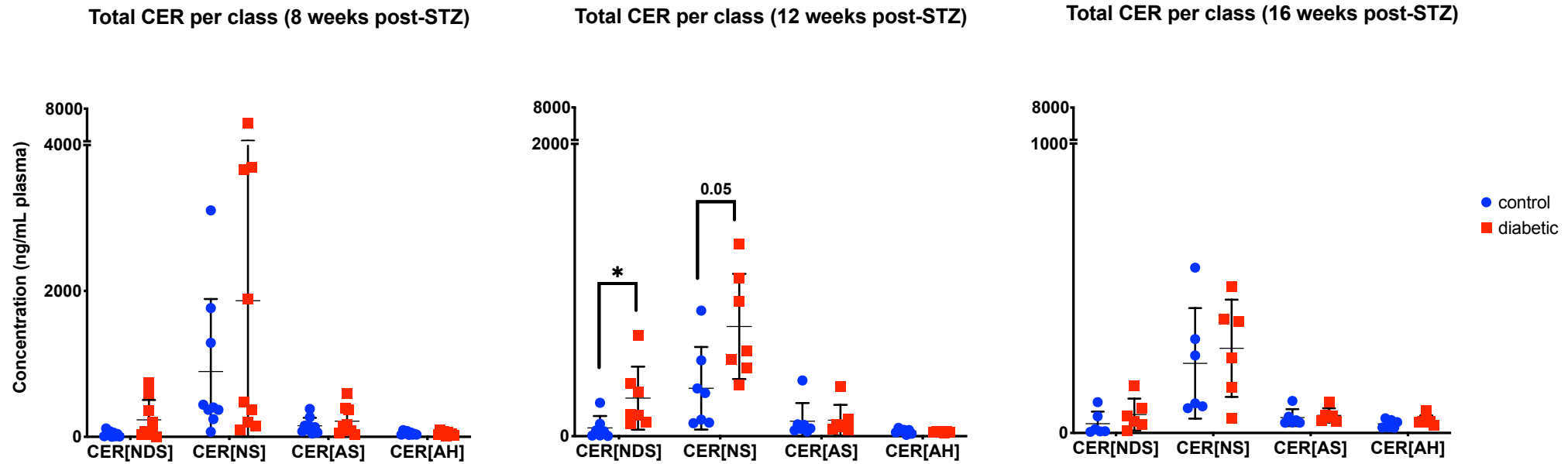


Figure 5.11 Total CER per class measured in control and STZ-diabetic rat plasma. Total ceramide classes were measured using UPLC/ESI-MS/MS in control and diabetic plasma collected at 8,12 and 16 weeks post-STZ., data are presented as absolute concentration in ng/mL plasma (mean \pm SD). Comparisons were performed between the control and diabetic group of the same time point; 8 weeks post-STZ control n=9, diabetic n=9; 12 weeks post-STZ control n=7, diabetic n=7; 16 weeks post-STZ control n=6, diabetic n=6. Log transformed data were analysed by t-tests with corrections for multiple analyses using the Holm-Sidak method; *p < 0.05. STZ: streptozotocin; CER: ceramide; NDS: non-hydroxy dihydrosphingosine; NS: non-hydroxy sphingosine; AS: alpha-hydroxy sphingosine; AH: alpha-hydroxy 6-hydroxysphingosine.

5.3.2.3 Several CER[NDS] and CER[NS] species were elevated in diabetic plasma

Individual species were analysed to observe possible trends in plasma CER metabolism between control and diabetes with and without insulin treatment. **Figure 5.12, 5.13** shows the CER[NDS] (four species), CER[NS] (eight species), CER[AS] (three species), CER[AH] (three species) that were detected. There was significant increase in CER[NDS] and CER[NS] species at 12 weeks post-STZ. All CER[NDS] species were increased at 12 weeks post-STZ: N(18)DS(24) ($p=0.03$), N(22)DS(18) ($p=0.01$), N(24)DS(18) ($p=0.03$), N(25)DS(18) ($p=0.03$) (**Figure 5.12 A**). The following CER[NS] species were significantly increased in diabetic plasma at 12 weeks post-STZ as well; N(16)S(18) ($p=0.002$), N(18)S(18) ($p=0.04$), N(20)S(18) ($p=0.04$) (**Figure 5.12 B**). Additionally, there was a significant increase in the A(24) H(17) ceramide species at 8 week post-STZ ($p= 0.045$) (**Figure 5.13 B**). No difference was found between control and diabetes at 16 weeks post-STZ (**Figure 5.12, 5.13**).

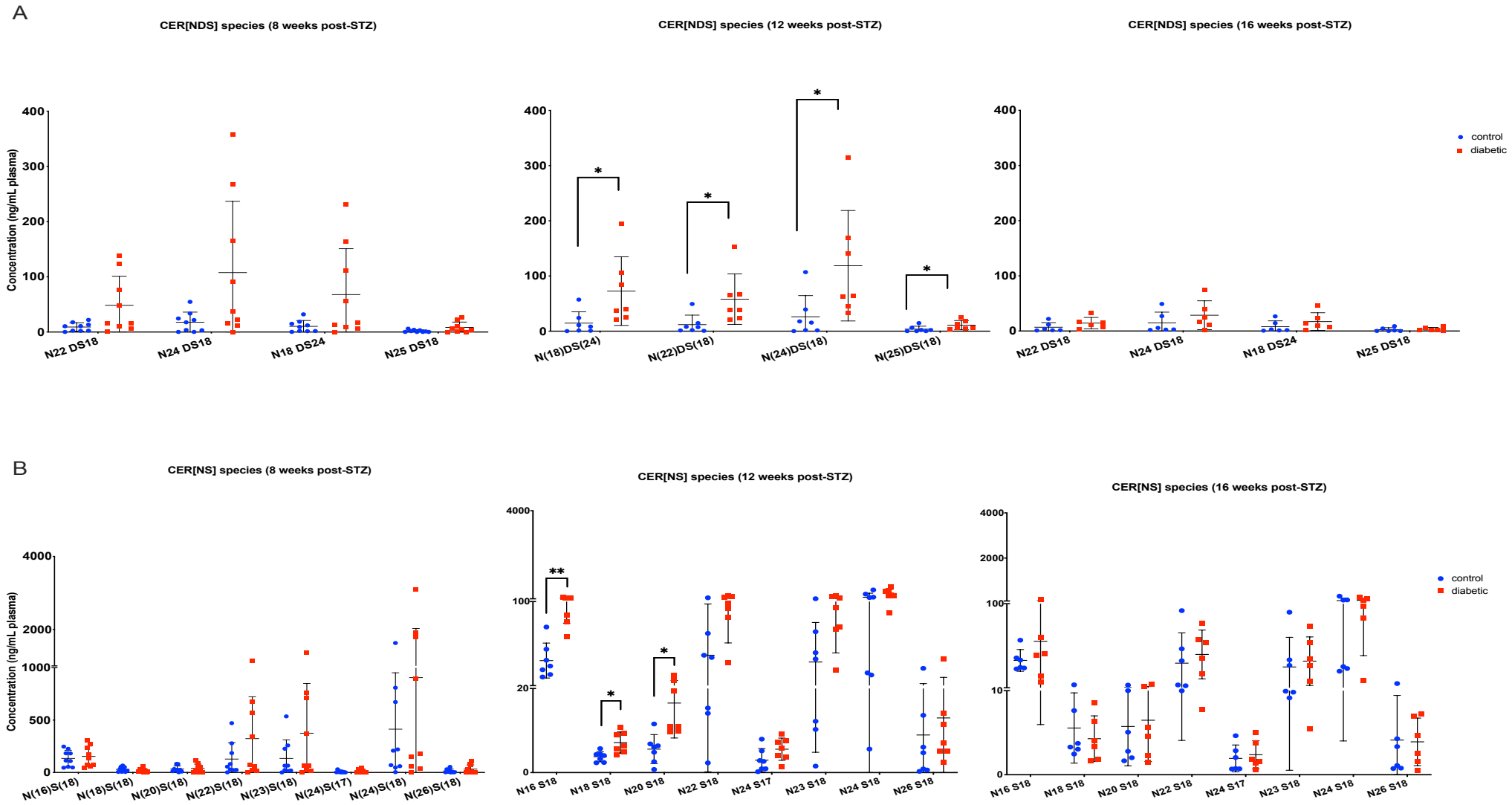


Figure 5.12 CER[NDS] and CER[NS] species measured in control and STZ-diabetic rat plasma. A) CER[NDS] species measured using UPLC/ESI-MS/MS in control and diabetic plasma collected at 8,12 and 16 weeks post-STZ; data are presented as absolute concentration in ng/mL plasma (mean \pm SD); B) CER[NS] species measured using UPLC/ESI-MS/MS in control and diabetic plasma collected at 8,12 and 16 weeks post-STZ; data are presented as absolute concentration in ng/mL plasma (mean \pm SD). Comparisons were performed between the control and diabetic group of the same time point; 8 weeks post-STZ control n=9, diabetic n=9; 12 weeks post-STZ control n=7, diabetic n=7; 16 weeks post-STZ control n=6, diabetic n=6. Log transformed data were analysed by t-tests with corrections for multiple analyses using the Holm-Sidak method; *p <0.05; **p<0.01. STZ: streptozotocin; CER: ceramide; NDS: non-hydroxy dihydrosphingosine; NS: non-hydroxy sphingosine.

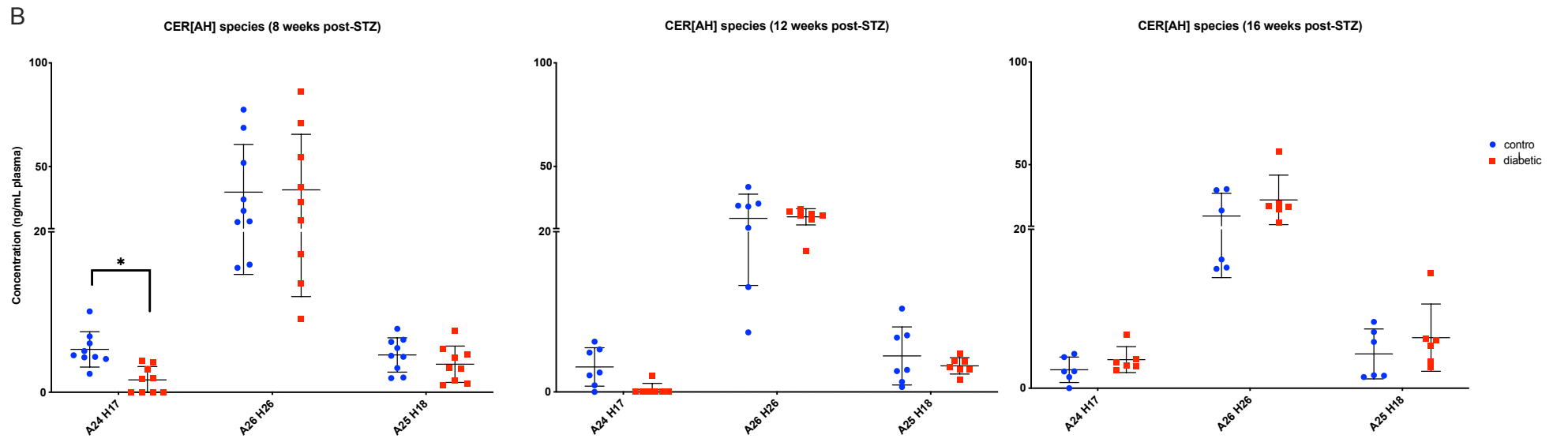
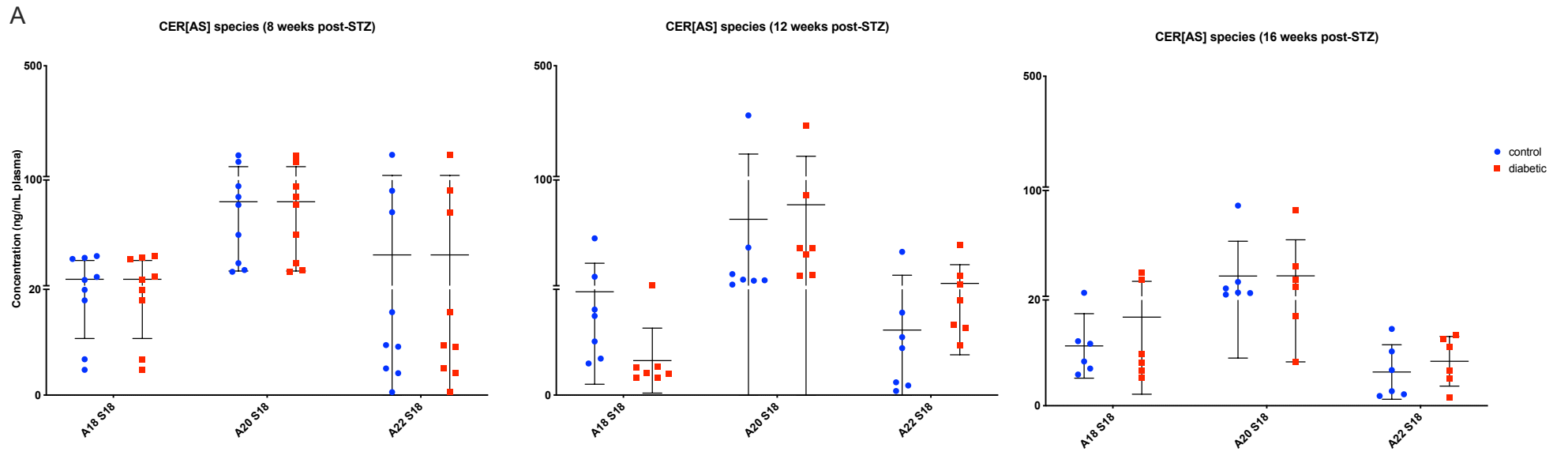


Figure 5.13 CER[AS] and CER[AH] species measured in control and STZ-diabetic rat plasma. A) CER[AS] species measured using UPLC/ESI-MS/MS in control and diabetic plasma collected at 8,12 and 16 weeks post-STZ; data presented as ng/mL plasma (mean \pm SD); B) CER[AH] species measured using UPLC/ESI-MS/MS in control and diabetic plasma collected at 8,12 and 16 weeks post-ST; presented as ng/mL plasma (mean \pm SD). Comparisons were performed between control and diabetic plasma of the same time point; 8 weeks post-STZ control n=9, diabetic n=9; 12 weeks post-STZ control n=7, diabetic n=7; 16 weeks post-STZ control n=6, diabetic n=6. Log transformed data were analysed by t-tests with corrections for multiple analyses using the Holm-Sidak method. *p <0.05. STZ: streptozotocin; CER: ceramide; AS: alpha-hydroxy sphingosine; AH: alpha-hydroxy 6-hydroxysphingosine.

5.3.2.4 Short chain ceramides were significantly increased in diabetic plasma

Analysing ceramide total chain lengths (carbon number of the fatty acyl-chain + carbon number of the sphingoid base-chain) is a useful way to observe changes in ceramide metabolism with disease. The ceramides that were measured, has a total carbon number that ranged from C34-C52. There was a significant increase in the short-chain ceramides with a C34 total carbon number at 12 weeks post-STZ (**Figure 5.14**).

5.3.2.5 Total C24 sphingoid base-chain was increased in diabetic plasma

Ceramides measured had either a dihydrosphingosine (DS), sphingosine (S), or 6-hydroxysphingosine (H) base chain. A total C18 sphingoid base-chain, for example, is calculated by taking the sum of all ceramides with a C18 sphingoid base-chain (all DS, S and H base-chains with a C18 carbon number). The base chains had a carbon number that ranged from C17-C26. There was a significant increase in ceramide levels with a C24 sphingoid base-chain at 12 weeks post-STZ ($p= 0.04$) (**Figure 5.15**).

5.3.2.6 Total C16 fatty acyl-chains were elevated in diabetic plasma

Another way to present the data is to group the ceramides according to fatty-acyl chain length, as it could help monitor activities of the fatty-acyl specific *de novo* biosynthesis enzymes (CerS1-6). The fatty acyl-chains that were detected were either non-hydroxy acyl-chains or α -hydroxy acyl-chains. A C18 total fatty acyl-chain carbon number for example, is calculated by taking the sum of all ceramides with a C18 fatty acyl-chain (non-hydroxy + α -hydroxy acyl-chains with a C18 carbon number). The ceramides measured had fatty acyl-chains that ranged from C16-C26. There was a significant increase in the C16 fatty acyl-chains at 12 weeks post-STZ ($p= 0.002$) (**Figure 5.16**).

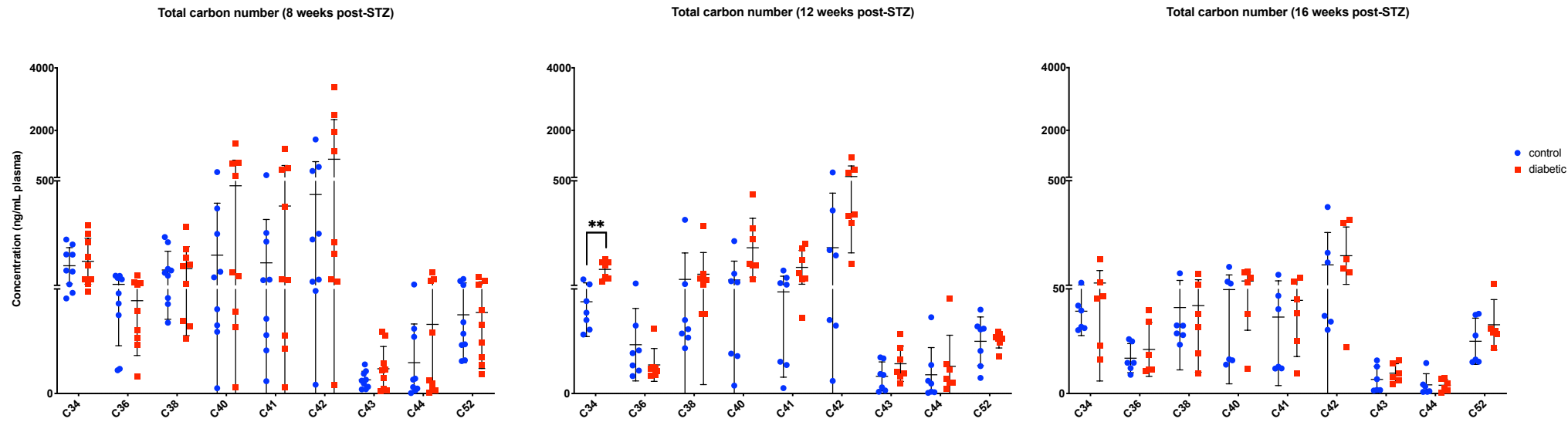


Figure 5.14 CER total carbon chains measured in control and STZ-diabetic rat plasma. Total carbon number in plasma ceramides measured using UPLC/ESI-MS/MS in control and diabetic plasma collected at 8,12 and 16 weeks post-STZ; data presented as absolute concentration in ng/mL plasma (mean \pm SD). Comparisons were performed between the control and diabetic group of the same time point; 8 weeks post-STZ control n=9, diabetic n=9; 12 weeks post-STZ control n=7, diabetic n=7; 16 weeks post-STZ control n=6, diabetic n=6. Log transformed data were analysed by t-tests with corrections for multiple analyses using the Holm-Sidak method; **p < 0.01. STZ: streptozotocin; C: carbon number.

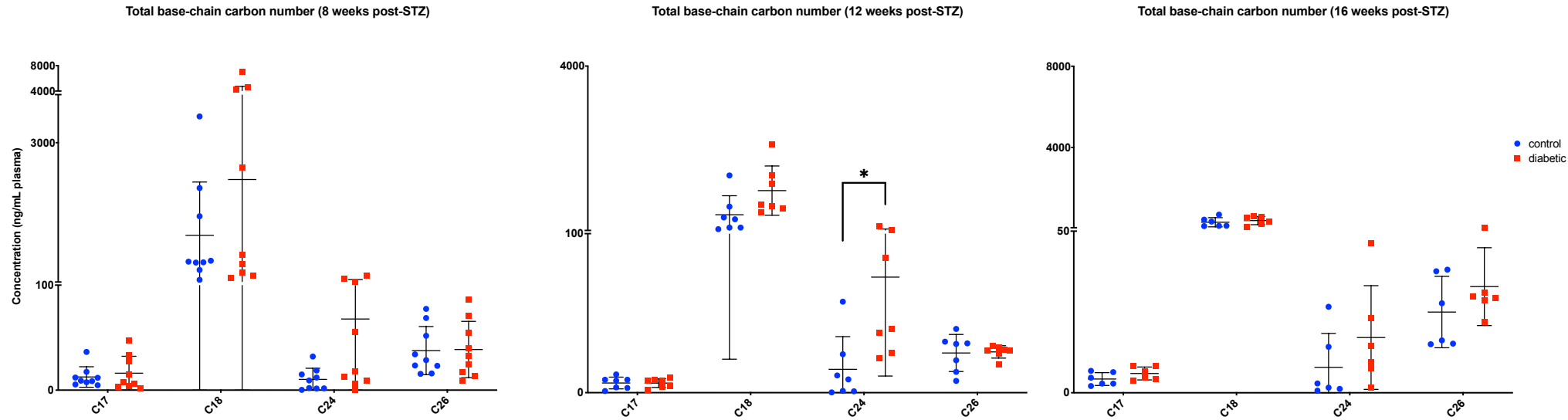


Figure 5.15 Total CER sphingoid base-chains measured in control and STZ-diabetic rat plasma. Total base-chain carbon number in plasma ceramides measured using UPLC/ESI-MS/MS in control and diabetic plasma collected at 8,12 and 16 weeks post-STZ; data presented as absolute concentration in ng/mL plasma (mean \pm SD). Comparisons were performed between the control and diabetic group of the same time point; 8 weeks post-STZ control n=9, diabetic n=9; 12 weeks post-STZ control n=7, diabetic n=7; 16 weeks post-STZ control n=6, diabetic n=6. Log transformed data were analysed by t-tests with corrections for multiple analyses using the Holm-Sidak method. STZ: streptozotocin; C: carbon number; DS: dihydrosphingosine; S: sphingosine; H: 6-hydroxysphingosine.

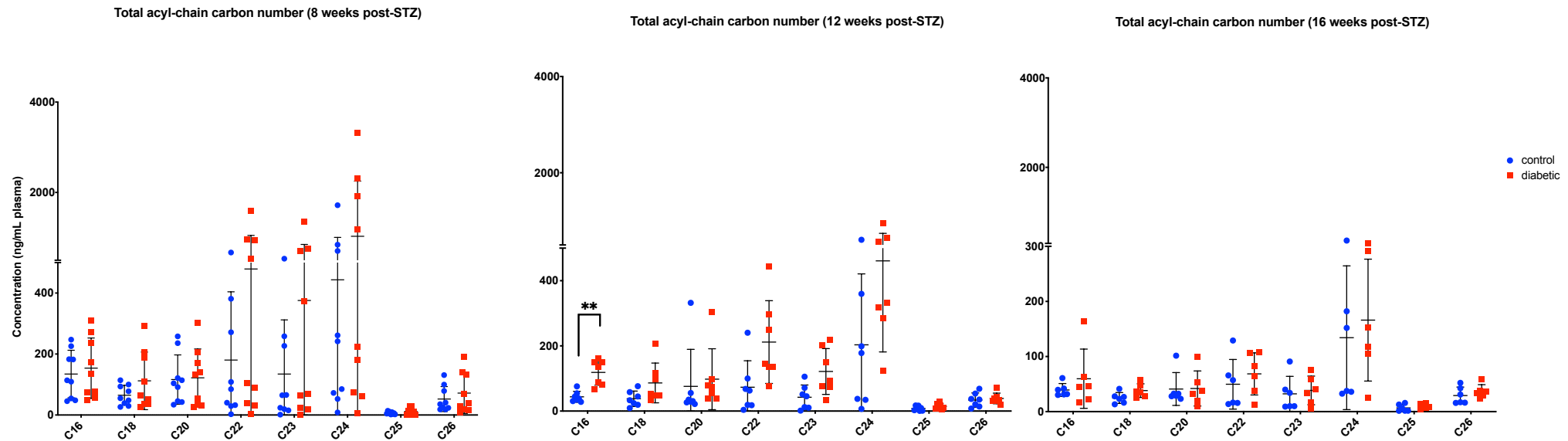


Figure 5.16 Total CER fatty-acyl-chains measured in control and STZ-diabetic rat plasma. Total fatty acyl-chain carbon number in plasma ceramides measured using UPLC/ESI-MS/MS in control and diabetic plasma collected at 8,12 and 16 weeks post-STZ; data presented as absolute concentration in ng/mL plasma (mean \pm SD). Comparisons were performed between the control and diabetic group of the same time point; 8 weeks post-STZ control n=9, diabetic n=9; 12 weeks post-STZ control n=7, diabetic n=7; 16 weeks post-STZ control n=6, diabetic n=6. Log transformed data were analysed by t-tests with corrections for multiple analyses using the Holm-Sidak method. **p < 0.01. STZ: streptozotocin; C: carbon number.

5.3.3 MAG and NAE species were reduced in diabetic skin

Differences in skin endocannabinoids, MAG and NAE levels between control and diabetes was analysed by UPLC/ESI-MS/MS (**Section 2.5.4**). The same samples used for the skin ceramides analysis were analysed for skin endocannabinoids, MAG and NAE. Foot pad skin from STZ-diabetic rats was arranged into three groups based on time of sampling post-STZ injection. Skin was sampled at 8 weeks (diabetic n=8, control n=9), 12 weeks (diabetic n=4, control n=4) and 16 weeks (diabetic n=6, control n=6) post-STZ. The 16 weeks diabetic group received insulin. Endocannabinoids, NAE and MAG concentrations were reported as absolute values in ng/mg protein (Mean \pm SD). All detected species in the diabetic skin samples were detected in/ and compared to the control skin samples.

2-AG was the only endocannabinoid detected. Analysing independent species revealed an increase in LG concentration at 8 weeks post-STZ ($p=0.03$) (**Figure 5.17 A**). At 16 weeks post-STZ, PDEA, OEA and VEA concentrations were significantly reduced ($p= 0.0$, $p= 0.02$, $p=0.001$) respectively (**Figure 5.17 B**).

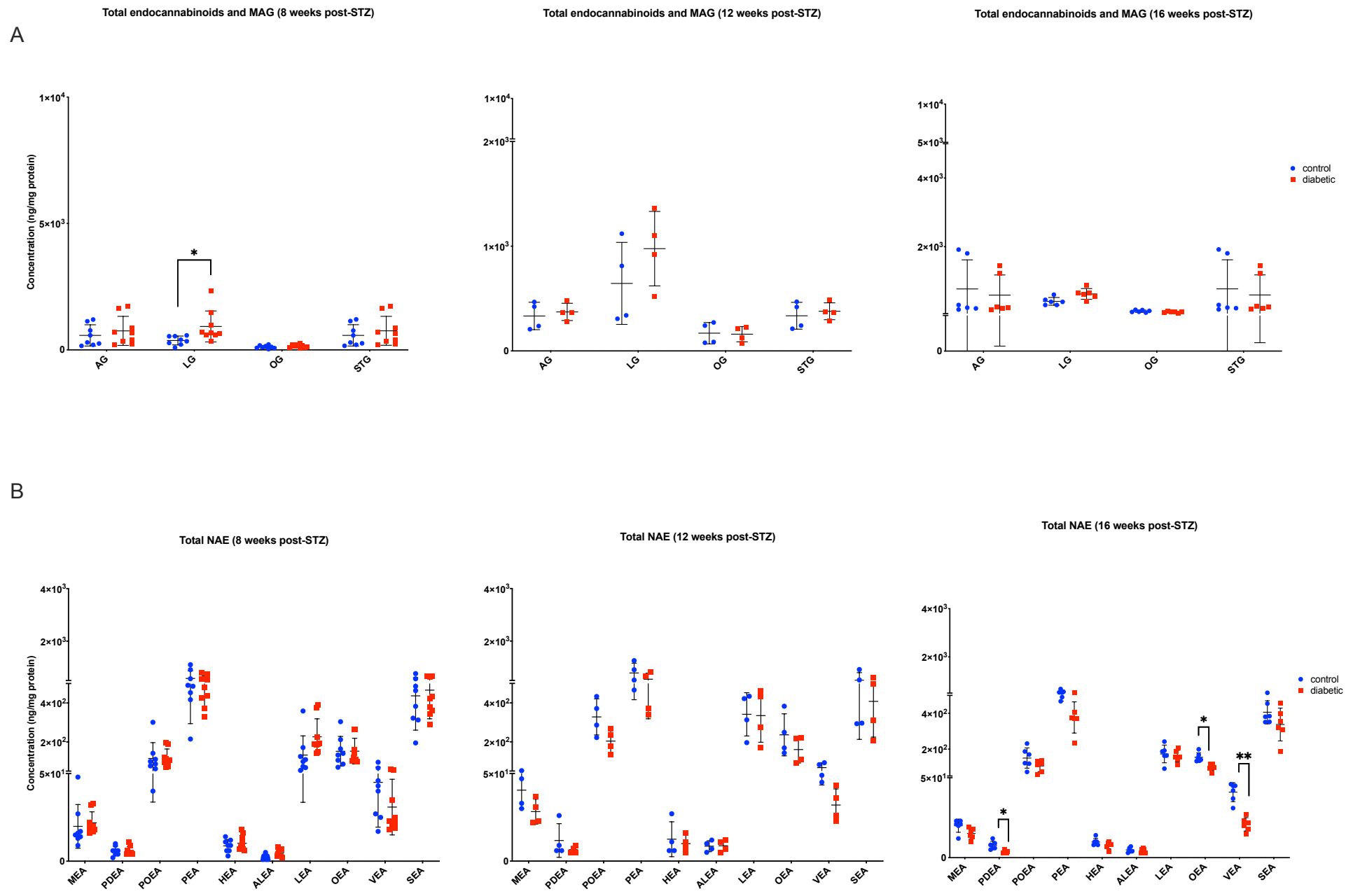


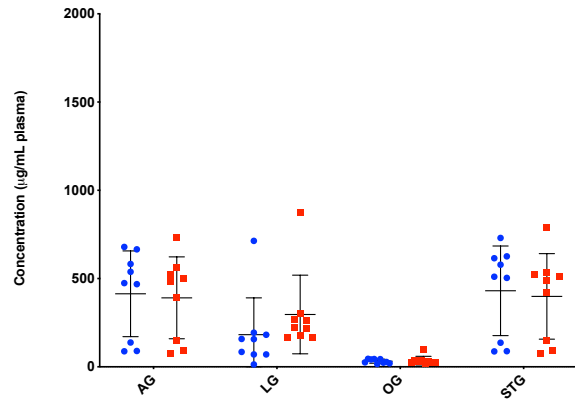
Figure 5.17 Endocannabinoid and NAE measured in control and STZ-diabetic rat skin. A) Total endocannabinoids and MAG measured using UPLC/ESI-MS/MS in control and diabetic skin collected at 8,12 and 16 weeks post-STZ; data presented as ng/mg protein (mean \pm SD); B) Total NAE measured using UPLC/ESI-MS/MS in control and diabetic skin collected at 8,12 and 16 weeks post-STZ; data presented as ng/mg protein (mean \pm SD). Comparisons were performed between control and diabetic skin of the same time point; 8 weeks post-STZ control n=8, diabetic n=9; 12 weeks post-STZ control n=4, diabetic n=4; 16 weeks post-STZ control n=6, diabetic n=6. Log transformed data were analysed by t-tests with corrections for multiple analyses using the Holm-Sidak method; *p <0.05; *** p<0.001. STZ: streptozotocin; NAE: N-acyl ethanolamine; MAG: monoacylglycerol; AG: arachidonoyl glycerol; LG: lineoleoyl glycerol; PAG: palmitoyl glycerol; OG: oleoyl glycerol; STG: stearoyl glycerol; MEA: myristoyl ethanolamine; PDEA: pentadecanoyl ethanolamine; POEA: palmitoleoyl ethanolamine; PEA: palmitoyl ethanolamine; HEA: heptadecanoyl ethanolamine; ALEA: α -linolenoyl ethanolamine; LEA: lineoleoyl ethanolamine; OEA: oleoyl ethanolamine; VEA: vaccenoyl ethanolamine; SEA: stearoyl ethanolamine; DEA: docosanoyl ethanolamine; NEA: nervonoyl ethanolamine.

5.3.4 There was a significant decrease in NAE species in diabetic plasma

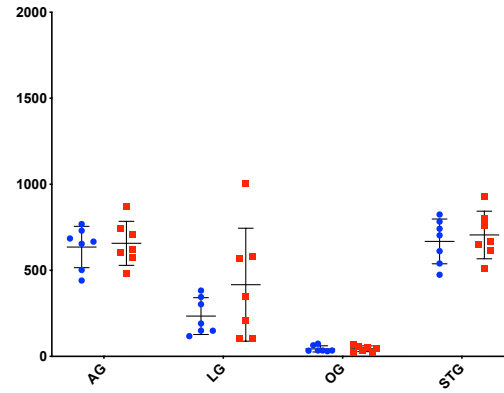
Differences in plasma endocannabinoids, MAG and NAE levels between control and diabetes was analysed by UPLC/ESI-MS/MS (**Section 2.5.4**). The same samples used for the plasma ceramides analysis were analysed for plasma endocannabinoids, MAG and NAE. Plasma from STZ-diabetic rats was arranged into three groups based on time of sample collection post-STZ injection. Plasma was sampled at 8 weeks (diabetic n=9, control n=9), 12 weeks (diabetic n=7, control n=7) and 16 weeks (diabetic n=6, control n=6) post-STZ. The 16 weeks diabetic group received insulin. Endocannabinoids, NAE and MAG concentrations were reported as absolute values in $\mu\text{g/ml}$ plasma (mean \pm SD). All detected species in the diabetic plasma samples were detected in and compared to the control plasma samples.

2-AG was the only endocannabinoid detected. Analysing individual species revealed a significant decrease in the concentration of the NAE species, POEA and VEA, in diabetes at 8, 12 and 16 weeks post-STZ; POEA ($p= 0.03$, $p= 0.01$, $p= 0.04$) at 8, 12 and 16 weeks post-STZ, respectively; VEA ($p= 0.002$, $p= 0.02$, $p= 0.048$) at 8, 12, and 16 weeks post-STZ, respectively (**Figure 5.18 B**). No differences were found in 2-AG and MAG species levels between control and diabetes (**Figure 5.18 A**).

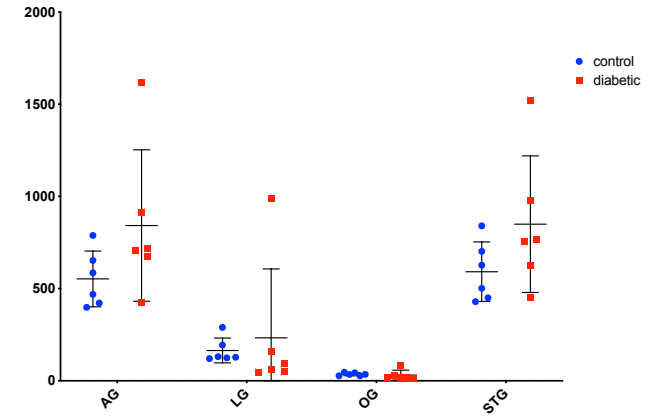
Total endocannabinoids and MAG (8 weeks post-STZ)



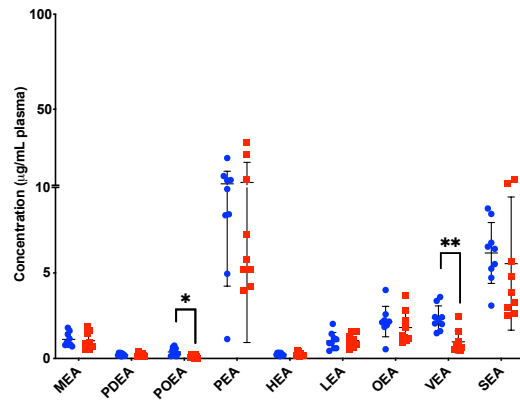
Total endocannabinoids and MAG (12 weeks post-STZ)



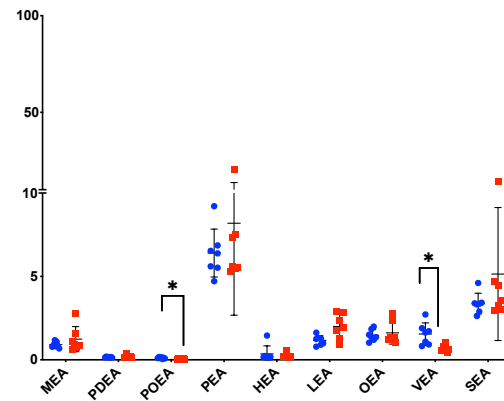
Total endocannabinoids and MAG (16 weeks post-STZ)



Total NAE (8 weeks post-STZ)



Total NAE (12 weeks post-STZ)



Total NAE (16 weeks post-STZ)

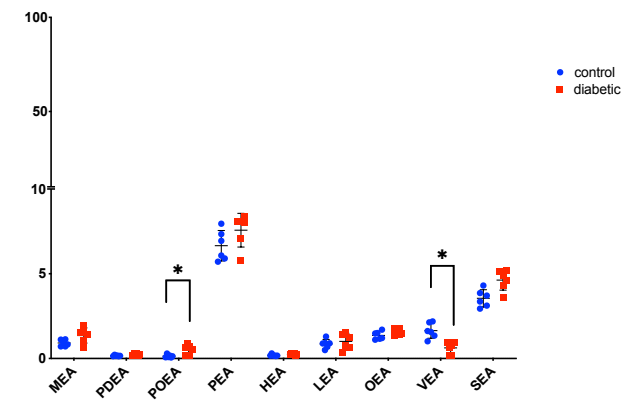


Figure 5.18 Endocannabinoids and N-acyl ethanolamines measured in control and STZ-diabetic rat plasma. A) Total endocannabinoids and MAG measured using UPLC/ESI-MS/MS in control and diabetic plasma collected at 8,12 and 16 weeks post-STZ; data presented as $\mu\text{g/mL}$ plasma (mean \pm SD); B) Total NAE measured using UPLC/ESI-MS/MS in control and diabetic plasma collected at 8,12 and 16 weeks post-STZ; data presented as $\mu\text{g/mL}$ plasma (mean \pm SD). Comparisons were performed between control and diabetic plasma of the same time point; 8 weeks post-STZ control n=9, diabetic n=9; 12 weeks post-STZ control n=7, diabetic n=7; 16 weeks post-STZ control n=6, diabetic n=6. Log transformed data were analysed by t-tests with corrections for multiple analyses using the Holm-Sidak method; *p <0.05; ** p<0.01. STZ: streptozotocin; NAE: N-acyl ethanolamine; MAG: monoacylglycerol; AG: arachidonoyl glycerol; LG: lineoleoyl glycerol; OG: oleoyl glycerol; STG: stearoyl glycerol; MEA: myristoyl ethanolamine; PDEA: pentadecanoyl ethanolamine; POEA: palmitoleoyl ethanolamine; PEA: palmitoyl ethanolamine; HEA: heptadecanoyl ethanolamine; LEA: lineoleoyl ethanolamine; OEA: oleoyl ethanolamine; VEA: vaccenoyl ethanolamine; SEA: stearoyl ethanolamine.

5.4 Discussion

In this study, changes in skin and plasma CER levels were assessed in the context of DPN in order to investigate the potential involvement of skin lipids in the development of associated dermopathies, and how alterations in circulating lipids could reflect that. The STZ-diabetic rat is the preferred animal model in diabetic neuropathy studies as it has been shown to present structural peripheral nerve damage and neuropathic symptoms similar to those seen in DPN patients as previously shown in (Sima and Sugimoto, 1999, Gardiner et al., 2007, Zherebitskaya et al., 2012, Biessels et al., 2014). The rats are made diabetic by injecting STZ intraperitoneally to cause β -cell damage and insulin deficiency (Calcutt and Chaplan, 1997). The intended outcome from this animal model of type-1 DM was to display structural peripheral nerve changes and negative DPN symptoms, such as loss of sensation. The required duration of STZ-induced diabetes to initiate peripheral nerve damage is from 8 to 16 weeks as found in (Biessels et al., 2014). It should be noted that the 16 weeks batch of STZ-diabetic rats received insulin in order to maintain the animals for the duration of the experiment as STZ-induced diabetes could cause cachexia (extreme weight loss and muscle wasting) (Biessels et al., 2014). Therefore, CER analysis was conducted at individual time-points (8, 12 and 16 weeks) after the induction of diabetes to monitor possible changes in CER levels with disease progression.

Foot pad skin from STZ-induced diabetic rats were compared to samples from age-matched naïve rats. Rat skin has been found to be comparable in structure, permeability properties, lipid class and drug penetration rate to that in human skin (Aoki et al., 2019, Marjukka Suhonen et al., 2003, Pappinen et al., 2008). The present study revealed alterations in CER[NH] at 16 weeks post-STZ. There was a close to significant decrease in total CER[NH] levels ($p= 0.05$) and statistically significant decreases in individual CER[NH] species at 16 weeks post-STZ. The exact enzymes involved in the biosynthesis of these CERs remain to be identified. Skin specific 6-hydroxysphingosine CERs have been found to be essential for skin barrier permeability protection and thermal stability (Kovacik et al., 2017). Additionally, in a study on the effect of seasonal changes on skin CERs, it was suggested that 6-hydroxysphingosine CERs might be involved in thermal

adaptation (Pappas et al., 2018). Therefore, the present study could suggest a role for the reduction observed in these ceramides in the development of DPN associated barrier dysfunction. However, functional tests are required to further investigate the effect of decreased CER[NH] in rat foot pad skin on the barrier.

The lack of statistical significance at 12 weeks post-STZ could be attributed to the short duration of the disease at that time-point, as it has been found that the degree of skin barrier disruption and nerve loss corresponds to the duration of hyperglycemia and diabetes (Park et al., 2011, Shun et al., 2004). Similarly, intraepidermal nerve fibre damage in STZ-diabetic rat hind paws occurs at 12 weeks post the induction of diabetes onwards (Freeman et al., 2016). This could suggest that more time was required to observe significant changes in CER levels following the course of the systemic development of DPN which leads to peripheral tissue injury with disease progression. One study on skin CERs in type-2 diabetic mice reported a reduction in SPT expression and CER levels (Kim et al., 2018). In this study, although the reduction in CER synthesis was not significant, it was suggested to be a main factor for barrier and wound healing impairment. In addition, it was mentioned that the duration of hyperglycemia was not sufficient to produce statistically significant alterations.

Furthermore, plasma from STZ-induced diabetic rats were compared to samples from age-matched naïve rats. The data showed significant alterations in plasma CER levels with diabetes at 12 weeks post-STZ administration. Although nerve damage assessment was not done for this study, it has been previously shown that sensory and motor nerve conduction velocities were decreased, in addition to intraepidermal nerve fibre damage in STZ-diabetic rat hind paws at ≥ 12 weeks post-STZ (Freeman et al., 2016). Similarly, levels of the neurotrophic factor, neuritin, which promotes axonal regeneration were found to be reduced in the nerves of STZ-diabetic rats at 12 weeks post-STZ (Karamoysoyli et al., 2008). From this, it could be shown that alterations in plasma CER levels were observed at the same time-point that DPN would usually occur.

In plasma, a significantly higher total CER[NDS] levels were reported with diabetes at 12 weeks-post STZ ($p= 0.03$), when compared with control animals (**Figure 5.3**). When analysing individual CER species, several CER[NDS] and CER[NS] species were significantly elevated at 12 weeks post-STZ (**Figure 5.4**). Dihydroceramides are precursors for all ceramide classes and their *de novo* synthesis is regulated by SPT, the rate-limiting enzyme in the *de novo* CER biosynthesis pathway, and CerS1-6. From CER[NDS], the fatty acyl-chain specific CerS and sphingosine specific Des1, produce CER[NS] as discussed in (**Chapter 1**) (Airoola and Hannun, 2013). *De novo* ceramide synthesis has been shown to be involved in lipotoxic β -cell apoptosis, which was significantly reduced by blocking this pathway (Galadari et al., 2013, Boslem et al., 2012). For example, it has been found that blocking SPT activity, using inhibitors such as myriocin, improved glucose homeostasis, insulin sensitivity and prevented diabetes in rodents (Holland et al., 2007, Sokolowska and Blachnio-Zabielska, 2019, Ussher et al., 2010).

Although CER biosynthesis in DPN is largely unexplored, neurotoxic deoxy-CER[NS], which are produced due to mutations in SPTLC1 that alter SPT substrate preference, have been reported in DPN (Hammad et al., 2017). In addition to this, L-serine level, the preferred SPT substrate, was found to be reduced in STZ-diabetic rats with DPN, whereas L-serine supplementation lowered deoxy-CER[NS] levels and reduced DPN outcomes (Othman et al., 2015). Moreover, in a study on neurogenesis, it was suggested that elevated CER levels in neurons due to high SPT activity could lead to apoptosis (Herget et al., 2000). This could suggest a major role for the *de novo* CER biosynthesis pathway in the development and progression of the nerve loss through apoptosis. However, the exact pathological significance of CER in DPN is not fully understood. For example, the mechanism by which mutations in the ubiquitous enzyme, SPT, specifically target peripheral nerves remains to be explained (Herget et al., 2000).

One way to help explain this could be by investigating changes in CER species containing specific sphingoid base-chain lengths to DPN development to help monitor changes in SPT and Des1,2 activity. In addition to shifts in SPT substrate preference seen in DPN and HSN1, alterations in SPT acyl-CoA specificity have been reported in HSN1. In the CER *de novo* biosynthesis pathway, SPT utilises L-

serine (C2) and the most abundant acyl-CoA, palmitoyl-CoA (C16) to produce a C18 dihydrosphingosine (**Figure 1.4**). In the present study, a significant increase in the total C24 base-chains was observed at 12 weeks post-STZ ($p= 0.04$), and were found in CER[NDS] (**Figure 5.5, 5.2**). It has been found that C20 dihydrosphingosine was elevated in human embryonic kidney cells (HEK293) expressing particular SPTLC mutations and in plasma from patients with a specific HSN1 subclass, and the C18 dihydrosphingosine levels were not reduced (Bode et al., 2016). Bode and colleagues explained that the C20 sphingoid bases are a product of L-serine and stearyl-CoA, and were observed in one specific HSN1 subclass. Additionally, in other HEK293 SPTLC mutations both the C18 and C20 sphingoid bases were elevated where the activity of SPT was increased (Bode et al., 2016). SPT activity is subjected to several variables such as tissue type, the developmental stage of the tissue and diet (Hanada, 2003). Furthermore, there are various SPT mutations that produce distinct sphingoid base profiles and pathological symptoms, making neuropathy investigations using sphingoid base profiles both challenging and valuable (Bode et al., 2016).

Moreover, correlating CER species containing specific fatty acyl-chain lengths to distinct disease mechanisms has been mentioned in previous studies establishing the effect of plasma and tissue CERs on diabetes and DPN (Hammad et al., 2017, Véret et al., 2011). When analysing total fatty-acyl chain carbon number (e.g. Total C18 fatty acyl-chain= concentration of all CERs containing a C18 non-hydroxy fatty acyl-chain + concentration of all CERs containing a C18 α -hydroxy fatty acyl-chains) and total carbon number (fatty acyl-chain carbon number + sphingoid base-chain carbon number), a significant increase in the C16 short fatty acyl-chain ($p= 0.002$), and the short chain CERs (C34) CER ($p= 0.002$) were found, respectively (**Figure 5.4, 5.6**). These short chain CERs are produced by the C14-C16 specific CER synthases, CerS5 and CerS6, which are expressed ubiquitously across tissues (**Table 1.2**). These findings are consistent with previous studies that reported increases in plasma CERs with short and medium fatty acyl-chains in diabetes. It has been demonstrated that CERs with a C16, C22 and C24 fatty acyl-chain were increased in STZ-diabetic rats and were suggested to promote apoptosis (van Blitterswijk et al., 2003). Additionally, C16 and C18 CERs were found to play a

major role in insulin signalling (Stith et al., 2019, Raichur et al., 2014). Moreover, in addition to deoxy-CER[NS], naturally occurring CERs with a C24 and C26 fatty acyl-chain were found to be increased in the plasma in of type-1 diabetic patients with neuropathy, but were not elevated in that of diabetic patients without neuropathy (Hammad et al., 2017). The exact pathogenic role of these CER species in diabetes and DPN is not fully understood. Therefore, comparing the data highlighted in this animal model with that in the literature that focuses on the effect of specific CER species in diabetes and neuropathy could help elucidate underlying mechanisms.

Although we did not obtain the glucose levels for the STZ-diabetic rats, glucose was measured by study collaborators to confirm diabetes (**Section 5.2**). This model is characterized by STZ-induced β -cell damage and insulin deficiency and establishes hyperglycemia within 2-3 days (Freeman et al., 2016, Calcutt and Chaplan, 1997). Interestingly, accumulation of CER[NDS] and CER[NS] that were observed in the present study are in agreement with a study which found these CER classes to be involved in β -cell apoptosis in a rat pancreatic β -cell line (Véret et al., 2011). The same study suggests that accumulation of these CERs was triggered by glucolipotoxicity due to palmitate and hyperglycemia. Palmitic acid has been found to mediate various inflammatory mechanisms in obesity and diabetes either directly through high circulating levels or through its utilisation to produce CERs *de novo* (Korbecki and Bajdak-Rusinek, 2019). Véret et al. reported that palmitate supplementation with high glucose levels elevated CER[NDS] with a C18, C22 and C24 fatty acyl-chain, upregulated *CERS4* and increased CER[NS] with fatty-acyl chains that ranged from C16-C22. Additionally, the impact of glucolipotoxicity on CER recycling through the salvage pathway was examined. No effect on sphingosine levels in β -cells was seen with palmitate supplementation and hyperglycemia independently or combined, whereas dihydrosphingosine was significantly elevated with palmitate and high glucose, confirming a specific impact on the *de novo* biosynthesis pathway (Véret et al., 2011).

Another study comparing lipid levels in diabetic mice that received insulin with control diabetic mice, found that insulin withdrawal in the first group further increased the levels of C16-C24 CERs in plasma and muscles, whereas *SPT*, *CERS1*

and *CERS5* expression in muscle was increased in the *de novo* biosynthesis fraction, the sarcoplasmic reticulum (Zabielski et al., 2014). Zabielski and colleagues also showed that there was an increase in all C18 plasma FFAs and in C16-C18 muscle FFAs, which could be due to the diet composition used for the STZ-diabetic rat model, which contains oleate (C18) and linoleate (C18) fatty acids (80%) and 20% palmitate (C16), linolenate (C18) and stearate (18) (Zabielski et al., 2014). Consistent with the mentioned observations, CER[NDS] species were found to be elevated in STZ-diabetic rat plasma and contained C18, C22, C24 and C25 fatty acyl-chains, in addition to CER[NS] with a C16-C20 fatty acyl-chain. This could imply a connection between hyperglycemia and insulin deficiency and the CER *de novo* biosynthesis pathway, by mediating utilisation of endogenous FFAs to produce these specific apoptotic CER species through the upregulation of CER *de novo* biosynthesis enzymes.

Finally, endocannabinoids and their congeners were analysed in skin and plasma to examine their levels in a model of DPN and elucidate their potential role in the development of the disease. In plasma, there was a significant decrease in POEA and VEA levels at all time points post-STZ. In skin, however, the changes were significant at 16 weeks post-STZ where PDEA, OEA and VEA were reduced. In addition to endocannabinoids, their related lipid mediators play a crucial role in inflammatory signaling pathways. It has been found that VEA is the primary and second most abundant C18 FA-ethanolamine in rat and human plasma, respectively (Röhrig et al., 2016). Interestingly they were significantly decreased in STZ-diabetic rat plasma even at the earliest time-point (8 weeks post-STZ). Additionally, the reduced levels in plasma C18 VEA and C16 palmitoleic acid derived-EA (POEA), could reflect the increase observed in plasma short fatty acyl-CER levels. It has been mentioned that the bioavailability of endocannabinoid precursors, FFAs, has an effect on their levels (Phinney, 1996, Annuzzi et al., 2010). These studies were on obesity and obesity-related diabetes where endocannabinoids were found to be increased. However, the animal model that was used in the present study was fed regular chow diet. This could reflect the competitive lipid metabolism process in the STZ-induced diabetes, in which the CER *de novo* biosynthesis pathway is activated to utilise C16-C18 FFAs and produce apoptotic CERs. Furthermore, there was a wider range of skin lipid mediators that were reduced with diabetes. Both

CB₁ and CB₂ receptors are expressed in skin cells and nerve fibers, and are involved in regulating nociceptive pathways and skin cell functions (Barrie and Manolios, 2017, Tóth et al., 2019). The reduction in skin lipid mediators could be explained by the diabetes-related dyslipidemia. Again, this could show the highly interlinked lipid metabolism mechanisms in skin, and that these specific alterations in skin bioactive lipids in DPN could be a major contributor for skin injury and delayed healing.

5.5 Conclusion

In conclusion, this study showed alterations in skin and plasma CERs and endocannabinoid-related bioactive lipids in an animal model of DPN. These alterations could show a specific role of CER[NH] ceramides in the development of DPN. As concluded from this study, the accumulation of circulating C16-C24 CERs may be involved in the development of diabetes and DPN, through the induction of inflammatory, apoptotic and neurotoxic mechanisms. Additionally, we showed alterations in skin CER and lipid mediator profiles in DPN, which have not been previously explored. These alterations could disrupt skin homeostasis and cell signaling, which in the context of DPN could render the skin susceptible to injury, affect cutaneous nerve development, and impair wound healing. Further investigation is required to elucidate the potential pathogenic role of individual cutaneous and circulating CER species and lipid mediators on diabetic dermopathies.

Chapter 6

General discussion, conclusions and further work

6.1 Thesis aims and objectives

Ceramides are a dynamic group of bioactive lipids, which are considered a major constituent of the epidermal permeability barrier. Alterations in ceramide levels have been reported in several skin disorders. However, the exact roles of individual CER species in health and disease remain unclear. Additionally, a recent study reported that *n*-3 PUFA have been found to influence ceramide levels in human skin (Kendall et al., 2017). The exact mechanisms, however, by which these fatty acids can manipulate ceramide metabolism are not fully understood. Understanding how cutaneous ceramides could be targeted by PUFA could help in the development of therapeutic approaches for inflammatory skin disorders. The primary aim of this thesis was to explore mechanisms involved in the metabolism of cutaneous lipids in normal skin cells treated with PUFAs, and to examine differences in cutaneous and systemic lipid profiles in diabetes when compared with control.

The epidermis and dermis are structurally and functionally distinct, and the majority of studies examining cutaneous CERs include the epidermis, specifically the SC where CER concentration is the highest. The lipid composition of the epidermis and dermis differ, and *n*-3 PUFAs have been found to have a differential effect on ceramide levels in these layers (Uchida et al., 1988, Kendall et al., 2015, Kendall et al., 2017). Therefore, it was hypothesised that *n*-3 and *n*-6 PUFA may have specific effects on ceramide metabolism in cultured primary human keratinocytes and fibroblasts. In order to elucidate the individual action of DHA, EPA and LA on CER metabolism in different compartments of human skin, proliferating keratinocytes representing the basal layers and differentiating keratinocytes which represent the granular epidermis were used, in addition to dermal fibroblasts. To achieve this, ceramide levels, CER biosynthesis enzyme gene expression and membrane lipid levels were analysed in PUFA-treated and control normal human skin cells.

Furthermore, diabetes is a global metabolic disease with complications that could present in the skin. For example, DPN is a major diabetic complication that leads to diabetic foot due to loss of sensation, repeated tissue injury and dysfunctional

wound healing (Volmer-Thole and Lobmann, 2016, Feldman et al., 2017). However, changes in cutaneous ceramides have not been previously investigated in DPN. Therefore, the project assessed likely alterations in skin CER levels in a diabetic animal model of DPN. An STZ-diabetic rat model of DPN was used as a tool to investigate changes in cutaneous ceramides that could be involved in the susceptibility of diabetic skin to injury. Studies on cutaneous functional properties in diabetes, although limited, have reported barrier impairment and changes in SC CERs (Sakai et al., 2003, Kim et al., 2018). It was, therefore, hypothesised that cutaneous CER levels would be altered in DPN. Accumulation of circulating and tissue CERs have been found to be involved in pathogenic processes such as insulin resistance and β -cell dysfunction in diabetes (Hage Hassan et al., 2016, Yaribeygi et al., 2020, Guo et al., 2010). Therefore, plasma CERs, in addition to skin and plasma lipid mediators were analysed, which could reflect systemic factors that may be involved in diabetic dermopathies.

6.2 Exploring the pathways mediating PUFA regulation of ceramide biosynthesis in primary human skin cells

The individual effects of DHA, EPA and LA supplementation on CER biosynthesis at different stages of epidermal cellular growth were reported in this study. In the epidermis, both proliferating and differentiating NHEK responded to DHA supplementation, whereas LA induced a response in differentiating cells. Lipid metabolism in HDF showed a differential effect of *n*-3 and *n*-6 PUFA. **Figure 6.1** summarises the main findings observed.

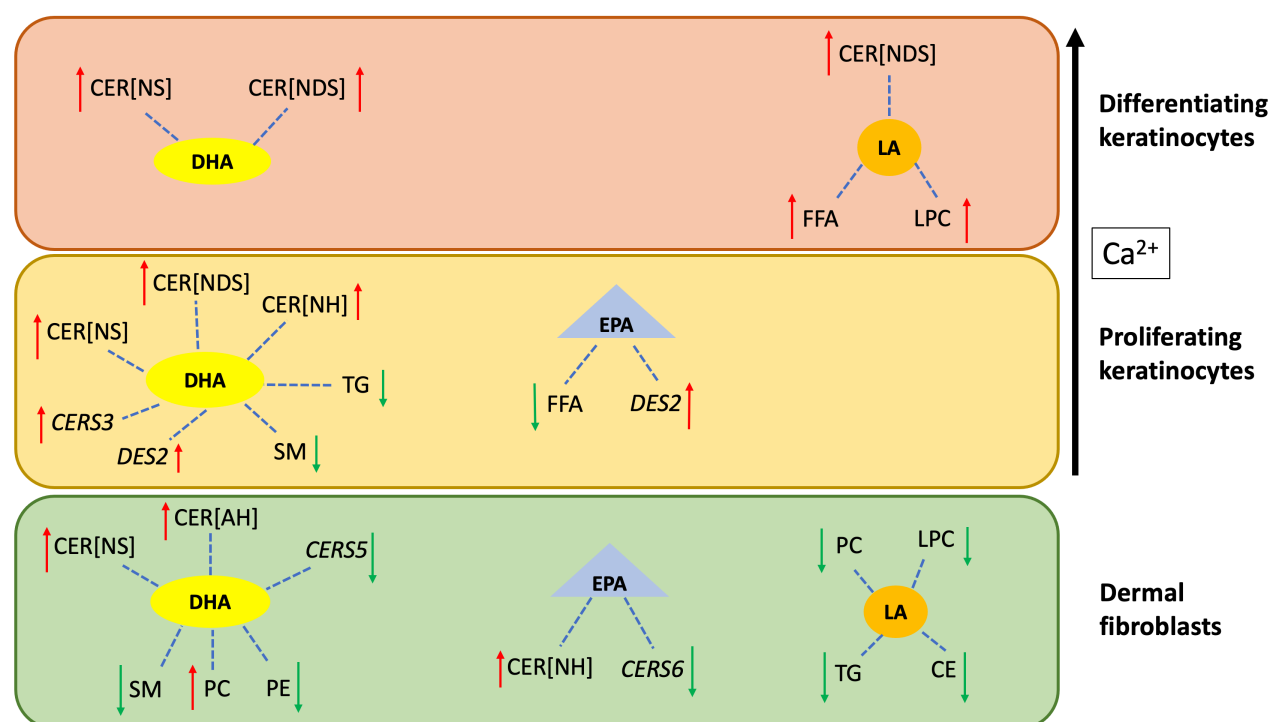


Figure 6.1 Summary of the effects of PUFA treatment on lipid metabolism in NHEK and HDF. The figure summarises the main increases (red arrow) and decreases (green arrow) found in CER and membrane lipid levels, in addition to CER biosynthesis gene expression, measured in differentiating NHEK (High Ca^{2+} , $n=3$ donors), proliferating NHEK (Low Ca^{2+} , $n=3$ donors) and HDF ($n=3$ donors) treated with DHA, EPA and LA ($10\ \mu\text{M}$) compared to control. Ceramides and membrane lipids were measured using UPLC-MS/MS; CER biosynthesis enzyme gene expression was measured by RT-qPCR. NHEK: normal human epidermal keratinocytes; Ca^{2+} : calcium; HDF: human dermal fibroblasts; PUFA: polyunsaturated fatty acid; DHA: docosahexaenoic acid; EPA: eicosapentaenoic acid; LA: linoleic acid; CER: ceramide; CER[NS]: non-hydroxy ceramide; CER[NDS]: non-hydroxy dihydroceramide; CER[NH]: non-hydroxy 6-hydroxyceramide; CER[AH]: alpha-hydroxy 6-hydroxyceramide; *CERS3*: ceramide synthase 3; *CERS5*: ceramide synthase 5; *CERS6*: ceramide synthase 6; *DES2*: dihydroceramide desaturase 2; FFA: free fatty acids; SM: sphingomyelin; CE: cholesterol ester; TG: triacylglycerol; PE: phosphatidylethanolamine; PC: phosphatidylcholine; LPC: lysophosphatidylcholine.

6.2.1 Proliferating NHEK

In proliferating NHEK, which represent the basal layers, DHA enhanced the levels of the majority of CER classes, which was accompanied by an upregulation in *CERS3* and *DES2* gene expression and a reduction in SM levels (**Chapter 3**). This suggests an action of DHA on the CER *de novo* biosynthesis and SM recycling pathway. DHA stimulated the *de novo* synthesis of CERs that are involved in skin health. The FA preference of CerS3 includes CERs with medium (C18-C21) and

long (C22-C25) carbon chains which are essential for normal barrier function (Mizutani et al., 2004). In addition to this, Des2 produces phytoceramides, which are also critical for barrier integrity (Choi et al., 2018). This could suggest a protective role for DHA in the epidermis. Moreover, it has been found that SM is a precursor for CER[NS] and CER[AS] species (Uchida et al., 2000). Therefore, the reduction in SM with DHA and the observed increase in CER[NS] and CER[AS] classes could indicate the action of DHA on an additional CER synthesis pathway involving the breakdown of SM in the basal epidermal layers. Furthermore, DHA altered membrane lipid levels were TG, CE and proapoptotic PC and LPC levels were reduced. The decrease in proapoptotic glycerophospholipids and energy producing glycerolipids in proliferating cells with DHA could reflect the anti-inflammatory effect of *n*-3 PUFA, and suggests a proliferative effect on the basal cells where these membrane lipids are utilised for cellular growth.

6.2.2 Differentiating NHEK

In differentiated NHEK, which represents the granular layers, the increase in CER concentrations with PUFAs was not accompanied by changes in CER *de novo* biosynthesis enzyme gene expression, SM and membrane lipid metabolism (**Chapter 3**). Since the significant increase in CER[NS] and CER[AS] in differentiated cells with DHA was not accompanied with changes in SM or other membrane lipids, DHA could increase CER levels through alternative pathways linked to differentiation. Interestingly, CER signaling pathways which regulate keratinocyte differentiation were highly enriched in differentiated NHEK. Activation of PPAR- α with DHA treatment has been found to induce differentiation and to normalise SC lipid ratio in a filaggrin deficient mouse skin model (Wallmeyer et al., 2015). Similarly, activating PPAR- α has been found to upregulated β -glucocerebrosidase, but not SM related enzymes in SC of skin equivalents (Takeda et al., 2018). Moreover, gene sequencing analysis showed an upregulation in the glucosylceramide metabolism genes in differentiated NHEK. In addition to SM, glucosylceramides are precursors for SC CERs which are converted back to CER by β -glucocerebrosidase (Uchida et al., 2000, Holleran et al., 1994). Additionally, glucosylceramide synthesis is stimulated during differentiation of keratinocytes (Sando et al., 1996). Therefore, this could suggest a role for PPAR-

α activation in keratinocyte differentiation and CER synthesis through utilization of glucosylceramide, and the differential effect of DHA on CER synthesis according to the developmental stage of the epidermis.

LA supplementation increased non-hydroxy CER levels in differentiated cells, without affecting CER *de novo* biosynthesis enzymes or SM levels. LA-containing omega-hydroxy CERs, which are essential for a healthy barrier, are produced from glucosylceramides (Holleran et al., 1993). In addition to this, LA is a PPAR- α activator used to initiate keratinocyte differentiation, which upregulates differentiation markers and β -glucocerebrosidase (Hanley et al., 1998, Breiden et al., 2007a). Taken together, it is suggested that LA could stimulate CER synthesis in granular epidermal layers through glucosylceramide degradation. Additionally, it could be shown that *n*-3 and *n*-6 PUFAs play a crucial role in modulating the epidermal differentiation process, and ultimately the biosynthesis of SC CERs from glucosylceramide. **Figure 6.2** summarises the expression of lipid metabolism genes in differentiated NHEK compared to proliferating NHEK.

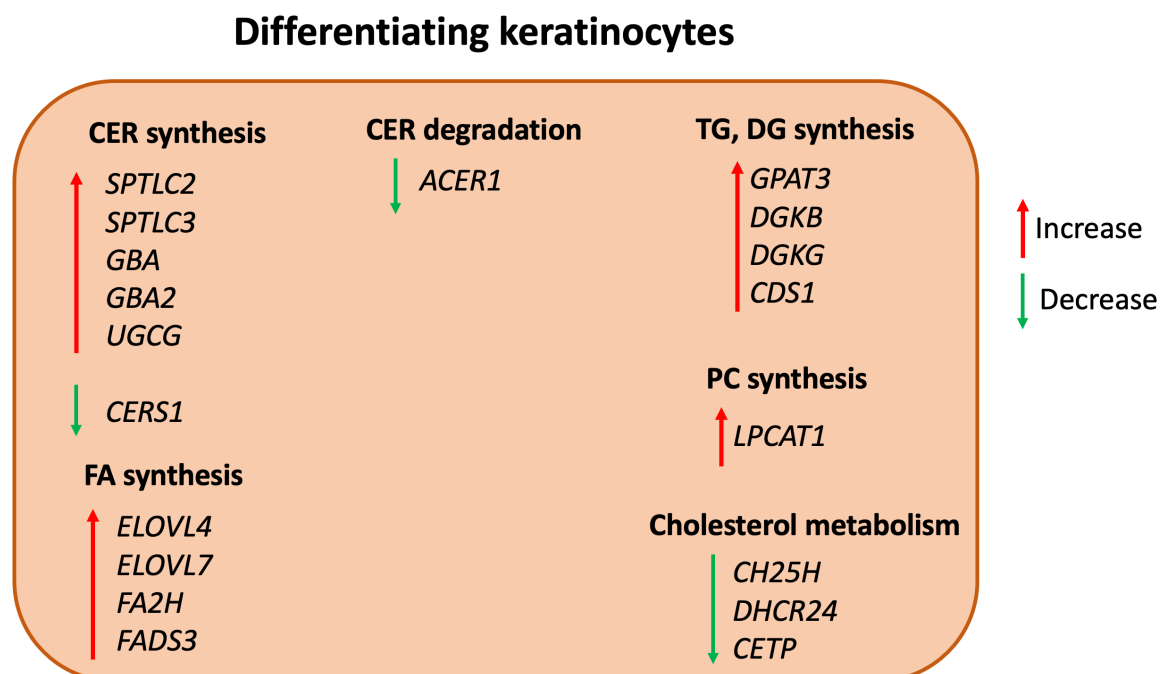


Figure 6.2 Summary lipid metabolism genes found altered in differentiating NHEK. The figure summarises the main increases (red arrow) and decreases (green arrow) found in the expression of CER, sterols, FA, glycerolipids and glycerophospholipids metabolism genes measured in differentiating NHEK (High Ca^{2+} , $n=3$ donors) compared to proliferating NHEK (Low Ca^{2+} , $n=3$ donors). Lipid metabolism gene expression was

measured using next generation sequencing; data were analysed using Ingenuity Pathway Analysis software (IPA[®], Qiagen). NHEK: normal human epidermal keratinocytes; Ca²⁺: calcium; CER: ceramide; *CERS1*: ceramide synthase 1; FA: fatty acids; *UGCG*: UDP-glucose ceramide glucosyltransferase; *GBA*: Glucosylceramidase beta; *GBA2*: Glucosylceramidase beta 2; *SIPRI*: Sphingosine-1-phosphate receptor 1; *ACER1*: Alkaline ceramidase 1; *SPTLC2*: Serine palmitoyltransferase long chain base subunit 2; *SPTLC3*: Serine palmitoyltransferase long chain base subunit 3; *DHCR24*: 24-dehydrocholesterol reductase; *CH25H*: Cholesterol 25-hydroxylase; *CETP*: Cholesteryl ester transfer protein; *GPAT3*: Glycerol-3-phosphate acyltransferase 3; *DGKB*: Diacylglycerol kinase beta; *DGKG*: Diacylglycerol kinase gamma; *CDS1*: CDP-diacylglycerol synthase 1; *LPCAT1*: Lysophosphatidylcholine acyltransferase 1; *ELOVL 4*: Fatty acid elongase 4; *ELOVL 7*: Fatty acid elongase 7; *FADS3*: Fatty acid desaturase 3; *FA2H*: Fatty acid 2-hydroxylase.

6.2.3 Primary HDF

Studies investigating lipid metabolism in the dermis are limited. In this study, DHA and EPA stimulated CER synthesis and altered membrane lipid levels, whereas LA significantly reduced membrane lipid concentrations without changing CER concentrations (**Chapter 4**). DHA mainly targeted long-chain CERs with a fatty-acyl chain length of C23-C25. Additionally, DHA and EPA downregulated the expression of *CERS5* and *CERS6*, which have a fatty-acyl preference for the short-chain C14-C16 CERs. This suggests a protective role of DHA in the dermis by stimulating the production of long-chain CERs, which are crucial for skin health. Furthermore, DHA seemed to utilise membrane SM in favor of CER and which indicates the involvement of SM pathways in CER production in the dermis. Since with LA supplementation there was a significant reduction in membrane lipids used for energy production, inflammatory response and apoptosis, this shows a proliferative role of LA in HDF. Treating HDF with AA and LA has been found to stimulate fibroblast growth and proliferation (Ejiri et al., 2015). Therefore, the alteration in CE and TG levels are a sign of cellular growth.

6.3 Investigating changes in cutaneous ceramide levels in an STZ-diabetic rat model of DPN

This study showed alterations in skin and plasma CERs and endocannabinoid-related bioactive lipids in diabetic model of DPN. The main finding was the reduction in CER[NH] in skin with diabetes (**Chapter 5**). The enzymes involved in the biosynthesis of the 6-hydroxysphingosine CERs have not been identified to date. However, skin specific CER[NH] have been found to be essential for skin

barrier permeability protection and thermal stability (Kovacik et al., 2017). Another study reported that 6-hydroxysphingosine CERs may be involved in thermal adaptation (Pappas et al., 2018). Therefore, the reduction in CER[NH] that was observed could indicate a disruption in barrier function. Studies on skin CERs in diabetes suggest a role for altered CERs in barrier impairment (Kim et al., 2018, Sakai et al., 2003).

The accumulation of circulating short-chain (C16-C24) CERs may be involved in the development of diabetes. These short chain CERs are produced by the C14-C16 specific CER synthases, CerS5 and CerS6, which are expressed ubiquitously across tissues. Previous studies have reported increases in plasma CERs with short and medium fatty acyl-chains in diabetes. For example, CERs with a C16, C22 and C24 fatty acyl-chain were increased in STZ-diabetic rats and were suggested to promote apoptosis (van Blitterswijk et al., 2003). Additionally, C16 and C18 CERs were found to play a major role in insulin signalling (Stith et al., 2019, Raichur et al., 2014). Similarly, accumulation of CER was found to be involved in β -cell apoptosis in rat pancreatic β -cell line (Véret et al., 2011).

Regarding lipid mediators, skin and plasma endocannabinoid congeners were significantly reduced with diabetes. In skin, PDEA, OEA and VEA were the main species reduced, whereas POEA and VEA were the main species affected in plasma. Lipid mediators play a crucial role in inflammatory signaling pathways. It has been found that VEA is the primary and second most abundant C18 FA-ethanolamine in rat and human plasma, respectively (Röhrig et al., 2016). Additionally, the reduced levels in plasma C18 VEA and C16 POEA, could reflect the increase observed in plasma short fatty acyl-CER levels. Diabetes is a metabolic disorder involving pathogenic processes such as hyperglycemia and dyslipidemia. Furthermore, competitive lipid metabolism could be a possible mechanism where the CER biosynthesis pathway is activated to utilise C16-C18 FFAs to produce short-chain CERs. It has been mentioned that the bioavailability of endocannabinoid precursors, FFAs, has an effect on their levels (Phinney, 1996, Annuzzi et al., 2010). Both CB₁ and CB₂ receptors are expressed in skin cells and nerve fibers, and are involved in regulating nociceptive pathways and skin cell

functions (Barrie and Manolios, 2017, Tóth et al., 2019). The reduction in skin lipid mediators could be explained by the diabetes-related dyslipidemia. Again, this could show the highly interlinked lipid metabolism mechanisms in skin, and that these specific alterations in skin bioactive lipids in DPN could be a major contributor for skin injury and delayed healing. It has been found that in diabetes, dysfunctional insulin signaling affects the proliferation, differentiation and migration of CER producing keratinocytes, which leads to barrier function impairment and consequently, impaired wound healing (Wertheimer et al., 2000).

6.4 Conclusion and future directions

The different responses of epidermal and dermal skin cells to *n*-3 and *n*-6 PUFA supplementation observed in this study show compartmental differences in lipid metabolism in the skin. This includes differences in the CER metabolism pathways targeted by the fatty acids and in the response of the epidermal and dermal cells to the fatty acid treatments. The keratinocyte data showed that DHA and LA mainly targeted the CER generating pathways. In proliferating cells, DHA works through activating the *de novo* biosynthesis and sphingomyelin recycling pathway. On the other hand, stimulation of ceramide synthesis in differentiating cells may suggest the involvement of DHA and LA in the differentiation process which could activate the glucosylceramide recycling pathway. In fibroblasts, *n*-3 PUFA acids seemed to utilise membrane lipids in favor of ceramide and anti-inflammatory lipid mediator generation, which could indicate its protective role in the dermis. On the other hand, LA was involved in stimulation of fibroblast growth. Finally, the barrier critical CER[NH] were reduced in diabetic rat skin suggesting their potential role as therapeutic targets in the treatment of cutaneous issues associated with diabetes.

The number of samples was one limitation in this study as the PUFA experiments were conducted with cultured primary human skin cells from three biological replicates (n=3 donors). This could have affected variability between donors, which was also the case in the diabetic lipidomics study. Therefore a larger sample size would reduce the interference of such factors with the results. Additionally, the PUFA study used primary human skin cells, which are useful in investigating specific metabolic pathways in different cells types individually. However, cells cultured independently in a monolayer do not accurately represent biological

mechanisms occurring in whole tissue were different cells and molecules interact. Therefore, future studies could replicate the preliminary findings from this study in an *in vivo* model such as skin biopsy.

The metabolism and individual role of PUFAs in different skin compartments in addition to cutaneous CER metabolism are not fully explored. In differentiated NHEK, gene sequencing analysis showed an upregulation in the genes involved in the synthesis of very long-chain fatty acids and PUFA. Future studies could focus on investigating the effect of DHA on the SM degradation pathway in proliferating keratinocytes, and on the effect of DHA and LA supplementation on glucosylceramide metabolism in differentiated NHEK. In addition to this, the role of DHA in keratinocyte differentiation requires further investigation. This could be investigated *in vitro* using mass spectrometry-based lipidomics, CER gene expression analysis and differentiation assays such as western blot and TEER assay. Moreover, since DHA had a broad effect on CER synthesis in NHEK, affecting both keratinocyte types, DHA may have a wider therapeutic benefit in the epidermis as it could affect CER metabolism at basal and differentiated epidermal layers. On the other hand, LA's specific action on differentiated NHEK could suggest its involvement in improving skin barrier function.

It has been found that dihydrosphingosine supplementation in differentiating NHEK increased very-long chain CERs and could, therefore, be used for cosmetic applications which improve the barrier (Sigruener et al., 2013). Similarly, the specific effect of LA, in the present study, on differentiated NHEK, was based on direct supplementation of LA in cell culture. Therefore, clinical studies using LA topical application on skin could be considered to confirm the *in vitro* results and to investigate its effectiveness compared to epidermal uptake of LA through circulation and the dermis. Moreover, further investigation using *in vivo* models such as skin biopsy could be used to elucidate the therapeutic role of DHA and LA in the epidermis and dermis. This could be achieved by comparing CER profile and enzyme activity in healthy and injured skin, in addition to blood samples with and without PUFA supplementation. Furthermore, there are limited functional studies that explore barrier dysfunction and changes in SC lipids in diabetic skin (Sakai et al., 2003, Sakai et al., 2005, Kim et al., 2018). In addition to this, the potential

pathogenetic role of individual skin and plasma CER species on nerve damage and sensory loss associated with diabetes has not been fully investigated. This project did not include functional tests on the STZ-diabetic rat foot pads to measure barrier function. Therefore, it would be interesting to further investigate the effect of the reduction in CER[NH] on the skin barrier using the same animal model. To achieve this, mass spectrometry lipidomics, in addition to techniques comparing barrier structure and function in healthy and diseased skin could be used, such as skin permeability assay and electron microscopy which have been performed on rat skin as described in (Li et al., 2007). In addition to this, correlation studies could be useful to determine the involvement of pathogenic mechanisms such as hyperglycemia with skin CER alterations in diabetes. Finally, since DHA enhanced CER profile and gene expression in both proliferating and differentiating NHEK, in addition to HDF (**Figure 6.1**), exploring the the effect of this major anti-inflammatory agent on CER concentration and CER enzyme activity in diabetic skin could help develop therapeutic approaches for cutaneous inflammatory diseases. Future clinical studies using diabetic skin could investigate whether DHA supplementation or topical application could correct the CER profile in diabetic skin.

References

- AIROLA, M. V. & HANNUN, Y. A. 2013. Sphingolipid metabolism and neutral sphingomyelinases. *Handb Exp Pharmacol*, 57-76.
- ALAM, U., SLOAN, G. & TESFAYE, S. 2020. Treating Pain in Diabetic Neuropathy: Current and Developmental Drugs. *Drugs*, 80, 363-384.
- ALPHONSE, P. A. & JONES, P. J. 2016. Revisiting Human Cholesterol Synthesis and Absorption: The Reciprocity Paradigm and its Key Regulators. *Lipids*, 51, 519-36.
- ANNUZZI, G., PISCITELLI, F., DI MARINO, L., PATTI, L., GIACCO, R., COSTABILE, G., BOZZETTO, L., RICCARDI, G., VERDE, R., PETROSINO, S., RIVELLESE, A. A. & DI MARZO, V. 2010. Differential alterations of the concentrations of endocannabinoids and related lipids in the subcutaneous adipose tissue of obese diabetic patients. *Lipids Health Dis*, 9, 43.
- AOKI, M., OGAI, K., KOBAYASHI, M., MINEMATSU, T., NAKATANI, T., OKUWA, M., SANADA, H. & SUGAMA, J. 2019. Comparison of ceramide retention in the stratum corneum between dry skin and normal skin using animal model with fluorescent imaging method. *Skin Research and Technology*, 25, 158-164.
- ARGENZIANO, M., TORTORA, C., BELLINI, G., DI PAOLA, A., PUNZO, F. & ROSSI, F. 2019. The Endocannabinoid System in Pediatric Inflammatory and Immune Diseases. *Int J Mol Sci*, 20.
- ARLETT, C. F., GREEN, M. H., PRIESTLEY, A., HARCOURT, S. A. & MAYNE, L. V. 1988. Comparative human cellular radiosensitivity: I. The effect of SV40 transformation and immortalisation on the gamma-irradiation survival of skin derived fibroblasts from normal individuals and from ataxia-telangiectasia patients and heterozygotes. *Int J Radiat Biol*, 54, 911-28.
- BALAZS, L., OKOLICANY, J., FERREBEE, M., TOLLEY, B. & TIGYI, G. 2001. Topical application of the phospholipid growth factor lysophosphatidic acid promotes wound healing in vivo. *Am J Physiol Regul Integr Comp Physiol*, 280, R466-72.
- BANSAL, V., KALITA, J. & MISRA, U. K. 2006. Diabetic neuropathy. *Postgraduate medical journal*, 82, 95-100.
- BARRIE, N. & MANOLIOS, N. 2017. The endocannabinoid system in pain and inflammation: Its relevance to rheumatic disease. *Eur J Rheumatol*, 4, 210-218.
- BERMÚDEZ-SIVA, F. J., SERRANO, A., DIAZ-MOLINA, F. J., SÁNCHEZ VERA, I., JUAN-PICO, P., NADAL, A., FUENTES, E. & RODRÍGUEZ DE FONSECA, F. 2006. Activation of cannabinoid CB1 receptors induces glucose intolerance in rats. *European Journal of Pharmacology*, 531, 282-284.
- BERTEA, M., RÜTTI, M. F., OTHMAN, A., MARTI-JAUN, J., HERSBERGER, M., VON ECKARDSTEIN, A. & HORNEMANN, T. 2010. Deoxysphingoid bases as plasma markers in diabetes mellitus. *Lipids Health Dis*, 9, 84.
- BIESSELS, G. J., BRIL, V., CALCUTT, N. A., CAMERON, N. E., COTTER, M. A., DOBROWSKY, R., FELDMAN, E. L., FERNYHOUGH, P., JAKOBSEN, J., MALIK, R. A., MIZISIN, A. P., OATES, P. J., OBROSOVA, I. G., POP-BUSUI, R., RUSSELL, J. W., SIMA, A. A., STEVENS, M. J., SCHMIDT, R. E., TESFAYE, S.,

- VEVES, A., VINIK, A. I., WRIGHT, D. E., YAGIHASHI, S., YOREK, M. A., ZIEGLER, D. & ZOCHODNE, D. W. 2014. Phenotyping animal models of diabetic neuropathy: a consensus statement of the diabetic neuropathy study group of the EASD (Neurodiab). *J Peripher Nerv Syst*, 19, 77-87.
- BIKLE, D. D., XIE, Z. & TU, C. L. 2012. Calcium regulation of keratinocyte differentiation. *Expert Rev Endocrinol Metab*, 7, 461-472.
- BJÖRKHEM, I. 2013. Five decades with oxysterols. *Biochimie*, 95, 448-54.
- BLAYDON, D. C. & KELSELL, D. P. 2014. Defective channels lead to an impaired skin barrier. *J Cell Sci*, 127, 4343-50.
- BLIGH, E. G. & DYER, W. J. 1959. A rapid method of total lipid extraction and purification. *Can J Biochem Physiol*, 37, 911-7.
- BODE, H., BOURQUIN, F., SURIYANARAYANAN, S., WEI, Y., ALECU, I., OTHMAN, A., VON ECKARDSTEIN, A. & HORNE MANN, T. 2016. HSAN1 mutations in serine palmitoyltransferase reveal a close structure-function-phenotype relationship. *Hum Mol Genet*, 25, 853-65.
- BONNET-DUQUENNOY, M., ABAIBOU, H., TAILHARDAT, M., LAZOU, K., BOSSET, S., LE VARLET, B., CLEUZIAT, P. & KURFÜRST, R. 2006. Study of housekeeping gene expression in human keratinocytes using OLISA, a long-oligonucleotide microarray and q RT-PCR. *Eur J Dermatol*, 16, 136-40.
- BORODZICZ, S., RUDNICKA, L., MIROWSKA-GUZEL, D. & CUDNOCH-JEDRZEJEWSKA, A. 2016. The role of epidermal sphingolipids in dermatologic diseases. *Lipids Health Dis*, 15, 13.
- BOROWIEC, A. S., DELCOURT, P., DEWAILLY, E. & BIDAUX, G. 2013. Optimal differentiation of in vitro keratinocytes requires multifactorial external control. *PLoS One*, 8, e77507.
- BOSLEM, E., MEIKLE, P. J. & BIDEN, T. J. 2012. Roles of ceramide and sphingolipids in pancreatic β -cell function and dysfunction. *Islets*, 4, 177-87.
- BOUKAMP, P., PETRUSSEVSKA, R. T., BREITKREUTZ, D., HORNUNG, J., MARKHAM, A. & FUSENIG, N. E. 1988. Normal keratinization in a spontaneously immortalized aneuploid human keratinocyte cell line. *J Cell Biol*, 106, 761-71.
- BOURQUIN, F., CAPITANI, G. & GRUTTER, M. G. 2011. PLP-dependent enzymes as entry and exit gates of sphingolipid metabolism. *Protein Sci*, 20, 1492-508.
- BRADFORD, M. M. 1976. A rapid and sensitive method for the quantitation of microgram quantities of protein utilizing the principle of protein-dye binding. *Analytical Biochemistry*, 72, 248-254.
- BREIDEN, B., GALLALA, H., DOERING, T. & SANDHOFF, K. 2007a. Optimization of submerged keratinocyte cultures for the synthesis of barrier ceramides. *Eur J Cell Biol*, 86, 657-73.
- BREIDEN, B., GALLALA, H., DOERING, T. & SANDHOFF, K. 2007b. Optimization of submerged keratinocyte cultures for the synthesis of barrier ceramides. *European Journal of Cell Biology*, 86, 657-673.

- BREIDEN, B. & SANDHOFF, K. 2014. The role of sphingolipid metabolism in cutaneous permeability barrier formation. *Biochim Biophys Acta*, 1841, 441-52.
- BREM, H. & TOMIC-CANIC, M. 2007. Cellular and molecular basis of wound healing in diabetes. *The Journal of clinical investigation*, 117, 1219-1222.
- CALCUTT, N. A. & CHAPLAN, S. R. 1997. Spinal pharmacology of tactile allodynia in diabetic rats. *Br J Pharmacol*, 122, 1478-82.
- CALDERÓN, C., RUBARTH, L., CEBO, M., MERFORT, I. & LÄMMERHOFER, M. 2020. Lipid Atlas of Keratinocytes and Betulin Effects on its Lipidome Profiled by Comprehensive UHPLC–MS/MS with Data Independent Acquisition Using Targeted Data Processing. *PROTEOMICS*, 20, 1900113.
- CALLAGHAN, B. C., CHENG, H. T., STABLES, C. L., SMITH, A. L. & FELDMAN, E. L. 2012a. Diabetic neuropathy: clinical manifestations and current treatments. *Lancet Neurol*, 11, 521-34.
- CALLAGHAN, B. C., LITTLE, A. A., FELDMAN, E. L. & HUGHES, R. A. 2012b. Enhanced glucose control for preventing and treating diabetic neuropathy. *Cochrane Database Syst Rev*, 6, Cd007543.
- CARDOSO, C. R., SOUZA, M. A., FERRO, E. A., FAVORETO, S., JR. & PENA, J. D. 2004. Influence of topical administration of n-3 and n-6 essential and n-9 nonessential fatty acids on the healing of cutaneous wounds. *Wound Repair Regen*, 12, 235-43.
- CHARRUYER, A., BELL, S. M., KAWANO, M., DOUANGPANYA, S., YEN, T. Y., MACHER, B. A., KUMAGAI, K., HANADA, K., HOLLERAN, W. M. & UCHIDA, Y. 2008. Decreased ceramide transport protein (CERT) function alters sphingomyelin production following UVB irradiation. *J Biol Chem*, 283, 16682-92.
- CHENG, K., BOU, M., RUYTER, B., PICKOVA, J., EHTESHAM, E., DU, L., VENEGAS, C. & MOAZZAMI, A. A. 2018. Impact of Reduced Dietary Levels of Eicosapentaenoic Acid and Docosahexaenoic Acid on the Composition of Skin Membrane Lipids in Atlantic Salmon (*Salmo salar* L.). *J Agric Food Chem*, 66, 8876-8884.
- CHI, W., WU, E. & MORGAN, B. A. 2013. Dermal papilla cell number specifies hair size, shape and cycling and its reduction causes follicular decline. *Development*, 140, 1676-83.
- CHOI, H. K., KIM, H. J., LIU, K. H. & PARK, C. S. 2018. Phytosphingosine Increases Biosynthesis of Phytoceramide by Uniquely Stimulating the Expression of Dihydroceramide C4-desaturase (DES2) in Cultured Human Keratinocytes. *Lipids*, 53, 909-918.
- CHUONG, C. M., NICKOLOFF, B. J., ELIAS, P. M., GOLDSMITH, L. A., MACHER, E., MADERSON, P. A., SUNDBERG, J. P., TAGAMI, H., PLONKA, P. M., THESTRUP-PEDERSON, K., BERNARD, B. A., SCHRÖDER, J. M., DOTTO, P., CHANG, C. M., WILLIAMS, M. L., FEINGOLD, K. R., KING, L. E., KLIGMAN, A. M., REES, J. L. & CHRISTOPHERS, E. 2002. What is the 'true' function of skin? *Exp Dermatol*, 11, 159-87.
- CODERCH, L., LOPEZ, O., DE LA MAZA, A. & PARRA, J. L. 2003. Ceramides and skin function. *Am J Clin Dermatol*, 4, 107-29.

- COELHO, M., OLIVEIRA, T. & FERNANDES, R. 2013. Biochemistry of adipose tissue: an endocrine organ. *Arch Med Sci*, 9, 191-200.
- COLLIN, C., MOLL, R., KUBICKA, S., OUHAYOUN, J.-P. & FRANKE, W. W. 1992. Characterization of human cytokeratin 2, an Epidermal cytoskeletal protein synthesized late during differentiation. *Experimental Cell Research*, 202, 132-141.
- DAWKINS, J. L., HULME, D. J., BRAHMBHATT, S. B., AUER-GRUMBACH, M. & NICHOLSON, G. A. 2001. Mutations in SPTLC1, encoding serine palmitoyltransferase, long chain base subunit-1, cause hereditary sensory neuropathy type I. *Nat Genet*, 27, 309-12.
- DE JONGE, H. J. M., FEHRMANN, R. S. N., DE BONT, E. S. J. M., HOFSTRA, R. M. W., GERBENS, F., KAMPS, W. A., DE VRIES, E. G. E., VAN DER ZEE, A. G. J., TE MEERMAN, G. J. & TER ELST, A. 2007. Evidence Based Selection of Housekeeping Genes. *PLOS ONE*, 2, e898.
- DEBOSE-BOYD, R. A. 2008. Feedback regulation of cholesterol synthesis: sterol-accelerated ubiquitination and degradation of HMG CoA reductase. *Cell Research*, 18, 609-621.
- DOERING, T., PROIA, R. L. & SANDHOFF, K. 1999. Accumulation of protein-bound epidermal glucosylceramides in beta-glucocerebrosidase deficient type 2 Gaucher mice. *FEBS Lett*, 447, 167-70.
- DOHRN, M. F., OTHMAN, A., HIRSHMAN, S. K., BODE, H., ALECU, I., FÄHNDRICH, E., KARGES, W., WEIS, J., SCHULZ, J. B., HORNEMANN, T. & CLAEYS, K. G. 2015. Elevation of plasma 1-deoxy-sphingolipids in type 2 diabetes mellitus: a susceptibility to neuropathy? *Eur J Neurol*, 22, 806-14, e55.
- ECKL, K. M., TIDHAR, R., THIELE, H., OJI, V., HAUSSER, I., BRODESSER, S., PREIL, M. L., ONAL-AKAN, A., STOCK, F., MULLER, D., BECKER, K., CASPER, R., NURNBERG, G., ALTMULLER, J., NURNBERG, P., TRAUPE, H., FUTERMAN, A. H. & HENNIES, H. C. 2013. Impaired epidermal ceramide synthesis causes autosomal recessive congenital ichthyosis and reveals the importance of ceramide acyl chain length. *J Invest Dermatol*, 133, 2202-11.
- EJIRI, H., NOMURA, T., HASEGAWA, M., TATSUMI, C., IMAI, M., SAKAKIBARA, S. & TERASHI, H. 2015. Use of synthetic serum-free medium for culture of human dermal fibroblasts to establish an experimental system similar to living dermis. *Cytotechnology*, 67, 507-14.
- ENGLAND, J. D., GRONSETH, G. S., FRANKLIN, G., MILLER, R. G., ASBURY, A. K., CARTER, G. T., COHEN, J. A., FISHER, M. A., HOWARD, J. F., KINSELLA, L. J., LATOV, N., LEWIS, R. A., LOW, P. A. & SUMNER, A. J. 2005. Distal symmetric polyneuropathy: A definition for clinical research. *Report of the American Academy of Neurology, the American Association of Electrodiagnostic Medicine, and the American Academy of Physical Medicine and Rehabilitation*, 64, 199-207.
- FAHY, E., SUBRAMANIAM, S., BROWN, H. A., GLASS, C. K., MERRILL, A. H., JR., MURPHY, R. C., RAETZ, C. R., RUSSELL, D. W., SEYAMA, Y., SHAW, W., SHIMIZU, T., SPENER, F., VAN MEER, G., VANNIEUWENHZE, M. S., WHITE, S. H., WITZTUM, J. L. & DENNIS, E. A. 2005. A comprehensive classification system for lipids. *J Lipid Res*, 46, 839-61.

- FAHY, E., SUBRAMANIAM, S., MURPHY, R. C., NISHIJIMA, M., RAETZ, C. R., SHIMIZU, T., SPENER, F., VAN MEER, G., WAKELAM, M. J. & DENNIS, E. A. 2009. Update of the LIPID MAPS comprehensive classification system for lipids. *J Lipid Res*, 50 Suppl, S9-14.
- FELDMAN, E. L., NAVE, K.-A., JENSEN, T. S. & BENNETT, D. L. H. 2017. New Horizons in Diabetic Neuropathy: Mechanisms, Bioenergetics, and Pain. *Neuron*, 93, 1296-1313.
- FELTON, S. J., KENDALL, A. C., ALMAEDANI, A. F. M., URQUHART, P., WEBB, A. R., KIFT, R., VAIL, A., NICOLAOU, A. & RHODES, L. E. 2017. Serum endocannabinoids and N-acyl ethanolamines and the influence of simulated solar UVR exposure in humans in vivo. *Photochemical & Photobiological Sciences*, 16, 564-574.
- FERNANDES, I. R., RUSSO, F. B., PIGNATARI, G. C., EVANGELINELLIS, M. M., TAVOLARI, S., MUOTRI, A. R. & BELTRÃO-BRAGA, P. C. 2016. Fibroblast sources: Where can we get them? *Cytotechnology*, 68, 223-8.
- FRANCIS-GOFORTH, K. N., HARKEN, A. H. & SABA, J. D. 2010. Normalization of diabetic wound healing. *Surgery*, 147, 446-449.
- FREEMAN, O. J., UNWIN, R. D., DOWSEY, A. W., BEGLEY, P., ALI, S., HOLLYWOOD, K. A., RUSTOGI, N., PETERSEN, R. S., DUNN, W. B., COOPER, G. J. & GARDINER, N. J. 2016. Metabolic Dysfunction Is Restricted to the Sciatic Nerve in Experimental Diabetic Neuropathy. *Diabetes*, 65, 228-38.
- FUCHS, E. 1990. Epidermal differentiation: the bare essentials. *J Cell Biol*, 111, 2807-14.
- FUJII, M., NAKASHIMA, H., TOMOZAWA, J., SHIMAZAKI, Y., OHYANAGI, C., KAWAGUCHI, N., OHYA, S., KOHNO, S. & NABE, T. 2013. Deficiency of n-6 polyunsaturated fatty acids is mainly responsible for atopic dermatitis-like pruritic skin inflammation in special diet-fed hairless mice. *Experimental Dermatology*, 22, 272-277.
- FUJII, M., OHYANAGI, C., KAWAGUCHI, N., MATSUDA, H., MIYAMOTO, Y., OHYA, S. & NABE, T. 2018. Eicosapentaenoic acid ethyl ester ameliorates atopic dermatitis-like symptoms in special diet-fed hairless mice, partly by restoring covalently bound ceramides in the stratum corneum. *Experimental Dermatology*, 27, 837-840.
- G J SCHROEPFER, J. 1982. Sterol Biosynthesis. *Annual Review of Biochemistry*, 51, 555-585.
- GALADARI, S., RAHMAN, A., PALLICHANKANDY, S., GALADARI, A. & THAYYULLATHIL, F. 2013. Role of ceramide in diabetes mellitus: evidence and mechanisms. *Lipids Health Dis*, 12, 98.
- GALLALA, H., MACHELEIDT, O., DOERING, T., SCHREINER, V. & SANDHOFF, K. 2004. Nitric oxide regulates synthesis of gene products involved in keratinocyte differentiation and ceramide metabolism. *European Journal of Cell Biology*, 83, 667-679.
- GARDINER, N. J., WANG, Z., LUKE, C., GOTT, A., PRICE, S. A. & FERNYHOUGH, P. 2007. Expression of hexokinase isoforms in the dorsal root ganglion of the adult rat and effect of experimental diabetes. *Brain Res*, 1175, 143-54.
- GAULT, C. R., OBEID, L. M. & HANNUN, Y. A. 2010. An overview of sphingolipid metabolism: from synthesis to breakdown. *Adv Exp Med Biol*, 688, 1-23.

- GERSTEIN, W. 1963. The Phospholipids of Normal and Psoriatic Skin**This work was performed while the author was an Exchange Fellow at St. John's Hospital for Diseases of the Skin, London, England, from Department of Dermatology, University of Pennsylvania School of Medicine, Philadelphia, Pennsylvania. *Journal of Investigative Dermatology*, 40, 105-109.
- GILL, S., STEVENSON, J., KRISTIANA, I. & BROWN, A. J. 2011. Cholesterol-dependent degradation of squalene monooxygenase, a control point in cholesterol synthesis beyond HMG-CoA reductase. *Cell Metab*, 13, 260-73.
- GONI, F. M. & ALONSO, A. 2002. Sphingomyelinases: enzymology and membrane activity. *FEBS Lett*, 531, 38-46.
- GREGOIRE, F. M. 2001. Adipocyte Differentiation: From Fibroblast to Endocrine Cell. *Experimental Biology and Medicine*, 226, 997-1002.
- GRIFFIN, M. F., DESJARDINS-PARK, H. E., MASCHARAK, S., BORRELLI, M. R. & LONGAKER, M. T. 2020. Understanding the impact of fibroblast heterogeneity on skin fibrosis. *Disease Models & Mechanisms*, 13, dmm044164.
- GRUDEN, G., BARUTTA, F., KUNOS, G. & PACHER, P. 2016. Role of the endocannabinoid system in diabetes and diabetic complications. *Br J Pharmacol*, 173, 1116-27.
- GUO, J., QIAN, Y., XI, X., HU, X., ZHU, J. & HAN, X. 2010. Blockage of ceramide metabolism exacerbates palmitate inhibition of pro-insulin gene expression in pancreatic β -cells. *Molecular and Cellular Biochemistry*, 338, 283-290.
- HAGE HASSAN, R., PACHECO DE SOUSA, A. C., MAHFOUZ, R., HAINAULT, I., BLACHNIO-ZABIELSKA, A., BOURRON, O., KOSKAS, F., GÓRSKI, J., FERRÉ, P., FOUFELLE, F. & HAJDUCH, E. 2016. Sustained Action of Ceramide on the Insulin Signaling Pathway in Muscle Cells: IMPLICATION OF THE DOUBLE-STRANDED RNA-ACTIVATED PROTEIN KINASE. *J Biol Chem*, 291, 3019-29.
- HAMMAD, S. M., BAKER, N. L., EL ABIAD, J. M., SPASSIEVA, S. D., PIERCE, J. S., REMBIESA, B., BIELAWSKI, J., LOPES-VIRELLA, M. F. & KLEIN, R. L. 2017. Increased Plasma Levels of Select Deoxy-ceramide and Ceramide Species are Associated with Increased Odds of Diabetic Neuropathy in Type 1 Diabetes: A Pilot Study. *Neuromolecular Med*, 19, 46-56.
- HAN, G., GUPTA, S. D., GABLE, K., NIRANJANAKUMARI, S., MOITRA, P., EICHLER, F., BROWN, R. H., JR., HARMON, J. M. & DUNN, T. M. 2009. Identification of small subunits of mammalian serine palmitoyltransferase that confer distinct acyl-CoA substrate specificities. *Proc Natl Acad Sci U S A*, 106, 8186-91.
- HANADA, K. 2003. Serine palmitoyltransferase, a key enzyme of sphingolipid metabolism. *Biochim Biophys Acta*, 1632, 16-30.
- HANADA, K., HARA, T. & NISHIJIMA, M. 2000. Purification of the serine palmitoyltransferase complex responsible for sphingoid base synthesis by using affinity peptide chromatography techniques. *J Biol Chem*, 275, 8409-15.

- HANLEY, K., JIANG, Y., SHAN HE, S., FRIEDMAN, M., ELIAS, P. M., BIKLE, D. D., WILLIAMS, M. L. & FEINGOLD, K. R. 1998. Keratinocyte Differentiation is Stimulated by Activators of the Nuclear Hormone Receptor PPAR α . *Journal of Investigative Dermatology*, 110, 368-375.
- HANNUN, Y. A. & OBEID, L. M. 2008. Principles of bioactive lipid signalling: lessons from sphingolipids. *Nat Rev Mol Cell Biol*, 9, 139-50.
- HANNUN, Y. A. & OBEID, L. M. 2011. Many ceramides. *J Biol Chem*, 286, 27855-62.
- HARDING, C. R. 2004. The stratum corneum: structure and function in health and disease. *Dermatol Ther*, 17 Suppl 1, 6-15.
- HASANEIN, P. & SOLTANI, N. 2009. Effects of the endocannabinoid transport inhibitors AM404 and UCM707 on diabetic neuropathy in rats. *Clin Exp Pharmacol Physiol*, 36, 1127-31.
- HAWKSHAW, N. J., PILKINGTON, S. M., MURPHY, S. A., AL-GAZAQ, N., FARRAR, M. D., WATSON, R. E., NICOLAOU, A. & RHODES, L. E. 2020. UV radiation recruits CD4+GATA3+ and CD8+GATA3+ T cells while altering the lipid microenvironment following inflammatory resolution in human skin in vivo. *Clinical & Translational Immunology*, 9, e01104.
- HAYNES, C. A., ALLEGOOD, J. C., SIMS, K., WANG, E. W., SULLARDS, M. C. & MERRILL, A. H., JR. 2008. Quantitation of fatty acyl-coenzyme As in mammalian cells by liquid chromatography-electrospray ionization tandem mass spectrometry. *J Lipid Res*, 49, 1113-25.
- HERGET, T., ESDAR, C., OEHRLEIN, S. A., HEINRICH, M., SCHÜTZE, S., MAELICKE, A. & VAN ECHTEN-DECKERT, G. 2000. Production of ceramides causes apoptosis during early neural differentiation in vitro. *J Biol Chem*, 275, 30344-54.
- HO, K. H. & PATRIZI, A. 2021. Assessment of common housekeeping genes as reference for gene expression studies using RT-qPCR in mouse choroid plexus. *Scientific Reports*, 11, 3278.
- HOLLAND, W. L., BROZINICK, J. T., WANG, L. P., HAWKINS, E. D., SARGENT, K. M., LIU, Y., NARRA, K., HOEHN, K. L., KNOTTS, T. A., SIESKY, A., NELSON, D. H., KARATHANASIS, S. K., FONTENOT, G. K., BIRNBAUM, M. J. & SUMMERS, S. A. 2007. Inhibition of ceramide synthesis ameliorates glucocorticoid-, saturated-fat-, and obesity-induced insulin resistance. *Cell Metab*, 5, 167-79.
- HOLLERAN, W. M., GINNS, E. I., MENON, G. K., GRUNDMANN, J. U., FARTASCH, M., MCKINNEY, C. E., ELIAS, P. M. & SIDRANSKY, E. 1994. Consequences of beta-glucocerebrosidase deficiency in epidermis. Ultrastructure and permeability barrier alterations in Gaucher disease. *J Clin Invest*, 93, 1756-64.
- HOLLERAN, W. M., TAKAGI, Y., MENON, G. K., LEGLER, G., FEINGOLD, K. R. & ELIAS, P. M. 1993. Processing of epidermal glucosylceramides is required for optimal mammalian cutaneous permeability barrier function. *J Clin Invest*, 91, 1656-64.
- HOLLERAN, W. M., TAKAGI, Y. & UCHIDA, Y. 2006. Epidermal sphingolipids: metabolism, function, and roles in skin disorders. *FEBS Lett*, 580, 5456-66.

- HORNEMANN, T., RICHARD, S., RUTTI, M. F., WEI, Y. & VON ECKARDSTEIN, A. 2006. Cloning and initial characterization of a new subunit for mammalian serine-palmitoyltransferase. *J Biol Chem*, 281, 37275-81.
- HOUBEN, E., HOLLERAN, W. M., YAGINUMA, T., MAO, C., OBEID, L. M., ROGIERS, V., TAKAGI, Y., ELIAS, P. M. & UCHIDA, Y. 2006. Differentiation-associated expression of ceramidase isoforms in cultured keratinocytes and epidermis. *J Lipid Res*, 47, 1063-70.
- IBRAHIM, M. M., PORRECA, F., LAI, J., ALBRECHT, P. J., RICE, F. L., KHODOROVA, A., DAVAR, G., MAKRIYANNIS, A., VANDERAH, T. W., MATA, H. P. & MALAN, T. P., JR. 2005. CB2 cannabinoid receptor activation produces antinociception by stimulating peripheral release of endogenous opioids. *Proc Natl Acad Sci U S A*, 102, 3093-8.
- ICHIKAWA, S. & HIRABAYASHI, Y. 1998. Glucosylceramide synthase and glycosphingolipid synthesis. *Trends Cell Biol*, 8, 198-202.
- IGAWA, S., CHOI, J. E., WANG, Z., CHANG, Y.-L., WU, C.-C., WERBEL, T., ISHIDA-YAMAMOTO, A. & DI NARDO, A. 2019. Human Keratinocytes Use Sphingosine 1-Phosphate and its Receptors to Communicate Staphylococcus aureus Invasion and Activate Host Defense. *Journal of Investigative Dermatology*, 139, 1743-1752.e5.
- IMOKAWA, G., ABE, A., JIN, K., HIGAKI, Y., KAWASHIMA, M. & HIDANO, A. 1991. Decreased level of ceramides in stratum corneum of atopic dermatitis: an etiologic factor in atopic dry skin? *J Invest Dermatol*, 96, 523-6.
- ISHIDA-YAMAMOTO, A., HOHL, D., ROOP, D. R., IIZUKA, H. & EADY, R. A. J. 1993. Loricrin immunoreactivity in human skin: localization to specific granules (L-granules) in acrosyringia. *Archives of Dermatological Research*, 285, 491-498.
- IYER, A., FAIRLIE, D. P., PRINS, J. B., HAMMOCK, B. D. & BROWN, L. 2010. Inflammatory lipid mediators in adipocyte function and obesity. *Nature Reviews Endocrinology*, 6, 71-82.
- JANSSENS, M., VAN SMEDEN, J., GOORIS, G. S., BRAS, W., PORTALE, G., CASPERS, P. J., VREEKEN, R. J., HANKEMEIER, T., KEZIC, S., WOLTERBEEK, R., LAVRIJSEN, A. P. & BOUWSTRA, J. A. 2012. Increase in short-chain ceramides correlates with an altered lipid organization and decreased barrier function in atopic eczema patients. *J Lipid Res*, 53, 2755-66.
- JARAMILLO, M. L., AMMAR, D., QUISPE, R. L., GUZMAN, F., MARGIS, R., NAZARI, E. M. & MÜLLER, Y. M. R. 2017. Identification and evaluation of reference genes for expression studies by RT-qPCR during embryonic development of the emerging model organism, *Macrobrachium olfersii*. *Gene*, 598, 97-106.
- JEFFCOATE, W. J., VILEIKYTE, L., BOYKO, E. J., ARMSTRONG, D. G. & BOULTON, A. J. M. 2018. Current Challenges and Opportunities in the Prevention and Management of Diabetic Foot Ulcers. *Diabetes Care*, 41, 645-652.
- JENNEMANN, R., RABIONET, M., GORGAS, K., EPSTEIN, S., DALPKE, A., ROTHERMEL, U., BAYERLE, A., VAN DER HOEVEN, F., IMGRUND, S., KIRSCH, J., NICKEL, W., WILLECKE, K., RIEZMAN, H., GRONE, H. J. & SANDHOFF, R. 2012. Loss of ceramide synthase 3 causes lethal skin barrier disruption. *Hum Mol Genet*, 21, 586-608.

- JENSEN, J. M., FORL, M., WINOTO-MORBACH, S., SEITE, S., SCHUNCK, M., PROKSCH, E. & SCHUTZE, S. 2005. Acid and neutral sphingomyelinase, ceramide synthase, and acid ceramidase activities in cutaneous aging. *Exp Dermatol*, 14, 609-18.
- JUAN-PICÓ, P., FUENTES, E., JAVIER BERMÚDEZ-SILVA, F., JAVIER DÍAZ-MOLINA, F., RIPOLL, C., RODRÍGUEZ DE FONSECA, F. & NADAL, A. 2006. Cannabinoid receptors regulate Ca²⁺ signals and insulin secretion in pancreatic β -cell. *Cell Calcium*, 39, 155-162.
- JUNGERSTED, J. M., SCHEER, H., MEMPEL, M., BAURECHT, H., CIFUENTES, L., HOGH, J. K., HELLGREN, L. I., JEMEC, G. B., AGNER, T. & WEIDINGER, S. 2010. Stratum corneum lipids, skin barrier function and filaggrin mutations in patients with atopic eczema. *Allergy*, 65, 911-8.
- KAM, E., NIRUNSUKSIRI, W., HAGER, B., FLECKMAN, P. & DALE, B. A. 1997. Protein phosphatase activity in human keratinocytes cultured from normal epidermis and epidermis from patients with harlequin ichthyosis. *British Journal of Dermatology*, 137, 874-882.
- KARAMOYSOYLI, E., BURNAND, R. C., TOMLINSON, D. R. & GARDINER, N. J. 2008. Neuritin mediates nerve growth factor-induced axonal regeneration and is deficient in experimental diabetic neuropathy. *Diabetes*, 57, 181-9.
- KENDALL, A. C., KIEZEL-TSUGUNOVA, M., BROWNBRIDGE, L. C., HARWOOD, J. L. & NICOLAOU, A. 2017. Lipid functions in skin: Differential effects of n-3 polyunsaturated fatty acids on cutaneous ceramides, in a human skin organ culture model. *BBA - Biomembranes*.
- KENDALL, A. C., KOSZYCZAREK, M. M., JONES, E. A., HART, P. J., TOWERS, M., GRIFFITHS, C. E. M., MORRIS, M. & NICOLAOU, A. 2018. Lipidomics for translational skin research: A primer for the uninitiated. *Experimental Dermatology*, 27, 721-728.
- KENDALL, A. C. & NICOLAOU, A. 2013. Bioactive lipid mediators in skin inflammation and immunity. *Prog Lipid Res*, 52, 141-64.
- KENDALL, A. C., PILKINGTON, S. M., MASSEY, K. A., SASSANO, G., RHODES, L. E. & NICOLAOU, A. 2015. Distribution of bioactive lipid mediators in human skin. *J Invest Dermatol*, 135, 1510-20.
- KENDALL, A. C., PILKINGTON, S. M., SASSANO, G., RHODES, L. E. & NICOLAOU, A. 2016. N-Acyl ethanolamide and eicosanoid involvement in irritant dermatitis. *British Journal of Dermatology*, 175, 163-171.
- KIHARA, A. 2016. Synthesis and degradation pathways, functions, and pathology of ceramides and epidermal acylceramides. *Prog Lipid Res*, 63, 50-69.
- KIHARA, A., MITSUTAKE, S., MIZUTANI, Y. & IGARASHI, Y. 2007. Metabolism and biological functions of two phosphorylated sphingolipids, sphingosine 1-phosphate and ceramide 1-phosphate. *Prog Lipid Res*, 46, 126-44.
- KIM, J. H., YOON, N. Y., KIM, D. H., JUNG, M., JUN, M., PARK, H. Y., CHUNG, C. H., LEE, K., KIM, S., PARK, C. S., LIU, K. H. & CHOI, E. H. 2018. Impaired permeability and antimicrobial barriers in type 2 diabetes skin are linked to increased serum levels of advanced glycation end-product. *Exp Dermatol*, 27, 815-823.
- KIM, S., HONG, I., HWANG, J. S., CHOI, J. K., RHO, H. S., KIM, D. H., CHANG, I., LEE, S. H., LEE, M. O. & HWANG, J. S. 2006. Phytosphingosine stimulates the

- differentiation of human keratinocytes and inhibits TPA-induced inflammatory epidermal hyperplasia in hairless mouse skin. *Mol Med*, 12, 17-24.
- KITATANI, K., IDKOWIAK-BALDYS, J. & HANNUN, Y. A. 2008. The sphingolipid salvage pathway in ceramide metabolism and signaling. *Cell Signal*, 20, 1010-8.
- KORBECKI, J. & BAJDAK-RUSINEK, K. 2019. The effect of palmitic acid on inflammatory response in macrophages: an overview of molecular mechanisms. *Inflammation Research*, 68, 915-932.
- KOVACIK, A., ROH, J. & VAVROVA, K. 2014. The chemistry and biology of 6-hydroxyceramide, the youngest member of the human sphingolipid family. *Chembiochem*, 15, 1555-62.
- KOVACIK, A., SILAROVA, M., PULLMANNOVA, P., MAIXNER, J. & VAVROVA, K. 2017. Effects of 6-hydroxyceramides on the thermotropic phase behavior and permeability of model skin lipid membranes. *Langmuir*.
- KREDER, D., KRUT, O., ADAM-KLAGES, S., WIEGMANN, K., SCHERER, G., PLITZ, T., JENSEN, J. M., PROKSCH, E., STEINMANN, J., PFEFFER, K. & KRONKE, M. 1999. Impaired neutral sphingomyelinase activation and cutaneous barrier repair in FAN-deficient mice. *EMBO J*, 18, 2472-9.
- KUMAWAT, V. S. & KAUR, G. 2019. Therapeutic potential of cannabinoid receptor 2 in the treatment of diabetes mellitus and its complications. *Eur J Pharmacol*, 862, 172628.
- LAI-CHEONG, J. E. & MCGRATH, J. A. 2013. Structure and function of skin, hair and nails. *Medicine*, 41, 317-320.
- LAMPE, M. A., WILLIAMS, M. L. & ELIAS, P. M. 1983. Human epidermal lipids: characterization and modulations during differentiation. *J Lipid Res*, 24, 131-40.
- LASS, A., ZIMMERMANN, R., OBERER, M. & ZECHNER, R. 2011. Lipolysis - a highly regulated multi-enzyme complex mediates the catabolism of cellular fat stores. *Prog Lipid Res*, 50, 14-27.
- LAVKER, R. M. & MATOLTSY, A. G. 1971. Substructure of keratohyalin granules of the epidermis as revealed by high resolution electron microscopy. *J Ultrastruct Res*, 35, 575-81.
- LEONARD, A. E., PEREIRA, S. L., SPRECHER, H. & HUANG, Y. S. 2004. Elongation of long-chain fatty acids. *Prog Lipid Res*, 43, 36-54.
- LI, W., SANDHOFF, R., KONO, M., ZERFAS, P., HOFFMANN, V., DING, B. C., PROIA, R. L. & DENG, C. X. 2007. Depletion of ceramides with very long chain fatty acids causes defective skin permeability barrier function, and neonatal lethality in ELOVL4 deficient mice. *Int J Biol Sci*, 3, 120-8.
- LÍSA, M., CÍFKOVÁ, E., KHALIKOVA, M., OVČAČÍKOVÁ, M. & HOLČAPEK, M. 2017. Lipidomic analysis of biological samples: Comparison of liquid chromatography, supercritical fluid chromatography and direct infusion mass spectrometry methods. *J Chromatogr A*, 1525, 96-108.
- LÍSA, M. & HOLČAPEK, M. 2015. High-Throughput and Comprehensive Lipidomic Analysis Using Ultrahigh-Performance Supercritical Fluid Chromatography–Mass Spectrometry. *Analytical Chemistry*, 87, 7187-7195.

- LIVAK, K. J. & SCHMITTGEN, T. D. 2001. Analysis of Relative Gene Expression Data Using Real-Time Quantitative PCR and the $2^{-\Delta\Delta CT}$ Method. *Methods*, 25, 402-408.
- LU, B., JIANG, Y. J., KIM, P., MOSER, A., ELIAS, P. M., GRUNFELD, C. & FEINGOLD, K. R. 2010. Expression and regulation of GPAT isoforms in cultured human keratinocytes and rodent epidermis. *J Lipid Res*, 51, 3207-16.
- MACCARRONE, M., DI RIENZO, M., BATTISTA, N., GASPERI, V., GUERRIERI, P., ROSSI, A. & FINAZZI-AGRÒ, A. 2003. The endocannabinoid system in human keratinocytes. Evidence that anandamide inhibits epidermal differentiation through CB1 receptor-dependent inhibition of protein kinase C, activation protein-1, and transglutaminase. *J Biol Chem*, 278, 33896-903.
- MACHELEIDT, O., KAISER, H. W. & SANDHOFF, K. 2002. Deficiency of epidermal protein-bound omega-hydroxyceramides in atopic dermatitis. *J Invest Dermatol*, 119, 166-73.
- MAESHIGE, N., TORII, K., TABUCHI, H., IMAI, M., KOGA, Y., UEMURA, M., AOYAMA-ISHIKAWA, M., MIYOSHI, M., FUJINO, H., TERASHI, H. & USAMI, M. 2019. Inhibitory Effects of Short-Chain Fatty Acids and ω -3 Polyunsaturated Fatty Acids on Profibrotic Factors in Dermal Fibroblasts. *Eplasty*, 19, e4.
- MARINKOVICH, M. P., KEENE, D. R., RIMBERG, C. S. & BURGESSON, R. E. 1993. Cellular origin of the dermal-epidermal basement membrane. *Dev Dyn*, 197, 255-67.
- MARJUKKA SUHONEN, T., PASONEN-SEPPÄNEN, S., KIRJAVAINEN, M., TAMMI, M., TAMMI, R. & URTTI, A. 2003. Epidermal cell culture model derived from rat keratinocytes with permeability characteristics comparable to human cadaver skin. *European Journal of Pharmaceutical Sciences*, 20, 107-113.
- MARTINEZ-MONTANES, F., LONE, M. A., HSU, F. F. & SCHNEITER, R. 2016. Accumulation of long-chain bases in yeast promotes their conversion to a long-chain base vinyl ether. *J Lipid Res*, 57, 2040-2050.
- MARZO, V. D., BIFULCO, M. & PETROCELLIS, L. D. 2004. The endocannabinoid system and its therapeutic exploitation. *Nature Reviews Drug Discovery*, 3, 771-784.
- MASUKAWA, Y., NARITA, H., SATO, H., NAOE, A., KONDO, N., SUGAI, Y., OBA, T., HOMMA, R., ISHIKAWA, J., TAKAGI, Y. & KITAHARA, T. 2009. Comprehensive quantification of ceramide species in human stratum corneum. *J Lipid Res*, 50, 1708-19.
- MASUKAWA, Y., NARITA, H., SHIMIZU, E., KONDO, N., SUGAI, Y., OBA, T., HOMMA, R., ISHIKAWA, J., TAKAGI, Y., KITAHARA, T., TAKEMA, Y. & KITA, K. 2008. Characterization of overall ceramide species in human stratum corneum. *J Lipid Res*, 49, 1466-76.
- MATOLTSY, A. G. & MATOLTSY, M. N. 1966. The membrane protein of horny cells. *The Journal of investigative dermatology*, 46, 127-129.
- MATSUI, T. & AMAGAI, M. 2015. Dissecting the formation, structure and barrier function of the stratum corneum. *Int Immunol*, 27, 269-80.

- MATSUZAKI, S., HIRATSUKA, T., TANIGUCHI, M., SHINGAKI, K., KUBO, T., KIYA, K., FUJIWARA, T., KANAZAWA, S., KANEMATSU, R., MAEDA, T., TAKAMURA, H., YAMADA, K., MIYOSHI, K., HOSOKAWA, K., TOHYAMA, M. & KATAYAMA, T. 2015. Physiological ER Stress Mediates the Differentiation of Fibroblasts. *PLoS One*, 10, e0123578.
- MATUSZEWSKI, B. K., CONSTANZER, M. L. & CHAVEZ-ENG, C. M. 2003. Strategies for the Assessment of Matrix Effect in Quantitative Bioanalytical Methods Based on HPLC-MS/MS. *Analytical Chemistry*, 75, 3019-3030.
- MCCUSKER, M. M. & GRANT-KELS, J. M. 2010. Healing fats of the skin: the structural and immunologic roles of the omega-6 and omega-3 fatty acids. *Clin Dermatol*, 28, 440-51.
- MEANEY, S. 2014. Epigenetic regulation of cholesterol homeostasis. *Front Genet*, 5, 311.
- MECKFESSEL, M. H. & BRANDT, S. 2014. The structure, function, and importance of ceramides in skin and their use as therapeutic agents in skin-care products. *J Am Acad Dermatol*, 71, 177-84.
- MEHREL, T., HOHL, D., ROTHNAGEL, J. A., LONGLEY, M. A., BUNDMAN, D., CHENG, C., LICHTI, U., BISHER, M. E., STEVEN, A. C., STEINERT, P. M., YUSPA, S. H. & ROOP, D. R. 1990. Identification of a major keratinocyte cell envelope protein, loricrin. *Cell*, 61, 1103-1112.
- MENG, X., QIU, L., SONG, H. & DANG, N. 2018. MAPK Pathway Involved in Epidermal Terminal Differentiation of Normal Human Epidermal Keratinocytes. *Open Med (Wars)*, 13, 189-195.
- MENON, G. K. 2002. New insights into skin structure: scratching the surface. *Adv Drug Deliv Rev*, 54 Suppl 1, S3-17.
- MERRILL, A. H., JR. 2011. Sphingolipid and glycosphingolipid metabolic pathways in the era of sphingolipidomics. *Chem Rev*, 111, 6387-422.
- MICHEL, C., VAN ECHTEN-DECKERT, G., ROTHER, J., SANDHOFF, K., WANG, E. & MERRILL, A. H., JR. 1997. Characterization of ceramide synthesis. A dihydroceramide desaturase introduces the 4,5-trans-double bond of sphingosine at the level of dihydroceramide. *J Biol Chem*, 272, 22432-7.
- MIZUTANI, Y., KIHARA, A., CHIBA, H., TOJO, H. & IGARASHI, Y. 2008. 2-Hydroxy-ceramide synthesis by ceramide synthase family: enzymatic basis for the preference of FA chain length. *J Lipid Res*, 49, 2356-64.
- MIZUTANI, Y., KIHARA, A. & IGARASHI, Y. 2004. Identification of the human sphingolipid C4-hydroxylase, hDES2, and its up-regulation during keratinocyte differentiation. *FEBS Lett*, 563, 93-7.
- MIZUTANI, Y., MITSUTAKE, S., TSUJI, K., KIHARA, A. & IGARASHI, Y. 2009. Ceramide biosynthesis in keratinocyte and its role in skin function. *Biochimie*, 91, 784-90.
- MOESSINGER, C., KLIZAITÉ, K., STEINHAGEN, A., PHILIPPOU-MASSIER, J., SHEVCHENKO, A., HOCH, M., EJSING, C. S. & THIELE, C. 2014. Two different pathways of phosphatidylcholine synthesis, the Kennedy Pathway and the Lands Cycle, differentially regulate cellular triacylglycerol storage. *BMC Cell Biol*, 15, 43.
- MOJUMDAR, E. H., KARIMAN, Z., VAN KERCKHOVE, L., GOORIS, G. S. & BOUWSTRA, J. A. 2014. The role of ceramide chain length distribution on

- the barrier properties of the skin lipid membranes. *Biochim Biophys Acta*, 1838, 2473-83.
- MOSMANN, T. 1983. Rapid colorimetric assay for cellular growth and survival: Application to proliferation and cytotoxicity assays. *Journal of Immunological Methods*, 65, 55-63.
- MOTTA, S., MONTI, M., SESANA, S., CAPUTO, R., CARELLI, S. & GHIDONI, R. 1993. Ceramide composition of the psoriatic scale. *Biochim Biophys Acta*, 1182, 147-51.
- MUHL, L., GENOVÉ, G., LEPTIDIS, S., LIU, J., HE, L., MOCCI, G., SUN, Y., GUSTAFSSON, S., BUYANDELGER, B., CHIVUKULA, I. V., SEGERSTOLPE, Å., RASCHPERGER, E., HANSSON, E. M., BJÖRKEGREN, J. L. M., PENG, X.-R., VANLANDEWIJCK, M., LENDAHL, U. & BETSHOLTZ, C. 2020. Single-cell analysis uncovers fibroblast heterogeneity and criteria for fibroblast and mural cell identification and discrimination. *Nature Communications*, 11, 3953.
- MULLEN, T. D., HANNUN, Y. A. & OBEID, L. M. 2012. Ceramide synthases at the centre of sphingolipid metabolism and biology. *Biochem J*, 441, 789-802.
- MULLEN, T. D., JENKINS, R. W., CLARKE, C. J., BIELAWSKI, J., HANNUN, Y. A. & OBEID, L. M. 2011. Ceramide synthase-dependent ceramide generation and programmed cell death: involvement of salvage pathway in regulating postmitochondrial events. *J Biol Chem*, 286, 15929-42.
- MURPHREY, M. B., MIAO, J. H. & ZITO, P. M. 2020. Histology, Stratum Corneum. *StatPearls*. Treasure Island (FL): StatPearls Publishing
Copyright © 2020, StatPearls Publishing LLC.
- NELSON, W. G. & SUN, T. T. 1983. The 50- and 58-kdalton keratin classes as molecular markers for stratified squamous epithelia: cell culture studies. *J Cell Biol*, 97, 244-51.
- NEWTON, V. L., GUCK, J. D., COTTER, M. A., CAMERON, N. E. & GARDINER, N. J. 2017. Neutrophils Infiltrate the Spinal Cord Parenchyma of Rats with Experimental Diabetic Neuropathy. *Journal of Diabetes Research*, 2017, 4729284.
- NICOLAOU, A., PILKINGTON, S. M. & RHODES, L. E. 2011. Ultraviolet-radiation induced skin inflammation: dissecting the role of bioactive lipids. *Chem Phys Lipids*, 164, 535-43.
- NOMURA, T., TERASHI, H., OMORI, M., SAKURAI, A., SUNAGAWA, T., HASEGAWA, M. & TAHARA, S. 2007. Lipid analysis of normal dermis and hypertrophic scars. *Wound Repair and Regeneration*, 15, 833-837.
- OHMAN, H. & VAHLQUIST, A. 1994. In vivo studies concerning a pH gradient in human stratum corneum and upper epidermis. *Acta dermato-venereologica*, 74, 375-379.
- OTHMAN, A., BIANCHI, R., ALECU, I., WEI, Y., PORRETTA-SERAPIGLIA, C., LOMBARDI, R., CHIORAZZI, A., MEREGALLI, C., OGGIONI, N., CVALETTI, G., LAURIA, G., VON ECKARDSTEIN, A. & HORNEMANN, T. 2015. Lowering plasma 1-deoxysphingolipids improves neuropathy in diabetic rats. *Diabetes*, 64, 1035-45.
- PAPPAS, A., KENDALL, A. C., BROWNBRIDGE, L. C., BATCHVAROVA, N. & NICOLAOU, A. 2018. Seasonal changes in epidermal ceramides are linked

- to impaired barrier function in acne patients. *Experimental Dermatology*, 27, 833-836.
- PAPPINEN, S., HERMANSSON, M., KUNTSCHKE, J., SOMERHARJU, P., WERTZ, P., URTTI, A. & SUHONEN, M. 2008. Comparison of rat epidermal keratinocyte organotypic culture (ROC) with intact human skin: Lipid composition and thermal phase behavior of the stratum corneum. *Biochimica et Biophysica Acta (BBA) - Biomembranes*, 1778, 824-834.
- PARK, H. Y., KIM, J. H., JUNG, M., CHUNG, C. H., HASHAM, R., PARK, C. S. & CHOI, E. H. 2011. A long-standing hyperglycaemic condition impairs skin barrier by accelerating skin ageing process. *Exp Dermatol*, 20, 969-74.
- PARK, J. W., PARK, W. J. & FUTERMAN, A. H. 2014. Ceramide synthases as potential targets for therapeutic intervention in human diseases. *Biochim Biophys Acta*, 1841, 671-81.
- PEREZ-MATOS, M. C., MORALES-ALVAREZ, M. C. & MENDIVIL, C. O. 2017. Lipids: A Suitable Therapeutic Target in Diabetic Neuropathy? *J Diabetes Res*, 2017, 6943851.
- PHINNEY, S. D. 1996. Arachidonic acid maldistribution in obesity. *Lipids*, 31 Suppl, S271-4.
- PILKINGTON, S. M., WATSON, R. E., NICOLAOU, A. & RHODES, L. E. 2011. Omega-3 polyunsaturated fatty acids: photoprotective macronutrients. *Exp Dermatol*, 20, 537-43.
- POOLMAN, T. M., GIBBS, J., WALKER, A. L., DICKSON, S., FARRELL, L., HENSMAN, J., KENDALL, A. C., MAIDSTONE, R., WARWOOD, S., LOUDON, A., RATTRAY, M., BRUCE, I. N., NICOLAOU, A. & RAY, D. W. 2019. Rheumatoid arthritis reprograms circadian output pathways. *Arthritis Research & Therapy*, 21.
- POP-BUSUI, R., BOULTON, A. J. M., FELDMAN, E. L., BRIL, V., FREEMAN, R., MALIK, R. A., SOSENKO, J. M. & ZIEGLER, D. 2017. Diabetic Neuropathy: A Position Statement by the American Diabetes Association. *Diabetes Care*, 40, 136.
- PROKSCH, E., BRANDNER, J. M. & JENSEN, J. M. 2008. The skin: an indispensable barrier. *Exp Dermatol*, 17, 1063-72.
- PRUETT, S. T., BUSHNEV, A., HAGEDORN, K., ADIGA, M., HAYNES, C. A., SULLARDS, M. C., LIOTTA, D. C. & MERRILL, A. H., JR. 2008. Biodiversity of sphingoid bases ("sphingosines") and related amino alcohols. *J Lipid Res*, 49, 1621-39.
- RADNER, F. P., MARRAKCHI, S., KIRCHMEIER, P., KIM, G. J., RIBIERRE, F., KAMOUN, B., ABID, L., LEIPOLDT, M., TURKI, H., SCHEMPP, W., HEILIG, R., LATHROP, M. & FISCHER, J. 2013. Mutations in CERS3 cause autosomal recessive congenital ichthyosis in humans. *PLoS Genet*, 9, e1003536.
- RADNER, F. P. W. & FISCHER, J. 2014. The important role of epidermal triacylglycerol metabolism for maintenance of the skin permeability barrier function. *Biochimica et Biophysica Acta (BBA) - Molecular and Cell Biology of Lipids*, 1841, 409-415.
- RAICHUR, S., WANG, S. T., CHAN, P. W., LI, Y., CHING, J., CHAURASIA, B., DOGRA, S., ÖHMAN, M. K., TAKEDA, K., SUGII, S., PEWZNER-JUNG, Y., FUTERMAN, A. H. & SUMMERS, S. A. 2014. CerS2 haploinsufficiency inhibits β -

- oxidation and confers susceptibility to diet-induced steatohepatitis and insulin resistance. *Cell Metab*, 20, 687-95.
- RICE, R. H. & GREEN, H. 1979. Presence in human epidermal cells of a soluble protein precursor of the cross-linked envelope: Activation of the cross-linking by calcium ions. *Cell*, 18, 681-694.
- RÍO, C. D., MILLÁN, E., GARCÍA, V., APPENDINO, G., DEMESA, J. & MUÑOZ, E. 2018. The endocannabinoid system of the skin. A potential approach for the treatment of skin disorders. *Biochem Pharmacol*, 157, 122-133.
- RIVIER, M., SAFONOVA, I., LEBRUN, P., GRIFFITHS, C. E., AILHAUD, G. & MICHEL, S. 1998. Differential expression of peroxisome proliferator-activated receptor subtypes during the differentiation of human keratinocytes. *J Invest Dermatol*, 111, 1116-21.
- RIVIER, M., SAFONOVA, I., MICHEL, S., CASTIEL, I. & AILHAUD, G. 2000. Peroxisome Proliferator-Activated Receptor- α Enhances Lipid Metabolism in a Skin Equivalent Model. *Journal of Investigative Dermatology*, 114, 681-687.
- ROBSON, K. J., STEWART, M. E., MICHELSEN, S., LAZO, N. D. & DOWNING, D. T. 1994. 6-Hydroxy-4-sphingenine in human epidermal ceramides. *J Lipid Res*, 35, 2060-8.
- RÖHRIG, W., WAIBEL, R., PERLWITZ, C., PISCHETSRIEDER, M. & HOCH, T. 2016. Identification of the oleic acid ethanolamide (OEA) isomer cis-vaccenic acid ethanolamide (VEA) as a highly abundant 18:1 fatty acid ethanolamide in blood plasma from rats and humans. *Analytical and Bioanalytical Chemistry*, 408, 6141-6151.
- ROTTA, L. N., DA SILVA, C. G., PERRY, M. L. & TRINDADE, V. M. 1999. Undernutrition decreases serine palmitoyltransferase activity in developing rat hypothalamus. *Ann Nutr Metab*, 43, 152-8.
- RUSSO, B., BREMBILLA, N. C. & CHIZZOLINI, C. 2020. Interplay Between Keratinocytes and Fibroblasts: A Systematic Review Providing a New Angle for Understanding Skin Fibrotic Disorders. *Front Immunol*, 11, 648.
- SAID, G. 2007. Diabetic neuropathy—a review. *Nature Clinical Practice Neurology*, 3, 331-340.
- SAKAI, S., ENDO, Y., OZAWA, N., SUGAWARA, T., KUSAKA, A., SAYO, T., TAGAMI, H. & INOUE, S. 2003. Characteristics of the epidermis and stratum corneum of hairless mice with experimentally induced diabetes mellitus. *J Invest Dermatol*, 120, 79-85.
- SAKAI, S., KIKUCHI, K., SATOH, J., TAGAMI, H. & INOUE, S. 2005. Functional properties of the stratum corneum in patients with diabetes mellitus: similarities to senile xerosis. *Br J Dermatol*, 153, 319-23.
- SANDO, G. N., HOWARD, E. J. & MADISON, K. C. 1996. Induction of ceramide glucosyltransferase activity in cultured human keratinocytes. Correlation with culture differentiation. *J Biol Chem*, 271, 22044-51.
- SCHÄFER, L. & KRAGBALLE, K. 1991. Abnormalities in Epidermal Lipid Metabolism in Patients with Atopic Dermatitis. *Journal of Investigative Dermatology*, 96, 10-15.
- SCHMIDT, M., GOEBELER, M., POSERN, G., FELLER, S. M., SEITZ, C. S., BROCKER, E. B., RAPP, U. R. & LUDWIG, S. 2000. Ras-independent activation of the

- Raf/MEK/ERK pathway upon calcium-induced differentiation of keratinocytes. *J Biol Chem*, 275, 41011-7.
- SEGRELLES, C., HOLGUÍN, A., HERNÁNDEZ, P., ARIZA, J. M., PARAMIO, J. M. & LORZ, C. 2011. Establishment of a murine epidermal cell line suitable for in vitro and in vivo skin modelling. *BMC Dermatol*, 11, 9.
- SHAKESPEARE, P. G. & STRANGE, R. E. 1982. Linoleic acid in hypertrophic scars. *Burns*, 9, 7-12.
- SHUN, C. T., CHANG, Y. C., WU, H. P., HSIEH, S. C., LIN, W. M., LIN, Y. H., TAI, T. Y. & HSIEH, S. T. 2004. Skin denervation in type 2 diabetes: correlations with diabetic duration and functional impairments. *Brain*, 127, 1593-1605.
- SIDDIQUE, M. M., LI, Y., CHAURASIA, B., KADDAI, V. A. & SUMMERS, S. A. 2015. Dihydroceramides: From Bit Players to Lead Actors. *J Biol Chem*, 290, 15371-9.
- SIGRUENER, A., TARABIN, V., PARAGH, G., LIEBISCH, G., KOEHLER, T., FARWICK, M. & SCHMITZ, G. 2013. Effects of sphingoid bases on the sphingolipidome in early keratinocyte differentiation. *Exp Dermatol*, 22, 677-9.
- SIMA, A. A. F. & SUGIMOTO, K. 1999. Experimental diabetic neuropathy: an update. *Diabetologia*, 42, 773-788.
- SINGH, S., JAJOO, S., SHUKLA, S. & ACHARYA, S. 2020. Educating patients of diabetes mellitus for diabetic foot care. *J Family Med Prim Care*, 9, 367-373.
- SKOLOVA, B., KOVACIK, A., TESAR, O., OPALKA, L. & VAVROVA, K. 2017. Phytosphingosine, sphingosine and dihydrosphingosine ceramides in model skin lipid membranes: permeability and biophysics. *Biochim Biophys Acta*, 1859, 824-834.
- SOETHOUDT, M., GREYER, U., FINGERLE, J., GRIM, T. W., FEZZA, F., DE PETROCELLIS, L., ULLMER, C., ROTHENHÄUSLER, B., PERRET, C., VAN GILS, N., FINLAY, D., MACDONALD, C., CHICCA, A., GENS, M. D., STUART, J., DE VRIES, H., MASTRANGELO, N., XIA, L., ALACHOUZOS, G., BAGGELAAR, M. P., MARTELLA, A., MOCK, E. D., DENG, H., HEITMAN, L. H., CONNOR, M., DI MARZO, V., GERTSCH, J., LICHTMAN, A. H., MACCARRONE, M., PACHER, P., GLASS, M. & VAN DER STELT, M. 2017. Cannabinoid CB2 receptor ligand profiling reveals biased signalling and off-target activity. *Nature Communications*, 8, 13958.
- SOKOLOWSKA, E. & BLACHNIO-ZABIELSKA, A. 2019. The Role of Ceramides in Insulin Resistance. *Frontiers in Endocrinology*, 10.
- SORRELL, J. M., BABER, M. A. & CAPLAN, A. I. 2004. Site-matched papillary and reticular human dermal fibroblasts differ in their release of specific growth factors/cytokines and in their interaction with keratinocytes. *Journal of Cellular Physiology*, 200, 134-145.
- SORRELL, J. M., BABER, M. A. & CAPLAN, A. I. 2007. Clonal characterization of fibroblasts in the superficial layer of the adult human dermis. *Cell and Tissue Research*, 327, 499-510.
- SORRELL, J. M. & CAPLAN, A. I. 2004. Fibroblast heterogeneity: more than skin deep. *Journal of Cell Science*, 117, 667-675.

- STÄNDER, S., SCHMELZ, M., METZE, D., LUGER, T. & RUKWIED, R. 2005. Distribution of cannabinoid receptor 1 (CB1) and 2 (CB2) on sensory nerve fibers and adnexal structures in human skin. *J Dermatol Sci*, 38, 177-88.
- STITH, J. L., VELAZQUEZ, F. N. & OBEID, L. M. 2019. Advances in determining signaling mechanisms of ceramide and role in disease. *J Lipid Res*, 60, 913-918.
- SUN, T. T. & GREEN, H. 1976. Differentiation of the epidermal keratinocyte in cell culture: formation of the cornified envelope. *Cell*, 9, 511-21.
- SUZUKI, J., AKAHANE, K., NAKAMURA, J., NARUSE, K., KAMIYA, H., HIMENO, T., NAKAMURA, N., SHIBATA, T., KONDO, M., NAGASAKI, H., FUJIYA, A., OISO, Y. & HAMADA, Y. 2011. Palmitate induces apoptosis in Schwann cells via both ceramide-dependent and independent pathways. *Neuroscience*, 176, 188-98.
- T'KINDT, R., JORGE, L., DUMONT, E., COUTURON, P., DAVID, F., SANDRA, P. & SANDRA, K. 2012. Profiling and characterizing skin ceramides using reversed-phase liquid chromatography-quadrupole time-of-flight mass spectrometry. *Anal Chem*, 84, 403-11.
- TAKAHASHI, H., HONMA, M., ISHIDA-YAMAMOTO, A., NAMIKAWA, K., KIYAMA, H. & IIZUKA, H. 2001. Expression of human cystatin A by keratinocytes is positively regulated via the Ras/MEKK1/MKK7/JNK signal transduction pathway but negatively regulated via the Ras/Raf-1/MEK1/ERK pathway. *J Biol Chem*, 276, 36632-8.
- TAKEDA, S., SHIMODA, H., TAKARADA, T. & IMOKAWA, G. 2018. Strawberry seed extract and its major component, tiliroside, promote ceramide synthesis in the stratum corneum of human epidermal equivalents. *PLoS One*, 13, e0205061.
- TAKEDA, Y., HARADA, Y., YOSHIKAWA, T. & DAI, P. 2017. Direct conversion of human fibroblasts to brown adipocytes by small chemical compounds. *Scientific Reports*, 7, 4304.
- TANNO, O., OTA, Y., KITAMURA, N., KATSUBE, T. & INOUE, S. 2000. Nicotinamide increases biosynthesis of ceramides as well as other stratum corneum lipids to improve the epidermal permeability barrier. *Br J Dermatol*, 143, 524-31.
- TERNES, P., FRANKE, S., ZHRINGER, U., SPERLING, P. & HEINZ, E. 2002. Identification and characterization of a sphingolipid delta 4-desaturase family. *J Biol Chem*, 277, 25512-8.
- TOBIN, D. J. 2017. Introduction to skin aging. *Journal of Tissue Viability*, 26, 37-46.
- TÓTH, K. F., ÁDÁM, D., BÍRÓ, T. & OLÁH, A. 2019. Cannabinoid Signaling in the Skin: Therapeutic Potential of the "C(ut)annabinoid" System. *Molecules*, 24.
- TRAN, S. L., PUHAR, A., NGO-CAMUS, M. & RAMARAO, N. 2011. Trypan blue dye enters viable cells incubated with the pore-forming toxin HlyII of *Bacillus cereus*. *PLoS One*, 6, e22876.
- UCHIDA, Y. 2014. Ceramide signaling in mammalian epidermis. *Biochim Biophys Acta*, 1841, 453-62.

- UCHIDA, Y., HARA, M., NISHIO, H., SIDRANSKY, E., INOUE, S., OTSUKA, F., SUZUKI, A., ELIAS, P. M., HOLLERAN, W. M. & HAMANAKA, S. 2000. Epidermal sphingomyelins are precursors for selected stratum corneum ceramides. *J Lipid Res*, 41, 2071-82.
- UCHIDA, Y., IWAMORI, M. & NAGAI, Y. 1988. Distinct differences in lipid composition between epidermis and dermis from footpad and dorsal skin of guinea pigs. *Jpn J Exp Med*, 58, 153-61.
- UCHIDA, Y., NARDO, A. D., COLLINS, V., ELIAS, P. M. & HOLLERAN, W. M. 2003. De novo ceramide synthesis participates in the ultraviolet B irradiation-induced apoptosis in undifferentiated cultured human keratinocytes. *J Invest Dermatol*, 120, 662-9.
- USSHER, J. R., KOVES, T. R., CADETE, V. J., ZHANG, L., JASWAL, J. S., SWYRD, S. J., LOPASCHUK, D. G., PROCTOR, S. D., KEUNG, W., MUOIO, D. M. & LOPASCHUK, G. D. 2010. Inhibition of de novo ceramide synthesis reverses diet-induced insulin resistance and enhances whole-body oxygen consumption. *Diabetes*, 59, 2453-64.
- VALASEK, M. A. & REPA, J. J. 2005. The power of real-time PCR. *Advances in Physiology Education*, 29, 151-159.
- VAN BLITTERSWIJK, W. J., VAN DER LUIT, A. H., VELDMAN, R. J., VERHEIJ, M. & BORST, J. 2003. Ceramide: second messenger or modulator of membrane structure and dynamics? *Biochem J*, 369, 199-211.
- VAN DER VEEN, J. N., KENNELLY, J. P., WAN, S., VANCE, J. E., VANCE, D. E. & JACOBS, R. L. 2017. The critical role of phosphatidylcholine and phosphatidylethanolamine metabolism in health and disease. *Biochim Biophys Acta Biomembr*, 1859, 1558-1572.
- VAN SMEDEN, J., HOPPEL, L., VAN DER HEIJDEN, R., HANKEMEIER, T., VREEKEN, R. J. & BOUWSTRA, J. A. 2011. LC/MS analysis of stratum corneum lipids: ceramide profiling and discovery. *J Lipid Res*, 52, 1211-21.
- VAN SMEDEN, J., JANSSENS, M., BOITEN, W. A., VAN DRONGELEN, V., FURIO, L., VREEKEN, R. J., HOVNANIAN, A. & BOUWSTRA, J. A. 2014. Intercellular skin barrier lipid composition and organization in Netherton syndrome patients. *J Invest Dermatol*, 134, 1238-45.
- VÉRET, J., COANT, N., BERDYSHEV, E. V., SKOBELEVA, A., THERVILLE, N., BAILBÉ, D., GORSHKOVA, I., NATARAJAN, V., PORTHA, B. & LE STUNFF, H. 2011. Ceramide synthase 4 and de novo production of ceramides with specific N-acyl chain lengths are involved in glucolipotoxicity-induced apoptosis of INS-1 β -cells. *Biochem J*, 438, 177-89.
- VETTOR, R. & PAGANO, C. 2009. The role of the endocannabinoid system in lipogenesis and fatty acid metabolism. *Best Practice & Research Clinical Endocrinology & Metabolism*, 23, 51-63.
- VOLMER-THOLE, M. & LOBMANN, R. 2016. Neuropathy and Diabetic Foot Syndrome. *Int J Mol Sci*, 17.
- WALLMEYER, L., LEHNEN, D., EGER, N., SOCHOROVÁ, M., OPÁLKA, L., KOVÁČIK, A., VÁVROVÁ, K. & HEDTRICH, S. 2015. Stimulation of PPAR α normalizes the skin lipid ratio and improves the skin barrier of normal and filaggrin deficient reconstructed skin. *J Dermatol Sci*, 80, 102-10.

- WANG, E., NORRED, W. P., BACON, C. W., RILEY, R. T. & MERRILL, A. H., JR. 1991. Inhibition of sphingolipid biosynthesis by fumonisins. Implications for diseases associated with *Fusarium moniliforme*. *J Biol Chem*, 266, 14486-90.
- WEERHEIM, A. & PONEC, M. 2001. Determination of stratum corneum lipid profile by tape stripping in combination with high-performance thin-layer chromatography. *Archives of Dermatological Research*, 293, 191-199.
- WEGNER, M. S., SCHIFFMANN, S., PARNHAM, M. J., GEISLINGER, G. & GROSCH, S. 2016. The enigma of ceramide synthase regulation in mammalian cells. *Prog Lipid Res*, 63, 93-119.
- WERTHEIMER, E., TREBICZ, M., ELGAR, T., GARTSBEIN, M., NOFEH-MOSES, S. & TENNENBAUM, T. 2000. Differential roles of insulin receptor and insulin-like growth factor-1 receptor in differentiation of murine skin keratinocytes. *J Invest Dermatol*, 115, 24-9.
- WERTZ, P. W. 1992. Epidermal lipids. *Semin Dermatol*, 11, 106-13.
- WERTZ, P. W., CHO, E. S. & DOWNING, D. T. 1983. Effect of essential fatty acid deficiency on the epidermal sphingolipids of the rat. *Biochimica et Biophysica Acta (BBA) - Lipids and Lipid Metabolism*, 753, 350-355.
- WERTZ, P. W. & VAN DEN BERGH, B. 1998. The physical, chemical and functional properties of lipids in the skin and other biological barriers. *Chem Phys Lipids*, 91, 85-96.
- WIGGER, L., CRUCIANI-GUGLIEMACCI, C., NICOLAS, A., DENOM, J., FERNANDEZ, N., FUMERON, F., MARQUES-VIDAL, P., KTORZA, A., KRAMER, W., SCHULTE, A., LE STUNFF, H., LIECHTI, R., XENARIOS, I., VOLLENWEIDER, P., WAEBER, G., UPHUES, I., ROUSSEL, R., MAGNAN, C., IBERSON, M. & THORENS, B. 2017. Plasma Dihydroceramides Are Diabetes Susceptibility Biomarker Candidates in Mice and Humans. *Cell Reports*, 18, 2269-2279.
- WIJESINGHE, D. S., WARNCKE, U. O. & DIEGELMANN, R. F. 2016. Human as the Ultimate Wound Healing Model: Strategies for Studies Investigating the Dermal Lipidome. *Curr Dermatol Rep*, 5, 244-251.
- WIKRAMANAYAKE, T. C., STOJADINOVIC, O. & TOMIC-CANIC, M. 2014. Epidermal Differentiation in Barrier Maintenance and Wound Healing. *Adv Wound Care (New Rochelle)*, 3, 272-280.
- WILLIAMS, R., KARURANGA, S., MALANDA, B., SAEEDI, P., BASIT, A., BESANÇON, S., BOMMER, C., ESTEGHAMATI, A., OGURTSOVA, K., ZHANG, P. & COLAGIURI, S. 2020. Global and regional estimates and projections of diabetes-related health expenditure: Results from the International Diabetes Federation Diabetes Atlas, 9th edition. *Diabetes Res Clin Pract*, 162, 108072.
- WOODLEY, D. T. 2017. Distinct Fibroblasts in the Papillary and Reticular Dermis: Implications for Wound Healing. *Dermatologic Clinics*, 35, 95-100.
- YAMAGUCHI, Y., HEARING, V. J., ITAMI, S., YOSHIKAWA, K. & KATAYAMA, I. 2005. Mesenchymal-epithelial interactions in the skin: aiming for site-specific tissue regeneration. *J Dermatol Sci*, 40, 1-9.
- YAMAMURA, T. & TEZUKA, T. 1990. Change in sphingomyelinase activity in human epidermis during aging. *J Dermatol Sci*, 1, 79-83.

- YARD, B. A., CARTER, L. G., JOHNSON, K. A., OVERTON, I. M., DORWARD, M., LIU, H., MCMAHON, S. A., OKE, M., PUECH, D., BARTON, G. J., NAISMITH, J. H. & CAMPOPIANO, D. J. 2007. The structure of serine palmitoyltransferase; gateway to sphingolipid biosynthesis. *J Mol Biol*, 370, 870-86.
- YARIBEYGI, H., BO, S., RUSCICA, M. & SAHEBKAR, A. 2020. Ceramides and diabetes mellitus: an update on the potential molecular relationships. *Diabetic Medicine*, 37, 11-19.
- YOON, J. S., NISHIFUJI, K. & IWASAKI, T. 2020. Supplementation with eicosapentaenoic acid and linoleic acid increases the production of epidermal ceramides in in vitro canine keratinocytes. *Vet Dermatol*.
- YUSPA, S. H., KILKENNY, A. E., STEINERT, P. M. & ROOP, D. R. 1989. Expression of murine epidermal differentiation markers is tightly regulated by restricted extracellular calcium concentrations in vitro. *J Cell Biol*, 109, 1207-17.
- ZABIELSKI, P., BLACHNIO-ZABIELSKA, A., LANZA, I. R., GOPALA, S., MANJUNATHA, S., JAKAITIS, D. R., PERSSON, X.-M., GRANSEE, J., KLAUS, K. A., SCHIMKE, J. M., JENSEN, M. D. & NAIR, K. S. 2014. Impact of insulin deprivation and treatment on sphingolipid distribution in different muscle subcellular compartments of streptozotocin-diabetic C57Bl/6 mice. *American Journal of Physiology-Endocrinology and Metabolism*, 306, E529-E542.
- ZAINUDDIN, A., MAKPOL, S., CHUA, K. H., ABDUL RAHIM, N., YUSOF, Y. A. M. & NGAH, W. Z. W. 2008. GAPDH as housekeeping gene for human skin fibroblast senescent model. *The Medical journal of Malaysia*, 63 Suppl A, 73-74.
- ZHANG, Y., RANTA, F., TANG, C., SHUMILINA, E., MAHMUD, H., FÖLLER, M., ULLRICH, S., HÄRING, H.-U. & LANG, F. 2009. Sphingomyelinase dependent apoptosis following treatment of pancreatic beta-cells with amyloid peptides A β 1-42 or IAPP. *Apoptosis*, 14, 878-889.
- ZHANG, Y., WANG, Y., YANNI, J., QURESHI, M. A., LOGANTHA, S. J. R. J., KASSAB, S., BOYETT, M. R., GARDINER, N. J., SUN, H., HOWARTH, F. C. & DOBRZYNSKI, H. 2019. Electrical Conduction System Remodeling in Streptozotocin-Induced Diabetes Mellitus Rat Heart. *Frontiers in Physiology*, 10.
- ZHEREBITSKAYA, E., SCHAPANESKY, J., AKUDE, E., SMITH, D. R., VAN DER PLOEG, R., SOLOVYOVA, N., VERKHRATSKY, A. & FERNYHOUGH, P. 2012. Sensory neurons derived from diabetic rats have diminished internal Ca²⁺ stores linked to impaired re-uptake by the endoplasmic reticulum. *ASN Neuro*, 4.
- ZUO, Y., ZHUANG, D. Z., HAN, R., ISAAC, G., TOBIN, J. J., MCKEE, M., WELTI, R., BRISSETTE, J. L., FITZGERALD, M. L. & FREEMAN, M. W. 2008. ABCA12 maintains the epidermal lipid permeability barrier by facilitating formation of ceramide linoleic esters. *J Biol Chem*, 283, 36624-35.

Appendices

Appendix 1

Sample #	cDNA concentration (μl)	Reaction Volume (μl)	cDNA (μl)	TaqMan (μl)	Primer (μl)	Water (μl)	GAPDH Ct	CERS4 Ct
33- 1a	20	20	2	10	1	5	18.92	29.79
33- 1b	20	10	1	5	0.5	2.5	19.70	30.62
33- 2a	200	20	4	10	1	5	21.28	32.11
33- 2b	200	10	2	5	0.5	2.5	21.42	32.27
34- 1a	20	20	2	10	1	5	19.04	30.07
34- 1b	20	10	1	5	0.5	2.5	19.81	30.70
34- 2a	200	20	4	10	1	5	21.37	32.19
34- 2b	200	10	2	5	0.5	2.5	21.32	32.24

Table A 1.1 Determination of cDNA concentration and reaction volume. The concentration of cDNA samples and the reaction volume of the RT-qPCR reaction were optimized. NHEK samples from two individual donors were cultured in duplicates and RNA was extracted. RNA samples were converted to cDNA (20 μl), then one cDNA from each donor was diluted to give a final volume of 200 μl. RT-qPCR using both cDNA concentrations was performed using two final reaction volumes (20 μl and 10 μl). Diluting cDNA and working with a reaction volume of 10 μl did not affect the Ct of housekeeping gene, GAPDH, and test gene, CERS4 when compared to 20 μl reaction volume.

Appendix 2

Several experiments were designed and carried out to test ceramide extraction protocols from human plasma and skin cells and to choose the best ceramide UPLC/ESI-MS/MS method parameters. This would allow the identification of the most reliable protocol for optimum lipid extraction and internal standards (IS) recovery from human plasma and primary skin cells. Process efficiency (PE) was assessed following (Matuszewski et al., 2003) study, where $PE(\%) = C/A \times 100$. A: IS dried then reconstituted in acidified methanol; C= Sample spiked with IS before the extraction.

Experiment 1: Process efficiency (%) was calculated for three methods tested using different extraction solvents: chloroform/methanol (CHCl₃/CH₃OH) and isopropanol: water: ethyl acetate (30:10:60 (v/v/v)) using 3 types of matrices (deionized water, HaCaT keratinocytes and human plasma). After choosing the best

solvents, our laboratory further assessed PE, matrix effect (ME) and recovery (RE) and modified plasma and skin ceramide extraction assays. $ME(\%) = B/A \times 100$; $RE(\%) = C/B \times 100$. A: IS dried then reconstituted in acidified methanol; B: Sample spiked with IS after the extraction; C= Sample spiked with IS before the extraction.

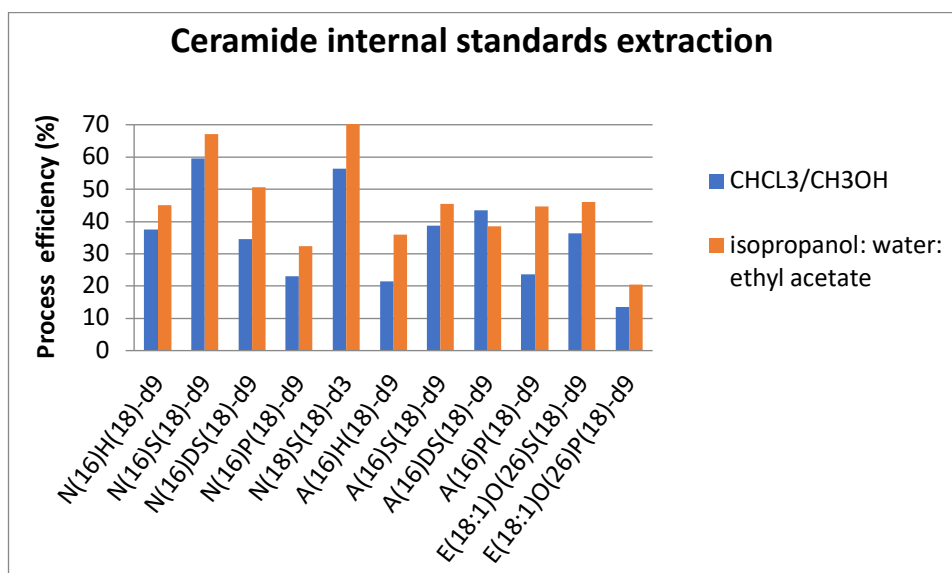
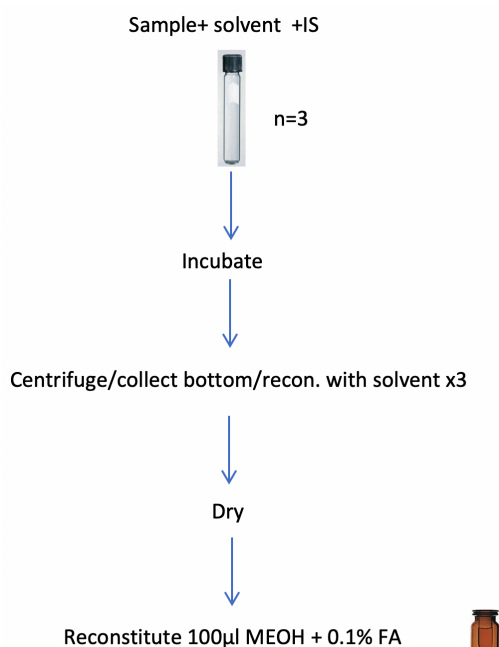


Figure A 2.1 Experiment 1-a. Internal standards extraction from deionized water where there is minimum matrix effect, using two extraction solvents: CHCL₃/CH₃OH or isopropanol: water: ethyl acetate. Both solvents showed good process efficiency when there is minimum matrix effect as the sample here was deionized water.

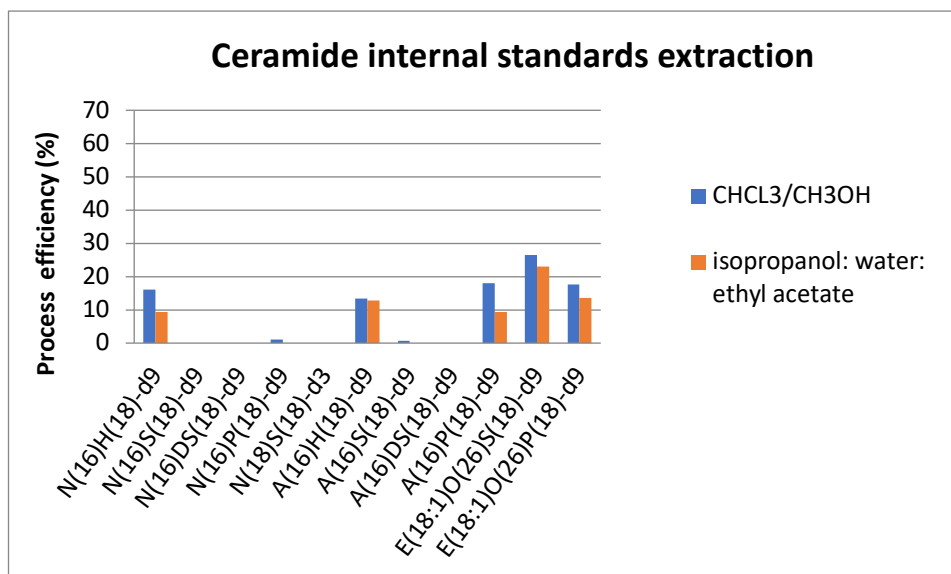


Figure A 2.2 Experiment 1-b. The figure summarizes the process efficiency for the same extraction method as above using HaCaT keratinocyte samples (n=3). When using HaCaT keratinocytes, CHCL₃/CH₃OH recovery was better than isopropanol: water: ethyl acetate.

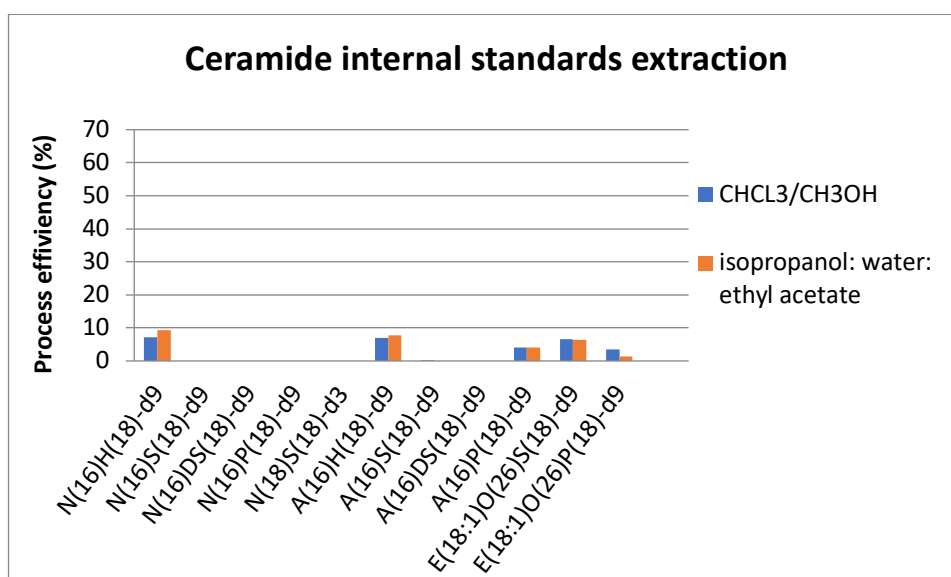


Figure A 2.3 Experiment 1-c. The figure summarizes the process efficiency for the same extraction method as above using human plasma samples. Plasma also showed less recovery for the internal standards extracted using the two solvents.

Experiment 2: As CHCL₃/CH₃OH showed better PE(%), the effect of using acidified CHCL₃/CH₃OH as an extraction solvent on the recovery of the internal standards was examined and compared with the results to those from using only CHCL₃/CH₃OH. Deionised water was used as the sample.

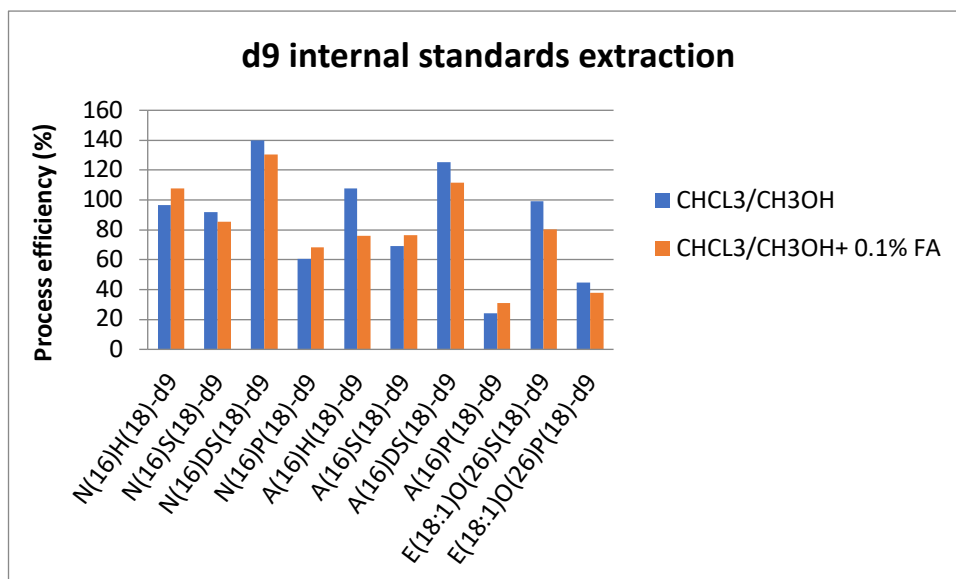


Figure A 2.4 Experiment 2. Process efficiency percentage for internal standards extraction from deionized water using CHCL₃/CH₃OH or CHCL₃/CH₃OH + 0.1% formic acid. Dried samples were reconstituted in methanol + 0.1% formic acid. CHCL₃/CH₃OH was found to be a more efficient extracting solvent than acidified CHCL₃/CH₃OH.

Since the type of sample had an effect on the recovery of internal standards, additional experiments were designed to examine matrix effect and develop a method using the solvent of choice (CHCL₃/CH₃OH) that would recover all internal standards. For these experiments human pooled plasma and HDF samples were used to test matrix effect on the internal standards recovery. Further developments to the extraction protocol were then made by members of our laboratory team.

Experiment 3: Optimising collision energy (CE) and capillary voltage (CV). Samples run in duplicates and peak area averaged.

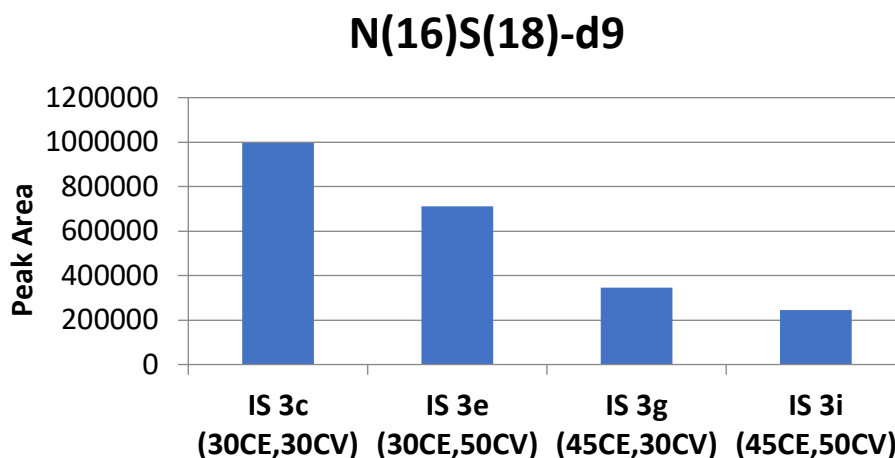


Figure A 2.8 Experiment 3-a. Using transition 547.576>264.4

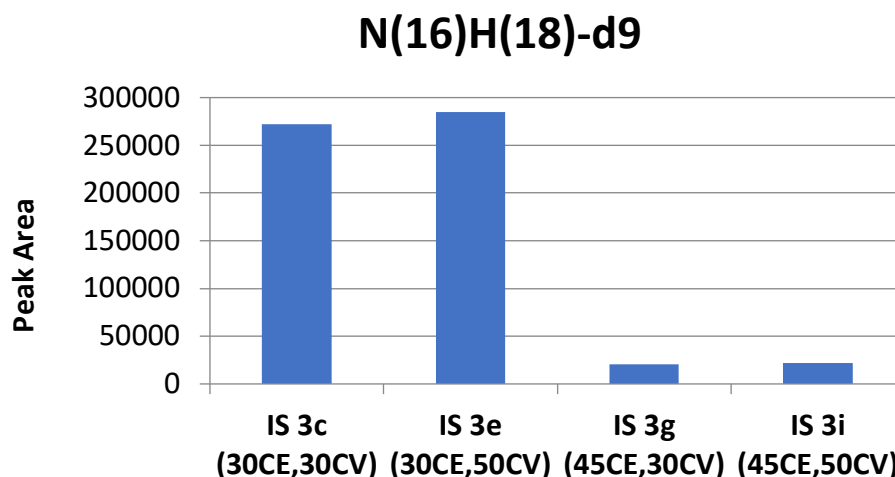


Figure A 2.9 Experiment 3-b. Using transition 545.615>280.4

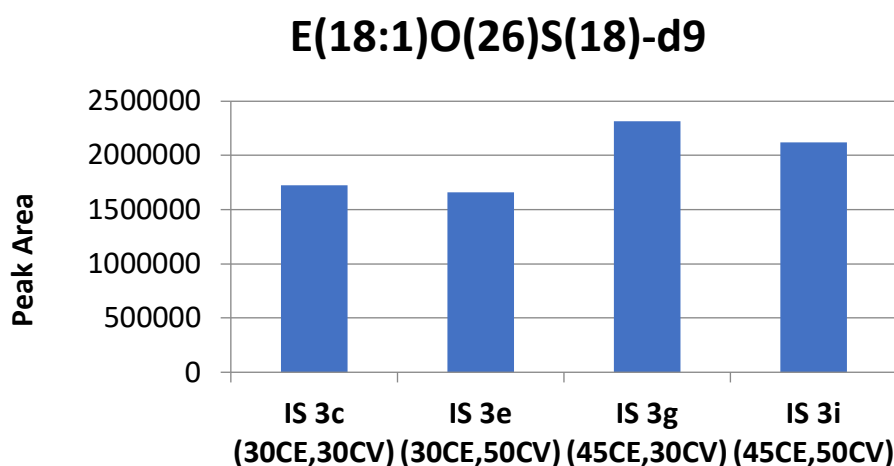


Figure A 2.10 Experiment 3-c. Using transition 967.973>264.4

Appendix 3

Table A 3.1 MRM transitions and retention times used for the ceramide assay. Ceramides were analysed using LC-MS/MS. MRM: multiple reaction monitoring; NDS: non-hydroxy dihydroceramide; NS: non-hydroxy ceramide; NP: non-hydroxy phytoceramide; NH: non-hydroxy 6-hydroxyceramide; AS: alpha-hydroxy ceramide; AP: alpha-hydroxy phytoceramide; AH: alpha-hydroxy 6-hydroxyceramide; EODS: ester-linked omega-hydroxy dihydroceramide; EOS: ester-linked omega-hydroxy ceramide; EOP: ester-linked omega-hydroxy phytoceramide; EOH: ester-linked omega-hydroxy 6-hydroxyceramide.

Compound	Precursor Ion	Product Ion	Retention Time (min)
N(16)DS(18)-d9	549.592	284.4	10.96
N(24)DS(16)	624.629	256.4	12
N(25)DS(16)	638.645	256.4	12.26
N(26)DS(16)	652.661	256.4	12.48
N(22)DS(17)	610.614	270.4	11.79
N(23)DS(17)	624.629	270.4	12.02
N(24)DS(17)	638.645	270.4	12.27
N(25)DS(17)	652.661	270.4	12.55
N(26)DS(17)	666.676	270.4	12.71
N(27)DS(17)	680.692	270.4	13.1
N(28)DS(17)	694.708	270.4	13.44
N(14)DS(18)	512.504	284.4	10.72
N(15)DS(18)	526.520	284.4	10.84
N(16)DS(18)	540.536	284.4	10.96
N(17)DS(18)	554.551	284.4	11.1
N(18)DS(18)	568.567	284.4	11.25
N(19)DS(18)	582.583	284.4	11.41
N(20)DS(18)	596.598	284.4	11.57
N(22)DS(18)	624.629	284.4	11.99
N(23)DS(18)	638.645	284.4	12.24
N(24)DS(18)	652.661	284.4	12.47
N(25)DS(18)	666.676	284.4	12.76
N(26)DS(18)	680.692	284.4	13.05
N(27)DS(18)	694.708	284.4	13.37
N(28)DS(18)	708.723	284.4	13.7
N(14)DS(19)	526.520	298.4	10.84
N(15)DS(19)	540.536	298.4	10.94
N(16)DS(19)	554.551	298.4	11.1
N(18)DS(19)	582.583	298.4	11.41
N(20)DS(19)	610.614	298.4	11.75
N(21)DS(19)	624.629	298.4	11.98
N(22)DS(19)	638.645	298.4	12.2
N(23)DS(19)	652.661	298.4	12.45
N(24)DS(19)	666.676	298.4	12.72
N(25)DS(19)	680.692	298.4	13.07
N(26)DS(19)	694.708	298.4	13.31
N(28)DS(19)	722.739	298.4	(Expected ~14.00)
N(14)DS(20)	540.536	312.4	10.99
N(15)DS(20)	554.551	312.4	11.11
N(16)DS(20)	568.567	312.4	11.24
N(17)DS(20)	582.583	312.4	11.42
N(18)DS(20)	596.598	312.4	11.6

N(19)DS(20)	610.614	312.4	11.77
N(20)DS(20)	624.629	312.4	11.98
N(21)DS(20)	638.645	312.4	12.19
N(22)DS(20)	652.661	312.4	12.45
N(23)DS(20)	666.676	312.4	12.71
N(24)DS(20)	680.692	312.4	12.99
N(25)DS(20)	694.708	312.4	13.31
N(26)DS(20)	708.723	312.4	13.65
N(27)DS(20)	722.739	312.4	(Expected ~14.02)
N(28)DS(20)	736.755	312.4	14.33
N(29)DS(20)	750.770	312.4	(Expected ~14.63)
N(30)DS(20)	764.786	312.4	(Expected ~14.90)
N(18)DS(21)	610.614	326.4	11.77
N(20)DS(21)	638.645	326.4	12.17
N(21)DS(21)	652.661	326.4	12.46
N(22)DS(21)	666.676	326.4	12.7
N(23)DS(21)	680.692	326.4	12.98
N(24)DS(21)	694.708	326.4	13.29
N(25)DS(21)	708.723	326.4	13.65
N(26)DS(21)	722.739	326.4	13.97
N(28)DS(21)	750.770	326.4	(Expected ~14.60)
N(30)DS(21)	778.802	326.4	(Expected ~15.40)
N(15)DS(22)	582.583	340.4	11.42
N(16)DS(22)	596.598	340.4	11.6
N(17)DS(22)	610.614	340.4	11.8
N(18)DS(22)	624.629	340.4	11.98
N(19)DS(22)	638.645	340.4	12.18
N(20)DS(22)	652.661	340.4	12.45
N(21)DS(22)	666.676	340.4	12.66
N(22)DS(22)	680.692	340.4	12.98
N(23)DS(22)	694.708	340.4	13.3
N(24)DS(22)	708.723	340.4	13.62
N(25)DS(22)	722.739	340.4	(Expected ~13.95)
N(26)DS(22)	736.755	340.4	(Expected ~14.27)
N(15)DS(23)	596.598	354.4	11.61
N(16)DS(23)	610.614	354.4	11.79
N(18)DS(23)	638.645	354.4	12.21
N(20)DS(23)	666.676	354.4	12.69
N(22)DS(23)	694.708	354.4	13.29
N(14)DS(24)	596.598	368.4	11.63

N(15)DS(24)	610.614	368.4	11.8
N(16)DS(24)	624.629	368.4	12.01
N(17)DS(24)	638.645	368.4	12.25
N(18)DS(24)	652.661	368.4	12.46
N(19)DS(24)	666.676	368.4	12.73
N(20)DS(24)	680.692	368.4	13.01
N(21)DS(24)	694.708	368.4	13.27
N(22)DS(24)	708.723	368.4	13.59
N(23)DS(24)	722.739	368.4	13.92
N(24)DS(24)	736.755	368.4	14.3
N(25)DS(24)	750.770	368.4	14.71
N(16)DS(26)	652.661	396.4	12.49
N(18)DS(26)	680.692	396.4	13.01
N(20)DS(26)	708.723	396.4	13.63
N(16)S(18)-d9	529.566	264.4	10.88
N(14)S(16)	482.457	236.4	10.44
N(15)S(16)	496.473	236.4	10.54
N(16)S(16)	510.489	236.4	10.64
N(17)S(16)	524.504	236.4	10.79
N(18)S(16)	538.520	236.4	10.91
N(19)S(16)	552.536	236.4	11.03
N(20)S(16)	566.551	236.4	11.2
N(21)S(16)	580.567	236.4	11.35
N(22)S(16)	594.583	236.4	11.53
N(23)S(16)	608.598	236.4	11.75
N(24)S(16)	622.614	236.4	11.94
N(25)S(16)	636.629	236.4	12.18
N(26)S(16)	650.645	236.4	12.43
N(27)S(16)	664.661	236.4	12.7
N(28)S(16)	678.676	236.4	12.99
N(29)S(16)	692.692	236.4	13.3
N(30)S(16)	706.708	236.4	13.64
N(14)S(17)	496.473	250.4	10.56
N(15)S(17)	510.489	250.4	10.63
N(16)S(17)	524.504	250.4	10.76
N(17)S(17)	538.520	250.4	10.88
N(18)S(17)	552.536	250.4	11.03
N(19)S(17)	566.551	250.4	11.18
N(20)S(17)	580.567	250.4	11.34
N(21)S(17)	594.583	250.4	11.51
N(22)S(17)	608.598	250.4	11.72
N(23)S(17)	622.614	250.4	11.91
N(24)S(17)	636.629	250.4	12.13
N(25)S(17)	650.645	250.4	12.39

N(26)S(17)	664.661	250.4	12.67
N(27)S(17)	678.676	250.4	12.93
N(28)S(17)	692.692	250.4	13.24
N(29)S(17)	706.708	250.4	13.57
N(30)S(17)	720.723	250.4	13.94
N(14)S(18)	510.489	264.4	10.63
N(15)S(18)	524.504	264.4	10.76
N(16)S(18)	538.520	264.4	10.88
N(17)S(18)	552.536	264.4	11.02
N(18)S(18)	566.551	264.4	11.15
N(19)S(18)	580.567	264.4	11.31
N(20)S(18)	594.583	264.4	11.5
N(21)S(18)	608.598	264.4	11.68
N(22)S(18)	622.614	264.4	11.9
N(23)S(18)	636.629	264.4	12.11
N(24)S(18)	650.645	264.4	12.36
N(25)S(18)	664.661	264.4	12.61
N(26)S(18)	678.676	264.4	12.91
N(27)S(18)	692.692	264.4	13.19
N(28)S(18)	706.708	264.4	13.53
N(29)S(18)	720.723	264.4	13.88
N(14)S(19)	524.504	278.4	10.78
N(15)S(19)	538.520	278.4	10.9
N(16)S(19)	552.536	278.4	11
N(17)S(19)	566.551	278.4	11.16
N(18)S(19)	580.567	278.4	11.3
N(19)S(19)	594.583	278.4	11.49
N(20)S(19)	608.598	278.4	11.68
N(21)S(19)	622.614	278.4	11.84
N(22)S(19)	636.629	278.4	12.06
N(23)S(19)	650.645	278.4	12.32
N(24)S(19)	664.661	278.4	12.57
N(25)S(19)	678.676	278.4	12.86
N(26)S(19)	692.692	278.4	13.19
N(27)S(19)	706.708	278.4	13.48
N(28)S(19)	720.723	278.4	13.86
N(30)S(19)	748.755	278.4	14.6
N(14)S(20)	538.520	292.4	10.9
N(15)S(20)	552.536	292.4	11.01
N(16)S(20)	566.551	292.4	11.15
N(17)S(20)	580.567	292.4	11.3
N(18)S(20)	594.583	292.4	11.48
N(19)S(20)	608.598	292.4	11.68
N(20)S(20)	622.614	292.4	11.85
N(21)S(20)	636.629	292.4	12.04

N(22)S(20)	650.645	292.4	12.29
N(23)S(20)	664.661	292.4	12.57
N(24)S(20)	678.676	292.4	12.82
N(25)S(20)	692.692	292.4	13.15
N(26)S(20)	706.708	292.4	13.44
N(27)S(20)	720.723	292.4	13.8
N(28)S(20)	734.739	292.4	14.14
N(29)S(20)	748.755	292.4	14.53
N(30)S(20)	762.770	292.4	14.95
N(14)S(21)	552.536	306.4	11.03
N(15)S(21)	566.551	306.4	11.17
N(16)S(21)	580.567	306.4	11.3
N(18)S(21)	608.598	306.4	11.61
N(20)S(21)	636.629	306.4	12.01
N(21)S(21)	650.645	306.4	12.27
N(22)S(21)	664.661	306.4	12.5
N(23)S(21)	678.676	306.4	12.79
N(24)S(21)	692.692	306.4	13.12
N(25)S(21)	706.708	306.4	13.44
N(26)S(21)	720.723	306.4	13.78
N(27)S(21)	734.739	306.4	14.1
N(28)S(21)	748.755	306.4	14.48
N(30)S(21)	776.786	306.4	-
N(14)S(22)	566.551	320.4	11.19
N(15)S(22)	580.567	320.4	11.32
N(16)S(22)	594.583	320.4	11.5
N(17)S(22)	608.598	320.4	11.6
N(18)S(22)	622.614	320.4	11.85
N(19)S(22)	636.629	320.4	12.07
N(20)S(22)	650.645	320.4	12.29
N(21)S(22)	664.661	320.4	12.51
N(22)S(22)	678.676	320.4	12.81
N(23)S(22)	692.692	320.4	13.11
N(24)S(22)	706.708	320.4	13.4
N(25)S(22)	720.723	320.4	13.76
N(26)S(22)	734.739	320.4	14.08
N(27)S(22)	748.755	320.4	14.46
N(28)S(22)	762.770	320.4	14.86
N(29)S(22)	776.786	320.4	15.3
N(18)S(23)	636.629	334.4	12.09
N(19)S(23)	650.645	334.4	12.31
N(20)S(23)	664.661	334.4	12.57
N(24)S(23)	720.723	334.4	13.77
N(25)S(23)	734.739	334.4	14.11
N(26)S(23)	748.755	334.4	14.5

N(17)S(24)	636.629	348.4	12.13
N(18)S(24)	650.645	348.4	12.33
N(19)S(24)	664.661	348.4	12.56
N(20)S(24)	678.676	348.4	12.81
N(21)S(24)	692.692	348.4	13.08
N(22)S(24)	706.708	348.4	13.43
N(23)S(24)	720.723	348.4	13.75
N(24)S(24)	734.739	348.4	14.1
N(25)S(24)	748.755	348.4	14.5
N(26)S(24)	762.770	348.4	14.88
N(16)P(18)-d9	565.65	282.4	10.73
N(22)P(16)	612.593	254.4	11.31
N(23)P(16)	626.609	254.4	11.49
N(24)P(16)	640.624	254.4	11.7
N(25)P(16)	654.640	254.4	11.9
N(26)P(16)	668.656	254.4	12.13
N(27)P(16)	682.671	254.4	12.38
N(28)P(16)	696.687	254.4	12.61
N(29)P(16)	710.703	254.4	12.94
N(30)P(16)	724.718	254.4	13.22
N(14)P(17)	514.484	268.4	10.41
N(15)P(17)	528.499	268.4	10.5
N(16)P(17)	542.515	268.4	10.62
N(17)P(17)	556.530	268.4	10.74
N(18)P(17)	570.546	268.4	10.85
N(22)P(17)	626.609	268.4	11.47
N(23)P(17)	640.624	268.4	11.66
N(24)P(17)	654.640	268.4	11.87
N(25)P(17)	668.656	268.4	12.08
N(26)P(17)	682.671	268.4	12.34
N(27)P(17)	696.687	268.4	12.61
N(28)P(17)	710.703	268.4	12.85
N(29)P(17)	724.718	268.4	13.15
N(14)P(18)	528.499	282.4	10.52
N(15)P(18)	542.515	282.4	10.63
N(16)P(18)	556.530	282.4	10.73
N(17)P(18)	570.546	282.4	10.83
N(18)P(18)	584.562	282.4	10.98
N(19)P(18)	598.577	282.4	11.12
N(20)P(18)	612.593	282.4	11.28
N(21)P(18)	626.609	282.4	11.46
N(22)P(18)	640.624	282.4	11.62
N(23)P(18)	654.640	282.4	11.83
N(24)P(18)	668.656	282.4	12.04

N(25)P(18)	682.671	282.4	12.29
N(26)P(18)	696.687	282.4	12.53
N(27)P(18)	710.703	282.4	12.8
N(28)P(18)	724.718	282.4	13.13
N(14)P(19)	542.515	296.4	10.6
N(15)P(19)	556.530	296.4	10.72
N(16)P(19)	570.546	296.4	10.86
N(20)P(19)	626.609	296.4	11.43
N(21)P(19)	640.624	296.4	11.58
N(22)P(19)	654.640	296.4	11.81
N(23)P(19)	668.656	296.4	12.03
N(24)P(19)	682.671	296.4	12.25
N(25)P(19)	696.687	296.4	12.51
N(26)P(19)	710.703	296.4	12.77
N(27)P(19)	724.718	296.4	13.06
N(14)P(20)	556.530	310.4	10.72
N(15)P(20)	570.546	310.4	10.85
N(16)P(20)	584.562	310.4	10.98
N(20)P(20)	640.624	310.4	11.6
N(21)P(20)	654.640	310.4	11.77
N(22)P(20)	668.656	310.4	12
N(23)P(20)	682.671	310.4	12.23
N(24)P(20)	696.687	310.4	12.48
N(25)P(20)	710.703	310.4	12.74
N(26)P(20)	724.718	310.4	13.04
N(20)P(21)	654.640	324.4	11.77
N(21)P(21)	668.656	324.4	11.97
N(22)P(21)	682.671	324.4	12.21
N(23)P(21)	696.687	324.4	12.44
N(24)P(21)	710.703	324.4	12.72
N(25)P(21)	724.718	324.4	13
N(26)P(21)	738.734	324.4	13.32
N(14)P(22)	584.562	338.4	11.01
N(15)P(22)	598.577	338.4	11.12
N(16)P(22)	612.593	338.4	11.25
N(18)P(22)	640.624	338.4	11.56
N(19)P(22)	654.640	338.4	11.76
N(20)P(22)	668.656	338.4	11.99
N(21)P(22)	682.671	338.4	12.22
N(22)P(22)	696.687	338.4	12.41
N(23)P(22)	710.703	338.4	12.69
N(24)P(22)	724.718	338.4	13.01
N(25)P(22)	738.734	338.4	13.31
N(26)P(22)	752.750	338.4	13.62
N(27)P(22)	766.765	338.4	13.95

N(28)P(22)	780.781	338.4	14.36
N(20)P(23)	682.671	352.4	12.22
N(22)P(23)	710.703	352.4	12.7
N(23)P(23)	724.718	352.4	13
N(16)P(24)	640.624	366.4	11.63
N(18)P(24)	668.656	366.4	11.99
N(20)P(24)	696.687	366.4	12.46
N(21)P(24)	710.703	366.4	12.7
N(22)P(24)	724.718	366.4	12.98
N(16)H(18)-d9	545.615	280.4	10.53
N(17)H(15)	508.473	238.4	10.35
N(18)H(15)	522.489	238.4	10.44
N(19)H(15)	536.504	238.4	10.53
N(20)H(15)	550.520	238.4	10.62
N(21)H(15)	564.536	238.4	10.74
N(23)H(15)	592.567	238.4	11.01
N(24)H(15)	606.583	238.4	11.18
N(25)H(15)	620.598	238.4	11.34
N(26)H(15)	634.614	238.4	11.52
N(27)H(15)	648.629	238.4	11.67
N(28)H(15)	662.645	238.4	11.9
N(29)H(15)	676.661	238.4	12.09
N(30)H(15)	690.676	238.4	12.34
N(31)H(15)	704.692	238.4	12.58
N(16)H(16)	508.473	252.4	10.34
N(17)H(16)	522.489	252.4	10.43
N(18)H(16)	536.504	252.4	10.53
N(19)H(16)	550.520	252.4	10.61
N(20)H(16)	564.536	252.4	10.73
N(22)H(16)	592.567	252.4	11.06
N(23)H(16)	606.583	252.4	11.2
N(24)H(16)	620.598	252.4	11.37
N(25)H(16)	634.614	252.4	11.55
N(26)H(16)	648.629	252.4	11.74
N(27)H(16)	662.645	252.4	11.89
N(28)H(16)	676.661	252.4	12.1
N(29)H(16)	690.676	252.4	12.35
N(30)H(16)	704.692	252.4	12.62
N(16)H(17)	522.489	266.4	10.44
N(17)H(17)	536.504	266.4	10.53
N(18)H(17)	550.520	266.4	10.63
N(19)H(17)	564.536	266.4	10.72
N(20)H(17)	578.551	266.4	10.88
N(21)H(17)	592.567	266.4	10.99

N(22)H(17)	606.583	266.4	11.16
N(23)H(17)	620.598	266.4	11.35
N(24)H(17)	634.614	266.4	11.52
N(25)H(17)	648.629	266.4	11.72
N(26)H(17)	662.645	266.4	11.91
N(27)H(17)	676.661	266.4	12.13
N(28)H(17)	690.676	266.4	12.4
N(29)H(17)	704.692	266.4	12.56
N(16)H(18)	536.504	280.4	10.53
N(17)H(18)	550.520	280.4	10.62
N(18)H(18)	564.536	280.4	10.73
N(19)H(18)	578.551	280.4	10.85
N(20)H(18)	592.567	280.4	10.99
N(21)H(18)	606.583	280.4	11.14
N(22)H(18)	620.598	280.4	11.31
N(23)H(18)	634.614	280.4	11.48
N(24)H(18)	648.629	280.4	11.67
N(25)H(18)	662.645	280.4	11.88
N(26)H(18)	676.661	280.4	12.09
N(27)H(18)	690.676	280.4	12.33
N(28)H(18)	704.692	280.4	12.58
N(30)H(18)	732.723	280.4	13.1
N(16)H(19)	550.520	294.4	10.62
N(17)H(19)	564.536	294.4	10.71
N(18)H(19)	578.551	294.4	10.85
N(19)H(19)	592.567	294.4	10.98
N(20)H(19)	606.583	294.4	11.13
N(21)H(19)	620.598	294.4	11.26
N(22)H(19)	634.614	294.4	11.44
N(23)H(19)	648.629	294.4	11.63
N(24)H(19)	662.645	294.4	11.83
N(25)H(19)	676.661	294.4	12.05
N(26)H(19)	690.676	294.4	12.29
N(27)H(19)	704.692	294.4	12.57
N(28)H(19)	718.708	294.4	12.83
N(30)H(19)	746.739	294.4	13.44
N(16)H(20)	564.536	308.4	10.72
N(17)H(20)	578.551	308.4	10.83
N(18)H(20)	592.567	308.4	10.97
N(19)H(20)	606.583	308.4	11.12
N(20)H(20)	620.598	308.4	11.24
N(21)H(20)	634.614	308.4	11.42
N(22)H(20)	648.629	308.4	11.61
N(23)H(20)	662.645	308.4	11.82
N(24)H(20)	676.661	308.4	12.02

N(25)H(20)	690.676	308.4	12.26
N(26)H(20)	704.692	308.4	12.5
N(27)H(20)	718.708	308.4	12.77
N(28)H(20)	732.723	308.4	13.06
N(29)H(20)	746.739	308.4	13.41
N(30)H(20)	760.755	308.4	13.73
N(22)H(21)	662.645	322.4	11.82
N(23)H(21)	676.661	322.4	12
N(24)H(21)	690.676	322.4	12.21
N(25)H(21)	704.692	322.4	12.48
N(26)H(21)	718.708	322.4	12.74
N(28)H(21)	746.739	322.4	13.33
N(16)H(22)	592.567	336.4	10.97
N(17)H(22)	606.583	336.4	11.1
N(18)H(22)	620.598	336.4	11.25
N(19)H(22)	634.614	336.4	11.38
N(20)H(22)	648.629	336.4	11.57
N(22)H(22)	676.661	336.4	11.96
N(23)H(22)	690.676	336.4	12.17
N(24)H(22)	704.692	336.4	12.44
N(26)H(22)	732.723	336.4	12.97
N(28)H(22)	760.755	336.4	13.6
A(16)S(18)-d9	545.561	264.4	10.79
A(16)S(16)	526.4835348	236.4	10.58
A(17)S(16)	540.4991848	236.4	10.67
A(18)S(16)	554.5148349	236.4	10.8
A(20)S(16)	582.546135	236.4	11.08
A(21)S(16)	596.5617851	236.4	11.22
A(22)S(16)	610.5774352	236.4	11.38
A(23)S(16)	624.5930853	236.4	11.56
A(24)S(16)	638.6087353	236.4	11.77
A(25)S(16)	652.6243854	236.4	11.99
A(26)S(16)	666.6400355	236.4	12.23
A(27)S(16)	680.6556855	236.4	12.45
A(28)S(16)	694.6713356	236.4	12.75
A(16)S(17)	540.4991848	250.4	10.65
A(17)S(17)	554.5148349	250.4	10.8
A(18)S(17)	568.530485	250.4	10.92
A(19)S(17)	582.546135	250.4	11.05
A(20)S(17)	596.5617851	250.4	11.22
A(22)S(17)	624.5930853	250.4	11.56
A(24)S(17)	652.6243854	250.4	11.96
A(25)S(17)	666.6400355	250.4	12.19
A(26)S(17)	680.6556855	250.4	12.44

A(27)S(17)	694.6713356	250.4	12.71
A(28)S(17)	708.6869857	250.4	12.99
A(15)S(18)	540.4991848	264.4	10.65
A(16)S(18)	554.5148349	264.4	10.79
A(17)S(18)	568.530485	264.4	10.91
A(18)S(18)	582.546135	264.4	11.04
A(19)S(18)	596.5617851	264.4	11.19
A(20)S(18)	610.5774352	264.4	11.35
A(21)S(18)	624.5930853	264.4	11.5
A(22)S(18)	638.6087353	264.4	11.75
A(23)S(18)	652.6243854	264.4	11.93
A(24)S(18)	666.6400355	264.4	12.17
A(25)S(18)	680.6556855	264.4	12.39
A(26)S(18)	694.6713356	264.4	12.66
A(27)S(18)	708.6869857	264.4	12.96
A(28)S(18)	722.7026357	264.4	13.26
A(15)S(19)	554.5148349	278.4	10.77
A(16)S(19)	568.530485	278.4	10.91
A(17)S(19)	582.546135	278.4	11
A(18)S(19)	596.5617851	278.4	11.19
A(24)S(19)	680.6556855	278.4	12.38
A(25)S(19)	694.6713356	278.4	12.62
A(26)S(19)	708.6869857	278.4	12.9
A(27)S(19)	722.7026357	278.4	13.25
A(15)S(20)	568.530485	292.4	10.88
A(16)S(20)	582.546135	292.4	11.05
A(17)S(20)	596.5617851	292.4	11.18
A(18)S(20)	610.5774352	292.4	11.33
A(22)S(20)	666.6400355	292.4	12.09
A(23)S(20)	680.6556855	292.4	12.34
A(24)S(20)	694.6713356	292.4	12.61
A(25)S(20)	708.6869857	292.4	12.87
A(26)S(20)	722.7026357	292.4	13.19
A(27)S(20)	736.7182858	292.4	13.48
A(16)S(21)	596.5617851	306.4	11.19
A(18)S(21)	624.5930853	306.4	11.51
A(24)S(21)	708.6869857	306.4	12.86
A(25)S(21)	722.7026357	306.4	13.17
A(26)S(21)	736.7182858	306.4	13.5
A(16)S(22)	610.5774352	320.4	11.38
A(17)S(22)	624.5930853	320.4	11.49
A(18)S(22)	638.6087353	320.4	11.69
A(23)S(22)	708.6869857	320.4	12.83
A(24)S(22)	722.7026357	320.4	13.14
A(25)S(22)	736.7182858	320.4	13.46

A(16)P(18)-d9	581.629	282.4	10.63
A(18)P(16)	572.525	254.4	10.65
A(19)P(16)	586.541	254.4	10.76
A(20)P(16)	600.557	254.4	10.89
A(21)P(16)	614.572	254.4	11.02
A(22)P(16)	628.588	254.4	11.18
A(23)P(16)	642.604	254.4	11.34
A(24)P(16)	656.619	254.4	11.54
A(25)P(16)	670.635	254.4	11.72
A(26)P(16)	684.651	254.4	11.92
A(17)P(17)	572.525	268.4	10.63
A(18)P(17)	586.541	268.4	10.76
A(19)P(17)	600.557	268.4	10.89
A(20)P(17)	614.572	268.4	11.01
A(21)P(17)	628.588	268.4	11.16
A(22)P(17)	642.604	268.4	11.33
A(23)P(17)	656.619	268.4	11.49
A(24)P(17)	670.635	268.4	11.7
A(25)P(17)	684.651	268.4	11.9
A(26)P(17)	698.666	268.4	12.11
A(16)P(18)	572.525	282.4	10.63
A(17)P(18)	586.541	282.4	10.75
A(18)P(18)	600.557	282.4	10.88
A(19)P(18)	614.572	282.4	11
A(20)P(18)	628.588	282.4	11.14
A(22)P(18)	656.619	282.4	11.47
A(23)P(18)	670.635	282.4	11.63
A(24)P(18)	684.651	282.4	11.86
A(25)P(18)	698.666	282.4	12.07
A(26)P(18)	712.682	282.4	12.32
A(27)P(18)	726.698	282.4	12.57
A(15)P(19)	572.525	296.4	10.63
A(16)P(19)	586.541	296.4	10.74
A(17)P(19)	600.557	296.4	10.85
A(18)P(19)	614.572	296.4	10.99
A(19)P(19)	628.588	296.4	11.13
A(20)P(19)	642.604	296.4	11.27
A(21)P(19)	656.619	296.4	11.42
A(22)P(19)	670.635	296.4	11.63
A(23)P(19)	684.651	296.4	11.83
A(24)P(19)	698.666	296.4	12.04
A(25)P(19)	712.682	296.4	12.26
A(26)P(19)	726.698	296.4	12.52
A(16)P(20)	600.557	310.4	10.88

A(17)P(20)	614.572	310.4	10.99
A(18)P(20)	628.588	310.4	11.14
A(19)P(20)	642.604	310.4	11.29
A(20)P(20)	656.619	310.4	11.44
A(21)P(20)	670.635	310.4	11.62
A(22)P(20)	684.651	310.4	11.83
A(23)P(20)	698.666	310.4	12.02
A(24)P(20)	712.682	310.4	12.26
A(25)P(20)	726.698	310.4	12.52
A(26)P(20)	740.713	310.4	12.78
A(17)P(21)	628.588	324.4	11.13
A(18)P(21)	642.604	324.4	11.27
A(20)P(21)	670.635	324.4	11.6
A(24)P(21)	726.698	324.4	12.48
A(16)P(22)	628.588	338.4	11.14
A(17)P(22)	642.604	338.4	11.26
A(18)P(22)	656.619	338.4	11.43
A(19)P(22)	670.635	338.4	11.61
A(20)P(22)	684.651	338.4	11.78
A(22)P(22)	712.682	338.4	12.21
A(23)P(22)	726.698	338.4	12.44
A(24)P(22)	740.713	338.4	12.68
A(26)P(22)	768.745	338.4	13.1
A(14)P(23)	614.572	352.4	10.95
A(15)P(23)	628.588	352.4	11.11
A(16)P(23)	642.604	352.4	11.22
A(17)P(23)	656.619	352.4	11.41
A(15)P(24)	642.604	366.4	11.23
A(16)H(18)-d9	561.587	280.4	10.42
A(24)H(14)	608.562	224.4	10.9
A(25)H(14)	622.577	224.4	11.02
A(26)H(14)	636.593	224.4	11.18
A(28)H(14)	664.624	224.4	11.5
A(26)H(15)	650.609	238.4	11.31
A(27)H(15)	664.624	238.4	11.47
A(28)H(15)	678.640	238.4	11.68
A(29)H(15)	692.656	238.4	11.86
A(18)H(16)	552.499	252.4	10.41
A(19)H(16)	566.515	252.4	10.52
A(20)H(16)	580.530	252.4	10.63
A(21)H(16)	594.546	252.4	10.72
A(22)H(16)	608.562	252.4	10.89
A(23)H(16)	622.577	252.4	11.04
A(24)H(16)	636.593	252.4	11.18

A(25)H(16)	650.609	252.4	11.36
A(26)H(16)	664.624	252.4	11.54
A(27)H(16)	678.640	252.4	11.65
A(28)H(16)	692.656	252.4	11.84
A(29)H(16)	706.671	252.4	12.07
A(30)H(16)	720.687	252.4	12.28
A(16)H(17)	538.484	266.4	10.35
A(17)H(17)	552.499	266.4	10.42
A(18)H(17)	566.515	266.4	10.53
A(19)H(17)	580.530	266.4	10.63
A(20)H(17)	594.546	266.4	10.74
A(21)H(17)	608.562	266.4	10.85
A(22)H(17)	622.577	266.4	11.01
A(23)H(17)	636.593	266.4	11.16
A(24)H(17)	650.609	266.4	11.32
A(25)H(17)	664.624	266.4	11.5
A(26)H(17)	678.640	266.4	11.7
A(27)H(17)	692.656	266.4	11.89
A(28)H(17)	706.671	266.4	12.04
A(29)H(17)	720.687	266.4	12.23
A(16)H(18)	552.499	280.4	10.42
A(17)H(18)	566.515	280.4	10.51
A(18)H(18)	580.530	280.4	10.62
A(19)H(18)	594.546	280.4	10.75
A(20)H(18)	608.562	280.4	10.87
A(21)H(18)	622.577	280.4	10.96
A(22)H(18)	636.593	280.4	11.12
A(23)H(18)	650.609	280.4	11.29
A(24)H(18)	664.624	280.4	11.46
A(25)H(18)	678.640	280.4	11.64
A(26)H(18)	692.656	280.4	11.85
A(27)H(18)	706.671	280.4	12.07
A(28)H(18)	720.687	280.4	12.32
A(16)H(19)	566.515	294.4	10.51
A(17)H(19)	580.530	294.4	10.6
A(18)H(19)	594.546	294.4	10.72
A(19)H(19)	608.562	294.4	10.81
A(20)H(19)	622.577	294.4	10.96
A(21)H(19)	636.593	294.4	11.1
A(22)H(19)	650.609	294.4	11.25
A(23)H(19)	664.624	294.4	11.42
A(24)H(19)	678.640	294.4	11.61
A(25)H(19)	692.656	294.4	11.81
A(26)H(19)	706.671	294.4	12.03
A(27)H(19)	720.687	294.4	12.24

A(28)H(19)	734.702	294.4	12.52
A(16)H(20)	580.530	308.4	10.61
A(17)H(20)	594.546	308.4	10.72
A(18)H(20)	608.562	308.4	10.83
A(19)H(20)	622.577	308.4	10.96
A(20)H(20)	636.593	308.4	11.11
A(21)H(20)	650.609	308.4	11.24
A(22)H(20)	664.624	308.4	11.4
A(23)H(20)	678.640	308.4	11.6
A(24)H(20)	692.656	308.4	11.78
A(25)H(20)	706.671	308.4	12.01
A(26)H(20)	720.687	308.4	12.22
A(27)H(20)	734.702	308.4	12.47
A(28)H(20)	748.718	308.4	12.73
A(15)H(21)	580.530	322.4	10.62
A(16)H(21)	594.546	322.4	10.73
A(18)H(21)	622.577	322.4	10.97
A(22)H(21)	678.640	322.4	11.57
A(23)H(21)	692.656	322.4	11.77
A(24)H(21)	706.671	322.4	11.98
A(25)H(21)	720.687	322.4	12.19
A(26)H(21)	734.702	322.4	12.46
A(16)H(22)	608.562	336.4	10.84
A(17)H(22)	622.577	336.4	10.93
A(18)H(22)	636.593	336.4	11.09
A(22)H(22)	692.656	336.4	11.74
A(23)H(22)	706.671	336.4	11.93
A(24)H(22)	720.687	336.4	12.2
A(26)H(22)	748.718	336.4	12.69
E(18:2)O(33)DS(16)	1028.995	238.4	16.14
E(18:2)O(34)DS(16)	1043.011	238.4	16.69
E(18:2)O(32)DS(17)	1028.995	252.4	16.18
E(18:2)O(33)DS(17)	1043.011	252.4	16.61
E(18:2)O(34)DS(17)	1057.026	252.4	17.08
E(18:2)O(30)DS(18)	1014.979	266.4	15.81
E(18:2)O(31)DS(18)	1028.995	266.4	16.26
E(18:2)O(32)DS(18)	1043.011	266.4	16.7
E(18:2)O(33)DS(18)	1057.026	266.4	16.95
E(18:2)O(34)DS(18)	1071.042	266.4	17.38
E(18:2)O(28)DS(19)	1000.964	280.4	15.31
E(18:2)O(29)DS(19)	1014.979	280.4	15.7
E(18:2)O(30)DS(19)	1028.995	280.4	16.13
E(18:2)O(31)DS(19)	1043.011	280.4	16.6
E(18:2)O(32)DS(19)	1057.026	280.4	17.05

E(18:2)O(33)DS(19)	1071.042	280.4	17.55
E(18:2)O(34)DS(19)	1085.058	280.4	17.98
E(18:2)O(28)DS(20)	1014.979	294.4	15.66
E(18:2)O(29)DS(20)	1028.995	294.4	16.09
E(18:2)O(30)DS(20)	1043.011	294.4	16.53
E(18:2)O(31)DS(20)	1057.026	294.4	16.96
E(18:2)O(32)DS(20)	1071.042	294.4	17.43
E(18:2)O(27)DS(21)	1014.979	308.4	15.55
E(18:2)O(28)DS(21)	1028.995	308.4	15.95
E(18:2)O(29)DS(21)	1043.011	308.4	16.42
E(18:2)O(30)DS(21)	1057.026	308.4	16.89
E(18:2)O(31)DS(21)	1071.042	308.4	17.39
E(18:2)O(32)DS(21)	1085.058	308.4	17.85
E(18:2)O(33)DS(21)	1099.073	308.4	18.33
E(18:2)O(28)DS(22)	1043.011	322.4	16.38
E(18:2)O(29)DS(22)	1057.026	322.4	16.8
E(18:2)O(30)DS(22)	1071.042	322.4	17.25
E(18:2)O(31)DS(22)	1085.058	322.4	17.79
E(18:2)O(32)DS(22)	1099.073	322.4	18.26
E(18:2)O(28)DS(23)	1057.026	336.4	16.75
E(18:2)O(29)DS(23)	1071.042	336.4	17.25
E(18:2)O(30)DS(23)	1085.058	336.4	17.71
E(18:2)O(31)DS(23)	1099.073	336.4	18.19
E(18:1)O(26)S(18)-d9	967.973	264.4	15.64
E(18:2)O(29)S(16)	970.917	236.4	16.24
E(18:2)O(30)S(16)	984.932	236.4	16.72
E(18:2)O(31)S(16)	998.948	236.4	17.17
E(18:2)O(32)S(16)	1012.964	236.4	17.64
E(18:2)O(28)S(17)	970.917	250.4	16.18
E(18:2)O(29)S(17)	984.932	250.4	16.57
E(18:2)O(30)S(17)	998.948	250.4	17.08
E(18:2)O(31)S(17)	1012.964	250.4	17.56
E(18:2)O(32)S(17)	1026.979	250.4	18.01
E(18:2)O(33)S(17)	1040.995	250.4	18.53
E(18:2)O(34)S(17)	1055.011	250.4	19.06
E(18:2)O(27)S(18)	970.917	264.4	16.2
E(18:2)O(28)S(18)	984.932	264.4	16.54
E(18:2)O(29)S(18)	998.948	264.4	16.98
E(18:2)O(30)S(18)	1012.964	264.4	17.43
E(18:2)O(31)S(18)	1026.979	264.4	17.95
E(18:2)O(32)S(18)	1040.995	264.4	18.44
E(18:2)O(33)S(18)	1055.011	264.4	18.95
E(18:2)O(34)S(18)	1069.026	264.4	19.44
E(18:2)O(28)S(19)	998.948	278.4	16.93

E(18:2)O(29)S(19)	1012.964	278.4	17.43
E(18:2)O(30)S(19)	1026.979	278.4	17.9
E(18:2)O(31)S(19)	1040.995	278.4	18.39
E(18:2)O(32)S(19)	1055.011	278.4	18.86
E(18:2)O(33)S(19)	1069.026	278.4	19.39
E(18:2)O(34)S(19)	1083.042	278.4	19.9
E(18:2)O(26)S(20)	984.932	292.4	16.36
E(18:2)O(27)S(20)	998.948	292.4	16.87
E(18:2)O(28)S(20)	1012.964	292.4	17.36
E(18:2)O(29)S(20)	1026.979	292.4	17.81
E(18:2)O(30)S(20)	1040.995	292.4	18.34
E(18:2)O(31)S(20)	1055.011	292.4	18.83
E(18:2)O(32)S(20)	1069.026	292.4	19.33
E(18:2)O(33)S(20)	1083.042	292.4	19.79
E(18:2)O(34)S(20)	1097.058	292.4	20.31
E(18:2)O(26)S(21)	998.948	306.4	16.8
E(18:2)O(27)S(21)	1012.964	306.4	17.32
E(18:2)O(28)S(21)	1026.979	306.4	17.75
E(18:2)O(29)S(21)	1040.995	306.4	18.28
E(18:2)O(30)S(21)	1055.011	306.4	18.74
E(18:2)O(31)S(21)	1069.026	306.4	19.28
E(18:2)O(32)S(21)	1083.042	306.4	19.74
E(18:2)O(33)S(21)	1097.058	306.4	20.31
E(18:2)O(24)S(22)	984.932	320.4	16.25
E(18:2)O(26)S(22)	1012.964	320.4	17.21
E(18:2)O(27)S(22)	1026.979	320.4	17.69
E(18:2)O(28)S(22)	1040.995	320.4	18.22
E(18:2)O(29)S(22)	1055.011	320.4	18.71
E(18:2)O(30)S(22)	1069.026	320.4	19.21
E(18:2)O(31)S(22)	1083.042	320.4	19.74
E(18:2)O(32)S(22)	1097.058	320.4	20.18
E(18:1)O(26)P(18)-d9	986.031	282.4	15.09
E(18:2)O(30)P(16)	1002.943	254.4	16.08
E(18:2)O(30)P(17)	1016.959	268.4	16.48
E(18:2)O(31)P(17)	1030.974	268.4	16.97
E(18:2)O(32)P(17)	1044.990	268.4	17.45
E(18:2)O(28)P(18)	1002.943	282.4	15.9
E(18:2)O(29)P(18)	1016.959	282.4	16.41
E(18:2)O(30)P(18)	1030.974	282.4	16.85
E(18:2)O(31)P(18)	1044.990	282.4	17.3
E(18:2)O(32)P(18)	1059.005	282.4	17.8
E(18:2)O(30)P(19)	1044.990	296.4	17.27
E(18:2)O(32)P(19)	1073.021	296.4	18.26
E(18:2)O(28)P(20)	1030.974	310.4	16.71

E(18:2)O(29)P(20)	1044.990	310.4	17.18
E(18:2)O(30)P(20)	1059.005	310.4	17.67
E(18:2)O(31)P(20)	1073.021	310.4	18.15
E(18:2)O(32)P(20)	1087.037	310.4	18.62
E(18:2)O(28)P(21)	1044.990	324.4	17.21
E(18:2)O(29)P(21)	1059.005	324.4	17.68
E(18:2)O(30)P(21)	1073.021	324.4	18.1
E(18:2)O(31)P(21)	1087.037	324.4	18.56
E(18:2)O(32)P(21)	1101.052	324.4	19.12
E(18:2)O(28)P(22)	1059.005	338.4	17.53
E(18:2)O(29)P(22)	1073.021	338.4	18.04
E(18:2)O(30)P(22)	1087.037	338.4	18.52
E(18:2)O(31)P(22)	1101.052	338.4	19.08
E(18:2)O(32)P(22)	1115.068	338.4	19.57
E(18:2)O(28)H(17)	968.901	266.4	14.86
E(18:2)O(29)H(17)	982.917	266.4	15.24
E(18:2)O(30)H(17)	996.932	266.4	15.67
E(18:2)O(31)H(17)	1010.948	266.4	16.11
E(18:2)O(32)H(17)	1024.964	266.4	16.57
E(18:2)O(28)H(18)	982.917	280.4	15.16
E(18:2)O(29)H(18)	996.932	280.4	15.58
E(18:2)O(30)H(18)	1010.948	280.4	16.05
E(18:2)O(31)H(18)	1024.964	280.4	16.51
E(18:2)O(32)H(18)	1038.979	280.4	16.9
E(18:2)O(33)H(18)	1052.995	280.4	17.41
E(18:2)O(29)H(19)	1010.948	294.4	15.96
E(18:2)O(30)H(19)	1024.964	294.4	16.37
E(18:2)O(31)H(19)	1038.979	294.4	16.85
E(18:2)O(32)H(19)	1052.995	294.4	17.3
E(18:2)O(28)H(20)	1010.948	308.4	15.85
E(18:2)O(29)H(20)	1024.964	308.4	16.32
E(18:2)O(30)H(20)	1038.979	308.4	16.78
E(18:2)O(31)H(20)	1052.995	308.4	17.25
E(18:2)O(32)H(20)	1067.011	308.4	17.69
E(18:2)O(27)H(21)	1010.948	322.4	16.02
E(18:2)O(28)H(21)	1024.964	322.4	16.23
E(18:2)O(29)H(21)	1038.979	322.4	16.65
E(18:2)O(30)H(21)	1052.995	322.4	17.16
E(18:2)O(31)H(21)	1067.011	322.4	17.68
E(18:2)O(28)H(22)	1038.979	336.4	16.64
E(18:2)O(29)H(22)	1052.995	336.4	17.05
E(18:2)O(30)H(22)	1067.011	336.4	17.58

Appendix 4

Table A 4.1 MRM transitions and retention times used for the endocannabinoid assay.

Lipid mediators were analysed using LC-MS/MS. MRM: multiple reaction monitoring; NAE: N-acyl ethanolamine; MAG: monoacylglycerol; AEA: arachidonoyl ethanolamine; AG: arachidonoyl glycerol; LG: lineoleoyl glycerol; PAG: palmitoyl glycerol; OG: oleoyl glycerol; STG: stearoyl glycerol; MEA: myristoyl ethanolamine; PDEA: pentadecanoyl ethanolamine; POEA: palmitoleoyl ethanolamine; PEA: palmitoyl ethanolamine; HEA: heptadecanoyl ethanolamine; ALEA: α -linolenoyl ethanolamine; LEA: lineoleoyl ethanolamine; OEA: oleoyl ethanolamine; VEA: vaccenoyl ethanolamine; SEA: stearoyl ethanolamine; DEA: docosanoyl ethanolamine; NEA: nervonoyl ethanolamine.

Compound	MRM	Retention time (min)
AEA-d8	356>63	5.41
2-AG-d8	387>293	6.19
MEA	272>62	4.66
PDEA	286>62	5.32
POEA	298>62	4.97
PEA	300>62	6.15
HEA	314>62	7.15
STEA	328>62	8.27
OEA	326>62	6.58
VEA	326>62	≈6.50
LEA	324>62	5.41
ALEA	322>62	4.68
DGLEA	350>62	6.00
AEA	348>62	5.48
EPEA	346>62	4.74
DPEA	374>62	5.69
DHEA	372>62	5.38
DEA	384>62	13.63
NEA	410>62	13.69
LGEA	412>62	12.70 (2nd injection)
PGE₂-EA	378>360	2.16
PGD₂-EA	378>360	2.50
15 HETE EA	364>62	3.61
PGF₂-EA	380>344	2.10
5(6) EET EA	364>346	4.29
8(9) EET EA	364>346	4.20
11(12) EET EA	364>346	4.04
14(15) EET EA	364>346	3.79
2-STG	359>341	9.63
2-OG	357>265	7.71
2-LG	355>263	6.29
2-AG	379>287	6.24
2-PG	331>239	7.30
NAT	412>126	4.19

Appendix 5

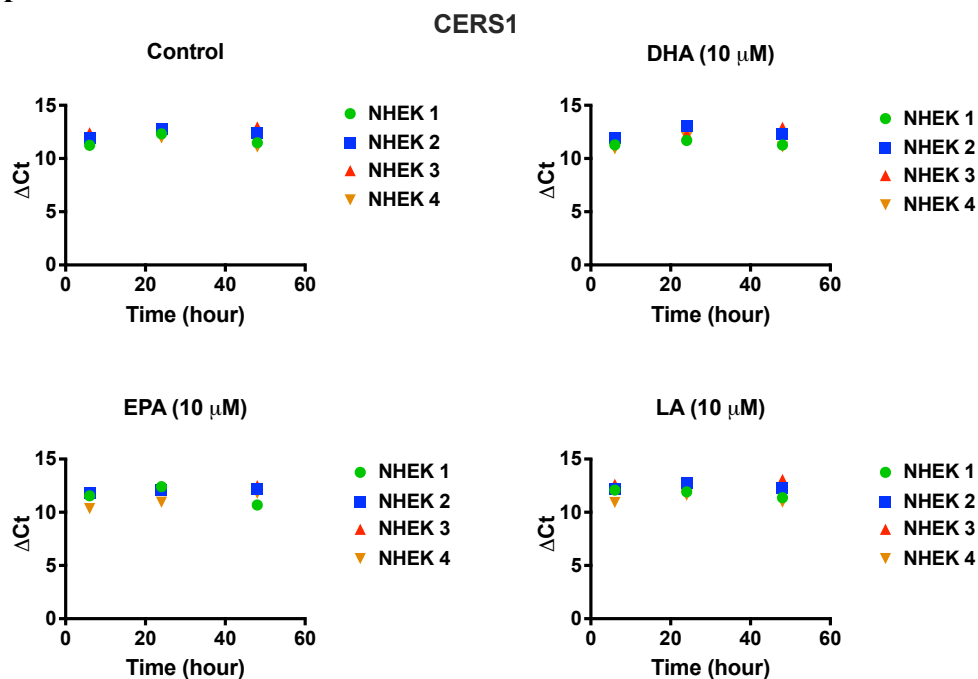


Figure A 5.1 The individual ΔCt values for CERS1 expression in proliferating NHEK. Cells were treated with 10 μM DHA, EPA and LA for six, 24 and 48 hours. NHEK: normal epidermal keratinocytes; DHA: docosahexaenoic acid; EPA: eicosapentaenoic acid; LA: linoleic acid; ΔCt : delta cycle threshold; CERS1: ceramide synthase 1.

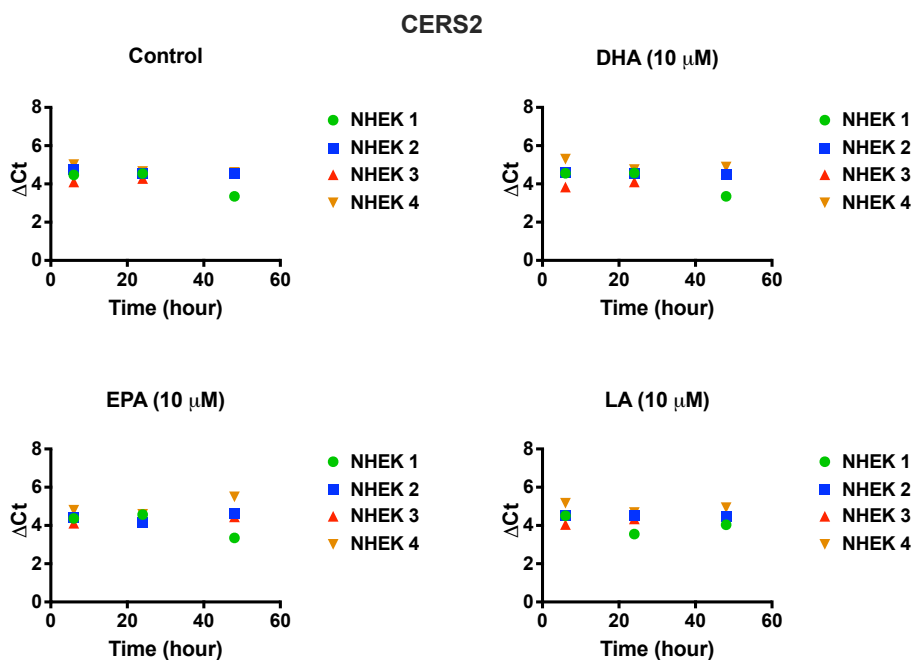


Figure A 5.2 The individual ΔCt values for CERS2 expression in proliferating NHEK. Cells were treated with 10 μM DHA, EPA and LA for six, 24 and 48 hours. NHEK: normal epidermal keratinocytes; DHA: docosahexaenoic acid; EPA: eicosapentaenoic acid; LA: linoleic acid; ΔCt : delta cycle threshold; CERS2: ceramide synthase 2.

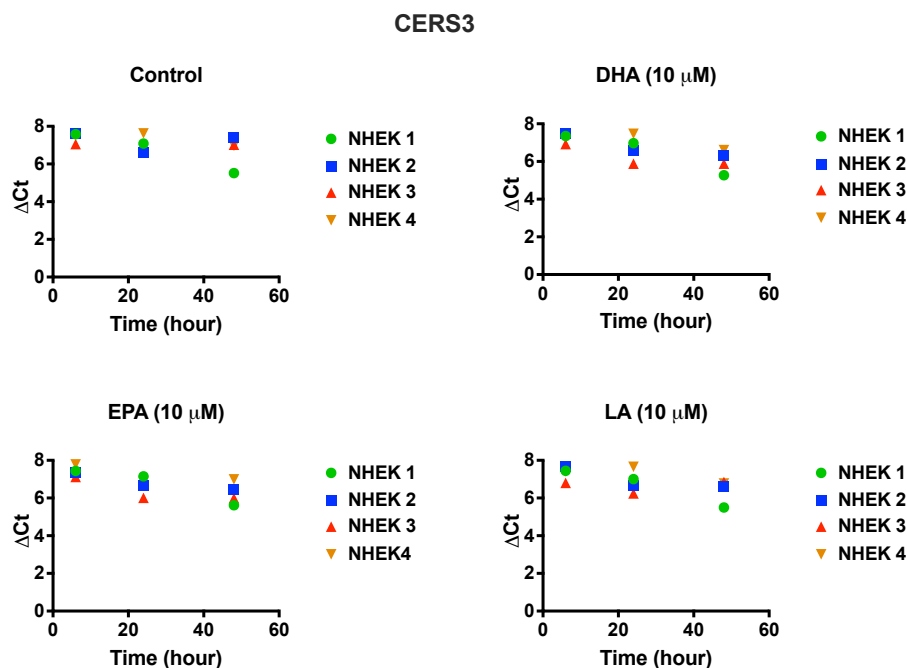


Figure A 5.3 The individual ΔCt values for CERS3 expression in proliferating NHEK. Cells were treated with 10 μM DHA, EPA and LA for six, 24 and 48 hours. NHEK: normal epidermal keratinocytes; DHA: docosahexaenoic acid; EPA: eicosapentaenoic acid; LA: linoleic acid; ΔCt : delta cycle threshold; CERS3: ceramide synthase 3.

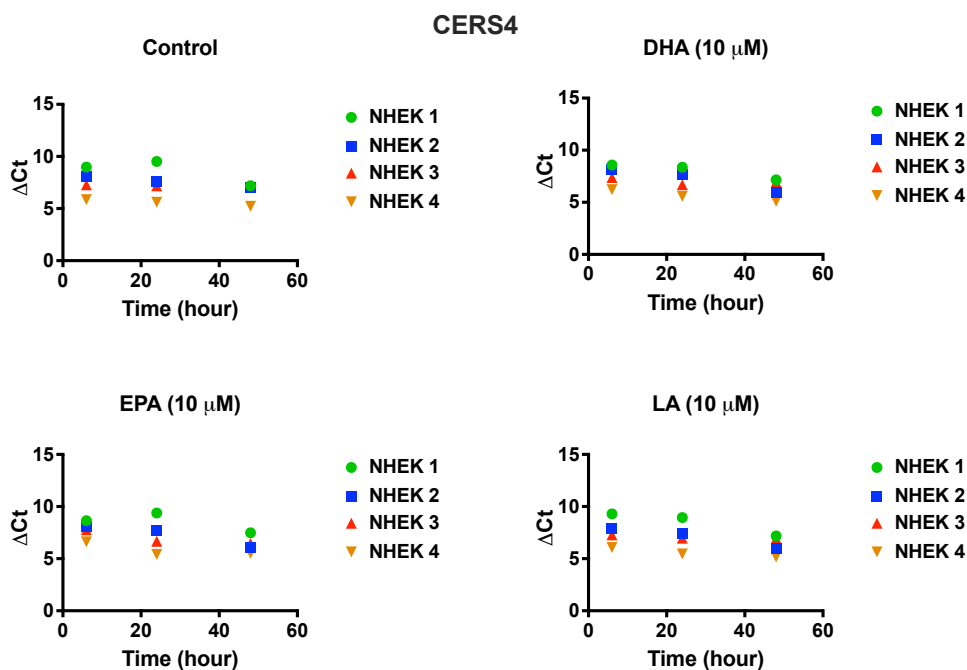


Figure A 5.4 The individual ΔCt values for CERS4 expression in proliferating NHEK. Cells were treated with 10 μM DHA, EPA and LA for six, 24 and 48 hours. NHEK: normal epidermal keratinocytes; DHA: docosahexaenoic acid; EPA: eicosapentaenoic acid; LA: linoleic acid; ΔCt : delta cycle threshold; CERS4: ceramide synthase 4.

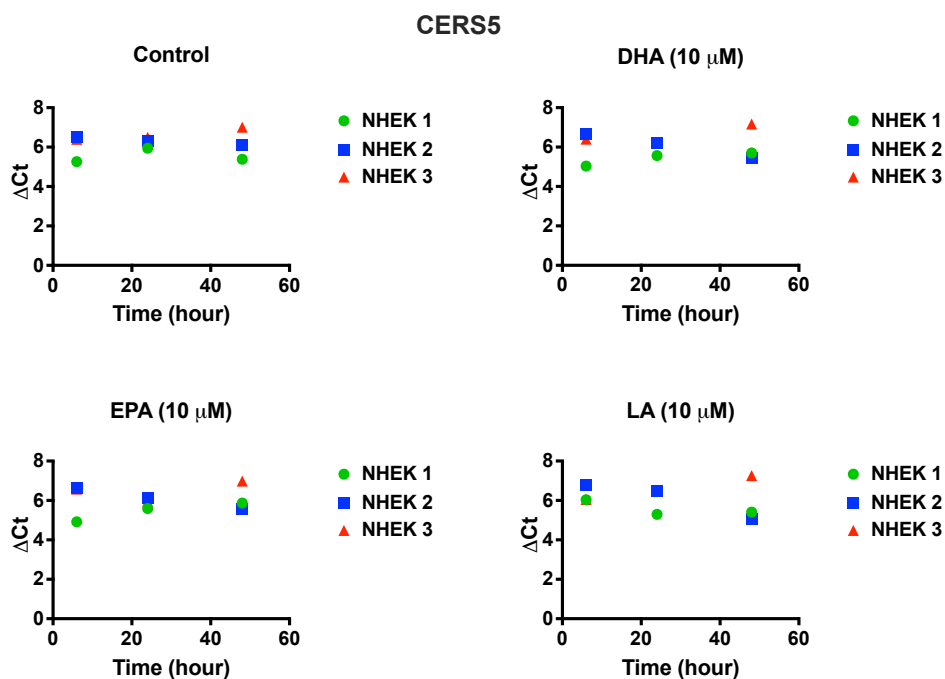


Figure A 5.5 The individual ΔCt values for CERS5 expression in proliferating NHEK. Cells were treated with 10 μM DHA, EPA and LA for six, 24 and 48 hours. NHEK: normal epidermal keratinocytes; DHA: docosahexaenoic acid; EPA: eicosapentaenoic acid; LA: linoleic acid; ΔCt : delta cycle threshold; CERS5: ceramide synthase 5.

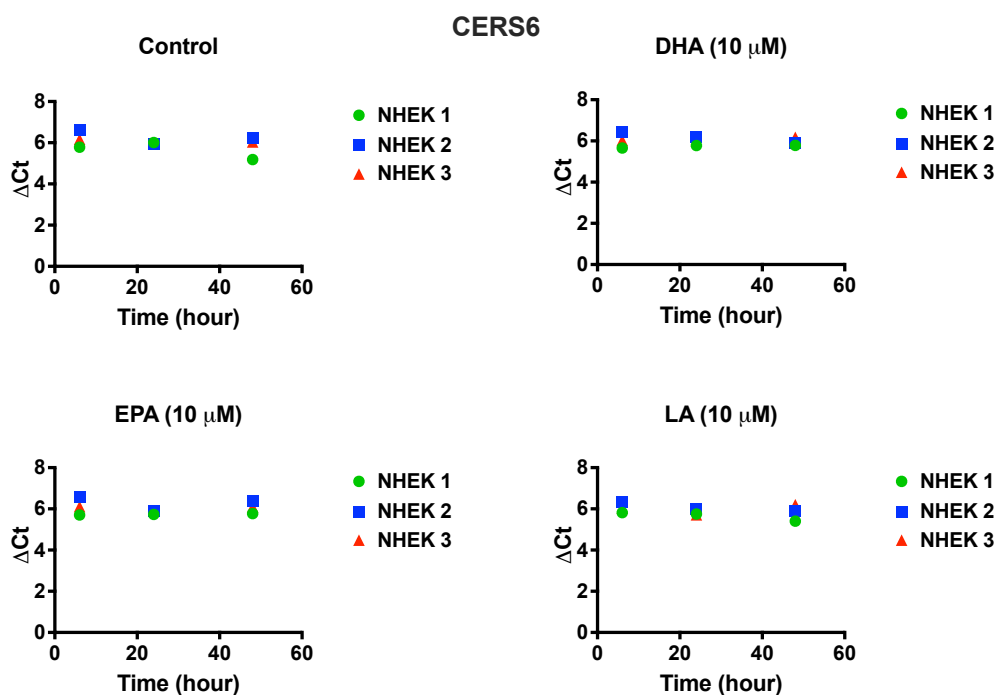


Figure A 5.6 The individual ΔCt values for CERS6 expression in proliferating NHEK. Cells were treated with 10 μM DHA, EPA and LA for six, 24 and 48 hours. NHEK: normal epidermal keratinocytes; DHA: docosahexaenoic acid; EPA: eicosapentaenoic acid; LA: linoleic acid; ΔCt : delta cycle threshold; CERS6: ceramide synthase 6.

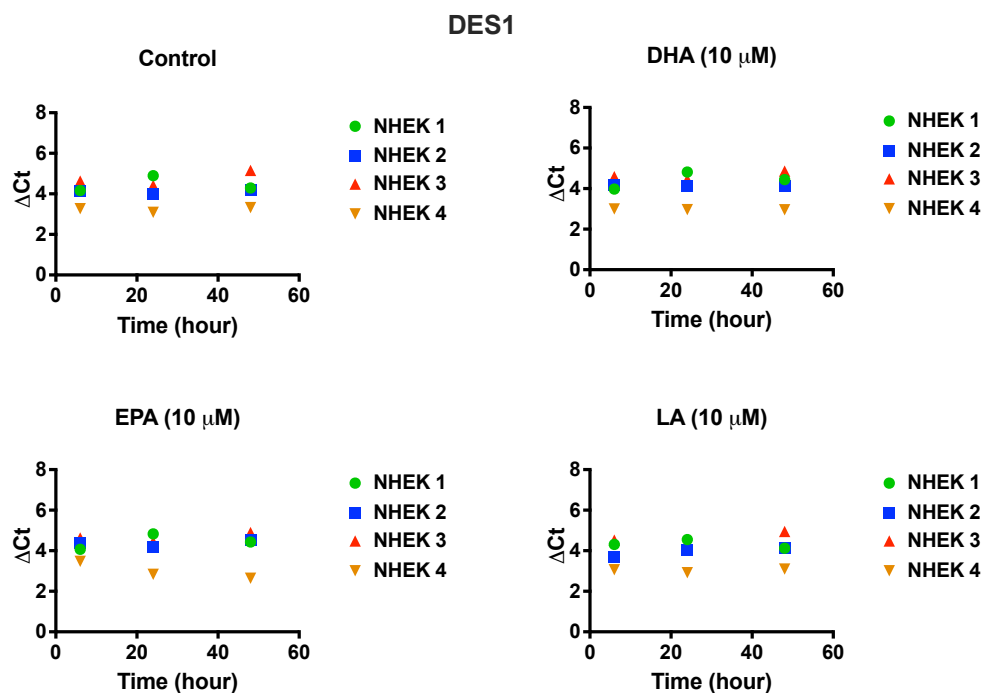


Figure A 5.7 The individual ΔCt values for DES1 expression in proliferating NHEK. Cells were treated with 10 μM DHA, EPA and LA for six, 24 and 48 hours. NHEK: normal epidermal keratinocytes; DHA: docosahexaenoic acid; EPA: eicosapentaenoic acid; LA: linoleic acid; ΔCt : delta cycle threshold; DES1: desaturase 1.

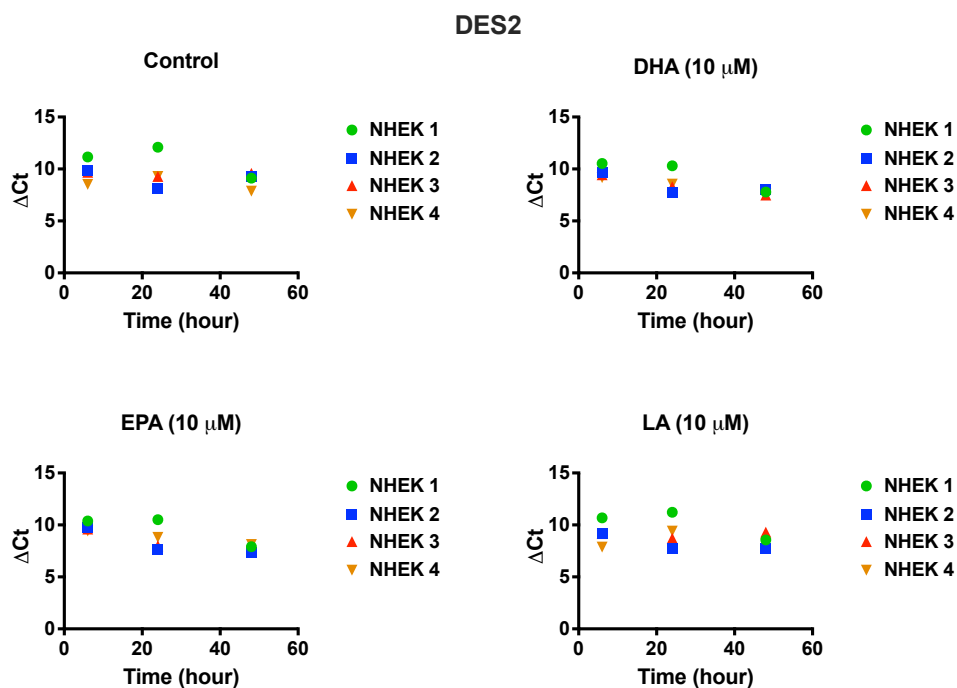


Figure A 5.8 The individual ΔCt values for DES2 expression in proliferating NHEK. Cells were treated with 10 μM DHA, EPA and LA for six, 24 and 48 hours. NHEK: normal epidermal keratinocytes; DHA: docosahexaenoic acid; EPA: eicosapentaenoic acid; LA: linoleic acid; ΔCt : delta cycle threshold; DES2: desaturase 2.

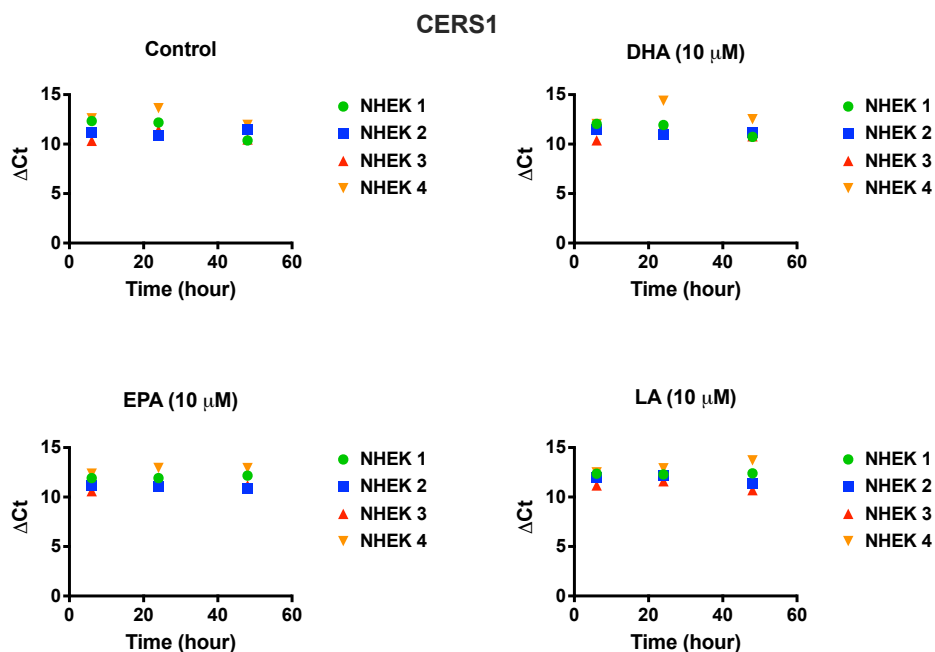


Figure A 5.9 The individual ΔCt values for CERS1 expression in differentiating NHEK. Cells were treated with 10 μM DHA, EPA and LA for six, 24 and 48 hours. NHEK: normal epidermal keratinocytes; DHA: docosahexaenoic acid; EPA: eicosapentaenoic acid; LA: linoleic acid; ΔCt : delta cycle threshold; CERS1: ceramide synthase 1.

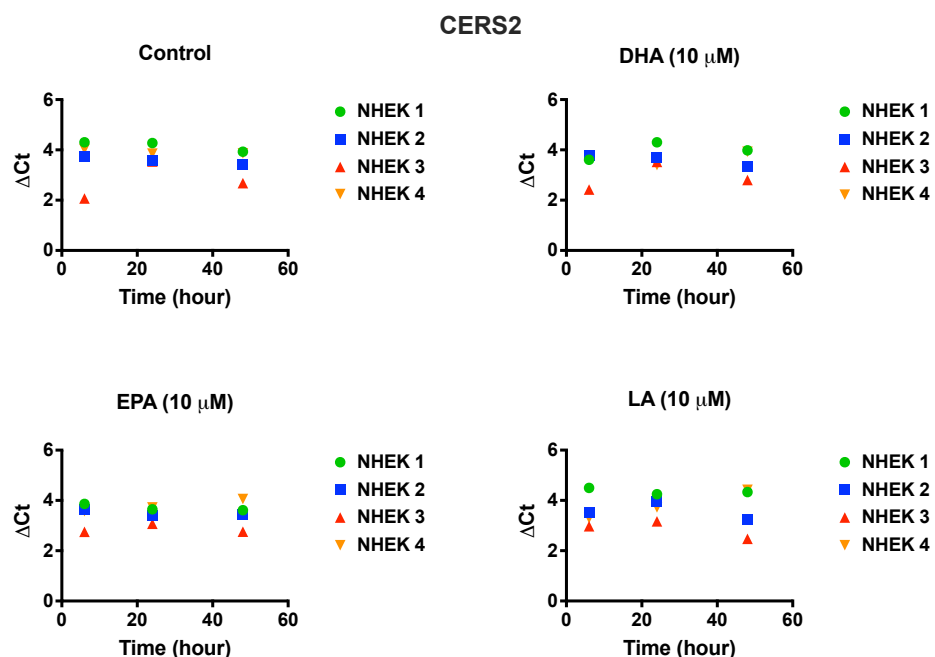


Figure A 5.10 The individual ΔCt values for CERS2 expression in differentiating NHEK. Cells were treated with 10 μM DHA, EPA and LA for six, 24 and 48 hours. NHEK: normal epidermal keratinocytes; DHA: docosahexaenoic acid; EPA: eicosapentaenoic acid; LA: linoleic acid; ΔCt : delta cycle threshold; CERS2: ceramide synthase 2.

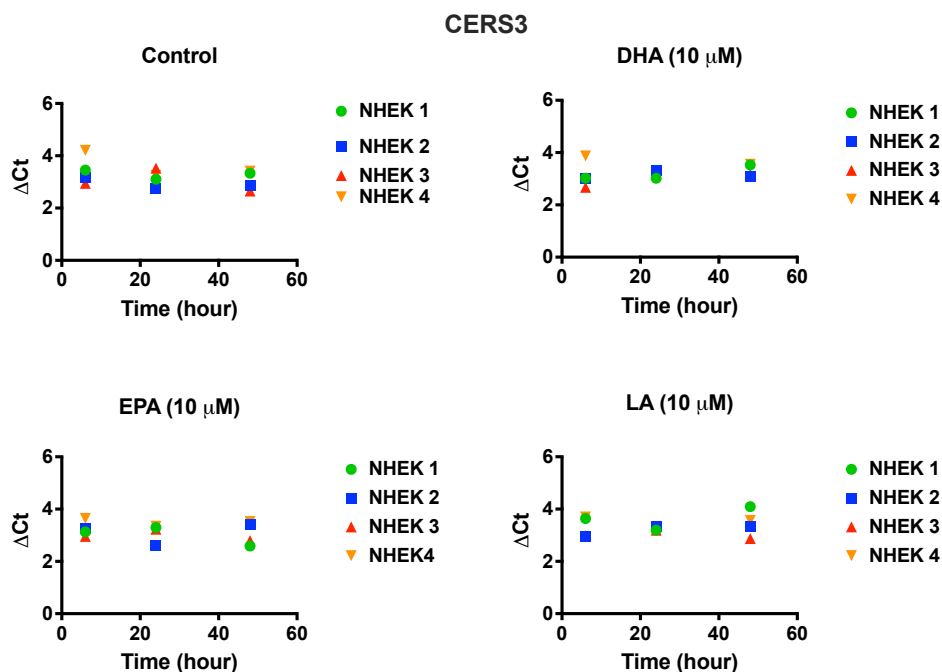


Figure A 5.11 The individual ΔCt values for CERS3 expression in differentiating NHEK. Cells were treated with 10 μM DHA, EPA and LA for six, 24 and 48 hours. NHEK: normal epidermal keratinocytes; DHA: docosahexaenoic acid; EPA: eicosapentaenoic acid; LA: linoleic acid; ΔCt : delta cycle threshold; CERS3: ceramide synthase 3.

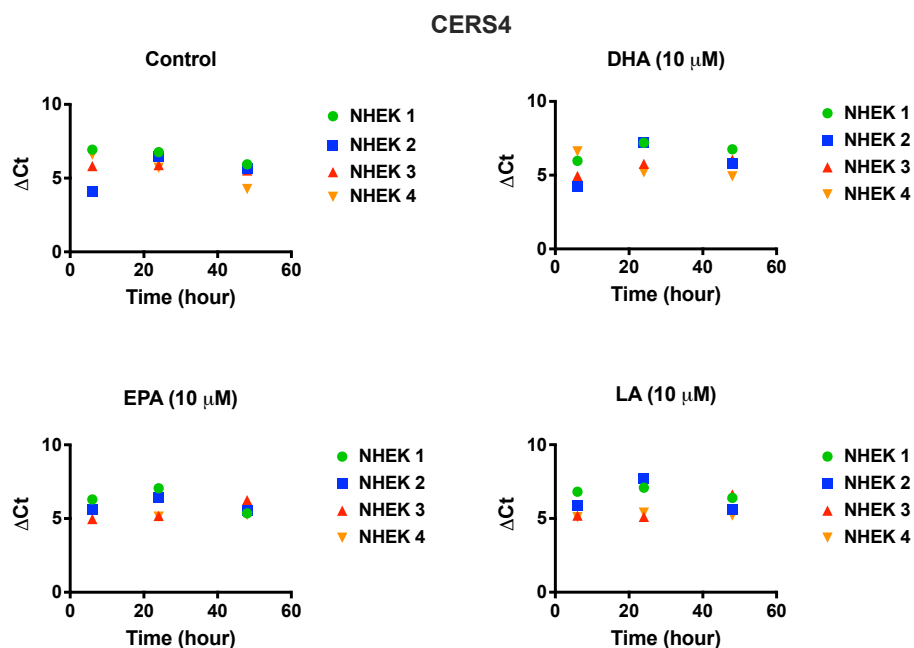


Figure A 5.12 The individual ΔCt values for CERS4 expression in differentiating NHEK. Cells were treated with 10 μM DHA, EPA and LA for six, 24 and 48 hours. NHEK: normal epidermal keratinocytes; DHA: docosahexaenoic acid; EPA: eicosapentaenoic acid; LA: linoleic acid; ΔCt : delta cycle threshold; CERS4: ceramide synthase 4.

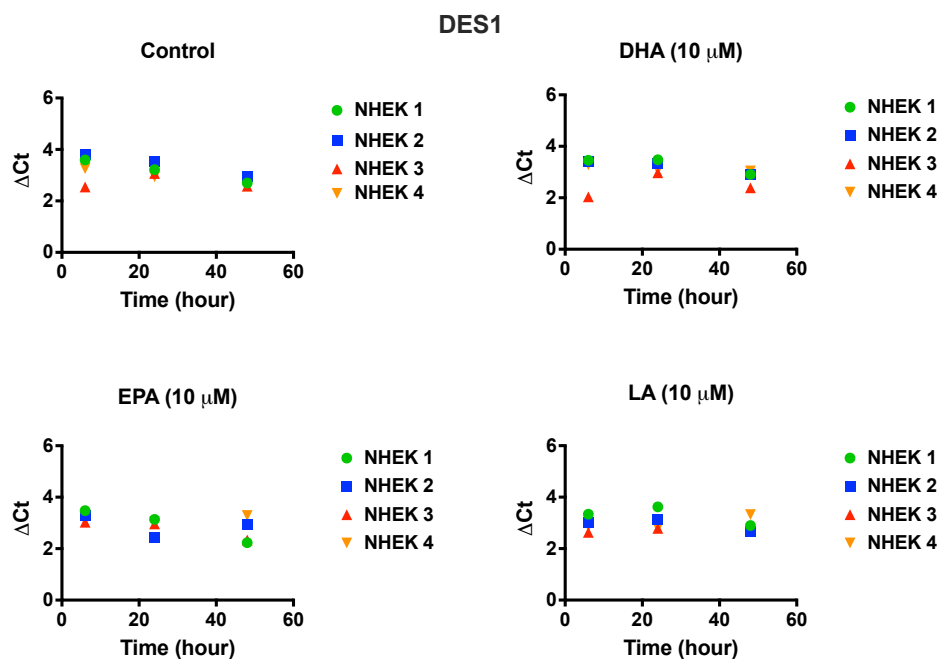


Figure A 5.13 The individual ΔCt values for **DES1** expression in differentiating NHEK. Cells were treated with 10 μM DHA, EPA and LA for six, 24 and 48 hours. NHEK: normal epidermal keratinocytes; DHA: docosahexaenoic acid; EPA: eicosapentaenoic acid; LA: linoleic acid; ΔCt : delta cycle threshold; DES1: desaturase 1.

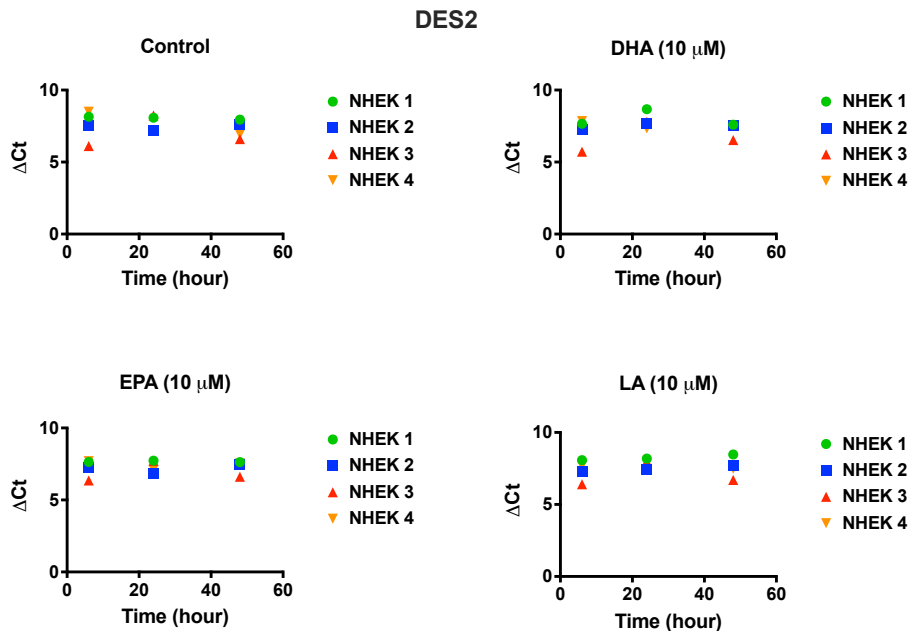


Figure A 5.14 The individual ΔCt values for **DES2** expression in differentiating NHEK. Cells were treated with 10 μM DHA, EPA and LA for six, 24 and 48 hours. NHEK: normal epidermal keratinocytes; DHA: docosahexaenoic acid; EPA: eicosapentaenoic acid; LA: linoleic acid; ΔCt : delta cycle threshold; DES2: desaturase 2.

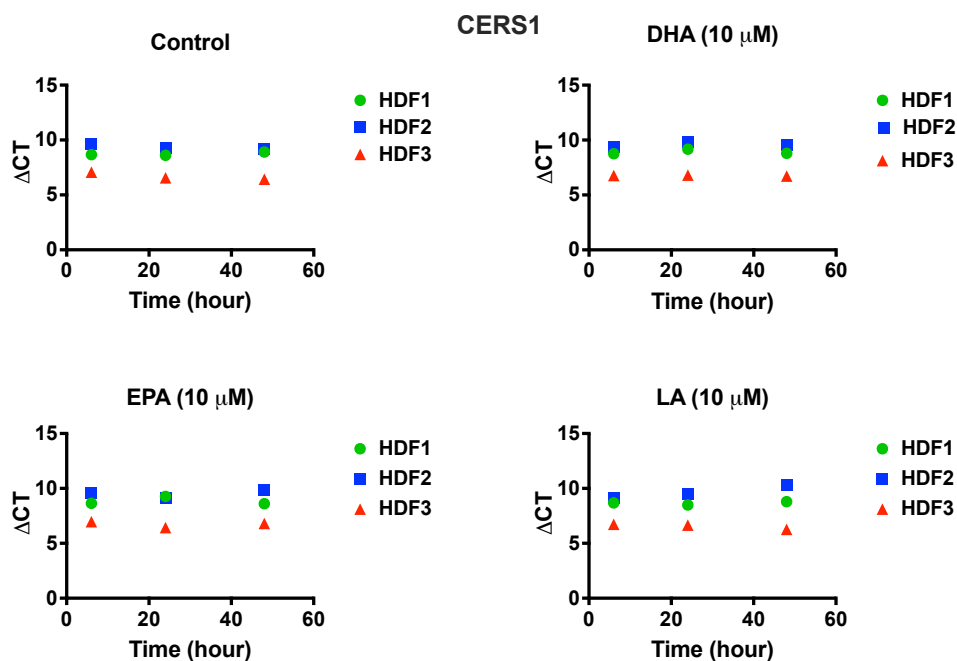


Figure A 5.15 The individual ΔC_t values for CERS1 expression in HDF. Cells were treated with 10 μM DHA, EPA and LA for six, 24 and 48 hours. HDF: human dermal fibroblast; DHA: docosahexaenoic acid; EPA: eicosapentaenoic acid; LA: linoleic acid; ΔC_t : delta cycle threshold; CERS1: ceramide synthase 1.

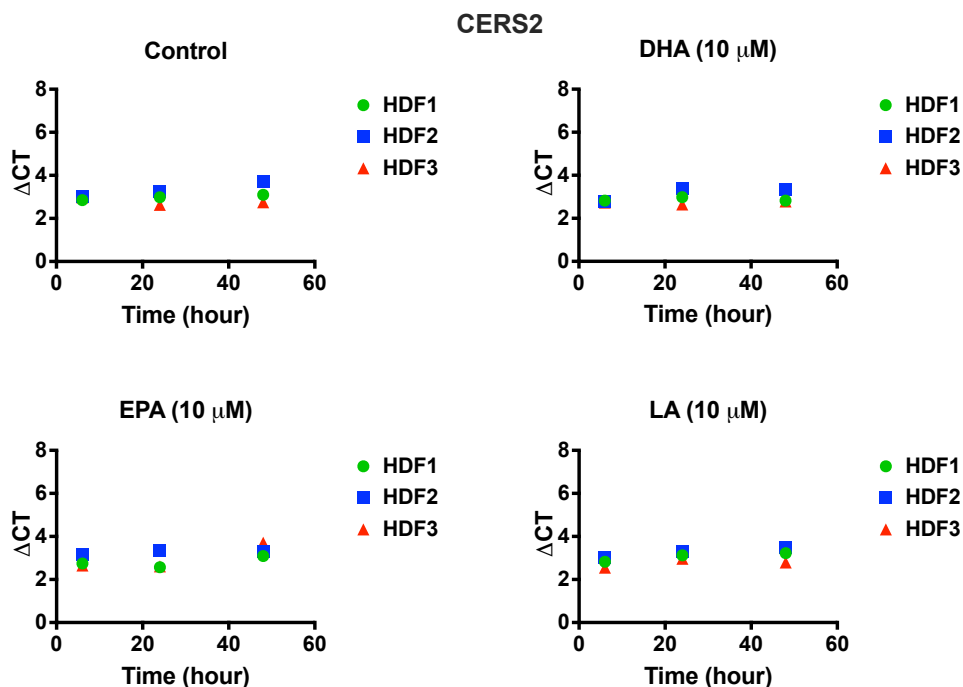


Figure A 5.16 The individual ΔC_t values for CERS2 expression in HDF. Cells were treated with 10 μM DHA, EPA and LA for six, 24 and 48 hours. HDF: human dermal fibroblast; DHA: docosahexaenoic acid; EPA: eicosapentaenoic acid; LA: linoleic acid; ΔC_t : delta cycle threshold; CERS2: ceramide synthase 2.

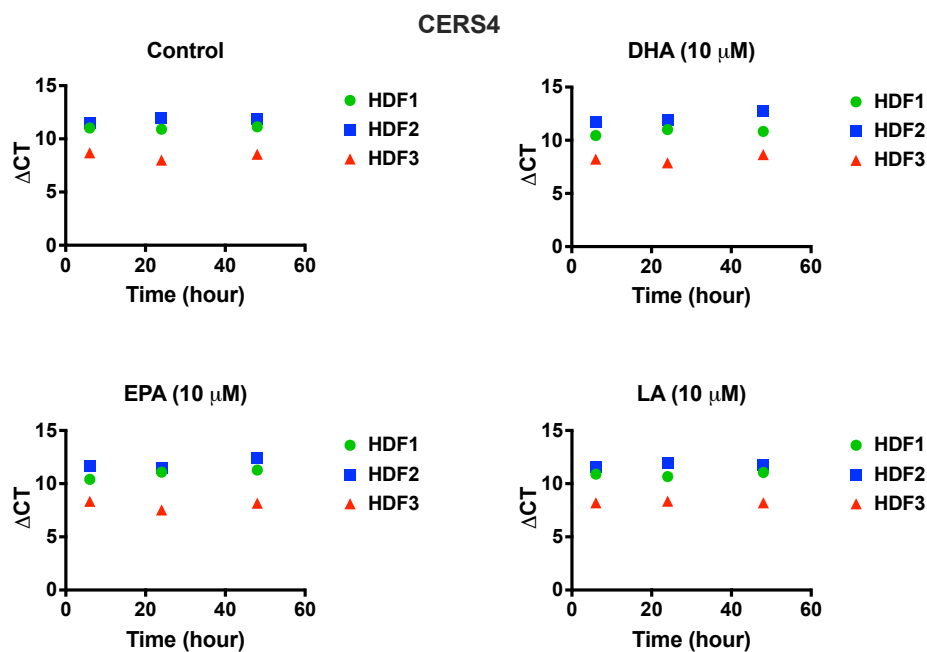


Figure A 5.17 The individual ΔCt values for CERS4 expression in HDF. Cells were treated with 10 μM DHA, EPA and LA for six, 24 and 48 hours. HDF: human dermal fibroblast; DHA: docosahexaenoic acid; EPA: eicosapentaenoic acid; LA: linoleic acid; ΔCt : delta cycle threshold; CERS4: ceramide synthase 4.

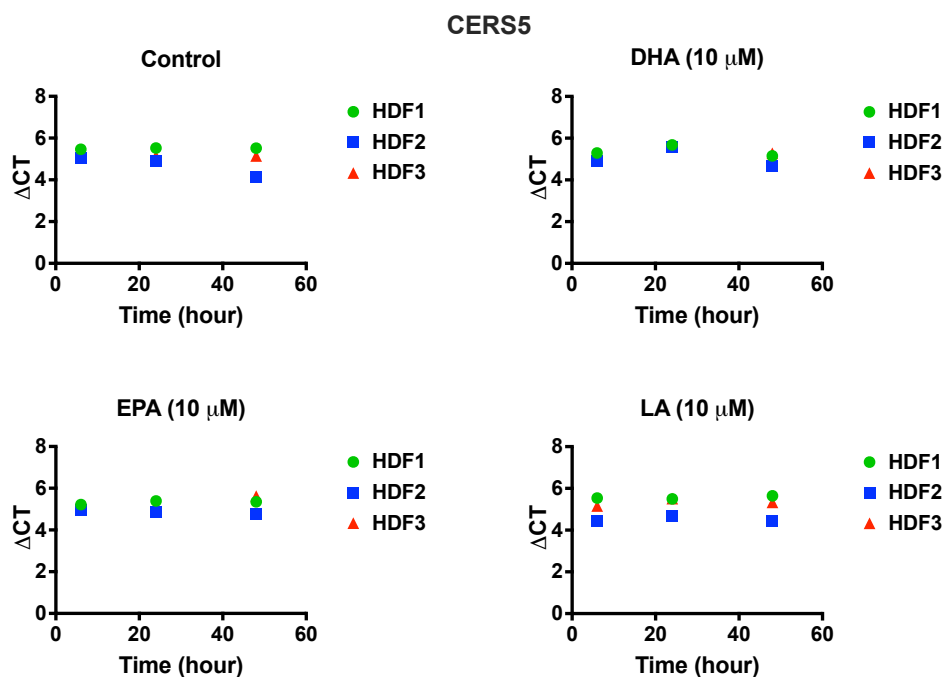


Figure A 5.18 The individual ΔCt values for CERS5 expression in HDF. Cells were treated with 10 μM DHA, EPA and LA for six, 24 and 48 hours. HDF: human dermal fibroblast; DHA: docosahexaenoic acid; EPA: eicosapentaenoic acid; LA: linoleic acid; ΔCt : delta cycle threshold; CERS5: ceramide synthase 5.

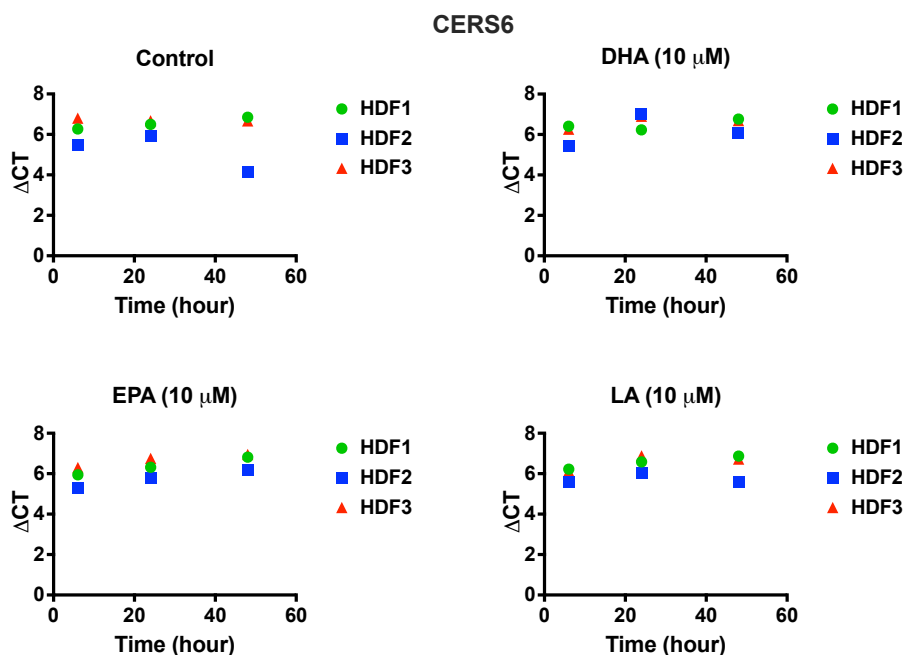


Figure A 5.19 The individual ΔC_t values for CERS6 expression in HDF. Cells were treated with 10 μ M DHA, EPA and LA for six, 24 and 48 hours. HDF: human dermal fibroblast; DHA: docosahexaenoic acid; EPA: eicosapentaenoic acid; LA: linoleic acid; ΔC_t : delta cycle threshold; CERS6: ceramide synthase 6.

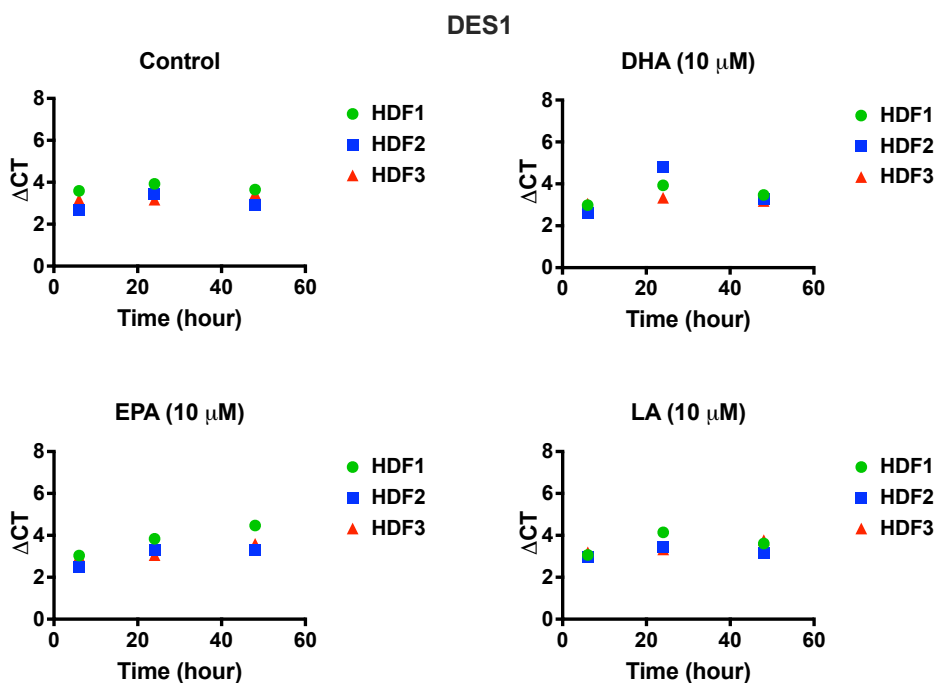


Figure A 5.20 The individual ΔC_t values for DES1 expression in HDF. Cells were treated with 10 μ M DHA, EPA and LA for six, 24 and 48 hours. HDF: human dermal fibroblast; DHA: docosahexaenoic acid; EPA: eicosapentaenoic acid; LA: linoleic acid; ΔC_t : delta cycle threshold; DES1: desaturase 1.

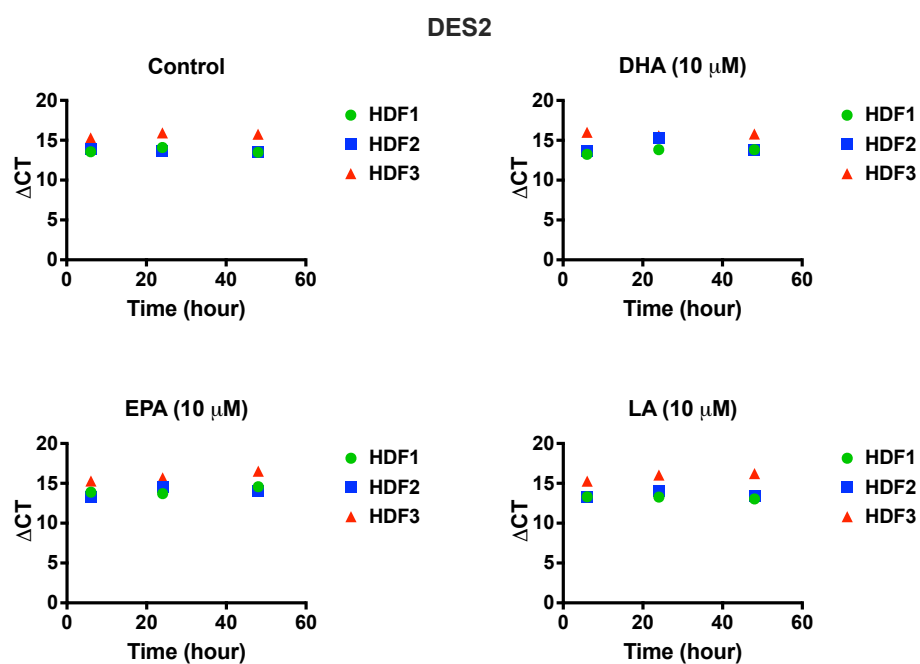
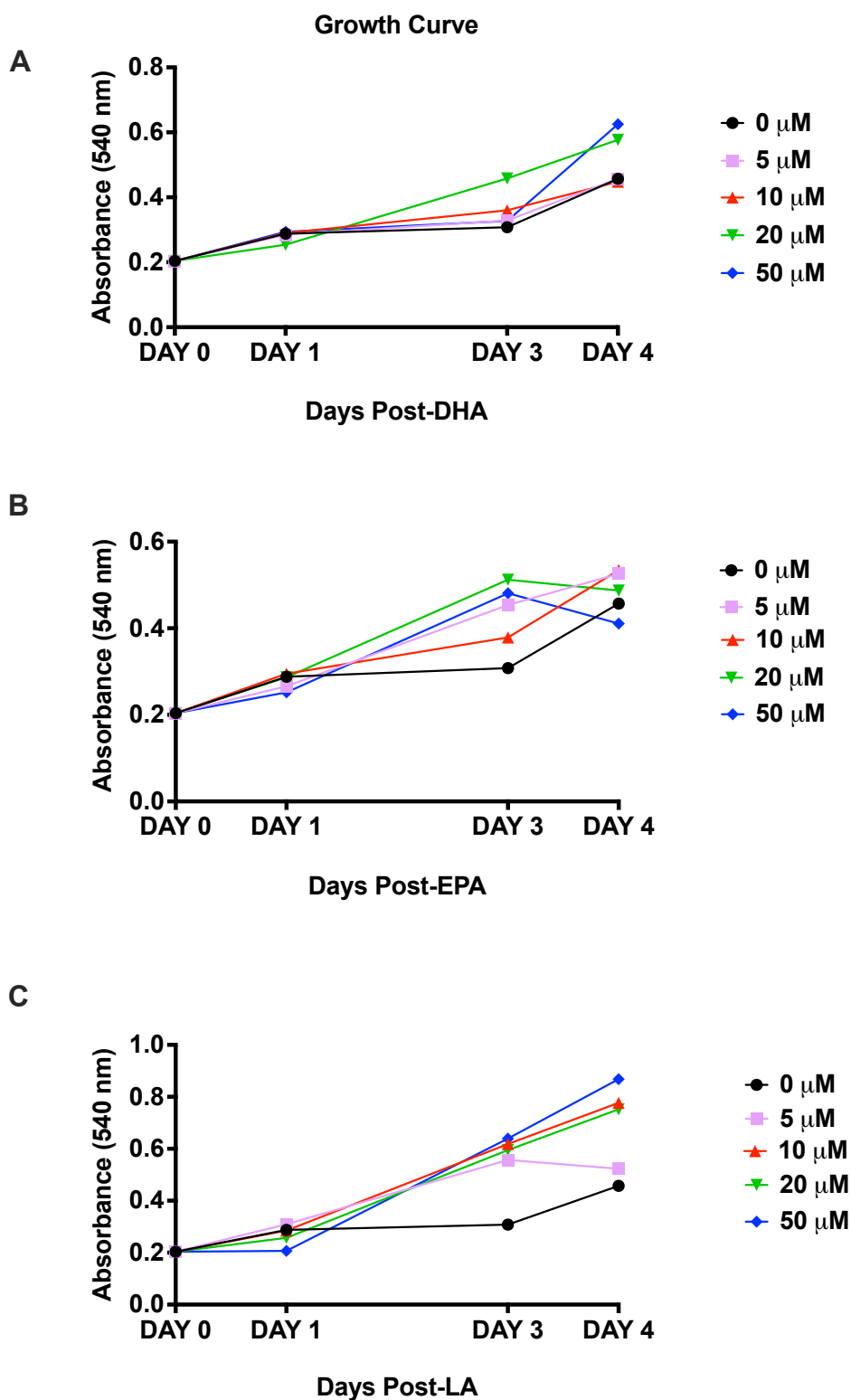


Figure A 5.21 The individual ΔCt values for DES2 expression in HDF. Cells were treated with 10 μM DHA, EPA and LA for six, 24 and 48 hours. HDF: human dermal fibroblast; DHA: docosahexaenoic acid; EPA: eicosapentaenoic acid; LA: linoleic acid; ΔCt : delta cycle threshold; DES2: desaturase 2.

Appendix 6



Appendix 7

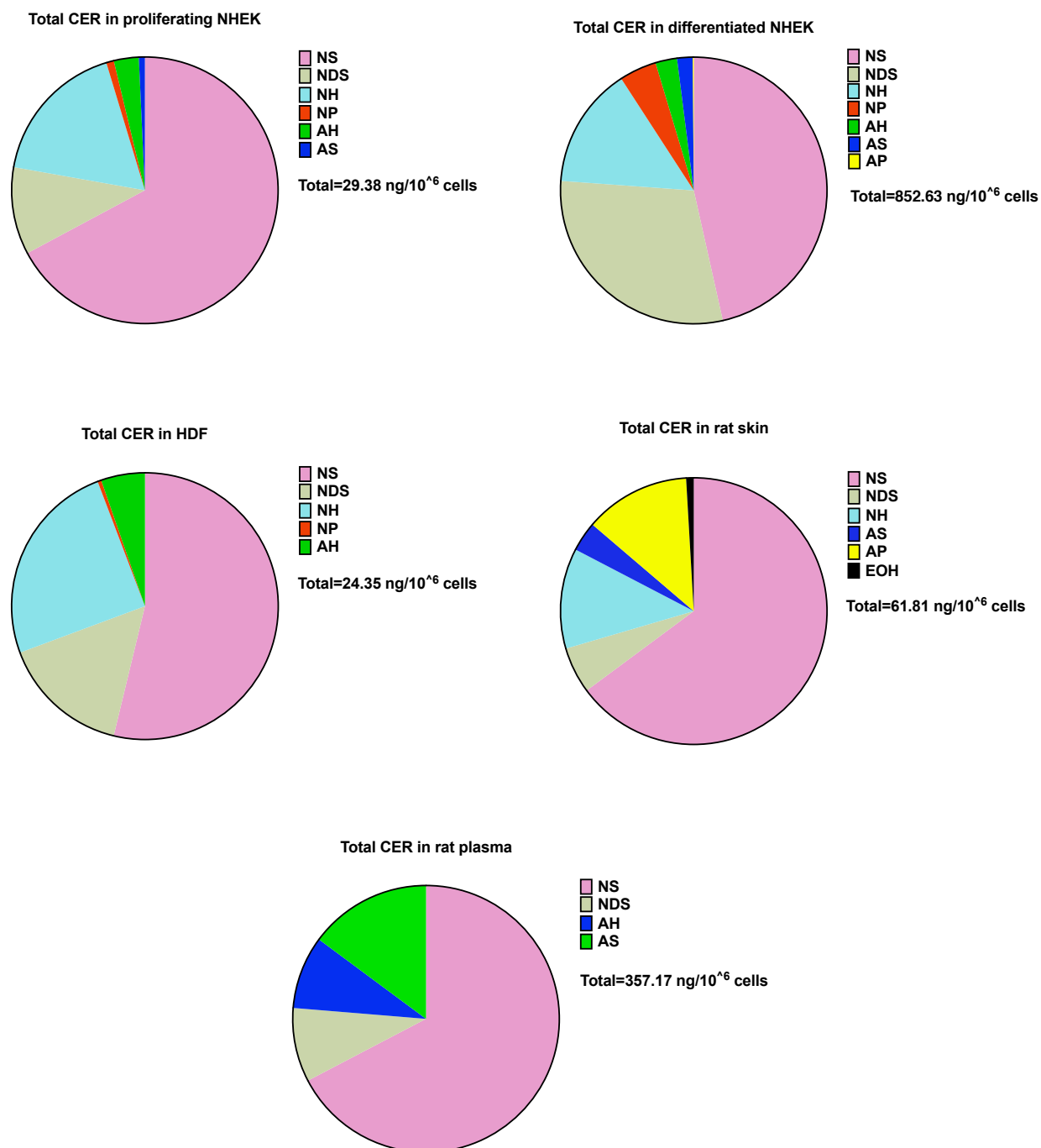
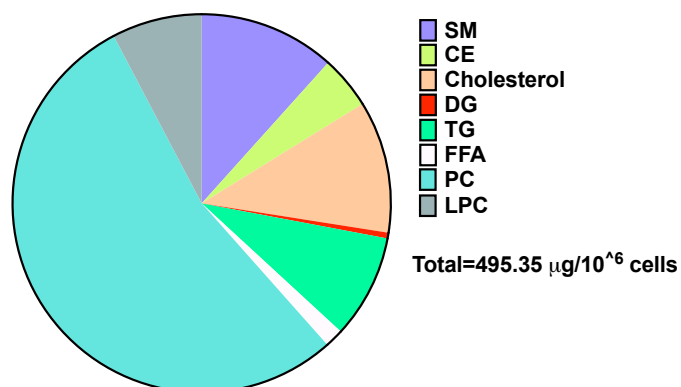
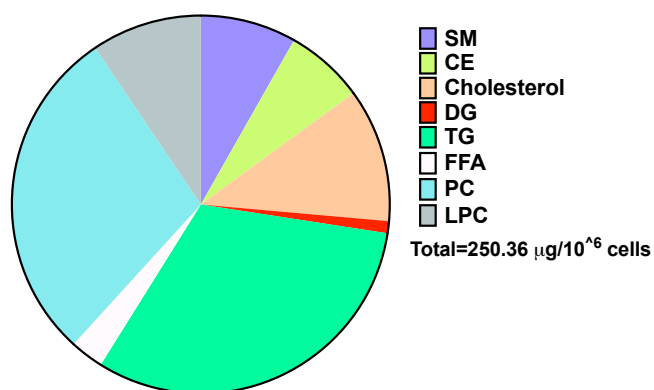


Figure A 7.1 Total CER measured in proliferating and differentiated NHEK, HDF, rat skin and plasma. NHEK: normal human epidermal keratinocyte; HDF: human dermal fibroblast; CER: ceramide; NS: non-hydroxy ceramide; NDS: non-hydroxy dihydroceramide; NH: non-hydroxy 6-hydroxyceramide; NP: non-hydroxy phytoceramide; AH: alpha-hydroxy 6-hydroxyceramide; AS: alpha-hydroxy ceramide; AP: alpha-hydroxy phytoceramide; EOH: ester-linked omega hydroxy 6-hydroxyceramide.

Total membrane lipids in proliferating NHEK



Total membrane lipids in differentiated NHEK



Total membrane lipids in HDF

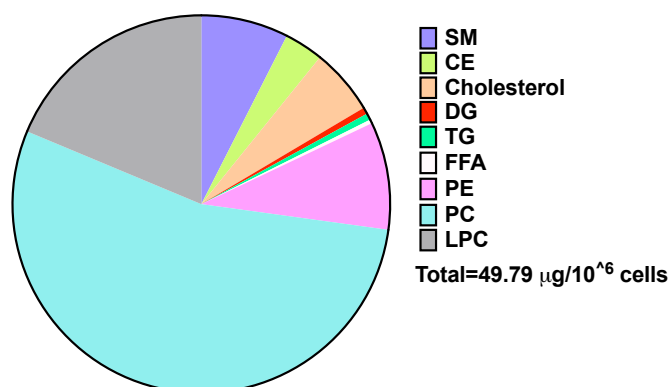


Figure A 7.2 Total membrane lipids measured in proliferating NHEK, differentiated NHEK and HDF. NHEK: normal human epidermal keratinocyte; HDF: human dermal fibroblast; CER: ceramide; SM: sphingomyelin; CE: cholesterol ester; DG: diacylglycerol; TG: triacylglycerol; FFA: free fatty acids; PE: phosphatidylethanolamine; PC: phosphatidylcholine; LPC: lysophosphatidylcholine.

Appendix 8

Table A 8.1 Ceramide species measured in proliferating NHEK (n= 3 individual donors).

Species	Control		DHA		EPA		LA	
	Mean	SD	Mean	SD	Mean	SD	Mean	SD
N(24)S(16)	3.61	2.82	8.14	5.75	3.91	2.06	2.90	1.27
N(22)S(18)	1.40	0.56	3.72	1.74	1.96	0.82	1.71	0.55
N(25)S(16)	0.13	0.12	0.24	0.18	0.11	0.13	0.09	0.05
N(24)S(17)	0.11	0.10	0.25	0.17	0.12	0.07	0.10	0.04
N(23)S(18)	0.09	0.06	0.22	0.06	0.11	0.12	0.09	0.04
N(26)S(16)	1.55	1.38	3.21	2.48	1.71	0.96	1.36	0.54
N(24)S(18)	5.77	3.51	14.65	8.08	7.76	2.66	8.06	2.77
N(26)S(17)	0.13	0.13	0.31	0.18	0.15	0.09	0.14	0.07
N(25)S(18)	0.34	0.28	0.79	0.49	0.44	0.54	0.39	0.25
N(24)S(19)	0.02	0.02	0.06	0.02	0.04	0.01	0.03	0.02
N(28)S(16)	0.12	0.09	0.23	0.14	0.13	0.12	0.13	0.07
N(26)S(18)	5.24	3.44	12.57	6.33	7.30	3.55	7.06	2.37
N(24)S(20)	0.21	0.15	0.61	0.39	0.26	0.21	0.34	0.15
N(27)S(18)	0.06	0.06	0.12	0.09	0.09	0.12	0.07	0.06
N(26)S(19)	0.03	0.03	0.08	0.05	0.06	0.03	0.05	0.03
N(28)S(18)	0.50	0.34	1.17	0.59	0.64	0.64	0.72	0.29
N(26)S(20)	0.29	0.24	0.87	0.52	0.41	0.41	0.44	0.20
N(24)S(22)	0.02	0.02	0.07	0.05	0.04	0.05	0.04	0.03
N(28)S(20)	0.06	0.06	0.12	0.08	0.08	0.11	0.06	0.03
N(26)S(22)	0.03	0.03	0.10	0.06	0.06	0.09	0.05	0.04
N(24)DS(16)	0.30	0.17	0.64	0.42	0.31	0.13	0.34	0.19
N(22)DS(18)	0.37	0.12	0.76	0.19	0.40	0.17	0.48	0.22
N(18)DS(22)	0.34	0.12	0.64	0.22	0.39	0.19	0.38	0.18
N(16)DS(24)	0.16	0.08	0.34	0.20	0.16	0.06	0.46	0.40
N(24)DS(18)	0.83	0.35	1.82	0.71	0.98	0.49	1.30	0.61
N(23)DS(18)	0.02	0.01	0.06	0.01	0.02	0.01	0.02	0.01
N(26)DS(16)	0.11	0.06	0.25	0.13	0.11	0.07	0.15	0.07
N(18)DS(24)	0.37	0.14	0.86	0.30	0.46	0.22	0.63	0.35
N(16)DS(26)	0.05	0.03	0.14	0.06	0.06	0.04	0.07	0.05
N(25)DS(18)	0.03	0.02	0.08	0.03	0.04	0.04	0.04	0.03

N(26)DS(18)	0.35	0.08	1.03	0.18	0.59	0.30	0.66	0.42
N(18)DS(26)	0.18	0.08	0.50	0.11	0.21	0.11	0.28	0.14
N(26)H(14)	0.18	0.07	0.34	0.13	0.19	0.04	0.18	0.06
N(26)H(16)	2.74	0.75	5.21	1.56	3.01	0.68	3.33	1.36
N(24)H(18)	0.16	0.12	0.26	0.11	0.14	0.09	0.13	0.06
N(28)H(16)	2.01	1.03	4.32	2.05	2.22	0.43	2.59	1.27
N(26)H(18)	0.06	0.04	0.10	0.04	0.06	0.04	0.07	0.03
N(24)P(16)	0.10	0.09	0.23	0.21	0.08	0.01	0.13	0.10
N(24)P(18)	0.13	0.09	0.28	0.19	0.10	0.02	0.23	0.20
N(26)P(18)	0.04	0.03	0.10	0.07	0.03	0.01	0.08	0.06
A(25)H(16)	0.26	0.08	0.49	0.07	0.32	0.09	0.32	0.12
A(26)H(16)	0.32	0.05	0.39	0.14	0.33	0.06	0.33	0.13
A(24)H(18)	0.19	0.10	0.32	0.20	0.15	0.01	0.15	0.08
A(26)H(18)	0.12	0.06	0.22	0.14	0.10	0.01	0.13	0.09
A(24)S(16)	0.05	0.05	0.11	0.09	0.04	0.03	0.05	0.03
A(24)S(18)	0.08	0.05	0.19	0.11	0.08	0.08	0.11	0.07
A(26)S(18)	0.08	0.05	0.17	0.11	0.08	0.06	0.11	0.07

Table A 8.2 Ceramide species measured in differentiating NHEK (n= 3 individual donors).

Species	Control		DHA		EPA		LA	
	Mean	SD	Mean	SD	Mean	SD	Mean	SD
N(24)S(16)	44.93	36.49	72.68	53.76	48.47	23.36	50.36	4.08
N(22)S(18)	49.62	42.83	104.69	116.16	58.19	29.02	63.87	23.64
N(25)S(16)	3.08	3.90	4.25	5.03	1.75	0.89	1.91	0.44
N(24)S(17)	5.15	5.79	8.11	8.98	3.96	1.84	4.34	1.61
N(23)S(18)	6.36	7.32	11.45	15.19	4.00	2.35	4.81	2.42
N(22)S(19)	0.05	0.07	0.22	0.22	0.11	0.06	0.16	0.10
N(26)S(16)	17.54	15.03	30.02	22.82	19.84	9.69	21.19	3.14
N(24)S(18)	109.27	81.69	204.70	161.48	132.77	62.01	159.48	54.20
N(22)S(20)	0.93	0.81	2.15	2.45	1.31	0.86	1.46	0.83
N(26)S(17)	4.98	5.97	7.07	7.52	4.42	2.80	4.06	0.70
N(25)S(18)	16.87	20.37	25.94	32.93	11.54	5.49	12.75	4.40
N(24)S(19)	0.76	0.69	1.33	1.36	0.82	0.36	0.96	0.46
N(23)S(20)	0.17	0.19	0.30	0.37	0.14	0.09	0.17	0.09
N(28)S(16)	2.51	2.47	3.85	3.62	2.23	1.04	2.75	0.60

N(26)S(18)	97.54	79.22	189.10	148.89	118.99	53.69	133.87	36.69
N(24)S(20)	9.35	8.17	21.96	21.12	14.18	7.39	15.79	7.39
N(28)S(17)	0.29	0.39	0.37	0.45	0.17	0.09	0.20	0.08
N(27)S(18)	1.73	2.21	2.60	3.35	1.09	0.55	1.14	0.40
N(26)S(19)	0.53	0.51	0.90	0.79	0.68	0.41	0.66	0.28
N(25)S(20)	0.43	0.47	0.68	0.75	0.43	0.24	0.42	0.18
N(28)S(18)	13.93	14.15	23.53	22.54	16.62	8.58	17.71	3.82
N(26)S(20)	6.45	6.27	13.26	11.81	10.63	6.36	9.81	3.96
N(24)S(22)	0.76	0.74	1.87	1.92	1.07	0.51	1.13	0.47
N(28)S(19)	0.10	0.11	0.12	0.12	0.08	0.04	0.09	0.03
N(27)S(20)	0.17	0.21	0.21	0.24	0.13	0.08	0.11	0.04
N(28)S(20)	1.63	1.87	2.28	2.05	1.92	1.25	1.78	0.63
N(26)S(22)	0.74	0.78	1.35	1.07	1.13	0.82	1.03	0.32
N(24)S(24)	0.16	0.17	0.42	0.47	0.19	0.08	0.25	0.12
N(28)S(22)	0.27	0.31	0.43	0.39	0.26	0.18	0.26	0.07
N(24)S(26)	0.11	0.11	0.49	0.68	0.14	0.07	0.16	0.09
N(28)S(24)	0.04	0.04	0.18	0.26	0.03	0.01	0.04	0.02
N(24)DS(16)	19.94	13.75	35.86	24.21	21.02	6.07	29.68	19.05
N(22)DS(18)	31.56	22.86	61.77	47.87	36.29	18.24	52.55	33.52
N(20)DS(20)	1.97	1.56	3.51	2.90	2.42	1.59	3.56	2.83
N(18)DS(22)	24.75	18.10	47.92	37.59	28.19	13.90	40.56	26.40
N(16)DS(24)	13.68	9.50	24.58	16.60	14.08	4.11	21.28	14.39
N(25)DS(16)	0.44	0.35	0.85	0.87	0.34	0.06	0.51	0.33
N(24)DS(17)	1.52	1.22	2.55	2.24	1.31	0.42	2.10	1.53
N(23)DS(18)	1.95	1.44	3.67	3.89	1.68	0.68	2.50	1.87
N(22)DS(19)	0.12	0.10	0.23	0.15	0.14	0.05	0.20	0.17
N(26)DS(16)	7.04	5.24	13.67	9.42	7.69	2.01	11.38	7.78
N(24)DS(18)	50.76	37.51	100.47	72.75	60.56	17.11	87.94	57.74
N(20)DS(22)	0.97	0.77	1.75	1.44	1.23	0.83	2.06	1.74
N(18)DS(24)	31.54	23.58	63.54	48.01	38.44	12.79	56.61	39.95
N(16)DS(26)	4.16	3.11	8.22	5.84	4.73	1.31	7.27	5.44
N(26)DS(17)	0.74	0.59	1.15	1.00	0.71	0.32	0.91	0.64
N(25)DS(18)	2.53	1.92	4.86	4.57	2.43	0.70	3.33	2.38
N(24)DS(19)	0.56	0.41	1.00	0.68	0.68	0.24	0.96	0.74
N(23)DS(20)	0.35	0.28	0.63	0.61	0.41	0.22	0.55	0.41

N(26)DS(18)	16.33	14.33	33.98	23.20	20.82	5.09	31.30	22.94
N(24)DS(20)	7.26	5.94	13.42	10.25	9.21	4.63	15.22	13.02
N(22)DS(22)	0.37	0.29	0.53	0.29	0.46	0.26	0.75	0.55
N(20)DS(24)	5.14	4.17	9.54	7.58	6.49	3.37	10.73	9.32
N(18)DS(26)	10.59	8.11	21.12	15.08	12.53	3.22	18.98	13.87
N(27)DS(18)	0.13	0.11	0.23	0.25	0.10	0.01	0.19	0.15
N(26)DS(19)	0.08	0.06	0.17	0.09	0.10	0.04	0.19	0.14
N(25)DS(20)	0.29	0.25	0.49	0.43	0.26	0.16	0.45	0.39
N(24)DS(21)	0.06	0.07	0.14	0.10	0.09	0.06	0.09	0.08
N(28)DS(18)	2.59	2.01	4.28	3.41	2.39	0.60	3.81	2.76
N(26)DS(20)	4.90	3.84	8.36	6.45	5.90	2.41	9.45	7.47
N(24)DS(22)	2.66	2.04	4.15	2.76	3.08	0.97	4.30	3.00
N(22)DS(24)	1.97	1.53	3.21	2.23	2.38	0.88	3.28	2.40
N(20)DS(26)	3.05	2.44	5.24	4.08	3.64	1.48	5.69	4.52
N(27)DS(20)	0.04	0.04	0.04	0.05	0.03	0.01	0.06	0.04
N(28)DS(20)	0.37	0.31	0.55	0.39	0.43	0.24	0.69	0.64
N(26)DS(22)	0.98	0.72	1.35	0.82	1.01	0.36	1.56	1.26
N(22)DS(26)	0.60	0.45	0.96	0.50	0.66	0.21	1.05	0.86
N(24)DS(24)	0.71	0.54	0.87	0.50	0.78	0.28	1.20	0.93
N(26)DS(26)	0.05	0.04	0.06	0.01	0.08	0.04	0.49	0.73
N(24)H(16)	17.06	15.06	25.03	22.37	16.65	7.16	18.71	9.08
N(26)H(14)	4.01	3.36	7.94	9.00	4.98	4.24	6.31	4.50
N(25)H(16)	1.40	0.91	2.35	1.58	0.71	0.56	0.89	0.63
N(26)H(16)	67.31	52.37	106.94	96.95	75.45	45.58	87.57	46.59
N(24)H(18)	1.77	1.84	2.09	1.91	1.36	0.52	1.44	0.96
N(28)H(16)	30.79	24.57	49.95	43.22	35.54	14.64	39.79	20.61
N(26)H(18)	1.32	1.15	1.64	1.33	1.05	0.38	1.03	0.58
N(28)H(17)	0.19	0.17	0.30	0.28	0.22	0.10	0.26	0.17
N(30)H(19)	1.46	1.22	2.41	2.04	2.13	0.99	2.31	1.60
N(24)P(16)	5.42	4.80	11.44	6.63	7.88	5.02	7.83	4.84
N(24)P(17)	0.67	0.68	0.91	0.62	0.76	0.55	0.63	0.39
N(26)P(16)	2.51	2.11	5.16	2.77	3.45	2.02	3.65	2.10
N(24)P(18)	18.10	14.84	35.43	20.33	25.33	11.75	27.54	15.18
N(26)P(17)	0.22	0.21	0.24	0.17	0.21	0.14	0.19	0.12
N(25)P(18)	0.68	0.63	1.24	0.90	0.66	0.40	0.91	0.71

N(28)P(16)	0.69	0.67	1.07	0.69	0.72	0.50	0.83	0.56
N(26)P(18)	6.00	5.21	11.87	7.42	8.39	5.27	8.81	5.51
N(24)P(20)	1.15	1.02	2.01	1.40	1.61	0.91	1.69	1.02
N(25)P(20)	0.15	0.17	0.23	0.14	0.26	0.18	0.16	0.08
N(28)P(18)	0.80	0.75	1.12	0.72	0.86	0.57	0.98	0.56
N(26)P(20)	0.84	0.74	1.39	0.79	1.08	0.83	1.15	0.74
N(24)P(22)	0.51	0.47	0.86	0.31	0.86	0.75	0.71	0.26
N(28)P(20)	0.20	0.20	0.20	0.08	0.22	0.21	0.16	0.09
N(26)P(22)	0.57	0.57	0.79	0.30	1.00	0.85	0.69	0.25
N(24)P(24)	0.12	0.13	0.15	0.07	0.17	0.14	0.14	0.06
A(22)H(16)	2.55	1.96	3.02	1.95	2.62	2.17	2.80	1.68
A(28)H(14)	0.88	1.01	0.82	0.72	0.49	0.19	0.68	0.50
A(26)H(16)	9.11	5.83	11.31	5.65	9.51	8.11	9.96	5.36
A(24)H(18)	0.78	0.72	1.31	0.92	0.87	0.46	0.89	0.64
A(28)H(16)	2.65	2.78	3.32	3.10	2.01	1.17	2.85	2.08
A(26)H(18)	0.53	0.40	0.78	0.30	0.92	0.72	0.52	0.16
A(24)H(20)	0.12	0.04	0.12	0.05	0.19	0.15	0.08	0.03
A(28)H(18)	0.20	0.15	0.27	0.15	0.25	0.15	0.20	0.12
A(26)H(20)	0.06	0.02	0.13	0.05	0.20	0.17	0.07	0.03
A(30)H(18)	5.31	4.40	7.62	5.64	5.46	2.84	6.76	5.09
A(28)H(20)	0.08	0.05	0.14	0.06	0.14	0.10	0.09	0.05
A(26)H(22)	0.06	0.05	0.10	0.03	0.11	0.10	0.06	0.03
A(24)S(16)	1.52	1.68	1.57	1.66	0.97	0.37	1.31	0.87
A(25)S(16)	0.34	0.36	0.37	0.31	0.24	0.16	0.27	0.10
A(24)S(17)	0.16	0.20	0.16	0.11	0.05	0.02	0.06	0.03
A(23)S(18)	0.44	0.39	0.65	0.58	0.40	0.22	0.42	0.16
A(26)S(16)	0.72	0.82	0.74	0.72	0.46	0.17	0.61	0.31
A(24)S(18)	6.13	5.59	9.64	6.78	4.42	2.33	6.38	4.21
A(27)S(16)	0.07	0.07	0.09	0.08	0.06	0.05	0.07	0.03
A(26)S(18)	5.71	5.91	6.91	7.70	4.23	1.63	5.65	3.27
A(24)S(20)	0.42	0.37	0.67	0.43	0.33	0.19	0.50	0.35
A(27)S(18)	0.23	0.20	0.32	0.30	0.18	0.08	0.26	0.12
A(26)S(20)	0.32	0.31	0.48	0.33	0.26	0.11	0.39	0.25
A(24)S(22)	0.04	0.04	0.08	0.04	0.04	0.02	0.04	0.02
A(26)S(22)	0.04	0.04	0.09	0.06	0.04	0.03	0.04	0.01

A(24)P(16)	0.16	0.20	0.18	0.17	0.18	0.14	0.13	0.09
A(24)P(17)	0.04	0.05	0.04	0.04	0.15	0.17	0.04	0.02
A(24)P(18)	0.52	0.51	0.56	0.49	0.73	0.69	0.50	0.31
A(24)P(20)	0.11	0.10	0.11	0.06	0.20	0.23	0.09	0.03
A(26)P(20)	0.06	0.05	0.08	0.03	0.14	0.18	0.06	0.04
A(24)P(22)	0.09	0.07	0.13	0.06	0.27	0.35	0.10	0.04

Table A 8.3 Ceramide species measured in HDF (n= 3 individual donors).

Species	Control		DHA		EPA		LA	
	Mean	SD	Mean	SD	Mean	SD	Mean	SD
N(24)S(16)	0.37	0.10	0.55	0.07	0.68	0.56	0.61	0.26
N(22)S(18)	3.70	1.25	5.71	0.59	6.25	4.22	7.31	2.24
N(24)S(17)	0.33	0.10	0.51	0.10	0.59	0.51	0.58	0.22
N(23)S(18)	1.12	0.47	1.74	0.32	1.94	1.54	2.15	0.77
N(24)S(18)	7.03	1.97	10.56	1.14	10.75	8.01	10.23	2.74
N(25)S(18)	0.28	0.12	0.41	0.09	0.57	0.52	0.49	0.22
N(24)S(19)	0.12	0.05	0.19	0.05	0.23	0.20	0.21	0.10
N(26)S(18)	0.17	0.06	0.25	0.01	0.39	0.40	0.24	0.10
N(24)DS(16)	0.10	0.06	0.20	0.13	0.22	0.10	0.21	0.11
N(22)DS(18)	1.16	0.82	2.54	1.56	2.42	0.66	2.82	1.46
N(18)DS(22)	0.79	0.53	1.76	1.04	1.73	0.32	2.00	0.99
N(24)DS(17)	0.04	0.03	0.12	0.10	0.14	0.04	0.13	0.08
N(23)DS(18)	0.19	0.22	0.38	0.43	0.46	0.22	0.56	0.40
N(24)DS(18)	0.98	0.84	1.95	1.51	1.77	0.52	1.72	1.26
N(18)DS(24)	0.49	0.45	0.98	0.90	0.92	0.32	0.95	0.72
N(26)DS(18)	0.04	0.03	0.08	0.08	0.10	0.04	0.04	0.02
N(25)H(16)	0.38	0.01	0.56	0.09	0.57	0.03	0.61	0.13
N(26)H(16)	5.37	0.75	7.51	1.94	6.93	0.88	7.83	0.68
N(24)H(18)	0.16	0.02	0.26	0.05	0.29	0.13	0.20	0.02
N(28)H(16)	0.16	0.02	0.23	0.08	0.21	0.06	0.13	0.10
N(24)P(18)	0.09	0.12	0.16	0.22	0.29	0.44	0.07	0.09
N(26)P(18)	0.02	0.01	0.02	0.01	0.04	0.03	0.02	0.00
A(26)H(16)	1.23	1.15	1.84	1.67	1.72	1.84	1.57	1.51
A(24)H(18)	0.05	0.02	0.07	0.02	0.10	0.09	0.05	0.01
A(26)H(18)	0.02	0.01	0.03	0.02	0.04	0.03	0.04	0.03

Table A 8.4 Ceramide species measured in rat skin (n=6 individual donors).

Species	Control		Diabetic	
	Mean	SD	Mean	SD
N(24)S(16)	2.74	1.32	2.52	1.24
N(22)S(18)	8.84	2.04	10.05	0.99
N(25)S(16)	0.19	0.08	0.19	0.10
N(24)S(17)	1.00	0.38	0.92	0.34
N(23)S(18)	2.74	1.17	3.76	1.40
N(26)S(16)	0.83	0.41	0.74	0.37
N(24)S(18)	17.09	6.56	22.00	8.46
N(22)S(20)	0.15	0.05	0.28	0.16
N(26)S(17)	0.18	0.09	0.15	0.07
N(25)S(18)	1.72	0.97	1.93	1.00
N(24)S(19)	0.20	0.11	0.17	0.08
N(26)S(18)	3.87	2.51	3.55	1.85
N(24)S(20)	0.34	0.20	0.49	0.39
N(28)S(18)	0.20	0.14	0.23	0.12
N(24)DS(16)	0.21	0.12	0.20	0.13
N(22)DS(18)	0.71	0.46	1.25	0.51
N(18)DS(22)	0.59	0.40	1.06	0.45
N(16)DS(24)	0.17	0.09	0.16	0.10
N(24)DS(18)	0.97	0.46	1.73	0.96
N(18)DS(24)	0.69	0.32	1.21	0.66
N(25)H(16)	0.24	0.08	0.18	0.02
N(24)H(17)	0.17	0.07	0.07	0.01
N(23)H(18)	0.12	0.01	0.07	0.01
N(26)H(16)	2.11	2.38	1.23	0.69
N(24)H(18)	3.23	1.24	1.60	0.34
N(25)H(18)	0.15	0.04	0.08	0.01
N(28)H(16)	0.17	0.12	0.21	0.14
N(26)H(18)	0.99	0.37	0.51	0.09
N(28)H(18)	0.24	0.11	0.16	0.06
N(30)H(19)	0.12	0.06	0.12	0.04
A(24)S(16)	0.29	0.16	0.15	0.10

A(23)S(18)	0.68	0.18	0.74	0.23
A(24)S(18)	1.11	0.48	1.30	0.81
A(26)S(18)	0.15	0.08	0.21	0.17
A(22)P(16)	0.10	0.04	0.12	0.05
A(24)P(16)	1.10	0.49	0.73	0.35
A(22)P(18)	0.97	0.31	1.24	0.29
A(24)P(17)	0.15	0.08	0.19	0.05
A(26)P(16)	0.20	0.05	0.17	0.06
A(24)P(18)	4.70	0.44	4.02	0.78
A(22)P(20)	0.11	0.04	0.16	0.03
A(25)P(18)	0.14	0.03	0.15	0.04
A(26)P(18)	0.36	0.17	0.48	0.18
A(24)P(20)	0.12	0.05	0.23	0.10
E(18:2)O(30)H(18)	0.29	0.14	0.15	0.06
E(18:2)O(32)H(18)	0.28	0.14	0.22	0.08

Species	Control		Diabetic	
	Mean	SD	Mean	SD
N16 S18	39.34	11.65	59.71	53.74
N18 S18	5.56	4.18	4.29	2.72
N20 S18	5.74	4.68	6.49	4.93
N22 S18	36.42	32.34	45.71	26.12
N24 S17	1.95	1.59	2.38	1.68
N23 S18	32.29	31.75	38.55	25.96
N24 S18	115.07	111.05	131.51	87.10
N26 S18	4.13	5.30	3.92	2.83
N22 DS18	6.87	8.38	14.35	10.30
N24 DS18	14.85	19.34	28.62	26.18
N18 DS24	7.87	10.50	17.09	16.04
N25 DS18	3.61	3.93	3.34	3.12
A18 S18	11.31	6.10	16.75	14.58
A20 S18	35.34	26.32	35.51	27.22
A22 S18	6.38	5.16	8.41	4.69
A24 H17	2.32	1.60	3.60	1.63
A26 H26	24.97	11.05	32.85	12.04
A25 H18	4.31	3.14	6.36	4.23

Table A 8.5 Ceramides measured in rat plasma (n= 6 individual donors).

Appendix 9

Table A 9.1 Membrane lipids measured in proliferating NHEK (n= 3 individual donors).

Species	Control		DHA		EPA		LA	
	Mean	SD	Mean	SD	Mean	SD	Mean	SD
CE 16:1	3.58	1.77	1.93	1.25	1.35	0.18	2.09	0.92
CE 18:1	2.75	0.95	1.11	0.50	0.80	0.16	1.51	0.48
CE 18:2	0.40	0.34	0.56	0.78	2.04	1.36	0.27	0.13
CE 20:5	0.44	0.56	0.84	1.15	2.72	1.16	0.41	0.19
CE 22:5	6.10	3.32	3.03	0.52	2.67	0.55	0.04	0.00
DG 34:2	0.05	0.03	0.03	0.02	3.49	0.76	0.04	0.01

DG 35:1	0.06	0.02	0.04	0.01	0.03	0.01	0.03	0.01
DG 36:2	0.05	0.04	0.03	0.02	0.03	0.01	0.79	0.23
DG 37:4	1.15	0.50	0.63	0.12	0.02	0.01	0.09	0.04
DG 38:3	0.13	0.07	0.07	0.02	0.58	0.16	2.65	0.87
LPC 16:0	4.53	1.75	2.21	0.99	0.06	0.02	0.68	0.31
LPC 16:1	1.55	0.46	0.60	0.28	2.15	0.30	0.39	0.18
LPC 18:0	0.54	0.30	0.34	0.23	0.52	0.13	5.74	1.12
LPC 18:1	11.27	5.96	4.98	1.98	0.26	0.12	3.12	0.85
LPC 24:1	4.67	2.23	2.62	0.30	4.43	0.43	0.65	0.22
PC 28:0	0.89	0.45	0.55	0.24	2.46	0.55	5.56	1.79
PC 30:0	6.74	2.97	4.57	1.78	0.47	0.13	0.32	0.18
PC 30:0e	0.37	0.21	0.19	0.10	4.23	0.94	0.03	0.02
PC 30:0p/PC 30:1e	0.04	0.03	0.02	0.01	0.14	0.08	2.17	0.69
PC 30:1	3.35	1.49	1.99	0.72	0.01	0.01	1.76	0.96
PC 32:0p/PC 32:1e	2.24	1.15	1.04	0.52	1.72	0.31	18.81	5.48
PC 32:1	26.00	10.16	16.91	5.76	0.80	0.45	0.09	0.03
PC 32:1p/PC 32:2e	0.13	0.05	0.07	0.03	15.44	2.78	3.99	0.94
PC 32:2	6.50	2.76	3.98	1.49	0.05	0.02	0.14	0.04
PC 32:3	0.18	0.10	0.12	0.05	3.36	0.35	1.57	0.81
PC 33:1/34:0p/34:1e	2.11	0.91	1.07	0.43	0.11	0.03	0.52	0.17
PC 33:2/34:1p/34:2e	0.65	0.24	0.37	0.12	0.82	0.40	24.67	7.02
PC 34:1	35.75	13.53	22.63	7.34	0.29	0.05	17.98	3.82
PC 34:2	29.12	12.80	16.92	6.33	19.47	4.14	0.13	0.03
PC 34:3	0.13	0.05	0.09	0.04	13.60	2.08	0.10	0.07
PC 34:3p/PC 34:4e	0.13	0.09	0.05	0.04	0.10	0.02	0.56	0.11
PC 34:4	0.67	0.30	0.49	0.25	0.04	0.04	0.10	0.02
PC 34:5	0.17	0.09	0.13	0.07	0.54	0.09	0.43	0.08
PC 35:2/36:1p/36:2e	0.67	0.24	0.33	0.10	0.18	0.03	0.09	0.06
PC 35:4/36:3p/36:4e	0.13	0.07	0.06	0.03	0.26	0.03	22.10	2.84

PC 36:2/38:8p/38:9 e	36.90	17.82	21.21	8.13	0.05	0.04	0.72	0.16
PC 36:5	0.97	0.42	0.75	0.42	16.29	1.65	1.14	0.19
PC 38:2/40:8p/30:9 e	1.86	0.96	1.13	0.48	1.16	0.29	1.52	0.44
PC 40:3/42:9p/42:1 0e	0.08	0.04	0.04	0.01	0.04	0.00	0.07	0.03
PC 42:2/44:8p/44:9 e	0.07	0.01	0.05	0.02	0.03	0.01	0.06	0.03
PC 44:2/46:8p/46:9 e	0.06	0.01	0.04	0.02	0.05	0.01	0.02	0.01
PC 46:3/48:9p	0.03	0.02	0.01	0.01	0.05	0.01	0.02	0.01
PC 46:5p/46:6e	0.03	0.02	0.02	0.01	0.01	0.00	5.14	3.83
SM 32:1	1.19	0.56	0.69	0.26	0.27	0.12	0.04	0.01
SM 33:2	0.06	0.04	0.03	0.01	0.54	0.07	10.77	3.02
SM 34:1	16.44	8.74	9.78	4.60	0.03	0.01	0.12	0.03
SM 34:2	0.21	0.12	0.11	0.05	7.82	1.46	0.15	0.01
SM 36:1	0.23	0.08	0.14	0.05	0.09	0.02	0.03	0.01
SM 38:3	0.04	0.02	0.02	0.00	0.12	0.02	0.73	0.17
SM 40:1	1.02	0.26	0.66	0.13	0.02	0.01	0.41	0.05
SM 40:2	0.65	0.16	0.36	0.07	0.55	0.12	0.01	0.01
SM 41:1	0.03	0.03	0.02	0.02	0.28	0.05	0.03	0.01
SM 41:2	0.05	0.03	0.03	0.01	0.01	0.01	5.70	1.34
SM 42:2	7.66	1.88	5.14	1.31	0.02	0.01	0.38	0.08
SM 42:3	0.43	0.14	0.27	0.08	4.16	0.72	0.04	0.01
SM 42:4	0.05	0.02	0.03	0.01	0.20	0.04	0.07	0.01
SM 42:5	0.10	0.03	0.06	0.02	0.03	0.01	0.03	0.02
SM 43:1	0.06	0.04	0.04	0.03	0.04	0.01	0.07	0.02
SM 43:2	0.10	0.07	0.06	0.04	0.03	0.02	2.78	0.39
SM 44:2	3.73	1.35	2.77	1.06	0.04	0.03	0.35	0.04
SM 44:3	0.46	0.18	0.32	0.11	2.19	0.40	0.07	0.01
SM 44:4	0.12	0.03	0.08	0.01	0.25	0.03	0.45	0.13
SM 44:5	0.58	0.16	0.38	0.10	0.06	0.01	0.40	0.08
SM 46:2	0.54	0.29	0.33	0.14	0.33	0.07	0.07	0.01
SM 46:3	0.09	0.05	0.05	0.03	0.24	0.03	0.06	0.01

SM 46:4	0.07	0.03	0.06	0.02	0.04	0.00	0.15	0.03
SM 46:5	0.21	0.08	0.15	0.06	0.05	0.02	0.02	0.01
TG 42:1	0.03	0.02	0.02	0.01	0.12	0.02	0.18	0.11
TG 44:1	0.27	0.11	0.18	0.07	0.01	0.01	0.07	0.03
TG 44:2	0.11	0.03	0.07	0.02	0.12	0.04	0.60	0.35
TG 46:1	0.87	0.27	0.59	0.14	0.05	0.01	0.33	0.14
TG 46:2	0.56	0.12	0.37	0.07	0.41	0.12	0.08	0.02
TG 46:3	0.13	0.03	0.08	0.02	0.25	0.04	0.03	0.02
TG 47:1	0.04	0.01	0.02	0.01	0.06	0.01	0.02	0.01
TG 47:2	0.03	0.01	0.01	0.01	0.01	0.00	2.01	0.98
TG 48:2	3.04	0.64	2.01	0.33	0.01	0.00	0.36	0.11
TG 48:3	0.55	0.11	0.35	0.08	1.43	0.32	0.05	0.01
TG 48:4	0.06	0.02	0.04	0.02	0.25	0.04	0.06	0.03
TG 49:2	0.10	0.02	0.05	0.01	0.04	0.01	0.02	0.01
TG 49:3	0.03	0.01	0.02	0.01	0.03	0.01	2.48	1.18
TG 50:2	3.63	0.55	2.40	0.34	0.01	0.00	1.11	0.35
TG 50:3	1.66	0.33	1.05	0.22	1.70	0.48	0.22	0.06
TG 50:4	0.23	0.07	0.15	0.05	0.74	0.14	0.03	0.01
TG 50:5	0.03	0.01	0.03	0.03	0.14	0.03	0.03	0.01
TG 51:3	0.04	0.02	0.02	0.01	0.06	0.03	3.80	1.43
TG 52:3	6.15	1.48	3.78	0.57	0.02	0.01	0.04	0.03
TG 53:2	0.02	0.01	0.08	0.11	2.77	0.61	0.04	0.01
TG 53:3	0.07	0.03	0.04	0.01	0.11	0.09	0.02	0.01
TG 53:4	0.03	0.01	0.02	0.01	0.03	0.00	2.73	0.88
TG 54:3	4.96	1.62	2.86	0.62	0.01	0.00	1.43	0.42
TG 54:4	1.33	0.44	0.73	0.20	1.96	0.43	0.53	0.26
TG 54:5	0.27	0.09	0.20	0.13	0.47	0.08	0.14	0.09
TG 54:6	0.05	0.02	0.09	0.10	0.21	0.10	0.02	0.02
TG 55:2	0.01	0.01	0.09	0.13	0.20	0.14	0.51	0.21
TG 56:3	0.90	0.27	0.56	0.15	0.06	0.05	0.38	0.09
TG 56:4	0.51	0.15	0.29	0.08	0.36	0.07	0.27	0.07
TG 56:5	0.23	0.07	0.14	0.06	0.17	0.02	0.12	0.06
TG 56:6	0.07	0.03	0.09	0.09	0.11	0.03	0.05	0.02
TG 56:7	0.02	0.02	0.10	0.13	0.15	0.10	0.36	0.16
FFA 16:0	0.49	0.18	0.28	0.06	0.15	0.11	0.10	0.02

FFA 16:1	0.14	0.10	0.09	0.04	0.28	0.04	1.73	0.11
FFA 18:1	2.83	1.54	1.63	0.65	0.07	0.01	0.16	0.02
FFA 18:2	0.08	0.05	0.06	0.05	1.12	0.21	0.06	0.02
FFA 20:1	0.07	0.08	0.05	0.05	0.03	0.01	0.18	0.16
FFA 24:0	0.34	0.27	0.15	0.10	0.03	0.02	0.11	0.07
FFA 24:1	0.12	0.04	0.08	0.03	0.13	0.08	0.29	0.23
FFA 26:1	0.35	0.19	0.25	0.14	0.06	0.03	0.09	0.10
FFA 28:1	0.14	0.09	0.08	0.06	0.19	0.11	0.08	0.07

Table A 9.2 Membrane lipids measured in differentiating NHEK (n= 3 individual donors).

Species	Control		DHA		EPA		LA	
	Mean	SD	Mean	SD	Mean	SD	Mean	SD
CE 16:1	3.10	1.15	2.02	0.93	1.23	0.73	1.66	0.53
CE 18:1	2.73	1.54	2.69	1.16	1.16	0.55	1.98	0.28
CE 18:2	0.22	0.28	0.47	0.67	6.23	9.97	0.28	0.09
CE 20:5	0.21	0.22	0.39	0.54	11.13	18.53	0.21	0.17
CE 22:5	12.43	3.93	13.53	5.79	7.02	4.02	14.28	13.21
DG 34:2	0.09	0.06	0.09	0.03	0.08	0.04	0.08	0.03
DG 35:1	0.13	0.10	0.13	0.06	0.12	0.08	0.11	0.05
DG 36:2	0.04	0.02	0.05	0.00	0.04	0.02	0.05	0.01
DG 37:4	2.42	1.60	2.21	0.94	2.26	1.67	1.76	0.66
DG 38:3	0.16	0.06	0.15	0.07	0.16	0.09	0.11	0.02
LPC 16:0	1.46	1.70	2.24	2.52	3.74	4.86	2.37	1.48
LPC 16:1	0.82	1.40	1.45	2.11	1.94	2.79	1.18	1.08
LPC 18:0	0.06	0.08	0.12	0.18	0.70	1.13	0.24	0.10
LPC 18:1	10.95	3.70	14.15	6.60	16.42	9.75	13.46	1.37
LPC 24:1	12.80	9.14	10.85	2.47	11.41	9.96	10.10	5.03
PC 28:0	0.17	0.13	0.20	0.12	0.49	0.61	0.23	0.06
PC 30:0	1.73	1.13	2.02	0.89	4.93	6.01	2.28	0.57
PC 30:0e	0.16	0.13	0.15	0.08	0.30	0.39	0.22	0.06
PC 30:0p/PC 30:1e	0.02	0.02	0.02	0.01	0.04	0.05	0.01	0.01
PC 30:1	1.02	0.70	1.14	0.61	2.32	2.55	1.27	0.31
PC 32:0p/PC 32:1e	1.40	0.95	1.20	0.41	2.08	2.24	1.62	0.36

PC 32:1	11.42	6.19	12.90	4.51	24.62	25.96	13.42	2.19
PC 32:1p/PC 32:2e	0.10	0.04	0.10	0.03	0.13	0.08	0.10	0.02
PC 32:2	2.82	1.60	3.13	1.35	5.98	6.33	3.49	0.58
PC 32:3	0.05	0.04	0.06	0.05	0.12	0.11	0.07	0.02
PC 33:1/34:0p/34:1e	1.55	0.85	1.47	0.51	2.23	2.11	1.78	0.41
PC 33:2/34:1p/34:2e	0.58	0.21	0.58	0.13	0.64	0.37	0.76	0.25
PC 34:1	19.92	8.80	22.42	5.03	34.93	31.66	21.29	3.11
PC 34:2	13.71	5.86	15.01	3.38	23.51	20.78	17.00	2.55
PC 34:3	0.06	0.04	0.08	0.05	0.15	0.12	0.09	0.02
PC 34:3p/PC 34:4e	0.06	0.09	0.03	0.03	0.11	0.16	0.06	0.02
PC 34:4	0.43	0.15	0.46	0.08	0.71	0.49	0.48	0.07
PC 34:5	0.10	0.05	0.11	0.05	0.26	0.23	0.09	0.01
PC 35:2/36:1p/36:2e	0.56	0.18	0.60	0.19	0.69	0.46	0.69	0.24
PC 35:4/36:3p/36:4e	0.07	0.08	0.06	0.05	0.11	0.16	0.07	0.02
PC 36:2/38:8p/38:9e	20.82	6.61	23.63	3.83	30.79	21.43	23.15	5.09
PC 36:5	0.67	0.20	0.74	0.05	1.85	1.57	0.76	0.22
PC 38:2/40:8p/30:9e	1.19	0.37	1.43	0.22	1.73	1.18	1.36	0.34
PC 38:3/40:9p	0.85	0.27	0.95	0.18	1.07	0.64	1.36	0.45
PC 40:2/42:8p/42:9e	0.06	0.03	0.09	0.01	0.11	0.07	0.10	0.04
PC 40:3/42:9p/42:10e	0.04	0.02	0.04	0.01	0.06	0.04	0.08	0.03
PC 42:2/44:8p/44:9e	0.05	0.03	0.06	0.03	0.09	0.09	0.08	0.02
PC 44:2/46:8p/46:9e	0.02	0.01	0.04	0.03	0.06	0.07	0.02	0.02
PC 48:7/48:0e	0.02	0.01	0.02	0.01	0.02	0.02	0.03	0.02
SM 32:1	0.82	0.30	0.89	0.15	1.29	1.07	0.91	0.10
SM 33:2	0.04	0.01	0.05	0.02	0.06	0.07	0.06	0.01
SM 34:1	9.53	3.66	9.89	1.35	14.19	11.23	10.11	1.60
SM 34:2	0.13	0.13	0.14	0.07	0.28	0.35	0.14	0.04
SM 36:1	0.30	0.13	0.32	0.02	0.41	0.29	0.31	0.04
SM 36:2	0.02	0.01	0.02	0.01	0.02	0.01	0.03	0.01
SM 38:3	0.18	0.15	0.15	0.08	0.17	0.20	0.14	0.08
SM 40:1	1.00	0.51	1.12	0.27	1.69	1.61	1.13	0.18

SM 40:2	0.70	0.25	0.72	0.09	0.96	0.74	0.82	0.11
SM 41:1	0.01	0.01	0.01	0.00	0.03	0.03	0.02	0.00
SM 41:2	0.04	0.02	0.05	0.01	0.05	0.06	0.07	0.01
SM 42:2	6.21	2.54	6.94	1.11	10.46	9.43	7.38	1.04
SM 42:3	0.40	0.18	0.46	0.08	0.67	0.62	0.67	0.15
SM 42:4	0.06	0.03	0.08	0.02	0.08	0.07	0.07	0.02
SM 42:5	0.12	0.04	0.13	0.01	0.17	0.10	0.16	0.05
SM 43:1	0.02	0.01	0.01	0.01	0.03	0.03	0.02	0.01
SM 43:2	0.03	0.03	0.03	0.02	0.06	0.07	0.05	0.02
SM 44:2	1.79	0.84	1.95	0.44	3.25	3.32	1.93	0.39
SM 44:3	0.16	0.13	0.20	0.09	0.40	0.50	0.21	0.06
SM 44:4	0.06	0.04	0.07	0.05	0.14	0.13	0.08	0.02
SM 44:5	0.67	0.22	0.78	0.04	0.88	0.44	0.77	0.19
SM 44:6	0.01	0.01	0.03	0.01	0.03	0.03	0.04	0.01
SM 46:2	0.24	0.10	0.28	0.05	0.36	0.30	0.30	0.07
SM 46:3	0.02	0.01	0.02	0.01	0.04	0.06	0.02	0.01
SM 46:4	0.03	0.02	0.03	0.02	0.06	0.07	0.03	0.02
SM 46:5	0.12	0.07	0.13	0.04	0.17	0.13	0.12	0.02
TG 42:1	0.04	0.03	0.05	0.02	0.04	0.01	0.04	0.03
TG 42:2	0.01	0.01	0.02	0.01	0.01	0.00	0.02	0.01
TG 44:1	0.57	0.49	0.65	0.34	0.57	0.29	0.50	0.32
TG 44:2	0.24	0.18	0.29	0.13	0.25	0.14	0.23	0.14
TG 44:3	0.04	0.02	0.05	0.01	0.04	0.02	0.05	0.03
TG 45:1	0.05	0.06	0.06	0.05	0.06	0.05	0.07	0.05
TG 45:2	0.04	0.04	0.04	0.03	0.04	0.03	0.05	0.03
TG 46:1	2.43	2.20	2.61	1.42	2.18	1.23	1.99	1.28
TG 46:2	1.42	1.18	1.60	0.75	1.33	0.75	1.22	0.71
TG 46:3	0.29	0.20	0.35	0.14	0.29	0.17	0.29	0.15
TG 46:4	0.02	0.02	0.02	0.01	0.03	0.02	0.03	0.02
TG 47:1	0.19	0.19	0.18	0.12	0.14	0.11	0.16	0.12
TG 47:2	0.13	0.12	0.12	0.08	0.10	0.09	0.12	0.08
TG 48:2	9.93	8.79	10.00	4.98	8.22	5.20	7.48	4.36
TG 48:3	1.51	1.18	1.59	0.65	1.39	0.86	1.36	0.70
TG 48:4	0.15	0.10	0.16	0.05	0.16	0.11	0.17	0.09
TG 49:2	0.47	0.44	0.44	0.28	0.34	0.27	0.38	0.25

TG 49:3	0.11	0.09	0.10	0.05	0.08	0.06	0.10	0.06
TG 49:4	0.05	0.04	0.05	0.03	0.05	0.03	0.04	0.02
TG 50:2	13.43	12.29	12.93	6.48	10.74	7.21	9.29	5.27
TG 50:3	5.42	4.56	5.46	2.44	4.60	3.13	4.36	2.34
TG 50:4	0.58	0.41	0.60	0.21	0.58	0.42	0.77	0.40
TG 50:5	0.06	0.04	0.07	0.02	0.13	0.10	0.10	0.06
TG 51:1	0.69	0.84	0.74	0.62	0.75	0.74	0.68	0.54
TG 51:2	0.61	0.74	0.68	0.57	0.49	0.50	0.75	0.59
TG 51:3	0.17	0.15	0.16	0.09	0.13	0.11	0.15	0.09
TG 52:3	20.82	16.95	20.75	9.19	16.95	12.64	13.98	7.29
TG 53:2	1.80	2.19	1.95	1.54	1.86	1.85	1.97	1.56
TG 53:3	0.30	0.27	0.29	0.18	0.24	0.20	0.21	0.13
TG 53:4	0.09	0.08	0.09	0.05	0.08	0.06	0.10	0.06
TG 53:5	0.03	0.02	0.03	0.02	0.04	0.03	0.04	0.03
TG 54:3	14.80	11.88	15.10	7.18	11.39	8.76	9.51	4.99
TG 54:4	2.61	1.86	2.67	1.20	2.08	1.65	4.10	2.30
TG 54:5	0.52	0.35	0.52	0.22	0.65	0.48	1.39	0.83
TG 54:6	0.19	0.17	0.22	0.10	0.78	0.62	0.35	0.20
TG 55:2	1.06	1.29	1.26	0.94	0.99	0.98	1.18	0.93
TG 55:3	0.66	0.80	0.74	0.60	0.55	0.55	0.91	0.71
TG 55:4	0.10	0.12	0.11	0.09	0.13	0.13	0.22	0.17
TG 55:5	0.03	0.02	0.03	0.01	0.03	0.02	0.03	0.02
TG 56:3	3.10	2.62	3.39	1.80	2.48	1.67	2.44	1.51
TG 56:4	1.09	0.80	1.14	0.50	0.87	0.69	1.07	0.61
TG 56:5	0.45	0.31	0.47	0.19	0.47	0.35	0.65	0.38
TG 56:6	0.16	0.13	0.19	0.07	0.54	0.41	0.26	0.16
TG 56:7	0.17	0.18	0.24	0.09	0.81	0.76	0.16	0.10
TG 57:3	0.25	0.30	0.30	0.23	0.29	0.26	0.29	0.24
TG 58:8	0.07	0.07	0.17	0.05	0.30	0.25	0.08	0.07
FFA 16:0	1.18	0.89	0.94	0.20	0.89	0.30	0.80	0.23
FFA 16:1	0.17	0.14	0.20	0.18	0.24	0.27	0.21	0.08
FFA 18:1	4.38	2.42	3.92	0.50	4.10	1.85	3.50	0.43
FFA 18:2	0.06	0.05	0.08	0.06	0.11	0.14	0.30	0.03
FFA 20:0	0.04	0.05	0.03	0.01	0.01	0.01	0.03	0.02
FFA 20:1	0.10	0.07	0.09	0.03	0.10	0.06	0.10	0.01

FFA 20:3	0.03	0.03	0.05	0.08	0.15	0.24	0.05	0.06
FFA 22:0	0.31	0.36	0.29	0.18	0.22	0.19	0.29	0.19
FFA 22:1	0.15	0.18	0.11	0.02	0.07	0.05	0.11	0.06
FFA 24:0	1.46	1.38	1.42	0.67	1.04	0.67	1.41	0.82
FFA 24:1	1.22	1.30	1.03	0.43	0.70	0.55	0.94	0.47
FFA 26:1	1.28	1.05	1.21	0.22	0.93	0.46	1.11	0.43
FFA 28:1	0.60	0.56	0.54	0.15	0.43	0.25	0.56	0.29
FFA 30:1	0.73	0.68	0.63	0.27	0.46	0.27	0.65	0.34
FFA 32:1	0.52	0.55	0.43	0.23	0.29	0.16	0.49	0.31

Table A 9.3 Membrane lipids measured in HDF (n= 3 individual donors).

Species	Control		DHA		EPA		LA	
	Mean	SD	Mean	SD	Mean	SD	Mean	SD
CE 16:1	0.41	0.05	0.68	0.27	0.88	0.48	0.61	0.26
CE 18:1	2.97	0.59	3.59	1.25	4.42	2.31	3.60	1.48
CE 18:2	0.39	0.13	0.45	0.41	0.73	0.57	1.77	1.74
CE 20:5	1.13	0.34	1.15	0.20	2.63	0.63	1.81	0.15
CE 22:5	0.43	0.34	0.66	0.40	2.42	2.90	0.39	0.50
CE 22:6	0.76	0.38	1.97	0.99	1.09	1.32	0.41	0.43
DG 35:1	0.04	0.01	0.04	0.01	0.04	0.02	0.03	0.01
DG 37:4	0.87	0.27	0.94	0.31	1.06	0.45	0.67	0.27
DG 38:3	0.12	0.04	0.12	0.05	0.13	0.06	0.08	0.04
LPC 16:0	8.83	1.85	8.96	2.36	9.85	3.05	5.81	2.14
LPC 18:0	15.93	3.16	17.96	5.30	21.21	7.77	14.70	4.88
LPC 18:1	4.93	0.96	4.72	1.69	5.32	2.09	2.78	0.85
LPC 20:3	1.02	0.14	0.96	0.19	1.25	0.54	0.92	0.59
LPC 24:1	3.57	1.65	3.62	1.47	3.95	1.78	2.84	1.29
PC 28:0	0.06	0.02	0.08	0.04	0.08	0.03	0.06	0.04
PC 30:0	2.22	0.44	2.51	0.57	3.10	0.81	2.32	0.80
PC 30:0e	0.12	0.03	0.16	0.04	0.19	0.07	0.11	0.04
PC 30:1	0.30	0.09	0.34	0.11	0.40	0.15	0.20	0.09
PC 32:0	7.72	1.24	8.68	1.53	10.45	1.64	9.26	2.09
PC 32:0e	1.21	0.17	1.47	0.31	1.70	0.44	1.22	0.35
PC 32:0p/PC 32:1e	0.53	0.15	0.64	0.23	0.72	0.34	0.37	0.10

PC 32:1	6.65	1.17	7.74	1.42	8.64	2.64	4.46	1.02
PC 32:2	0.72	0.18	0.83	0.21	0.93	0.38	0.90	0.33
PC 32:3	0.13	0.04	0.14	0.05	0.17	0.09	0.13	0.05
PC 33:1/34:0p/34:1e	2.45	0.58	2.72	0.68	3.12	0.83	1.82	0.58
PC 33:2/34:1p/34:2e	0.47	0.11	0.52	0.14	0.59	0.22	0.58	0.22
PC 33:3/34:2p/34:3e	0.04	0.01	0.05	0.02	0.06	0.02	0.07	0.03
PC 34:1	26.94	4.23	30.13	5.09	33.47	6.34	18.92	5.37
PC 34:2	5.52	0.91	6.53	1.26	7.36	2.14	10.96	3.38
PC 34:3	0.85	0.18	1.00	0.26	1.19	0.48	1.94	0.63
PC 34:5	0.02	0.01	0.03	0.01	0.08	0.04	0.05	0.03
PC 35:0/36:0e	0.04	0.02	0.03	0.01	0.05	0.02	0.05	0.05
PC 35:1/36:0p/36:1e	1.40	0.27	1.55	0.38	1.80	0.40	1.03	0.41
PC 35:2/36:1p/36:2e	1.01	0.20	1.14	0.26	1.27	0.37	1.01	0.36
PC 35:4/36:3p/36:4e	0.12	0.03	0.14	0.05	0.14	0.07	0.09	0.02
PC 35:5/36:4p/36:5e	0.15	0.07	0.16	0.08	0.25	0.15	0.08	0.02
PC 36:2/38:8p/38:9e	17.07	2.73	19.49	3.55	22.12	6.18	15.93	3.69
PC 36:5	0.98	0.21	1.23	0.23	2.52	0.94	0.78	0.15
PC 36:6	0.11	0.03	0.20	0.04	0.35	0.16	0.10	0.03
PC 37:0/38:0e	0.27	0.05	0.42	0.07	0.38	0.19	0.32	0.08
PC 37:1/38:0p/38:1e	0.06	0.01	0.08	0.03	0.15	0.04	0.07	0.04
PC 37:2/38:1p/38:2e	0.23	0.05	0.25	0.06	0.26	0.07	0.24	0.12
PC 37:5/38:4p/38:5e	1.31	0.24	1.37	0.41	1.57	0.64	0.97	0.16
PC 38:0/40:6p/40:7e	0.18	0.02	0.29	0.06	0.18	0.06	0.10	0.02

PC 38:1/40:7p/40: 8e	0.03	0.01	0.05	0.01	0.03	0.01	0.04	0.01
PC 38:3/40:9p	0.04	0.02	0.04	0.02	0.05	0.03	0.03	0.03
PC 38:5	12.34	2.59	12.80	2.70	17.35	5.76	10.37	1.33
PC 38:5p/38:6e	0.24	0.04	0.33	0.07	0.42	0.16	0.14	0.02
PC 38:6	1.75	0.22	2.89	0.33	3.48	1.19	1.44	0.11
PC 40:1p/40:2e	0.11	0.02	0.18	0.03	0.23	0.10	0.06	0.01
PC 40:4p/40:5e	0.44	0.05	0.45	0.09	0.58	0.13	0.33	0.12
PC 40:4p/40:6e	0.30	0.01	0.39	0.07	0.49	0.12	0.18	0.05
PC 40:6	4.00	0.14	4.64	0.71	7.21	1.65	3.34	0.80
PC 40:8/40:0p/40: 1e	0.35	0.06	0.40	0.08	0.59	0.21	0.31	0.03
PC 42:0p/42:1e	0.09	0.02	0.10	0.02	0.17	0.06	0.12	0.02
PC 42:1p/42:2e	0.18	0.04	0.22	0.04	0.36	0.13	0.11	0.01
PC 42:2p/42:3e	0.03	0.01	0.06	0.01	0.03	0.02	0.02	0.01
PC 42:5p/42:6e	0.04	0.01	0.04	0.01	0.07	0.01	0.03	0.01
PC 42:6	0.22	0.01	0.25	0.04	0.55	0.15	0.33	0.10
PC 42:7/42:0e	0.10	0.01	0.14	0.04	0.17	0.05	0.15	0.04
PC 44:2p/44:3e	0.02	0.01	0.03	0.01	0.13	0.05	0.02	0.01
PC 44:7/44:0e	0.02	0.01	0.02	0.01	0.05	0.03	0.05	0.01
PE 36:3	0.54	0.36	0.37	0.16	0.93	0.66	2.57	1.75
PE 36:4	0.82	0.47	0.54	0.20	0.86	0.37	1.13	0.63
PE 36:4p/36:5e	3.71	1.64	2.29	1.14	4.77	2.51	3.47	1.94
PE 36:5	0.59	0.24	0.33	0.11	0.91	0.43	0.61	0.30
PE 36:5p/36:6e	0.10	0.11	0.12	0.09	1.17	0.75	0.05	0.04
PE 38:0/40:6p/40: 7e	2.71	1.33	2.31	1.00	4.05	2.62	2.10	0.99
PE 38:0p/38:1e	0.30	0.10	0.35	0.15	0.22	0.09	0.27	0.11
PE 38:1/40:7p/40: 8e	1.10	0.47	1.14	0.60	0.98	0.37	1.11	0.50
PE 38:6	1.92	1.06	1.74	0.96	3.06	1.75	1.47	0.76
PE 40:1p/40:2e	0.28	0.13	0.30	0.17	0.42	0.24	0.19	0.10
PE 40:6	2.81	1.70	2.37	1.49	5.41	4.47	3.23	2.21
PE 40:7/40:0e	1.33	0.67	1.29	0.89	1.35	0.73	1.42	0.88
PE 42:2p/42:3e	0.09	0.05	0.16	0.12	0.08	0.07	0.10	0.04

PE 42:9/42:1p/42: 2e	0.31	0.19	0.33	0.27	0.69	0.70	0.36	0.25
PE 46:2/48:8p/48: 9e	0.29	0.30	0.19	0.14	0.57	0.56	0.40	0.37
SM 32:1	0.17	0.04	0.17	0.05	0.23	0.12	0.18	0.06
SM 33:2	0.16	0.03	0.17	0.05	0.22	0.09	0.15	0.04
SM 34:1	6.00	1.85	6.25	1.98	8.15	4.35	5.84	2.17
SM 34:2	0.22	0.10	0.23	0.12	0.32	0.23	0.20	0.10
SM 35:0	0.13	0.06	0.13	0.06	0.17	0.09	0.12	0.08
SM 35:1	0.19	0.06	0.18	0.05	0.25	0.11	0.19	0.06
SM 36:0	0.42	0.11	0.46	0.15	0.52	0.22	0.35	0.13
SM 36:1	0.22	0.03	0.22	0.02	0.27	0.07	0.17	0.03
SM 38:3	0.04	0.02	0.05	0.02	0.05	0.03	0.03	0.01
SM 40:1	0.59	0.26	0.63	0.27	0.82	0.51	0.40	0.09
SM 40:2	0.13	0.06	0.12	0.06	0.18	0.12	0.09	0.03
SM 41:2	0.29	0.10	0.30	0.10	0.38	0.21	0.25	0.08
SM 42:2	3.85	1.55	3.97	1.61	4.62	2.70	2.97	1.07
SM 44:2	0.03	0.03	0.04	0.03	0.05	0.05	0.03	0.02
SM 44:4	0.05	0.02	0.05	0.03	0.06	0.03	0.03	0.01
SM 44:5	0.40	0.13	0.43	0.15	0.53	0.35	0.42	0.22
SM 44:6	0.07	0.04	0.07	0.04	0.09	0.08	0.24	0.15
TG 48:1	0.08	0.02	0.09	0.01	0.06	0.01	0.03	0.02
TG 50:1	0.14	0.03	0.13	0.02	0.09	0.02	0.05	0.02
TG 50:2	0.06	0.02	0.05	0.02	0.04	0.00	0.05	0.02
TG 52:2	0.18	0.04	0.17	0.05	0.14	0.02	0.13	0.07
TG 52:3	0.13	0.04	0.14	0.05	0.15	0.06	0.18	0.08
TG 53:2	0.05	0.01	0.05	0.02	0.05	0.02	0.03	0.01
TG 54:5	0.18	0.04	0.19	0.08	0.21	0.06	0.41	0.29
TG 54:6	0.04	0.01	0.06	0.04	0.09	0.05	0.09	0.08
TG 56:6	0.13	0.03	0.16	0.10	0.25	0.13	0.31	0.24
TG 56:7	0.04	0.01	0.07	0.06	0.06	0.04	0.11	0.10
TG 58:8	0.03	0.01	0.05	0.05	0.06	0.04	0.13	0.13
FFA 16:0	0.16	0.11	0.28	0.07	0.29	0.12	0.19	0.09
FFA 18:1	0.45	0.12	0.47	0.15	0.53	0.18	0.27	0.19

Appendix 10

Table A 10.1 Endocannabinoids and their congeners measured in rat skin (n= 6 individual donors).

Species	Control		Diabetic	
	Mean	SD	Mean	SD
MEA	0.92	0.19	1.36	0.45
PDEA	0.16	0.03	0.22	0.06
POEA	0.14	0.09	0.52	0.27
PEA	6.65	0.90	7.57	0.99
HEA	0.19	0.06	0.24	0.03
LEA	0.86	0.27	1.01	0.48
OEA	1.36	0.24	1.55	0.18
VEA	1.65	0.45	0.63	0.35
SEA	3.55	0.51	4.63	0.59
AG	552.62	151.28	842.07	410.57
LG	164.49	67.12	232.95	373.42
OG	35.53	8.10	30.74	27.06
STG	591.59	161.13	849.46	370.48

Table A 10.2 Endocannabinoids and their congeners measured in rat plasma (n= 6 individual donors).

Species	Control		Diabetic	
	Mean	SD	Mean	SD
MEA	20.00	4.10	15.17	3.43
PDEA	7.67	2.58	3.83	0.75
POEA	150.33	56.57	106.50	31.59
PEA	539.50	71.62	376.83	87.05
HEA	9.83	2.23	7.67	2.07
ALEA	4.83	1.47	4.17	1.33
LEA	173.17	49.44	160.50	32.48
OEA	154.50	25.30	101.17	19.91
VEA	41.00	5.90	20.83	4.17
SEA	405.83	64.50	337.33	91.68
AG	770.67	847.17	591.67	584.72
LG	408.67	112.08	625.50	156.93
OG	122.83	32.82	92.17	20.70
STG	773.00	846.87	595.50	583.70